PHASE 2 INITIAL BOREHOLE DRILLING AND TESTING, SOUTH BRUCE

WP06: Hydraulic Testing Summary Report for SB_BH02

APM-REP-01332-0336 **October 2023**

Geofirma Engineering

nwmo
NUCLEAR WASTE MANAGEMENT ORGANIZATION
SOCIÉTÉ DE GESTION DES DÉCHETS NUCLÉAIRES

Phase 2 Initial Borehole Drilling and Testing, South Bruce

WP06: Hydraulic Testing Summary Report for SB_BH02

Revision: 1 (Final)

Prepared for:

Nuclear Waste Management Organization
22 St. Clair Avenue East. 6th Floor
Toronto, ON, M4T 2S3

Prepared by:

GEOFIRMA ENGINEERING
1 Raymond St. Suite 200, Ottawa, Ontario K1R 1A2
613.232.2525 613.232.7149 geofirma.com

AMP-REP-01332-0336

Project Number: 20-211-1

Document ID: WP06 Summary Report - Hydraulic Testing for SB_BH02_R0.docx

October 31, 2023

Title:	WP06: Hydraulic Testing Summary Report for SB_BH02	
Client:	Nuclear Waste Management Organization	
Project Number:	20-211-1	
Document ID:	WP06 Summary Report - Hydraulic Testing for SB_BH02_R0.docx	
Revision Number:	1	Date: October 31, 2023
Prepared by:	John Avis, B.A.Sc. P.Eng., Randy Roberts, M.Sc.	
Reviewed by:	Rick Beauheim, M.Sc., Sean Sterling, M.Sc., P.Eng., P.Geo.	
Approved by:	 Sean Sterling, M.Sc, P.Eng., P.Geo. – Project Manager - Principal	

Revision Tracking Table

Revision	Revision Release Date	Description of Modifications/Edits
R0	September 21, 2023	Initial release
R1	October 31, 2023	Revised for NWMO comments

TABLE OF CONTENTS

1 INTRODUCTION 1
1.1 Borehole SB_BH02 1
1.2 Hydraulic Testing Activities 4
1.3 Reported Analyses 4

2 EQUIPMENT 5
2.1 Mobile Integrated Aquifer Testing & Analysis (MIATA) Platform 5
2.2 Data Acquisition and Control System (DACS) 7
2.3 Pressure Maintenance System 8
2.4 Hydraulic Test Tool (HTT) 9
2.4.1 Packers 9
2.4.2 Downhole Shut-In Valve 10
2.4.3 Sensor Carrier 11
2.4.4 Piston Pulse Generators 11
2.4.5 Test Interval 12
2.4.6 Pressure Transducers 13
2.4.7 Temperature Transducers 13
2.4.8 Tubing String 13
2.4.9 Barometer 14
2.5 Summary of Measurement and Test Equipment 14

3 TESTING METHODOLOGY 17
3.1 Tool Assembly 17
3.2 HTT Installation and Leak Testing 17
3.3 Packer Inflation 18
3.4 System Stabilization 19
3.5 Slug Testing 20
3.6 Pulse Testing 20
3.7 Test Termination 20
3.8 Real-Time Analysis 20

4 ANALYSIS APPROACH 22
4.1 Conceptual Model 22
4.2 Parameters 23
4.3 Tests 24
4.4 Formation Specific Storage - Skin Conductivity - Skin Thickness 25
4.5 Pre-Test Borehole History 27
4.6 Test Zone Thermal Effects 28
4.7 Uncertainty Analysis 30

5 TEST INTERVALS 37

6 INDIVIDUAL TEST ANALYSES 40

7 ANALYSES SUMMARY 41
7.1 Summary Tables 41

7.2 Summary Figures 47

8 REFERENCES 51

APPENDIX A 52

A.1 HT01_05 Salina A2 Evaporite 53
A.1.1 Test Data Summary 53
A.1.2 Test Analyses 54
A.1.3 Uncertainty Analyses 56
A.1.4 Additional Figures 64
A.2 HT02_05 Guelph 67
A.2.1 Test Data Summary 67
A.2.2 Test Analyses 68
A.2.3 Uncertainty Analyses 70
A.2.4 Additional Figures 78
A.3 HT03_05 Blue Mountain - Lower 81
A.3.1 Test Data Summary 81
A.3.2 Test Analyses 82
A.3.3 Uncertainty Analyses 84
A.3.4 Additional Figures 92
A.4 HT04_05 Shadow Lake 95
A.4.1 Test Data Summary 95
A.4.2 Test Analyses 96
A.4.3 Uncertainty Analyses 98
A.4.4 Additional Figures 106
A.5 HT05_05 PreCambrian 109
A.5.1 Test Data Summary 109
A.5.2 Test Analyses 110
A.5.3 Uncertainty Analyses 113
A.5.4 Additional Figures 120
A.6 HT01_30 Salina F 123
A.6.1 Test Data Summary 123
A.6.2 Test Analyses 124
A.6.3 Uncertainty Analyses 126
A.6.4 Additional Figures 134
A.7 HT02_30 Salina A1 137
A.7.1 Test Data Summary 137
A.7.2 Test Analyses 138
A.7.3 Uncertainty Analyses 140
A.7.4 Additional Figures 148
A.8 HT03_30 Goat Island 151
A.8.1 Test Data Summary 151
A.8.2 Test Analyses 152
A.8.3 Uncertainty Analyses 154
A.8.4 Additional Figures 162
A.9 HT04_30 Cabot Head 165
A.9.1 Test Data Summary 165
A.9.2 Test Analyses 166
A.9.3 Uncertainty Analyses 168
A.9.4 Additional Figures 176

A.10 HT05_30 Upper Queenston 179
A.10.1 Test Data Summary 179
A.10.2 Test Analyses 180
A.10.3 Uncertainty Analyses 182
A.10.4 Additional Figures 190
A.11 HT06_30 Lower Queenston 193
A.11.1 Test Data Summary 193
A.11.2 Test Analyses 194
A.11.3 Uncertainty Analyses 196
A.11.4 Additional Figures 204
A.12 HT07_30 Upper Georgian Bay 207
A.12.1 Test Data Summary 207
A.12.2 Test Analyses 208
A.12.3 Uncertainty Analyses 210
A.12.4 Additional Figures 218
A.13 HT08_30 Lower Georgian Bay 221
A.13.1 Test Data Summary 221
A.13.2 Test Analyses 222
A.13.3 Uncertainty Analyses 224
A.13.4 Additional Figures 232
A.14 HT09_30 Blue Mountain 235
A.14.1 Test Data Summary 235
A.14.2 Test Analyses 236
A.14.3 Uncertainty Analyses 238
A.14.4 Additional Figures 246
A.15 HT10_30 Collingwood/Cobourg 249
A.15.1 Test Data Summary 249
A.15.2 Test Analyses 250
A.15.3 Uncertainty Analyses 252
A.15.4 Additional Figures 260
A.16 HT11_30 Lower Cobourg 263
A.16.1 Test Data Summary 263
A.16.2 Test Analyses 264
A.16.3 Uncertainty Analyses 266
A.16.4 Additional Figures 274
A.17 HT12_30 Sherman Fall 277
A.17.1 Test Data Summary 277
A.17.2 Test Analyses 278
A.17.3 Uncertainty Analyses 280
A.17.4 Additional Figures 288
A.18 HT13_30 Kirkfield 291
A.18.1 Test Data Summary 291
A.18.2 Test Analyses 292
A.18.3 Uncertainty Analyses 294
A.18.4 Additional Figures 302
A.19 HT14_30 Coboconk 305
A.19.1 Test Data Summary 305
A.19.2 Test Analyses 306
A.19.3 Uncertainty Analyses 308
A.19.4 Additional Figures 315

A.20 HT15_30 Gull River 318
A.20.1 Test Data Summary 318
A.20.2 Test Analyses 319
A.20.3 Uncertainty Analyses 322
A.20.4 Additional Figures 330

LIST OF TABLES

Table 2.1 Measurement and Test Equipment Calibration Summary. 14
Table 5.1 SB_BH02 hydraulic testing intervals. 38
Table 7.1 SB_BH02 Summary of Formation Hydraulic Conductivity Estimates. 41
Table 7.2 SB_BH02 Summary of Formation Pressure Estimates (Adjusted to Interval Midpoint). 42
Table 7.3 SB_BH02 Summary of Specific Storage Estimates. 43
Table 7.4 SB_BH02 Summary of Skin Hydraulic Conductivity Estimates. 44
Table 7.5 SB_BH02 Summary of Skin Thickness Estimates. 45
Table 7.6 SB_BH02 Summary of Calculated Skin Factor. 46
Table 7.7 SB_BH02 Summary of Simulation Input Parameters 47
Table A.1 - Summary of Test Events. 53
Table A.2 – nSIGHTS Input Parameters. 54
Table A.3 – nSIGHTS Parameter Optimization Ranges. 54
Table A.4 - Summary of the HT01_05 parameter estimates. 63
Table A.5 – Pearson cross-correlations of 5% to 95% parameters 63
Table A.6 - Summary of Test Events. 67
Table A.7 – nSIGHTS Input Parameters. 68
Table A.8 – nSIGHTS Parameter Optimization Ranges. 68
Table A.9 - Summary of the HT02_05 parameter estimates. 77
Table A.10 – Pearson cross-correlations of 5% to 95% parameters 77
Table A.11 - Summary of Test Events. 81
Table A.12 – nSIGHTS Input Parameters. 82
Table A.13 – nSIGHTS Parameter Optimization Ranges. 82
Table A.14 - Summary of the HT03_05 parameter estimates. 91
Table A.15 – Pearson cross-correlations of 5% to 95% parameters 91
Table A.16 - Summary of Test Events. 95
Table A.17 – nSIGHTS Input Parameters. 96
Table A.18 – nSIGHTS Parameter Optimization Ranges. 96
Table A.19 - Summary of the HT04_05 parameter estimates. 105
Table A.20 – Pearson cross-correlations of 5% to 95% parameters 105
Table A.21 - Summary of Test Events. 109
Table A.22 – nSIGHTS Input Parameters. 110
Table A.23 – nSIGHTS Parameter Optimization Ranges. 110
Table A.24 - Summary of the HT05_05 parameter estimates. 119
Table A.25 – Pearson cross-correlations of 5% to 95% parameters 119
Table A.26 - Summary of Test Events. 123
Table A.27 – nSIGHTS Input Parameters. 124
Table A.28 – nSIGHTS Parameter Optimization Ranges. 124
Table A.29 - Summary of the HT01_30 parameter estimates. 133
Table A.30 – Pearson cross-correlations of 5% to 95% parameters 133
Table A.31 - Summary of Test Events. 137
Table A.32 – nSIGHTS Input Parameters. 138
Table A.33 – nSIGHTS Parameter Optimization Ranges. 138
Table A.34 - Summary of the HT02_30 parameter estimates. 147
Table A.35 – Pearson cross-correlations of 5% to 95% parameters 147
Table A.36 - Summary of Test Events. 151
Table A.37 – nSIGHTS Input Parameters. 152
Table A.38 – nSIGHTS Parameter Optimization Ranges. 152
Table A.39 - Summary of the HT03_30 parameter estimates. 161
Table A.40 – Pearson cross-correlations of 5% to 95% parameters 161
Table A.41 - Summary of Test Events. 165

Table A.42 – nSIGHTS Input Parameters. 166
Table A.43 – nSIGHTS Parameter Optimization Ranges. 166
Table A.44 - Summary of the HT04_30 parameter estimates. 175
Table A.45 – Pearson cross-correlations of 5% to 95% parameters 175
Table A.46 - Summary of Test Events. 179
Table A.47 – nSIGHTS Input Parameters. 180
Table A.48 – nSIGHTS Parameter Optimization Ranges. 180
Table A.49 - Summary of the HT05_30 parameter estimates. 189
Table A.50 – Pearson cross-correlations of 5% to 95% parameters 189
Table A.51 - Summary of Test Events. 193
Table A.52 – nSIGHTS Input Parameters. 194
Table A.53 – nSIGHTS Parameter Optimization Ranges. 194
Table A.54 - Summary of the HT06_30 parameter estimates. 203
Table A.55 – Pearson cross-correlations of 5% to 95% parameters 203
Table A.56 - Summary of Test Events. 207
Table A.57 – nSIGHTS Input Parameters. 208
Table A.58 – nSIGHTS Parameter Optimization Ranges. 208
Table A.59 - Summary of the HT07_30 parameter estimates. 217
Table A.60 – Pearson cross-correlations of 5% to 95% parameters 217
Table A.61 - Summary of Test Events. 221
Table A.62 – nSIGHTS Input Parameters. 222
Table A.63 – nSIGHTS Parameter Optimization Ranges. 222
Table A.64 - Summary of the HT08_30 parameter estimates. 231
Table A.65 – Pearson cross-correlations of 5% to 95% parameters 231
Table A.66 - Summary of Test Events. 235
Table A.67 – nSIGHTS Input Parameters. 236
Table A.68 – nSIGHTS Parameter Optimization Ranges. 236
Table A.69 - Summary of the HT09_30 parameter estimates. 245
Table A.70 – Pearson cross-correlations of 5% to 95% parameters 245
Table A.71 - Summary of Test Events. 249
Table A.72 – nSIGHTS Input Parameters. 250
Table A.73 – nSIGHTS Parameter Optimization Ranges. 250
Table A.74 - Summary of the HT10_30 parameter estimates. 259
Table A.75 – Pearson cross-correlations of 5% to 95% parameters 259
Table A.76 - Summary of Test Events. 263
Table A.77 – nSIGHTS Input Parameters. 264
Table A.78 – nSIGHTS Parameter Optimization Ranges. 264
Table A.79 - Summary of the HT11_30 parameter estimates. 273
Table A.80 – Pearson cross-correlations of 5% to 95% parameters 273
Table A.81 - Summary of Test Events. 277
Table A.82 – nSIGHTS Input Parameters. 278
Table A.83 – nSIGHTS Parameter Optimization Ranges. 278
Table A.84 - Summary of the HT12_30 parameter estimates. 287
Table A.85 – Pearson cross-correlations of 5% to 95% parameters 287
Table A.86 - Summary of Test Events. 291
Table A.87 – nSIGHTS Input Parameters. 292
Table A.88 – nSIGHTS Parameter Optimization Ranges. 292
Table A.89 - Summary of the HT13_30 parameter estimates. 301
Table A.90 – Pearson cross-correlations of 5% to 95% parameters 301
Table A.91 - Summary of Test Events. 305
Table A.92 – nSIGHTS Input Parameters. 306
Table A.93 – nSIGHTS Parameter Optimization Ranges. 306
Table A.94 - Summary of the HT14_30 parameter estimates. 314

Table A.95 – Pearson cross-correlations of 5% to 95% parameters..... 314
Table A.96 - Summary of Test Events..... 318
Table A.97 – nSIGHTS Input Parameters. 319
Table A.98 – nSIGHTS Parameter Optimization Ranges. 319
Table A.99 - Summary of the HT15_30 parameter estimates..... 329
Table A.100 – Pearson cross-correlations of 5% to 95% parameters..... 329

LIST OF FIGURES

Figure 1.1 SB_BH02 Site Location. 2
Figure 1.2 Generalized Stratigraphic Bedrock Sequence in South Bruce Area (after Armstrong and Carter, 2010)..... 3
Figure 2.1 MIATA platform (white trailer) at the SB_BH01 testing site. A similar configuration was used at SB_BH02. 6
Figure 2.2 Interior of MIATA platform. 7
Figure 2.3 Schematic of Packer Pressure Maintenance System. 8
Figure 2.4 General Hydraulic Test Tool Schematic. 9
Figure 2.5 Baski Fracker Packer. 10
Figure 2.6 Downhole Shut-In Valve (DHSIV). 11
Figure 2.7 Hydraulic Pulse Generating Piston. 12
Figure 2.8 Perforated Pup Joints. 13
Figure 2.9 As-built 29.96-m test tool with measurements. 15
Figure 2.10 As-built 5.03-m test tool with measurements. 16
Figure 3.1 Analysis of leak test of 5.03 m HTT system. 17
Figure 3.2 Packer Inflation Pressure Ranges 19
Figure 4.1 An X-Y-Z scatter plot showing the correlation among skin thickness, skin hydraulic conductivity, and specific storage that can occur in a single-well test. 25
Figure 4.2 Ramey B diagnostic plots showing various combinations of skin factors and formation specific storage. 26
Figure 4.3 Pre-test borehole history for test HT10_30. 28
Figure 4.4 Test zone temperature during 5 m pulse tests in SB_BH02. 29
Figure 4.5 Initial parameter estimates for K_f, K_s, and P_f (HT13_30). 30
Figure 4.6 Initial parameter estimates for K_f, Ss, and t_s (HT13_30). 31
Figure 4.7 Converged parameter estimates for K_f, K_s, and P_f parameters (HT13_30). 31
Figure 4.8 Converged parameter estimates for K_f, Ss, and t_s (HT13_30). 32
Figure 4.9 Normalized fit CDF (HT13_30). 33
Figure 4.10 Fit distribution for K_f (HT13_30). 33
Figure 4.11 Accepted estimates for K_f, K_s, and P_f with fit values and best-fit (HT13_30). 34
Figure 4.12 Accepted estimates for K_f, Ss, and t_s with fit values and best-fit (HT13_30). 34
Figure 4.13 Cumulative distribution of accepted formation hydraulic conductivity (HT13_30). 35
Figure 4.14 Horsetail plot showing perturbation results. 35
Figure 4.15 Ramey B processed horsetail plot showing perturbation results (HT13_30). 36
Figure 5.1 SB_BH02 hydraulic testing test intervals. 39
Figure 7.1 Formation Hydraulic Conductivity, Specific Storage and Adjusted Formation Pressure. 48
Figure 7.2 Skin Hydraulic Conductivity, Skin Thickness and Skin Factor. 49
Figure 7.3 Simulation Parameters: Test Zone Compressibility, Test Zone Radius, Borehole Fluid Density. 50
Figure A.1 - Test events and pressures. 53
Figure A.2 - Annotated testing sequence showing best-fit simulation and parameter estimates. 54
Figure A.3 - Annotated testing sequence showing pre-test history, best-fit simulation and parameter estimates. 55
Figure A.4 - Log-log plot showing Ramey B and derivative response for best-fit simulation. 55
Figure A.5 - Normalized Jacobian for best-fit simulation. 56
Figure A.6 - Fit value cumulative distribution function. 56
Figure A.7 – Detail of fit value cumulative distribution function. 57
Figure A.8 - XY-scatter plot showing estimates of formation hydraulic conductivity (K_f) vs static formation pressure (P_f) (top panel) and specific storage (Ss) (bottom panel). 58

Figure A.9 - XY-scatter plot showing estimates of static formation pressure (P_f) vs specific storage (Ss) (top panel) and skin hydraulic conductivity (K_s) vs skin thickness (t_s) (bottom panel). . 59
Figure A.10 – Cumulative distribution functions and parameter limits for formation hydraulic conductivity (K_f) (top panel), static formation pressure (P_f) (middle panel) and specific storage (Ss) (bottom panel)..... 60
Figure A.11 – Cumulative distribution functions and parameter limits for skin hydraulic conductivity (K_s) (top panel), skin thickness (t_s) (middle panel) and skin factor (s) (bottom panel). 61
Figure A.12 – Perturbation results – all converged, accepted, and within 5% to 95% for all parameters. 62
Figure A.13 – Log-log plot showing Ramey B and derivative response for all converged optimizations and those within 5% to 95% for all parameters. 62
Figure A.14 - Hydraulics pressures and surface temperature/barometric pressure. 64
Figure A.15 - XY-scatter plot showing the formation parameter space normalized fit values. 65
Figure A.16 - XY-scatter plot showing the skin parameter space normalized fit values. 66
Figure A.17 - Test events and pressures. 67
Figure A.18 - Annotated testing sequence showing best-fit simulation and parameter estimates. 68
Figure A.19 - Annotated testing sequence showing pre-test history, best-fit simulation and parameter estimates. 69
Figure A.20 - Log-log plot showing Ramey B and derivative response for best-fit simulation. 69
Figure A.21 - Normalized Jacobian for best-fit simulation..... 70
Figure A.22 - Fit value cumulative distribution function..... 71
Figure A.23 – Detail of fit value cumulative distribution function. 71
Figure A.24 - XY-scatter plot showing estimates of formation hydraulic conductivity (K_f) vs static formation pressure (P_f) (top panel) and specific storage (Ss) (bottom panel). 72
Figure A.25 - XY-scatter plot showing estimates of static formation pressure (P_f) vs specific storage (Ss) (top panel) and skin hydraulic conductivity (K_s) vs skin thickness (t_s) (bottom panel). . 73
Figure A.26 – Cumulative distribution functions and parameter limits for formation hydraulic conductivity (K_f) (top panel), static formation pressure (P_f) (middle panel) and specific storage (Ss) (bottom panel)..... 74
Figure A.27 – Cumulative distribution functions and parameter limits for skin hydraulic conductivity (K_s) (top panel), skin thickness (t_s) (middle panel) and skin factor (s) (bottom panel). 75
Figure A.28 – Perturbation results – all converged, accepted, and within 5% to 95% for all parameters. 76
Figure A.29 – Log-log plot showing Ramey B and derivative response for all converged optimizations and those within 5% to 95% for all parameters. 76
Figure A.30 - Hydraulics pressures and surface temperature/barometric pressure. 78
Figure A.31 - XY-scatter plot showing the formation parameter space normalized fit values. 79
Figure A.32 - XY-scatter plot showing the skin parameter space normalized fit values. 80
Figure A.33 - Test events and pressures. 81
Figure A.34 - Annotated testing sequence showing best-fit simulation and parameter estimates. 82
Figure A.35 - Annotated testing sequence showing pre-test history, best-fit simulation and parameter estimates. 83
Figure A.36 - Log-log plot showing Ramey B and derivative response for best-fit simulation. 83
Figure A.37 - Normalized Jacobian for best-fit simulation..... 84
Figure A.38 - Fit value cumulative distribution function..... 85
Figure A.39 – Detail of fit value cumulative distribution function. 85
Figure A.40 - XY-scatter plot showing estimates of formation hydraulic conductivity (K_f) vs static formation pressure (P_f) (top panel) and specific storage (Ss) (bottom panel). 86
Figure A.41 - XY-scatter plot showing estimates of static formation pressure (P_f) vs specific storage (Ss) (top panel) and skin hydraulic conductivity (K_s) vs skin thickness (t_s) (bottom panel). . 87
Figure A.42 – Cumulative distribution functions and parameter limits for formation hydraulic conductivity (K_f) (top panel), static formation pressure (P_f) (middle panel) and specific storage (Ss) (bottom panel)..... 88

Figure A.43 – Cumulative distribution functions and parameter limits for skin hydraulic conductivity (K_s) (top panel), skin thickness (t_s) (middle panel) and skin factor (s) (bottom panel). 89
Figure A.44 – Perturbation results – all converged, accepted, and within 5% to 95% for all parameters. 90
Figure A.45 – Log-log plot showing Ramey B and derivative response for all converged optimizations and those within 5% to 95% for all parameters. 90
Figure A.46 - Hydraulics pressures and surface temperature/barometric pressure. 92
Figure A.47 - XY-scatter plot showing the formation parameter space normalized fit values. 93
Figure A.48 - XY-scatter plot showing the skin parameter space normalized fit values. 94
Figure A.49 - Test events and pressures. 95
Figure A.50 - Annotated testing sequence showing best-fit simulation and parameter estimates. 96
Figure A.51 - Annotated testing sequence showing pre-test history, best-fit simulation and parameter estimates. 97
Figure A.52 - Log-log plot showing Ramey B and derivative response for best-fit simulation. 97
Figure A.53 - Normalized Jacobian for best-fit simulation..... 98
Figure A.54 - Fit value cumulative distribution function..... 99
Figure A.55 – Detail of fit value cumulative distribution function. 99
Figure A.56 - XY-scatter plot showing estimates of formation hydraulic conductivity (K_f) vs static formation pressure (P_f) (top panel) and specific storage (Ss) (bottom panel). 100
Figure A.57 - XY-scatter plot showing estimates of static formation pressure (P_f) vs specific storage (Ss) (top panel) and skin hydraulic conductivity (K_s) vs skin thickness (t_s) (bottom panel). 101
Figure A.58 – Cumulative distribution functions and parameter limits for formation hydraulic conductivity (K_f) (top panel), static formation pressure (P_f) (middle panel) and specific storage (Ss) (bottom panel)..... 102
Figure A.59 – Cumulative distribution functions and parameter limits for skin hydraulic conductivity (K_s) (top panel), skin thickness (t_s) (middle panel) and skin factor (s) (bottom panel). 103
Figure A.60 – Perturbation results – all converged, accepted, and within 5% to 95% for all parameters. 104
Figure A.61 – Log-log plot showing Ramey B and derivative response for all converged optimizations and those within 5% to 95% for all parameters. 104
Figure A.62 - Hydraulics pressures and surface temperature/barometric pressure. 106
Figure A.63 - XY-scatter plot showing the formation parameter space normalized fit values. 107
Figure A.64 - XY-scatter plot showing the skin parameter space normalized fit values. 108
Figure A.65 - Test events and pressures. 109
Figure A.66 – Bottom zone pressure while sealed by inflated packers. 110
Figure A.67 - Annotated testing sequence showing best-fit simulation and parameter estimates. 111
Figure A.68 - Annotated testing sequence showing pre-test history, best-fit simulation and parameter estimates. 111
Figure A.69 - Log-log plot showing Ramey B and derivative response for best-fit simulation. 112
Figure A.70 - Normalized Jacobian for best-fit simulation..... 112
Figure A.71 - Fit value cumulative distribution function..... 113
Figure A.72 – Detail of fit value cumulative distribution function. 113
Figure A.73 - XY-scatter plot showing estimates of formation hydraulic conductivity (K_f) vs static formation pressure (P_f) (top panel) and specific storage (Ss) (bottom panel). 114
Figure A.74 - XY-scatter plot showing estimates of static formation pressure (P_f) vs specific storage (Ss) (top panel) and skin hydraulic conductivity (K_s) vs skin thickness (t_s) (bottom panel). 115
Figure A.75 – Cumulative distribution functions and parameter limits for formation hydraulic conductivity (K_f) (top panel), static formation pressure (P_f) (middle panel) and specific storage (Ss) (bottom panel)..... 116
Figure A.76 – Cumulative distribution functions and parameter limits for skin hydraulic conductivity (K_s) (top panel), skin thickness (t_s) (middle panel) and skin factor (s) (bottom panel). 117
Figure A.77 – Perturbation results – all converged, accepted, and within 5% to 95% for all parameters. 118

Figure A.78 – Log-log plot showing Ramey B and derivative response for all converged optimizations and those within 5% to 95% for all parameters. 118
Figure A.79 - Hydraulics pressures and surface temperature/barometric pressure. 120
Figure A.80 - XY-scatter plot showing the formation parameter space normalized fit values. 121
Figure A.81 - XY-scatter plot showing the skin parameter space normalized fit values. 122
Figure A.82 - Test events and pressures. 123
Figure A.83 - Annotated testing sequence showing best-fit simulation and parameter estimates. 124
Figure A.84 - Annotated HT01_30 testing sequence showing pre-test history, best-fit simulation and parameter estimates. 125
Figure A.85 - Log-log plot showing Ramey B and derivative response for best-fit simulation. 125
Figure A.86 - Normalized Jacobian for best-fit simulation..... 126
Figure A.87 - Fit value cumulative distribution function..... 127
Figure A.88 - Fit value cumulative distribution function (detail)..... 127
Figure A.89 - XY-scatter plot showing estimates of formation hydraulic conductivity (K_f) vs static formation pressure (P_f) (top panel) and specific storage (Ss) (bottom panel). 128
Figure A.90 - XY-scatter plot showing estimates of static formation pressure (P_f) vs specific storage (Ss) (top panel) and skin hydraulic conductivity (K_s) vs skin thickness (t_s) (bottom panel). 129
Figure A.91 – Cumulative distribution functions and parameter limits for formation hydraulic conductivity (K_f) (top panel), static formation pressure (P_f) (middle panel) and specific storage (Ss) (bottom panel)..... 130
Figure A.92 – Cumulative distribution functions and parameter limits for skin hydraulic conductivity (K_s) (top panel), skin thickness (t_s) (middle panel) and skin factor (s) (bottom panel). 131
Figure A.93 – Perturbation results – all converged, accepted, and within 5% to 95% for all parameters. 132
Figure A.94 – Log-log plot showing Ramey B and derivative response for all converged optimizations and those within 5% to 95% for all parameters. 132
Figure A.95 - Hydraulics pressures and surface temperature/barometric pressure. 134
Figure A.96 - XY-scatter plot showing the formation parameter space normalized fit values. 135
Figure A.97 - XY-scatter plot showing the skin parameter space normalized fit values. 136
Figure A.98 - Test events and pressures. 137
Figure A.99 - Annotated testing sequence showing best-fit simulation and parameter estimates. 138
Figure A.100 - Annotated HT02_30 testing sequence showing pre-test history, best-fit simulation and parameter estimates. 139
Figure A.101 - Log-log plot showing Ramey B and derivative response for best-fit simulation. 139
Figure A.102 - Normalized Jacobian for best-fit simulation..... 140
Figure A.103 - Fit value cumulative distribution function..... 141
Figure A.104 - XY-scatter plot showing estimates of formation hydraulic conductivity (K_f) vs static formation pressure (P_f) (top panel) and specific storage (Ss) (bottom panel). 142
Figure A.105 - XY-scatter plot showing estimates of static formation pressure (P_f) vs specific storage (Ss) (top panel) and skin hydraulic conductivity (K_s) vs skin thickness (t_s) (bottom panel). 143
Figure A.106 – Cumulative distribution functions and parameter limits for formation hydraulic conductivity (K_f) (top panel), static formation pressure (P_f) (middle panel) and specific storage (Ss) (bottom panel). 144
Figure A.107 – Cumulative distribution functions and parameter limits for skin hydraulic conductivity (K_s) (top panel), skin thickness (t_s) (middle panel) and skin factor (s) (bottom panel). 145
Figure A.108 – Perturbation results – all converged, accepted, and within 5% to 95% for all parameters. 146
Figure A.109 – Log-log plot showing Ramey B and derivative response for all converged optimizations and those within 5% to 95% for all parameters. 146
Figure A.110 - Hydraulics pressures and surface temperature/barometric pressure. 148
Figure A.111 - XY-scatter plot showing the formation parameter space normalized fit values. 149
Figure A.112 - XY-scatter plot showing the skin parameter space normalized fit values. 150

Figure A.113 - Test events and pressures..... 151
Figure A.114 - Annotated testing sequence showing best-fit simulation and parameter estimates.. 152
Figure A.115 - Annotated HT03_30 testing sequence showing pre-test history, best-fit simulation and parameter estimates. 153
Figure A.116 - Log-log plot showing Ramey B and derivative response for best-fit simulation. 153
Figure A.117 - Normalized Jacobian for best-fit simulation..... 154
Figure A.118 - Fit value cumulative distribution function..... 155
Figure A.119 – Detail - fit value cumulative distribution function..... 155
Figure A.120 - XY-scatter plot showing estimates of formation hydraulic conductivity (K_f) vs static formation pressure (P_f) (top panel) and specific storage (Ss) (bottom panel). 156
Figure A.121 - XY-scatter plot showing estimates of static formation pressure (P_f) vs specific storage (Ss) (top panel) and skin hydraulic conductivity (K_s) vs skin thickness (t_s) (bottom panel). 157
Figure A.122 – Cumulative distribution functions and parameter limits for formation hydraulic conductivity (K_f) (top panel), static formation pressure (P_f) (middle panel) and specific storage (Ss) (bottom panel). 158
Figure A.123 – Cumulative distribution functions and parameter limits for skin hydraulic conductivity (K_s) (top panel), skin thickness (t_s) (middle panel) and skin factor (s) (bottom panel). 159
Figure A.124 – Perturbation results – all converged, accepted, and within 5% to 95% for all parameters. 160
Figure A.125 – Log-log plot showing Ramey B and derivative response for all converged optimizations and those within 5% to 95% for all parameters. 160
Figure A.126 - Hydraulics pressures and surface temperature/barometric pressure. 162
Figure A.127 - XY-scatter plot showing the formation parameter space normalized fit values. 163
Figure A.128 - XY-scatter plot showing the skin parameter space normalized fit values. 164
Figure A.129 - Test events and pressures..... 165
Figure A.130 - Annotated testing sequence showing best-fit simulation and parameter estimates.. 166
Figure A.131 - Annotated HT04_30 testing sequence showing pre-test history, best-fit simulation and parameter estimates. 167
Figure A.132 - Log-log plot showing Ramey B and derivative response for best-fit simulation. 167
Figure A.133 - Normalized Jacobian for best-fit simulation..... 168
Figure A.134 - Fit value cumulative distribution function..... 169
Figure A.135 – Detail of fit value cumulative distribution function..... 169
Figure A.136 - XY-scatter plot showing estimates of formation hydraulic conductivity (K_f) vs static formation pressure (P_f) (top panel) and specific storage (Ss) (bottom panel). 170
Figure A.137 - XY-scatter plot showing estimates of static formation pressure (P_f) vs specific storage (Ss) (top panel) and skin hydraulic conductivity (K_s) vs skin thickness (t_s) (bottom panel). 171
Figure A.138 – Cumulative distribution functions and parameter limits for formation hydraulic conductivity (K_f) (top panel), static formation pressure (P_f) (middle panel) and specific storage (Ss) (bottom panel). 172
Figure A.139 – Cumulative distribution functions and parameter limits for skin hydraulic conductivity (K_s) (top panel), skin thickness (t_s) (middle panel) and skin factor (s) (bottom panel). 173
Figure A.140 – Perturbation results – all converged, accepted, and within 5% to 95% for all parameters. 174
Figure A.141 – Log-log plot showing Ramey B and derivative response for all converged optimizations and those within 5% to 95% for all parameters. 174
Figure A.142 - Hydraulics pressures and surface temperature/barometric pressure. 176
Figure A.143 - XY-scatter plot showing the formation parameter space normalized fit values. 177
Figure A.144 - XY-scatter plot showing the skin parameter space normalized fit values. 178
Figure A.145 - Test events and pressures..... 179
Figure A.146 - Annotated testing sequence showing best-fit simulation and parameter estimates.. 180

Figure A.147 - Annotated HT05_30 testing sequence showing pre-test history, best-fit simulation and parameter estimates. 181
Figure A.148 - Log-log plot showing Ramey B and derivative response for best-fit simulation. 181
Figure A.149 - Normalized Jacobian for best-fit simulation..... 182
Figure A.150 - Fit value cumulative distribution function..... 183
Figure A.151 - XY-scatter plot showing estimates of formation hydraulic conductivity (K_f) vs static formation pressure (P_f) (top panel) and specific storage (Ss) (bottom panel). 184
Figure A.152 - XY-scatter plot showing estimates of static formation pressure (P_f) vs specific storage (Ss) (top panel) and skin hydraulic conductivity (K_s) vs skin thickness (t_s) (bottom panel). 185
Figure A.153 – Cumulative distribution functions and parameter limits for formation hydraulic conductivity (K_f) (top panel), static formation pressure (P_f) (middle panel) and specific storage (Ss) (bottom panel). 186
Figure A.154 – Cumulative distribution functions and parameter limits for skin hydraulic conductivity (K_s) (top panel), skin thickness (t_s) (middle panel) and skin factor (s) (bottom panel). 187
Figure A.155 – Perturbation results – all converged, accepted, and within 5% to 95% for all parameters. 188
Figure A.156 – Log-log plot showing Ramey B and derivative response for all converged optimizations and those within 5% to 95% for all parameters. 188
Figure A.157 - Hydraulics pressures and surface temperature/barometric pressure. 190
Figure A.158 - XY-scatter plot showing the formation parameter space normalized fit values. 191
Figure A.159 - XY-scatter plot showing the skin parameter space normalized fit values. 192
Figure A.160 - Test events and pressures..... 193
Figure A.161 - Annotated testing sequence showing best-fit simulation and parameter estimates. .. 194
Figure A.162 - Annotated testing sequence showing pre-test history, best-fit simulation and parameter estimates. 195
Figure A.163 - Log-log plot showing Ramey B and derivative response for best-fit simulation. 195
Figure A.164 - Normalized Jacobian for best-fit simulation..... 196
Figure A.165 - Fit value cumulative distribution function..... 197
Figure A.166 – Detail of fit value cumulative distribution function. 197
Figure A.167 - XY-scatter plot showing estimates of formation hydraulic conductivity (K_f) vs static formation pressure (P_f) (top panel) and specific storage (Ss) (bottom panel). 198
Figure A.168 - XY-scatter plot showing estimates of static formation pressure (P_f) vs specific storage (Ss) (top panel) and skin hydraulic conductivity (K_s) vs skin thickness (t_s) (bottom panel). 199
Figure A.169 – Cumulative distribution functions and parameter limits for formation hydraulic conductivity (K_f) (top panel), static formation pressure (P_f) (middle panel) and specific storage (Ss) (bottom panel). 200
Figure A.170 – Cumulative distribution functions and parameter limits for skin hydraulic conductivity (K_s) (top panel), skin thickness (t_s) (middle panel) and skin factor (s) (bottom panel). 201
Figure A.171 – Perturbation results – all converged, accepted, and within 5% to 95% for all parameters. 202
Figure A.172 – Log-log plot showing Ramey B and derivative response for all converged optimizations and those within 5% to 95% for all parameters. 202
Figure A.173 - Hydraulics pressures and surface temperature/barometric pressure. 204
Figure A.174 - XY-scatter plot showing the formation parameter space normalized fit values. 205
Figure A.175 - XY-scatter plot showing the skin parameter space normalized fit values. 206
Figure A.176 - Test events and pressures..... 207
Figure A.177 - Annotated testing sequence showing best-fit simulation and parameter estimates. .. 208
Figure A.178 - Annotated HT07_30 testing sequence showing pre-test history, best-fit simulation and parameter estimates. 209
Figure A.179 - Log-log plot showing Ramey B and derivative response for best-fit simulation. 209
Figure A.180 - Normalized Jacobian for best-fit simulation..... 210

Figure A.181 - Fit value cumulative distribution function. 211
Figure A.182 – Detail of fit value cumulative distribution function. 211
Figure A.183 - XY-scatter plot showing estimates of formation hydraulic conductivity (K_f) vs static formation pressure (P_f) (top panel) and specific storage (Ss) (bottom panel). 212
Figure A.184 - XY-scatter plot showing estimates of static formation pressure (P_f) vs specific storage (Ss) (top panel) and skin hydraulic conductivity (K_s) vs skin thickness (t_s) (bottom panel). 213
Figure A.185 – Cumulative distribution functions and parameter limits for formation hydraulic conductivity (K_f) (top panel), static formation pressure (P_f) (middle panel) and specific storage (Ss) (bottom panel). 214
Figure A.186 – Cumulative distribution functions and parameter limits for skin hydraulic conductivity (K_s) (top panel), skin thickness (t_s) (middle panel) and skin factor (s) (bottom panel). 215
Figure A.187 – Perturbation results – all converged, accepted, and within 5% to 95% for all parameters. 216
Figure A.188 – Log-log plot showing Ramey B and derivative response for all converged optimizations and those within 5% to 95% for all parameters. 216
Figure A.189 - Hydraulics pressures and surface temperature/barometric pressure. 218
Figure A.190 - XY-scatter plot showing the formation parameter space normalized fit values. 219
Figure A.191 - XY-scatter plot showing the skin parameter space normalized fit values. 220
Figure A.192 - Test events and pressures. 221
Figure A.193 - Annotated testing sequence showing best-fit simulation and parameter estimates. 222
Figure A.194 - Annotated testing sequence showing pre-test history, best-fit simulation and parameter estimates. 223
Figure A.195 - Log-log plot showing Ramey B and derivative response for best-fit simulation. 223
Figure A.196 - Normalized Jacobian for best-fit simulation. 224
Figure A.197 - Fit value cumulative distribution function. 225
Figure A.198 – Detail fit value cumulative distribution function. 225
Figure A.199 - XY-scatter plot showing estimates of formation hydraulic conductivity (K_f) vs static formation pressure (P_f) (top panel) and specific storage (Ss) (bottom panel). 226
Figure A.200 - XY-scatter plot showing estimates of static formation pressure (P_f) vs specific storage (Ss) (top panel) and skin hydraulic conductivity (K_s) vs skin thickness (t_s) (bottom panel). 227
Figure A.201 – Cumulative distribution functions and parameter limits for formation hydraulic conductivity (K_f) (top panel), static formation pressure (P_f) (middle panel) and specific storage (Ss) (bottom panel). 228
Figure A.202 – Cumulative distribution functions and parameter limits for skin hydraulic conductivity (K_s) (top panel), skin thickness (t_s) (middle panel) and skin factor (s) (bottom panel). 229
Figure A.203 – Perturbation results – all converged, accepted, and within 5% to 95% for all parameters. 230
Figure A.204 – Log-log plot showing Ramey B and derivative response for all converged optimizations and those within 5% to 95% for all parameters. 230
Figure A.205 - Hydraulics pressures and surface temperature/barometric pressure. 232
Figure A.206 - XY-scatter plot showing the formation parameter space normalized fit values. 233
Figure A.207 - XY-scatter plot showing the skin parameter space normalized fit values. 234
Figure A.208 - Test events and pressures. 235
Figure A.209 - Annotated testing sequence showing best-fit simulation and parameter estimates. 236
Figure A.210 - Annotated testing sequence showing pre-test history, best-fit simulation and parameter estimates. 237
Figure A.211 - Log-log plot showing Ramey B and derivative response for best-fit simulation. 237
Figure A.212 - Normalized Jacobian for best-fit simulation. 238
Figure A.213 - Fit value cumulative distribution function. 239
Figure A.214 - XY-scatter plot showing estimates of formation hydraulic conductivity (K_f) vs static formation pressure (P_f) (top panel) and specific storage (Ss) (bottom panel). 240

Figure A.215 - XY-scatter plot showing estimates of static formation pressure (P_f) vs specific storage (Ss) (top panel) and skin hydraulic conductivity (K_s) vs skin thickness (t_s) (bottom panel). 241
Figure A.216 – Cumulative distribution functions and parameter limits for formation hydraulic conductivity (K_f) (top panel), static formation pressure (P_f) (middle panel) and specific storage (Ss) (bottom panel). 242
Figure A.217 – Cumulative distribution functions and parameter limits for skin hydraulic conductivity (K_s) (top panel), skin thickness (t_s) (middle panel) and skin factor (s) (bottom panel). 243
Figure A.218 – Perturbation results – all converged, accepted, and within 5% to 95% for all parameters. 244
Figure A.219 – Log-log plot showing Ramey B and derivative response for all converged optimizations and those within 5% to 95% for all parameters. 244
Figure A.220 - Hydraulics pressures and surface temperature/barometric pressure. 246
Figure A.221 - XY-scatter plot showing the formation parameter space normalized fit values. 247
Figure A.222 - XY-scatter plot showing the skin parameter space normalized fit values. 248
Figure A.223 - Test events and pressures. 249
Figure A.224 - Annotated testing sequence showing best-fit simulation and parameter estimates. .. 250
Figure A.225 - Annotated testing sequence showing pre-test history, best-fit simulation and parameter estimates. 251
Figure A.226 - Log-log plot showing Ramey B and derivative response for best-fit simulation. 251
Figure A.227 - Normalized Jacobian for best-fit simulation. 252
Figure A.228 - Fit value cumulative distribution function. 253
Figure A.229 - XY-scatter plot showing estimates of formation hydraulic conductivity (K_f) vs static formation pressure (P_f) (top panel) and specific storage (Ss) (bottom panel). 254
Figure A.230 - XY-scatter plot showing estimates of static formation pressure (P_f) vs specific storage (Ss) (top panel) and skin hydraulic conductivity (K_s) vs skin thickness (t_s) (bottom panel). 255
Figure A.231 – Cumulative distribution functions and parameter limits for formation hydraulic conductivity (K_f) (top panel), static formation pressure (P_f) (middle panel) and specific storage (Ss) (bottom panel). 256
Figure A.232 – Cumulative distribution functions and parameter limits for skin hydraulic conductivity (K_s) (top panel), skin thickness (t_s) (middle panel) and skin factor (s) (bottom panel). 257
Figure A.233 – Perturbation results – all converged, accepted, and within 5% to 95% for all parameters. 258
Figure A.234 – Log-log plot showing Ramey B and derivative response for all converged optimizations and those within 5% to 95% for all parameters. 258
Figure A.235 - Hydraulics pressures and surface temperature/barometric pressure. 260
Figure A.236 - XY-scatter plot showing the formation parameter space normalized fit values. 261
Figure A.237 - XY-scatter plot showing the skin parameter space normalized fit values. 262
Figure A.238 - Test events and pressures. 263
Figure A.239 - Annotated testing sequence showing best-fit simulation and parameter estimates. .. 264
Figure A.240 - Annotated testing sequence showing pre-test history, best-fit simulation and parameter estimates. 265
Figure A.241 - Log-log plot showing Ramey B and derivative response for best-fit simulation. 265
Figure A.242 - Normalized Jacobian for best-fit simulation. 266
Figure A.243 - Fit value cumulative distribution function. 267
Figure A.244 - XY-scatter plot showing estimates of formation hydraulic conductivity (K_f) vs static formation pressure (P_f) (top panel) and specific storage (Ss) (bottom panel). 268
Figure A.245 - XY-scatter plot showing estimates of static formation pressure (P_f) vs specific storage (Ss) (top panel) and skin hydraulic conductivity (K_s) vs skin thickness (t_s) (bottom panel). 269

Figure A.246 – Cumulative distribution functions and parameter limits for formation hydraulic conductivity (K_f) (top panel), static formation pressure (P_f) (middle panel) and specific storage (Ss) (bottom panel). 270
Figure A.247 – Cumulative distribution functions and parameter limits for skin hydraulic conductivity (K_s) (top panel), skin thickness (t_s) (middle panel) and skin factor (s) (bottom panel). 271
Figure A.248 – Perturbation results – all converged, accepted, and within 5% to 95% for all parameters. 272
Figure A.249 – Log-log plot showing Ramey B and derivative response for all converged optimizations and those within 5% to 95% for all parameters. 272
Figure A.250 - Hydraulics pressures and surface temperature/barometric pressure. 274
Figure A.251 - XY-scatter plot showing the formation parameter space normalized fit values. 275
Figure A.252 - XY-scatter plot showing the skin parameter space normalized fit values. 276
Figure A.253 - Test events and pressures. 277
Figure A.254 - Annotated testing sequence showing best-fit simulation and parameter estimates. .. 278
Figure A.255 - Annotated testing sequence showing pre-test history, best-fit simulation and parameter estimates. 279
Figure A.256 - Log-log plot showing Ramey B and derivative response for best-fit simulation. 279
Figure A.257 - Normalized Jacobian for best-fit simulation. 280
Figure A.258 - Fit value cumulative distribution function. 281
Figure A.259 - XY-scatter plot showing estimates of formation hydraulic conductivity (K_f) vs static formation pressure (P_f) (top panel) and specific storage (Ss) (bottom panel). 282
Figure A.260 - XY-scatter plot showing estimates of static formation pressure (P_f) vs specific storage (Ss) (top panel) and skin hydraulic conductivity (K_s) vs skin thickness (t_s) (bottom panel). 283
Figure A.261 – Cumulative distribution functions and parameter limits for formation hydraulic conductivity (K_f) (top panel), static formation pressure (P_f) (middle panel) and specific storage (Ss) (bottom panel). 284
Figure A.262 – Cumulative distribution functions and parameter limits for skin hydraulic conductivity (K_s) (top panel), skin thickness (t_s) (middle panel) and skin factor (s) (bottom panel). 285
Figure A.263 – Perturbation results – all converged, accepted, and within 5% to 95% for all parameters. 286
Figure A.264 – Log-log plot showing Ramey B and derivative response for all converged optimizations and those within 5% to 95% for all parameters. 286
Figure A.265 - Hydraulics pressures and surface temperature/barometric pressure. 288
Figure A.266 - XY-scatter plot showing the formation parameter space normalized fit values. 289
Figure A.267 - XY-scatter plot showing the skin parameter space normalized fit values. 290
Figure A.268 - Test events and pressures. 291
Figure A.269 - Annotated testing sequence showing best-fit simulation and parameter estimates. .. 292
Figure A.270 - Annotated testing sequence showing pre-test history, best-fit simulation and parameter estimates. 293
Figure A.271 - Log-log plot showing Ramey B and derivative response for best-fit simulation. 293
Figure A.272 - Normalized Jacobian for best-fit simulation. 294
Figure A.273 - Fit value cumulative distribution function. 295
Figure A.274 - XY-scatter plot showing estimates of formation hydraulic conductivity (K_f) vs static formation pressure (P_f) (top panel) and specific storage (Ss) (bottom panel). 296
Figure A.275 - XY-scatter plot showing estimates of static formation pressure (P_f) vs specific storage (Ss) (top panel) and skin hydraulic conductivity (K_s) vs skin thickness (t_s) (bottom panel). 297
Figure A.276 – Cumulative distribution functions and parameter limits for formation hydraulic conductivity (K_f) (top panel), static formation pressure (P_f) (middle panel) and specific storage (Ss) (bottom panel). 298
Figure A.277 – Cumulative distribution functions and parameter limits for skin hydraulic conductivity (K_s) (top panel), skin thickness (t_s) (middle panel) and skin factor (s) (bottom panel). 299

Figure A.278 – Perturbation results – all converged, accepted, and within 5% to 95% for all parameters. 300
Figure A.279 – Log-log plot showing Ramey B and derivative response for all converged optimizations and those within 5% to 95% for all parameters. 300
Figure A.280 - Hydraulics pressures and surface temperature/barometric pressure. 302
Figure A.281 - XY-scatter plot showing the formation parameter space normalized fit values. 303
Figure A.282 - XY-scatter plot showing the skin parameter space normalized fit values. 304
Figure A.283 - Test events and pressures. 305
Figure A.284 - Annotated testing sequence showing best-fit simulation and parameter estimates. .. 306
Figure A.285 - Annotated testing sequence showing pre-test history, best-fit simulation and parameter estimates. 307
Figure A.286 - Log-log plot showing Ramey B and derivative response for best-fit simulation. 307
Figure A.287 - Normalized Jacobian for best-fit simulation. 308
Figure A.288 - Fit value cumulative distribution function. 308
Figure A.289 - XY-scatter plot showing estimates of formation hydraulic conductivity (K_f) vs static formation pressure (P_f) (top panel) and specific storage (Ss) (bottom panel). 309
Figure A.290 - XY-scatter plot showing estimates of static formation pressure (P_f) vs specific storage (Ss) (top panel) and skin hydraulic conductivity (K_s) vs skin thickness (t_s) (bottom panel). 310
Figure A.291 – Cumulative distribution functions and parameter limits for formation hydraulic conductivity (K_f) (top panel), static formation pressure (P_f) (middle panel) and specific storage (Ss) (bottom panel). 311
Figure A.292 – Cumulative distribution functions and parameter limits for skin hydraulic conductivity (K_s) (top panel), skin thickness (t_s) (middle panel) and skin factor (s) (bottom panel). 312
Figure A.293 – Perturbation results – all converged, accepted, and within 5% to 95% for all parameters. 313
Figure A.294 – Log-log plot showing Ramey B and derivative response for all converged optimizations and those within 5% to 95% for all parameters. 313
Figure A.295 - Hydraulics pressures and surface temperature/barometric pressure. 315
Figure A.296 - XY-scatter plot showing the formation parameter space normalized fit values. 316
Figure A.297 - XY-scatter plot showing the skin parameter space normalized fit values. 317
Figure A.298 - Test events and pressures. 318
Figure A.299 - Annotated testing sequence showing best-fit simulation and parameter estimates. .. 319
Figure A.300 - Annotated testing sequence showing pre-test history, best-fit simulation and parameter estimates. 320
Figure A.301 - Log-log plot showing Ramey B and derivative response for best-fit simulation for test sequence PI1. 320
Figure A.302 - Log-log plot showing Ramey B and derivative response for best-fit simulation for test sequence PI2. 321
Figure A.303 - Normalized Jacobian for best-fit simulation for test sequence PI1. 321
Figure A.304 - Normalized Jacobian for best-fit simulation for test sequence PI2. 322
Figure A.305 - Fit value cumulative distribution function. 322
Figure A.306 - XY-scatter plot showing estimates of formation hydraulic conductivity (K_f) vs static formation pressure (P_f) (top panel) and specific storage (Ss) (bottom panel). 323
Figure A.307 - XY-scatter plot showing estimates of static formation pressure (P_f) vs specific storage (Ss) (top panel) and skin hydraulic conductivity (K_s) vs skin thickness (t_s) (bottom panel). 324
Figure A.308 – Cumulative distribution functions and parameter limits for formation hydraulic conductivity (K_f) (top panel), static formation pressure (P_f) (middle panel) and specific storage (Ss) (bottom panel). 325
Figure A.309 – Cumulative distribution functions and parameter limits for skin hydraulic conductivity (K_s) (top panel), skin thickness (t_s) (middle panel) and skin factor (s) (bottom panel). 326

Figure A.310 – Perturbation results – all converged, accepted, and within 5% to 95% for all parameters. 327
Figure A.311 – Log-log plot showing Ramey B and derivative response for all converged optimizations and those within 5% to 95% for all parameters for test sequence PI1. 327
Figure A.312 – Log-log plot showing Ramey B and derivative response for all converged optimizations and those within 5% to 95% for all parameters for test sequence PI2. 328
Figure A.313 - Hydraulics pressures and surface temperature/barometric pressure. 330
Figure A.314 - XY-scatter plot showing the formation parameter space normalized fit values. 331
Figure A.315 - XY-scatter plot showing the skin parameter space normalized fit values. 332

1 INTRODUCTION

Geofirma Engineering Ltd. (Geofirma) was retained by the Nuclear Waste Management Organization (NWMO) to complete a drilling and testing program for two deep bedrock boreholes (SB_BH01 and SB_BH02) as part of the NWMO's Phase 2 Geoscientific Preliminary Field Investigations. The full scope of this deep drilling and testing program is described in the Initial Borehole Characterization Plan.

Phase 1 of NWMO's APM plan included preliminary desktop studies using available geoscientific information and a set of key geoscientific characteristics and factors that can be realistically assessed at the desktop phase of the Preliminary Assessment. The Phase 1 Preliminary Assessment of the South Bruce area identified the Cobourg Formation as the preferred host formation for a deep geological repository for used nuclear fuel. The Initial Borehole Drilling and Testing study is a key component of the Phase 2 Geoscientific Preliminary Field Investigations of the NWMO's APM plan.

The activities described in this report constitute one component of the Geofirma geoscientific investigations as part of the NWMO Phase 2 Initial Borehole Drilling and Testing Program within the South Bruce site, near Teeswater, Ontario (Figure 1.1).

An important component of this geoscientific investigation is the acquisition of in situ estimates of rock mass hydraulic conductivity (K) and other hydrogeologic formation properties including formation pressure (P_f) and specific storage (S_s).

Specifically, this report presents the results of analyses of data collected during hydraulic testing in borehole SB_BH02 as described in Geofirma's WP06 Test Plan. Testing was conducted by subcontractor HydroResolutions LLC (HR) under the direction of senior Geofirma staff.

This report describes the results of the testing and analyses associated with SB_BH02. Figure 1.2 shows the stratigraphic sequence that was encountered in the subsurface while drilling SB_BH02. The subsurface nomenclature used was based on Armstrong and Carter (2010).

1.1 Borehole SB_BH02

Borehole SB_BH02 is located approximately 5.5 km northwest of the community of Teeswater, Ontario, and was drilled to 900.57 m below ground surface (mBGS). SB_BH02 was drilled through the entire sedimentary bedrock sequence to approximately 14 m into the Precambrian basement. SB_BH02 is located approximately 2.5 km west of SB_BH01. The borehole was drilled using PQ3 wireline coring equipment that produces a 123 mm nominal diameter borehole and 83 mm nominal diameter core over the period August 19, 2021 until March 22, 2022 using brine as a drilling fluid. Borehole geophysical logging was completed over the period April 15, 2022 until June 1, 2022

Figure 1.1 SB_BH02 Site Location.

Standard Reference		Area of South Bruce		SB_BH02 Final Fm. Top (mBGS)	SB_BH02 Final Thickness (m)	Lithology
				GS elevation = 294 mASL		
Devonian	Middle	Drift		0	34.60	n/a
		Detroit River Gp	Lucas Fm	34.60	54.13	dolostone
			Amherstburg Fm	88.73	41.77	dolostone
	Lower	Bois Blanc Fm		130.50	26.41	cherty dolostone
Silurian [b]	Upper	Bass Island Fm		156.91	28.82	dolostone
		Salina Fm	G Unit	185.73	6.82	argillaceous dolostone
			F Unit	192.55	45.58	dolomitic shale
			E Unit	238.13	25.51	brecciated dolostone and dolomitic shale
			D Unit	263.64	2.76	anhydritic dolostone
			C Unit	266.40	16.67	dolomitic shale and shale
			B Unit	283.07	7.53	argillaceous dolostone
			B Unit-Equivalent	290.60	14.39	salt
			B Unit-Evaporite	304.99	1.98	anhydrite
			A2 Unit-Carbonate	306.97	25.27	dolostone
			A2 Unit-Evaporite	332.24	5.34	anhydritic dolostone
			A1 Unit-Carbonate	337.58	38.52	argillaceous dolostone
			A1 Unit-Evaporate	376.10	7.08	anhydritic dolostone
			A0 Unit [c]	383.18	3.66	bituminous dolostone
	Lower	Guelph Fm		386.84	5.02	dolostone
		Goat Island Fm		391.86	16.14	dolostone
		Gasport Fm		408.00	7.30	dolostone and dolomitic dolostone
		Lions Head Fm		415.30	2.80	dolostone and dolomitic dolostone
		Fossil Hill Fm		418.10	1.18	dolostone and dolomitic dolostone
		Cabot Head Fm		419.28	20.82	shale
		Manitoulin Fm		440.10	9.15	cherty dolostone and minor shale
Ordovician [a]	Upper	Queenston Fm		449.25	85.45	red shale
		Georgian Bay Fm		534.70	86.16	grey shale
		Blue Mountain Fm		620.86	48.83	dark grey shale
		Trenton Gp	Cobourg Fm Collingwood Mb)	669.69	7.85	black calcareous shale
			Cobourg Fm [1]	677.54	38.83	argillaceous limestone
			Sherman Fall Fm [2]	716.37	45.66	argillaceous limestone
			Kirkfield Fm [3]	762.03	43.60	argillaceous limestone
		Black River Gp	Coboconk Fm [3]	805.63	21.08	bioturnated limestone
			Gull River Fm	826.71	54.87	lithographic limestone
			Shadow Lake Fm	881.58	5.35	siltstone and sandstone
Cambrian		Cambrian (Unsubdivided)		--	-- [d]	sandstone
Precambrian		Precambrian Basement		886.93		gneiss

Notes:

a - Strata traditionally referred to as Middle Ordovician (i.e., Black River and Trenton groups; Armstrong and Carter, 2006) are now considered Part of the Upper Ordovician.
b - The formal term Middle Silurian (e.g., Armstrong and Carter, 2006) has been abandoned so all strata have been re-assigned to either the Lower or Upper Silurian.
c - A0 Unit (Salina Formation) is recognized based on site characterization activities at the Bruce nuclear site (Intera, 2011).
d - Unit/Formation is not expected but may be present.

Surface Nomenclature Equivalent (approx.): 1 - Lindsay Fm; 2 - Verulam Fm; 3 - Bobcaygeon Fm

---------- Unconformity

Figure 1.2 Generalized Stratigraphic Bedrock Sequence in South Bruce site (after Armstrong and Carter, 2010).

1.2 Hydraulic Testing Activities

Straddle-packer hydraulic testing of South Bruce borehole SB_BH02 provided the data required to determine in situ values of hydrogeologic properties. A custom test tool and support trailer with a data-acquisition system was developed to address the unique requirements of low-permeability testing in deep boreholes. The test equipment was designed and constructed by HR staff and drew upon years of experience in testing of low-permeability strata at multiple locations around the globe.

The key components of the test tool are: two inflatable packers to isolate a test interval within a borehole; a downhole shut-in valve that connects or isolates the test interval from the tubing on which the test tool is suspended in the hole; a hydraulic piston that can be extended or retracted to cause a pressure increase or decrease in the test interval; and pressure transducers that measure the pressure in the test interval, in the bottom of the hole below the lower packer, in the tubing string above the test tool, and in the annulus between the tubing and borehole wall above the upper packer.

SB_BH02 testing was carried out between June 5, 2022, and August 24, 2022, in fifteen 29.96-m intervals and five 5.03-m intervals. These tests were performed under control of WP06 Test Plan.

1.3 Reported Analyses

This report summarizes the analyses of straddle-packer hydraulic testing performed in borehole SB_BH02. This testing included fourteen pulse tests and one slug test in the 29.96-m intervals and three pulse tests and two slug tests in the 5.03-m intervals.

Transient pressure data collected during straddle-packer hydraulic testing were analyzed using version 3.00T of the nSIGHTS (**n**-dimensional **S**tatistical **I**nverse **G**raphical **H**ydraulic **T**est **S**imulator) well-test-analysis software, a numerical well-test analysis code written in C++ and described in detail in the nSIGHTS User Manual (Geofirma and INTERA, 2011).

2 EQUIPMENT

Low-permeability testing is subject to non-ideal testing conditions that can have significant impact on testing results and suitability of results for analysis. The uncertainty associated with these conditions was minimized through effective equipment design for the SB_BH02 testing.

Most tests performed in the SB_BH02 borehole were pulse tests. The pressure response observed during a pulse test is directly proportional to the wellbore storage coefficient of the test interval. The wellbore storage coefficient has two components: the volume of fluid contained within the test zone (V_{tz}) and the compressibility of all the materials within or in contact with the test zone (C_{tz}). V_{tz} includes the volume of fluid between the packers, within any tubing or equipment components below the shut-in valve, and within the feedthrough line connected to the test-zone transducer. C_{tz} is a composite compressibility that includes contributions from the test equipment, the borehole fluid, and the geomechanical response of the borehole wall. To minimize the time required to complete a pulse test, the SB_BH02 equipment was carefully designed and selected to minimize both V_{tz} and C_{tz}. During the SB_BH02 borehole testing, V_{tz} was approximately 0.44 m^3 for 29.96-m test intervals and approximately 0.085 m^3 for 5.03-m test intervals. C_{tz} was minimized through use of extremely stiff packers with high inflation pressures and strong interconnecting components. Most tool feedthroughs and connections were custom-machined stainless-steel components.

During pulse tests in low-permeability formations, variations in packer pressures can cause perceptible changes in test-zone pressure that can mask the actual formation response. To minimize variations in packer pressures, a pressure maintenance system (PMS, see Section 2.3) was hydraulically connected to the packers during testing. The PMS was also connected to the shut-in valve and the pulse piston hydraulics.

Another important equipment design feature was to provide remote access to the test data in real time. This allowed for off-site supervision of testing and for continuous monitoring of the test response. Remote access also allowed for near real-time preliminary test analyses.

The testing equipment consisted of downhole and surface components. The downhole equipment was connected to surface with four stainless steel hydraulic lines (packer inflate/deflate, piston extend, piston retract, shut-in valve close) and an umbilical cable with transducer power and communication lines. The hydraulic lines and umbilical cable were clamped to the outside of a 2-3/8 inch tubing string that provided the overall mechanical connection between the service rig at surface and the downhole tool.

2.1 Mobile Integrated Aquifer Testing & Analysis (MIATA) Platform

The MIATA platform is a testing system developed by HR and provided capabilities for conducting the SB_BH02 hydraulic tests through a wide range of weather conditions. The MIATA platform provided a controlled environment from which personnel conducted the on-site operations required to successfully execute the hydraulic testing program. The MIATA platform protected all above-ground instrumentation and equipment from exposure to the weather and animals.

The MIATA platform was designed and developed to accommodate both low-permeability and conventional hydraulic testing activities. The operation of the hydraulic test tool (HTT) for low-

permeability hydraulic testing applications was one of its core capabilities. The MIATA platform design included:

- Internal hydraulic line control through a pressure manifold;
- Pressure maintenance system to minimize temperature-dependent pressure fluctuations in the packers and downhole hydraulic lines;
- Custom data acquisition and control system (DACS).

Figure 2.1 and Figure 2.2 show the exterior and interior of the MIATA platform, respectively.

Figure 2.1 MIATA platform (white trailer) at the SB_BH01 testing site. A similar configuration was used at SB_BH02.

Figure 2.2 Interior of MIATA platform.

2.2 Data Acquisition and Control System (DACS)

The DACS allowed for the collection of data associated with the hydraulic testing and for secure off-site remote access via the internet. This capability reduced the number of on-site personnel required by allowing real-time analysis of the hydraulic tests to be conducted remotely. This also allowed designated parties real-time access to the data and the ability to provide input to the hydraulic testing process as it took place.

The DACS consisted of a remote terminal unit (RTU) connected via ethernet to a field laptop running a real-time monitoring and control system (RTMCS). The RTU received digital and analog measurements from the sensors, converted the analog measurements to engineering units, and recorded the measurements with date-time timestamps to an ASCII file in internal memory using a time interval set by the operator. A file server then automatically transferred the data to the field laptop. If the connection to the field laptop was lost, the RTU continued to record the data until a connection was re-established, at which time it transferred all the buffered data to the field laptop where it was stored in a OneDrive directory accessible by remote staff. The RTMCS provided graphic and numeric read outs of the measurements and allowed the operator to set the recording interval. The RTMCS also maintained an independent database of the measurements, read directly from the RTU, and recorded with a 10-second interval.

2.3 Pressure Maintenance System

The pressure maintenance system (PMS) was a critical component in successfully conducting high quality hydraulic tests in very low-permeability systems. Diurnal temperature changes on the surface cause the expansion/contraction of fluid in the packer inflation lines. In low-permeability intervals, even small variations in packer pressure directly affect the pressure response in the test zone. The PMS virtually eliminated the pressure fluctuations, resulting in a much cleaner pressure response in the test zone.

The PMS had three principal components:

- A pressurised nitrogen source (bottle) with pressure regulator,
- An Alicat pressure controller, and
- A high-pressure hydraulic accumulator containing pressurised nitrogen in a bladder over packer-inflation fluid.

The Alicat pressure controller is connected to the nitrogen bottle and to the accumulator (see schematic diagram in Figure 2.3). The desired packer-inflation pressure ("set" point) is entered into the controller, which has an integral pressure sensor. The controller then adds nitrogen to the accumulator if the pressure drops below the set point or vents nitrogen from the accumulator if the pressure rises above the set point.

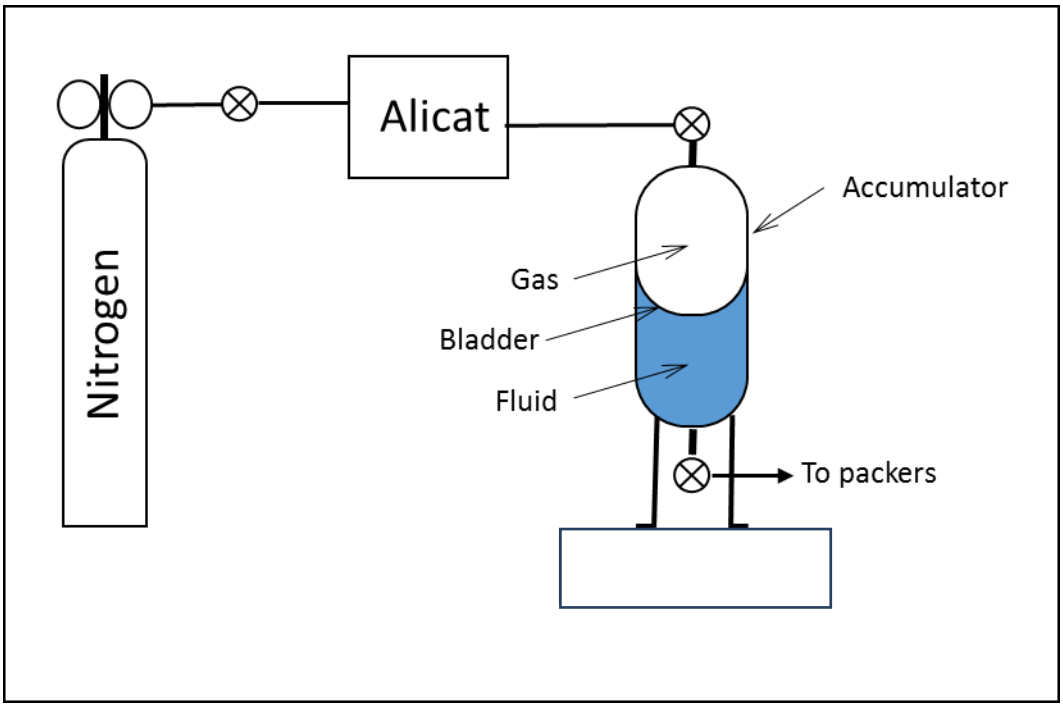

Figure 2.3 Schematic of Packer Pressure Maintenance System.

2.4 Hydraulic Test Tool (HTT)

The straddle-packer HTT (Figure 2.4) consisted of two inflatable packers, a downhole shut-in valve (DHSIV), a piston-pulse generator (PPG), a sensor (or Gauge) carrier, a perforated section, and miscellaneous subs and pass-throughs to connect the various pieces and minimize the fluid volume in the test zone.

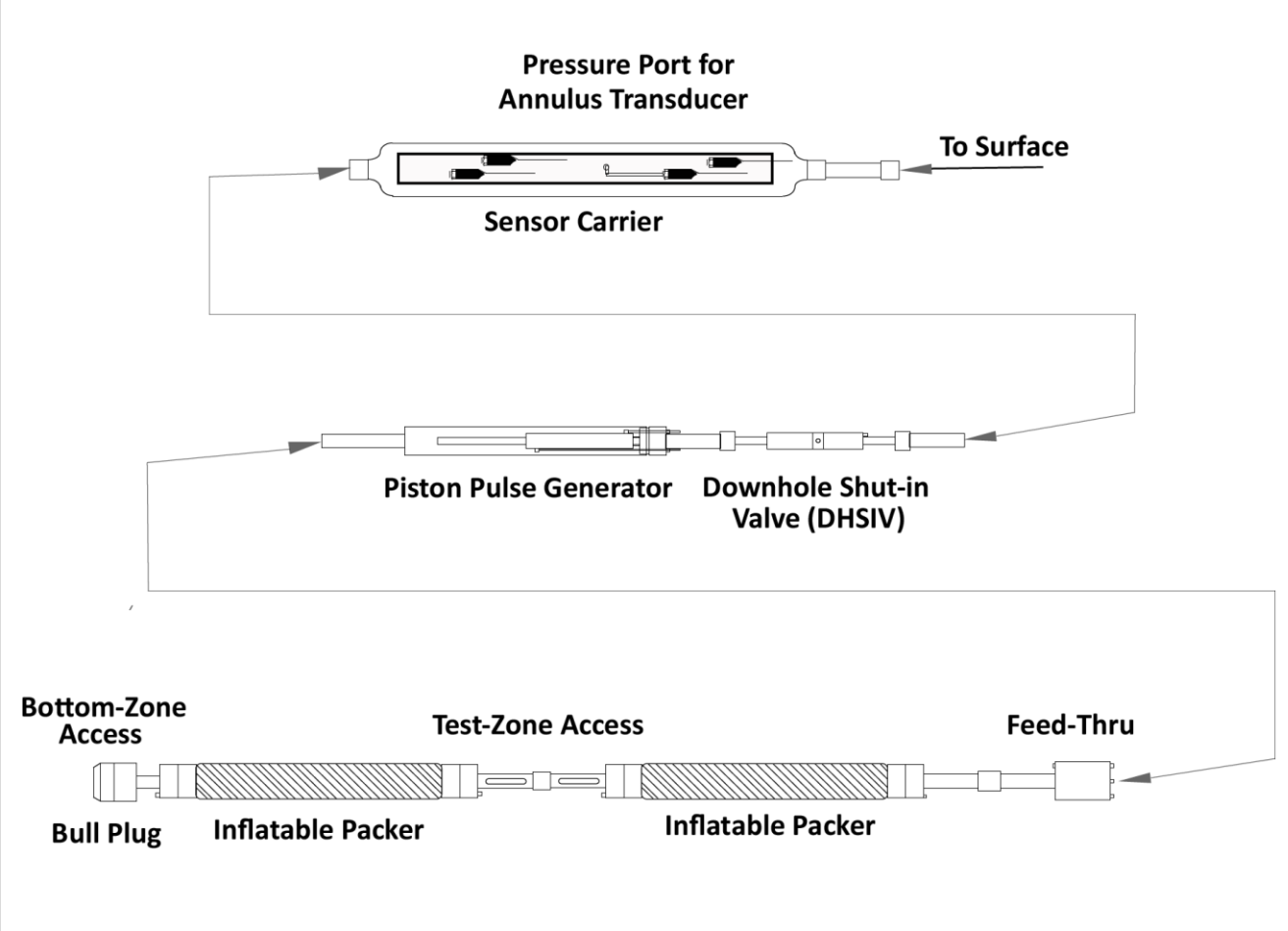

Figure 2.4 General Hydraulic Test Tool Schematic.

2.4.1 Packers

Baski 4.1-inch (104 mm) external-inflate sliding-end Fracker packers (Figure 2.5) were used in the HTT for testing in the PQ (123 mm) borehole. The packers had an uninflated diameter of 104 mm and an element length of 1.14 m, which provided a seal length of approximately 1.0 m in a 123-mm-diameter hole. The packers were capable of withstanding differential pressures of up to 20.7 MPa (3000 psi). The packers and packer-inflation line were filled with non-toxic antifreeze with a density less than 1 gm/cm^3 and inflated using a single ¼-inch stainless steel line by pressurizing a fluid reservoir at the surface with compressed nitrogen to 5 to 15 MPa (725 to 2175 psi), depending upon depth and formation properties. Actual packer inflation pressure depended upon interval depth. The packers were placed on the pressure maintenance system (PMS) once inflated to the desired initial pressure. The packers

were oriented so that their fixed ends were up and their sliding ends were down, to avoid putting inflation lines in tension and so that the packers didn't compress and expand during HTT removal.

Some element of abrasion protection for the packers was provided by the largest diameter (115 mm) components in the system, which were the bull plug below the bottom packer and the feedthrough above the top packer.

Figure 2.5 Baski Fracker Packer.

2.4.2 Downhole Shut-In Valve

A downhole shut-in valve (DHSIV) (Figure 2.6) was used to control the connection between the interior of the tubing string above the HTT and the test zone between the inflatable packers. The DHSIV was manufactured by Inflatable Packers International Pty. Ltd. (IPI) of Australia and used a piston-actuated ball valve within a stainless steel housing. The valve was set up in a normally open position and hydraulic pressure was applied to push an annular piston down, rotating the ball 90° to close the valve. A spring pushed the piston up, opening the valve, when the hydraulic pressure was relieved. The ball had a 1.27-cm-diameter opening and caused no displacement in the test interval when it was actuated. A single ¼ inch stainless steel line was used for DHSIV actuation. As for the packers, a lighter-than water non-toxic antifreeze (plumber's antifreeze) was used as the hydraulic fluid for operation of the DHSIV.

Figure 2.6 Downhole Shut-In Valve (DHSIV).

2.4.3 Sensor Carrier

The transducers (Section 2.4.6) used to monitor pressures were mounted in a sensor carrier that was located at the top of the HTT and enclosed and protected the transducers in the borehole.

2.4.4 Piston Pulse Generators

For pulse-testing applications, a pressure pulse was created by displacing a known volume of fluid in the test zone using a hydraulically actuated piston (Figure 2.7). Four versions of the PPG were available with displacement volumes of 15, 30, 60, and 100 cm^3 so that several hundred kPa pulses could be produced in test intervals with different volumes. For the SB_BH02 pulse tests, the 15 cm^3 piston was used in all the 5.03-m intervals and the 100 cm^3 piston was used in all the 29.96-m intervals. The hydraulically actuated pistons were located inside a custom housing that resided above the top packer (but was hydraulically connected to the test zone). The PPG was extended/retracted using two ¼ inch stainless steel hydraulic lines.

Figure 2.7 Hydraulic Pulse Generating Piston.

2.4.5 Test Interval

Two sections of the tool string between the straddle packers allowed flow from the straddled test zone into the tool string. Two perforated 1-ft (0.3048 m) long pup joints of 2-inch NUE stainless steel pipe were used for this purpose. The pup joints (Figure 2.8) had a total of 10,000 mm^2 (15 in^2) open area available to flow into the HTT.

In addition to the perforated sections, two nominal 10m tubing joints and 6 pup joints were used to create the 29.96 m test zone interval. In SB_BH01 the test interval was 30.05 m. However, one of the pup joints in SB_BH01 was damaged during tool disassembly at the completion of testing and replaced with a shorter joint, resulting in a 9 cm reduction in test zone length. The 5.03 m test zone interval was created with 2 pup joints and is the same size as the short SB_BH01 interval.

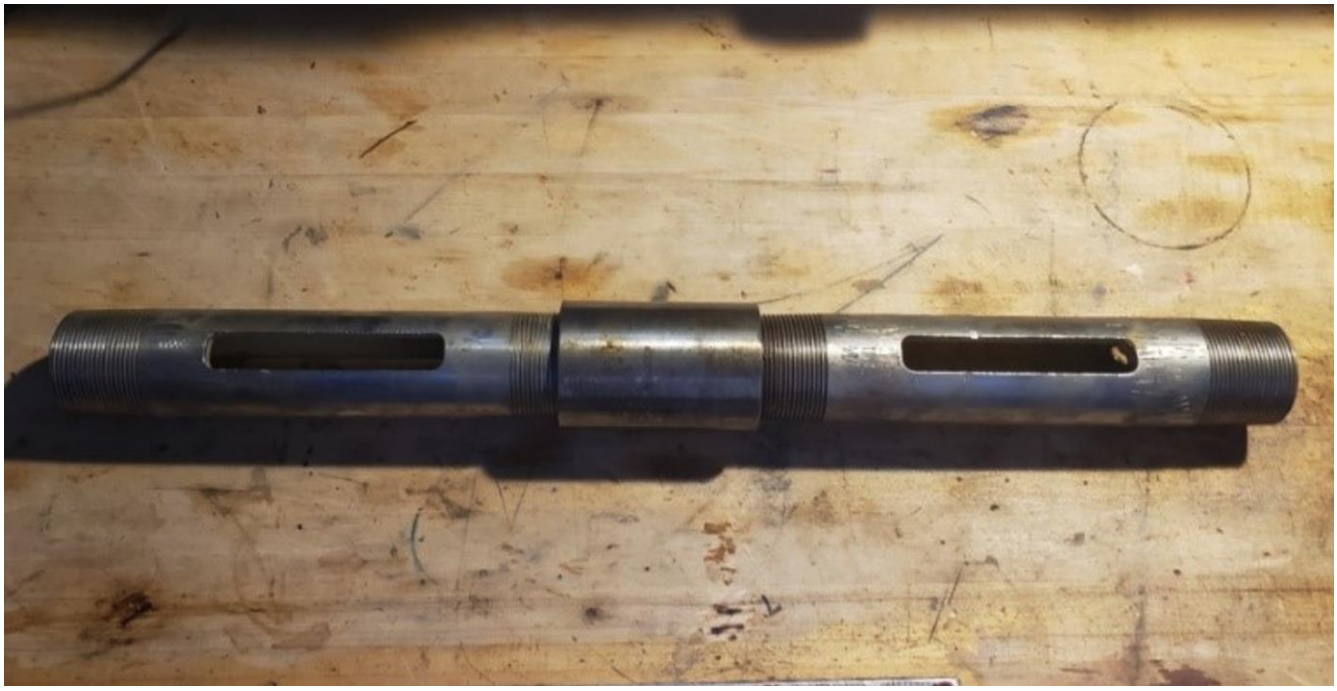

Figure 2.8 Perforated Pup Joints.

2.4.6 Pressure Transducers

For both the 29.96-m and 5.03-m straddle-packer tool configuration, four Keller PAA-33X 30 MPa (300 bar) pressure transducers were used to monitor pressure in the zone below the bottom packer (BZ), the zone in between the packers (TZ), the zone above the top packer between the tubing and borehole wall above the upper packer (Annulus), and inside the tubing string (Tubing). The transducers were housed in a sensor carrier (described above) positioned above the shut-in valve. The transducers had internal electronics that produce temperature-compensated floating point values that were transmitted as text to the data acquisition and control system (DACS) via RS485 Modbus serial data link. The Keller transducers were factory calibrated by Keller, Inc., in May 2020. A second calibration was performed at the conclusion of SB_BH01 testing (Table 2.1) and prior to the start of SB_BH02 testing.

The packer pressures, shut-in valve pressure, and piston pressures were monitored with Omegadyne pressure transducers with an operating range of 0-3000 psia (~0-20.7 MPaa). The Omegadyne transducers had a 4-20 mA output which was monitored by the DACS and converted to pressure in engineering units (psi). Hydraulic pressures are not quality-affecting data; the primary purpose of monitoring pressures is to verify that the packers have inflated and to keep their pressure constant.

2.4.7 Temperature Transducers

HOBO temperature logging transducers were installed in the test zone and bottom zone by taping the transducers to the tool below the top and bottom packers.

2.4.8 Tubing String

The test tool was raised and lowered in the borehole using a tubing string comprised of nominally 28 to 32 ft (8.5 to 9.8 m) long joints of 2-3/8” diameter EUE tubing, rated for pressures in excess of 75 MPa.

The 2-3/8" EUE tubing string threaded directly into the top of the sensor carrier. Shorter lengths of tubing (pup joints) were used for adjustment of the tool depth, allowing the open end of the tubing to be a reasonable length above the rig deck (nominally 1 m). All pup joints were measured and included in the recorded tubing tally.

2.4.9 Barometer

Barometric pressure was monitored during all hydraulic tests using an In-Situ BaroTroll with a useable pressure range of 16.5 psi (113.7 kPa). The BaroTroll has internal electronics that produce temperature-compensated floating point values that are transmitted to the DACS via RS485 Modbus.

2.5 Summary of Measurement and Test Equipment

Measurement and test equipment (M&TE) requiring calibration, and calibration status are listed in Table 2.1. With the exception of the Alicat and BaroTroll transducers, calibration dates listed in the table are for the post-calibration conducted at the completion of SB_BH01 testing.

Table 2.1 Measurement and Test Equipment Calibration Summary.

ID	Description	Serial #	Calibration Date	Calibration Renewal Date
Keller-1	TZ transducer	1096425	26 May 2022	26 May 2023
Keller-2	BZ transducer	1096424	26 May 2022	26 May 2023
Keller-3	Annulus transducer	1096427	26 May 2022	26 May 2023
Keller-4	Tubing transducer	1096426	26 May 2022	26 May 2023
Keller-5	Backup transducer	1096428	26 May 2022	26 May 2023
Alicat-1	PMS pressure controller	293473	29 Sep 2021	n/a
Alicat-2	Backup PMS pressure controller	293474	29 Sep 2021	n/a
In-Situ BaroTroll	Barometer	471449	12 Jul 2020T	n/a
HOBO-1	TZ temperature	21281229	2 Jun 2022	2 Jun 2023
HOBO-2	BZ temperature	21281231	2 Jun 2022	2 Jun 2023
Omegadyne-1	Packer inflation pressure transducer	430994	31 May 2022	31 May 2023
Omegadyne-2	DHSIV pressure transducer	432809	31 May 2022	31 May 2023
Omegadyne-3	Piston extend pressure transducer	432801	31 May 2022	31 May 2023
Omegadyne-4	Piston retract pressure transducer	430979	31 May 2022	31 May 2023

The as-built 29.96-m and 5.03-m test tool assembly schematics are shown in Figure 2.9 and Figure 2.10.

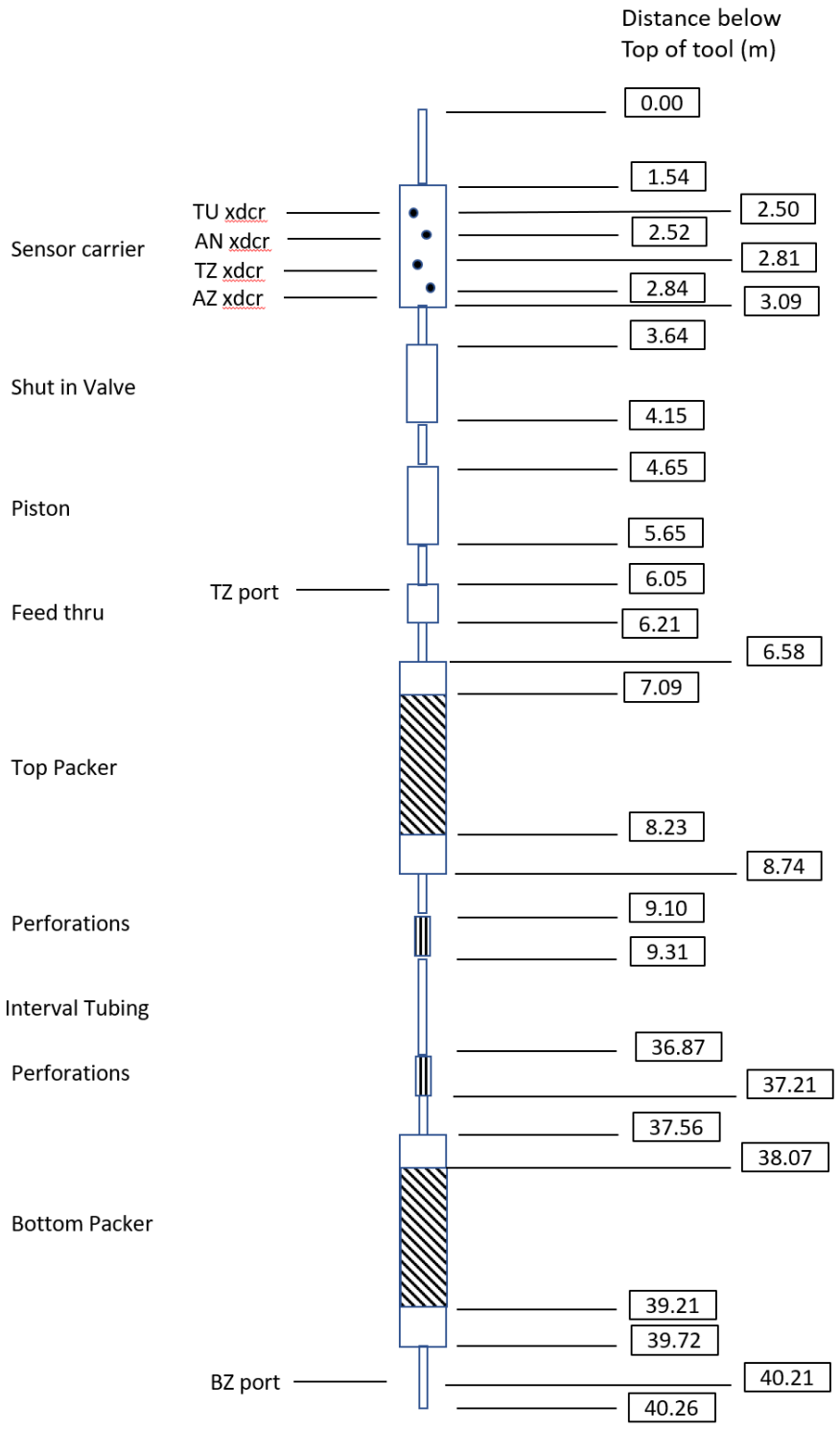

Figure 2.9 As-built 29.96-m test tool with measurements.

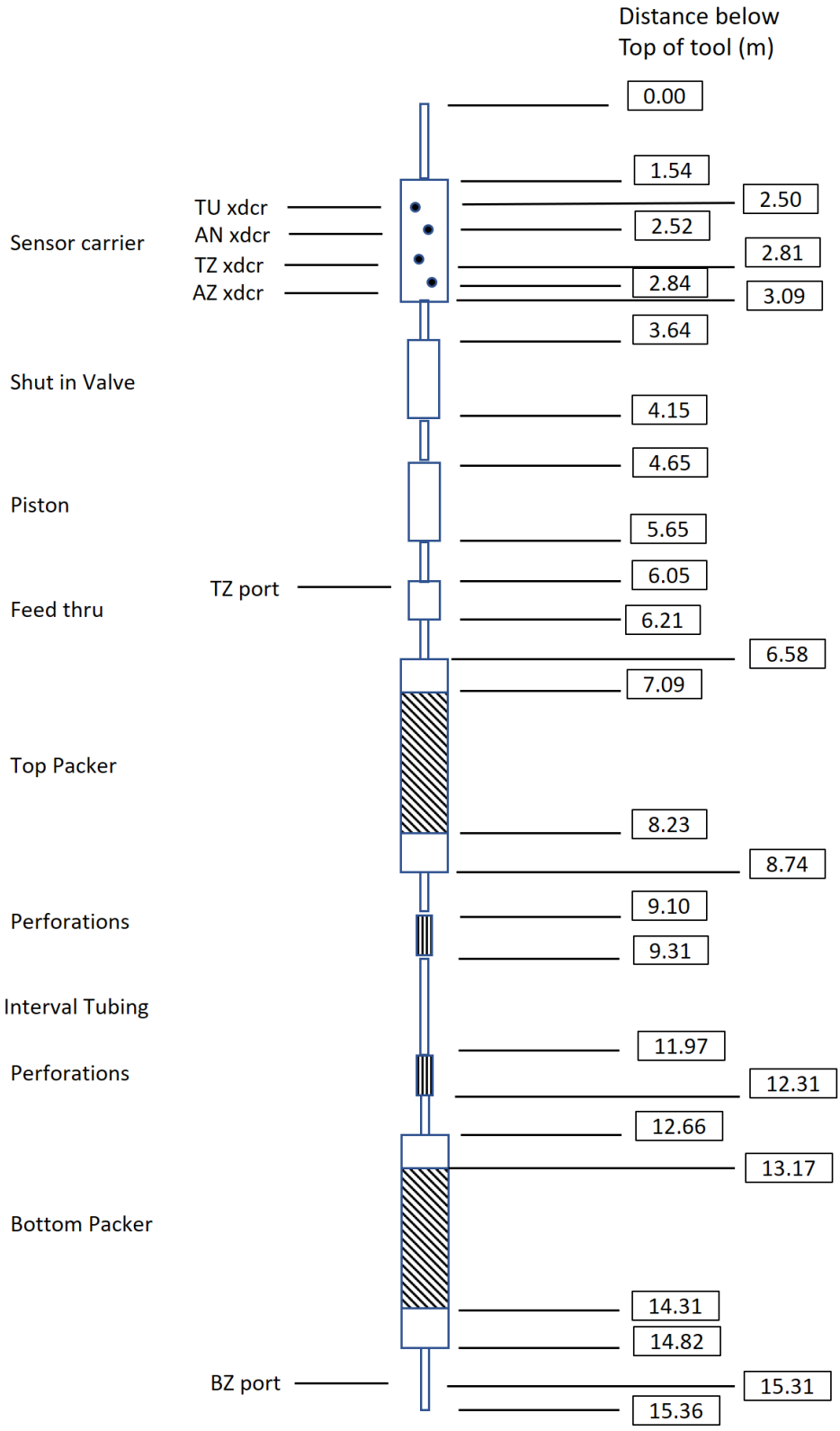

Figure 2.10 As-built 5.03-m test tool with measurements.

3 TESTING METHODOLOGY

3.1 Tool Assembly

The HTT was too long to be completely assembled at surface and then lowered in the hole. Consequently, the tool was assembled in sections (top of tool to upper packer, interval joints, lower packer and below) on surface with the individual sections assembled over the borehole. Hydraulic lines and fittings were pressure tested and “snooped” as the tool was assembled. “Snooping” involves squirting soapy water over the connection and visually monitoring for bubbles.

3.2 HTT Installation and Leak Testing

The HTT was lowered into the well on 2-3/8 inch tubing, with the shut-in valve open, to its desired position with respect to the first interval to be tested. Tubing joints were prepared with PTFE thread sealant and assembled with pipe wrenches to ensure a leak proof seal. For subsequent intervals, the tool was moved down to the specified interval position.

Leak testing in the surface casing was performed before the test tool was lowered to formation depths. The tool was typically lowered to a depth of 40 metres below the static water level in the BH. Packers were inflated with the DHSIV open and the pulse piston in retracted position. After inflation, the DHSIV was closed and the pressure monitored for fluctuations that indicate fluid leakage into the TZ. The pulse piston was extended producing a pulse , and the response monitored for several hours. The leak tests were analyzed in nSIGHTS to ensure the apparent hydraulic conductivity met the criterion of less than 10^{-13} m/s. Leak testing was also performed after each tool reconfiguration or repair during testing. All accepted leak tests were significantly tighter than the acceptance criterion, with apparent hydraulic conductivities down to 10^{-15} m/s. Results for initial leak testing on the 5 m tool configuration are shown in Figure 3.1.

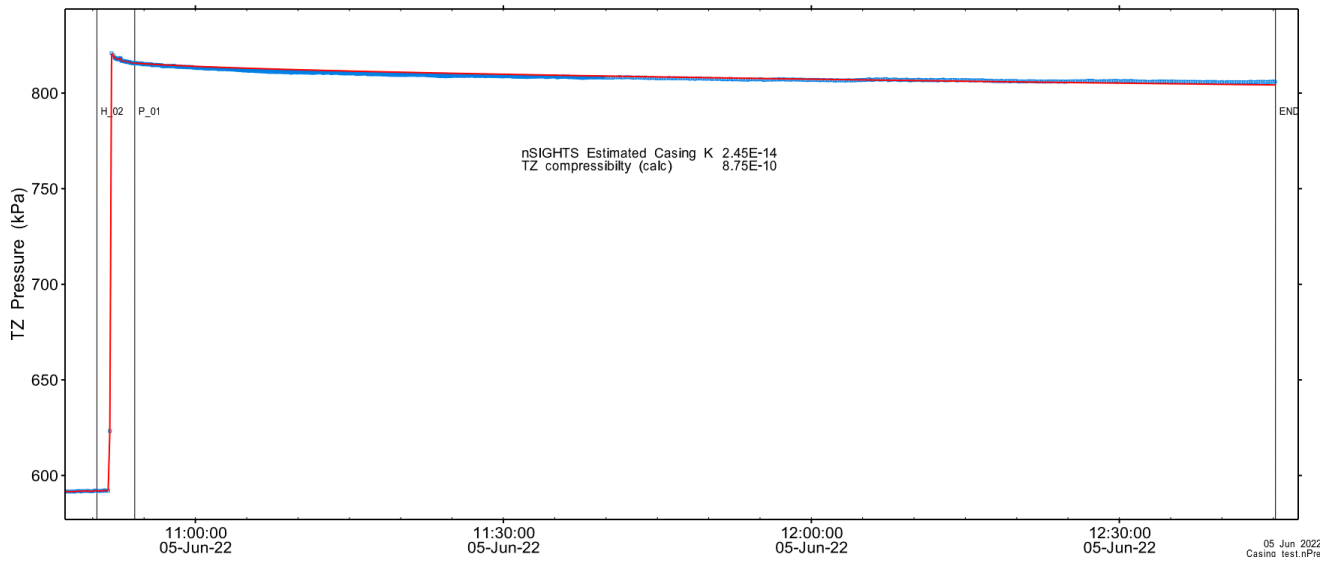

Figure 3.1 Analysis of leak test of 5.03 m HTT system.

Based on the target depth and tool measurements, the number of full joints of tubing needed for the HTT installation was calculated. Additional tubing joints and/or pup joints were added as needed to position the HTT precisely. In selecting and positioning pup joints, allowance was made for handling requirements at the surface. All tubing tallies and depth calculations were verified by a second individual and recorded before testing of an interval began. Tubing and pup joint calculations were recorded in the DQCW tubing tally sheet for each test.

Communication with the downhole pressure transducers was verified after every 10 joints (approximately 100 m) of tubing was installed.

Once the HTT was positioned at the desired depth, all transducers were connected to the DACS and data acquisition was initiated. The water levels in the annulus and the tubing string were measured at this time. The heights of the water columns in the tubing and annulus above the tubing and annulus transducer ports, respectively, combined with coincident pressure measurements allowed for two calculations of the effective water density, serving as a cross-check. All data relevant to these calculations and the calculation results were recorded in the DQCW. If calculated densities were significantly different, water level measurements were rechecked until reasonable agreement was established.

After all planned 5-m test intervals were completed, the HTT was tripped out of the borehole and a final leak test performed prior to reconfiguring the HTT for the 30-m testing.

3.3 Packer Inflation

Minimizing test-zone compressibility (C_{tz}) is imperative to maximize pulse test pressure response in low-permeability intervals. The most significant factor in test-zone compressibility is packer inflation pressure. Packers were inflated to the maximum pressure possible without impacting formation integrity and consistent with operational constraints. A geo-mechanical analysis of formation breakdown pressures (Figure 3.2) calculated maximum packer inflation system pressures at surface as a function of test interval depth. Formation breakdown pressure is an estimate of the radial pressure at which fracturing of the adjacent formation may occur. Combining the maximum calculated pressure with an operating pressure range (minimum required to inflate packers and maximum safe operating pressure of MIATA components) yielded a linearly varying range of maximum packer inflation from 6 MPa at 200 mBGS to 15 MPa below 560 mBGS.

Excessive N_2 consumption by the Alicat controller during testing required a reduction of maximum pressure to 11.7 MPa (1700 psi) which was used for all tests deeper than 430 mBGS. Calculated test zone compressibility was close to estimated borehole fluid compressibility for nearly all tests.

Packers were inflated to the desired pressures and PMS settings were recorded. The shut-in valve was maintained in an open position while the packers were inflated to avoid pressure squeeze in the test interval.

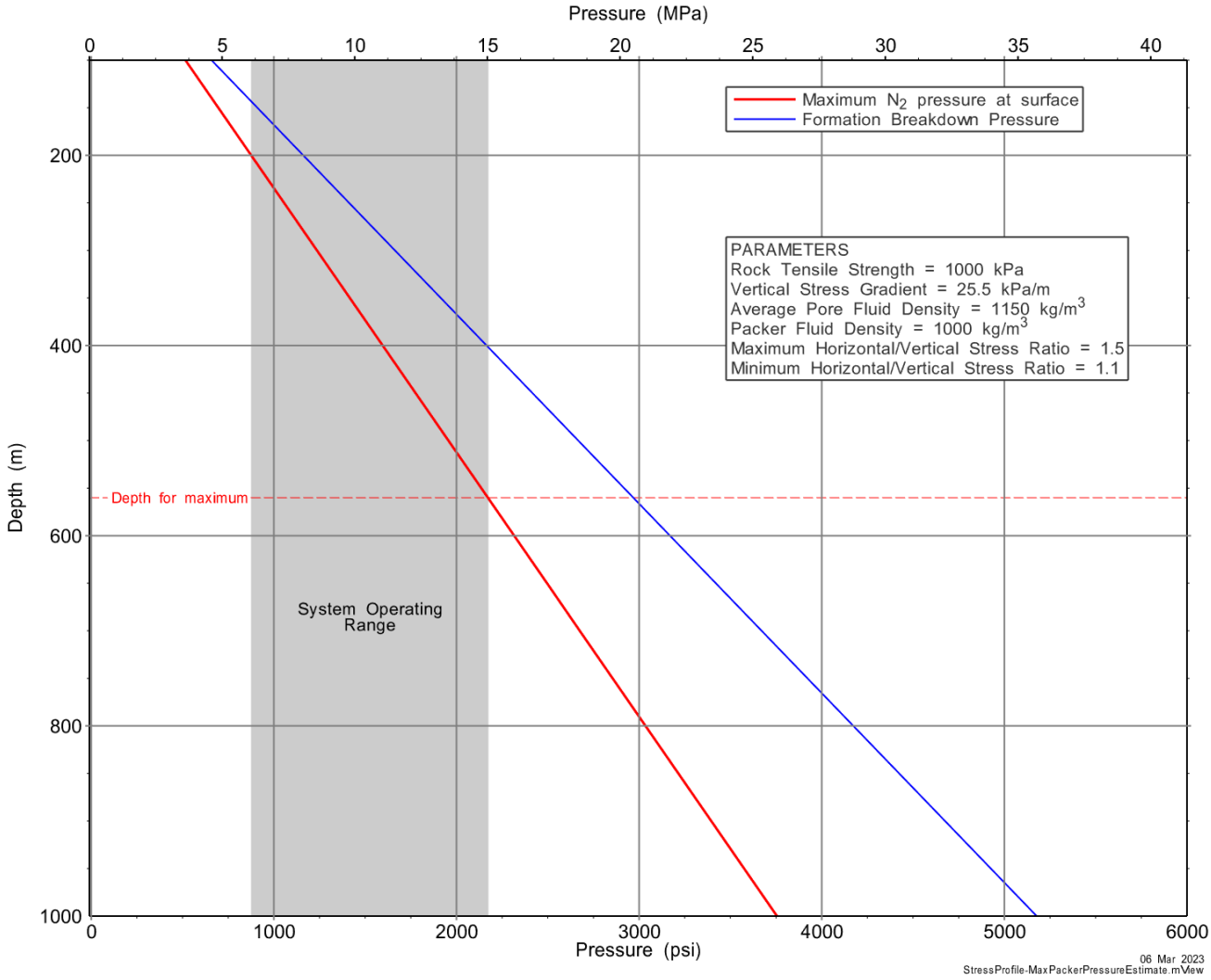

Figure 3.2 Packer Inflation Pressure Ranges

3.4 System Stabilization

Hydraulic pressures were reviewed to ensure the pulse piston position was “retracted” for testing to begin with a pulse injection.

After the pulse piston position was confirmed, the DHSIV was closed. Piston position and DHSIV closing time were recorded. The pressure in the now isolated test zone then began to change relative to the annulus pressure and the tubing pressure, as the test-zone pressure equilibrated with the far-field static pressure of the interval being tested. The bottom hole pressure typically showed a pressure increase during packer inflation due to “packer squeeze,” and then either increased or decreased depending on the natural formation pressure in the interval isolated below the bottom packer. Tubing string pressure remained constant apart from minor effects due to the atmospheric pressure changes once the DHSIV was closed.

Initially, the tubing pressure and annulus pressure were similar. Prior to initiating a slug test, enough water was removed from the tubing to lower the tubing pressure by approximately 150 to 350 kPa.

The system was then typically left to stabilize/equilibrate overnight. The stabilization period was sometimes shortened if relatively stable pressure conditions were obtained rapidly, as was the case in higher permeability test intervals. Note that equilibration did not necessarily mean a constant TZ pressure, as under-pressured or over-pressured formations and/or borehole history sometimes caused TZ pressure to rise and fall, and several hours of equilibration would not compensate for the effects of weeks of pre-test borehole history.

3.5 Slug Testing

After equilibration, the DHSIV was opened in certain intervals to initiate a slug withdrawal and the event was recorded. Slug tests were performed in three SB_BH02 intervals: HT01_05 (Salina A2 Evaporite); HT02_05 (Guelph); and HT03_30 (Goat Island).

3.6 Pulse Testing

After equilibration, pulse-injection tests were initiated in certain intervals by extending the piston. The pulse pressure differential (TZ pressure immediately before and after pulse initiation) was used along with the test-zone volume and pulse-piston displacement volume to calculate the test-zone compressibility (C_{tz}). Test-specific C_{tz} is an essential parameter for accurate simulation of pulse tests. C_{tz} integrates the essential components of the combined test tool, test zone and formation mechanical response. When combined with the actual test zone fluid volume, it forms the boundary condition term for pulse tests. It is not possible to accurately estimate C_{tz} without either a PPG or accurate measurements of tubing string fluid level changes in response to the DHSIV open/close sequences. Test-specific variables such as packer construction details, packer inflation pressure, formation rock compressibility, and test zone fluid compressibility preclude using estimated or generic values. Uncertainty in formation hydraulic parameter estimates is not quantifiable unless actual test-specific C_{tz} data are used.

At completion of the PI tests, the pulse piston was retracted to initiate a brief PW. This allowed verification that the same magnitude pulse was created by piston retraction as was created by piston extension at the start of the test. This confirmed that C_{tz} was constant over the test duration.

3.7 Test Termination

After a test was terminated, the DHSIV was opened, the packers were deflated, data acquisition terminated, and the raw test data file was produced. The file (CSV format) contained date/time stamps and pressure responses for all real-time transducers. The file was imported into nSIGHTS to produce a set of reference plots to be included with the DQC workbook.

3.8 Real-Time Analysis

The nSIGHTS well-test-analysis software (Section 4) was used to provide preliminary estimates of formation properties as testing progressed. Test-zone pressure histories were constructed for each testing sequence using the relevant data starting from drilling intercept to the start of the current sequence and were included in the analyses.

The measured test response for the equilibration/stabilization period during a testing sequence formed an additional pre-test history sequence. As a test progressed, measured TZ pressures were used to update the test sequence and the analysis continued. A final optimization with all the test data was performed immediately following test termination. These preliminary test analyses were recorded in the DQCW describing test results. All real-time analysis results are superseded by analyses presented in this report.

4 ANALYSIS APPROACH

A discussion of the conceptual flow models, descriptions of the types of hydraulic tests performed, definitions of the various fitting parameters, a discussion on borehole pressure history, and an overview of the analysis process, including the uncertainty calculations, are given below.

4.1 Conceptual Model

The term *conceptual model* in this report refers to the mathematical description of the hydrogeologic system. Selecting a conceptual model is the first step in the overall analysis process. The choice of conceptual model, along with the type of hydraulic test(s) performed, determines which parameters will be estimated, i.e., which parameters will be fitting parameters in the analysis process.

In a near horizontally layered sedimentary sequence, like that tested in borehole SB_BH02, where the borehole is drilled approximately perpendicular to the layers, the simplest conceptual model that is generally invoked in well-test analysis is described as an infinite-acting, radial-flow system with wellbore storage and skin. *Infinite-acting* means that the hydraulic parameters controlling the test response, such as transmissivity (T) and storativity (S), are constant within the region affected by the test and the test is not affected by external boundary conditions. The term radial indicates horizontal convergent flow toward and/or away from the test zone (depending on the gradient induced during a test). Note that all flow is assumed to be horizontal within the tested layer, i.e., flow with no vertical component. A further assumption made in the conceptual model is that the hydraulic properties of the tested interval do not vary vertically. This assumption may not hold true when multiple formations are included in the test interval.

Wellbore storage is that property of the testing system whereby some portion of the fluid injected/withdrawn during a hydraulic test is taken up by / derived from the test zone (shut-in valve is closed) or the tubing (shut-in valve is open) rather than the formation. During the wellbore-storage dominated period of a test, the formation properties of interest have little effect on the observed pressure response, meaning the formation properties are masked to some extent. The wellbore-storage dominated period of a test is that period in a test where the total system compressibility acts to mask the formation pressure response by absorbing/producing fluid unrelated to fluid movement in/out of the formation. Ideally, a test will proceed long enough such that the formation-flow component dominates the wellbore-storage component and the formation properties can be reliably estimated. The adequacy of the SB_BH02 test durations was determined by real-time analysis.

An area of altered hydraulic conductivity surrounding the wellbore that results from drilling activities (e.g., mud infiltration, stress relief, etc.) is termed a skin. A positive skin is a zone in which K has been decreased relative to the unaltered formation K. A negative skin is a zone in which K near the wellbore has been enhanced. Skin was included in all SB_BH02 simulations and was implemented using nSIGHTS' radially varying hydraulic conductivity functionality in which hydraulic conductivity changes logarithmically as a function of distance. A fixed radius point was placed at the wellbore with hydraulic conductivity optimized to represent initial skin conductivity. An adjustable radius point was placed to define the skin thickness and the optimized formation hydraulic conductivity. Formation hydraulic conductivity was constant beyond this adjustable radius point.

4.2 Parameters

Hydraulic conductivity (K) [L/T] is a constant of proportionality that was empirically derived by Darcy (1856) expressing the ratio of fluid flux to gradient within a porous medium. Darcy's empirical relationship is generally referred to as Darcy's Law, and can be written as follows:

$$Q = -K \frac{dh}{dl} A \qquad \textbf{Equation 4-1}$$

where:

Q	=	flow rate	[L^3/T]
dh/dl	=	hydraulic gradient	[ ]
A	=	flow area	[L^2]

The specific storage (Ss) [1/L] of a saturated geologic unit describes the amount of fluid released as a function of both the rock and fluid compressibility per unit decline in hydraulic head per unit volume of rock, and is given as:

$$S_s = \rho g(\alpha + n\beta) \qquad \textbf{Equation 4-2}$$

where:

ρ	=	fluid density	[M/L^3]
g	=	gravity	[L/T^2]
α	=	rock compressibility	[LT^2/M]
n	=	porosity	[ ]
β	=	fluid compressibility	[LT^2/M]

Well-test analysis does not provide estimates of K and Ss, but of their products when multiplied by the test-interval length, transmissivity (T) [L^2/T] and storativity (S) [-]. For the analyses presented in this report, K and Ss were calculated by assuming that all test intervals were vertically homogeneous and simply dividing the inferred values of T and S by the test-interval length. The validity of this assumption undoubtedly varies from test interval to test interval; when a test interval is wholly contained within a single formation, vertical homogeneity may be a reasonable assumption. But when a test interval spans portions of several formations, the assumption is less defensible. In such a case, other information must be used to try to infer what portion of the total T (or S) is contributed by the K (or Ss) and thickness of each formation in the test interval.

Static formation pressure (P_f) [M/LT^2] is the undisturbed fluid pressure within a formation prior to drilling and testing. "Raw", or uncorrected, formation pressures are those measured by the transducer, which is located some distance above the centre of the test zone. These "raw" numbers are used in the individual test analyses presented below. The raw values are subsequently corrected to represent the pressure in the centre of the test interval. Borehole fluid density estimates and measured transducer locations are used in calculating corrections. The corrected values are presented in the test summary tables and the borehole summary tables (Section 7).

The observed pressure change (*ΔPressure*) in the isolated test zone for a given amount of fluid (*ΔVolume*) that enters/leaves the test zone is controlled by the test-zone compressibility (C_{tz}), defined as follows:

$$C_{tz} = \frac{1}{TotalVolume} \frac{\Delta Volume}{\Delta Pressure} \qquad \textbf{Equation 4-3}$$

where: *Total Volume* = total volume of fluid within the isolated test zone

The skin factor (s) [ ] is a dimensionless parameter that indicates the relative degree to which skin hydraulic conductivity (K_s) near the borehole differs from the undisturbed formation hydraulic conductivity (K_f) at some distance away from the borehole. The skin factor is defined by Hawkins (1956) as:

$$s = \left(\frac{K_f}{K_s} - 1\right) \times \ln\left(\frac{(r_w + t_s)}{r_w}\right) \qquad \textbf{Equation 4-4}$$

where:

r_w = nominal well radius [L]
t_s = skin thickness [L]

In the case where the value of K_s is changing logarithmically with distance from the borehole wall to the value of K_f, the value of K_s used in Equation 4-4 is the log average of K_s at the borehole wall (which is the value fitted by nSIGHTS) and K_f.

4.3 Tests

A pulse injection (PI) or pulse withdrawal (PW) test is an instantaneous (within the limitations of the equipment) pressure increase or decrease induced in the test zone that is subsequently allowed to dissipate back toward static pressure conditions. The rate of pressure decay is used to infer the hydraulic properties of the tested geologic unit. During a pulse test, the test zone is shut-in, i.e., it is isolated from the fluid column in the tubing by closing the shut-in valve. Pulse tests are most suitable for testing formations with hydraulic conductivities less than 1E-10 m/s, and were performed in the majority of the test intervals.

Compressibility of the SB_BH02 test zones was calculated for each pulse test. All SB_BH02 pulse tests were initiated by rapidly extending the downhole pulse piston of known volume. The C_{tz} was then calculated from Equation 4-3 by measuring the initial pressure change, given that the test-zone fluid volume was known. (Note that the test-zone fluid volume comprises the fluid in the borehole between the two packers as well as all fluid contained within the test tool below the shut-in valve.) Note that hydraulic parameters such as K cannot be estimated accurately from pulse responses without knowing C_{tz}. All pulse tests performed in SB_BH02 used an initial PI, followed by a PW at the end of the test to confirm C_{tz}.

Slug withdrawal (SW) tests are similar to pulse tests, but the shut-in valve remains open during a slug test and fluid flowing out of the formation results in changing water levels within the tubing. Slug tests were initiated by removing water from the tubing to a desired level while the shut-in valve was closed, and then rapidly opening the shut-in valve. Analogous to C_{tz} in a pulse test, the tubing radius and fluid

density controlled the observed pressure change for a given amount of fluid that entered/left the tested formation. The tubing string radius must be known to estimate K from a slug-test response.

4.4 Formation Specific Storage - Skin Conductivity - Skin Thickness

Simultaneously estimating Ss, skin K (K_s), and skin thickness (t_s) values from analysis of single-well data (i.e., no cross-hole response) is complicated by the high degree of correlation among these fitting parameters in the regression process. Figure 4.1 shows 1345 estimates of these three parameters obtained from perturbation analysis (Section 4.6) of an example pulse test conducted in a low-permeability sedimentary formation. Note that each of the 1345 solution sets produced effectively equivalent matches (small change in the fit value) to the measured response. The values of K_s and t_s can be simultaneously increased/decreased over a range that results in approximately the same skin factor, s (Equation 4-4).

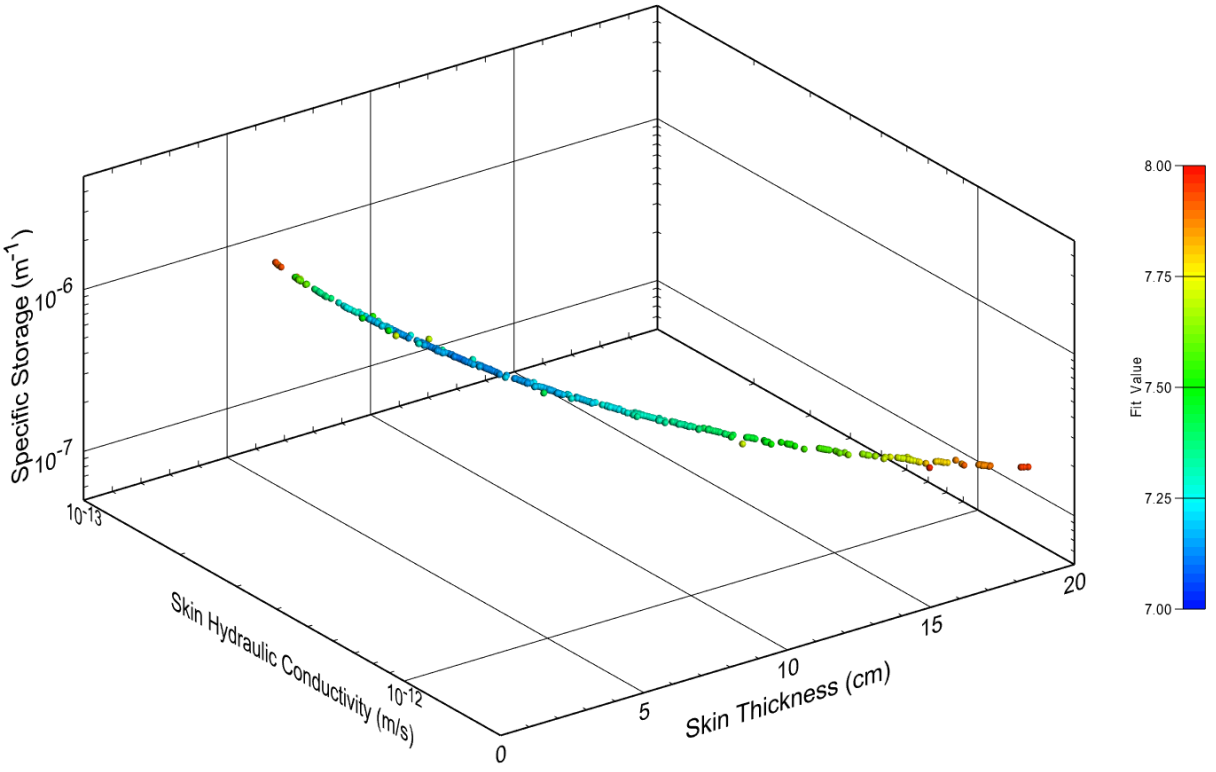

Figure 4.1 An X-Y-Z scatter plot showing the correlation among skin thickness, skin hydraulic conductivity, and specific storage that can occur in a single-well test.

In addition, Ss and s affect the match to a single-well pressure response in much the same way, so they can be simultaneously changed to produce a series of equivalent matches. Figure 4.2 shows simulated pulse-test responses assuming equilibrium initial conditions plotted on a log-log scale as a normalized pressure response and its derivative; a standard well-test diagnostic plot known as a Ramey B plot

(Ramey et al., 1975). Various parameter possibilities are simulated to illustrate the difficulty in distinguishing among variations in Ss and s.

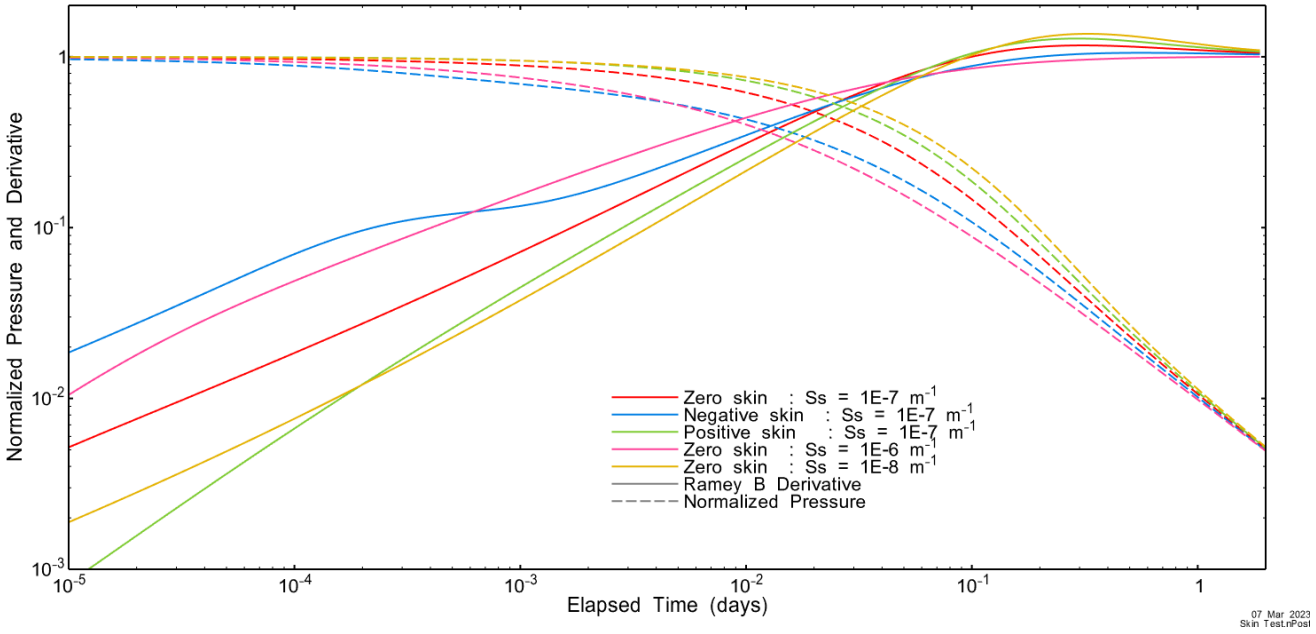

Figure 4.2 Ramey B diagnostic plots showing various combinations of skin factors and formation specific storage.

The baseline example shown in red in Figure 4.2 shows simulated responses when the hydraulic properties around the wellbore have not been altered – a condition known as a "zero" skin. Note that Ss for the baseline case is 1E-7 m^{-1} and the formation K (K_f) for all examples is constant. When the drilling process results in increased K_s over some distance t_s near the wellbore relative to the unaltered formation K_f, the condition is known as a "negative" skin, plotted as a blue line in Figure 4.2. Notice that the negative skin produces a distinctive downward inflection in that part of the Ramey B derivative that appears as an upward-sloping straight line when no skin is present (timing and magnitude of this inflection depend on the contrast between skin and formation properties). This inflection is observed in most of the DGR pulse responses. A decrease in K_s over some distance t_s around the wellbore is known as a "positive" skin, plotted in green in Figure 4.2. Unlike the negative skin, a positive skin causes no distinct inflection in the Ramey B derivative; it simply changes the slope of the derivative (the pulse recovery is slowed), effectively translating it to the right on the graph relative to the zero-skin case. Shown in magenta and gold are two zero-skin examples where Ss has been increased to 1E-6 m^{-1} and decreased to 1E-8 m^{-1}, respectively. As with the positive-skin case, simply changing the value of Ss does not result in a notable inflection in the derivative, it primarily changes the position of the derivative with respect to the baseline case. Figure 4.1 shows that changing K_s or Ss can result in similar responses, and consequently, estimates for each of these parameters can be paired in non-unique combinations to achieve similar matches to field data. In the case where the initial conditions at the start of a pulse are transient rather than in equilibrium (i.e., pressure is still responding to borehole history), the early-time derivative response may be altered from what is shown in Figure 4.2. Under these conditions, an inflection in the early-time derivative reflects the presence of a skin, but not whether it is positive or negative. Also note that any small transient changes in test-tool position or packer shape at the start of a pulse or slug test can affect the pressure response in such a way that these non-

formation responses resemble a skin effect. The approach used in these analyses for estimating Ss is discussed below in Section 4.7.

4.5 Pre-Test Borehole History

Each nSIGHTS simulation description includes a detailed specification of the sequence of borehole boundary conditions from the point at which the borehole perturbs the in situ, or formation, pressure. The sequence of pressures experienced by a test interval during the period between interception of the interval by drilling and the start of testing is denoted the "pressure history".

Pressure histories were included in the analyses performed for each test interval as specified-pressure boundary conditions in the test zone. Part of the pressure history consisted of the calculated pressure (not measured by transducer) at the centre of each test interval from the approximate time of drilling intercept to the time that the pressure at that interval was measured by a pressure transducer.

Fluid densities recorded during drilling and logging were nominally 1100 g/L with some measurements as low as 1046 g/L. There were drilling fluid losses after drilling through and below permeable Silurian formations, primarily the Guelph. After completion of drilling, borehole fluid equilibration occurred as native formation fluids from permeable intervals mixed with higher density drilling fluids that had migrated into these formations during drilling. It is assumed that borehole pressures would remain relatively constant as Guelph formation pressures dictated overall borehole response. Accordingly, the borehole pressure history prior to testing was fixed at the first measured pressure at the start of the first test (HT01_05).

After the start of straddle-packer testing in a given interval, pressure histories are extracted from measured pressures in the annulus and bottom zones of previous tests. As an illustrative example, the borehole history for the 29.96-m test conducted in the Collingwood/Upper Cobourg (HT10_30) is shown in Figure 4.3. The constant pressure from drilling intercept until start of HT testing reflects the TZ pressure measured at the beginning of HT01_05. Tests conducted above the permeable Guelph Formation did not result in significant BZ pressure changes. However, subsequent tests on lower intervals all showed an under-pressured response in the BZ which is included in the borehole history. Measured BZ pressures were adjusted to the center of the test interval using the average borehole fluid density.

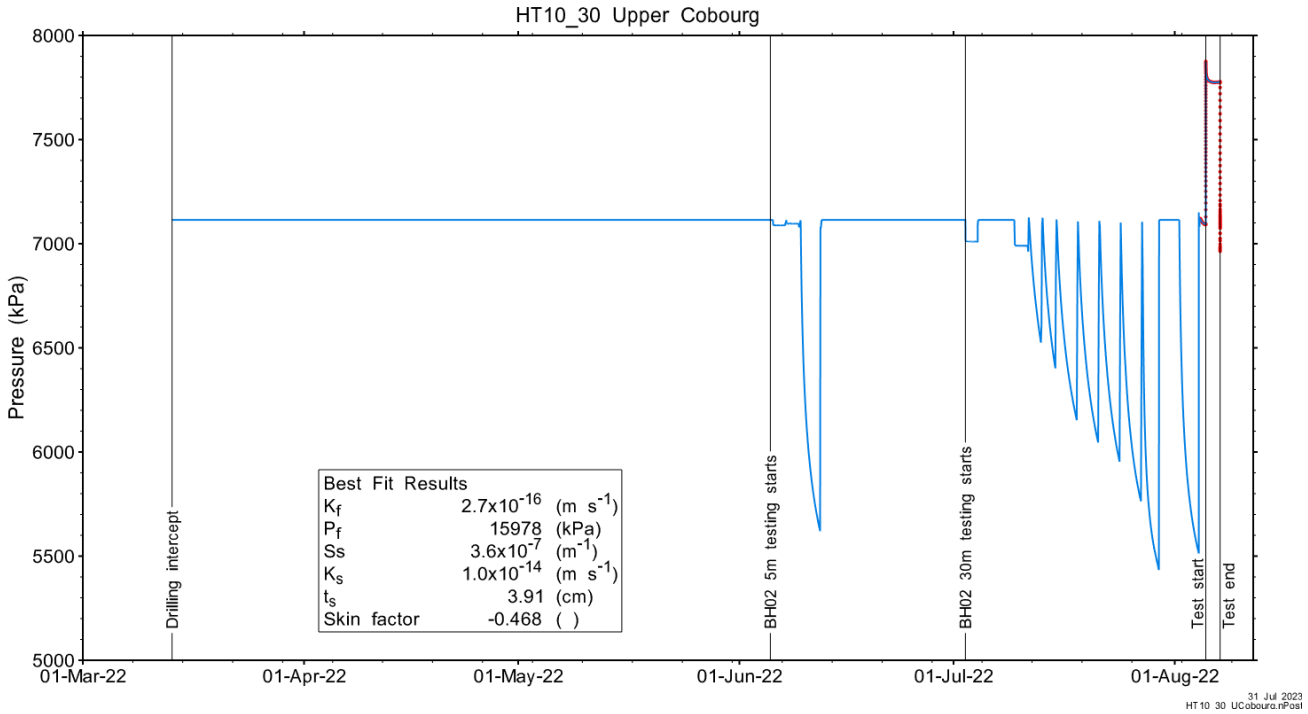

Figure 4.3 Pre-test borehole history for test HT10_30.

4.6 Test Zone Thermal Effects

Temperature changes in the shut-in test zone during pulse tests will cause thermal expansion or contraction of the borehole fluid, leading to pressure changes which complicate the analyses. Although nSIGHTS has the capability of including thermal effects in analyses, this leads to additional uncertainties in analysis results. Test zone temperatures for the three 5 m pulse tests in SB_BH02 (Figure 4.4) showed no evidence of thermal effects. All analyses were conducted as isothermal.

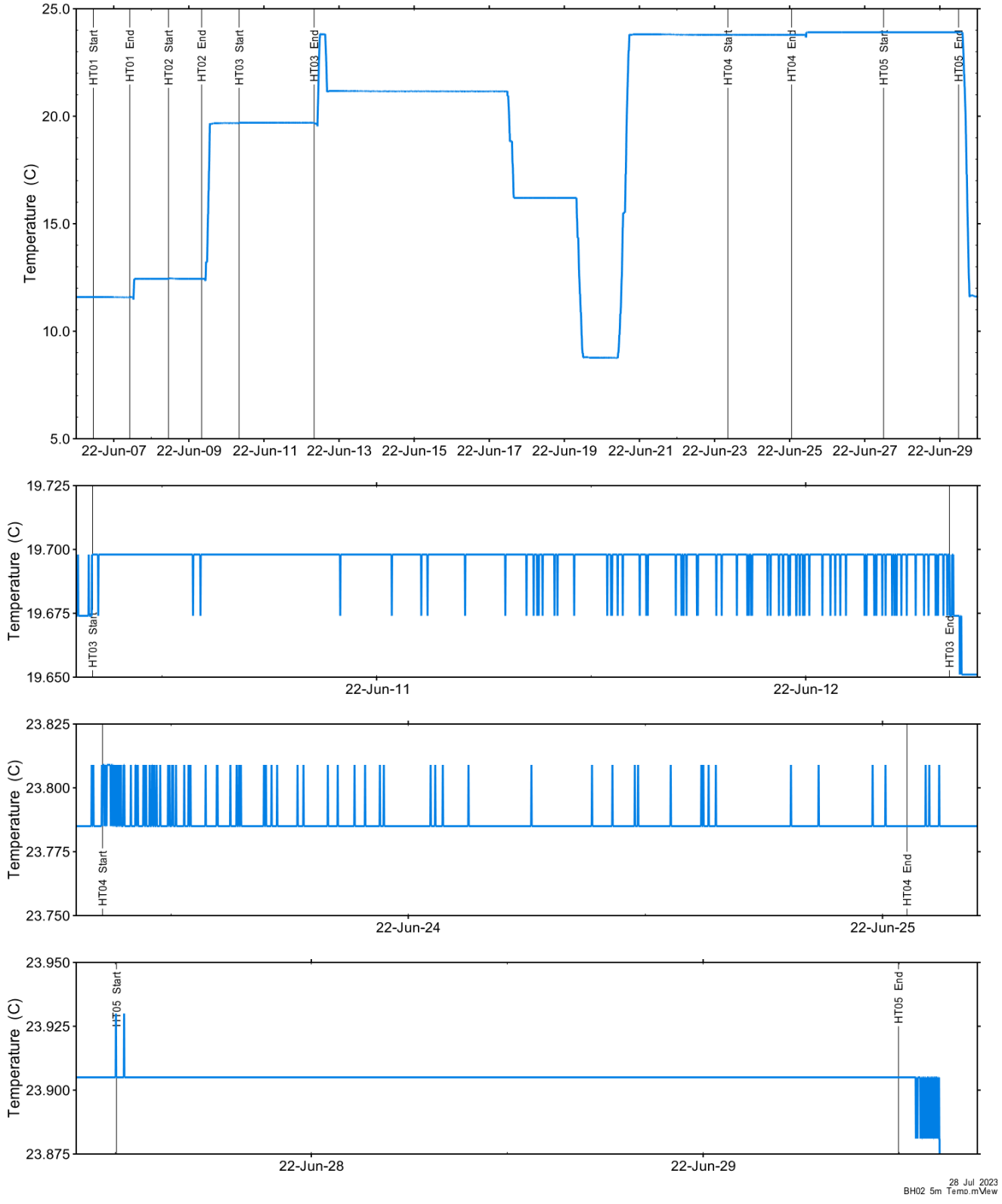

Figure 4.4 Test zone temperature during 5 m pulse tests in SB_BH02.

4.7 Uncertainty Analysis

All tests analyzed in this report assumed the skin conceptual model described in Section 4.1, which requires five fitting parameters: K_f, P_f, K_s, t_s, and Ss. Preliminary analyses obtained a single set of optimized baseline fitting-parameter values. These were used to determine limiting ranges, or domains, for each optimized parameter. Perturbation analyses were then performed to obtain the final best-fit parameter values and the corresponding uncertainty ranges.

For these analyses, 10,000 simulations were performed using randomized starting parameter estimates uniformly distributed over the potential parameter domain. Simulations which converged on an optimized solution (typically the vast majority of the 10,000 perturbations) were retained for further analyses. Initial and converged parameter estimates for selected parameters in the HT13_30 test analyses are shown in Figure 4.5 through Figure 4.8. Each figure shows data for three parameter domains – K_f is shown on all figures.

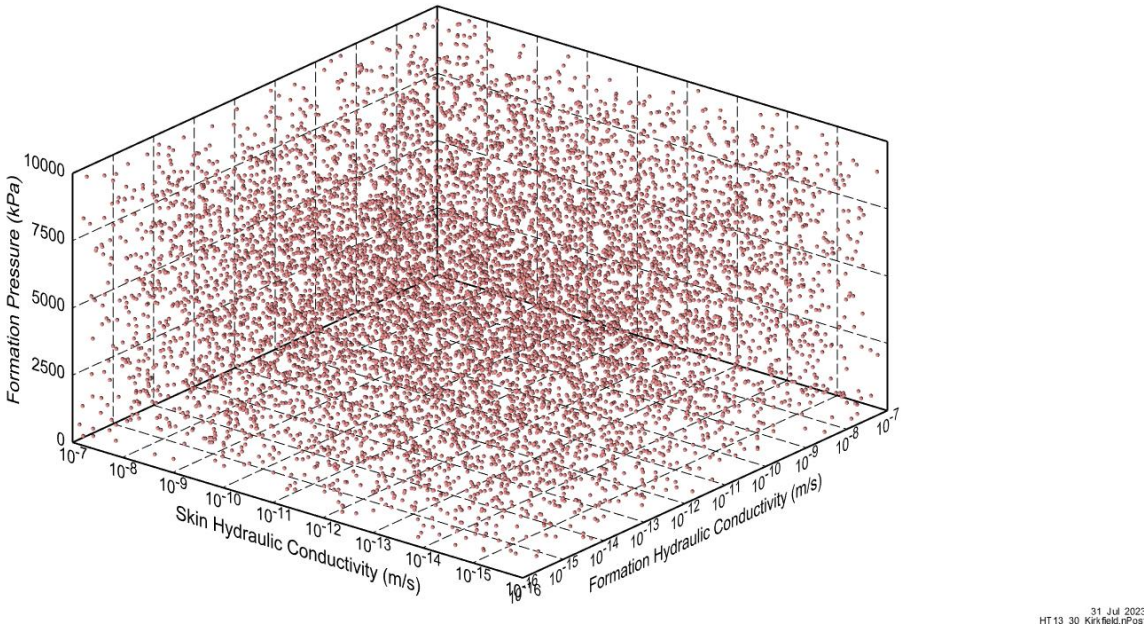

Figure 4.5 Initial parameter estimates for K_f, K_s, and P_f (HT13_30).

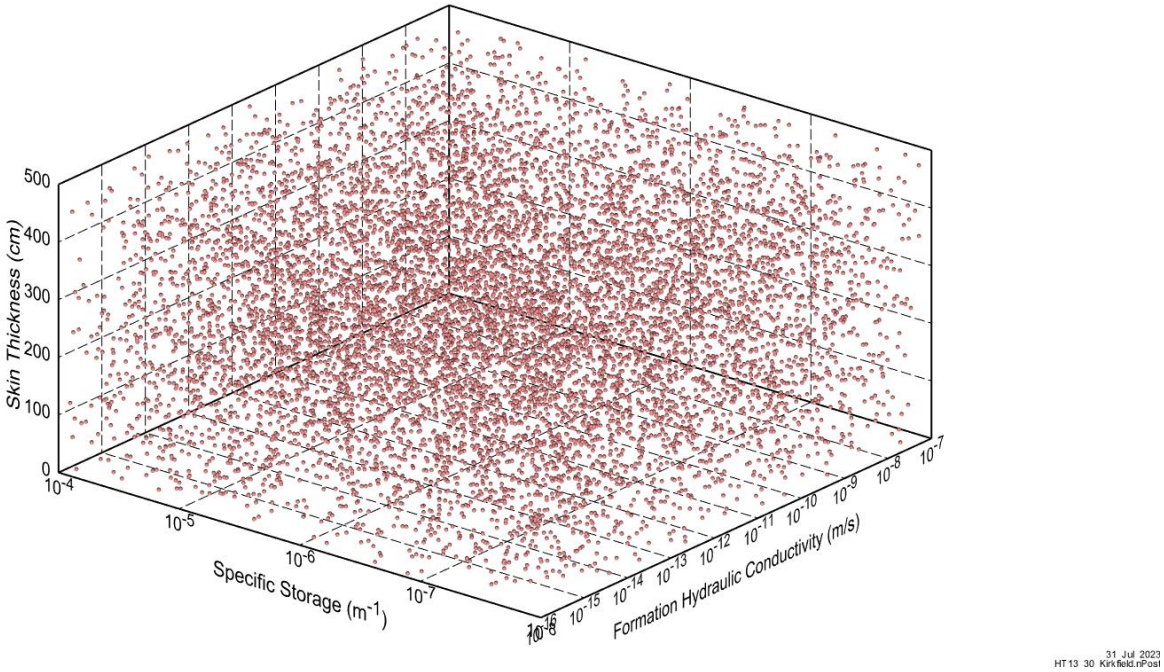

Figure 4.6 Initial parameter estimates for K_f, Ss, and t_s (HT13_30).

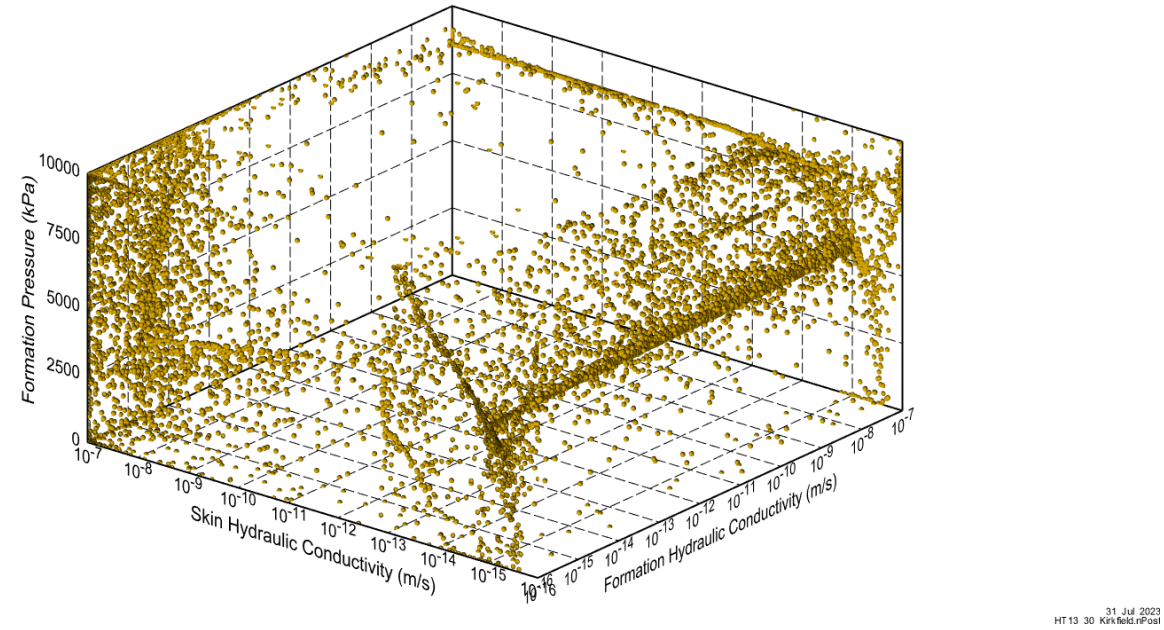

Figure 4.7 Converged parameter estimates for K_f, K_s, and P_f parameters (HT13_30).

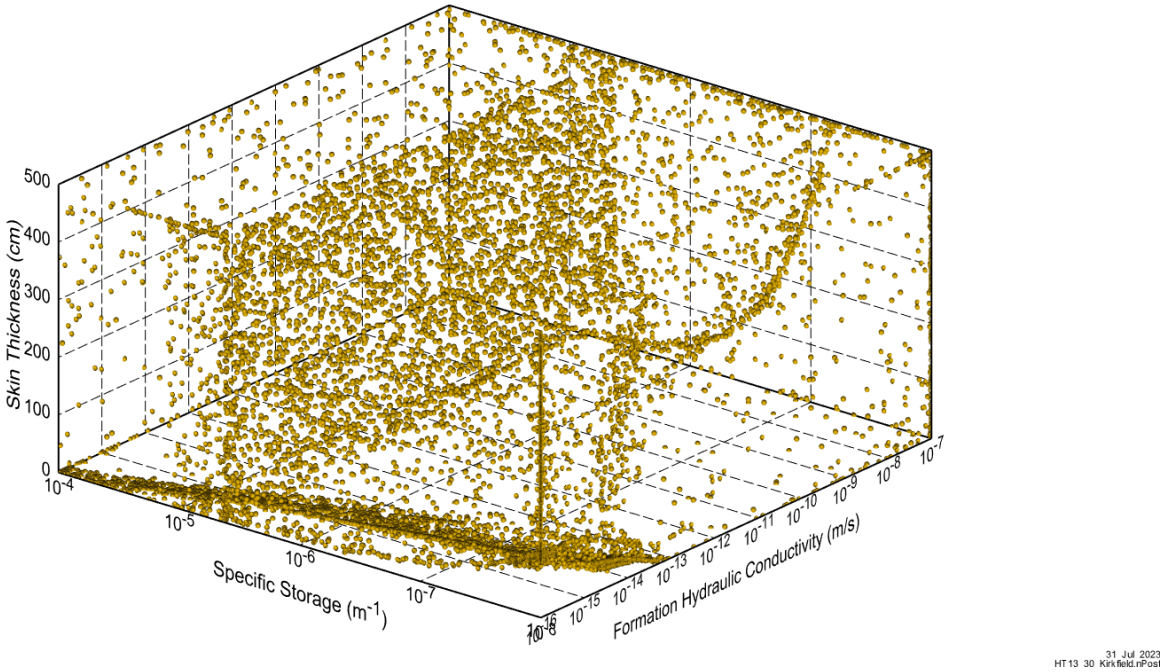

Figure 4.8 Converged parameter estimates for K_f, Ss, and t_s (HT13_30).

Goodness-of-fit is determined by the fit value, which is the sum-of-squared errors (SSE) between the simulated response and the TZ pressure data. Fit-values were normalized to the minimum (or best fit) value and the cumulative distribution function (CDF) calculated. The structure of the CDF was then examined and a "fit-discriminant" value determined. Generally, the fit discriminant was set at the first value where the CDF shape changes or inflects. A secondary criterion was to ensure that all selected fits closely matched the TZ field data. All fits with fit-values less than the discriminant were accepted as being representative of the formation response. This approach limits the fits to those within the apparent global minimum of the five-dimensional parameter space. Typically, at least several hundred perturbations were accepted for each test. Figure 4.9 shows the normalized fit CDF and the fit discriminant for the HT13_30 test.

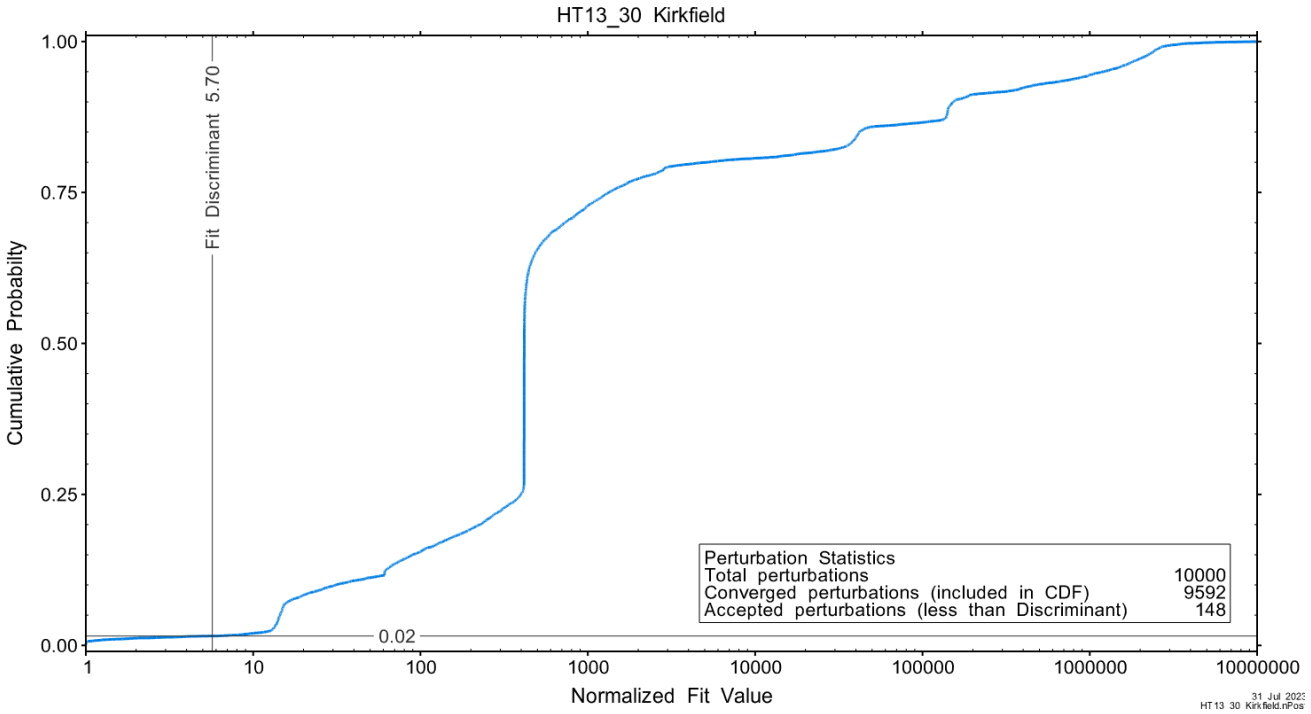

Figure 4.9 Normalized fit CDF (HT13_30).

Examination of individual fit distributions (Figure 4.10) provides confirmation that local minima are not included.

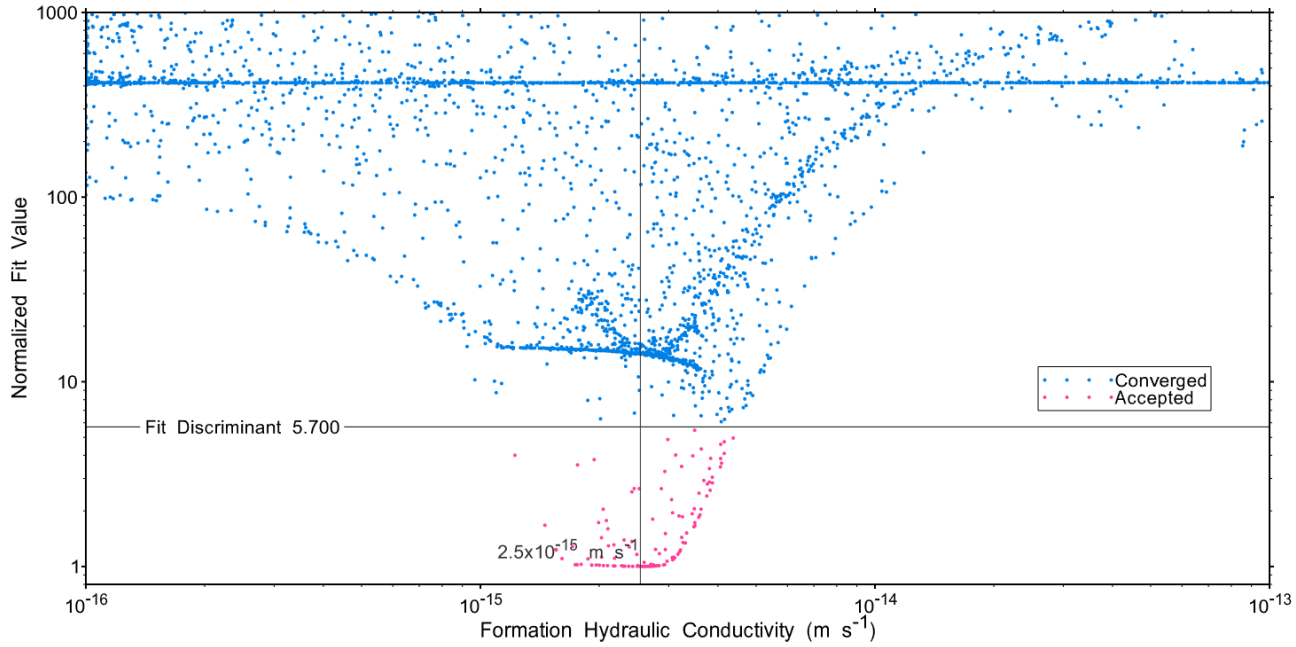

Figure 4.10 Fit distribution for K_f (HT13_30).

The parameter estimates and fit values for the 661 perturbations that met the fit-discriminant value are shown in Figure 4.11 and Figure 4.12.

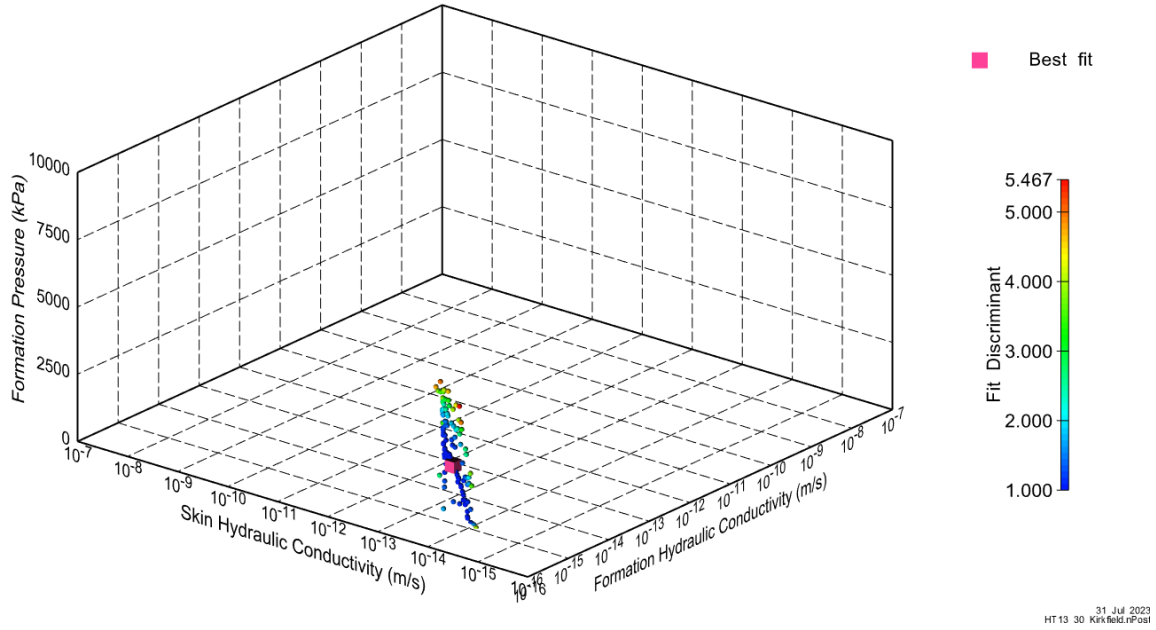

Figure 4.11 Accepted estimates for K_f, K_s, and P_f with fit values and best-fit (HT13_30).

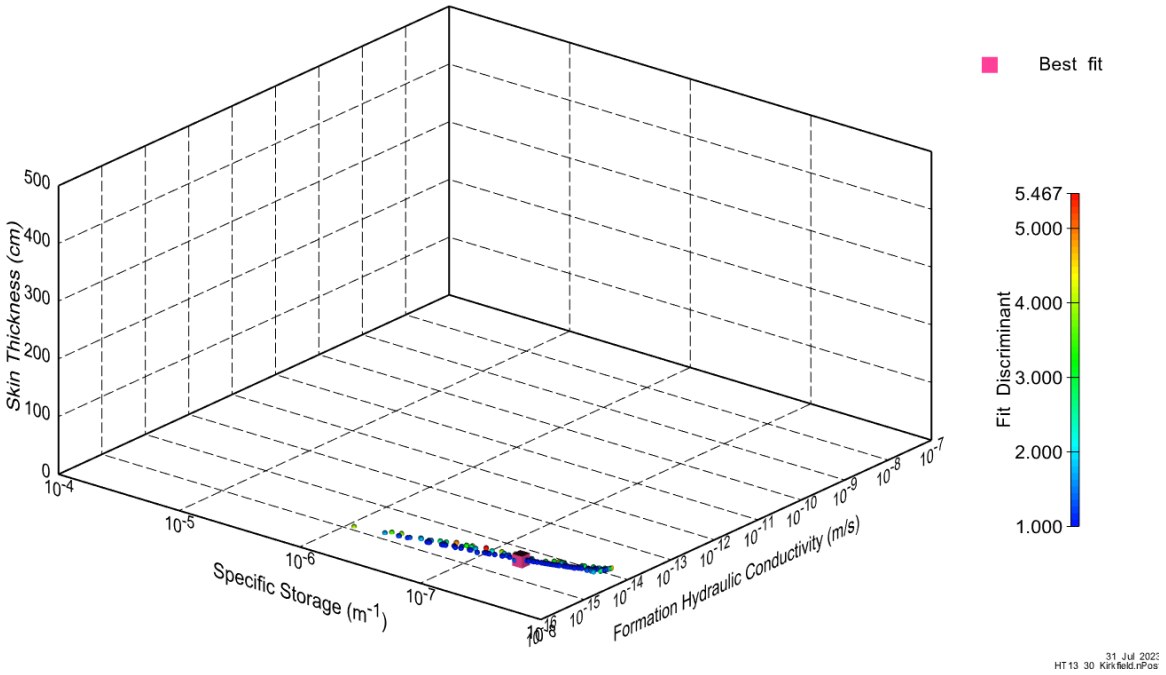

Figure 4.12 Accepted estimates for K_f, Ss, and t_s with fit values and best-fit (HT13_30).

CDFs were constructed for each of the estimated parameters from the accepted perturbations to determine parameter uncertainty. The parameter CDF for K_f is constructed for all accepted values below the fit-discriminant line in Figure 4.10, and is shown in Figure 4.13.

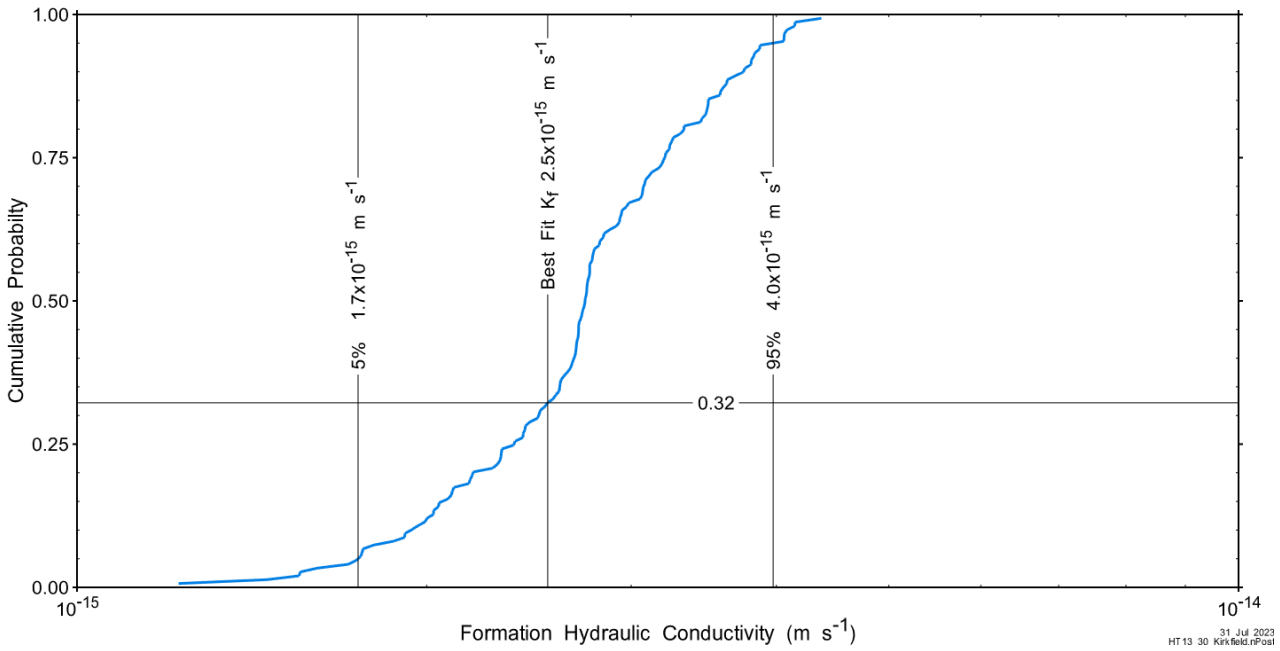

Figure 4.13 Cumulative distribution of accepted formation hydraulic conductivity (HT13_30).

Simulated results for all perturbations where all accepted parameter values were within the 5% to 95% range are shown in Figure 4.14. Note that the blue line shows results for all 123 perturbations with all parameters in the 5% to 95% range.

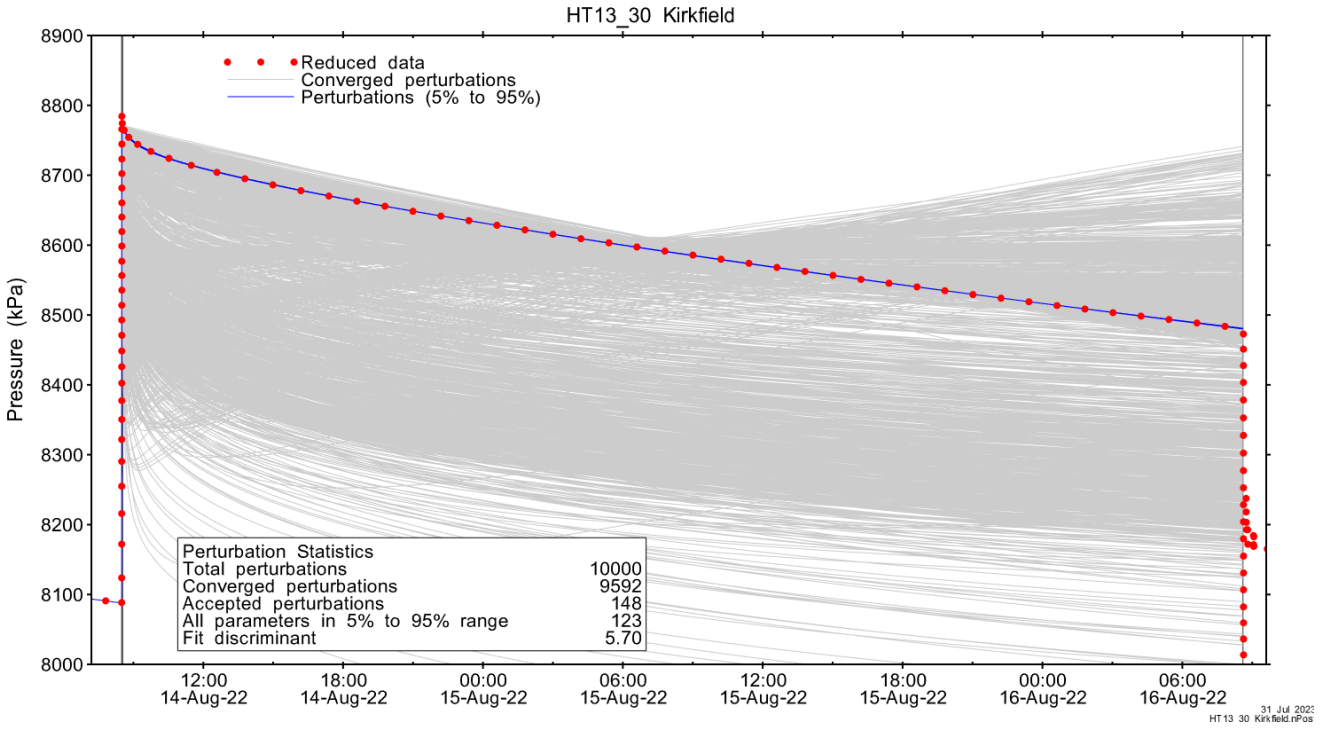

Figure 4.14 Horsetail plot showing perturbation results.

Ramey B processed results (Figure 4.15) illustrate the uncertainty range in processed derivatives.

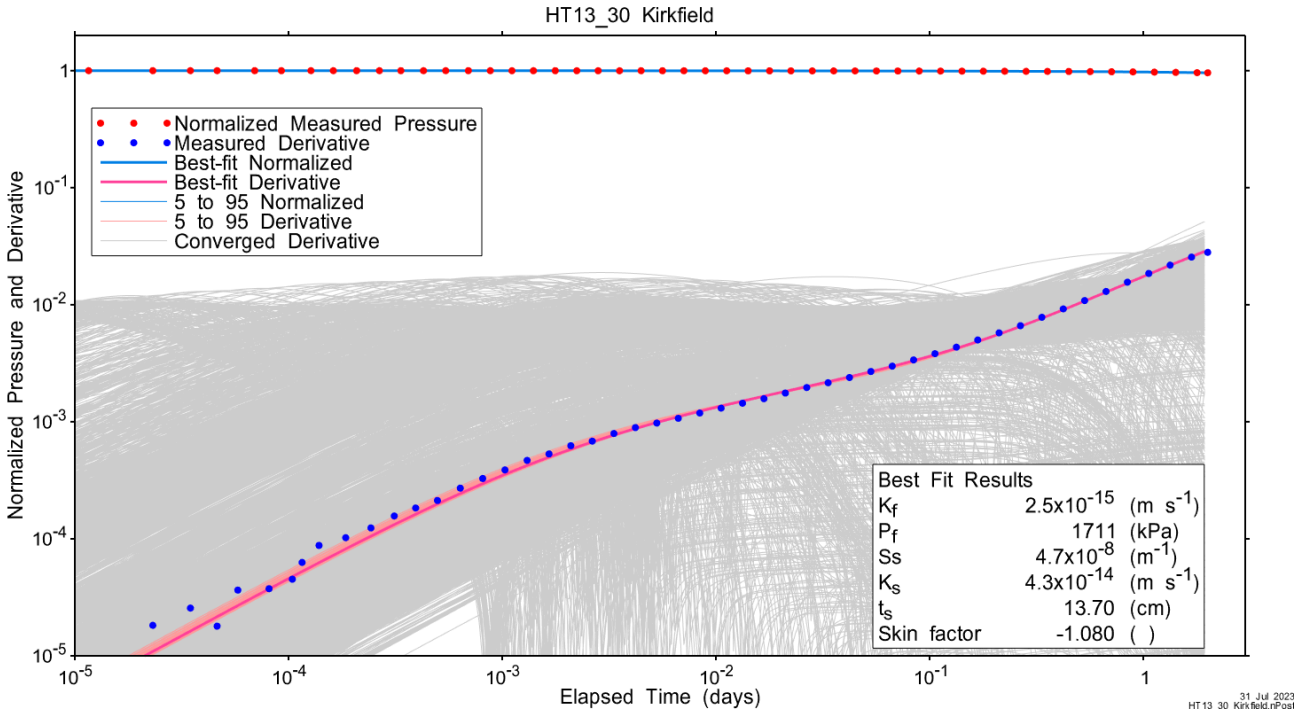

Figure 4.15 Ramey B processed horsetail plot showing perturbation results (HT13_30).

As a final analysis, fitted parameter correlations are calculated for all accepted optimizations (Table 4.1).

Table 4.1 Pearson cross-correlations of 5% to 95% parameters (HT13_30).

	Log(K_f)	P_f	Log(Ss)	Log(K_s)	t_s	s
Log(K_f)	1.000	0.965	-0.686	0.859	0.617	-0.647
P_f	0.965	1.000	-0.493	0.708	0.439	-0.452
Log(Ss)	-0.686	-0.493	1.000	-0.954	-0.976	0.998
Log(K_s)	0.859	0.708	-0.954	1.000	0.897	-0.936
t_s	0.617	0.439	-0.976	0.897	1.000	-0.984
s	-0.647	-0.452	0.998	-0.936	-0.984	1.000

5 TEST INTERVALS

Test intervals were selected by Geofirma in consultation with NWMO staff. In general, individual formations were targeted, with most testing focussed on the Ordovician-age formations. The shorter 5-m tests were assigned to relatively thin formations. Within individual formations, test intervals were adjusted vertically to ensure packer seats were located in zones with minimal borehole diameter changes as indicated by caliper logs. Borehole geophysical logs, core photos and core logging data were also reviewed during the interval selection process. Intervals were selected based on nominal 30-m and 5-m interval lengths. These have been corrected to the actual 29.96-m and 5.03-m test interval lengths resulting from selection of available tubing and pup joints during testing. Test durations were specified as 2 days for all tests above the Queenston Formation shale, and 3 days for Queenston Formation shale and deeper tests. This provided longer test response times for the lower permeability Ordovician formations.

The Cobourg Formation and Collingwood Member were targeted with three tests: two 30-m intervals which overlapped to give complete coverage of the Cobourg (HT10_30 and HT11_30), and a single 5-m test for the Collingwood Member (HT03_05). However, formation tops were subsequently revised and the Collingwood Member top adjusted downward by approximately 8 m, resulting in the 5-m "Collingwood" test interval being totally encompassed in the lower Blue Mountain Formation. Similarly, the 30-m test designed to cover the top 30 m of the Cobourg Formation (HT10_30) ended up consisting of 6.47 m of the Collingwood and the upper 23.53 m of the Cobourg. These tests have been renamed appropriately.

Table 5.1 and Figure 5.1 summarize the selected test intervals. The third panel of the figure presents caliper data and the mean caliper values for each test interval. Mean caliper values were used as the well radius in nSIGHTS analyses. Logged core features are presented in the fourth panel of the figure.

Table 5.1 SB_BH02 hydraulic testing intervals.

Test ID	Top (mBGS)	Bottom (mBGS)	Formation	Caliper Mean Diameter (cm)	Specified Packer Pressure (psi)
5-m Tests					
HT01_05	332.50	337.53	Salina A2 Evaporite	13.49	1150
HT02_05	386.80	391.83	Guelph	13.09	1700
HT03_05	663.50	668.53	Blue Mountain - Lower	12.77	1700
HT04_05	880.50	885.03	Shadow Lake	12.50	1700
HT05_05	887.00	892.03	Precambrian	12.24	1700
30-m Tests					
HT01_30	200.00	229.96	Salina F	13.26	1200
HT02_30	340.00	369.96	Salina A1 Carbonate	13.45	1250
HT03_30	393.00	422.96	Goat Island	13.42	1600
HT04_30	420.00	449.96	Cabot Head	13.34	1700
HT05_30	450.00	479.96	Queenston – Upper	14.90	1700
HT06_30	490.00	519.96	Queenston – Lower	15.21	1700
HT07_30	532.00	561.96	Georgian Bay – Upper	13.25	1700
HT08_30	580.00	609.96	Georgian Bay – Lower	12.94	1700
HT09_30	630.00	659.96	Blue Mountain	12.97	1700
HT10_30	671.00	700.96	Collingwood/Cobourg	12.64	1700
HT11_30	686.00	715.96	Cobourg	12.65	1700
HT12_30	725.00	754.96	Sherman Fall	12.67	1700
HT13_30	770.00	799.96	Kirkfield	12.73	1700
HT14_30	797.00	826.96	Coboconk	12.53	1700
HT15_30	840.00	869.96	Gull River	12.49	1700

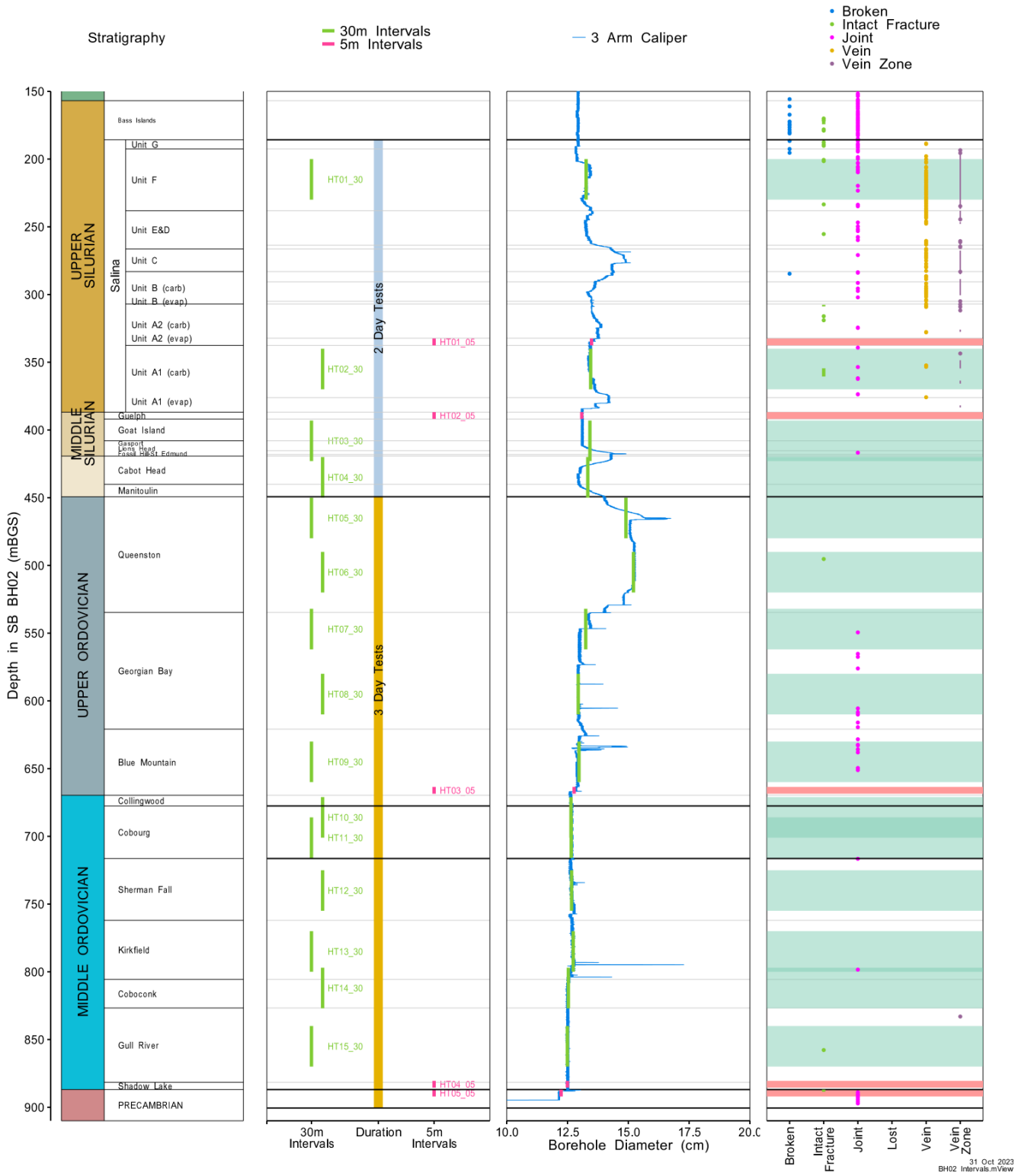

Figure 5.1 SB_BH02 hydraulic testing test intervals.

6 INDIVIDUAL TEST ANALYSES

All analyses follow a common structure:

1. Test Data Summary – a table describing timing and duration of test events and a figure displaying pressures for all downhole pressure transducers over the period of active testing.

2. Test Analyses – tables showing test-specific nSIGHTS input parameters and ranges for optimized fitting parameters. Figures are presented showing: a) the single-best fit result, b) the borehole history, c) the Ramey B plot for the best fit, and d) the normalized Jacobian parameter sensitivity plot.

3. Uncertainly Analyses – figures include: a) the CDF of normalized fit values annotated with the selected fit discriminant, b) cross plots (K_f vs P_f, K_f vs Ss, P_f vs Ss, and K_s vs t_s) showing initial parameter estimates, converged simulations and simulations meeting fit-discriminant criteria, c) parameter CDFs for all simulations meeting fit-discriminant criteria, d) horsetail Cartesian and Ramey B plots showing converged and accepted simulations, e) tables summarizing parameter ranges (best fit, 5%, median, and 95%) and fitted parameter correlations.

4. Additional Figures – includes: a) hydraulic system pressures and weather data (barometric pressure, surface temperature), and b) structure of normalized fit values for each fitted parameter.

Individual test analyses are presented in Appendix A.1 through A.20.

7 ANALYSES SUMMARY

Results from analyses documented in Appendix A are presented in summary form by test interval.

7.1 Summary Tables

CDFs of all accepted perturbations for each parameter represent the range of values for which analyses are visually indistinguishable on a Cartesian plot. The "Best Fit", 5%, Median (50%), and 95% CDF values are extracted for each parameter to indicate the possible range of parameter values. The "Best Fit" value represents the minimum SSE for all accepted perturbations but should not be considered as the most representative value, as occasionally the Best Fit falls outside the 5% and 95% confidence interval range. The Median value should be used as the representative single value for each parameter.

Table 7.1 through Table 7.6 provide the Best Fit, 5%, Median (50%), and 95% CDF values for each fitting parameter and for the calculated skin factor. Formation pressures (Table 7.2) are adjusted to the interval midpoint. A final table shows simulation input parameters (Table 7.7).

As described in Appendix A.15, the analyses of the HT10_30 test of the Collingwood and Upper Cobourg yielded anomalous formation pressure estimates and very low hydraulic conductivity estimates. We believe these results are due to the extremely low hydraulic conductivity which is below the lower limit of tool capability with the amount of time available for testing. Accordingly, the formation hydraulic conductivity estimate for this interval is reported as less than 10^{-15} m/s; other parameters for this interval are not reported.

Table 7.1 SB_BH02 Summary of Formation Hydraulic Conductivity Estimates.

Formation Hydraulic Conductivity (m/s)					
Test ID	**Formation**	**Best Fit**	**5%**	**Median**	**95%**
HT01_30	Salina F	1.8E-14	1.0E-14	5.7E-14	8.7E-14
HT02_30	Salina A1 Carbonate	7.8E-12	7.0E-12	1.1E-11	1.7E-11
HT03_30	Goat Island	1.4E-07	1.0E-07	1.5E-07	2.1E-07
HT04_30	Cabot Head	4.7E-14	3.5E-14	5.2E-14	9.9E-14
HT05_30	Queenston – Upper	3.0E-13	2.4E-13	1.1E-12	3.4E-12
HT06_30	Queenston – Lower	5.3E-12	5.1E-12	3.9E-10	8.6E-09
HT07_30	Georgian Bay – Upper	4.2E-14	1.3E-14	4.1E-14	4.2E-14
HT08_30	Georgian Bay – Lower	2.6E-09	3.3E-11	4.2E-09	8.1E-08
HT09_30	Blue Mountain	2.1E-15	3.9E-15	1.1E-13	1.6E-13
HT10_30	Collingwood/Cobourg	<1E-15			
HT11_30	Cobourg	1.6E-15	1.0E-15	1.7E-15	3.1E-15
HT12_30	Sherman Fall	2.8E-15	2.5E-15	3.0E-15	3.9E-15
HT13_30	Kirkfield	2.5E-15	1.7E-15	2.7E-15	4.0E-15
HT14_30	Coboconk	3.0E-12	2.7E-12	2.9E-12	3.0E-12
HT15_30	Gull River	4.9E-12	4.8E-12	5.0E-12	5.5E-12

Formation Hydraulic Conductivity (m/s)					
Test ID	**Formation**	**Best Fit**	**5%**	**Median**	**95%**
HT01_05	Salina A2 Evaporite	1.2E-07	1.2E-07	1.2E-07	1.2E-07
HT02_05	Guelph	6.4E-04	1.7E-05	1.7E-04	1.1E-03
HT03_05	Blue Mountain - Lower	2.9E-14	2.0E-14	2.8E-14	3.5E-14
HT04_05	Shadow Lake	1.4E-13	1.2E-13	1.3E-13	1.4E-13
HT05_05	Precambrian	5.1E-13	4.9E-13	5.2E-13	5.3E-13

Table 7.2 SB_BH02 Summary of Formation Pressure Estimates (Adjusted to Interval Midpoint).

Formation Pressure (kPa)					
Test ID	**Formation**	**Best Fit**	**5%**	**Median**	**95%**
HT01_30	Salina F	1402	1059	1931	2063
HT02_30	Salina A1 Carbonate	3651	3648	3658	3664
HT03_30	Goat Island	4251	4251	4251	4251
HT04_30	Cabot Head	5428	5264	5427	5518
HT05_30	Queenston – Upper	5390	5214	5266	5425
HT06_30	Queenston – Lower	5316	5316	5320	5320
HT07_30	Georgian Bay – Upper	5102	4601	5100	5103
HT08_30	Georgian Bay – Lower	5888	5883	5888	5888
HT09_30	Blue Mountain	5016	5141	6468	6555
HT10_30	Collingwood/Cobourg	not reported			
HT11_30	Cobourg	1005	218	2054	5013
HT12_30	Sherman Fall	230	218	600	2131
HT13_30	Kirkfield	1929	329	2251	4204
HT14_30	Coboconk	6469	6441	6462	6468
HT15_30	Gull River	6203	6187	6203	6211
HT01_05	Salina A2 Evaporite	3461	3461	3461	3461
HT02_05	Guelph	4035	4035	4035	4035
HT03_05	Blue Mountain - Lower	4058	3537	4051	4417
HT04_05	Shadow Lake	7734	7732	7733	7734
HT05_05	Precambrian	8977	8964	8983	8989

Table 7.3 SB_BH02 Summary of Specific Storage Estimates.

Specific Storage (m^{-1})					
Test ID	**Formation**	**Best Fit**	**5%**	**Median**	**95%**
HT01_30	Salina F	1.1E-05	4.6E-07	2.8E-06	1.8E-05
HT02_30	Salina A1 Carbonate	6.0E-08	1.8E-08	2.0E-08	3.2E-07
HT03_30	Goat Island	8.4E-06	8.4E-06	8.5E-06	8.5E-06
HT04_30	Cabot Head	1.7E-06	4.3E-07	1.5E-06	2.6E-06
HT05_30	Queenston – Upper	2.9E-05	2.1E-06	4.8E-06	5.7E-05
HT06_30	Queenston – Lower	5.2E-06	2.6E-06	2.6E-06	5.3E-06
HT07_30	Georgian Bay – Upper	5.9E-08	6.3E-08	2.4E-07	9.6E-06
HT08_30	Georgian Bay – Lower	1.8E-05	1.7E-05	1.7E-05	2.1E-05
HT09_30	Blue Mountain	3.0E-04	1.3E-08	1.4E-06	1.6E-04
HT10_30	Collingwood/Cobourg	not reported			
HT11_30	Cobourg	1.0E-08	1.0E-08	2.4E-08	4.9E-07
HT12_30	Sherman Fall	6.5E-08	1.0E-08	3.1E-08	2.8E-07
HT13_30	Kirkfield	4.7E-08	1.0E-08	2.7E-08	3.4E-07
HT14_30	Coboconk	8.4E-08	8.2E-08	8.5E-08	8.8E-08
HT15_30	Gull River	1.0E-08	1.0E-08	3.5E-08	1.4E-06
HT01_05	Salina A2 Evaporite	2.0E-08	2.0E-08	2.0E-08	2.0E-08
HT02_05	Guelph	1.0E-08	1.0E-08	8.9E-08	7.5E-06
HT03_05	Blue Mountain - Lower	1.3E-06	7.5E-07	1.4E-06	2.4E-06
HT04_05	Shadow Lake	9.7E-07	9.5E-07	1.2E-06	1.5E-06
HT05_05	Precambrian	4.7E-07	1.7E-08	2.0E-07	1.2E-06

Table 7.4 SB_BH02 Summary of Skin Hydraulic Conductivity Estimates.

Skin Hydraulic Conductivity (m/s)					
Test ID	**Formation**	**Best Fit**	**5%**	**Median**	**95%**
HT01_30	Salina F	1.3E-14	7.5E-15	4.4E-14	1.1E-13
HT02_30	Salina A1 Carbonate	2.2E-12	1.3E-12	3.2E-12	4.0E-12
HT03_30	Goat Island	1.7E-08	1.4E-08	1.7E-08	2.0E-08
HT04_30	Cabot Head	1.2E-13	7.7E-14	3.3E-12	1.9E-11
HT05_30	Queenston – Upper	3.6E-14	2.4E-14	1.6E-13	4.6E-13
HT06_30	Queenston – Lower	2.4E-13	2.3E-13	2.8E-12	1.4E-11
HT07_30	Georgian Bay – Upper	2.0E-11	6.6E-14	2.6E-12	1.8E-11
HT08_30	Georgian Bay – Lower	1.0E-11	1.1E-12	1.4E-11	5.9E-11
HT09_30	Blue Mountain	5.5E-15	1.2E-14	5.9E-13	2.5E-12
HT10_30	Collingwood/Cobourg	not reported			
HT11_30	Cobourg	5.0E-14	8.5E-15	4.5E-14	1.2E-13
HT12_30	Sherman Fall	7.2E-14	3.7E-14	1.1E-13	2.7E-13
HT13_30	Kirkfield	4.3E-14	1.5E-14	5.5E-14	9.5E-14
HT14_30	Coboconk	2.6E-12	2.5E-12	2.6E-12	2.6E-12
HT15_30	Gull River	2.5E-11	7.7E-12	1.9E-11	2.5E-11
HT01_05	Salina A2 Evaporite	5.6E-08	4.6E-08	5.4E-08	5.6E-08
HT02_05	Guelph	2.5E-06	4.9E-07	1.4E-06	3.3E-06
HT03_05	Blue Mountain - Lower	5.2E-11	6.9E-14	1.1E-11	5.2E-11
HT04_05	Shadow Lake	8.1E-11	4.3E-13	1.1E-11	9.0E-11
HT05_05	Precambrian	1.0E-12	6.8E-13	1.4E-12	3.3E-12

Table 7.5 SB_BH02 Summary of Skin Thickness Estimates.

Skin Thickness (cm)					
Test ID	**Formation**	**Best Fit**	**5%**	**Median**	**95%**
HT01_30	Salina F	0.48	0.25	1.88	20.92
HT02_30	Salina A1 Carbonate	73.75	13.66	362.38	813.75
HT03_30	Goat Island	5182.98	3202.93	5900.29	9495.34
HT04_30	Cabot Head	0.37	0.44	1.13	4.75
HT05_30	Queenston – Upper	1.34	0.73	8.28	24.52
HT06_30	Queenston – Lower	6.95	6.71	22.79	30.40
HT07_30	Georgian Bay – Upper	47.35	0.99	20.04	45.80
HT08_30	Georgian Bay – Lower	29.41	9.26	31.88	55.32
HT09_30	Blue Mountain	0.02	0.04	4.95	88.31
HT10_30	Collingwood/Cobourg	not reported			
HT11_30	Cobourg	32.39	1.84	18.00	31.72
HT12_30	Sherman Fall	12.43	4.03	19.75	39.33
HT13_30	Kirkfield	13.70	2.98	18.96	34.12
HT14_30	Coboconk	993.52	169.10	603.73	983.74
HT15_30	Gull River	360.25	29.69	190.60	395.68
HT01_05	Salina A2 Evaporite	9989.47	952.99	5922.25	9713.61
HT02_05	Guelph	6174.34	1450.23	6511.21	9991.59
HT03_05	Blue Mountain - Lower	1.94	0.38	1.27	3.01
HT04_05	Shadow Lake	3.05	0.67	1.99	3.11
HT05_05	Precambrian	25.29	16.63	39.11	138.45

Table 7.6 SB_BH02 Summary of Calculated Skin Factor.

Skin Factor ( )					
Test ID	**Formation**	**Best Fit**	**5%**	**Median**	**95%**
HT01_30	Salina F	0.030	-0.550	0.041	0.105
HT02_30	Salina A1 Carbonate	6.366	4.965	9.538	15.372
HT03_30	Goat Island	49.888	39.003	53.377	67.995
HT04_30	Cabot Head	-0.032	-0.228	-0.136	-0.030
HT05_30	Queenston – Upper	1.196	0.806	3.994	9.497
HT06_30	Queenston – Lower	13.865	13.422	187.910	1026.961
HT07_30	Georgian Bay – Upper	-2.093	-2.064	-1.370	-0.111
HT08_30	Georgian Bay – Lower	419.296	26.628	566.389	3130.148
HT09_30	Blue Mountain	-0.002	-2.515	-0.457	-0.004
HT10_30	Collingwood/Cobourg	not reported			
HT11_30	Cobourg	-1.752	-1.749	-1.276	-0.228
HT12_30	Sherman Fall	-1.043	-1.944	-1.373	-0.459
HT13_30	Kirkfield	-1.080	-1.777	-1.309	-0.337
HT14_30	Coboconk	0.721	0.317	0.586	0.718
HT15_30	Gull River	-3.263	-3.302	-2.543	-0.493
HT01_05	Salina A2 Evaporite	8.654	7.740	8.292	8.626
HT02_05	Guelph	1717.500	208.541	796.448	2326.190
HT03_05	Blue Mountain - Lower	-0.265	-0.379	-0.178	-0.035
HT04_05	Shadow Lake	-0.396	-0.404	-0.273	-0.074
HT05_05	Precambrian	-0.807	-2.655	-1.260	-0.361

Table 7.7 SB_BH02 Summary of Simulation Input Parameters

Simulation Input Parameters				
Test ID	**Formation**	**Test Zone Compressibility (Pa^{-1})**	**Test Zone Radius (cm)**	**Test Zone Fluid Density (g/L)**
HT01_30	Salina F	4.65E-10	6.63	1071
HT02_30	Salina A1 Carbonate	4.13E-10	6.73	1077
HT03_30	Goat Island	n/a – slug test	6.71	1083
HT04_30	Cabot Head	4.38E-10	6.67	1086
HT05_30	Queenston – Upper	4.58E-10	7.45	1086
HT06_30	Queenston – Lower	4.67E-10	7.61	1085
HT07_30	Georgian Bay – Upper	1.90E-09	6.62	1084
HT08_30	Georgian Bay – Lower	1.50E-09	6.47	1085
HT09_30	Blue Mountain	1.30E-09	6.49	1090
HT10_30	Collingwood/Cobourg	3.53E-10	6.32	1093
HT11_30	Cobourg	3.43E-10	6.33	1095
HT12_30	Sherman Fall	3.82E-10	6.33	1096
HT13_30	Kirkfield	3.91E-10	6.37	1095
HT14_30	Coboconk	4.27E-10	6.27	1096
HT15_30	Gull River	4.46E-10	6.25	1094
HT01_05	Salina A2 Evaporite	n/a - slug test	6.74	1046
HT02_05	Guelph	n/a - slug test	6.54	1056
HT03_05	Blue Mountain - Lower	3.59E-10	6.39	1077
HT04_05	Shadow Lake	4.28E-10	6.25	1076
HT05_05	Precambrian	4.18E-10	6.12	1076

7.2 Summary Figures

Figure 7.1 and Figure 7.2 show the Best Fit, 5%, Median, and 95% CDF values for each fitting parameter and for the calculated skin factor plotted against the stratigraphy. Formation pressures (Figure 7.1) are adjusted to the interval midpoint. The Silurian strata are generally normally pressured, whereas the majority of the lower Ordovician strata show significant under-pressures. Test-specific simulation input parameters are presented in Figure 7.3.

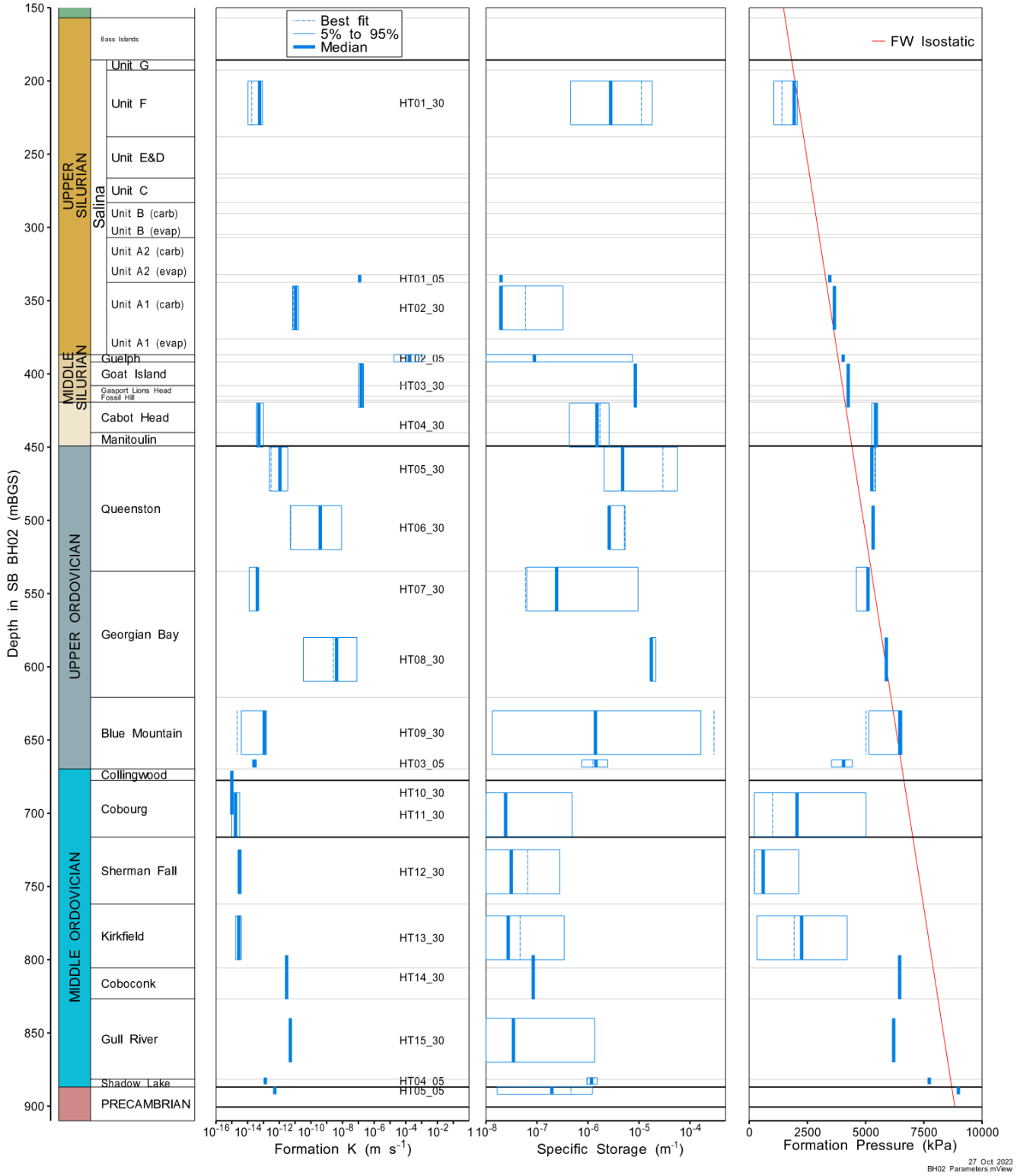

Figure 7.1 Formation Hydraulic Conductivity, Specific Storage and Adjusted Formation Pressure.

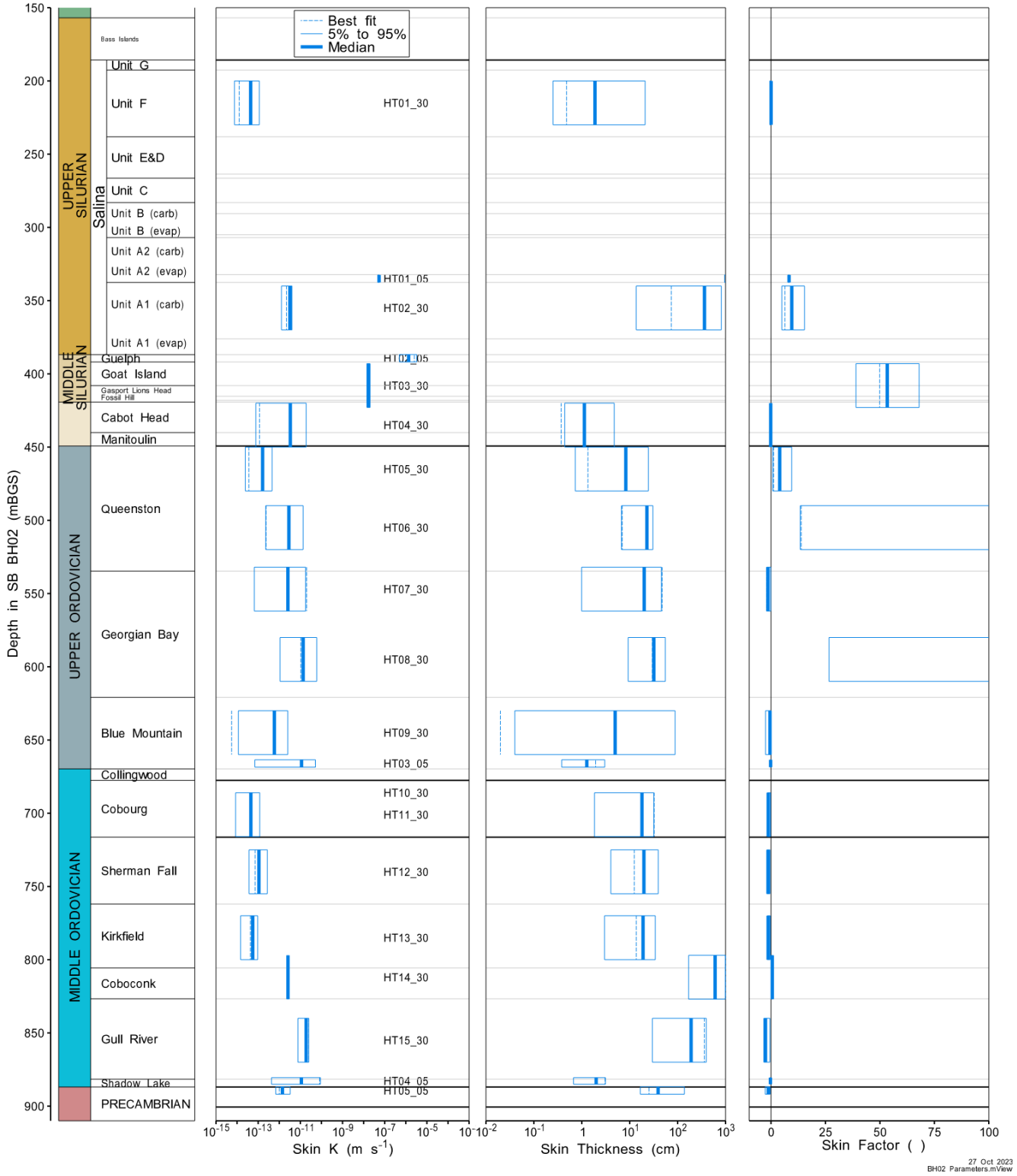

Figure 7.2 Skin Hydraulic Conductivity, Skin Thickness and Skin Factor.

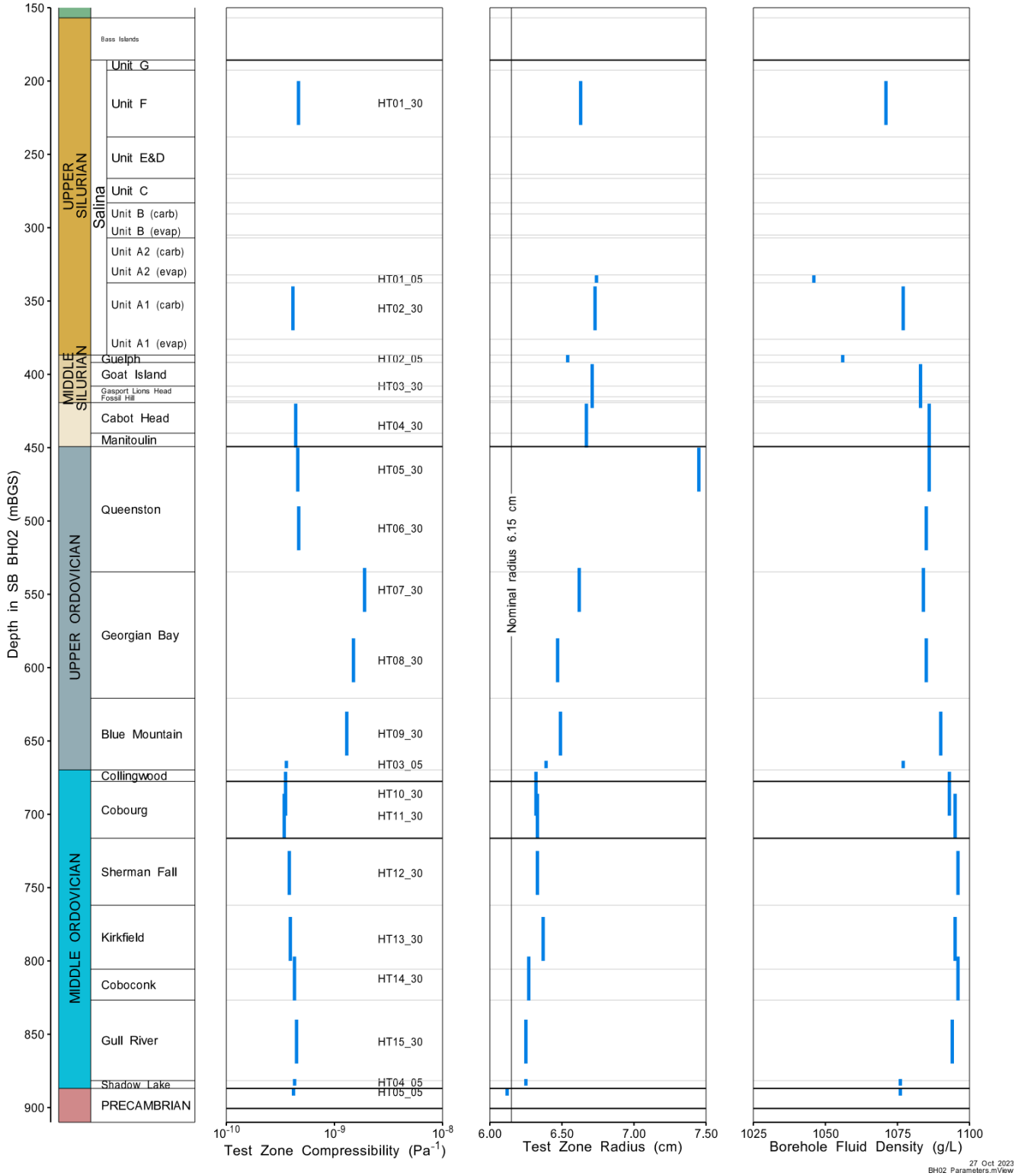

Figure 7.3 Simulation Parameters: Test Zone Compressibility, Test Zone Radius, Borehole Fluid Density.

8 REFERENCES

Armstrong, D.K., and T.R. Carter, 2010. The Subsurface Paleozoic Stratigraphy of Southern Ontario. Ontario Geological Survey – Special Volume 7; 301p.

Geofirma Engineering Ltd. and INTERA Inc. 2011. nSIGHTS Version 2.50 User Manual. INTERA Inc., Austin, TX, USA.

APPENDIX A

INDIVIDUAL TEST ANALYSES

A.1 HT01_05 Salina A2 Evaporite

The SB BH02 interval from 332.50 to 337.53 mBGS tested in HT01_05 covers the majority of the A2 Evaporite Unit of the Salina Group. Original testing plans called for a one day PI test. However, the test zone response to shut-in indicated relatively high hydraulic conductivity. A PI was attempted and it recovered completely in under 10 seconds. Subsequently, the tubing was swabbed and a SW test of one-day duration was performed. For analysis, the PI was treated as pressure history and only the SW was simulated. All figures presented in this chapter refer to the SW response.

A.1.1 Test Data Summary

Table A.1 and Figure A.1 provide a summary of test events and a plot of pressures measured while testing respectively.

Table A.1 - Summary of Test Events.

Event	Start Date & Time	Duration (days)	TZ Pressure (kPa)
Drilling intercept	22-01-03 14:47	153.13	3412
Shut-in	22-06-05 17:53	0.59	3409
Pulse injection	22-06-06 08:07	0.12	3459
Slug withdrawal	22-06-06 10:55	0.97	3177
Test end	22-06-07 10:13		3380

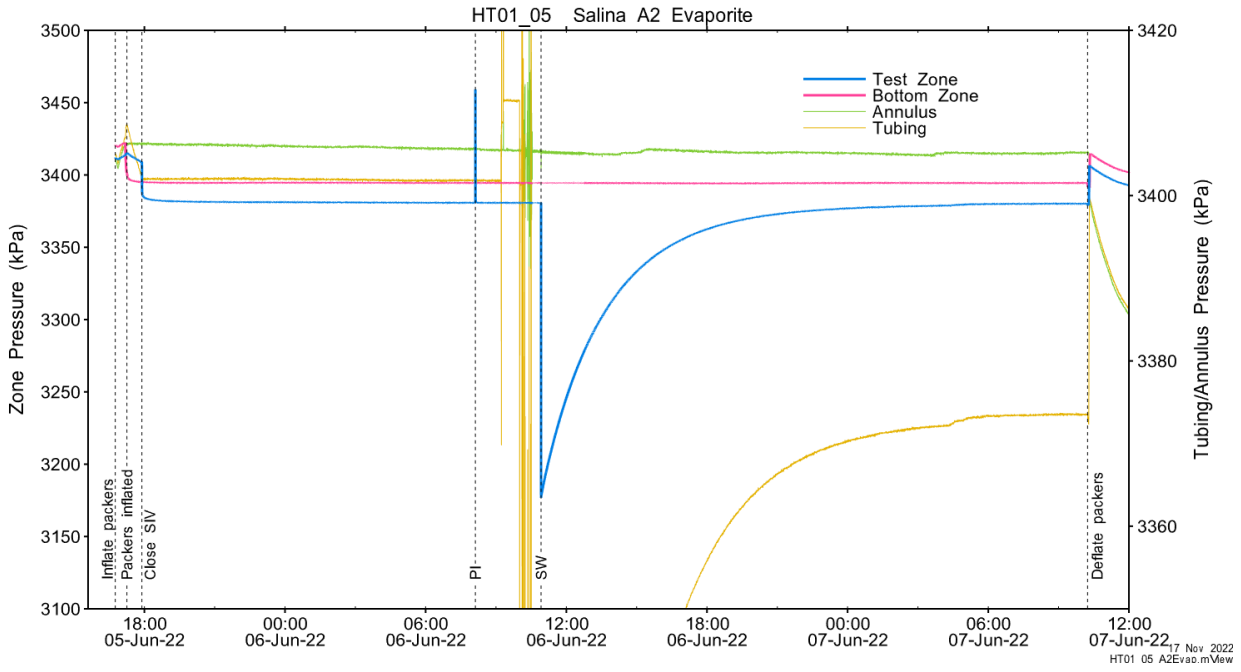

Figure A.1 - Test events and pressures.

A.1.2 Test Analyses

Table A.7 is a summary of test-specific input parameters used in the analyses, while Table A.8 presents the optimized parameters and allowed ranges. Perturbations were originally performed with wider conductivity range and a maximum 1000 cm skin thickness, however the skin thickness for the best fit was at the maximum skin thickness. Conductivity ranges were reduced and skin thickness increased to 2500 cm based on review of these initial results. Results from the second set also indicated a best-fit at the maximum thickness. A third set of permutations were run with maximum skin thickness of 100m.

Table A.2 – nSIGHTS Input Parameters.

Parameter	Value	Units
Test zone radius	6.74	cm
Tubing string radius	2.54	cm
Test zone length	5.03	m

Table A.3 – nSIGHTS Parameter Optimization Ranges.

Parameter	Minimum	Maximum	Units	Type
Formation hydraulic conductivity (K_f)	1E-10	1E-05	m/s	log
Formation pressure (P_f)	3000	4000	kPa	linear
Specific storage (S_s)	1E-08	1E-04	1/m	log
Skin hydraulic conductivity (K_s)	1E-10	1E-05	m/s	log
Skin thickness (t_s)	0.013	10000	cm	linear

Figure A.18 shows the measured test zone pressure record (with reduced data density for clarity) used in the analysis along with the best-fit simulation and parameter values. Figure A.19 presents the pre-test history, and Figure A.20 shows the Ramey B normalized best-fit pressure and pressure derivatives.

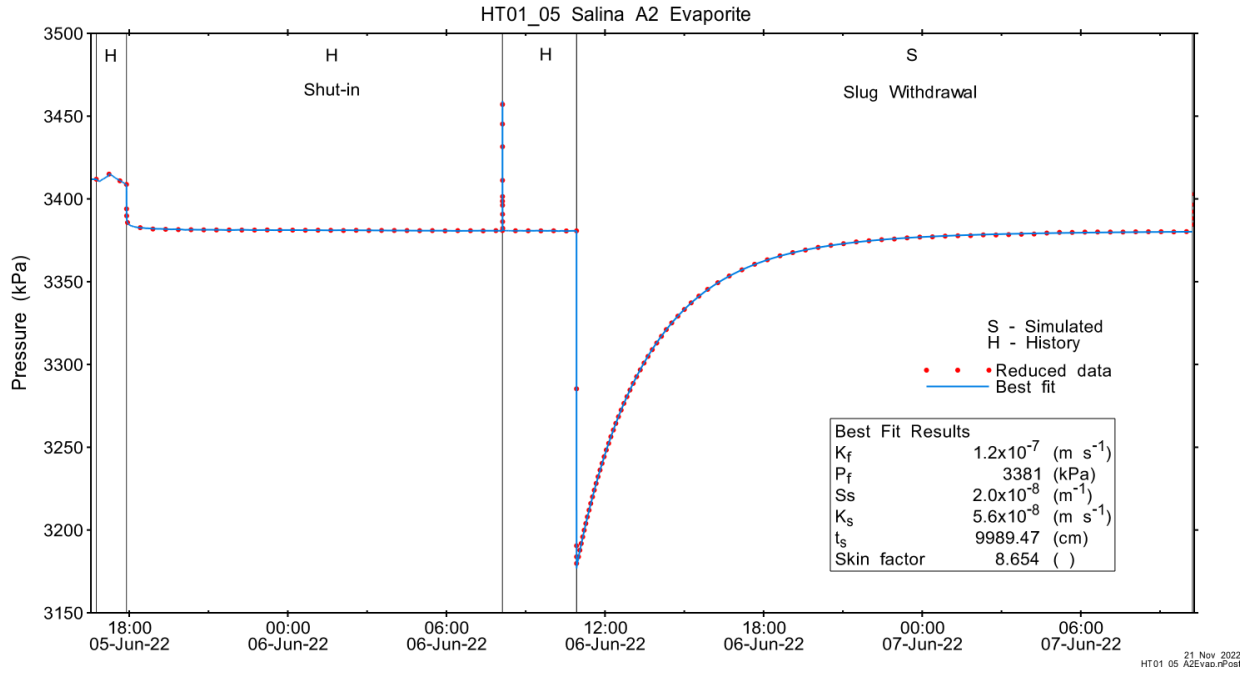

Figure A.2 - Annotated testing sequence showing best-fit simulation and parameter estimates.

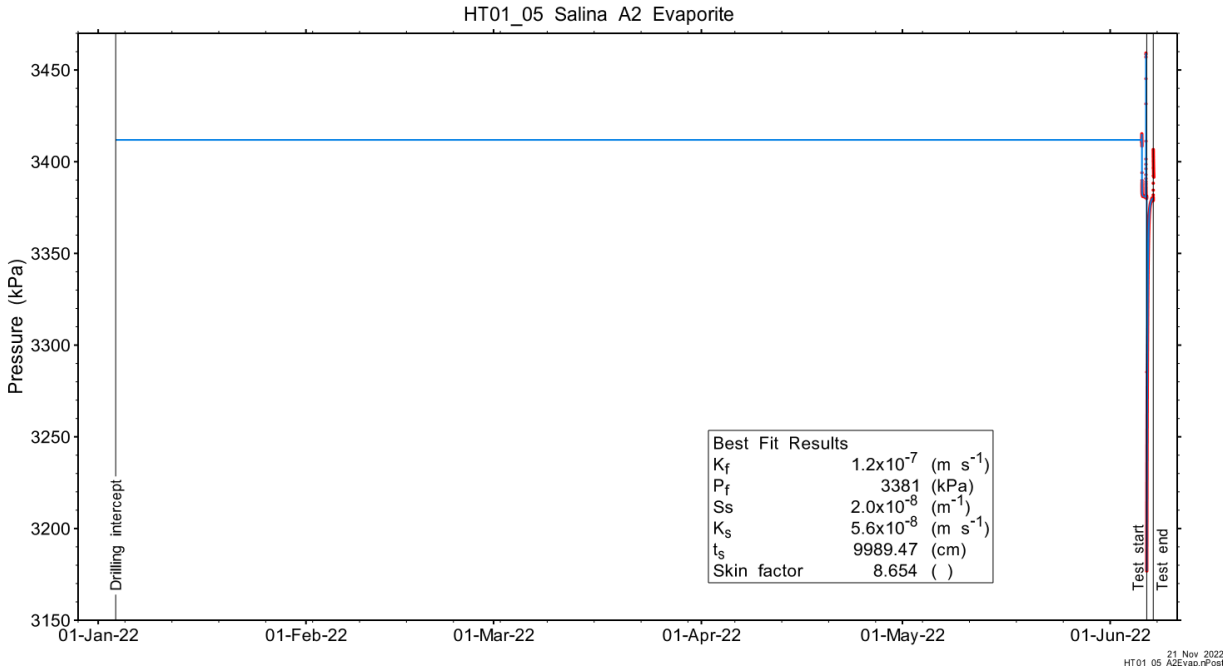

Figure A.3 - Annotated testing sequence showing pre-test history, best-fit simulation and parameter estimates.

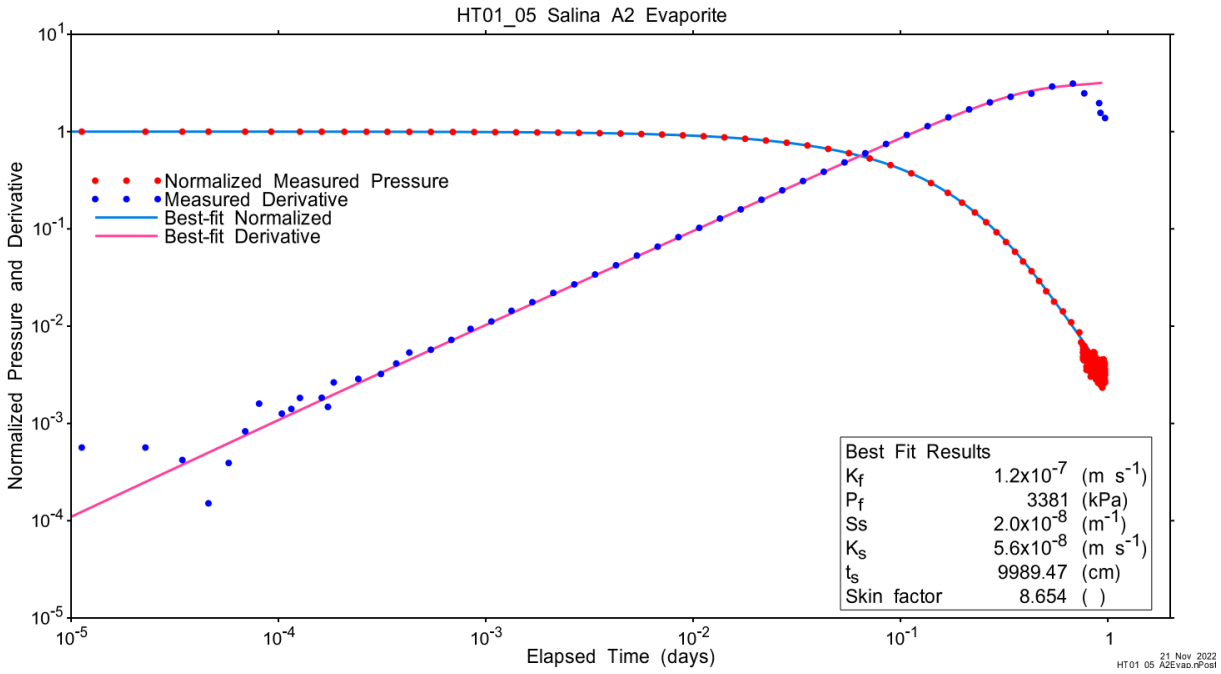

Figure A.4 - Log-log plot showing Ramey B and derivative response for best-fit simulation.

Figure A.21 shows the normalized parameter sensitivity response for the best fit. Sensitivity for fitting parameters is flat at the end of the test, indicating that test duration was sufficient.

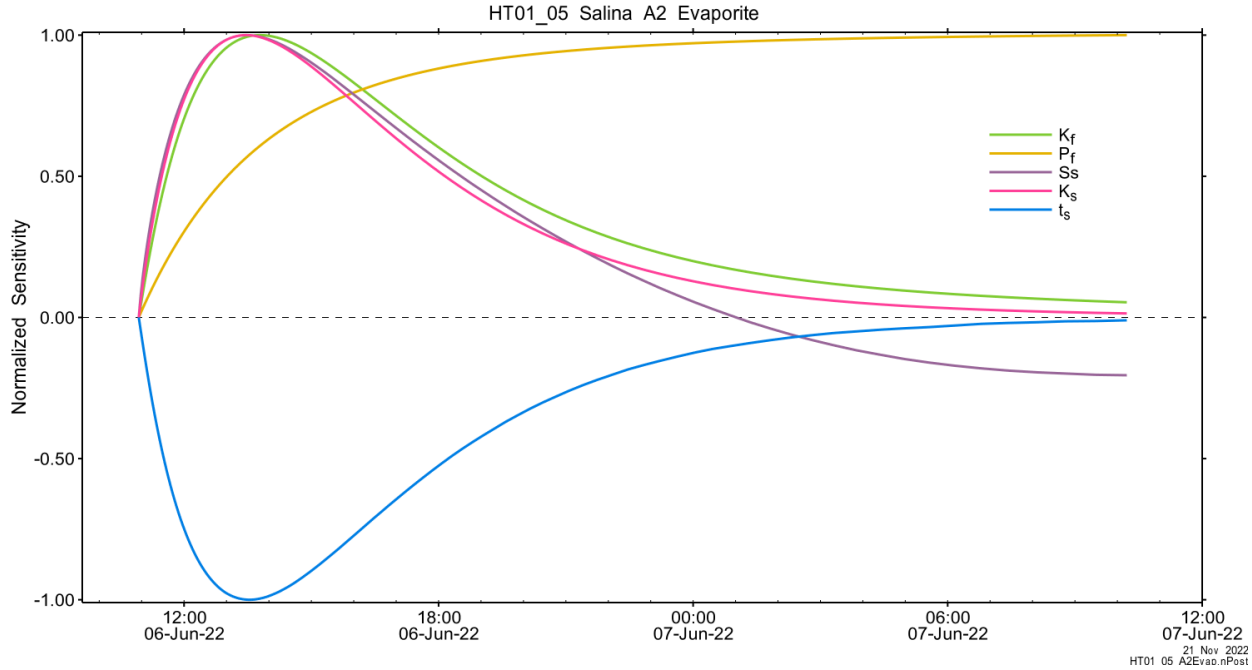

Figure A.5 - Normalized Jacobian for best-fit simulation.

A.1.3 Uncertainty Analyses

The CDF of normalized fit values for all converged simulations and the selected fit discriminant are shown in Figure A.22 and, in detail, in Figure A.7.

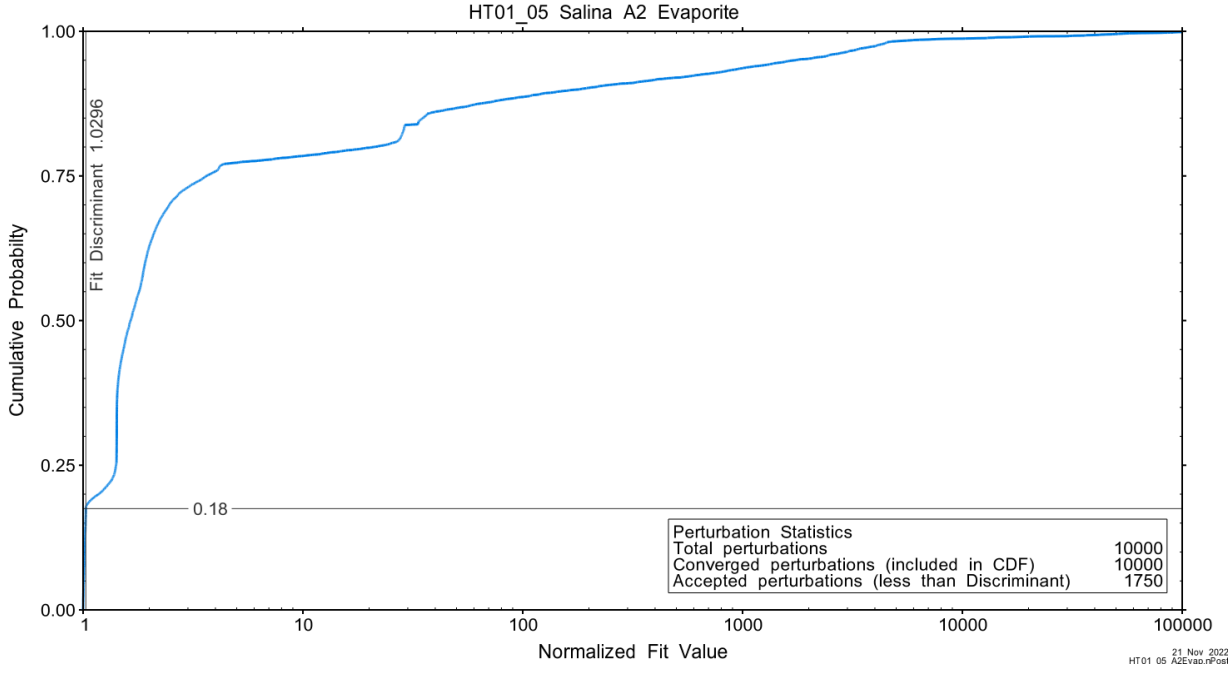

Figure A.6 - Fit value cumulative distribution function.

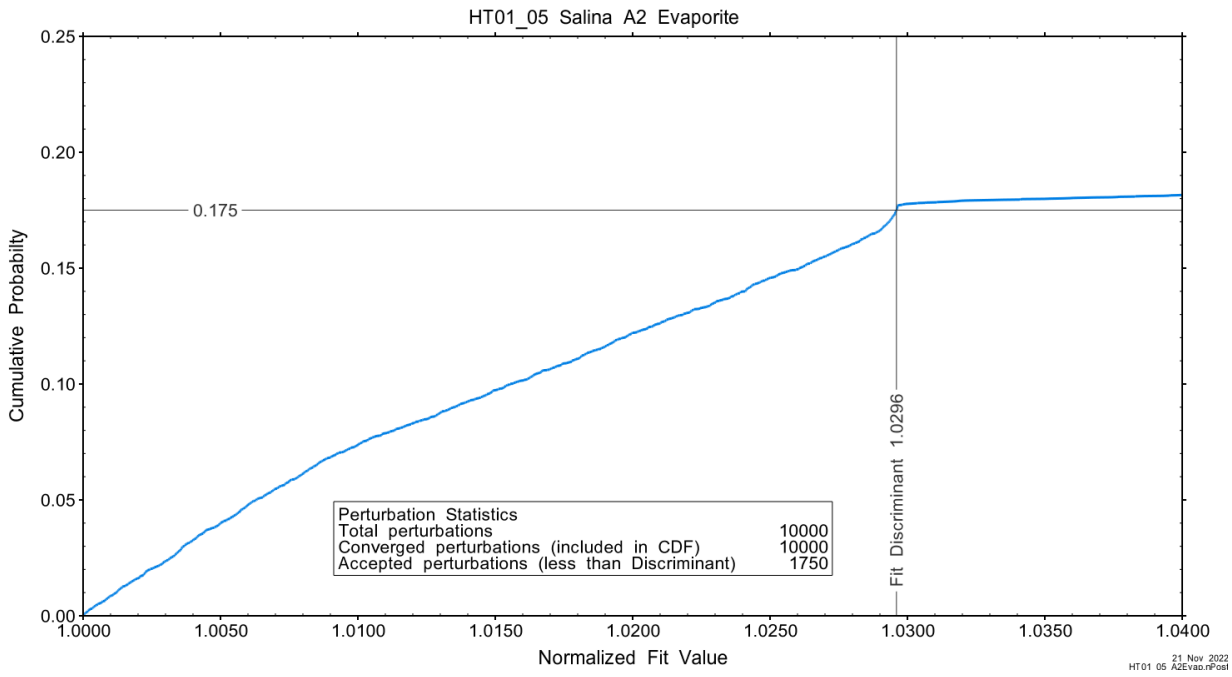

Figure A.7 – Detail of fit value cumulative distribution function.

Summary cross parameter scatter plots for selected formation and skin parameters are given in Figure A.24 and Figure A.25. The light pink dots on the figures are the initial parameter estimates, with red dots overlaying those initial parameter values that resulted in accepted optimization results. The grey dots are converged optimizations which did not meet the fit discriminant. Larger varying color symbols represent the fit value of accepted optimizations, with the blue values representing the best fit.

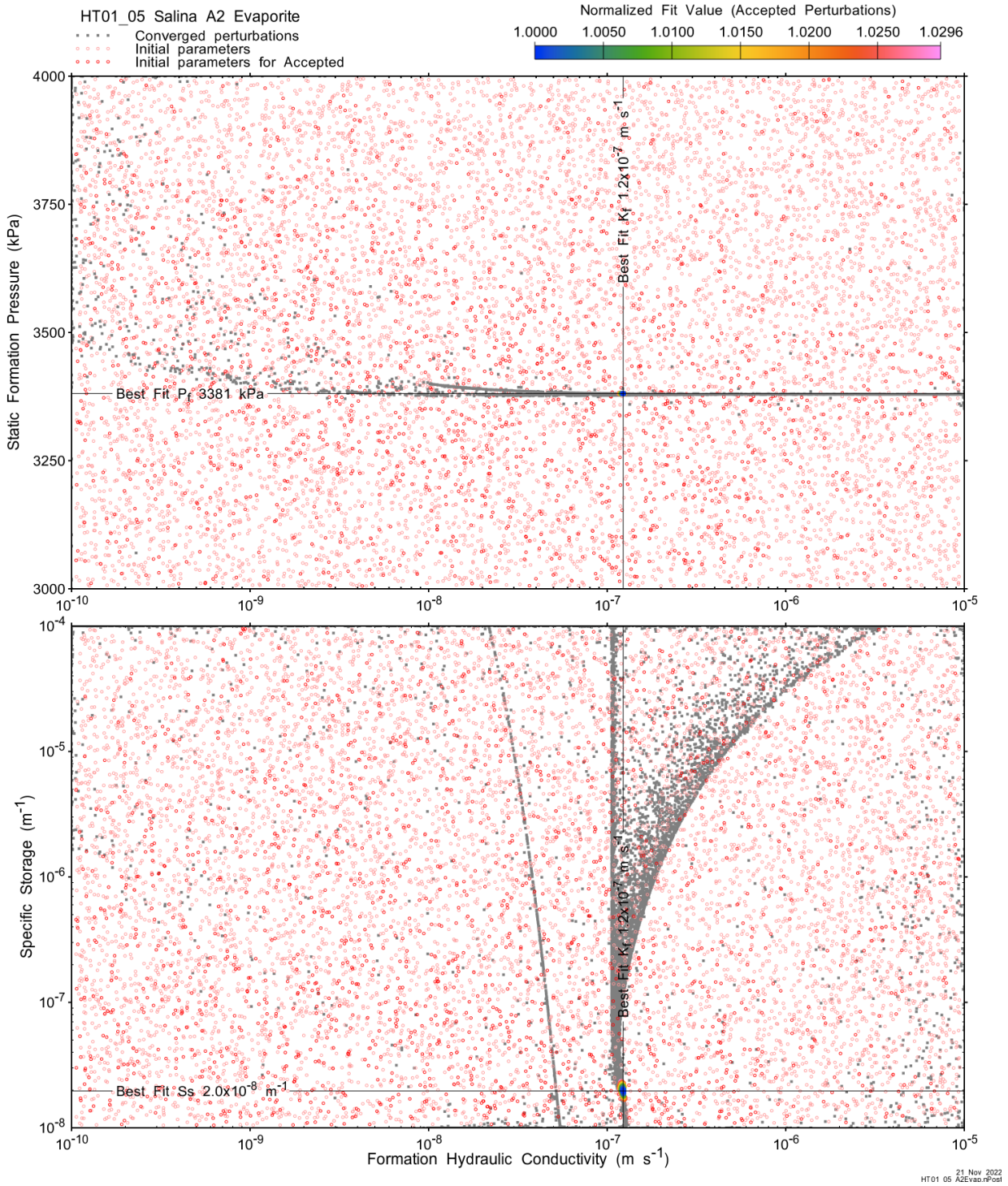

Figure A.8 - XY-scatter plot showing estimates of formation hydraulic conductivity (K_f) vs static formation pressure (P_f) (top panel) and specific storage (Ss) (bottom panel).

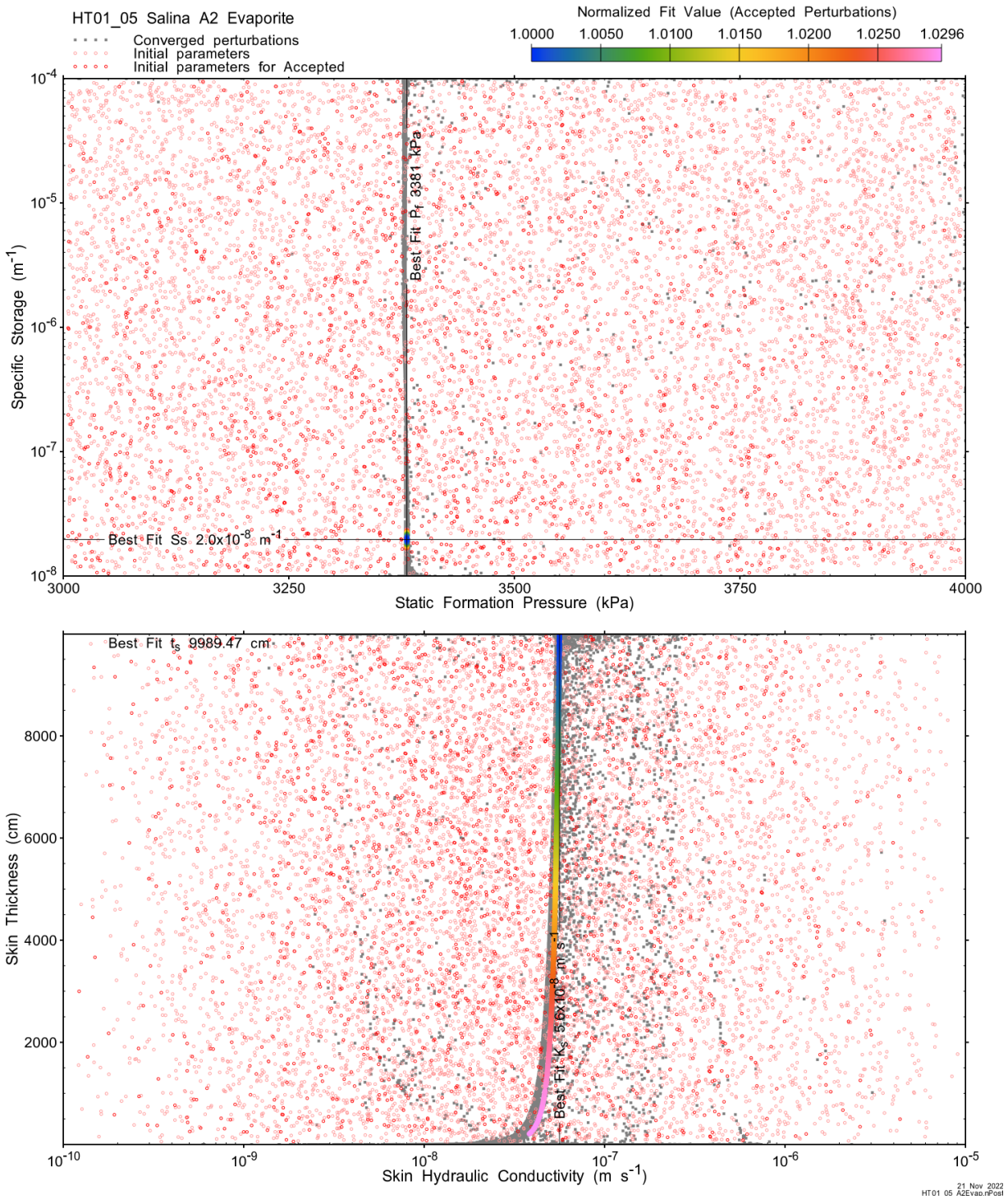

Figure A.9 - XY-scatter plot showing estimates of static formation pressure (P_f) vs specific storage (Ss) (top panel) and skin hydraulic conductivity (K_s) vs skin thickness (t_s) (bottom panel).

Confidence limits and median values are determined from the CDF of accepted optimization results (i.e. the varying color values in the above figures), with best fit value, 5% and 95% confidence indicated on Figure A.26 and Figure A.27.

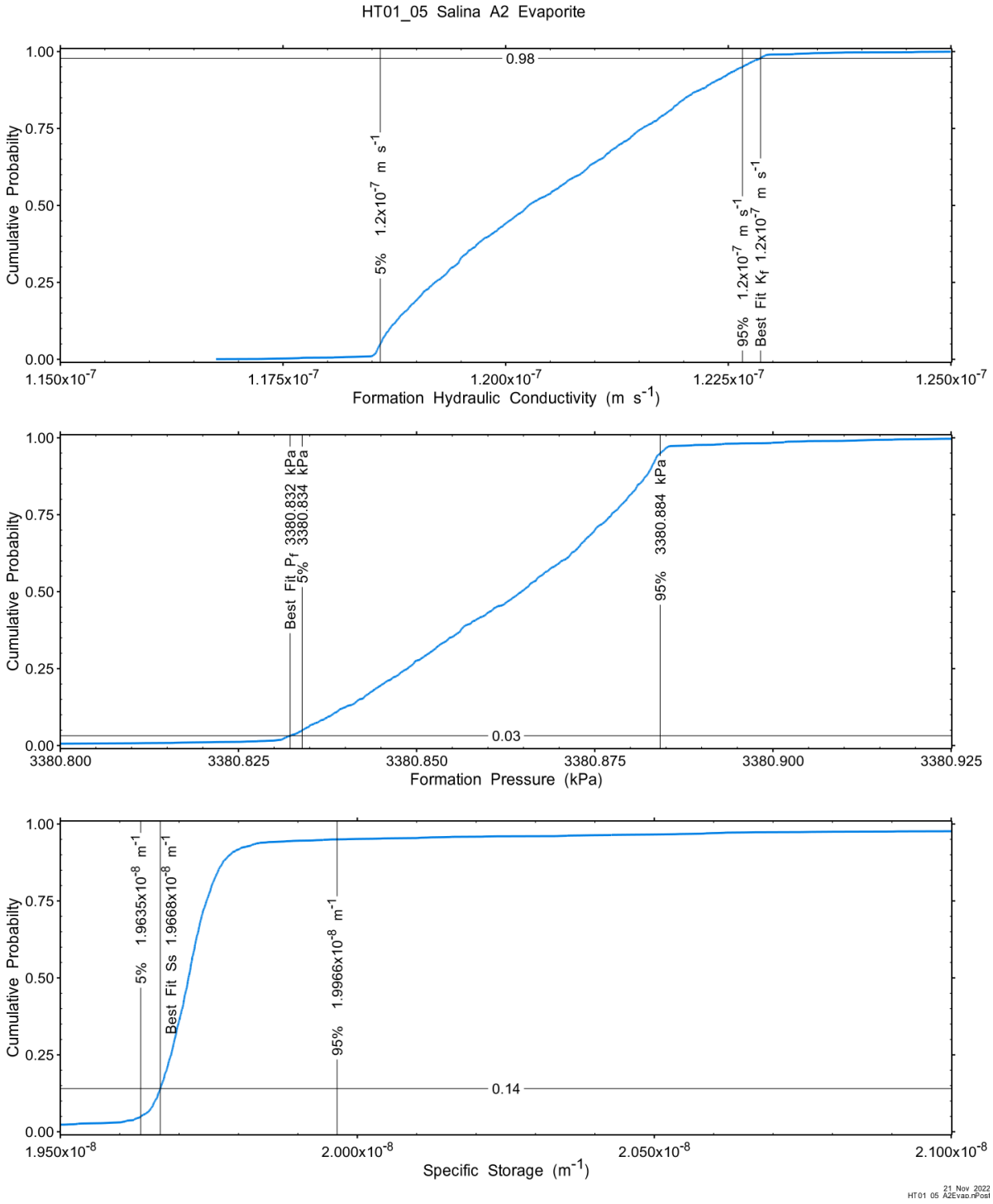

Figure A.10 – Cumulative distribution functions and parameter limits for formation hydraulic conductivity (K_f) (top panel), static formation pressure (P_f) (middle panel) and specific storage (Ss) (bottom panel).

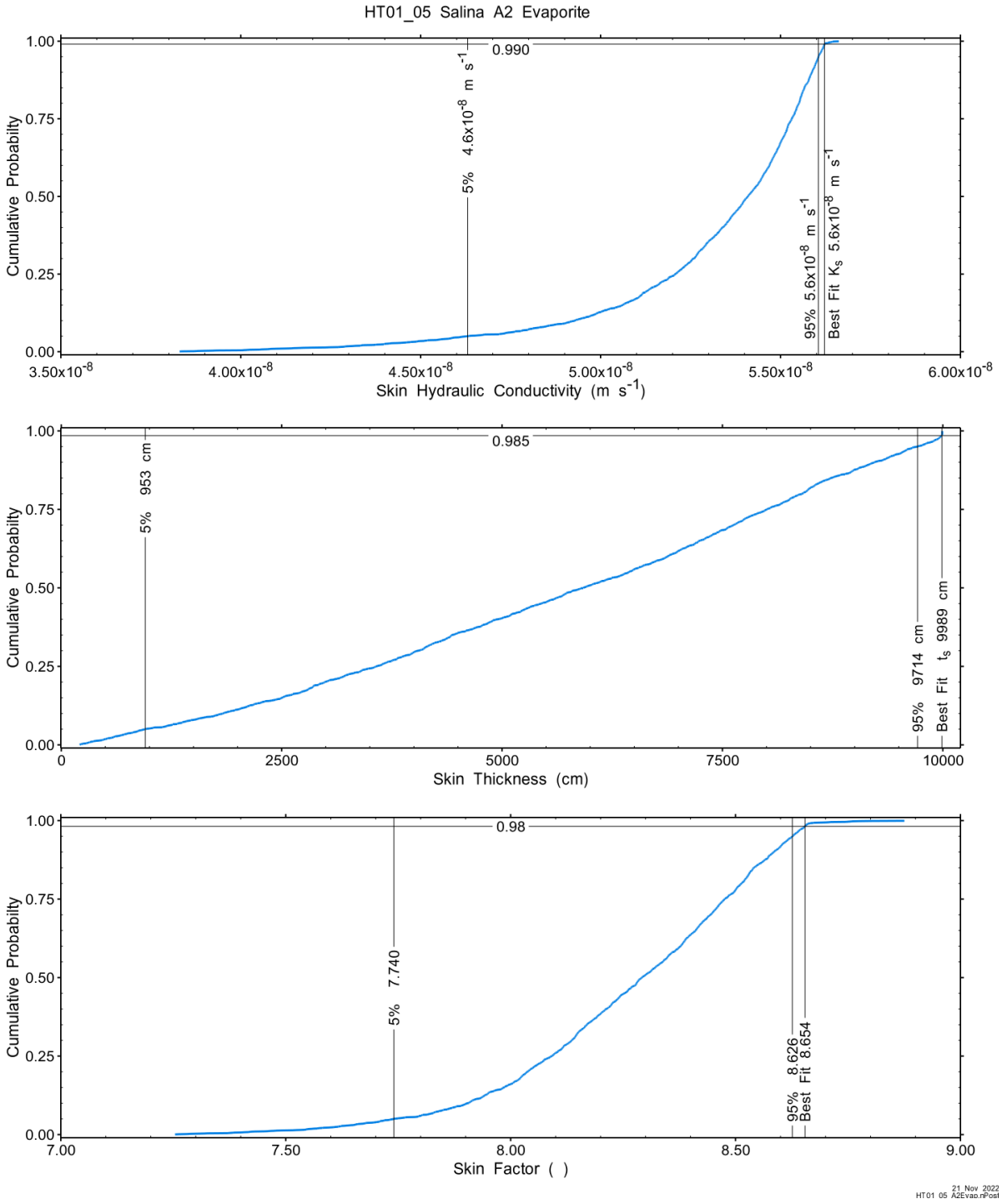

Figure A.11 – Cumulative distribution functions and parameter limits for skin hydraulic conductivity (K_s) (top panel), skin thickness (t_s) (middle panel) and skin factor (s) (bottom panel).

A summary of perturbation results is presented in Figure A.28, with Ramey-processed perturbations in Figure A.13. Those perturbations (1411 of 10,000) with all parameters within the 5% and 95% range present an excellent fit to the measured test zone data.

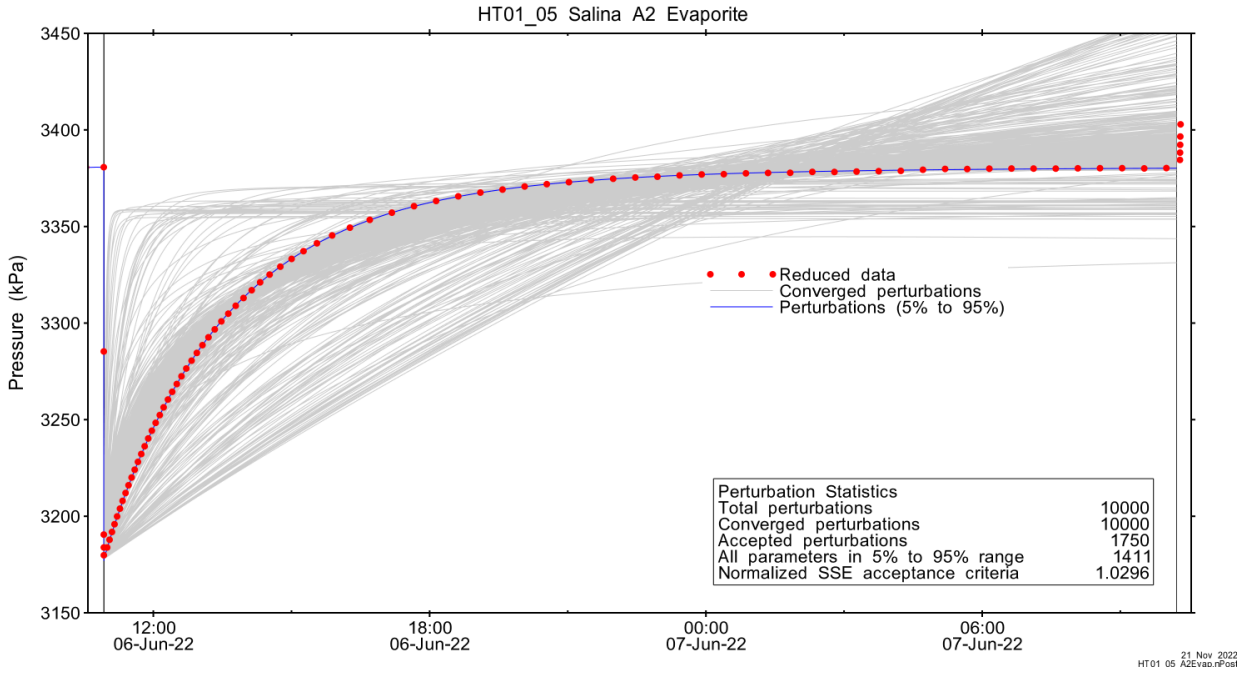

Figure A.12 – Perturbation results – all converged, accepted, and within 5% to 95% for all parameters.

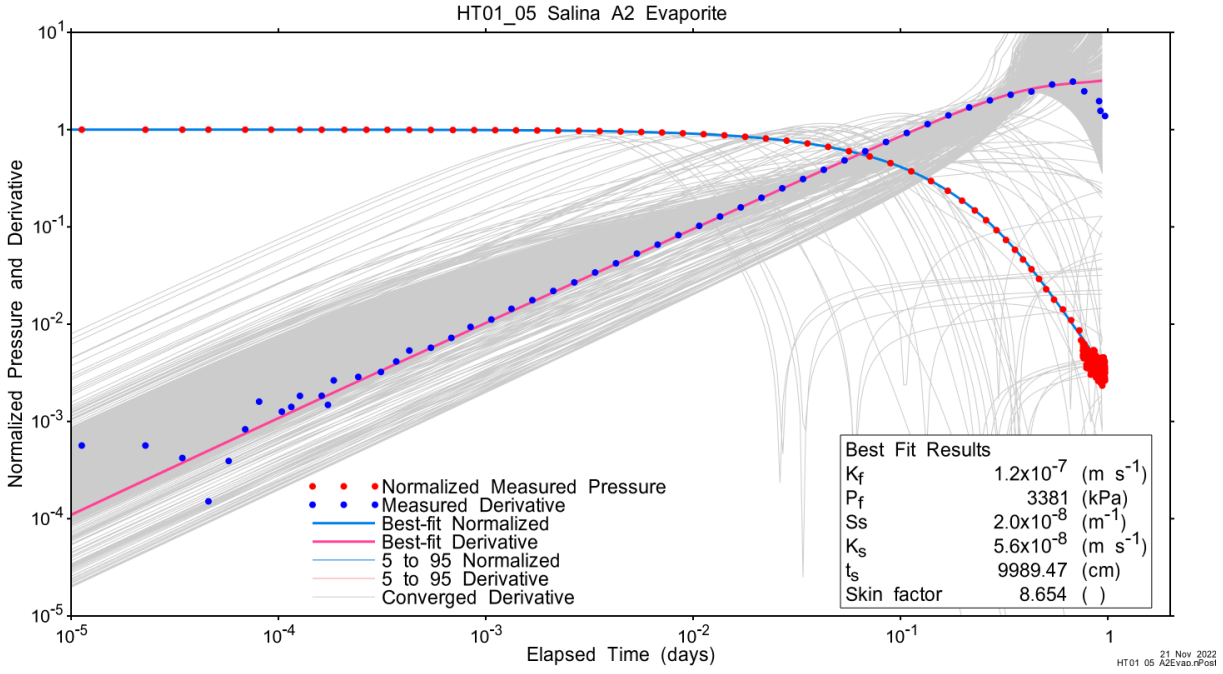

Figure A.13 – Log-log plot showing Ramey B and derivative response for all converged optimizations and those within 5% to 95% for all parameters.

A summary of best-fit and parameter ranges is given in Table A.9.

Table A.4 - Summary of the HT01_05 parameter estimates.

Parameter	Best Fit	5%	Median	95%
K_f (m/s)	1.2E-07	1.2E-07	1.2E-07	1.2E-07
P_f (kPa)	3381	3381	3381	3381
Ss (1/m)	2.0E-08	2.0E-08	2.0E-08	2.0E-08
K_s (m/s)	5.6E-08	4.6E-08	5.4E-08	5.6E-08
t_s (cm)	9989.47	952.99	5922.25	9713.61
s (-)	8.654	7.740	8.292	8.626

Parameter correlations for all perturbations with all parameters within the 5% to 95% limits are given in Table A.5.

Table A.5 – Pearson cross-correlations of 5% to 95% parameters

	Log(K_f)	P_f	Log(Ss)	Log(K_s)	t_s	s
Log(K_f)	1.000	-0.998	-0.244	0.908	0.989	0.982
Pf	-0.998	1.000	0.292	-0.899	-0.983	-0.977
Log(S_s)	-0.244	0.292	1.000	-0.048	-0.167	-0.157
Log(K_s)	0.908	-0.899	-0.048	1.000	0.956	0.971
t_s	0.989	-0.983	-0.167	0.956	1.000	0.998
s	0.982	-0.977	-0.157	0.971	0.998	1.000

A.1.4 Additional Figures

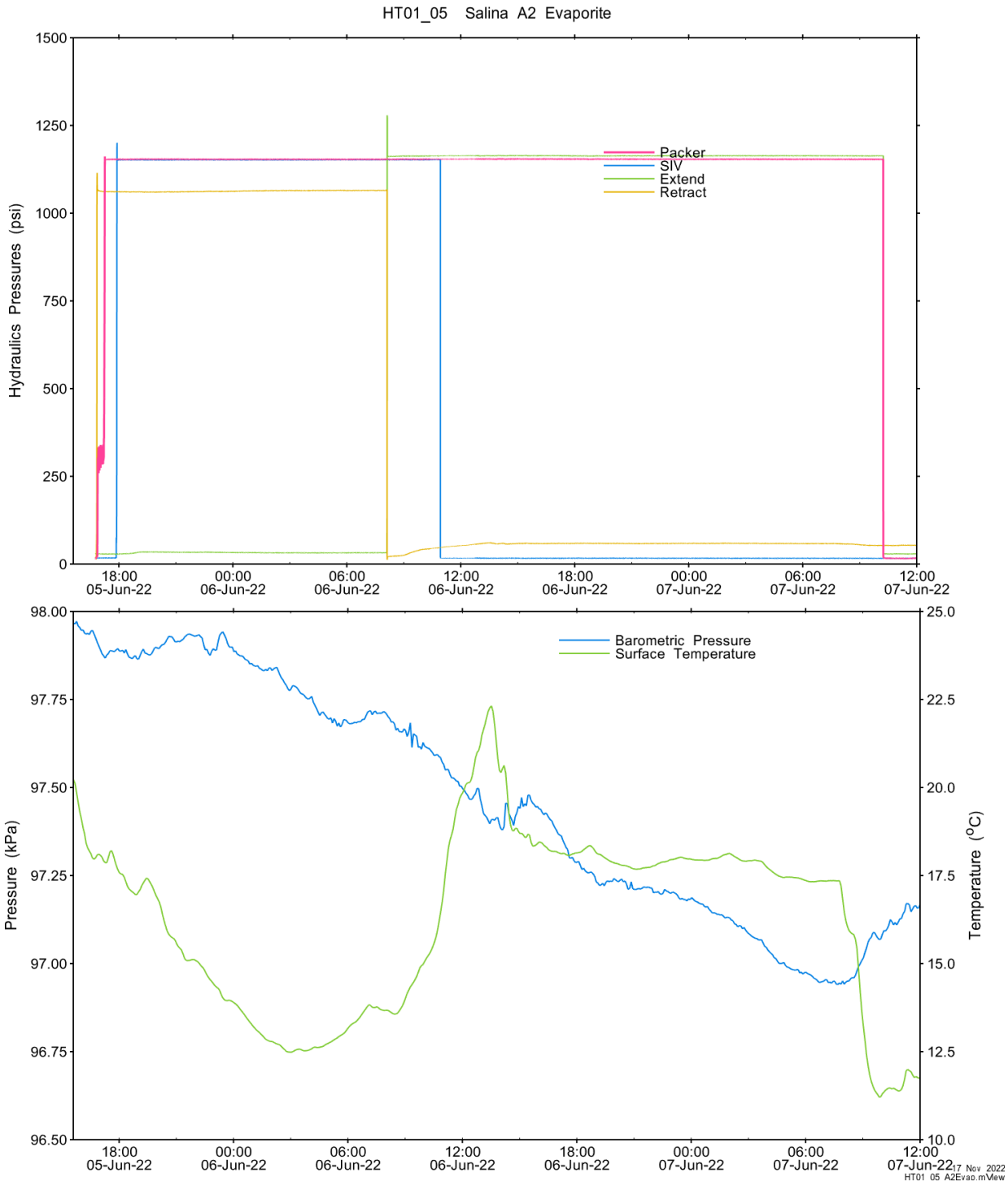

Figure A.14 - Hydraulics pressures and surface temperature/barometric pressure.

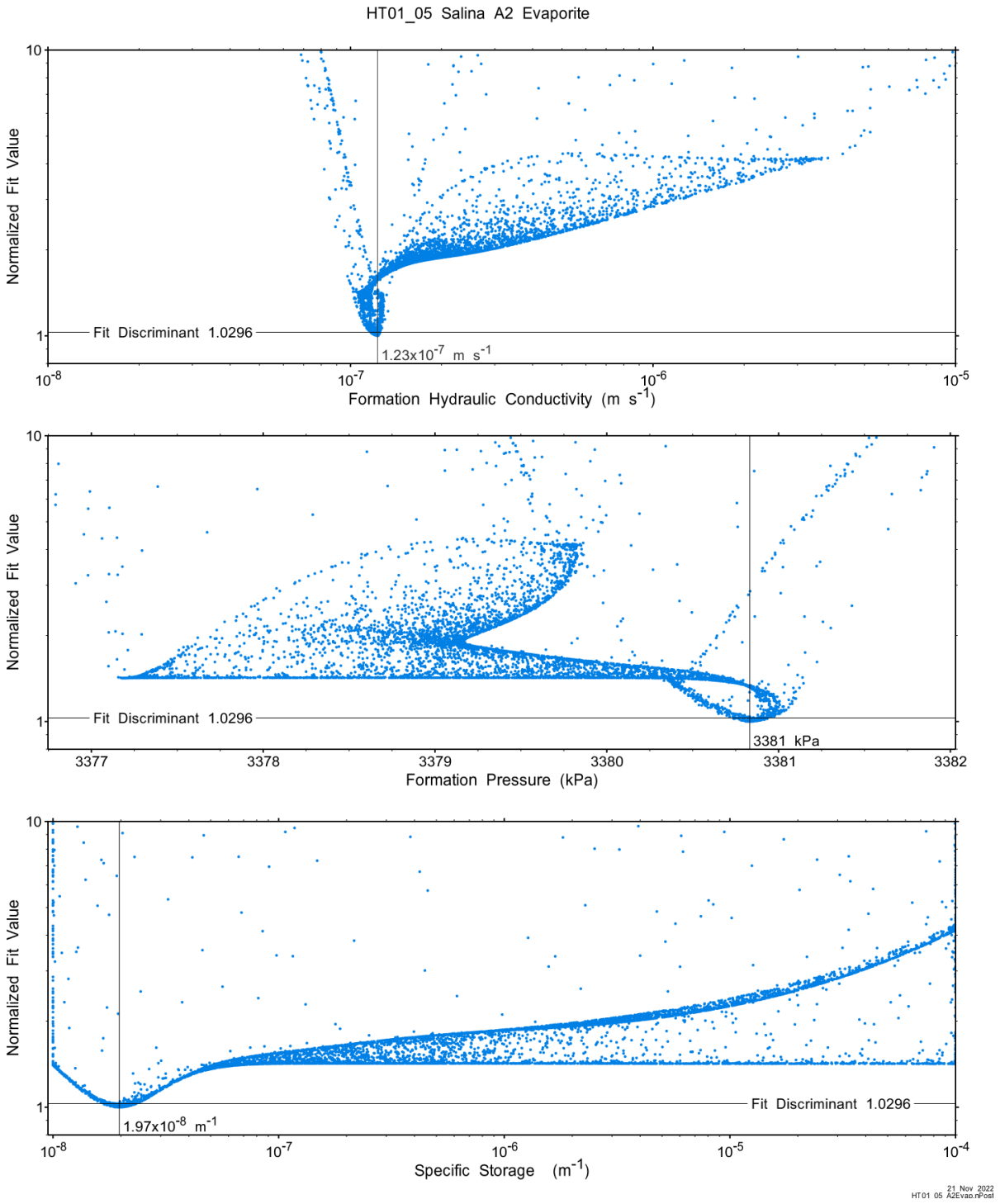

Figure A.15 - XY-scatter plot showing the formation parameter space normalized fit values.

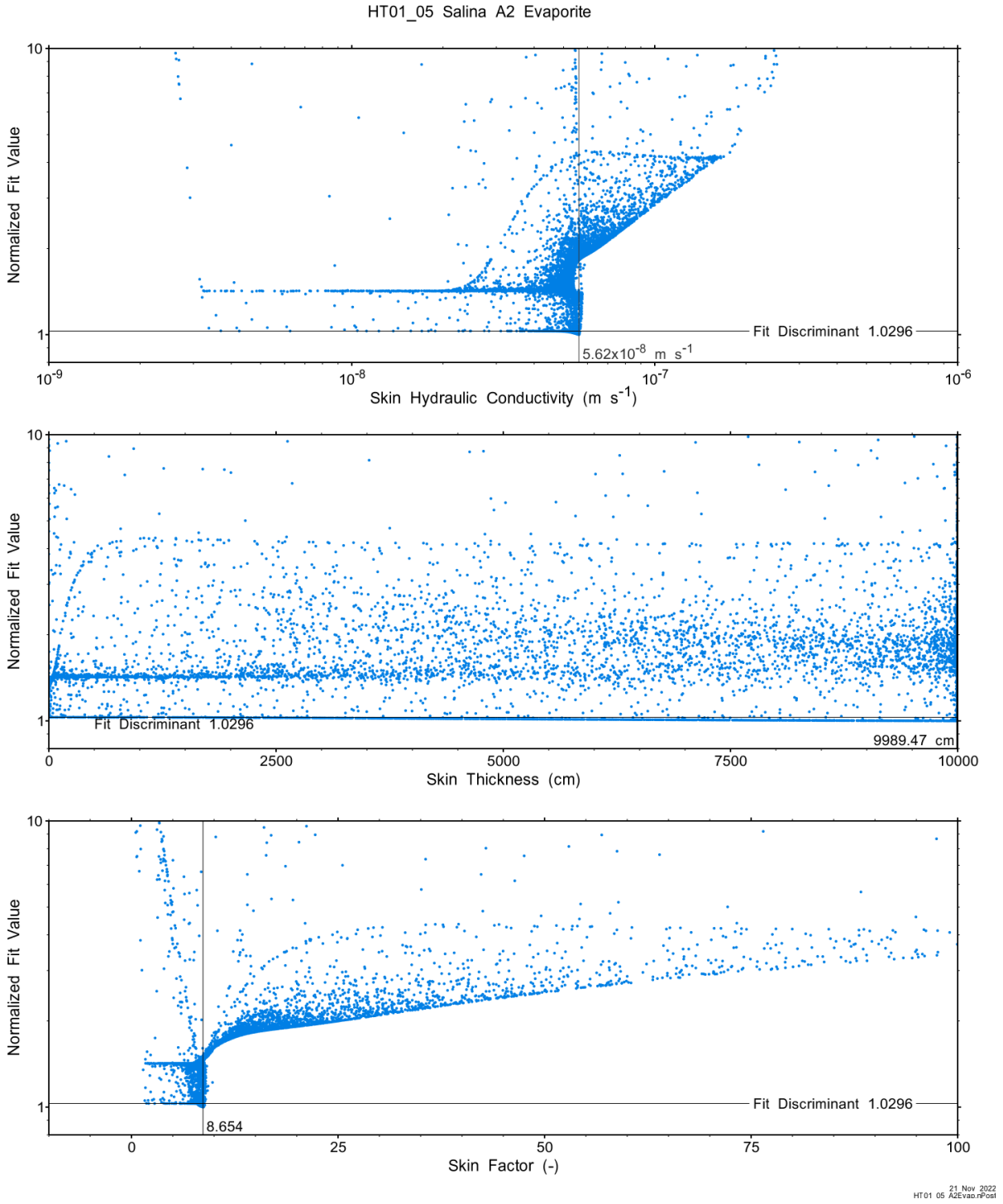

Figure A.16 - XY-scatter plot showing the skin parameter space normalized fit values.

A.2 HT02_05 Guelph

The SB BH02 interval from 386.80 to 391.83 mBGS tested in HT02_05 covers nearly the entirety of the Guelph Formation. A SW test of one-day duration was planned. However, the unit was very permeable and complete recovery was obtained within 20 hours, at which time the test was terminated.

A.2.1 Test Data Summary

Table A.6 and Figure A.1 provide a summary of test events and a plot of pressures measured while testing respectively.

Table A.6 - Summary of Test Events.

Event	Start Date & Time	Duration (days)	TZ Pressure (kPa)
Drilling intercept	22-01-04 23:22	153.64	3987
Shut-in	22-06-07 14:42	0.84	3976
Slug withdrawal	22-06-08 10:59	0.88	3691
Test end	22-06-09 08:08		3978

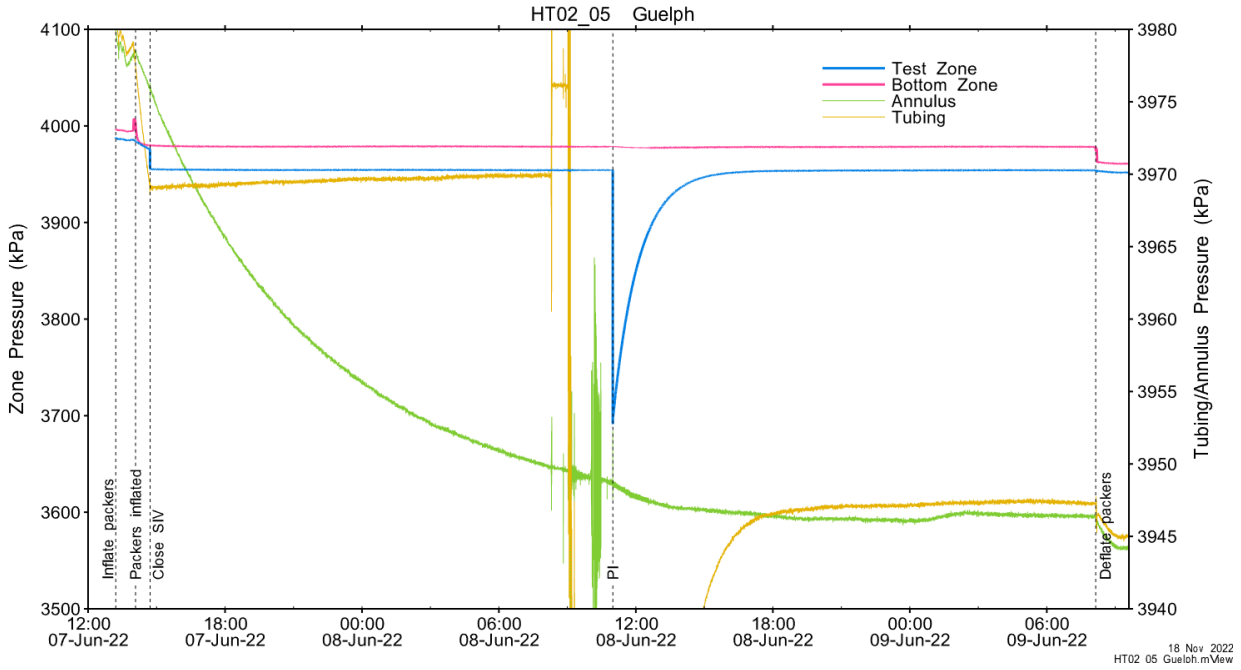

Figure A.17 - Test events and pressures.

A.2.2 Test Analyses

Table A.7 is a summary of test-specific input parameters used in the analyses, while Table A.8 presents the optimized parameters and allowed ranges. Perturbations were originally performed with wider conductivity and formation pressure ranges and a maximum 2500 cm skin thickness. Conductivity ranges were modified and skin thickness increased to 10000 cm based on review of initial results.

Table A.7 – nSIGHTS Input Parameters.

Parameter	Value	Units
Test zone radius	6.54	cm
Tubing string radius	2.54	cm
Test zone length	5.03	m

Table A.8 – nSIGHTS Parameter Optimization Ranges.

Parameter	Minimum	Maximum	Units	Type
Formation hydraulic conductivity (K_f)	1E-08	1E-02	m/s	log
Formation pressure (P_f)	3900	4000	kPa	linear
Specific storage (S_s)	1E-08	1E-04	1/m	log
Skin hydraulic conductivity (K_s)	1E-08	1E-02	m/s	log
Skin thickness (t_s)	0.013	10000	cm	linear

Figure A.18 shows the measured test zone pressure record (with reduced data density for clarity) used in the analysis along with the best-fit simulation and parameter values. Figure A.19 presents the pre-test history, and Figure A.20 shows the Ramey B normalized best-fit pressure and pressure derivatives.

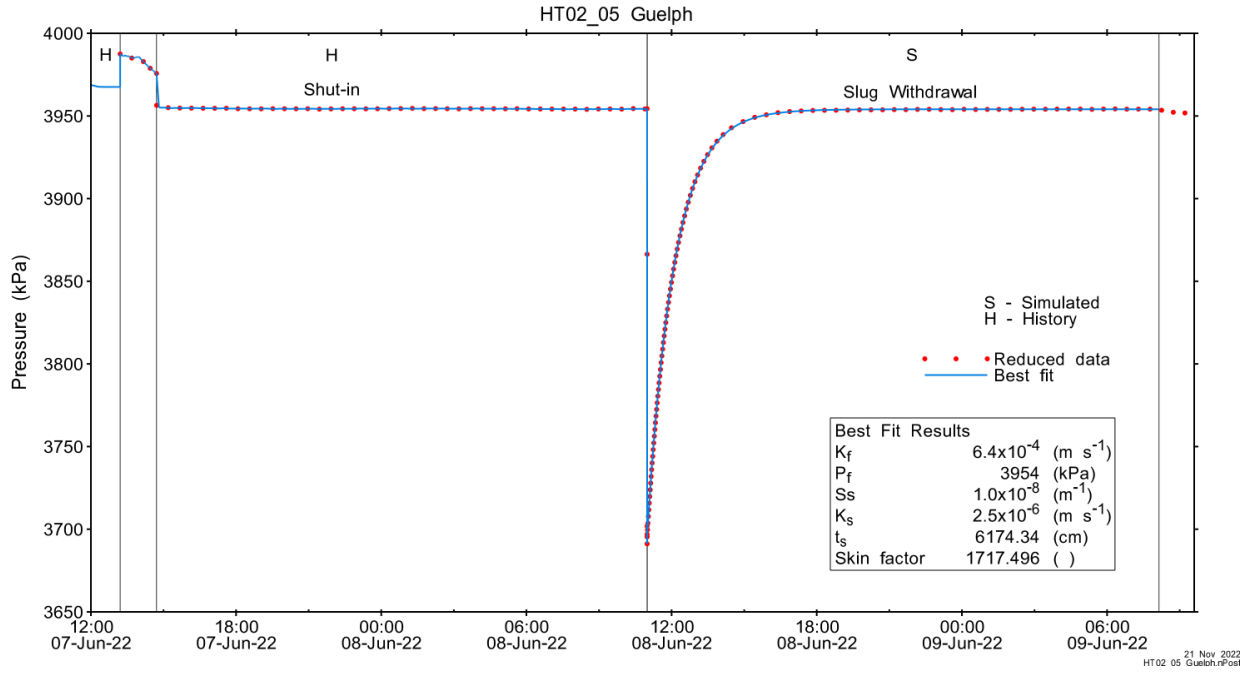

Figure A.18 - Annotated testing sequence showing best-fit simulation and parameter estimates.

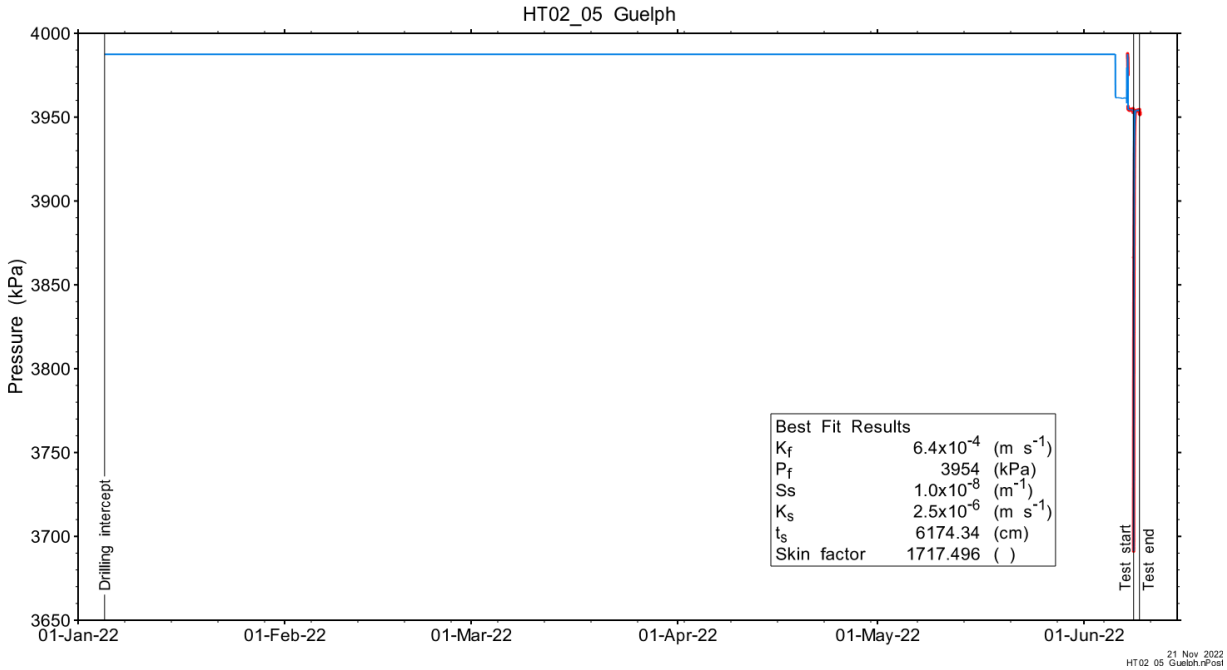

Figure A.19 - Annotated testing sequence showing pre-test history, best-fit simulation and parameter estimates.

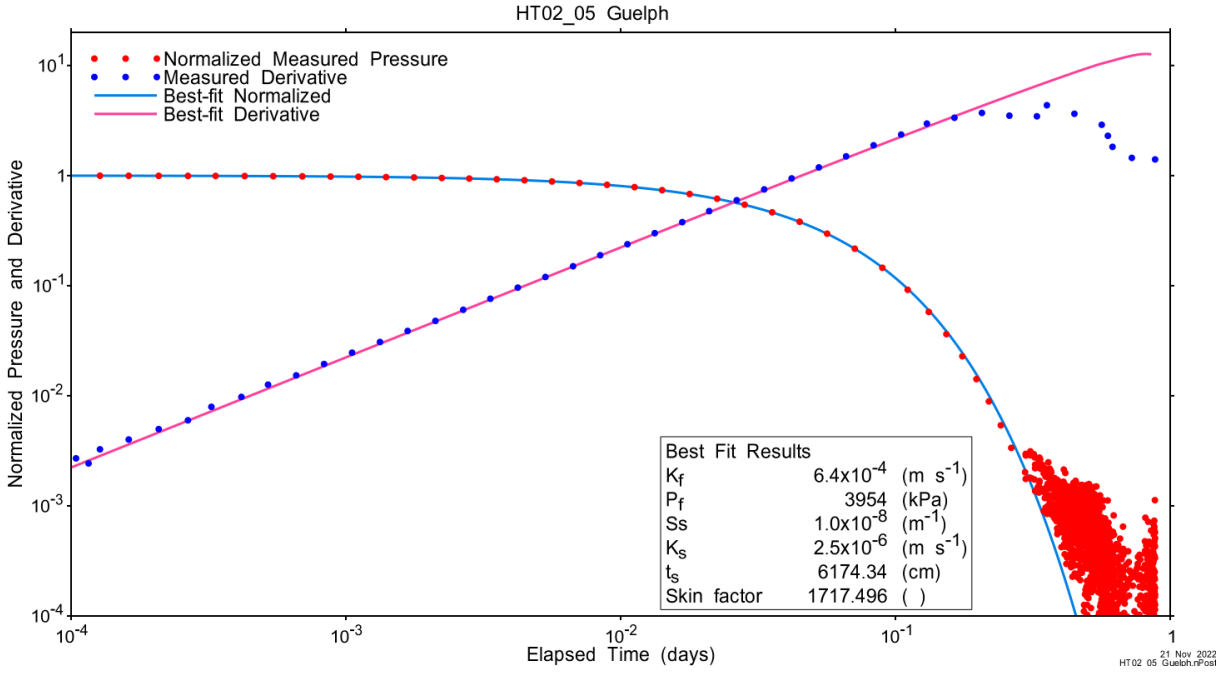

Figure A.20 - Log-log plot showing Ramey B and derivative response for best-fit simulation.

Figure A.21 shows the normalized parameter sensitivity response for the best fit. Sensitivity for fitting parameters is flat at the end of the test, indicating that test duration was sufficient. Results are not sensitive to the specific storage coefficient

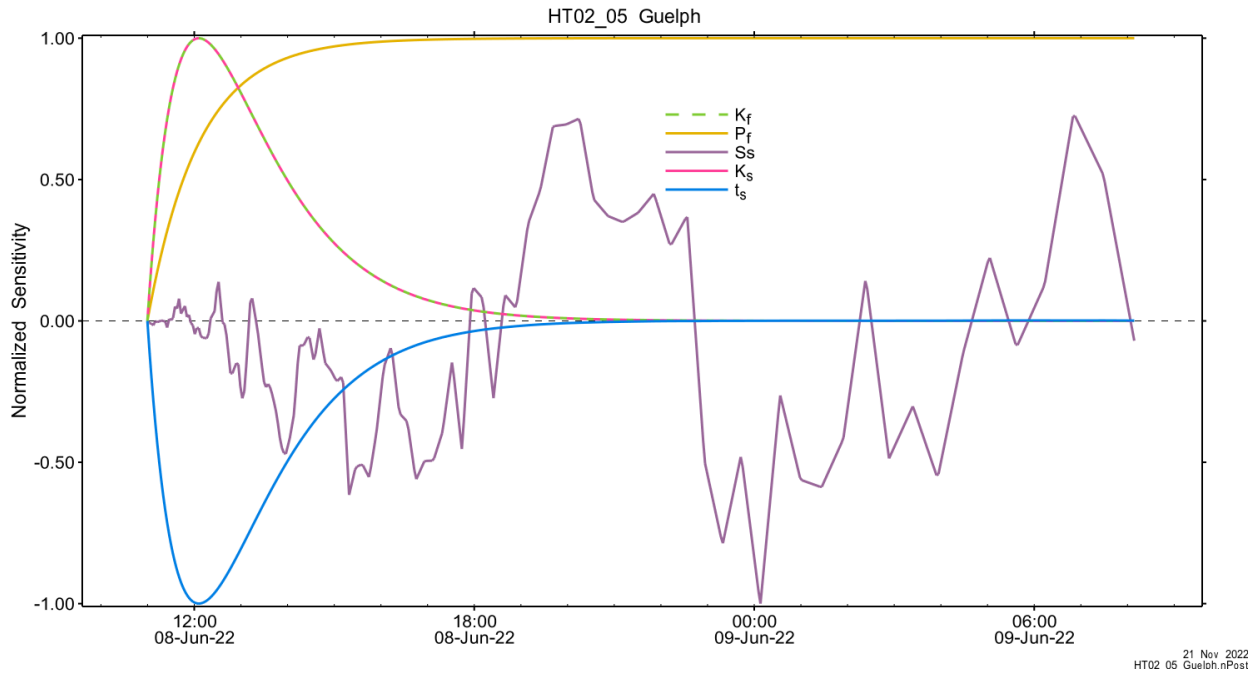

Figure A.21 - Normalized Jacobian for best-fit simulation.

A.2.3 Uncertainty Analyses

The CDF of normalized fit values for all converged simulations and the selected fit discriminant are shown in Figure A.22 and, in detail, in Figure A.23 .

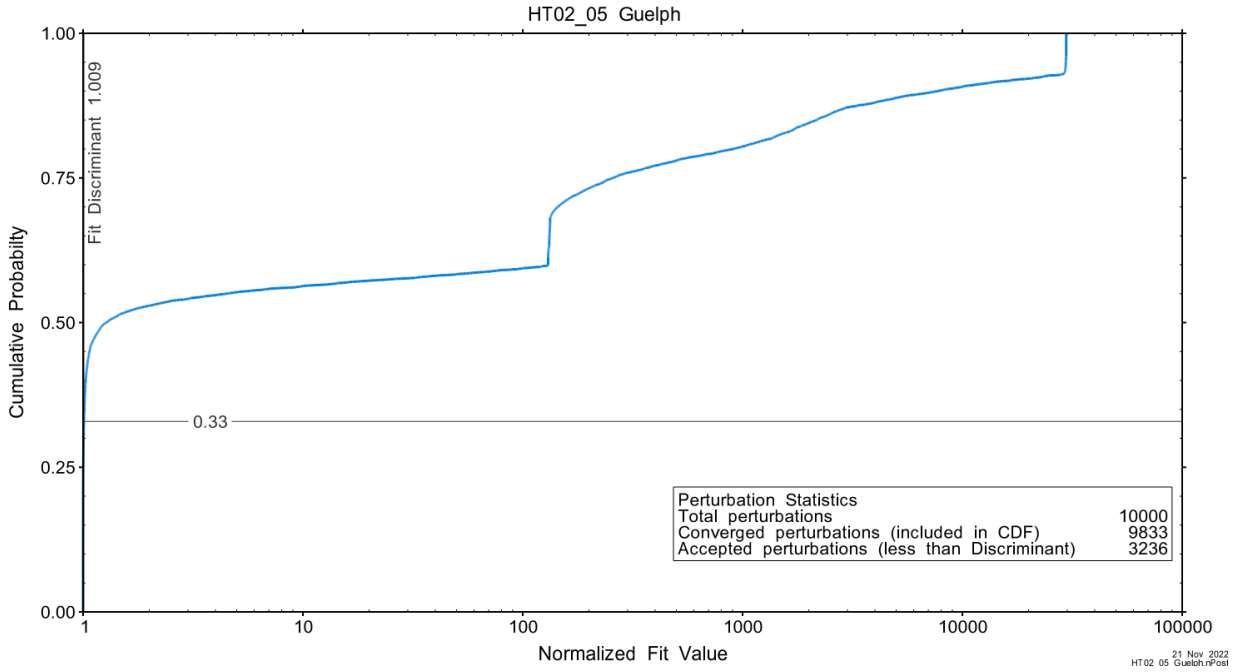

Figure A.22 - Fit value cumulative distribution function.

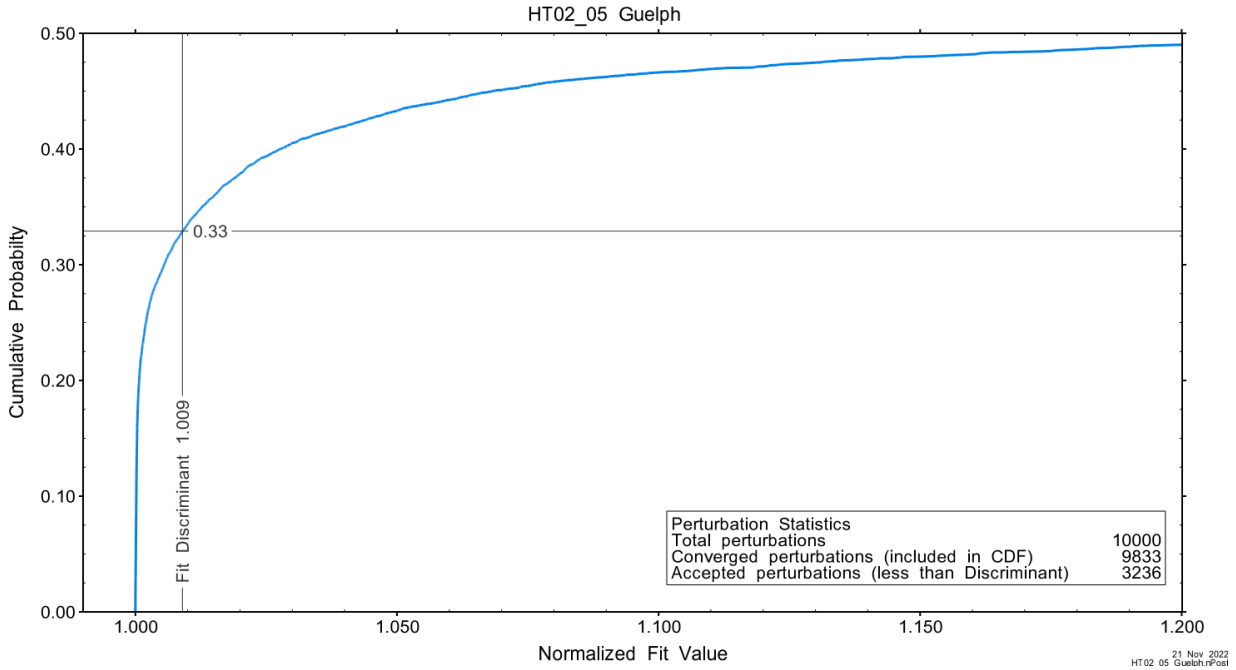

Figure A.23 – Detail of fit value cumulative distribution function.

Summary cross parameter scatter plots for selected formation and skin parameters are given in Figure A.24 and Figure A.25. The light pink dots on the figures are the initial parameter estimates, with red dots overlaying those initial parameter values that resulted in accepted optimization results. The grey dots are converged optimizations which did not meet the fit discriminant. Larger varying color symbols represent the fit value of accepted optimizations, with the blue values representing the best fit.

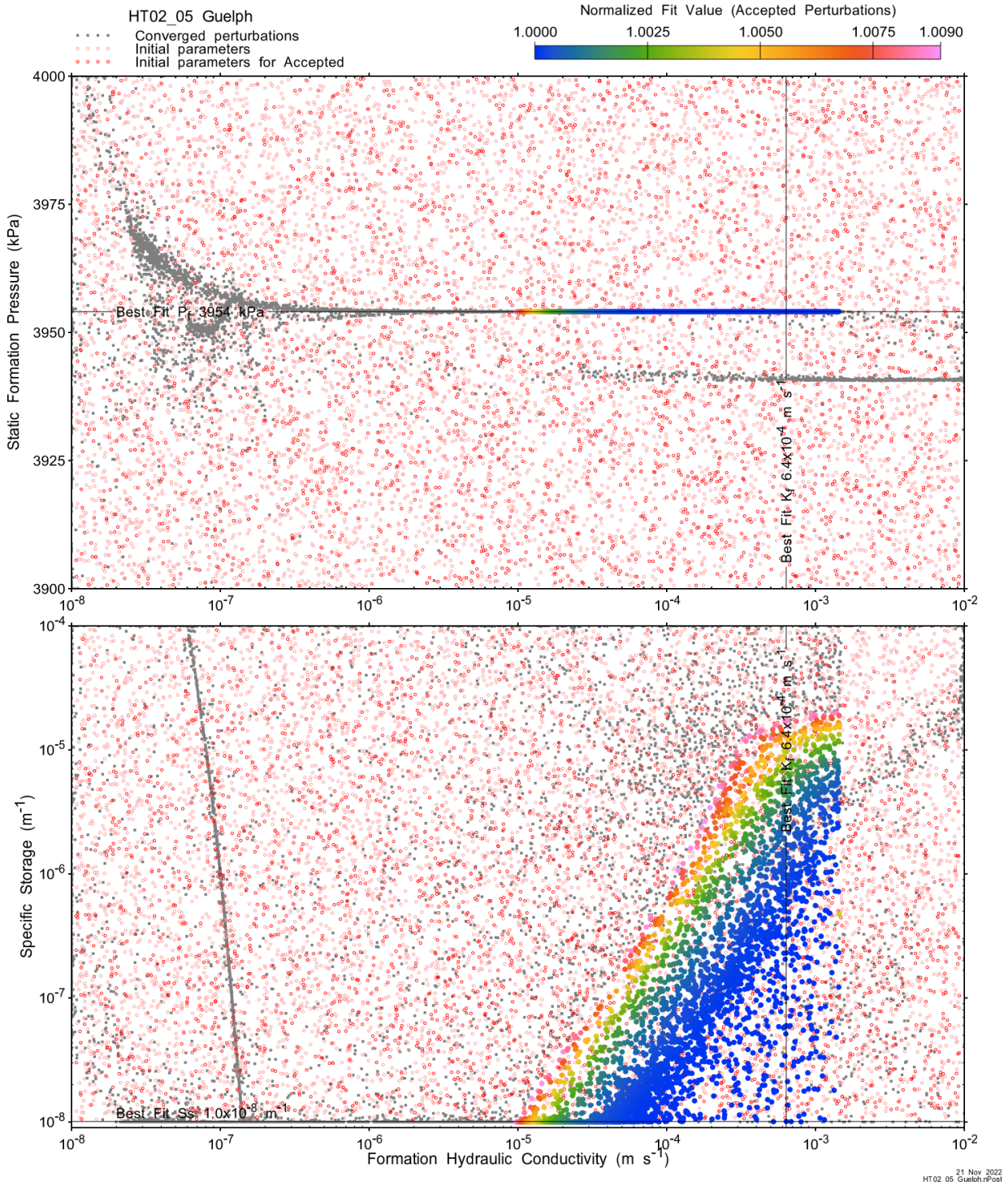

Figure A.24 - XY-scatter plot showing estimates of formation hydraulic conductivity (K_f) vs static formation pressure (P_f) (top panel) and specific storage (Ss) (bottom panel).

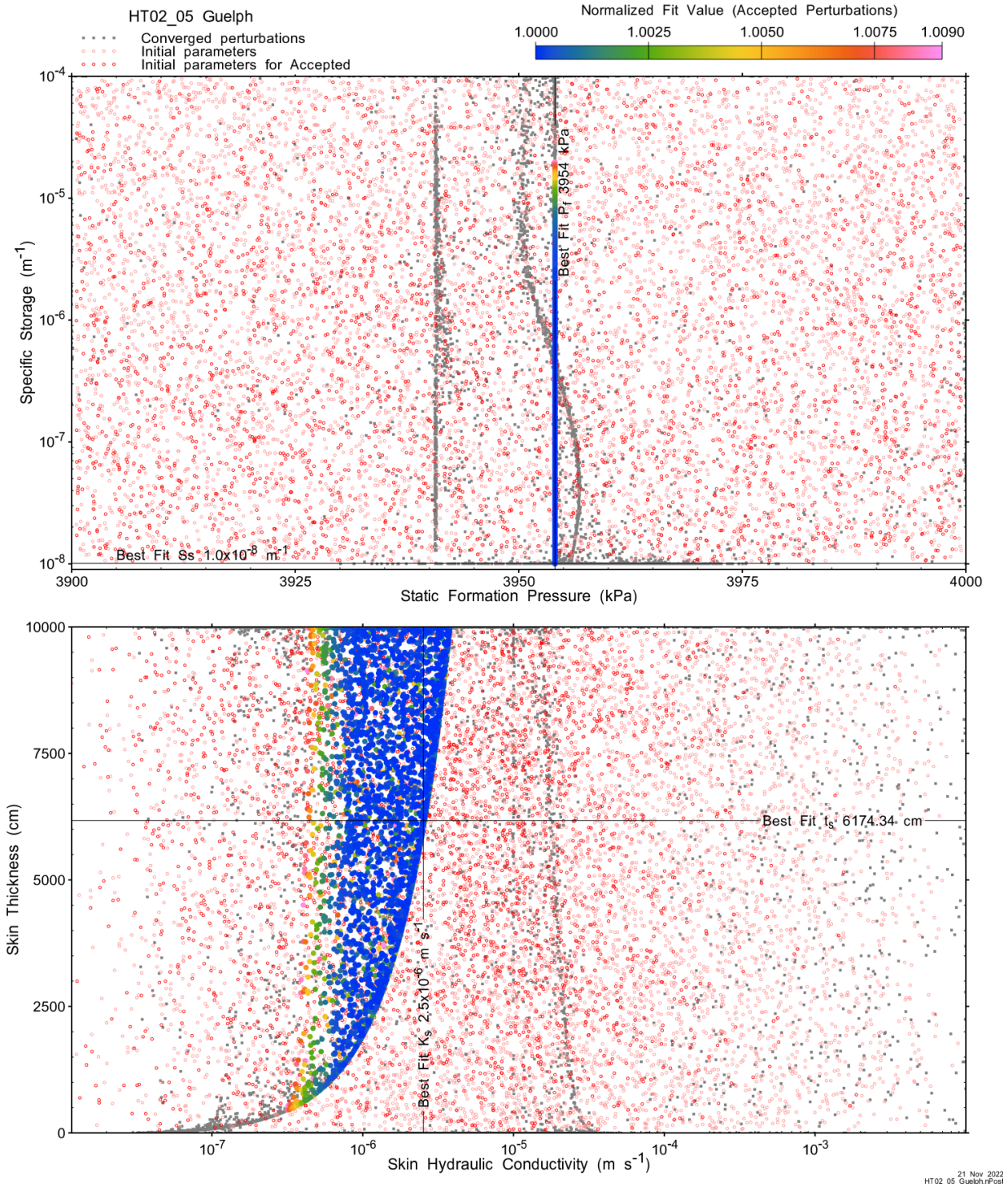

Figure A.25 - XY-scatter plot showing estimates of static formation pressure (P_f) vs specific storage (Ss) (top panel) and skin hydraulic conductivity (K_s) vs skin thickness (t_s) (bottom panel).

Confidence limits and median values are determined from the CDF of accepted optimization results (i.e. the varying color values in the above figures), with best fit value, 5% and 95% confidence indicated on Figure A.26 and Figure A.27.

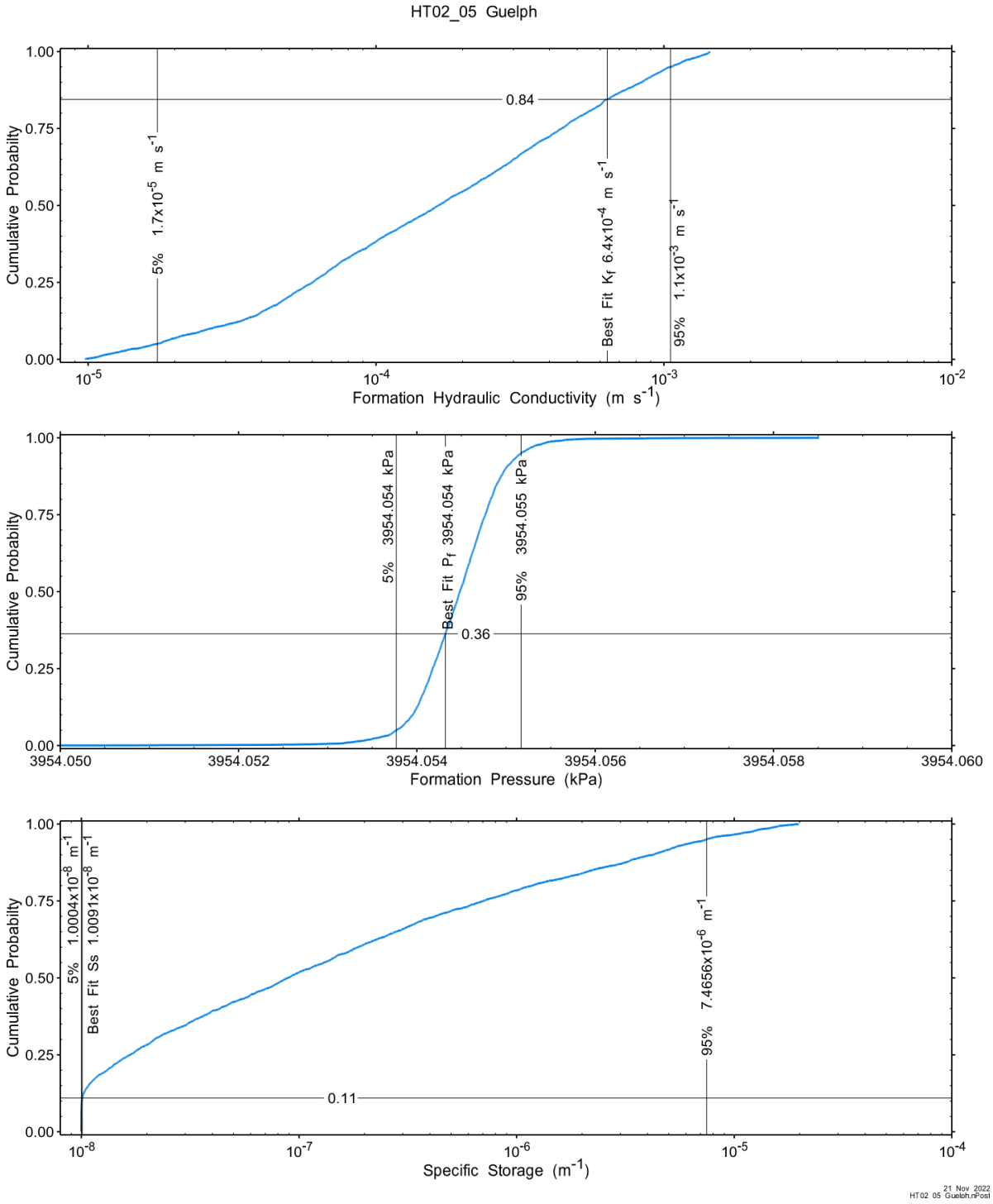

Figure A.26 – Cumulative distribution functions and parameter limits for formation hydraulic conductivity (K_f) (top panel), static formation pressure (P_f) (middle panel) and specific storage (Ss) (bottom panel).

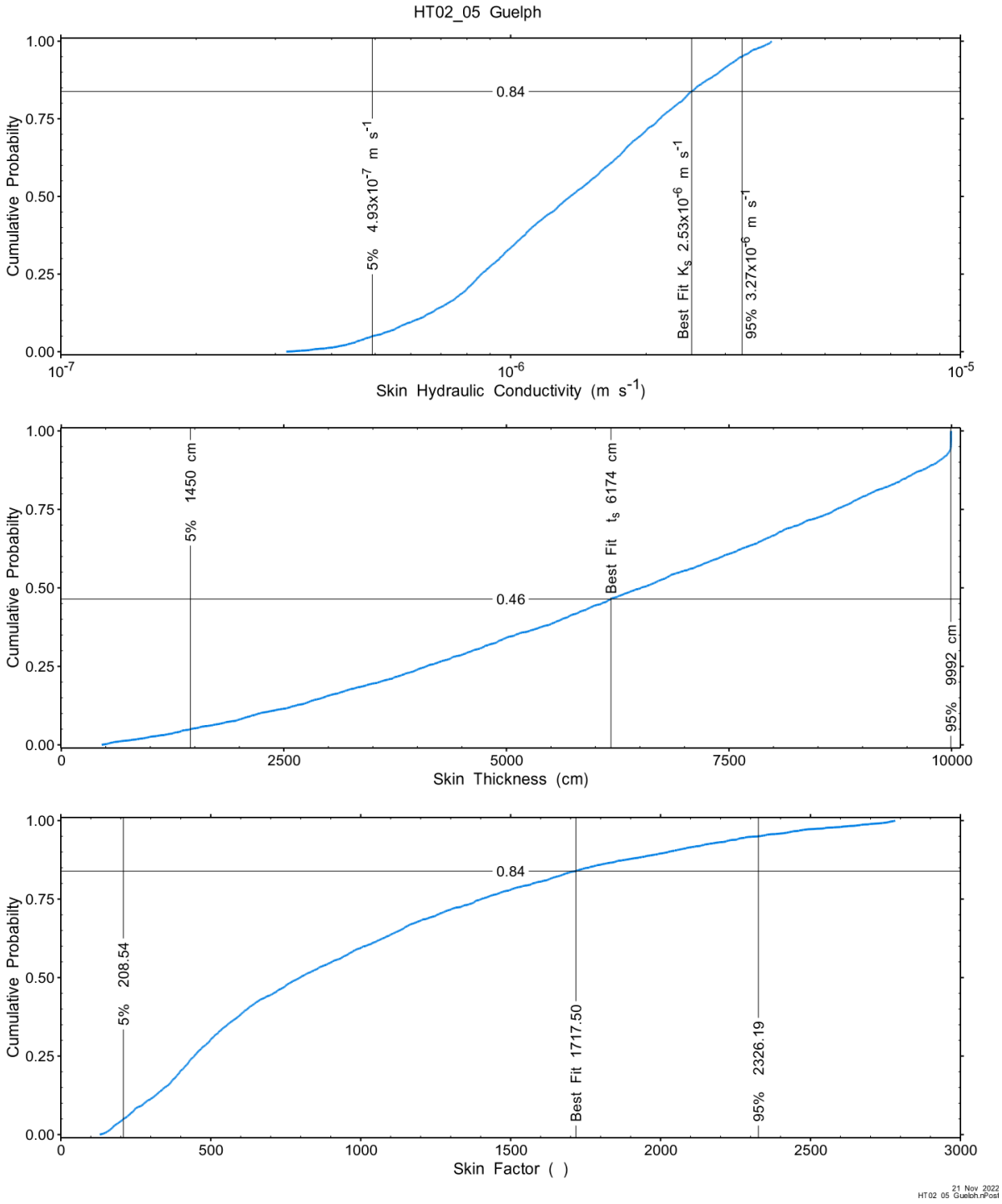

Figure A.27 – Cumulative distribution functions and parameter limits for skin hydraulic conductivity (K_s) (top panel), skin thickness (t_s) (middle panel) and skin factor (s) (bottom panel).

A summary of perturbation results is presented in Figure A.28, with Ramey-processed perturbations in Figure A.13. Those perturbations (2279 of 10,000) with all parameters within the 5% and 95% range present an excellent fit to the measured test zone data.

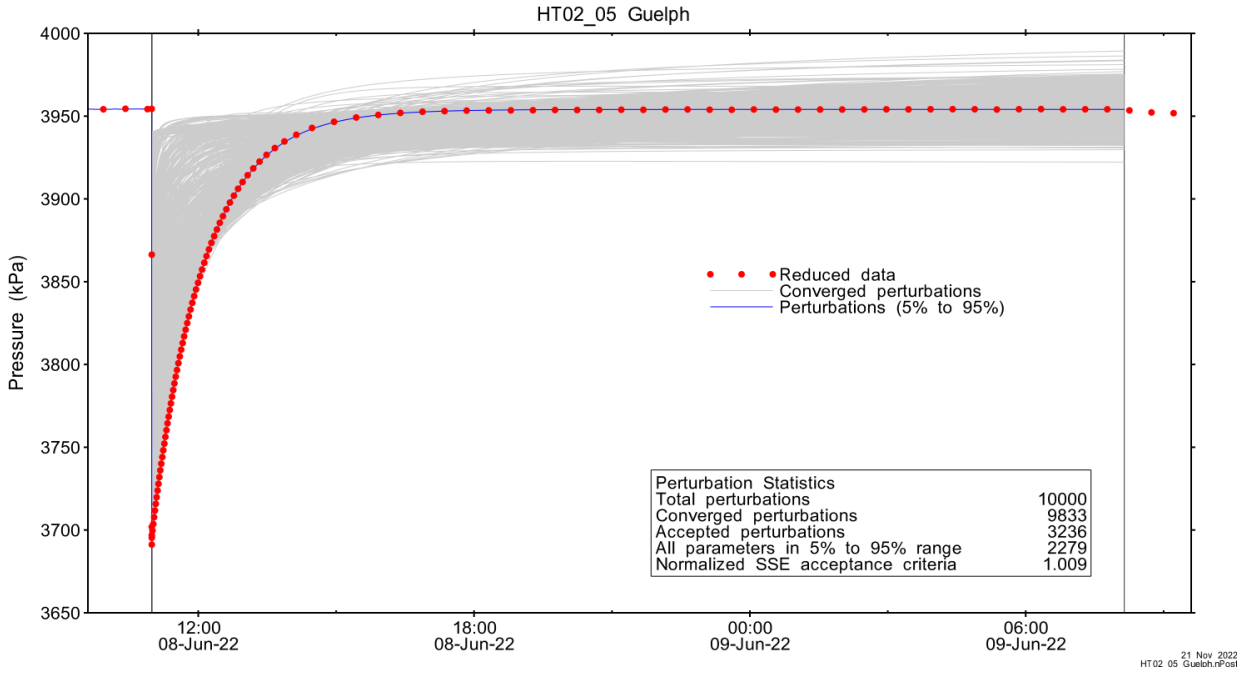

Figure A.28 – Perturbation results – all converged, accepted, and within 5% to 95% for all parameters.

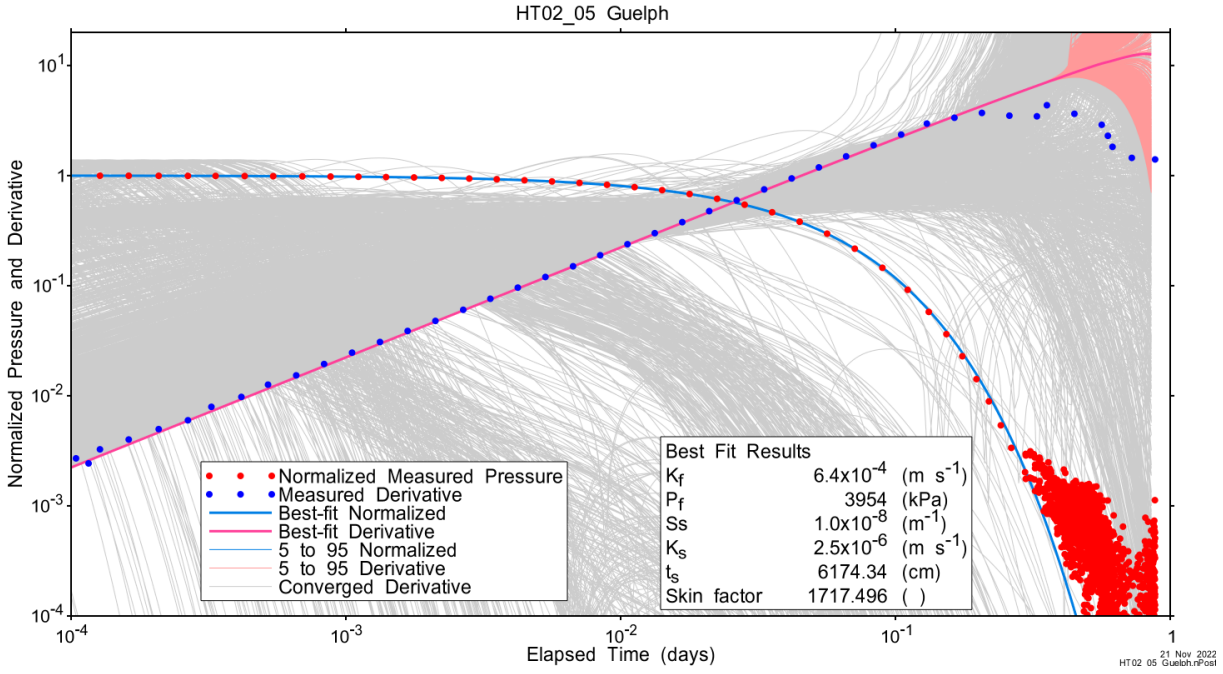

Figure A.29 – Log-log plot showing Ramey B and derivative response for all converged optimizations and those within 5% to 95% for all parameters.

A summary of best-fit and parameter ranges is given in Table A.9.

Table A.9 - Summary of the HT02_05 parameter estimates.

Parameter	Best Fit	5%	Median	95%
K_f (m/s)	6.4E-04	1.7E-05	1.6E-04	1.1E-03
P_f (kPa)	3954	3954	3954	3954
Ss (1/m)	1.0E-08	1.0E-08	8.9E-08	7.5E-06
K_s (m/s)	2.5E-06	4.9E-07	1.4E-06	3.3E-06
t_s (cm)	6174.34	1450.23	6511.21	9991.59
s (-)	1717.500	208.541	796.448	2326.190

Parameter correlations for all perturbations with all parameters within the 5% to 95% limits are given in Table A.5.

Table A.10 – Pearson cross-correlations of 5% to 95% parameters

	Log(K_f)	P_f	Log(Ss)	Log(K_s)	t_s	s
Log(K_f)	1.000	-0.006	0.727	0.996	0.217	0.962
Pf	-0.006	1.000	0.084	-0.011	-0.053	-0.013
Log(S_s)	0.727	0.084	1.000	0.712	0.009	0.683
Log(K_s)	0.996	-0.011	0.712	1.000	0.299	0.969
t_s	0.217	-0.053	0.009	0.299	1.000	0.317
s	0.962	-0.013	0.683	0.969	0.317	1.000

A.2.4 Additional Figures

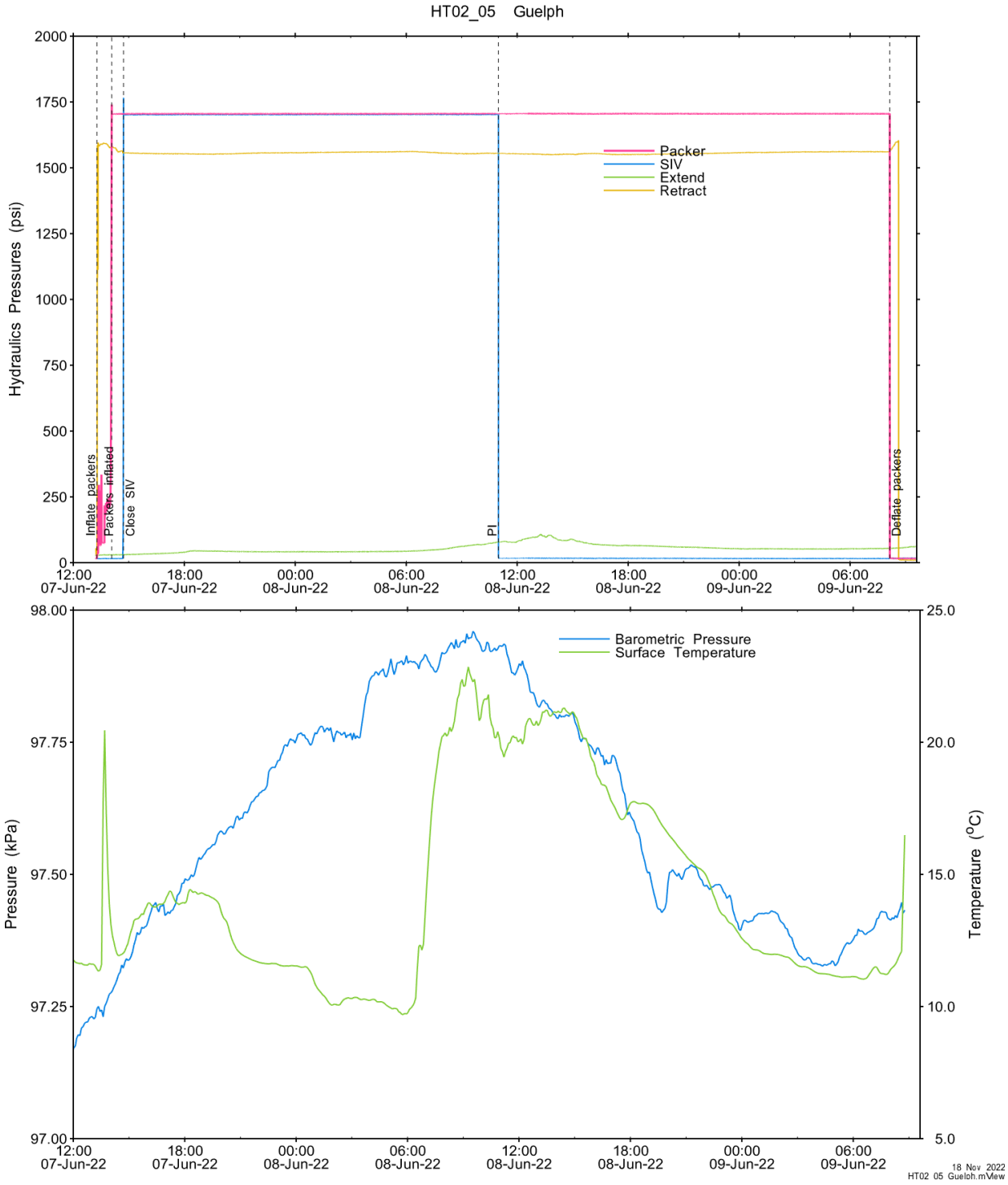

Figure A.30 - Hydraulics pressures and surface temperature/barometric pressure.

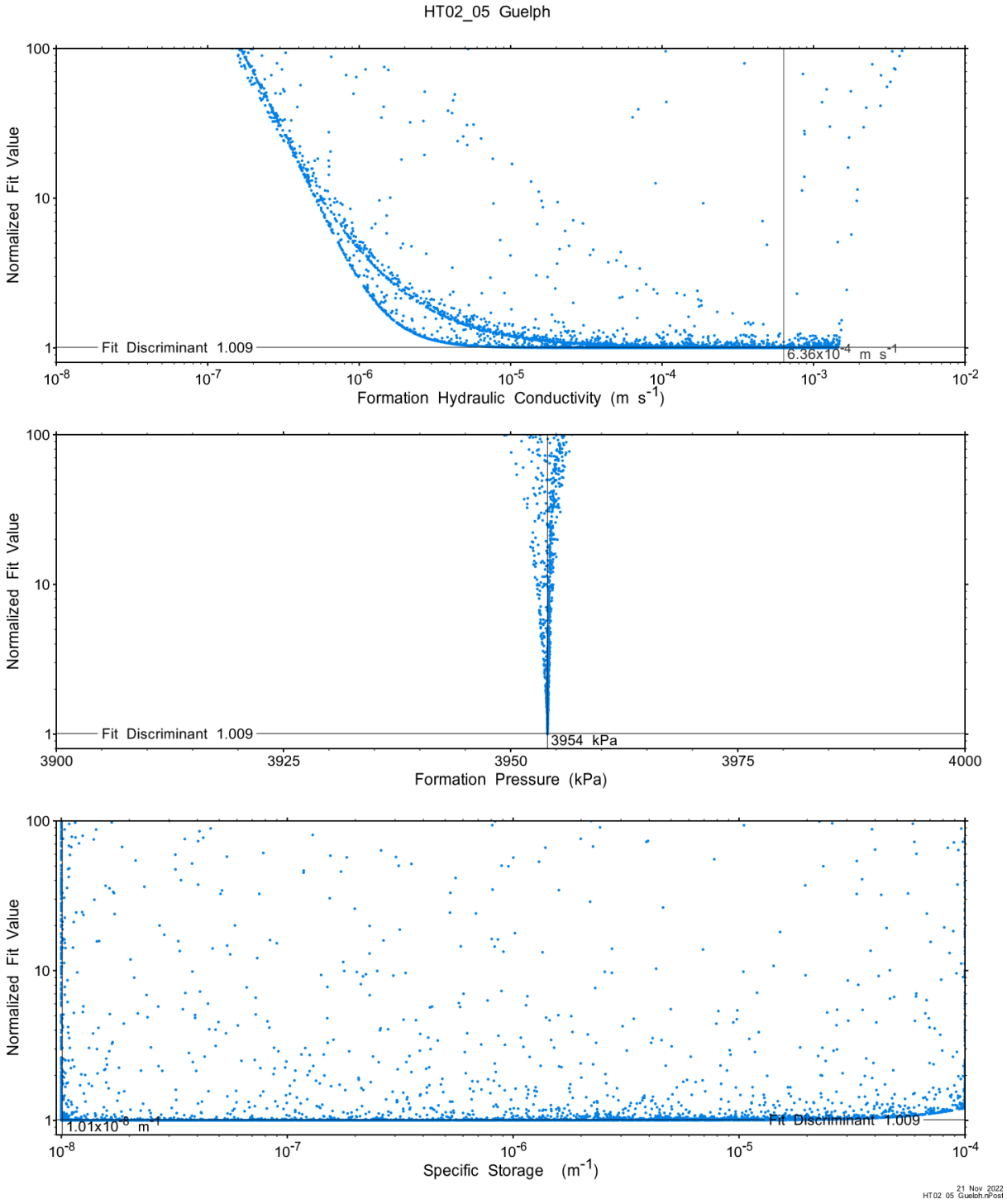

Figure A.31 - XY-scatter plot showing the formation parameter space normalized fit values.

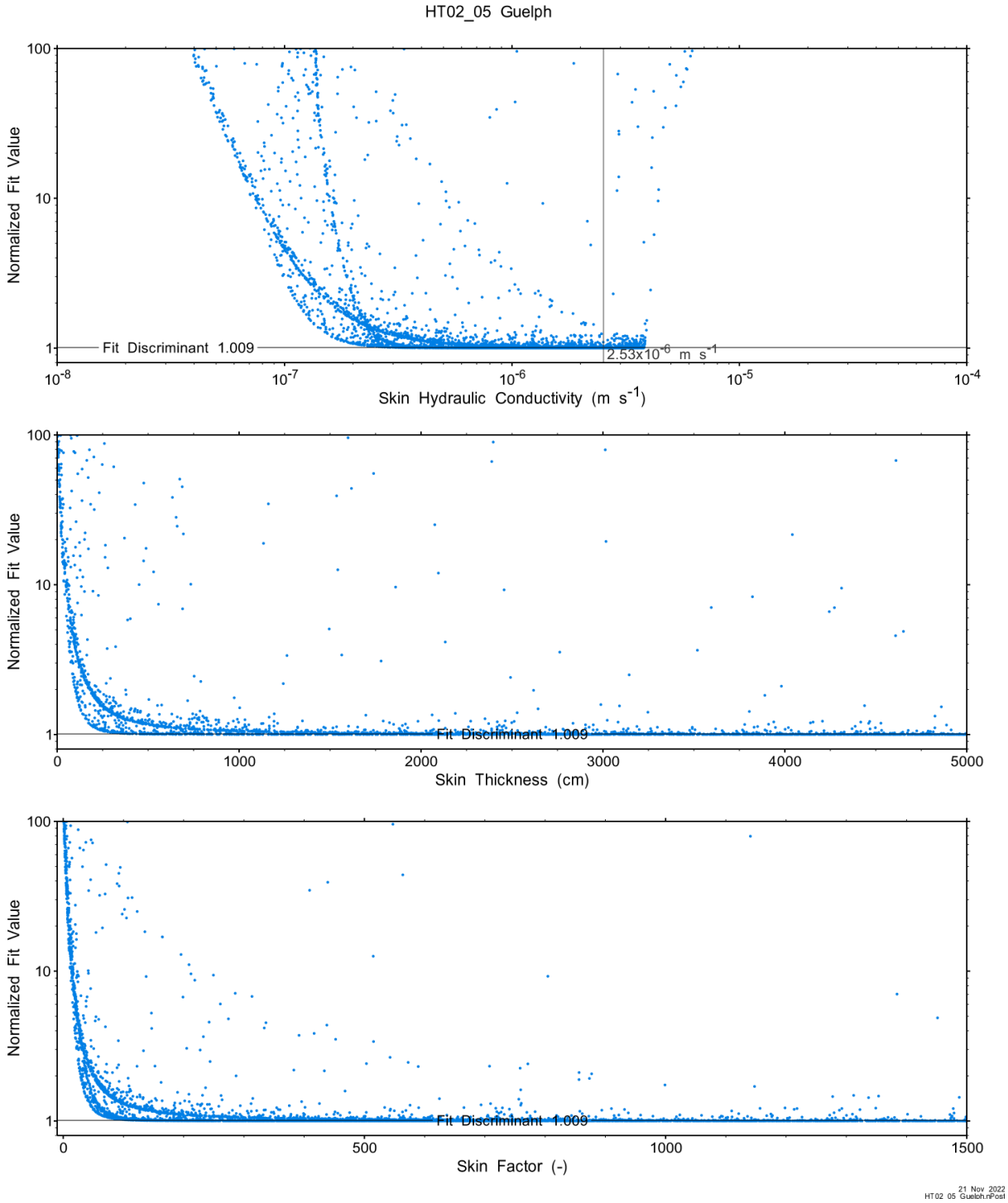

Figure A.32 - XY-scatter plot showing the skin parameter space normalized fit values.

A.3 HT03_05 Blue Mountain - Lower

The SB BH02 interval from 663.50 to 668.53 mBGS tested in HT03_05 covers the bottom 5 m of the Blue Mountain Formation. A two day duration PI was performed.

A.3.1 Test Data Summary

Table A.6 and Figure A.1 provide a summary of test events and a plot of pressures measured while testing respectively.

Table A.11 - Summary of Test Events.

Event	Start Date & Time	Duration (days)	TZ Pressure (kPa)
Drilling intercept	22-03-11 23:13	89.64	6992
Shut-in	22-06-09 14:33	0.73	6997
Pulse injection	22-06-10 08:05	2.00	7509
Test end	22-06-12 08:02		6842

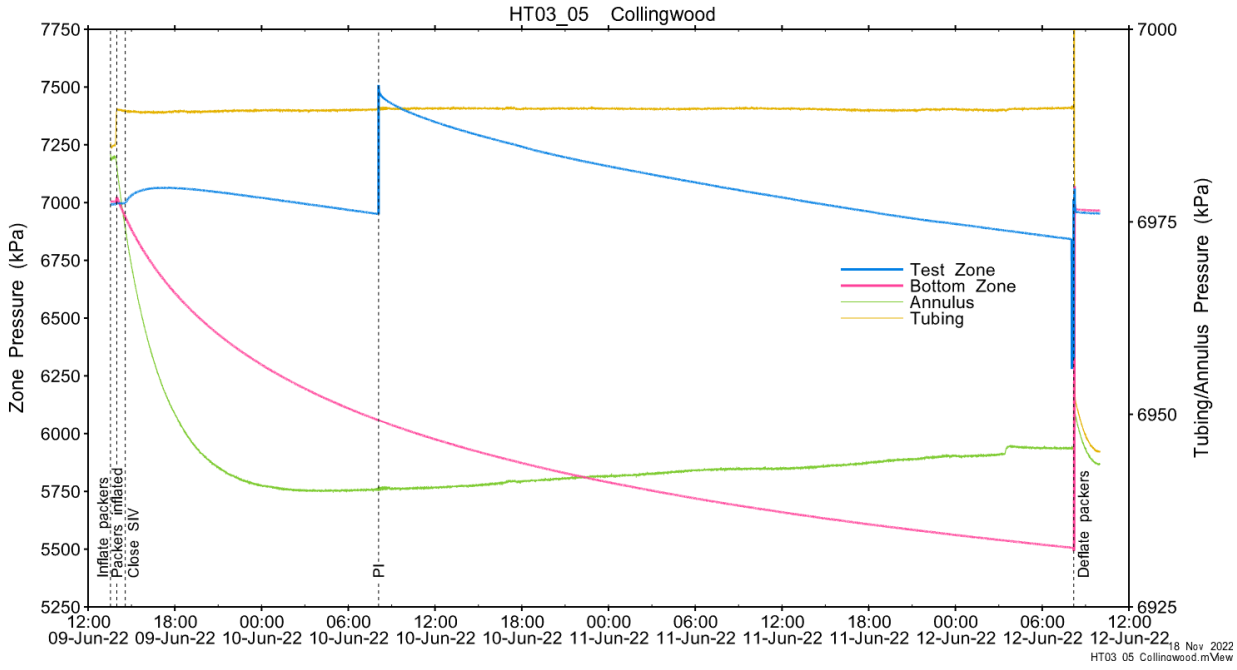

Figure A.33 - Test events and pressures.

A.3.2 Test Analyses

Table A.7 is a summary of test-specific input parameters used in the analyses, while Table A.8 presents the optimized parameters and allowed ranges.

Table A.12 – nSIGHTS Input Parameters.

Parameter	Value	Units
Test zone radius	6.39	cm
Test zone compressibility	3.59E-10	1/Pa
Test zone length	5.03	m

Table A.13 – nSIGHTS Parameter Optimization Ranges.

Parameter	Minimum	Maximum	Units	Type
Formation hydraulic conductivity (K_f)	1E-15	1E-07	m/s	log
Formation pressure (P_f)	0	7000	kPa	linear
Specific storage (S_s)	1E-08	1E-04	1/m	log
Skin hydraulic conductivity (K_s)	1E-15	1E-07	m/s	log
Skin thickness (t_s)	0.013	500	cm	linear

Figure A.18 shows the measured test zone pressure record (with reduced data density for clarity) used in the analysis along with the best-fit simulation and parameter values. Figure A.19 presents the pre-test history, and Figure A.20 shows the Ramey B normalized best-fit pressure and pressure derivatives.

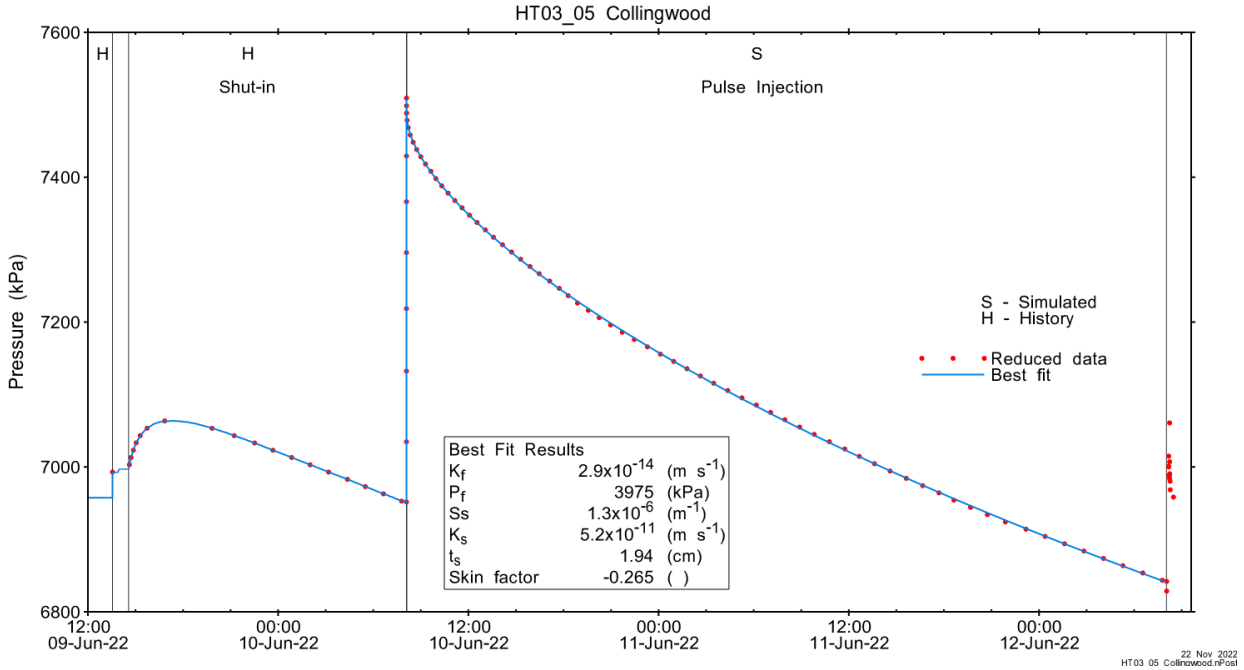

Figure A.34 - Annotated testing sequence showing best-fit simulation and parameter estimates.

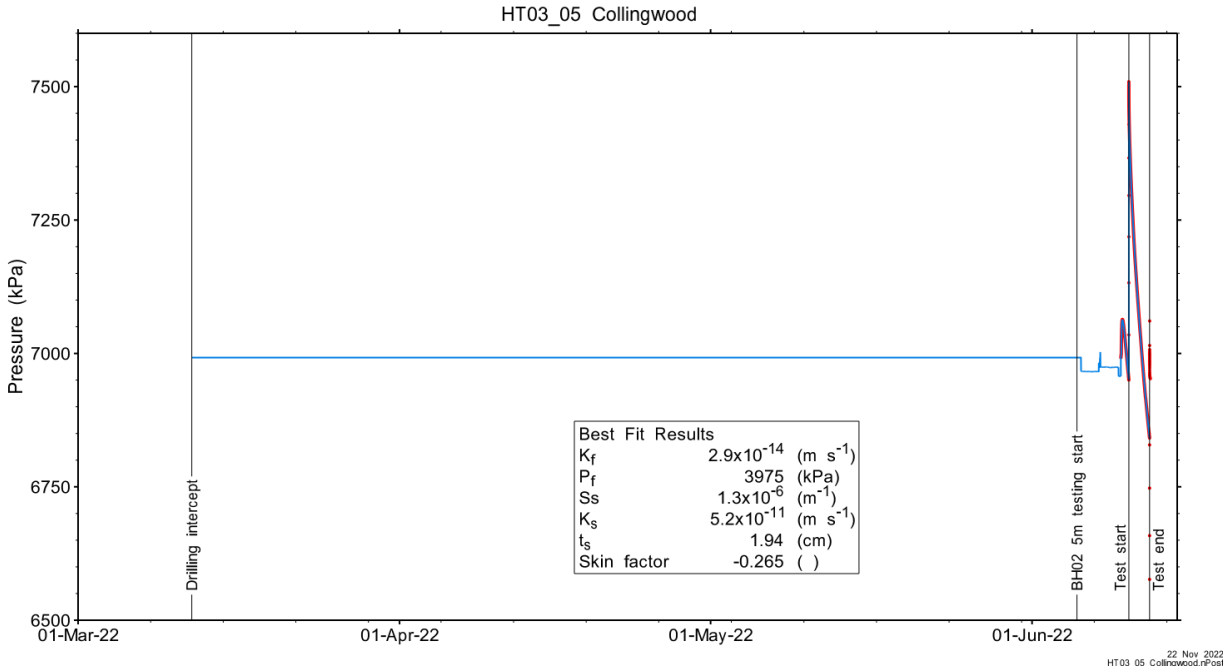

Figure A.35 - Annotated testing sequence showing pre-test history, best-fit simulation and parameter estimates.

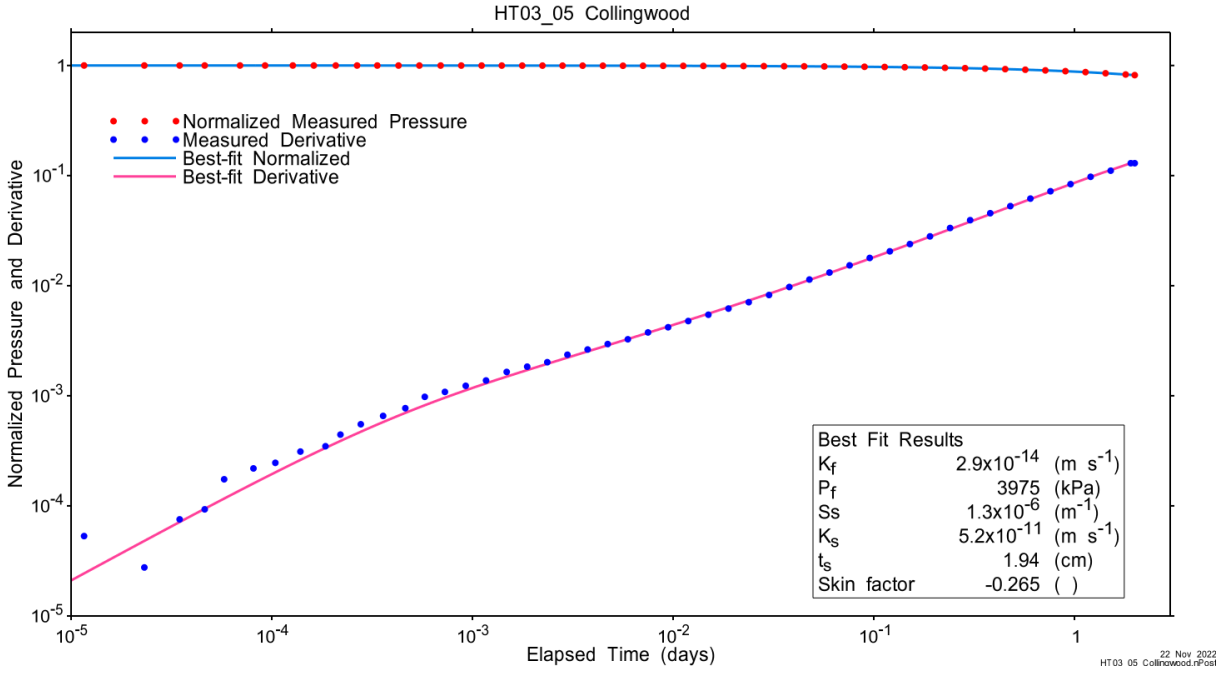

Figure A.36 - Log-log plot showing Ramey B and derivative response for best-fit simulation.

Figure A.21 shows the normalized parameter sensitivity response for the best fit. Sensitivity for most fitting parameters is increasing at the end of the test, indicating that more precise results may be obtained with a longer test duration.

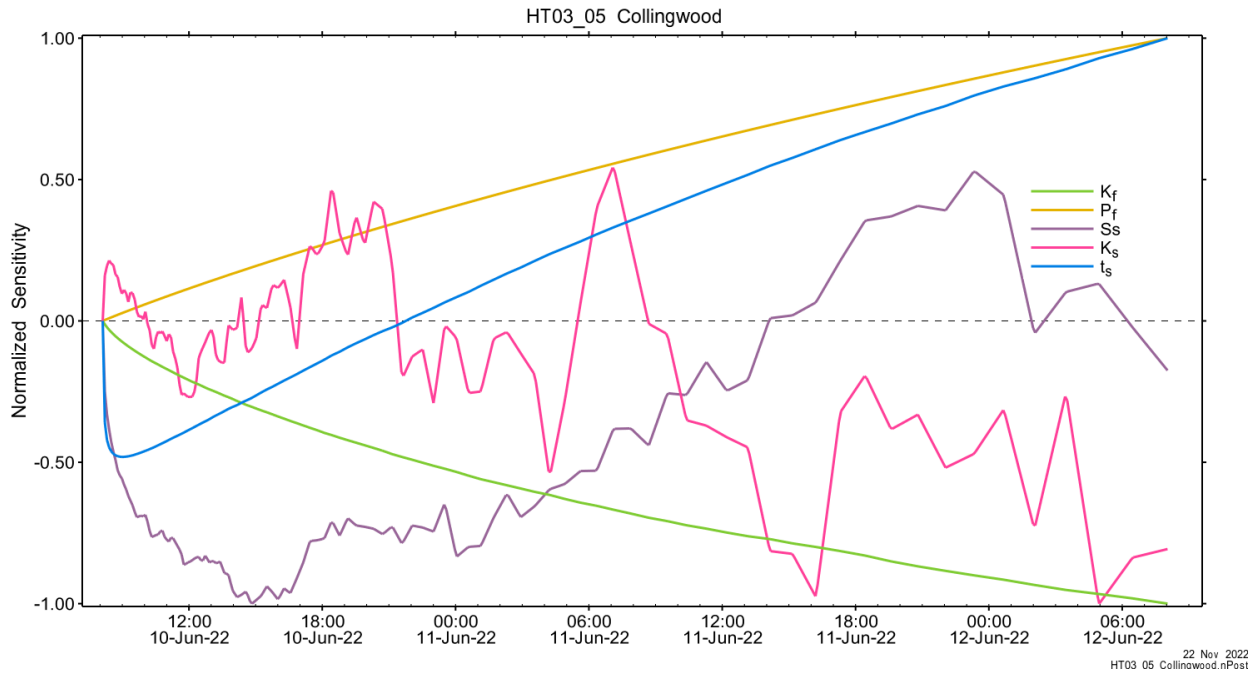

Figure A.37 - Normalized Jacobian for best-fit simulation.

A.3.3 Uncertainty Analyses

The CDF of normalized fit values for all converged simulations and the selected fit discriminant are shown in Figure A.22 and, in detail, in Figure A.23 .

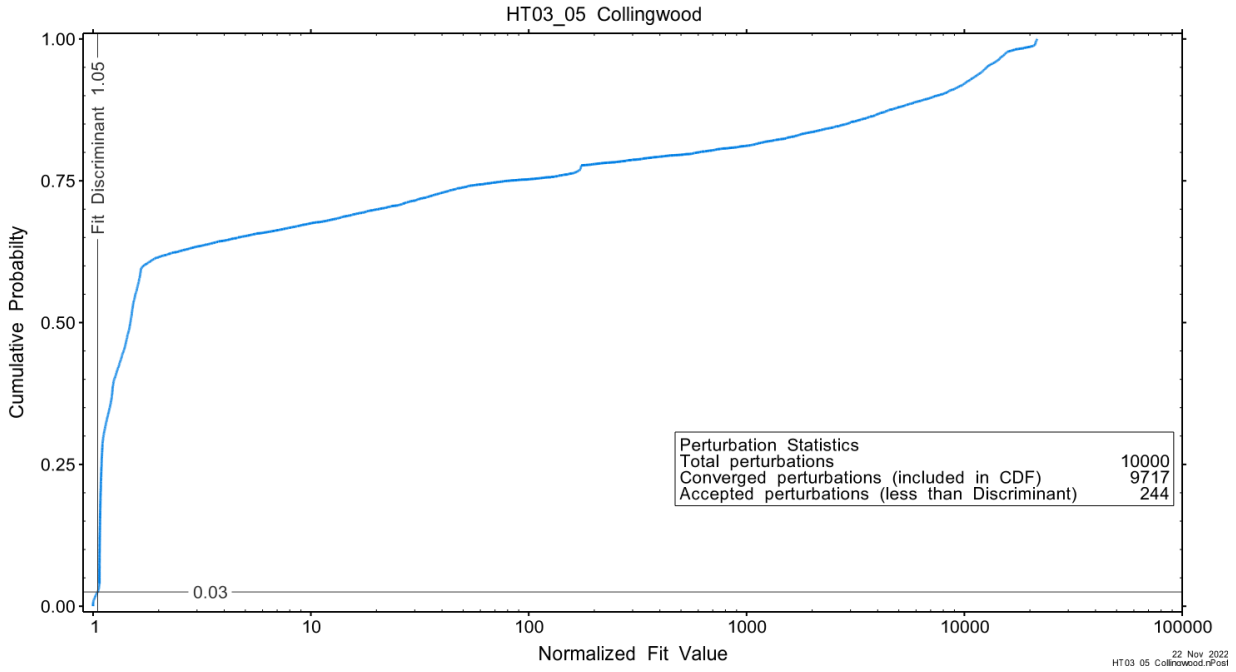

Figure A.38 - Fit value cumulative distribution function.

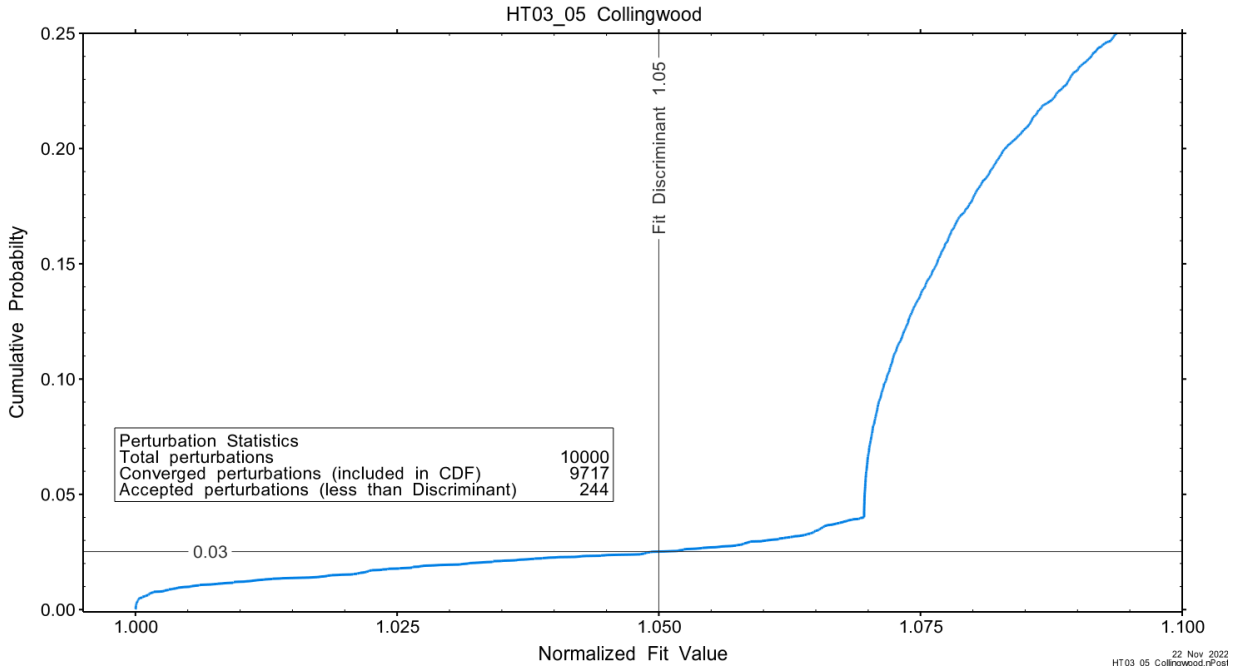

Figure A.39 – Detail of fit value cumulative distribution function.

Summary cross parameter scatter plots for selected formation and skin parameters are given in Figure A.24 and Figure A.25. The light pink dots on the figures are the initial parameter estimates, with red dots overlaying those initial parameter values that resulted in accepted optimization results. The grey dots are converged optimizations which did not meet the fit discriminant. Larger varying color symbols represent the fit value of accepted optimizations, with the blue values representing the best fit.

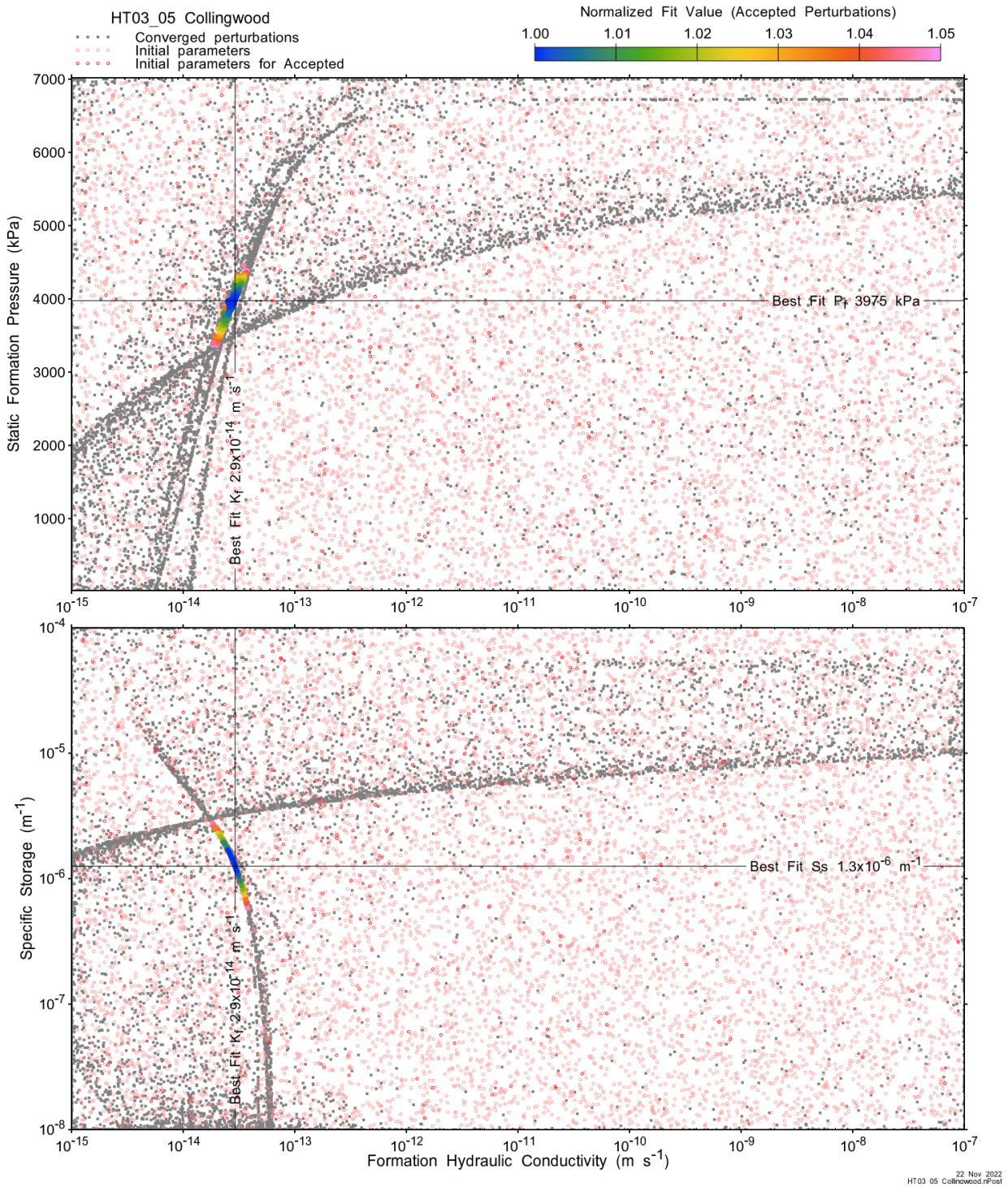

Figure A.40 - XY-scatter plot showing estimates of formation hydraulic conductivity (K_f) vs static formation pressure (P_f) (top panel) and specific storage (Ss) (bottom panel).

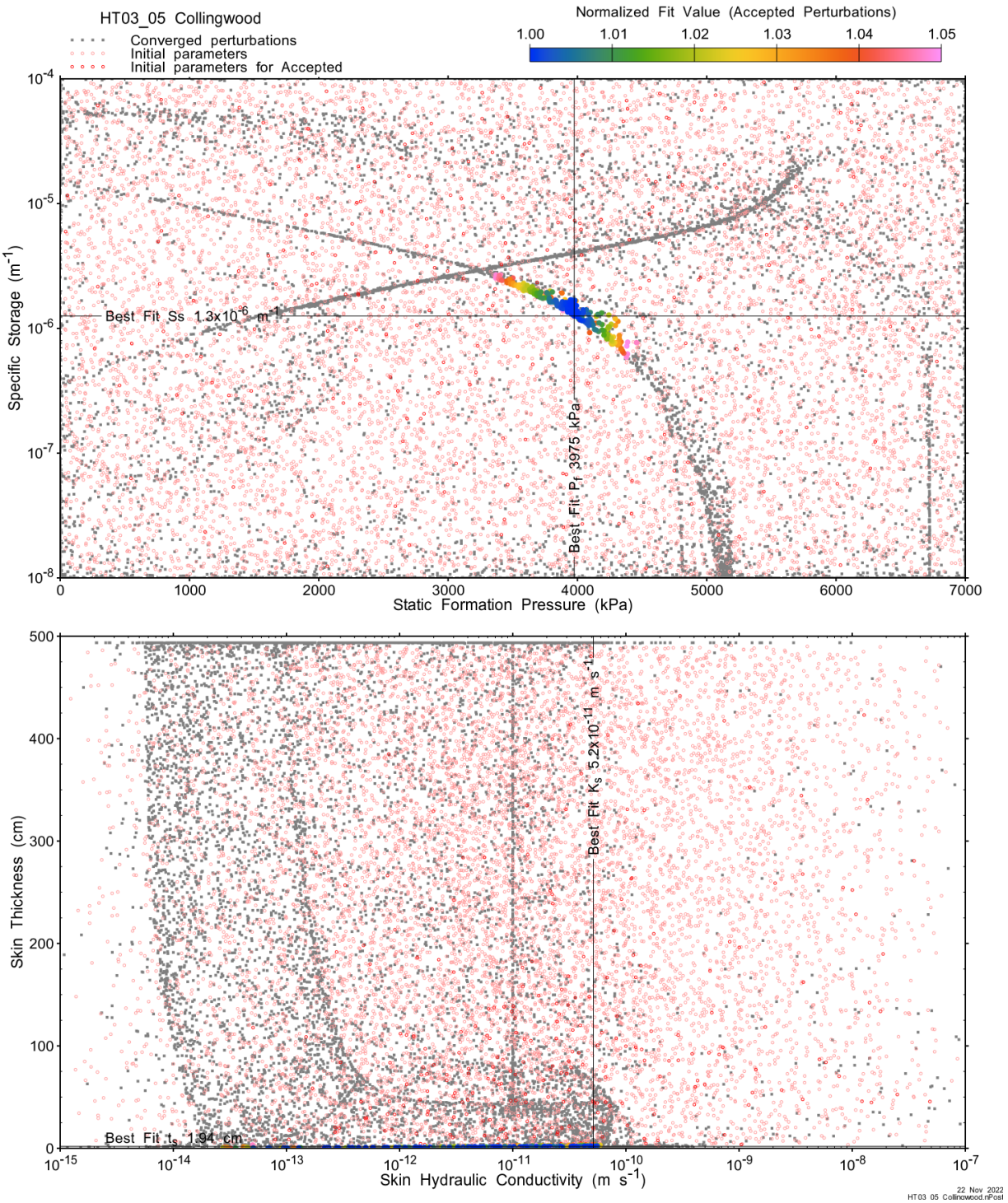

Figure A.41 - XY-scatter plot showing estimates of static formation pressure (P_f) vs specific storage (Ss) (top panel) and skin hydraulic conductivity (K_s) vs skin thickness (t_s) (bottom panel).

Confidence limits and median values are determined from the CDF of accepted optimization results (i.e. the varying color values in the above figures), with best fit value, 5% and 95% confidence indicated on Figure A.26 and Figure A.27.

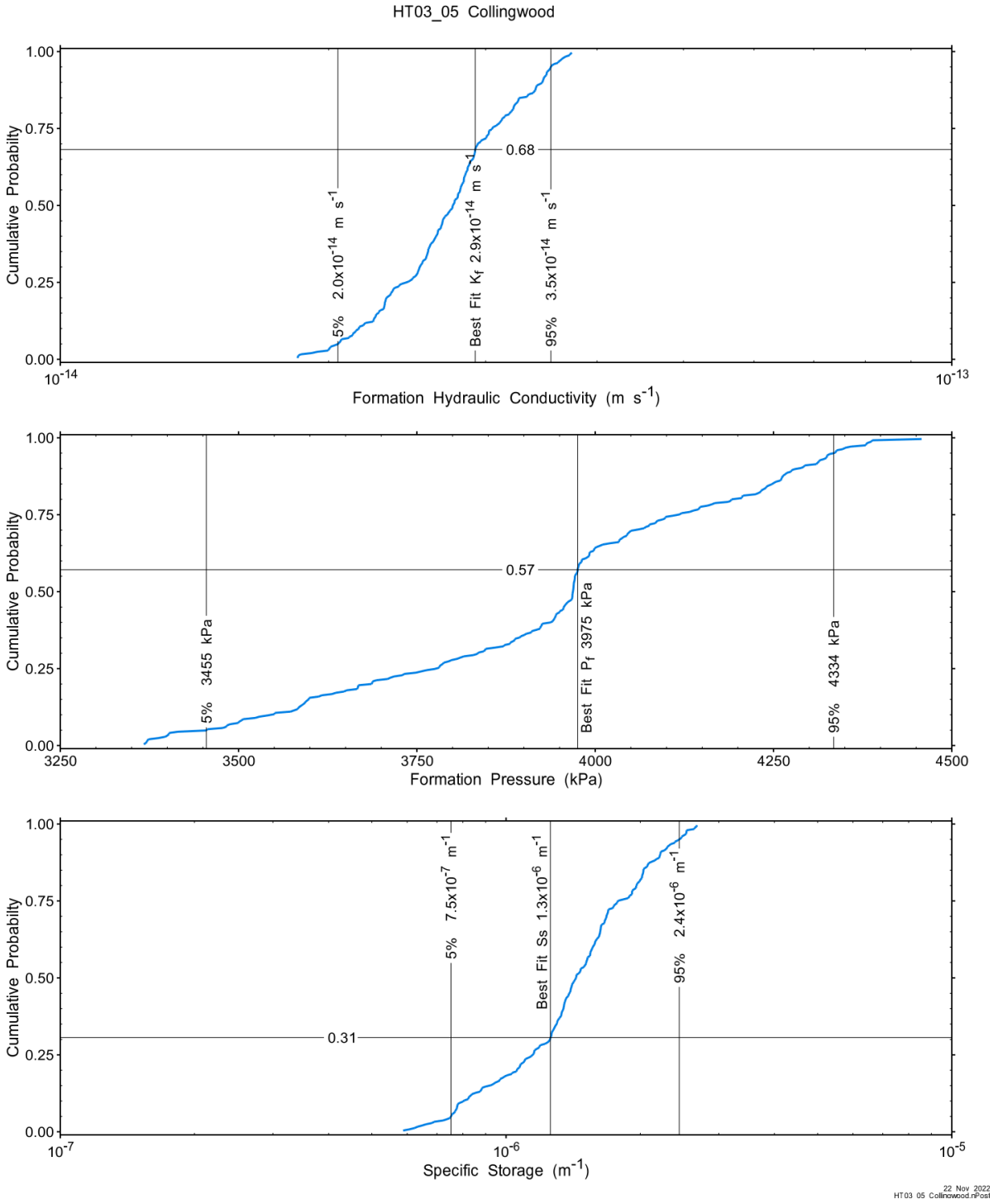

Figure A.42 – Cumulative distribution functions and parameter limits for formation hydraulic conductivity (K_f) (top panel), static formation pressure (P_f) (middle panel) and specific storage (Ss) (bottom panel).

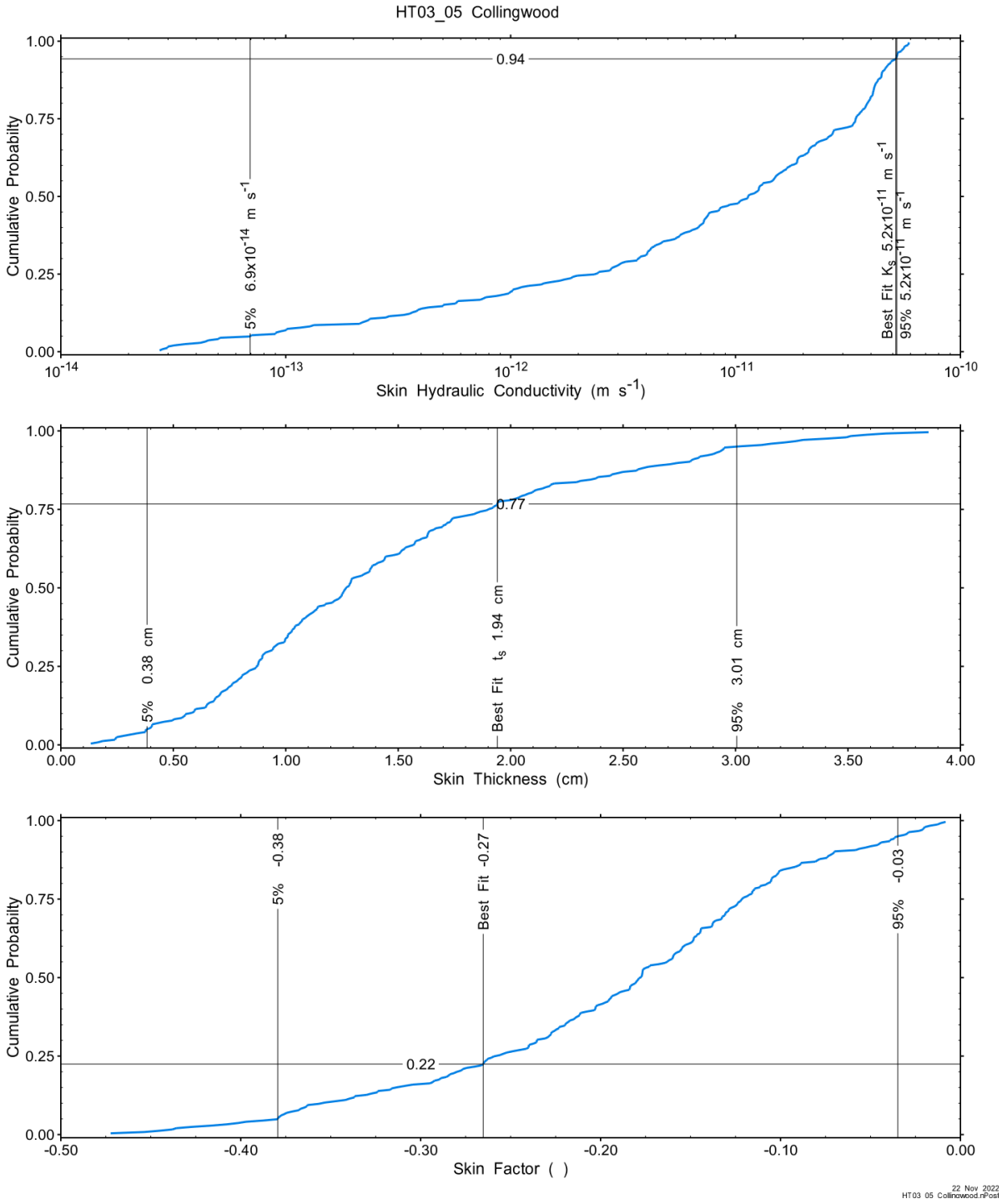

Figure A.43 – Cumulative distribution functions and parameter limits for skin hydraulic conductivity (K_s) (top panel), skin thickness (t_s) (middle panel) and skin factor (s) (bottom panel).

A summary of perturbation results is presented in Figure A.28, with Ramey-processed perturbations in Figure A.13. Those perturbations (192 of 10,000) with all parameters within the 5% and 95% range present a good fit to the measured test zone data.

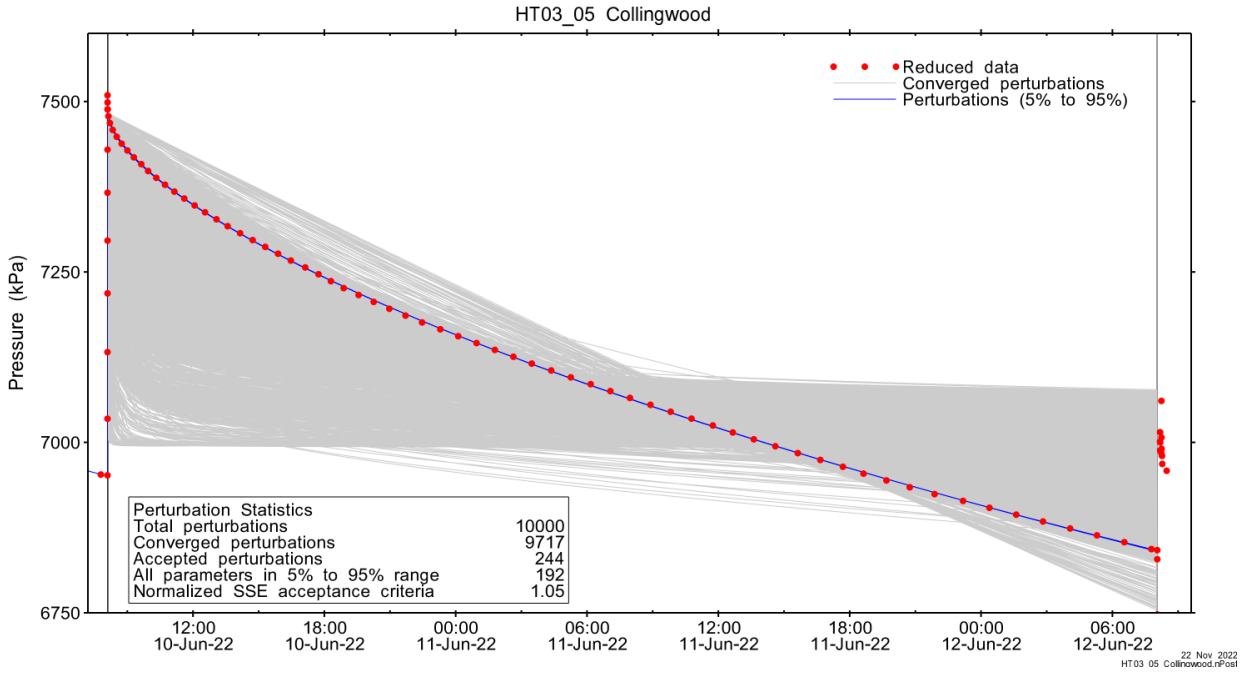

Figure A.44 – Perturbation results – all converged, accepted, and within 5% to 95% for all parameters.

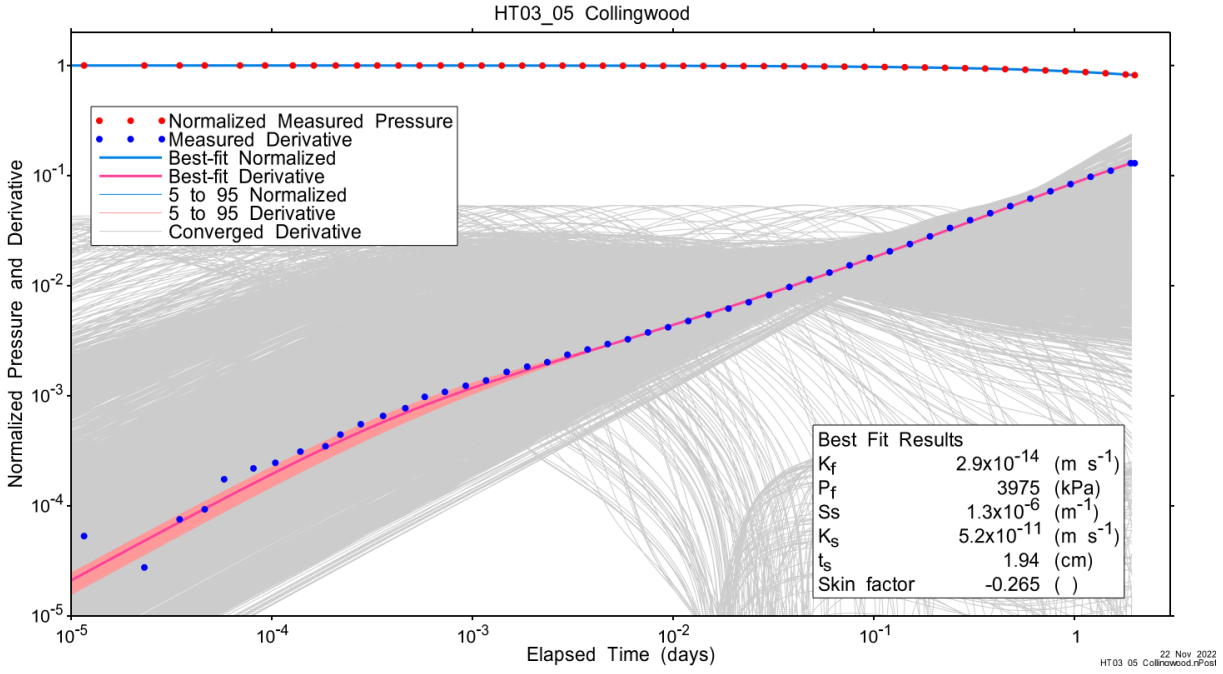

Figure A.45 – Log-log plot showing Ramey B and derivative response for all converged optimizations and those within 5% to 95% for all parameters.

A summary of best-fit and parameter ranges is given in Table A.9.

Table A.14 - Summary of the HT03_05 parameter estimates.

Parameter	Best Fit	5%	Median	95%
K_f (m/s)	2.9E-14	2.0E-14	2.8E-14	3.5E-14
P_f (kPa)	3975	3455	3969	4334
Ss (1/m)	1.3E-06	7.5E-07	1.4E-06	2.4E-06
K_s (m/s)	5.2E-11	6.9E-14	1.1E-11	5.2E-11
t_s (cm)	1.94	0.38	1.27	3.01
s (-)	-0.265	-0.379	-0.178	-0.035

Parameter correlations for all perturbations with all parameters within the 5% to 95% limits are given in Table A.5.

Table A.15 – Pearson cross-correlations of 5% to 95% parameters

	Log(K_f)	P_f	Log(Ss)	Log(K_s)	t_s	s
Log(K_f)	1.000	0.965	-0.992	0.164	0.830	-0.816
Pf	0.965	1.000	-0.949	-0.093	0.666	-0.643
Log(S_s)	-0.992	-0.949	1.000	-0.183	-0.864	0.845
Log(K_s)	0.164	-0.093	-0.183	1.000	0.628	-0.662
t_s	0.830	0.666	-0.864	0.628	1.000	-0.998
s	-0.816	-0.643	0.845	-0.662	-0.998	1.000

A.3.4 Additional Figures

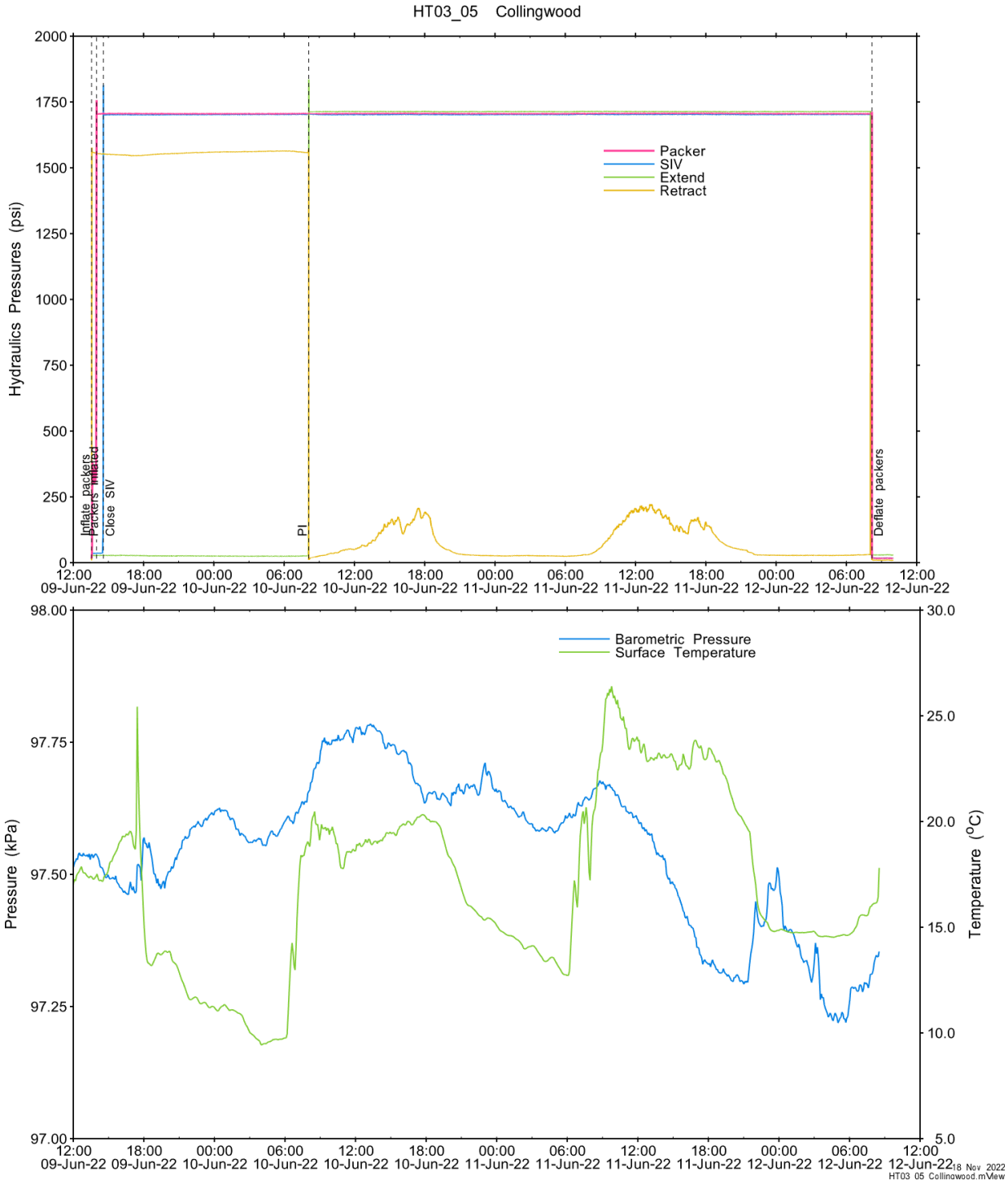

Figure A.46 - Hydraulics pressures and surface temperature/barometric pressure.

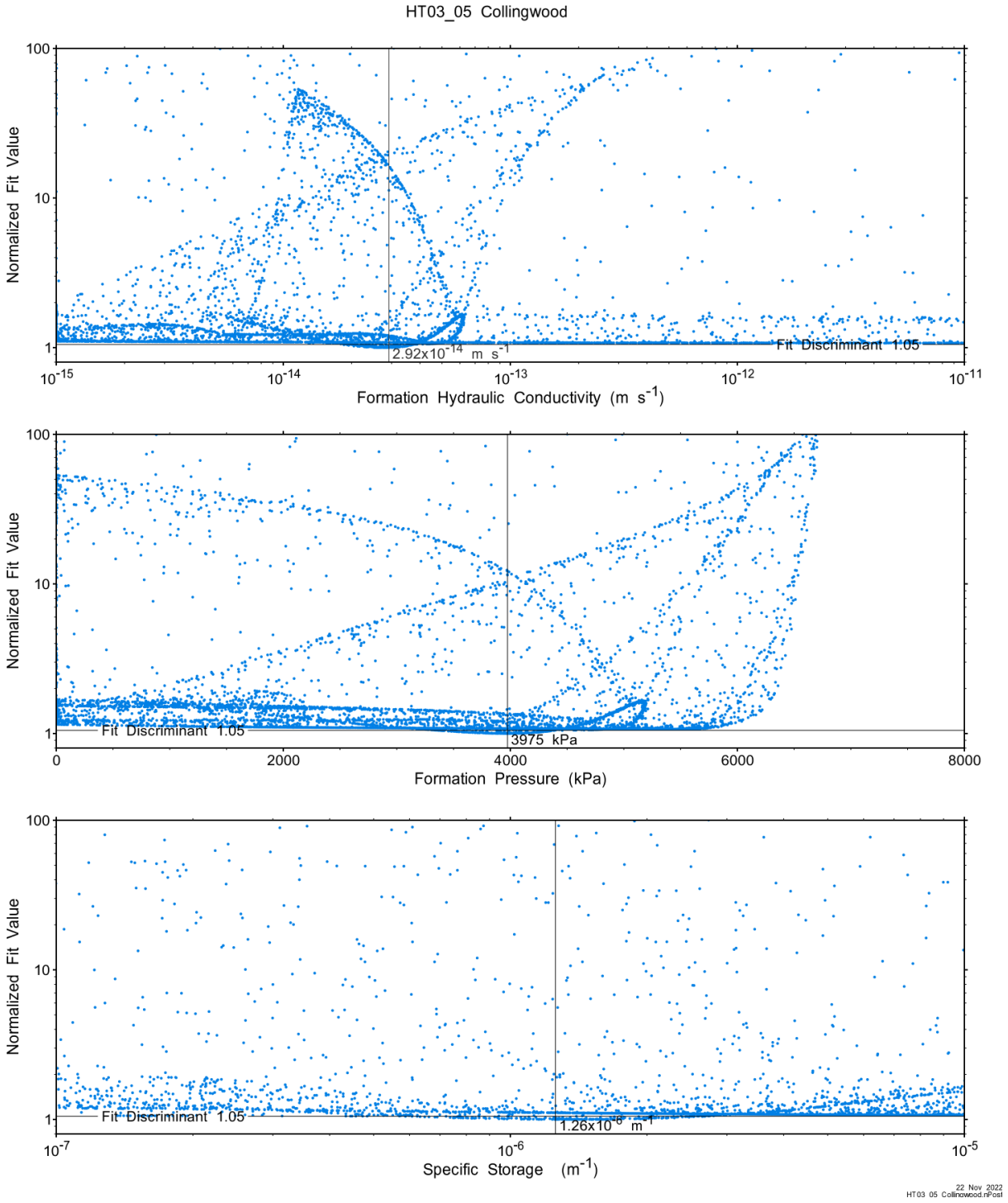

Figure A.47 - XY-scatter plot showing the formation parameter space normalized fit values.

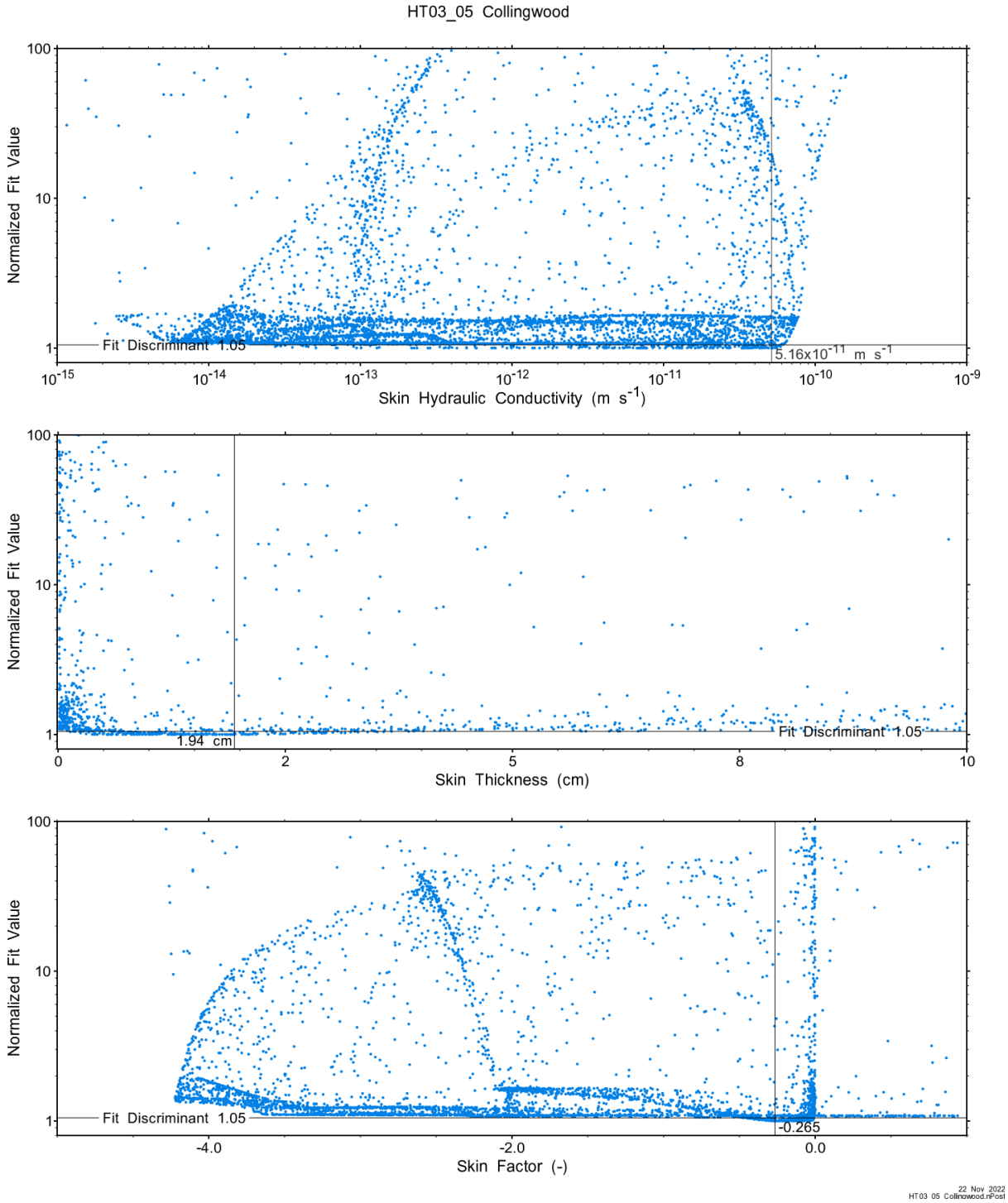

Figure A.48 - XY-scatter plot showing the skin parameter space normalized fit values.

A.4 HT04_05 Shadow Lake

The SB BH02 interval from 880.50 to 885.53 mBGS tested in HT04_05 covers the majority of the Shadow Lake Formation. An initial test was terminated early due to suspected leaks in the SIV. Packers remained inflated and the SIV was cycled several times. After shutting in, a two day duration PI was performed.

A.4.1 Test Data Summary

Table A.6 and Figure A.1 provide a summary of test events and a plot of pressures measured while testing respectively.

Table A.16 - Summary of Test Events.

Event	Start Date & Time	Duration (days)	TZ Pressure (kPa)
Drilling intercept	22-03-21 15:49	93.10	9205
Shut-in	22-06-22 18:08	0.60	9317
Pulse injection	22-06-23 08:29	2.00	9765
Test end	22-06-25 08:35		9060

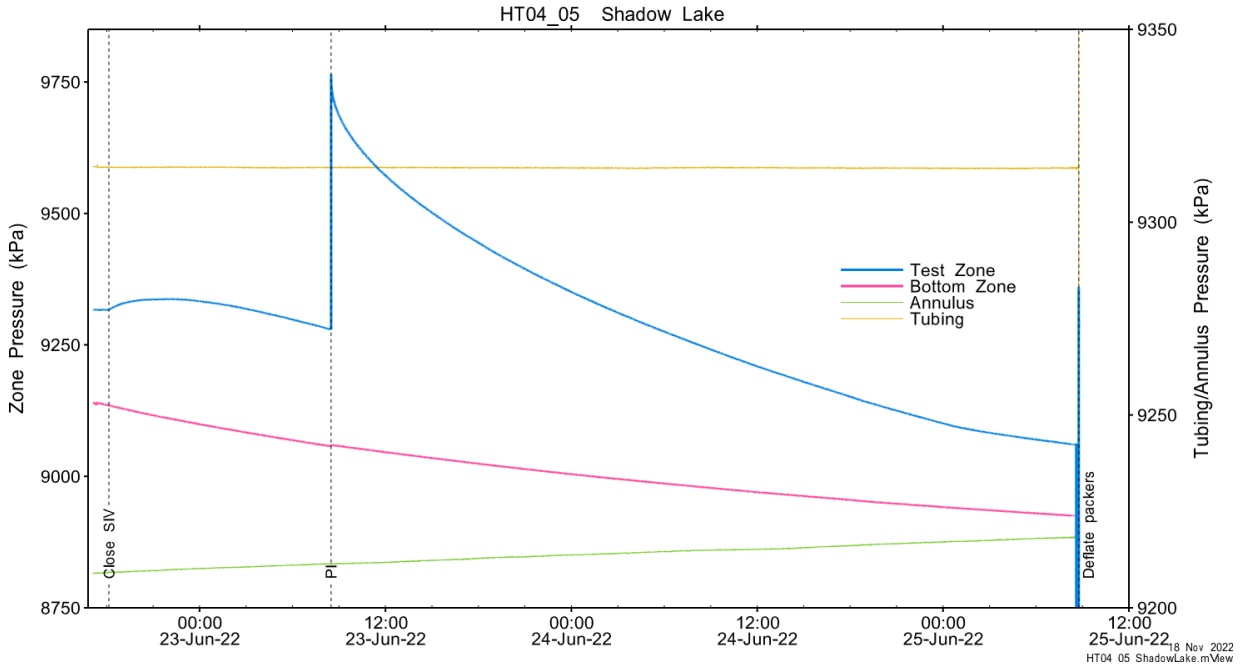

Figure A.49 - Test events and pressures.

A.4.2 Test Analyses

Table A.7 is a summary of test-specific input parameters used in the analyses, while Table A.8 presents the optimized parameters and allowed ranges.

Table A.17 – nSIGHTS Input Parameters.

Parameter	Value	Units
Test zone radius	6.25	cm
Test zone compressibility	4.28E-10	1/Pa
Test zone length	5.03	m

Table A.18 – nSIGHTS Parameter Optimization Ranges.

Parameter	Minimum	Maximum	Units	Type
Formation hydraulic conductivity (K_f)	1E-15	1E-07	m/s	log
Formation pressure (P_f)	4000	12000	kPa	linear
Specific storage (S_s)	1E-08	1E-04	1/m	log
Skin hydraulic conductivity (K_s)	1E-15	1E-07	m/s	log
Skin thickness (t_s)	0.013	1000	cm	linear

Figure A.18 shows the measured test zone pressure record (with reduced data density for clarity) used in the analysis along with the best-fit simulation and parameter values. The fitted test length was reduced by 7 hours to remove an anomalous late time response from the fit. Figure A.19 presents the pre-test history, and Figure A.20 shows the Ramey B normalized best-fit pressure and pressure derivatives.

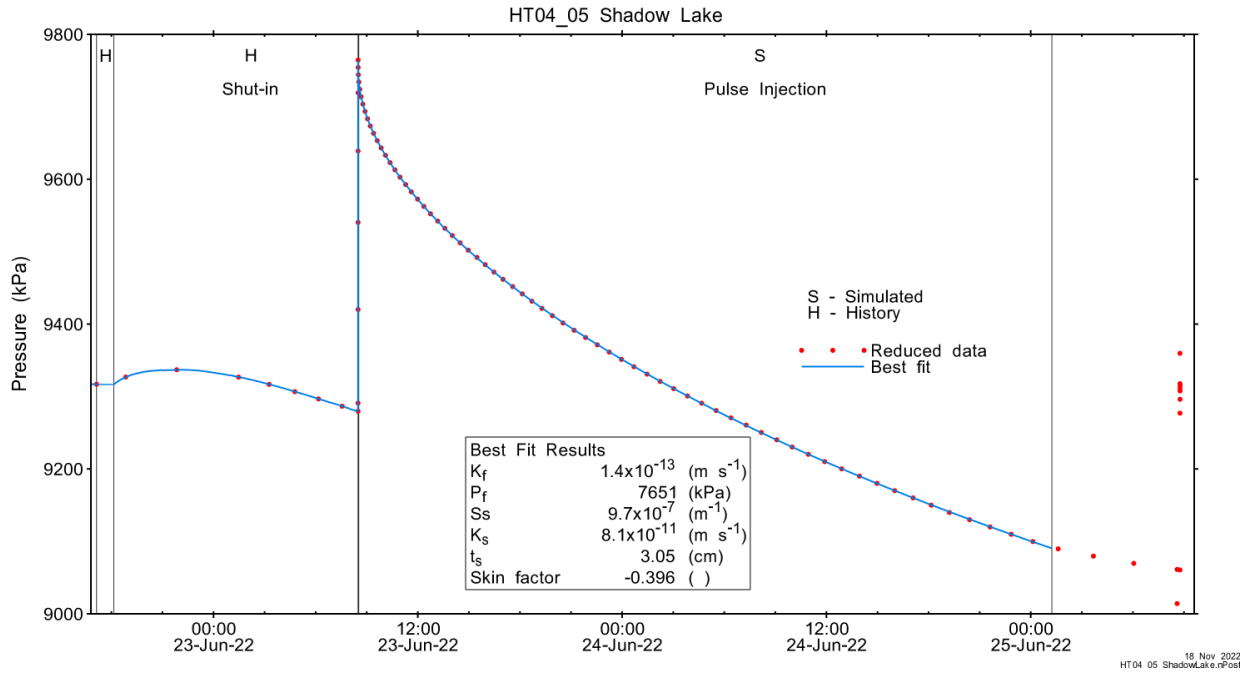

Figure A.50 - Annotated testing sequence showing best-fit simulation and parameter estimates.

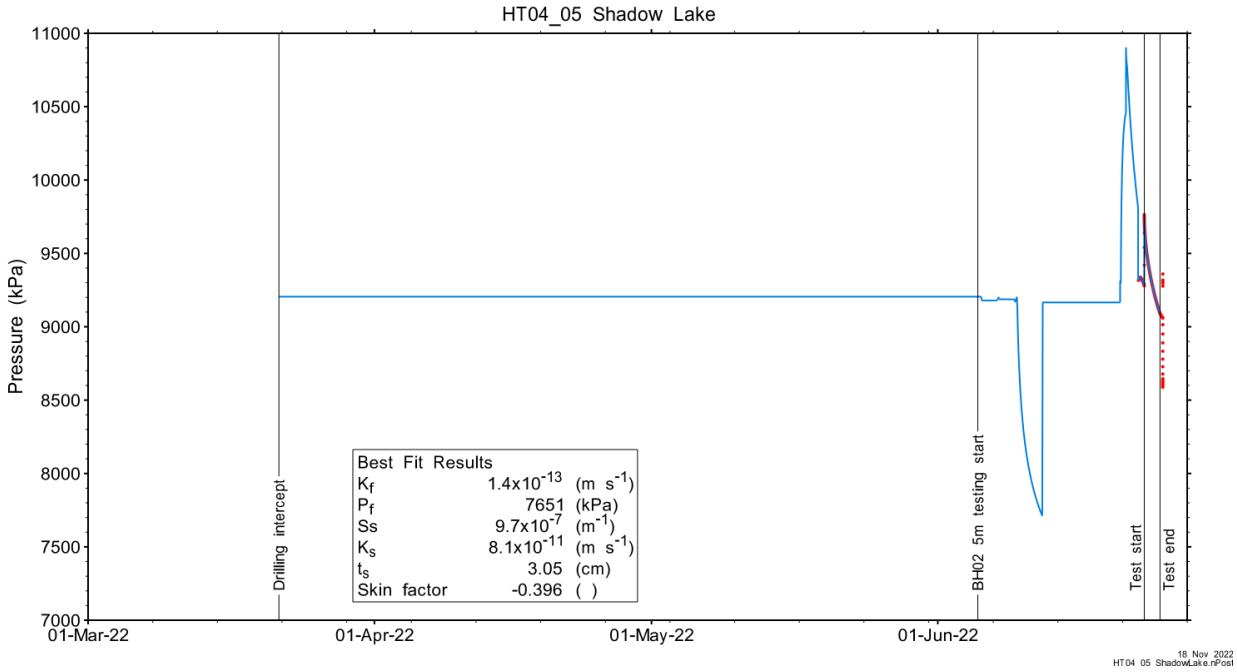

Figure A.51 - Annotated testing sequence showing pre-test history, best-fit simulation and parameter estimates.

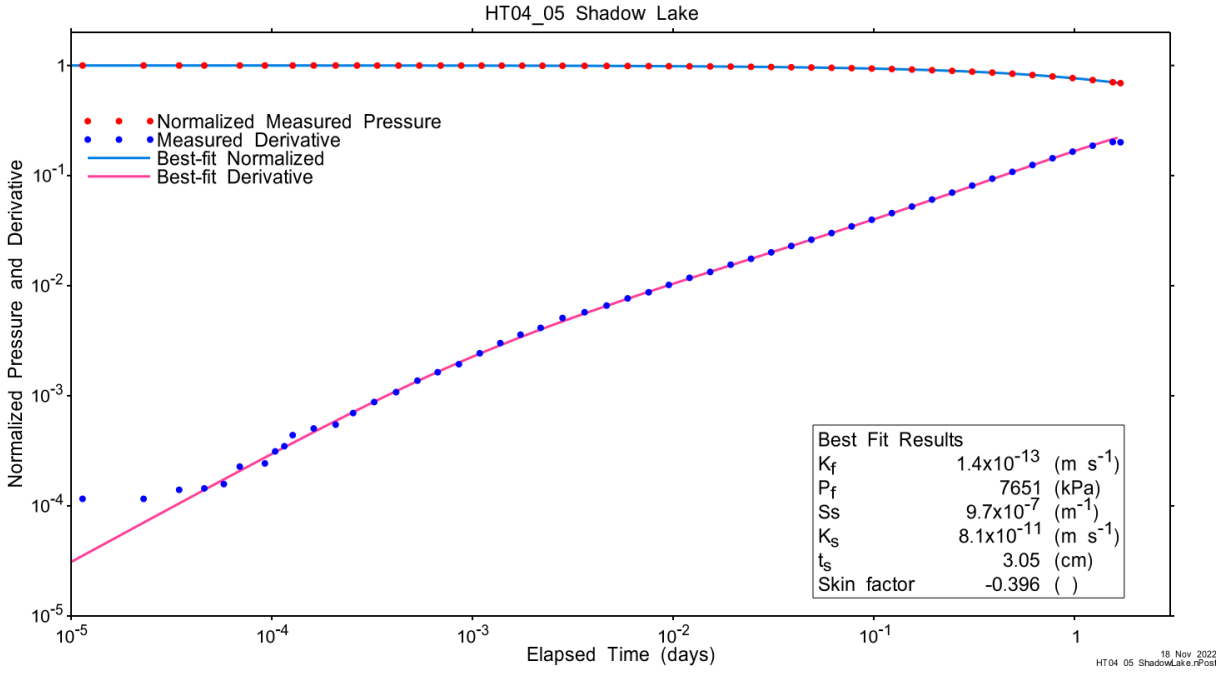

Figure A.52 - Log-log plot showing Ramey B and derivative response for best-fit simulation.

Figure A.21 shows the normalized parameter sensitivity response for the best fit. Sensitivity for most fitting parameters is increasing at the end of the test, indicating that more precise results may have been obtained with a longer test duration.

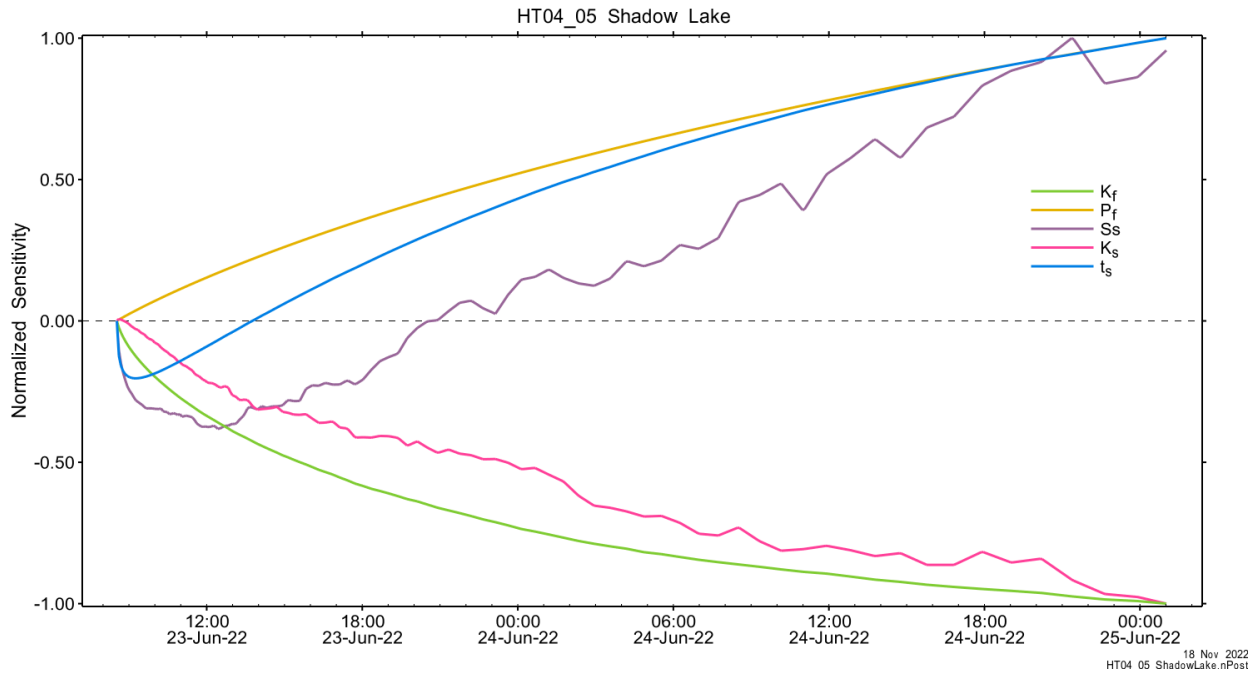

Figure A.53 - Normalized Jacobian for best-fit simulation.

A.4.3 Uncertainty Analyses

The CDF of normalized fit values for all converged simulations and the selected fit discriminant are shown in Figure A.22 and, in detail, in Figure A.23.

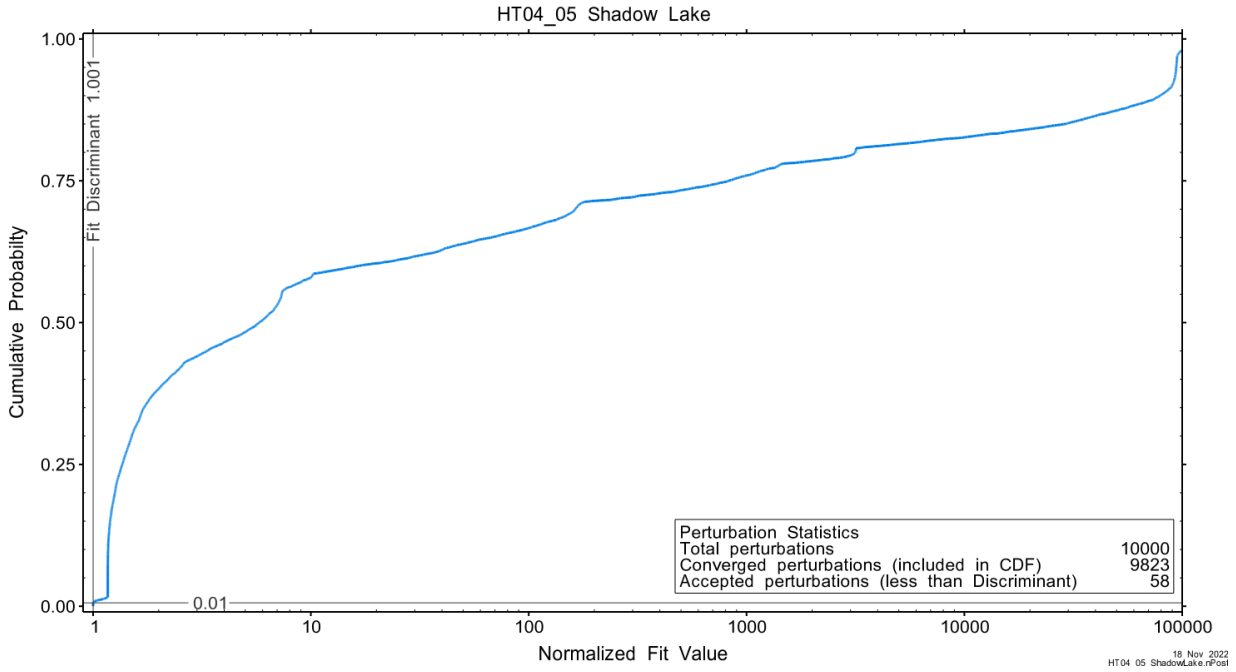

Figure A.54 - Fit value cumulative distribution function.

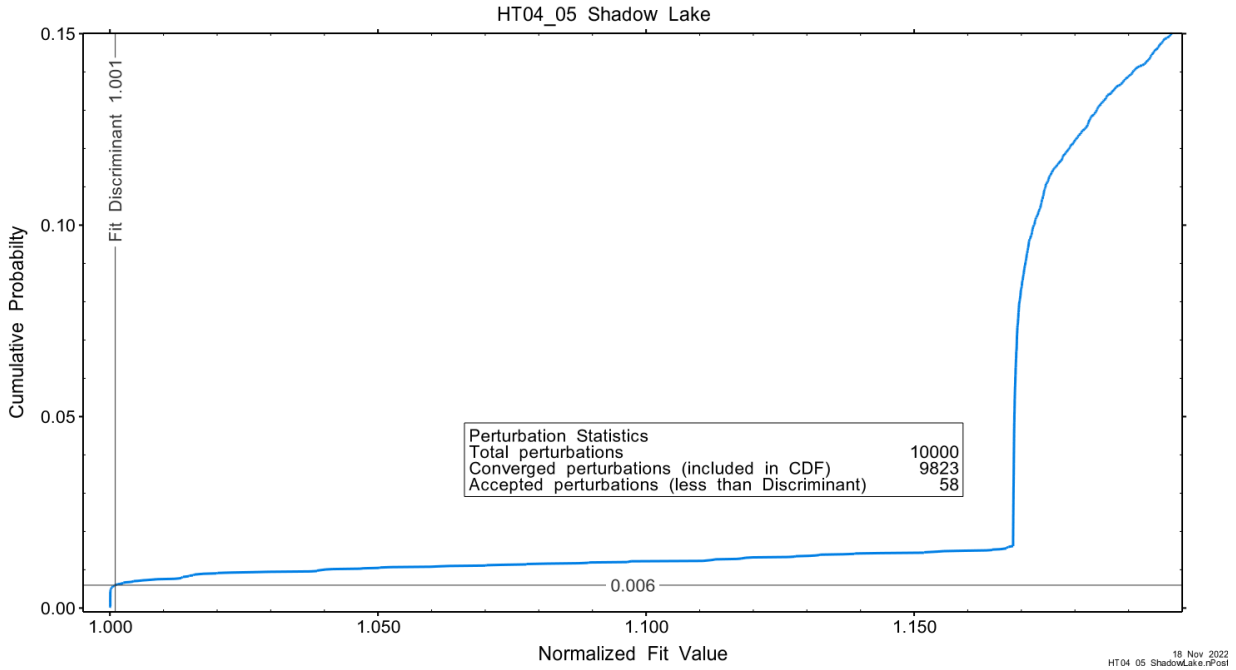

Figure A.55 – Detail of fit value cumulative distribution function.

Summary cross parameter scatter plots for selected formation and skin parameters are given in Figure A.24 and Figure A.25. The light pink dots on the figures are the initial parameter estimates, with red dots overlaying those initial parameter values that resulted in accepted optimization results. The grey dots are converged optimizations which did not meet the fit discriminant. Larger varying color symbols represent the fit value of accepted optimizations, with the blue values representing the best fit.

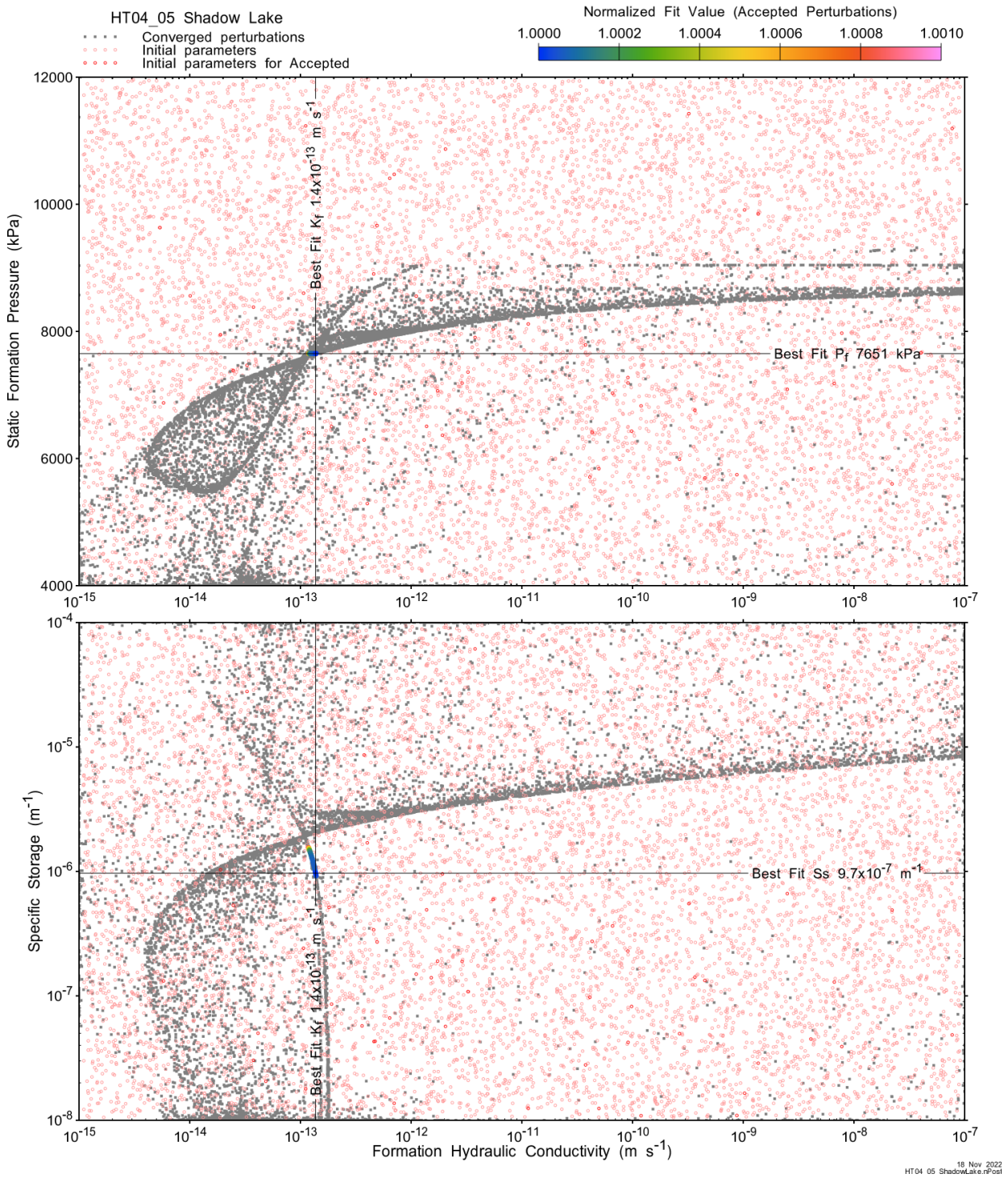

Figure A.56 - XY-scatter plot showing estimates of formation hydraulic conductivity (K_f) vs static formation pressure (P_f) (top panel) and specific storage (Ss) (bottom panel).

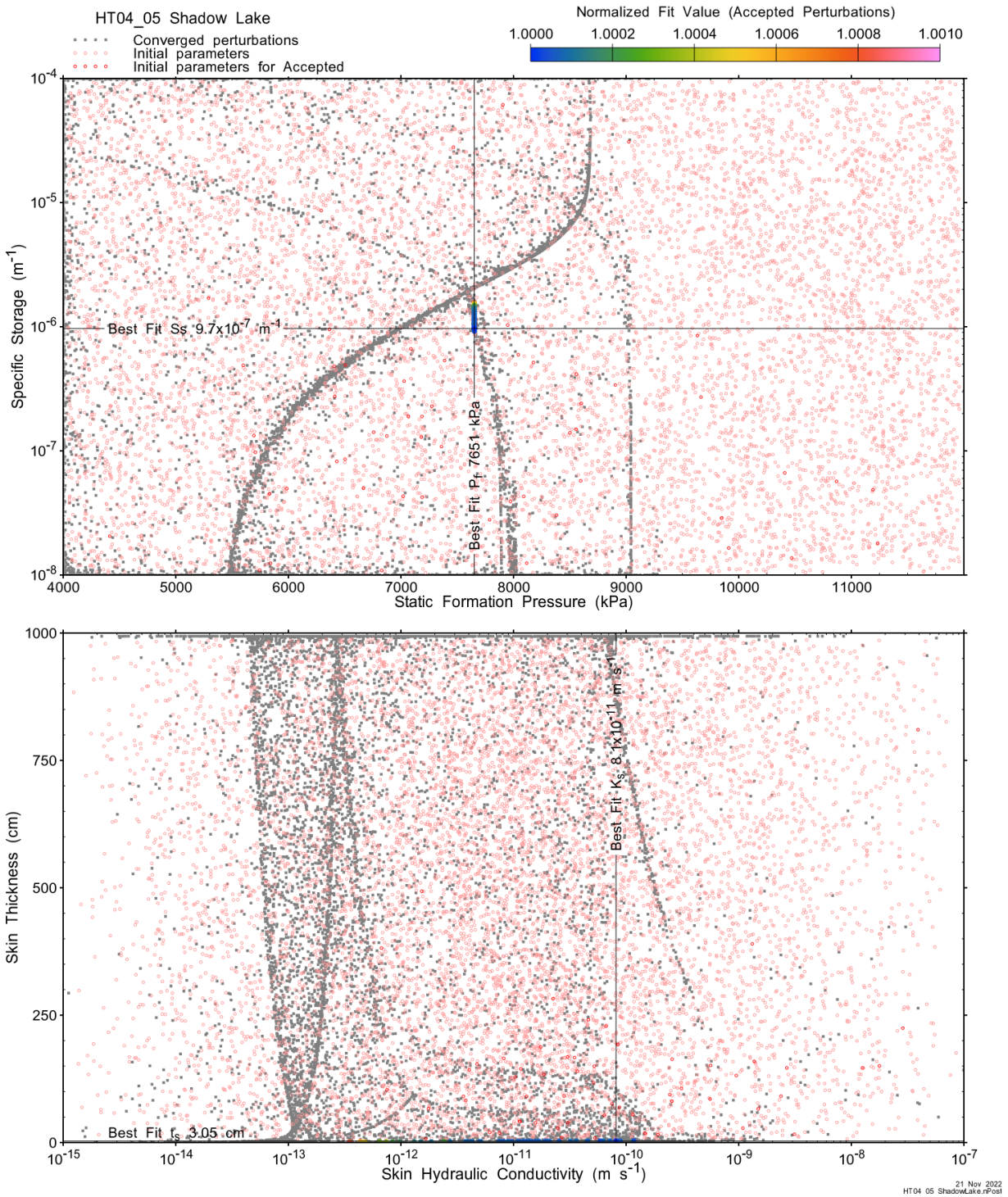

Figure A.57 - XY-scatter plot showing estimates of static formation pressure (P_f) vs specific storage (Ss) (top panel) and skin hydraulic conductivity (K_s) vs skin thickness (t_s) (bottom panel).

Confidence limits and median values are determined from the CDF of accepted optimization results (i.e. the varying color values in the above figures), with best fit value, 5% and 95% confidence indicated on Figure A.26 and Figure A.27.

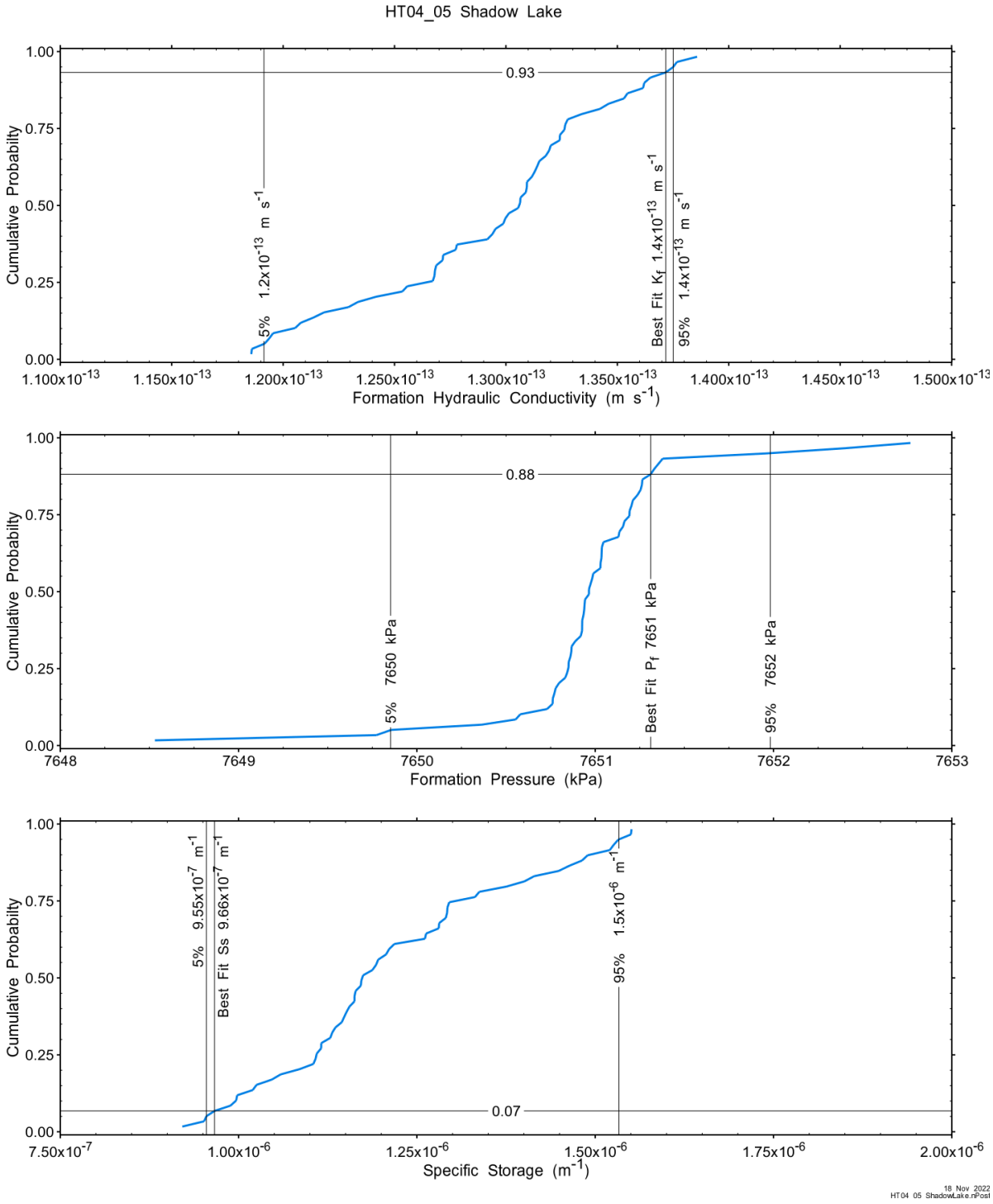

Figure A.58 – Cumulative distribution functions and parameter limits for formation hydraulic conductivity (K_f) (top panel), static formation pressure (P_f) (middle panel) and specific storage (Ss) (bottom panel).

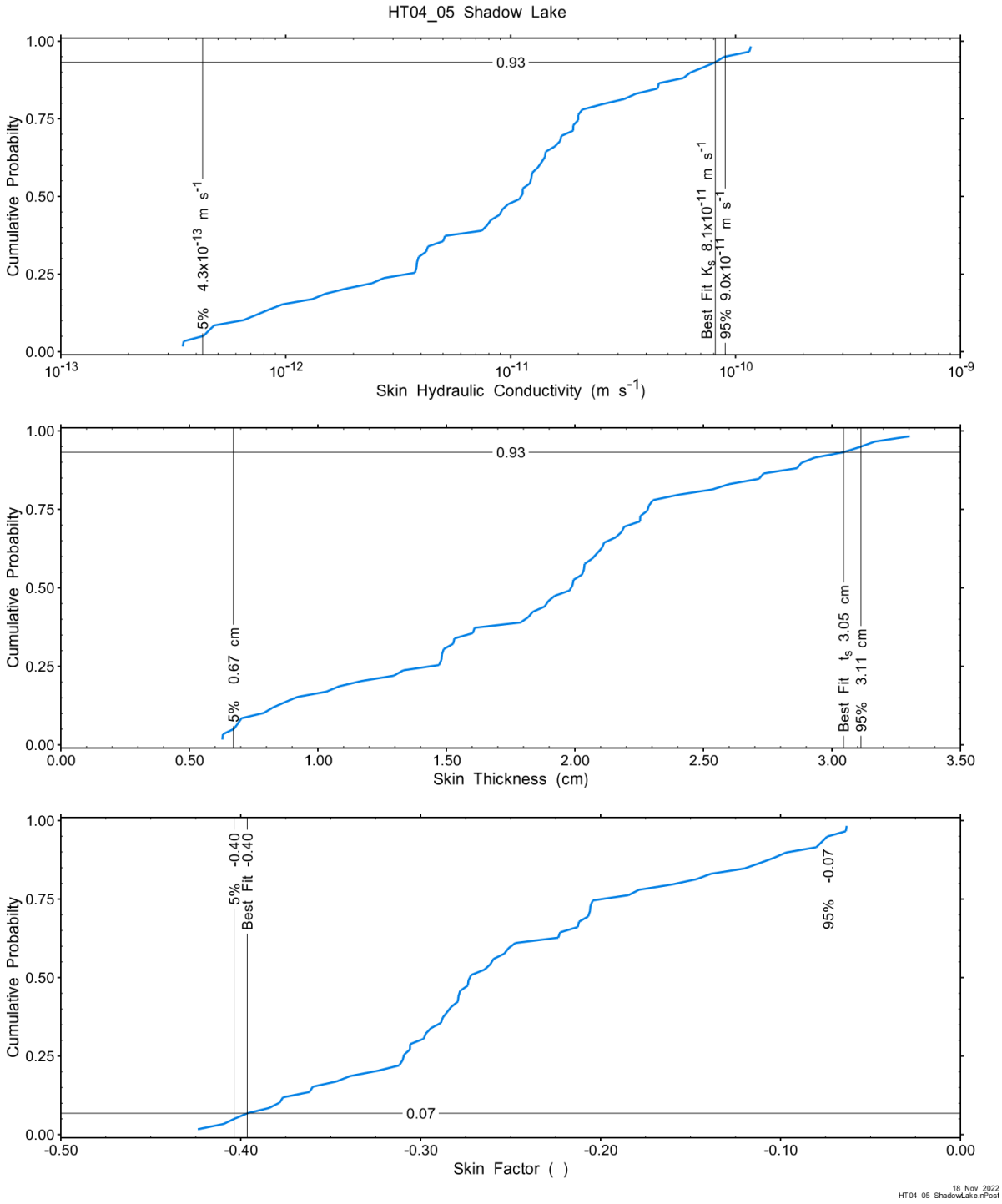

Figure A.59 – Cumulative distribution functions and parameter limits for skin hydraulic conductivity (K_s) (top panel), skin thickness (t_s) (middle panel) and skin factor (s) (bottom panel).

A summary of perturbation results is presented in Figure A.28, with Ramey-processed perturbations in Figure A.13. Those perturbations (52 of 10,000) with all parameters within the 5% and 95% range present an excellent fit to the measured test zone data.

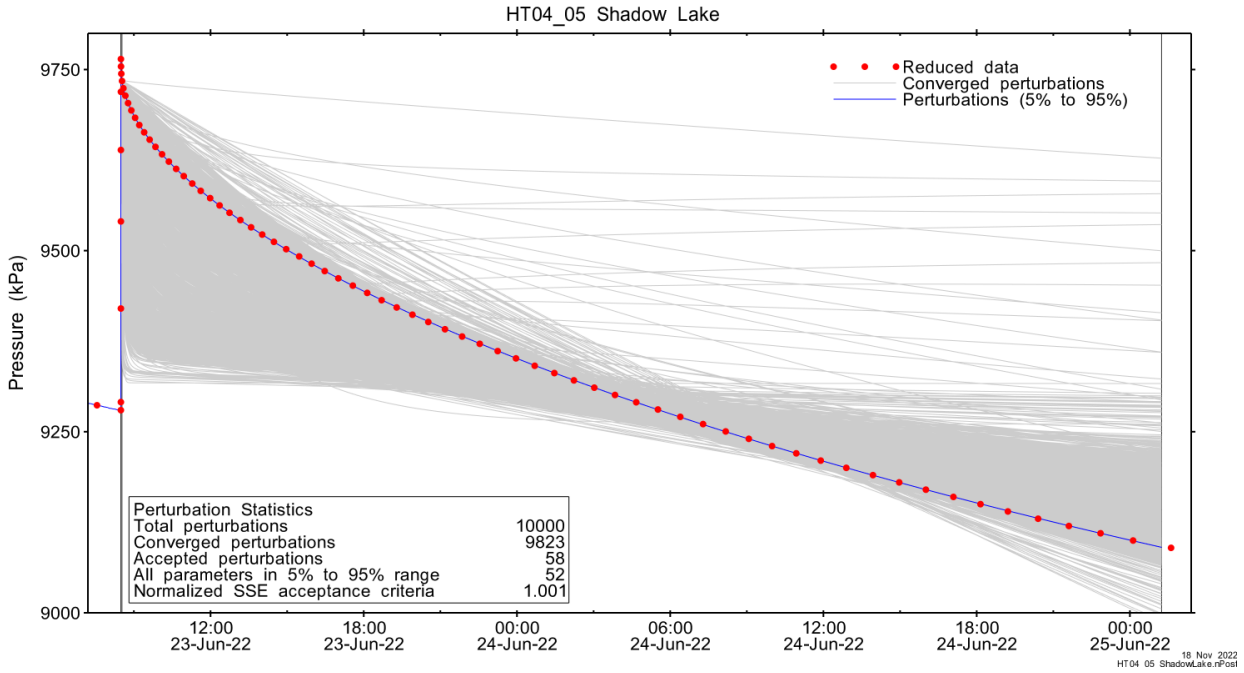

Figure A.60 – Perturbation results – all converged, accepted, and within 5% to 95% for all parameters.

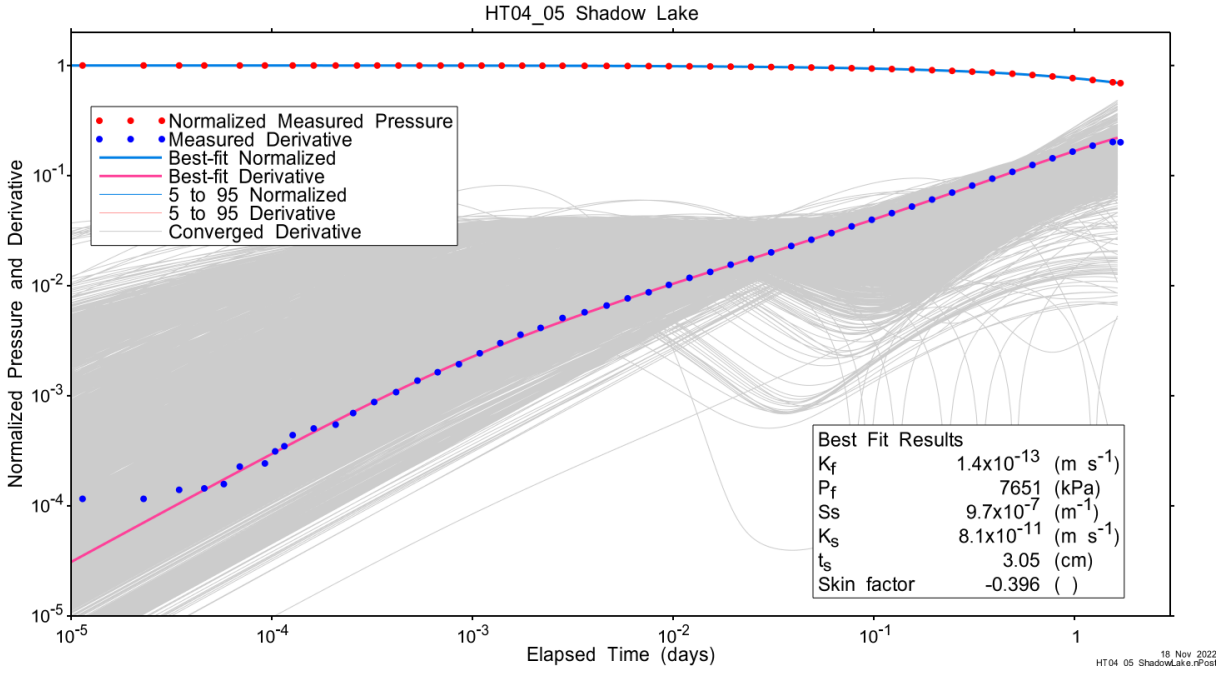

Figure A.61 – Log-log plot showing Ramey B and derivative response for all converged optimizations and those within 5% to 95% for all parameters.

A summary of best-fit and parameter ranges is given in Table A.9.

Table A.19 - Summary of the HT04_05 parameter estimates.

Parameter	Best Fit	5%	Median	95%
K_f (m/s)	1.4E-13	1.2E-13	1.3E-13	1.4E-13
P_f (kPa)	7651	7650	7651	7652
Ss (1/m)	9.7E-07	9.5E-07	1.2E-06	1.5E-06
K_s (m/s)	8.1E-11	4.3E-13	1.1E-11	9.0E-11
t_s (cm)	3.05	0.67	1.99	3.11
s (-)	-0.396	-0.404	-0.273	-0.074

Parameter correlations for all perturbations with all parameters within the 5% to 95% limits are given in Table A.5.

Table A.20 – Pearson cross-correlations of 5% to 95% parameters

	Log(K_f)	P_f	Log(Ss)	Log(K_s)	t_s	s
Log(K_f)	1.000	0.160	-0.996	0.999	0.992	-0.999
Pf	0.160	1.000	-0.183	0.160	0.187	-0.167
Log(S_s)	-0.996	-0.183	1.000	-0.998	-0.999	0.999
Log(K_s)	0.999	0.160	-0.998	1.000	0.996	-1.000
t_s	0.992	0.187	-0.999	0.996	1.000	-0.997
s	-0.999	-0.167	0.999	-1.000	-0.997	1.000

A.4.4 Additional Figures

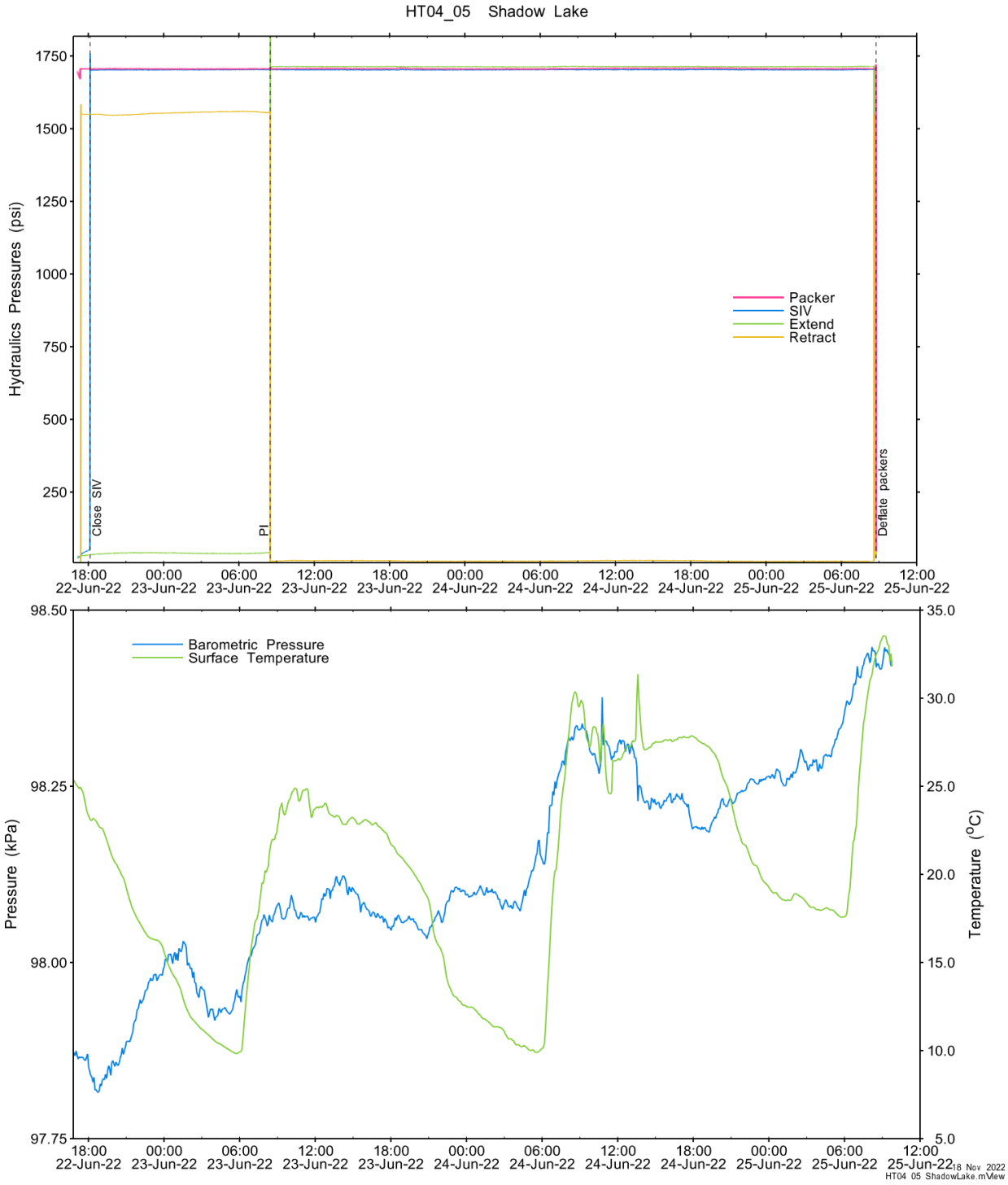

Figure A.62 - Hydraulics pressures and surface temperature/barometric pressure.

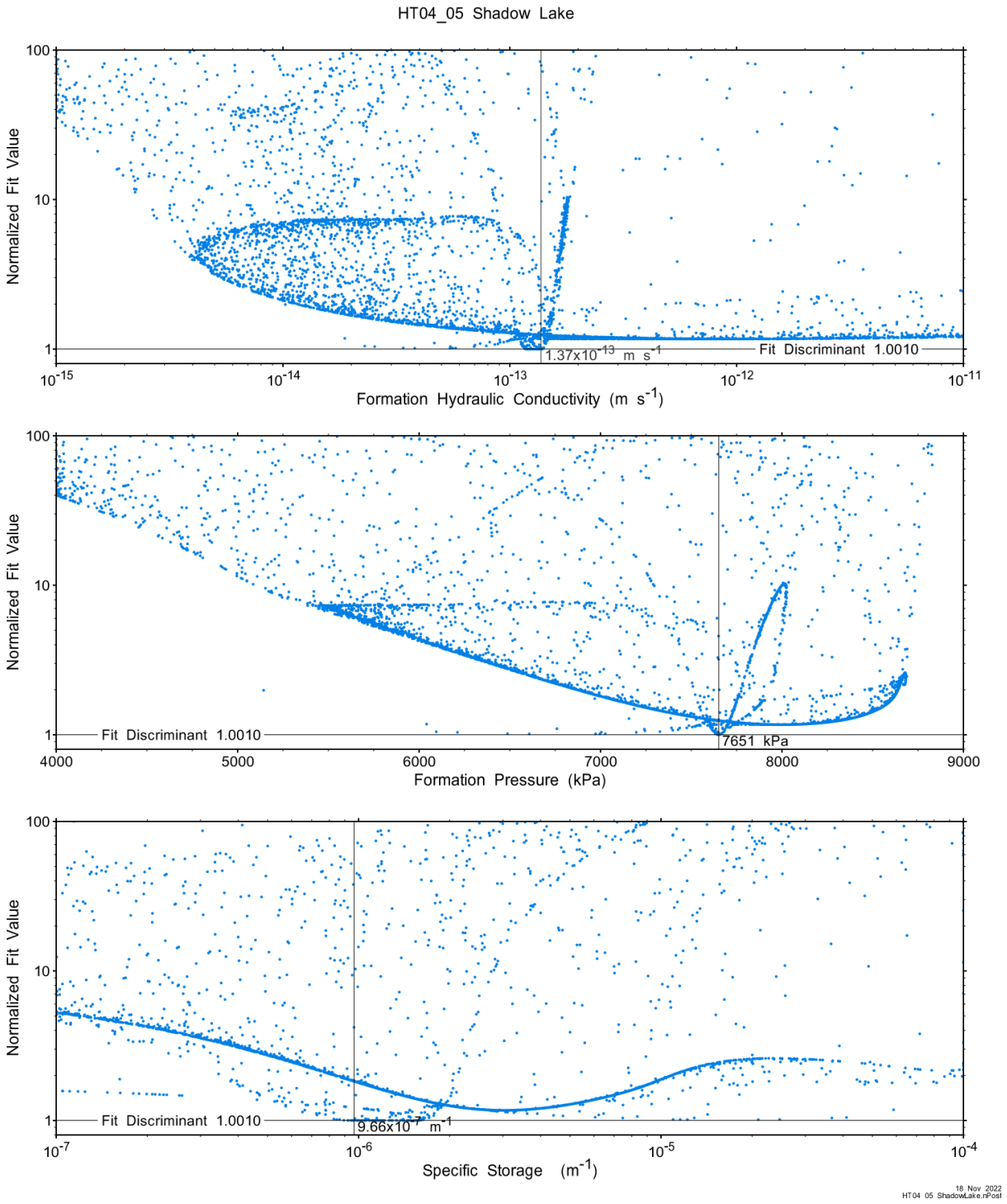

Figure A.63 - XY-scatter plot showing the formation parameter space normalized fit values.

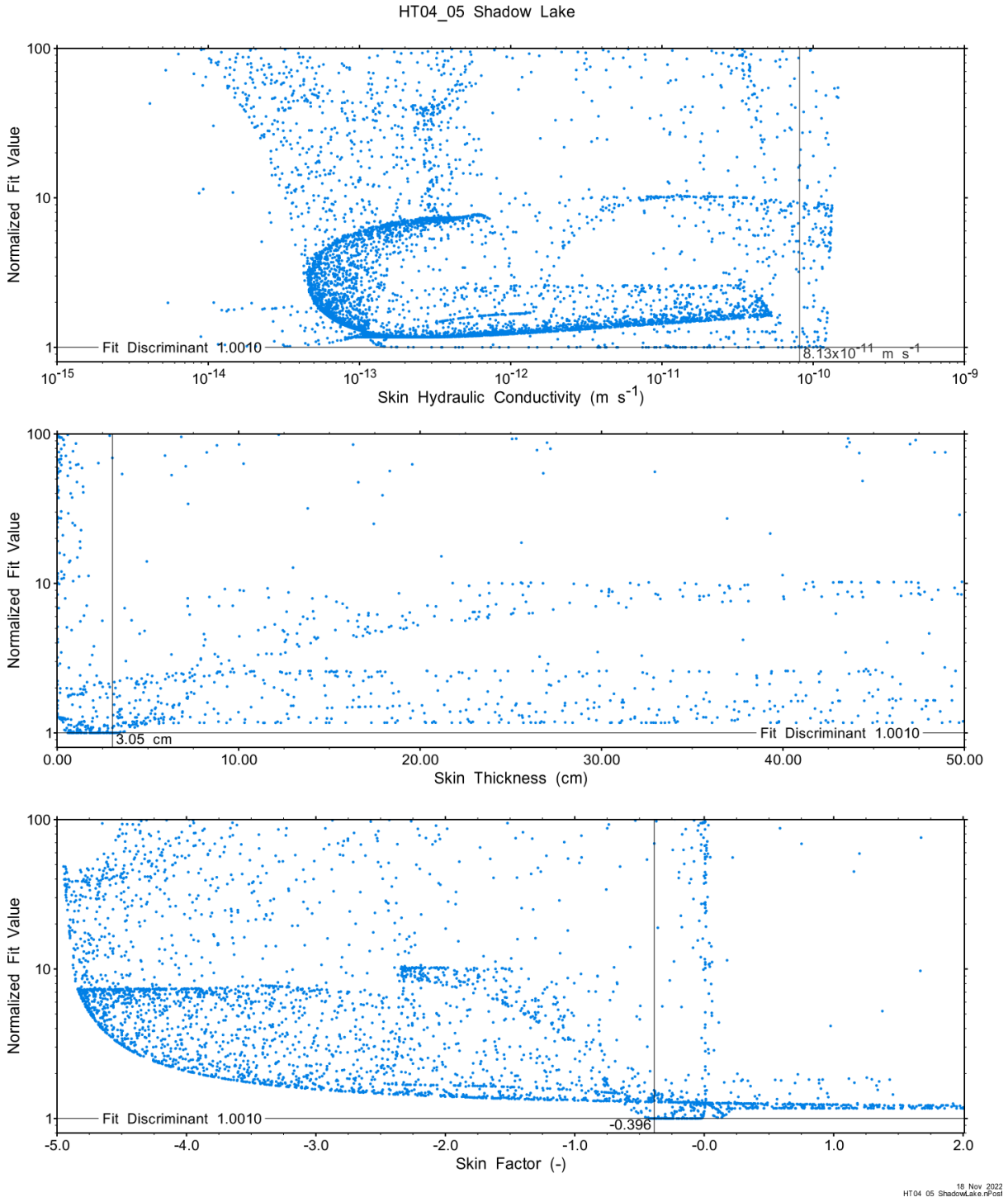

Figure A.64 - XY-scatter plot showing the skin parameter space normalized fit values.

A.5 HT05_05 PreCambrian

The SB BH02 HT05 test was originally planned to cover the interval from 887.00 to 892.03 mBGS. However, borehole conditions prevented access to the very bottom of the borehole, and the actual test interval was 886.81 to 891.48 mBGS. This covers the upper 5m of the PreCambrian. An initial test was terminated early due to suspected leaks in the SIV. Packers remained inflated and the SIV was cycled several times. After shutting in, a two day duration PI was performed.

A.5.1 Test Data Summary

Table A.6 and Figure A.1 provide a summary of test events and a plot of test-zone pressures measured while testing respectively. Figure A.66 shows the bottom zone pressure during the entire period the zone was isolated by inflated packers.

Table A.21 - Summary of Test Events.

Event	Start Date & Time	Duration (days)	TZ Pressure (kPa)
22-03-21 20:09	22-03-21 20:09	97.52	9294
22-06-27 08:42	22-06-27 08:42	0.14	9299
22-06-27 12:00	22-06-27 12:00	2.00	9877
22-06-29 11:58	22-06-29 11:58		9206

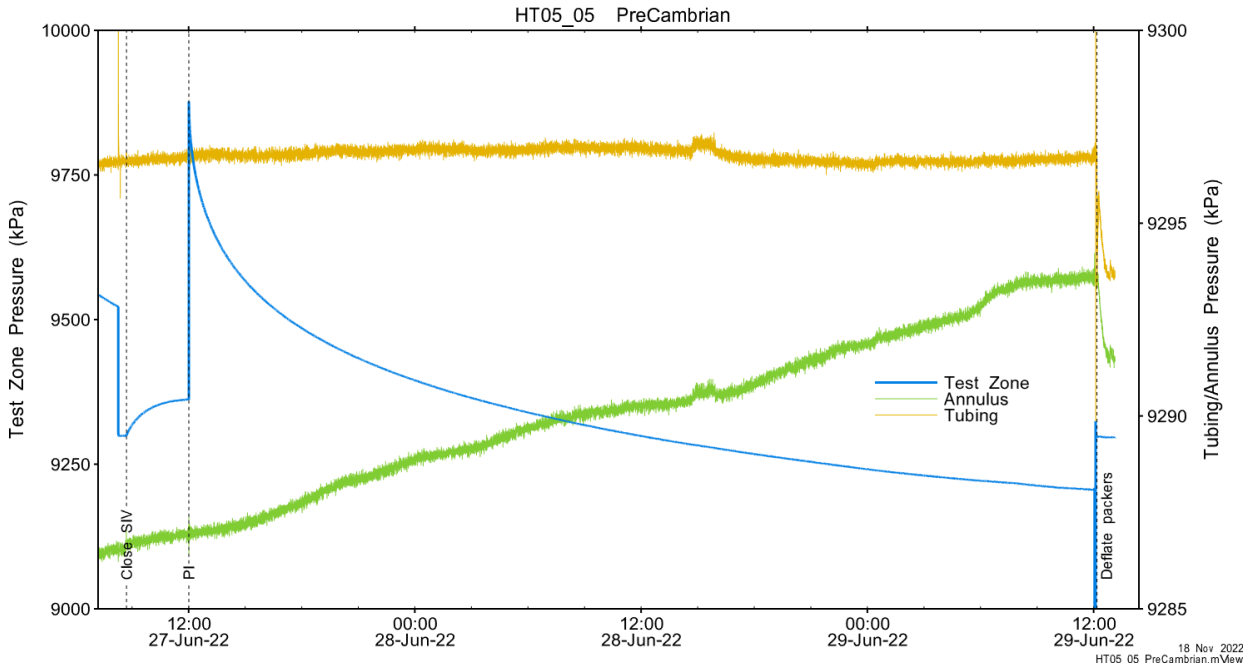

Figure A.65 - Test events and pressures.

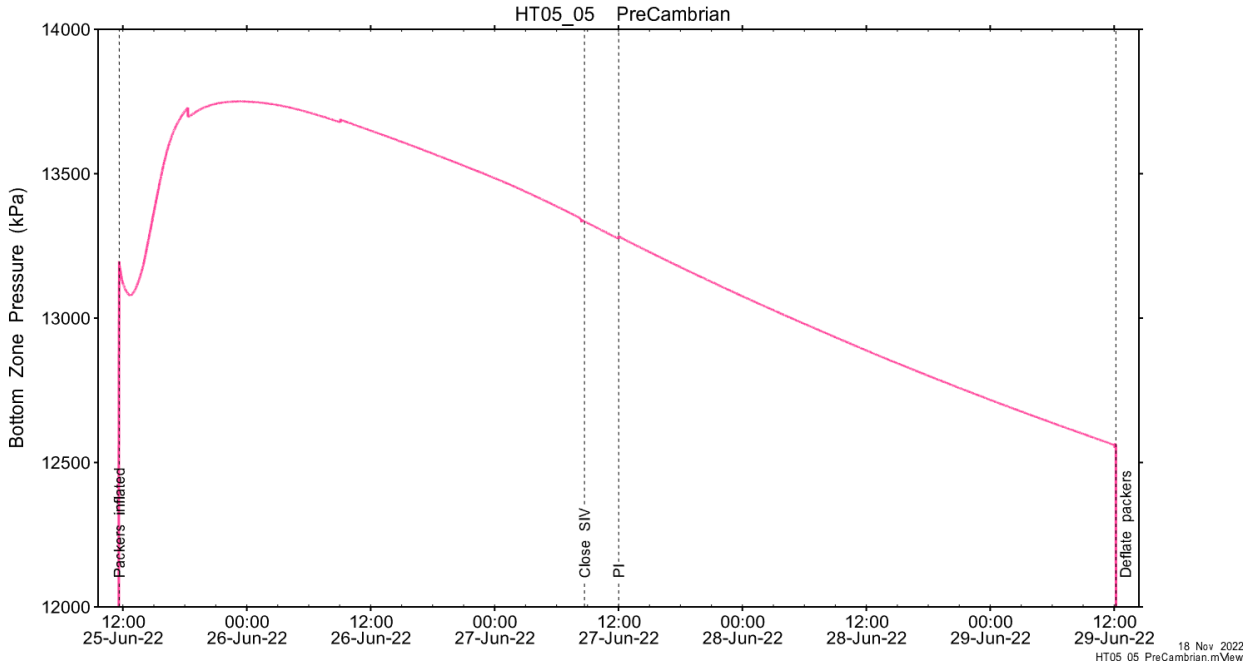

Figure A.66 – Bottom zone pressure while sealed by inflated packers.

A.5.2 Test Analyses

Table A.7 is a summary of test-specific input parameters used in the analyses, while Table A.8 presents the optimized parameters and allowed ranges.

Table A.22 – nSIGHTS Input Parameters.

Parameter	Value	Units
Test zone radius	6.12	cm
Test zone compressibility	4.18E-10	1/Pa
Test zone length	5.03	m

Table A.23 – nSIGHTS Parameter Optimization Ranges.

Parameter	Minimum	Maximum	Units	Type
Formation hydraulic conductivity (K_f)	1E-15	1E-06	m/s	log
Formation pressure (P_f)	4000	12000	kPa	linear
Specific storage (S_s)	1E-08	1E-04	1/m	log
Skin hydraulic conductivity (K_s)	1E-15	1E-06	m/s	log
Skin thickness (t_s)	0.013	1000	cm	linear

Figure A.18 shows the measured test zone pressure record (with reduced data density for clarity) used in the analysis along with the best-fit simulation and parameter values. Figure A.19 presents the pre-test history, and Figure A.20 shows the Ramey B normalized best-fit pressure and pressure derivatives.

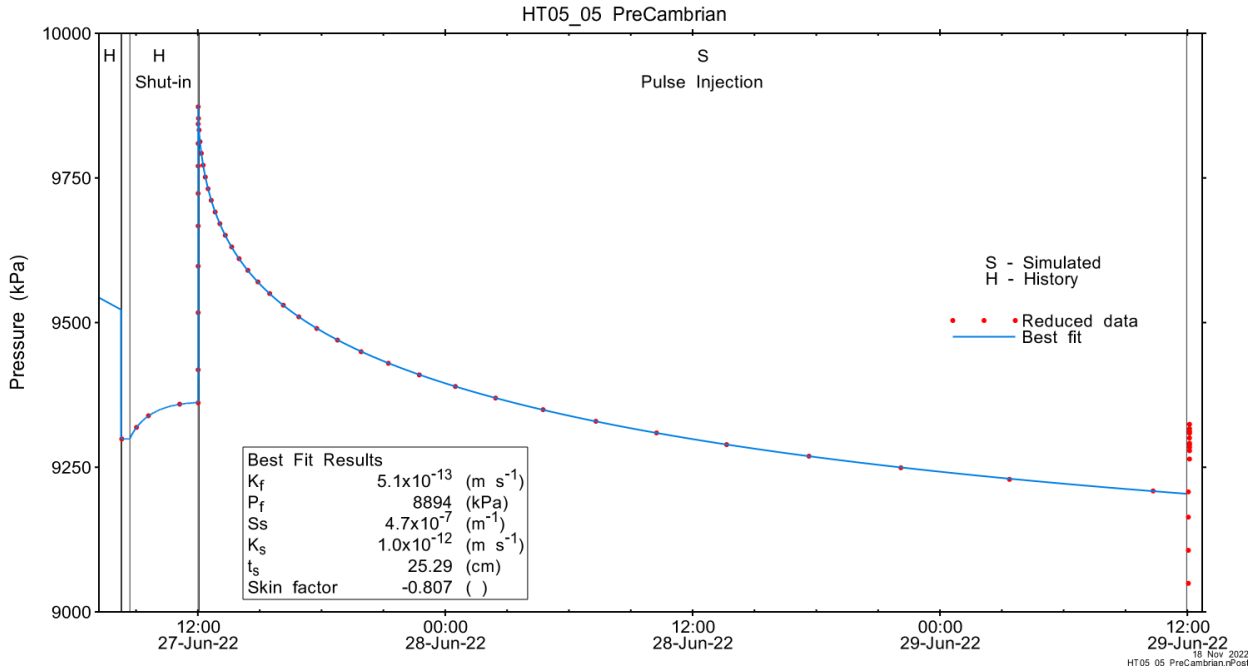

Figure A.67 - Annotated testing sequence showing best-fit simulation and parameter estimates.

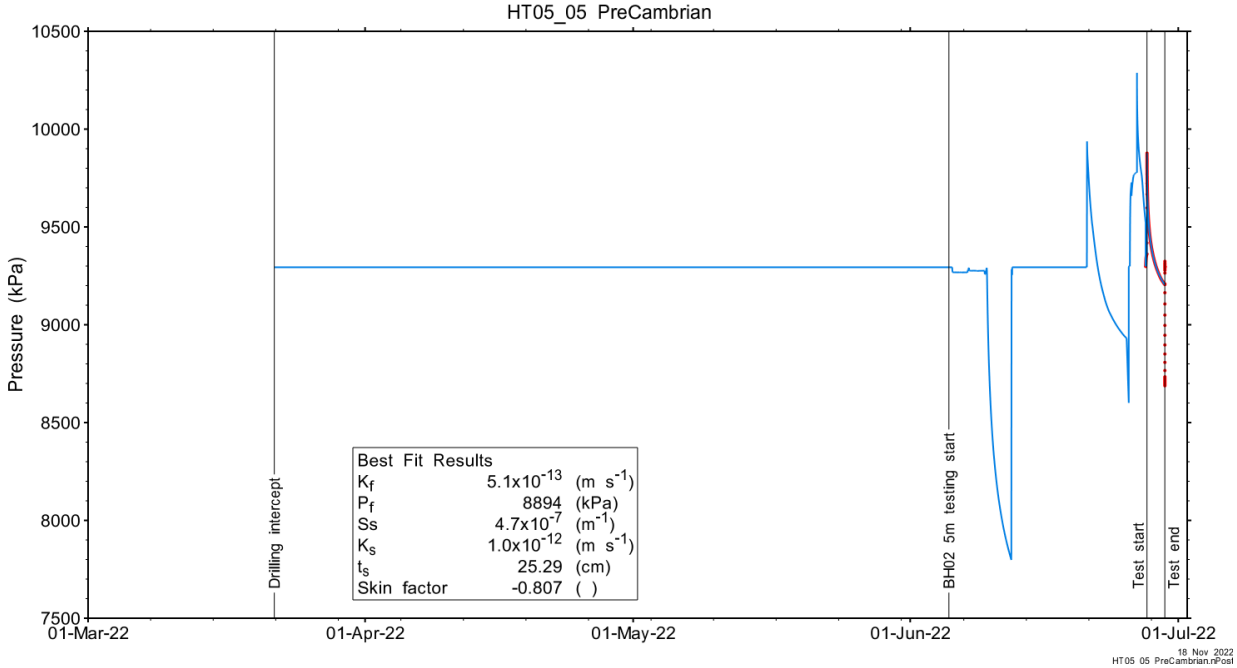

Figure A.68 - Annotated testing sequence showing pre-test history, best-fit simulation and parameter estimates.

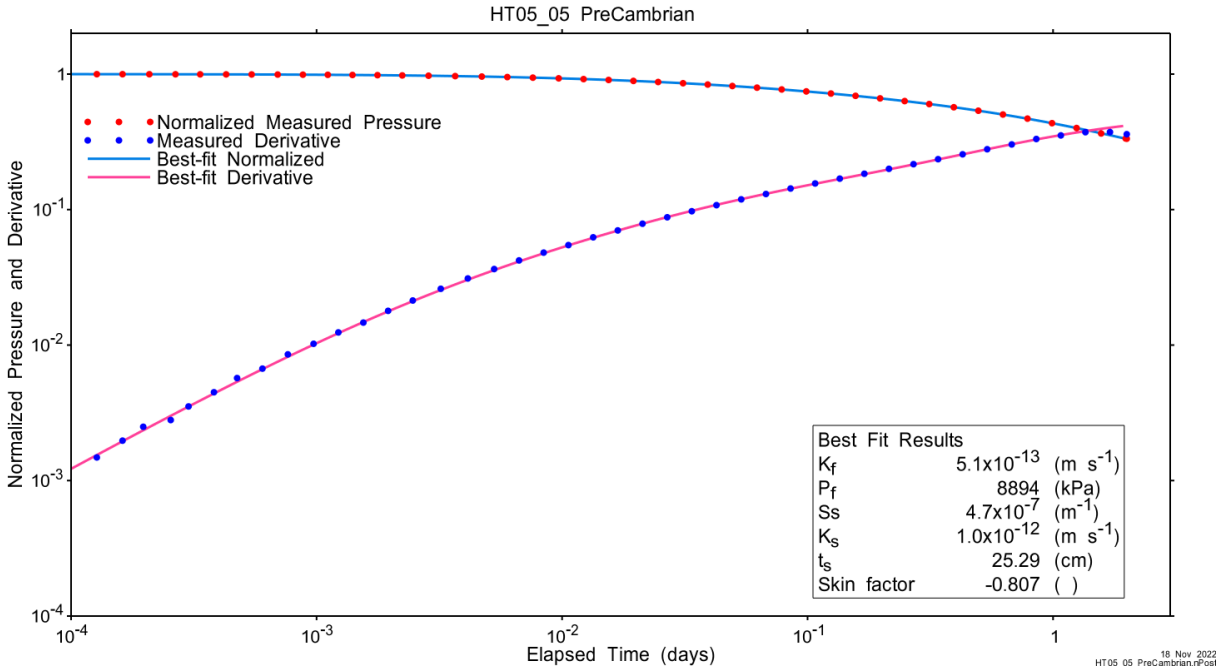

Figure A.69 - Log-log plot showing Ramey B and derivative response for best-fit simulation.

Figure A.21 shows the normalized parameter sensitivity response for the best fit. Sensitivity for most fitting parameters is increasing at the end of the test, indicating that more precise results may have been be obtained with a longer test duration.

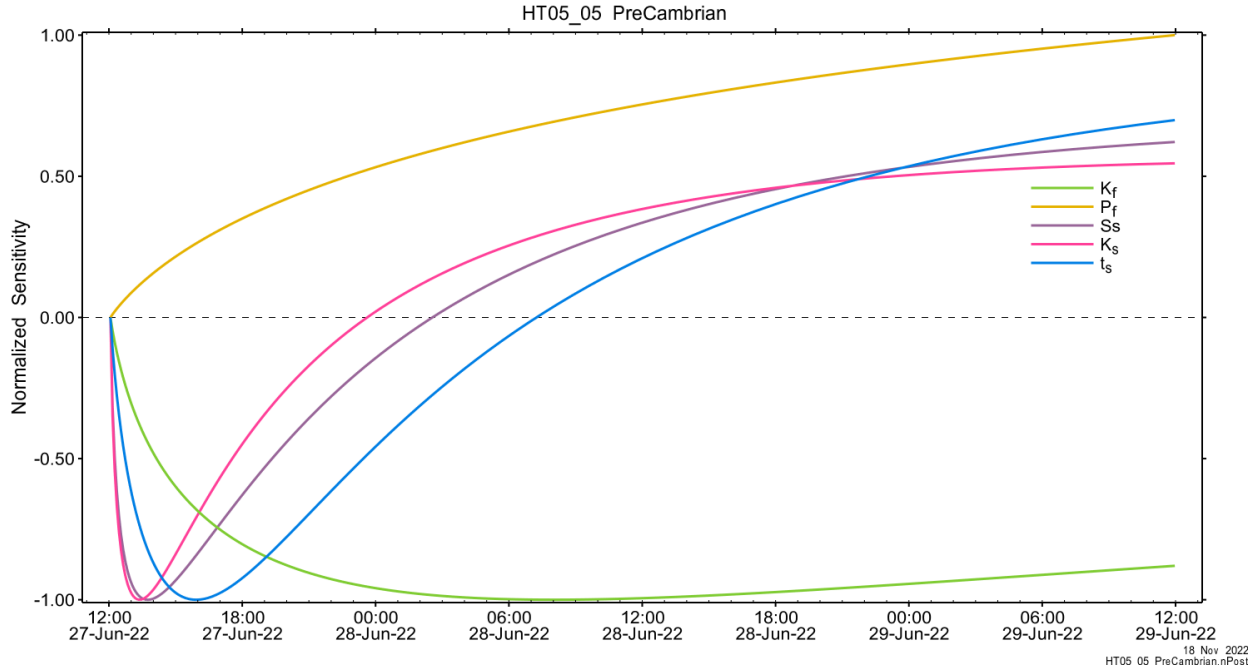

Figure A.70 - Normalized Jacobian for best-fit simulation.

A.5.3 Uncertainty Analyses

The CDF of normalized fit values for all converged simulations and the selected fit discriminant are shown in Figure A.22 and, in detail, in Figure A.23.

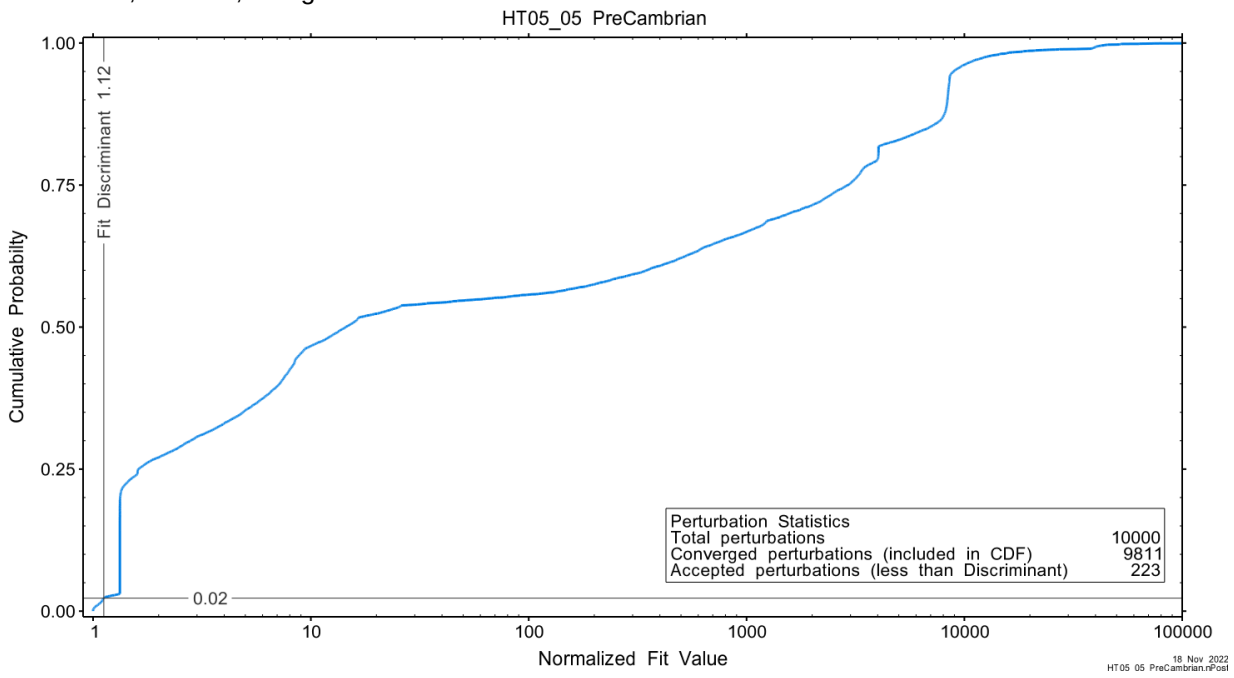

Figure A.71 - Fit value cumulative distribution function.

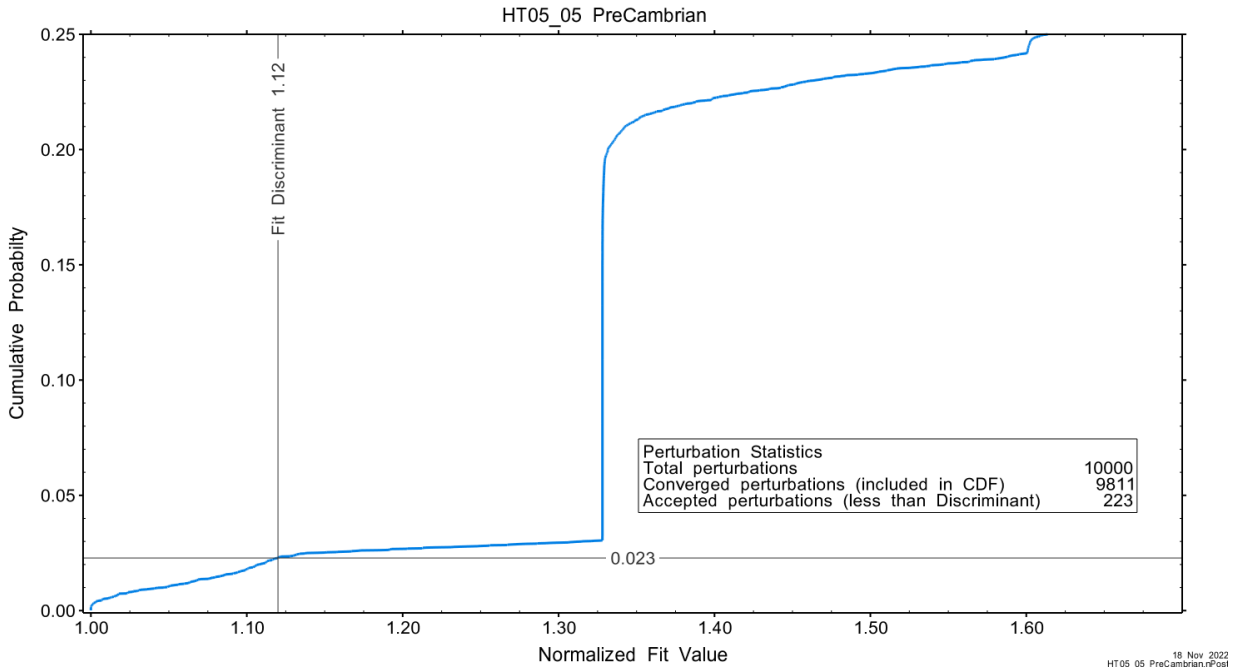

Figure A.72 – Detail of fit value cumulative distribution function.

Summary cross parameter scatter plots for selected formation and skin parameters are given in Figure A.24 and Figure A.25. The light pink dots on the figures are the initial parameter estimates, with red dots overlaying those initial parameter values that resulted in accepted optimization results. The grey dots are converged optimizations which did not meet the fit discriminant. Larger varying color symbols represent the fit value of accepted optimizations, with the blue values representing the best fit.

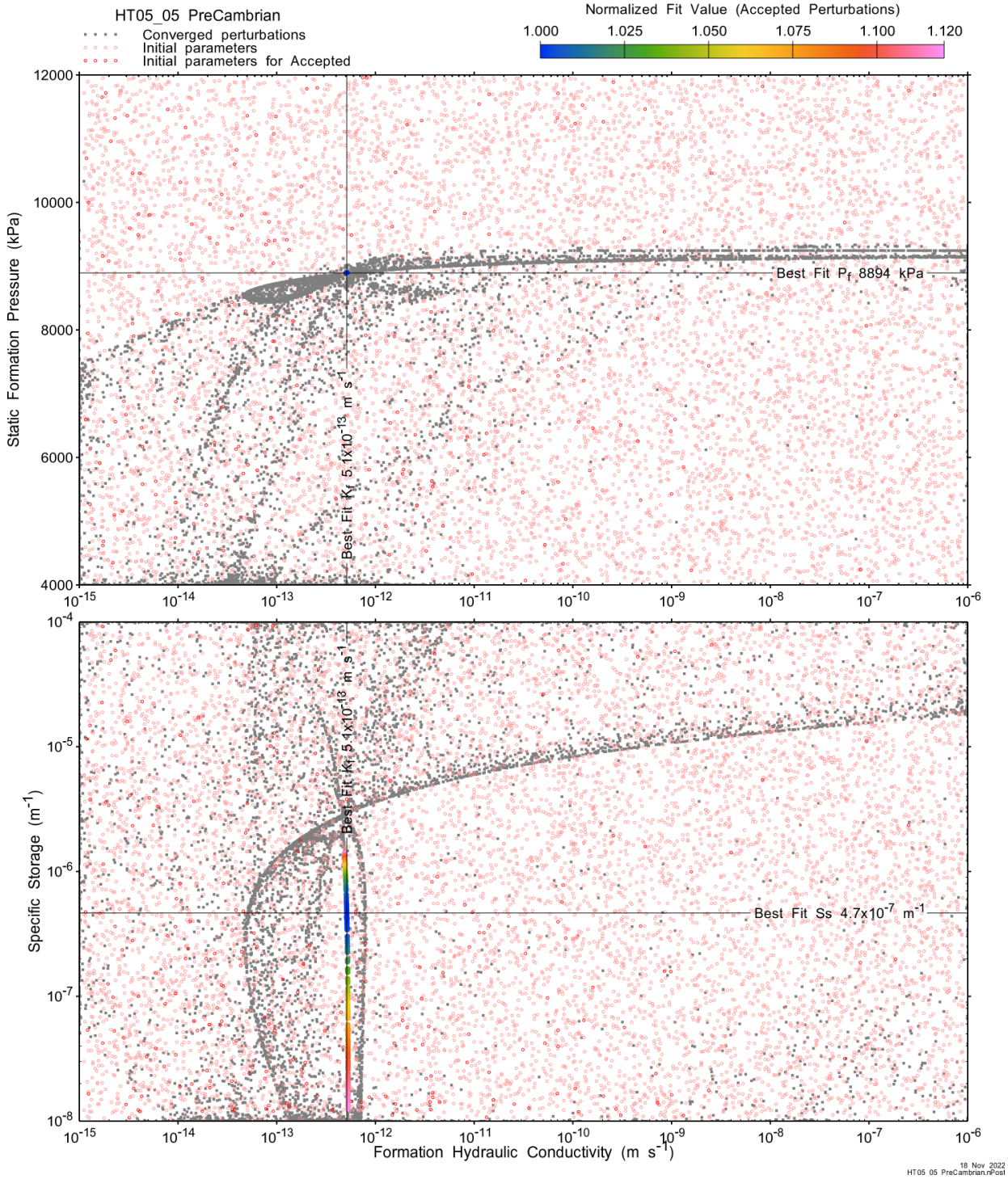

Figure A.73 - XY-scatter plot showing estimates of formation hydraulic conductivity (K_f) vs static formation pressure (P_f) (top panel) and specific storage (Ss) (bottom panel).

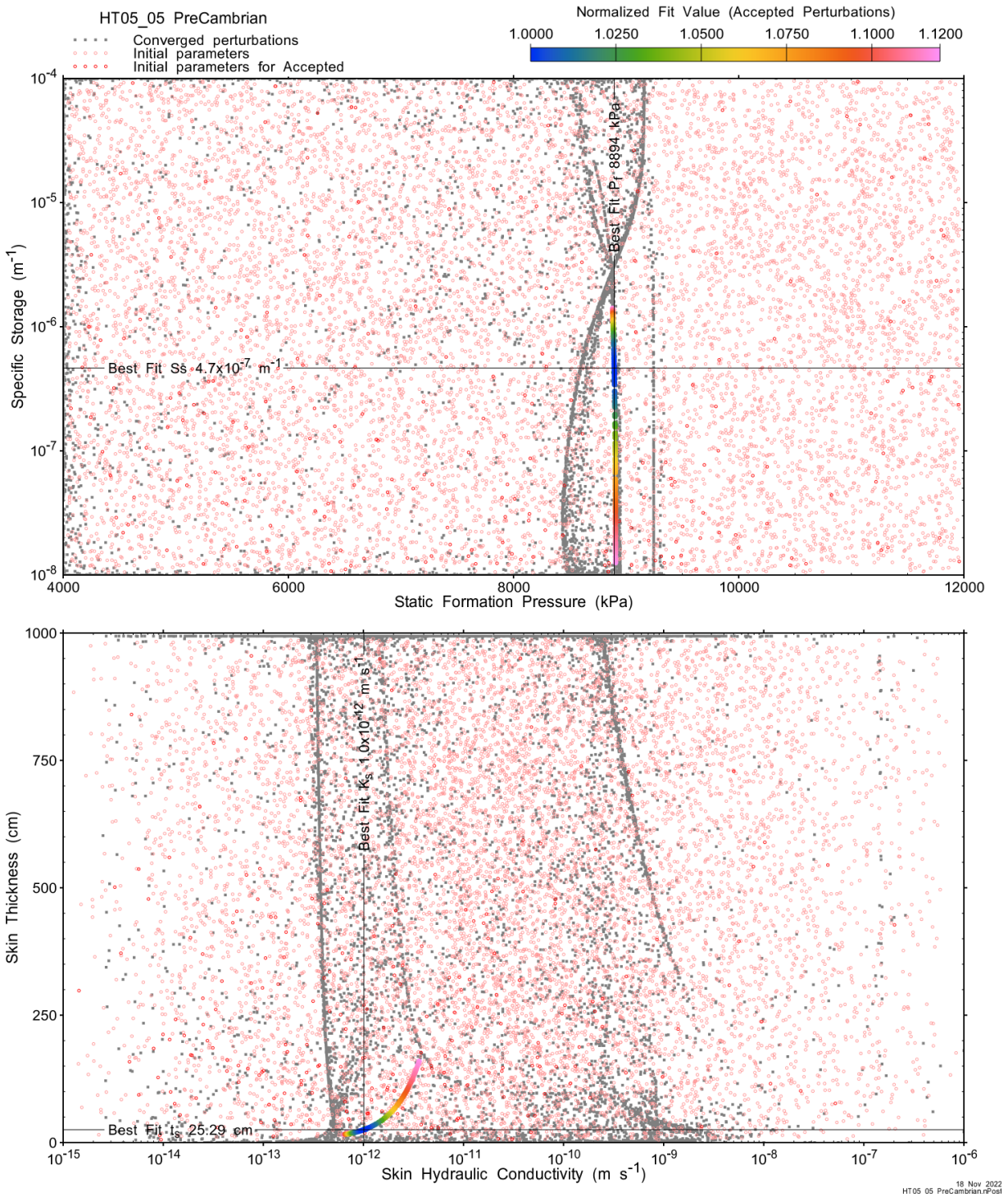

Figure A.74 - XY-scatter plot showing estimates of static formation pressure (P_f) vs specific storage (Ss) (top panel) and skin hydraulic conductivity (K_s) vs skin thickness (t_s) (bottom panel).

Confidence limits and median values are determined from the CDF of accepted optimization results (i.e. the varying color values in the above figures), with best fit value, 5% and 95% confidence indicated on Figure A.26 and Figure A.27.

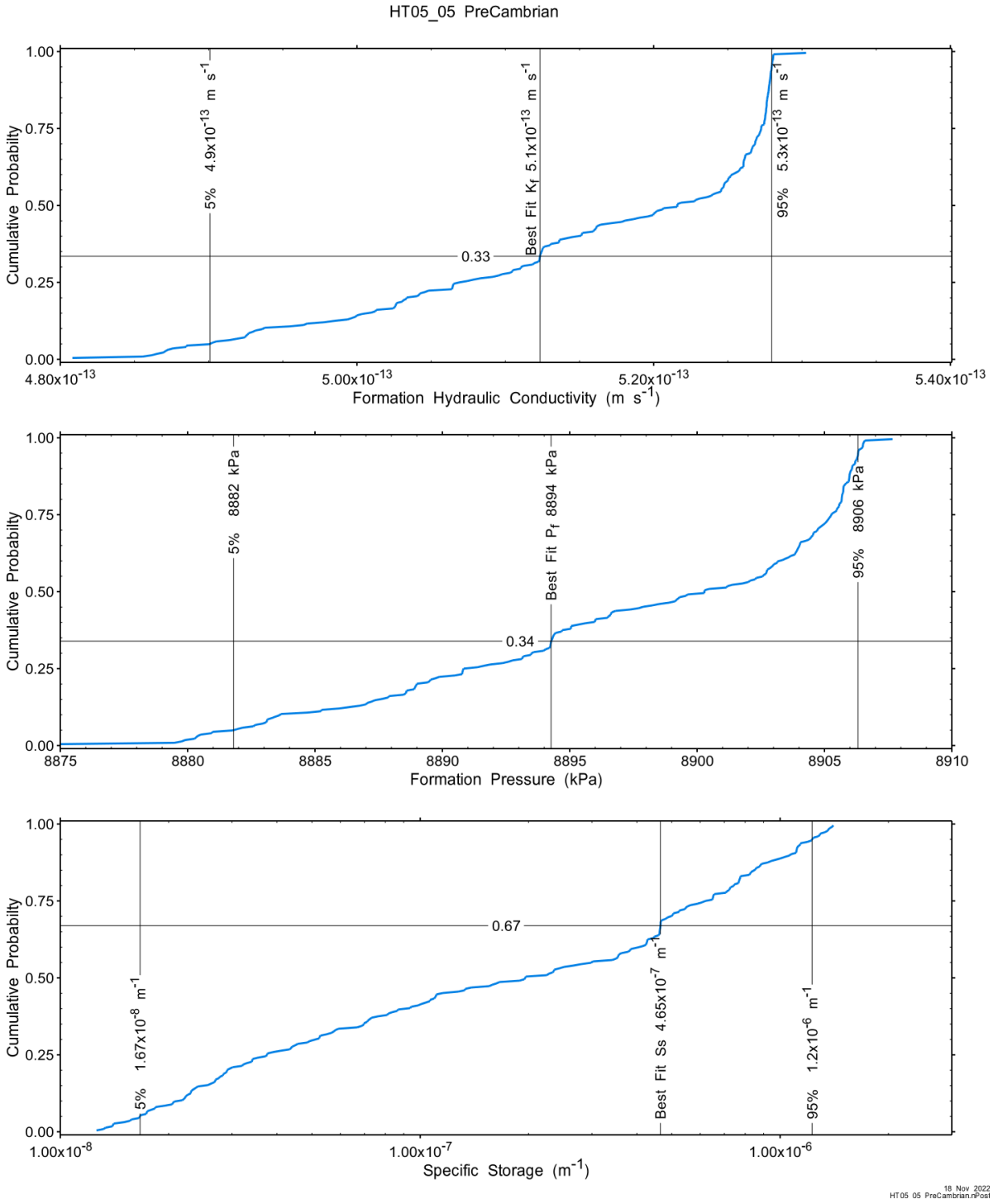

Figure A.75 – Cumulative distribution functions and parameter limits for formation hydraulic conductivity (K_f) (top panel), static formation pressure (P_f) (middle panel) and specific storage (Ss) (bottom panel).

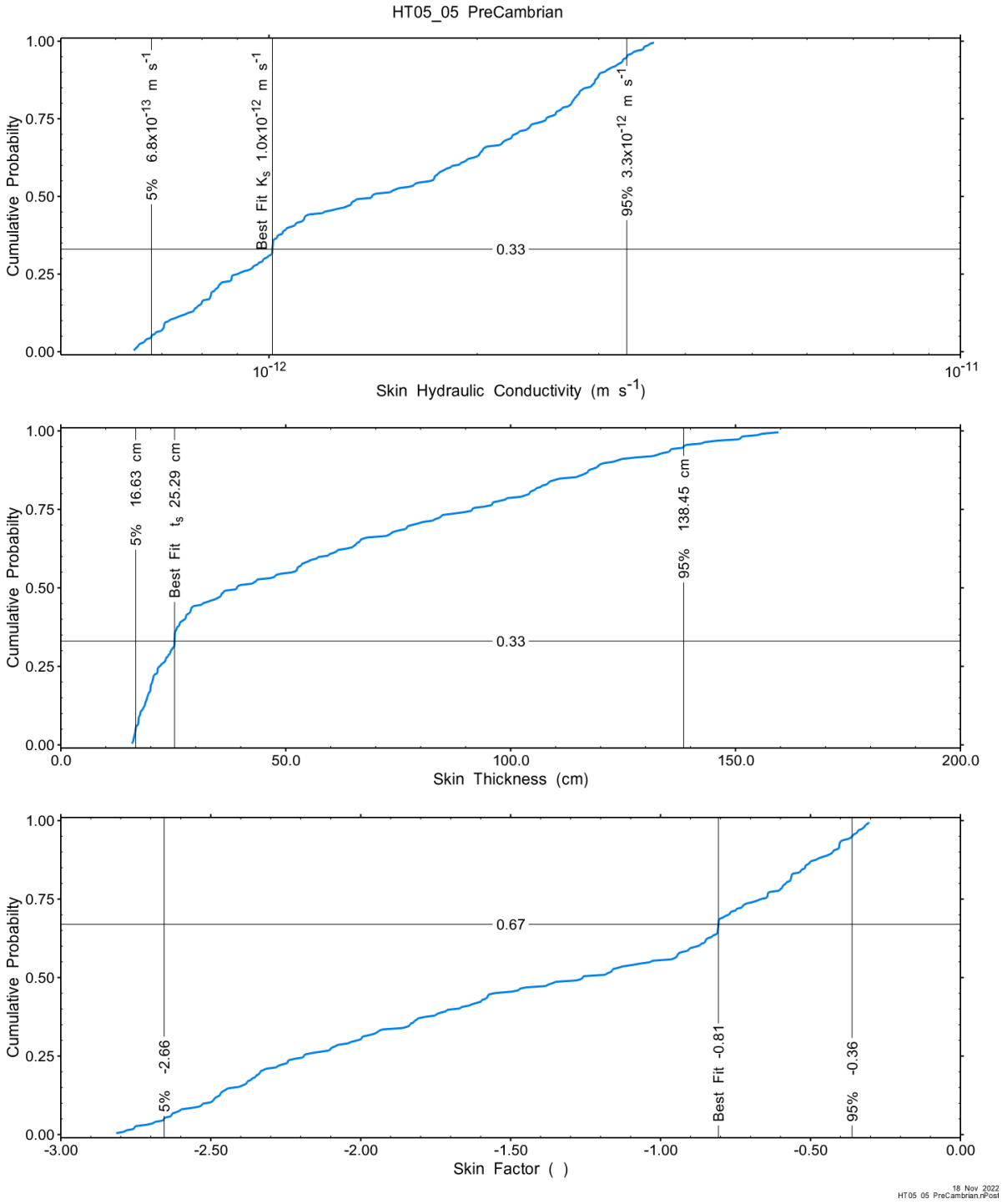

Figure A.76 – Cumulative distribution functions and parameter limits for skin hydraulic conductivity (K_s) (top panel), skin thickness (t_s) (middle panel) and skin factor (s) (bottom panel).

A summary of perturbation results is presented in Figure A.28, with Ramey-processed perturbations in Figure A.13. Those perturbations (195 of 10,000) with all parameters within the 5% and 95% range present an excellent fit to the measured test zone data.

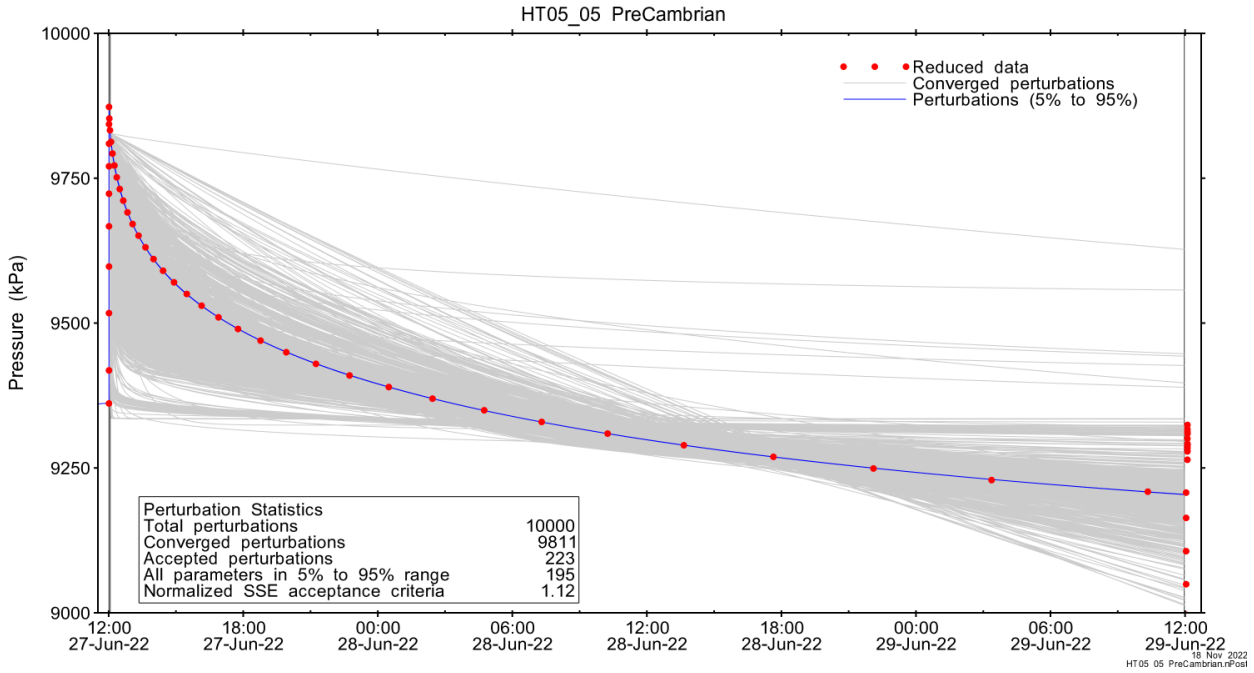

Figure A.77 – Perturbation results – all converged, accepted, and within 5% to 95% for all parameters.

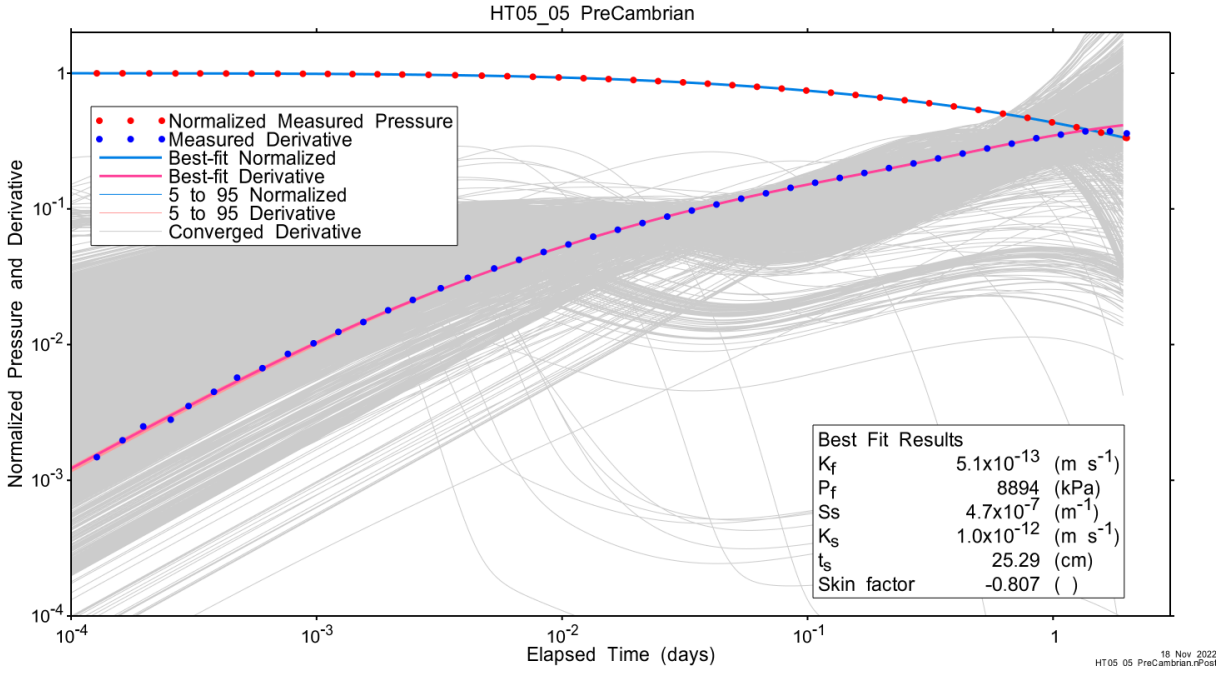

Figure A.78 – Log-log plot showing Ramey B and derivative response for all converged optimizations and those within 5% to 95% for all parameters.

A summary of best-fit and parameter ranges is given in Table A.9.

Table A.24 - Summary of the HT05_05 parameter estimates.

Parameter	Best Fit	5%	Median	95%
K_f (m/s)	5.1E-13	4.9E-13	5.2E-13	5.3E-13
P_f (kPa)	8894	8882	8900	8906
Ss (1/m)	4.7E-07	1.7E-08	2.0E-07	1.2E-06
K_s (m/s)	1.0E-12	6.8E-13	1.4E-12	3.3E-12
t_s (cm)	25.29	16.63	39.11	138.45
s (-)	-0.807	-2.655	-1.260	-0.361

Parameter correlations for all perturbations with all parameters within the 5% to 95% limits are given in Table A.5.

Table A.25 – Pearson cross-correlations of 5% to 95% parameters

	Log(K_f)	P_f	Log(Ss)	Log(K_s)	t_s	s
Log(K_f)	1.000	0.995	-0.915	0.928	0.800	-0.902
Pf	0.995	1.000	-0.949	0.959	0.850	-0.939
Log(S_s)	-0.915	-0.949	1.000	-0.999	-0.970	1.000
Log(K_s)	0.928	0.959	-0.999	1.000	0.961	-0.998
t_s	0.800	0.850	-0.970	0.961	1.000	-0.976
s	-0.902	-0.939	1.000	-0.998	-0.976	1.000

A.5.4 Additional Figures

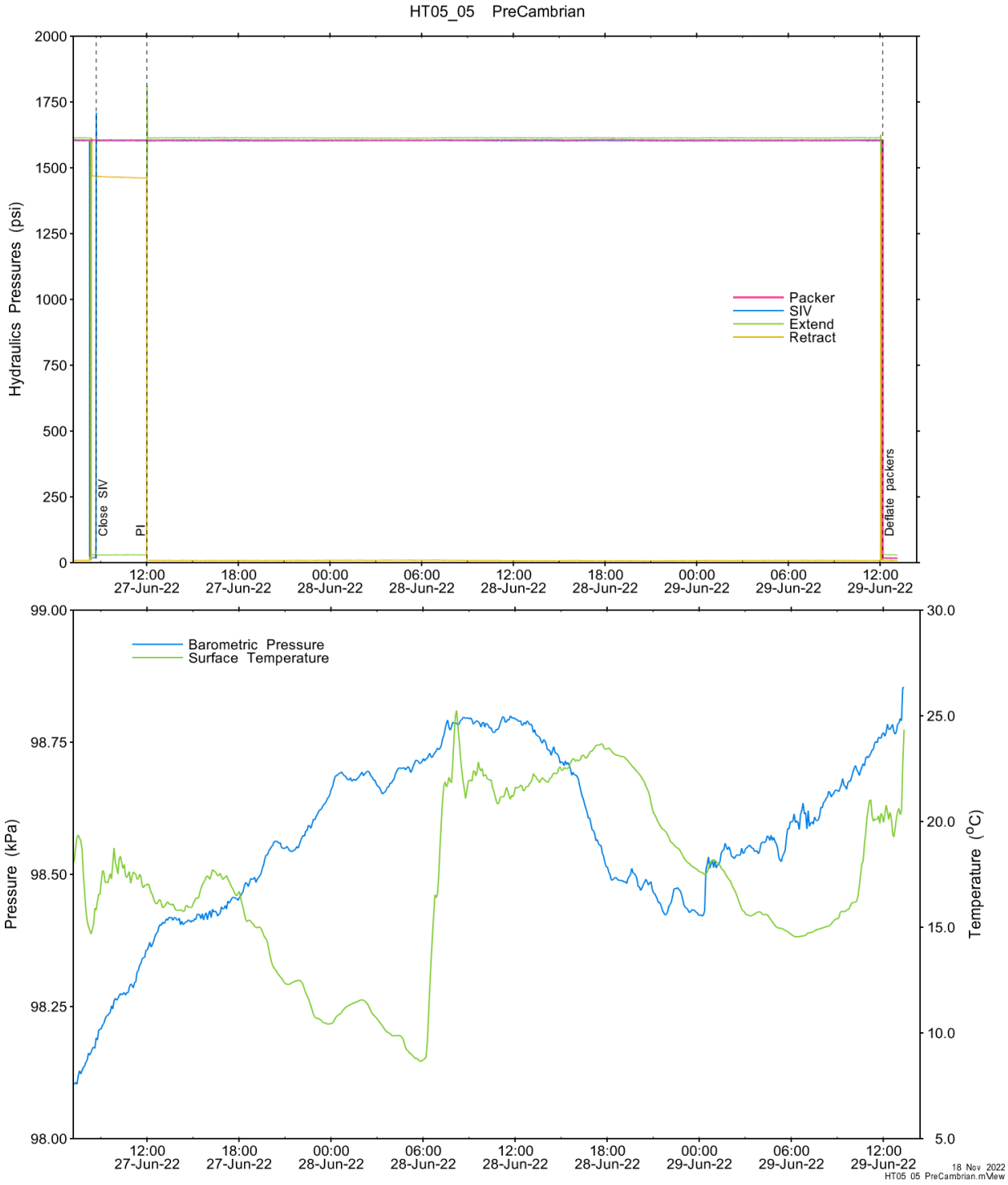

Figure A.79 - Hydraulics pressures and surface temperature/barometric pressure.

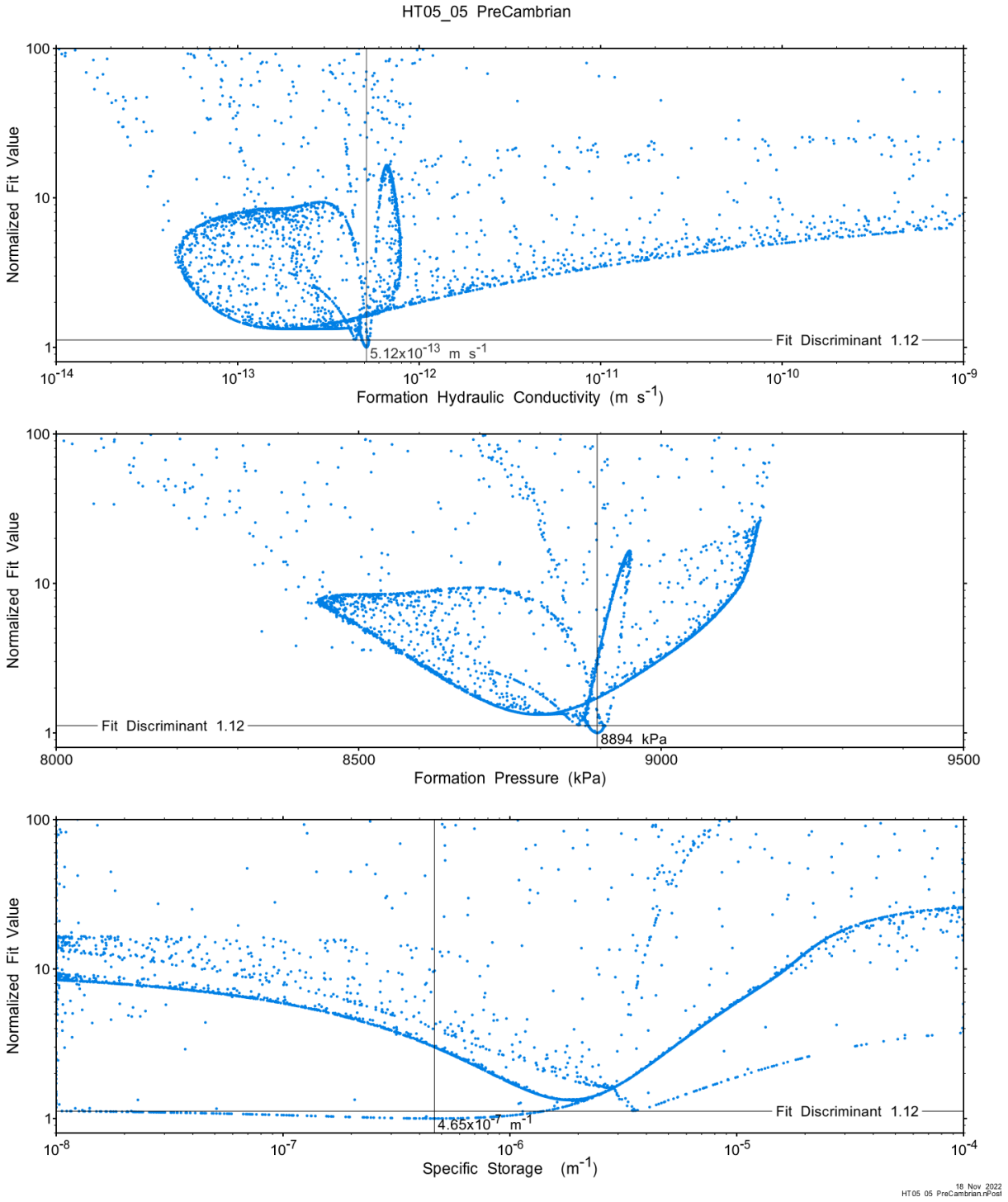

Figure A.80 - XY-scatter plot showing the formation parameter space normalized fit values.

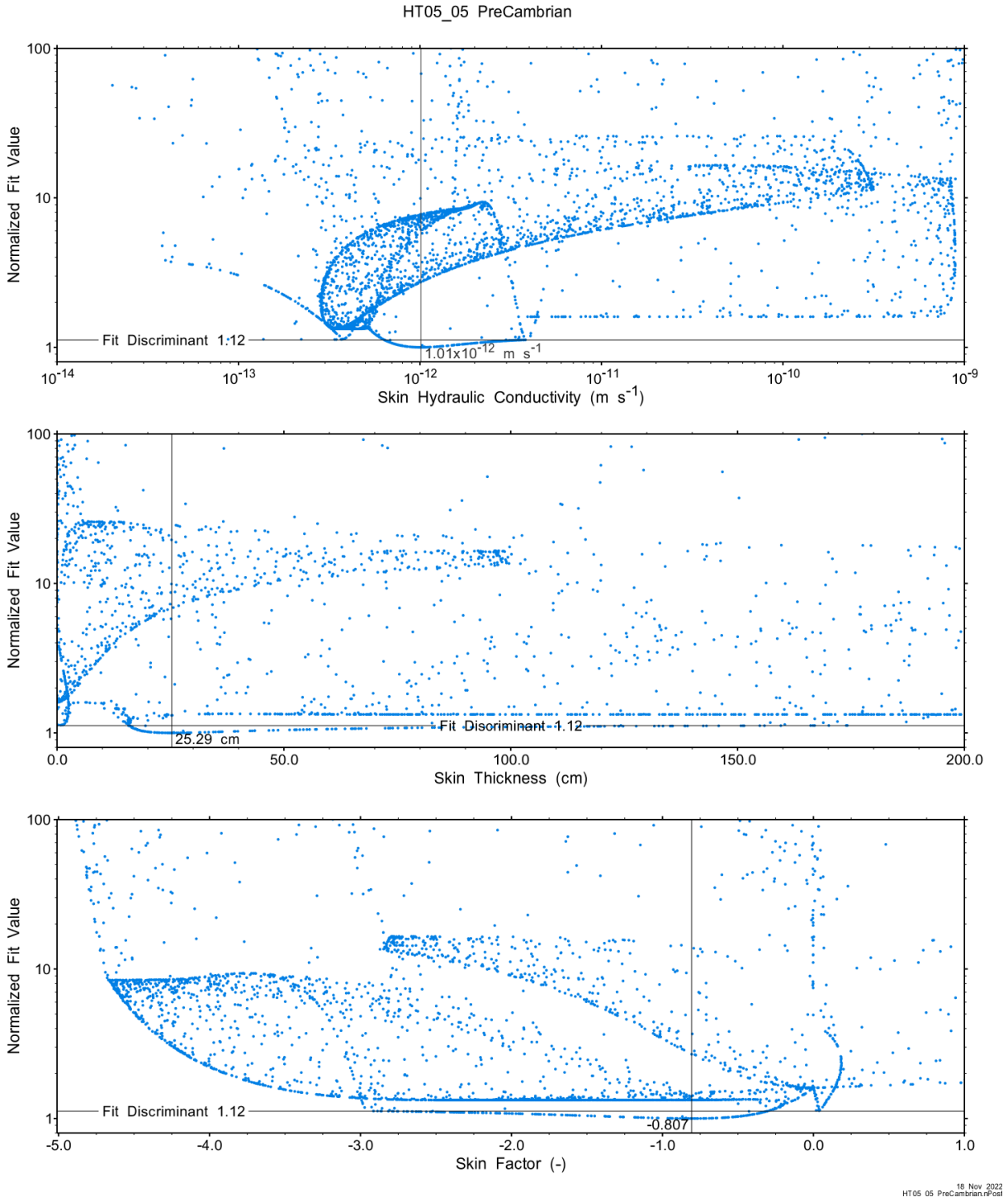

Figure A.81 - XY-scatter plot showing the skin parameter space normalized fit values.

A.6 HT01_30 Salina F

The SB BH02 interval from 200.00 to 229.96 mBGS tested in HT01_30 includes the majority of the F Unit of the Salina Group. A PI test with a duration of one day was conducted.

A.6.1 Test Data Summary

Table A.6 and Figure A.1 provide a summary of test events and a plot of pressures measured while testing respectively.

Table A.26 - Summary of Test Events.

Event	Start Date & Time	Duration (days)	TZ Pressure (kPa)
Drilling intercept	21-12-31 02:18	183.61	2085
Shut-in	22-07-02 16:52	0.66	2084
Pulse injection	22-07-03 08:37	1.02	2622
Test end	22-07-04 09:00		2290

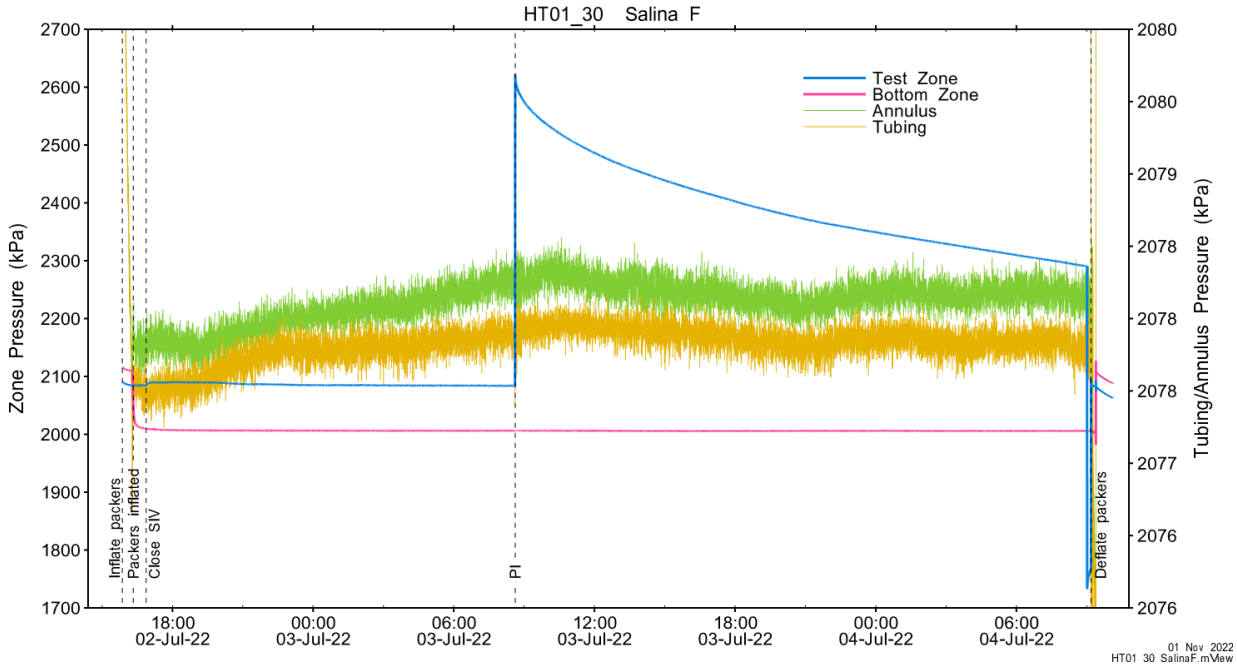

Figure A.82 - Test events and pressures.

A.6.2 Test Analyses

Table A.7 is a summary of test-specific input parameters used in the analyses, while Table A.8 presents the optimized parameters and allowed ranges.

Table A.27 – nSIGHTS Input Parameters.

Parameter	Value	Units
Test zone radius	6.63	cm
Test zone compressibility	4.65E-10	1/Pa
Test zone length	29.96	m

Table A.28 – nSIGHTS Parameter Optimization Ranges.

Parameter	Minimum	Maximum	Units	Type
Formation hydraulic conductivity (K_f)	1E-15	1E-09	m/s	log
Formation pressure (P_f)	0	2500	kPa	linear
Specific storage (S_s)	1E-08	1E-04	1/m	log
Skin hydraulic conductivity (K_s)	1E-15	1E-09	m/s	log
Skin thickness (t_s)	0.013	2500	cm	linear

Figure A.18 shows the measured test zone pressure record (with reduced data density for clarity) used in the analysis along with the best-fit simulation and parameter values. Figure A.19 presents the pre-test history, and Figure A.20 shows the Ramey B normalized best-fit pressure and pressure derivatives.

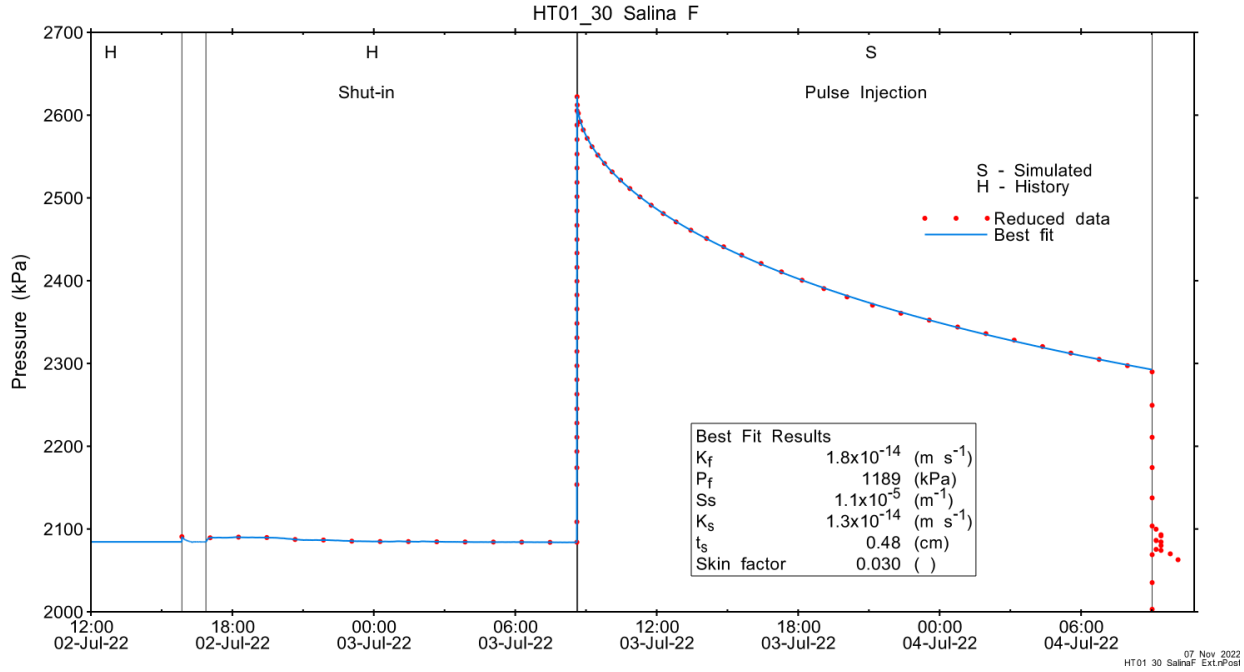

Figure A.83 - Annotated testing sequence showing best-fit simulation and parameter estimates.

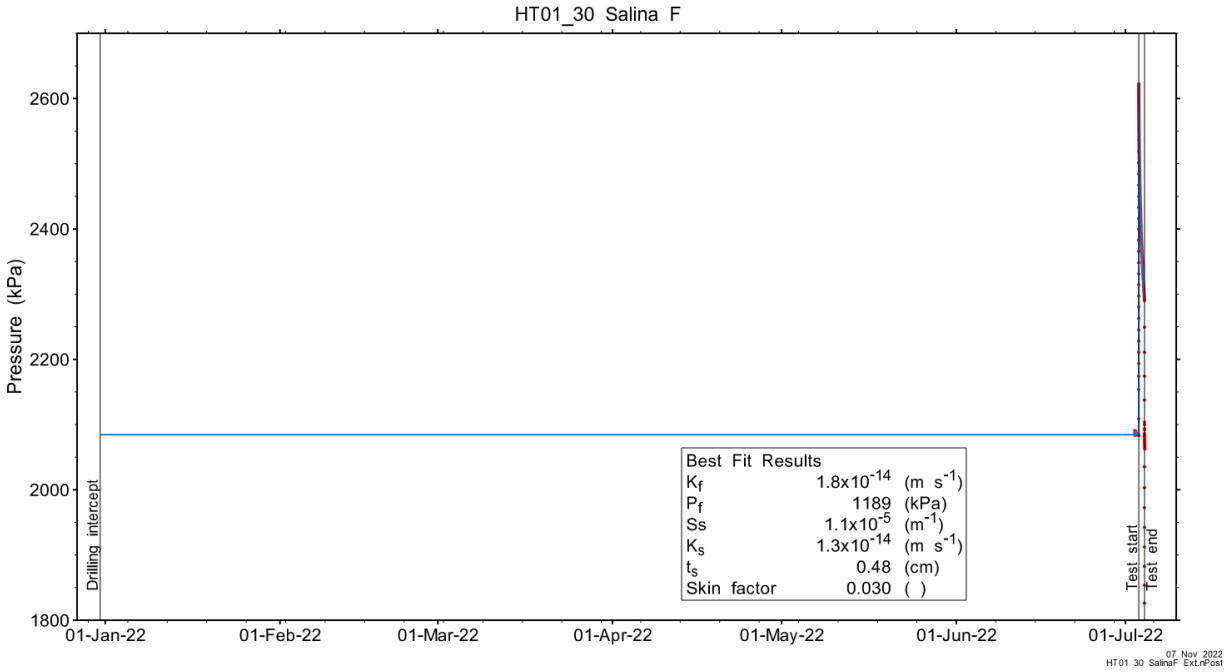

Figure A.84 - Annotated HT01_30 testing sequence showing pre-test history, best-fit simulation and parameter estimates.

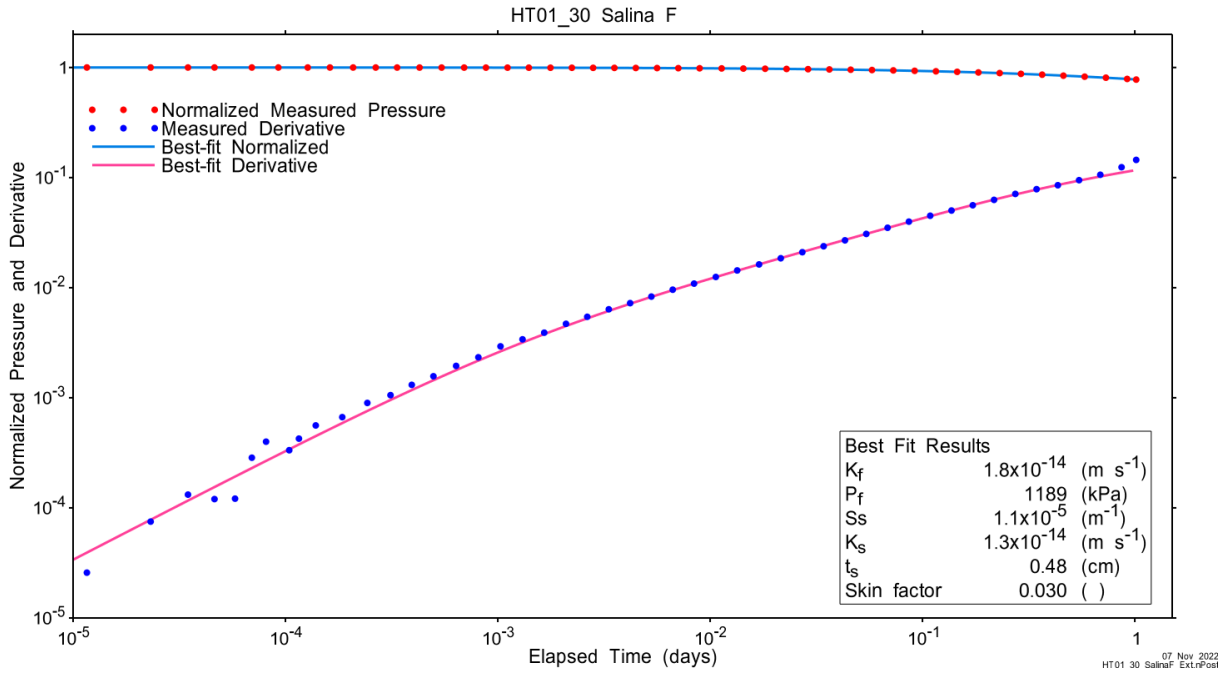

Figure A.85 - Log-log plot showing Ramey B and derivative response for best-fit simulation.

Figure A.21 shows the normalized parameter sensitivity response for the best fit. Sensitivity for K_f and P_f were still increasing at the end of the test, indicating that an increased test duration may have yielded improved estimates of these parameters.

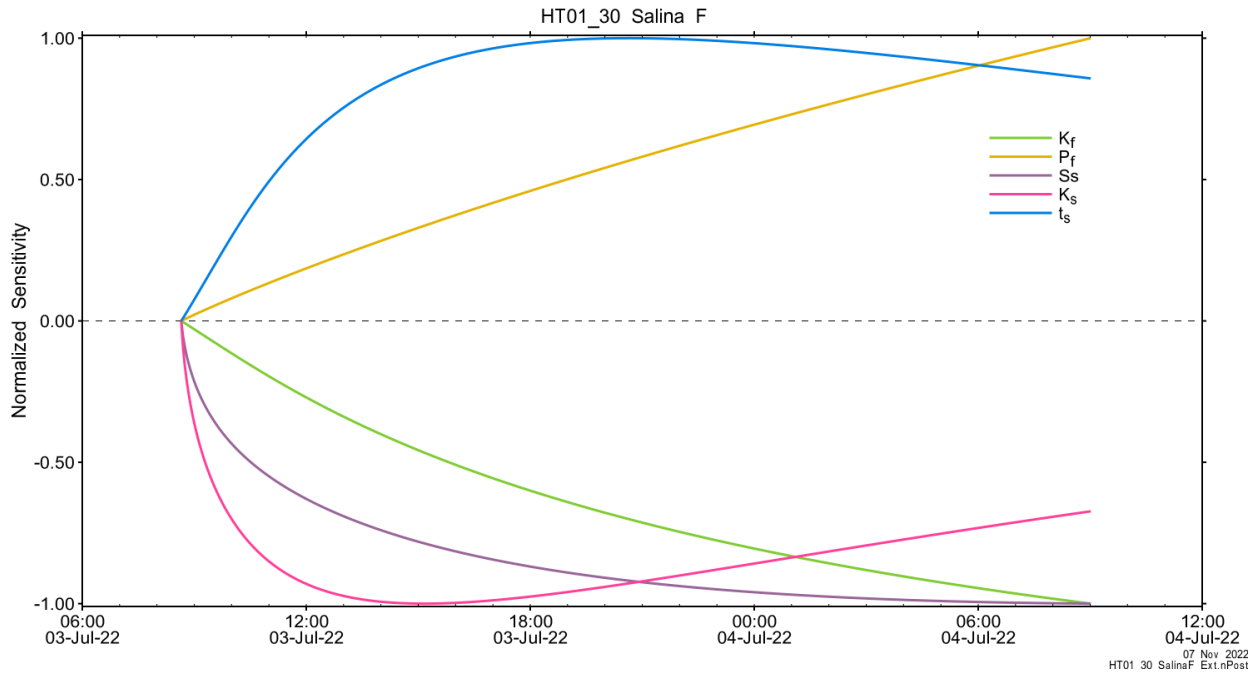

Figure A.86 - Normalized Jacobian for best-fit simulation.

A.6.3 Uncertainty Analyses

An initial uncertainty analyses was conducted with 10,000 perturbations. Results revealed a very small and poorly defined (less than 10 perturbations met fit criteria) global minimum. The parameter ranges were tightened slightly and a 50,000 perturbation analysis conducted, results of which are presented here. The CDF of normalized fit values for all converged simulations and the selected fit discriminant are shown in Figure A.22 and Figure A.88.

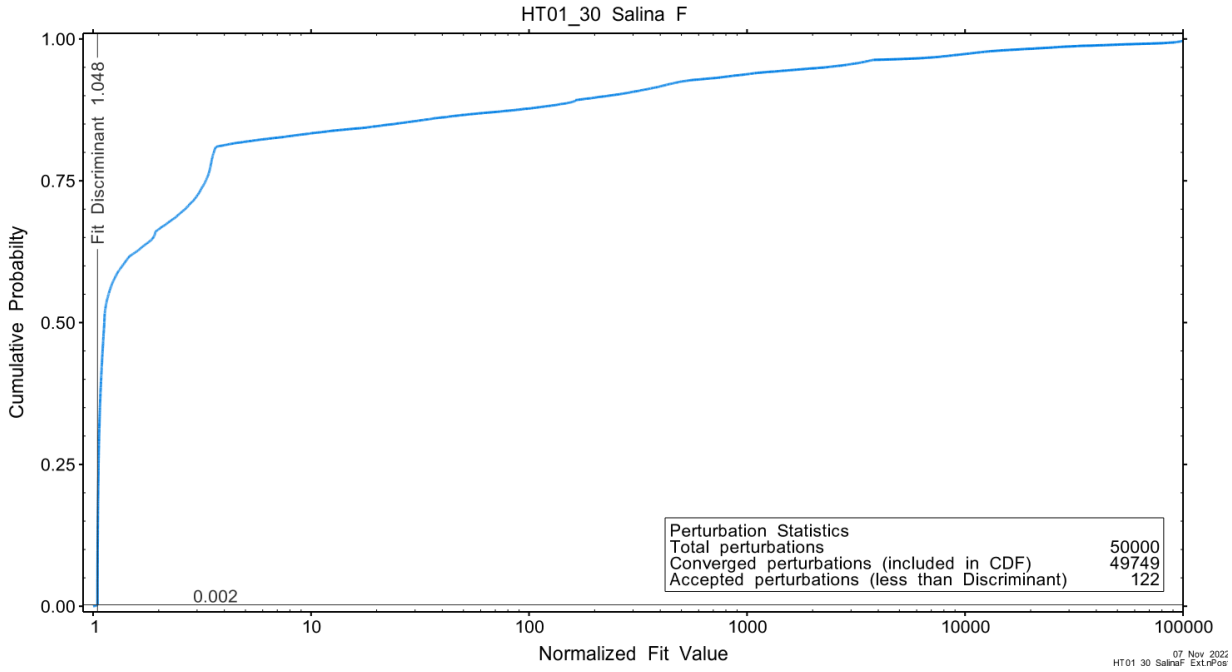

Figure A.87 - Fit value cumulative distribution function.

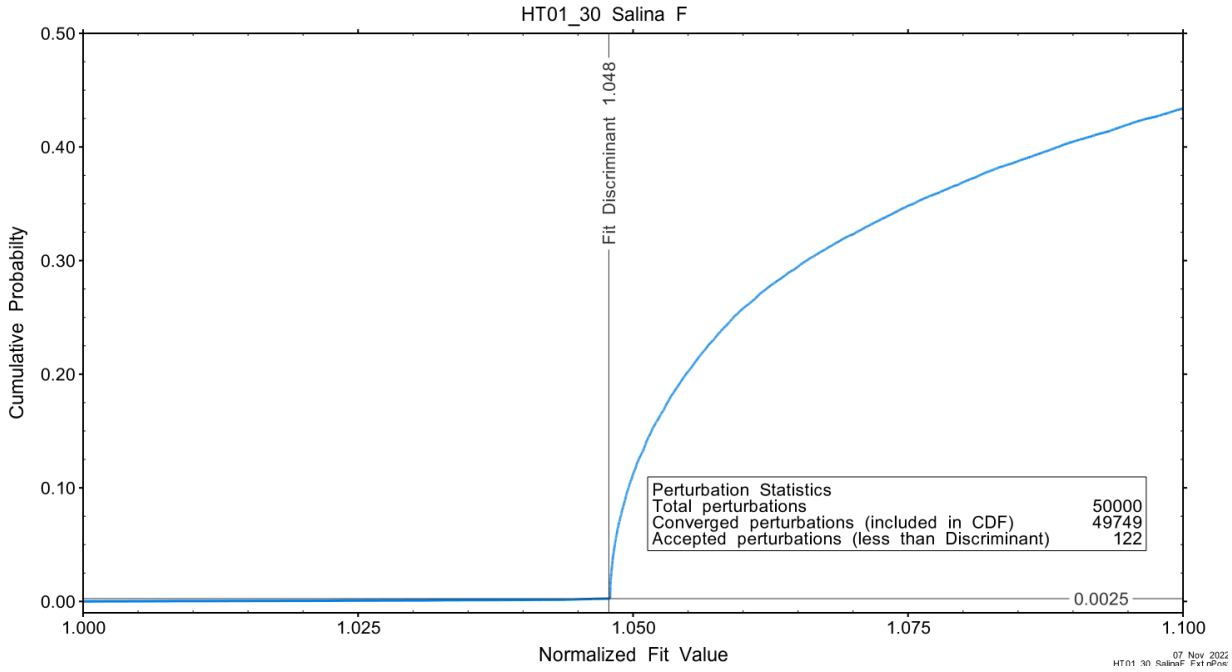

Figure A.88 - Fit value cumulative distribution function (detail).

Summary cross parameter scatter plots for selected formation and skin parameters are given in Figure A.24 and Figure A.25. The light pink dots on the figures are the initial parameter estimates, with red dots overlaying those initial parameter values that resulted in accepted optimization results. The grey dots are converged optimizations which did not meet the fit discriminant. Larger varying color symbols represent the fit value of accepted optimizations, with the blue values representing the best fit.

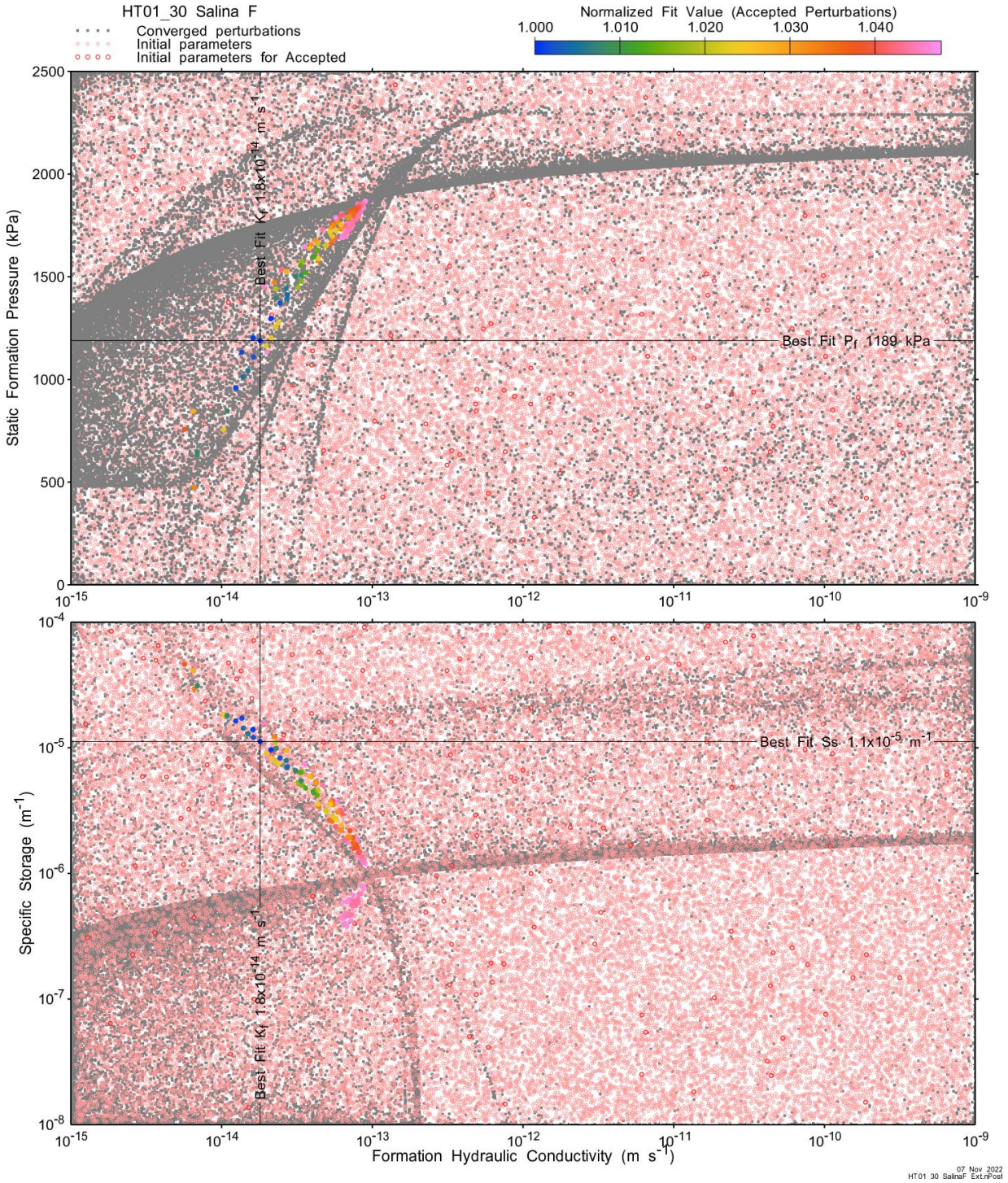

Figure A.89 - XY-scatter plot showing estimates of formation hydraulic conductivity (K_f) vs static formation pressure (P_f) (top panel) and specific storage (Ss) (bottom panel).

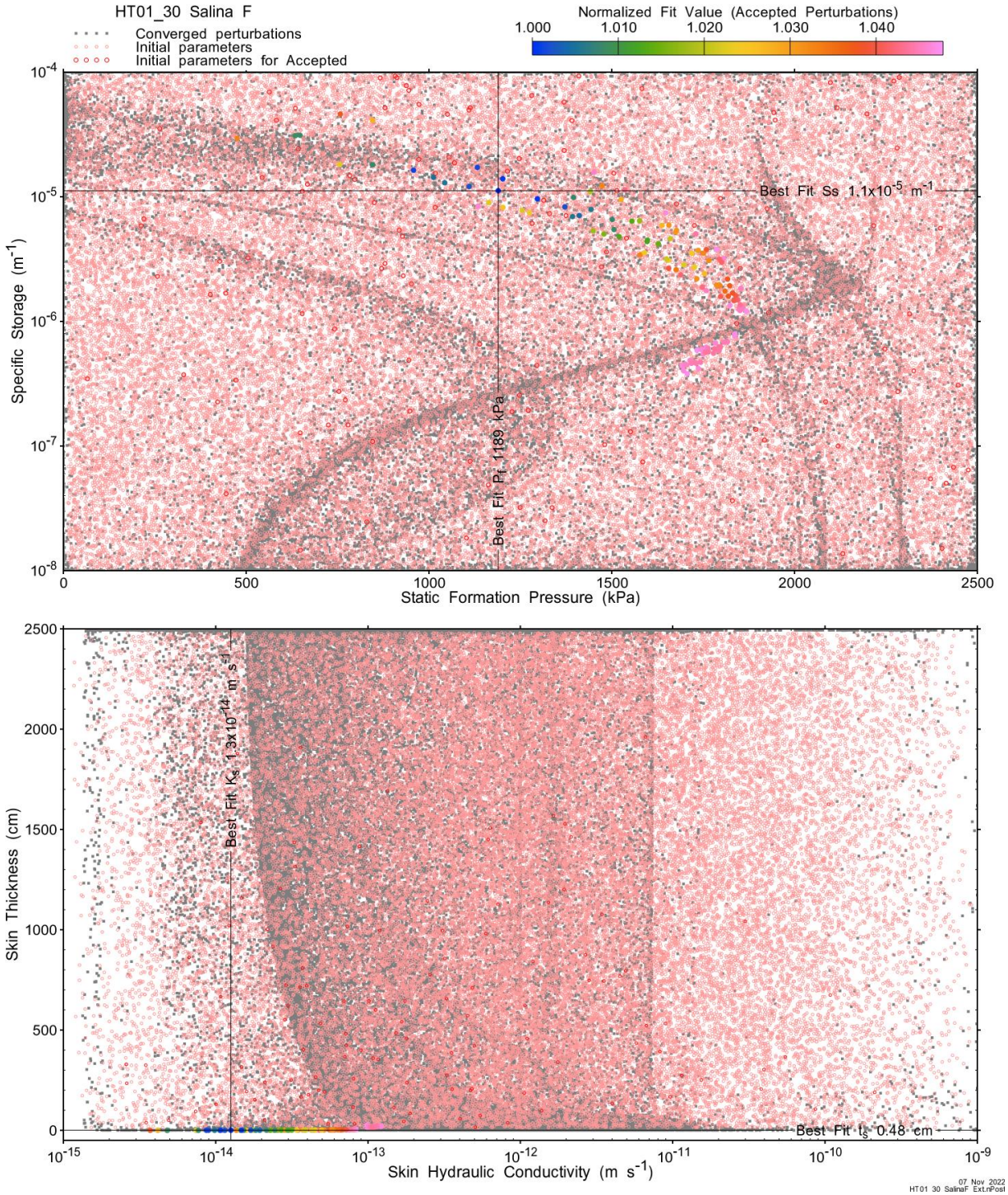

Figure A.90 - XY-scatter plot showing estimates of static formation pressure (P_f) vs specific storage (Ss) (top panel) and skin hydraulic conductivity (K_s) vs skin thickness (t_s) (bottom panel).

Confidence limits and median values are determined from the CDF of accepted optimization results (i.e. the varying color values in the above figures), with best fit value, 5% and 95% confidence indicated on Figure A.26 and Figure A.27.

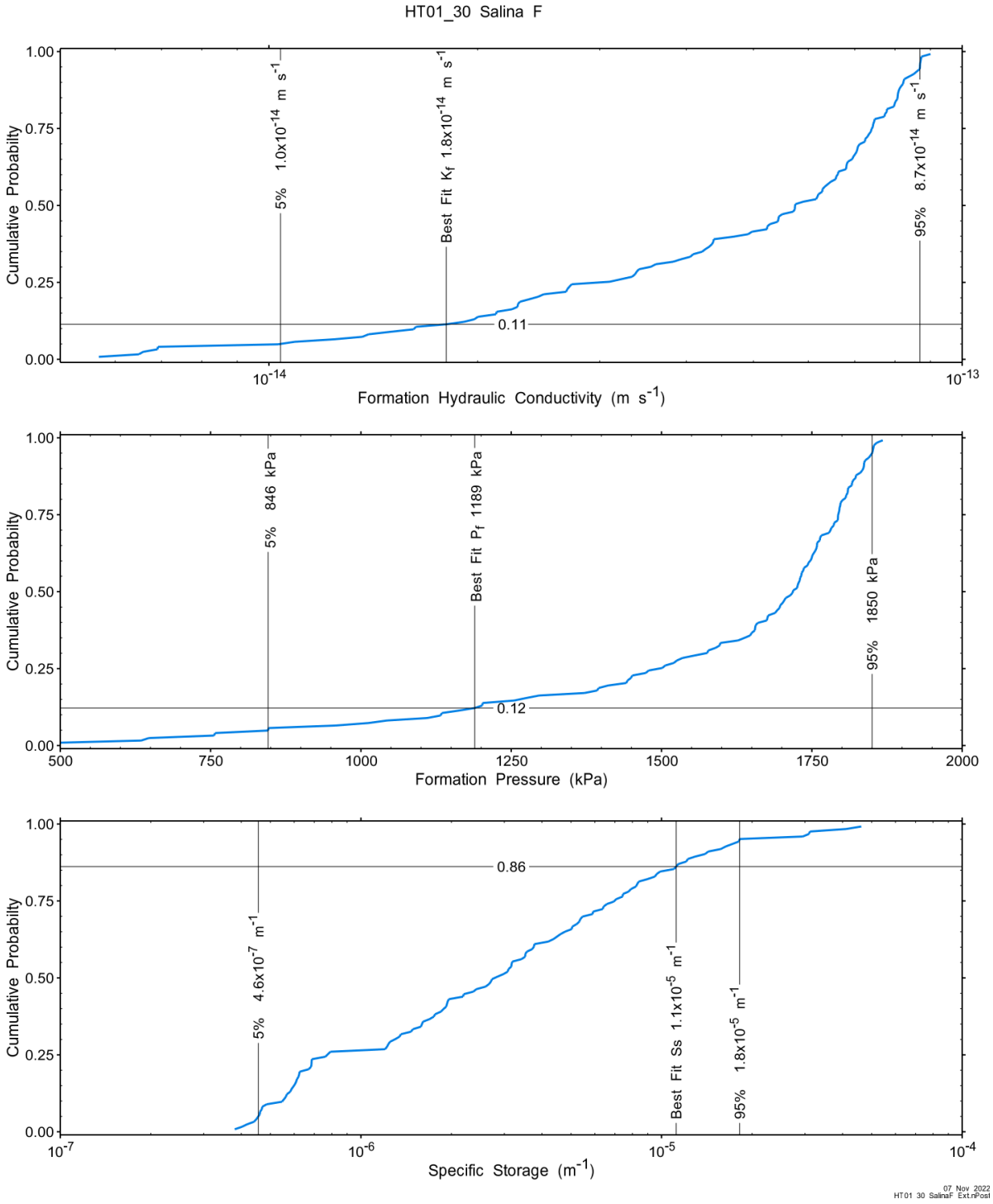

Figure A.91 – Cumulative distribution functions and parameter limits for formation hydraulic conductivity (K_f) (top panel), static formation pressure (P_f) (middle panel) and specific storage (Ss) (bottom panel).

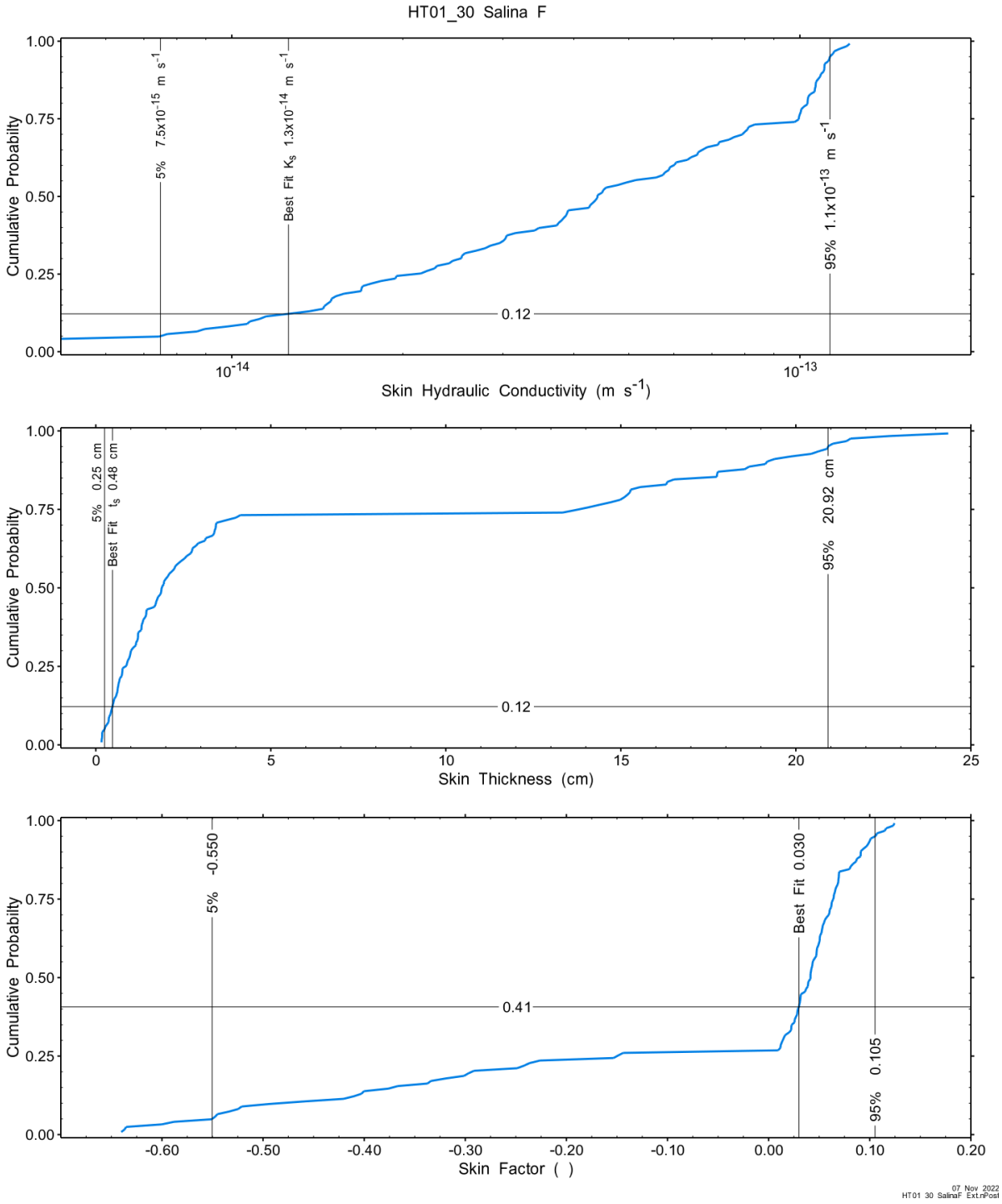

Figure A.92 – Cumulative distribution functions and parameter limits for skin hydraulic conductivity (K_s) (top panel), skin thickness (t_s) (middle panel) and skin factor (s) (bottom panel).

A summary of perturbation results is presented in Figure A.28, with Ramey-processed perturbations in Figure 12. Those perturbations (2548 of 10,000) with all parameters within the 5% and 95% range present a very good fit to the measured test zone data.

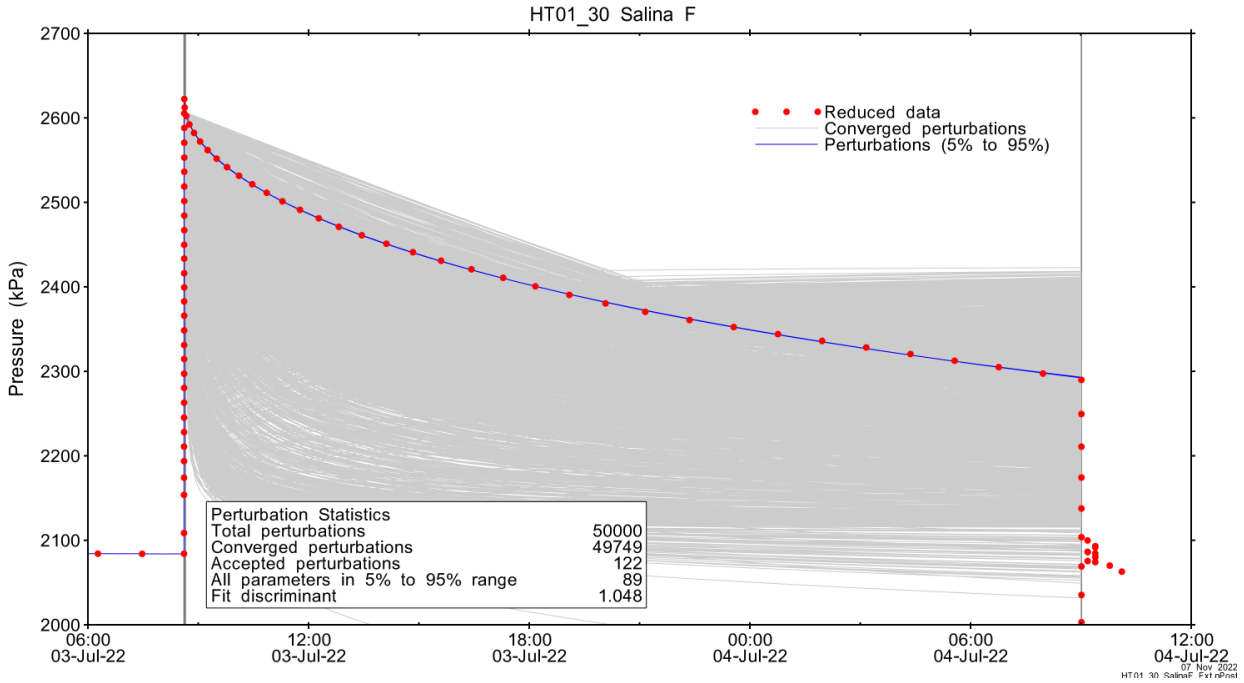

Figure A.93 – Perturbation results – all converged, accepted, and within 5% to 95% for all parameters.

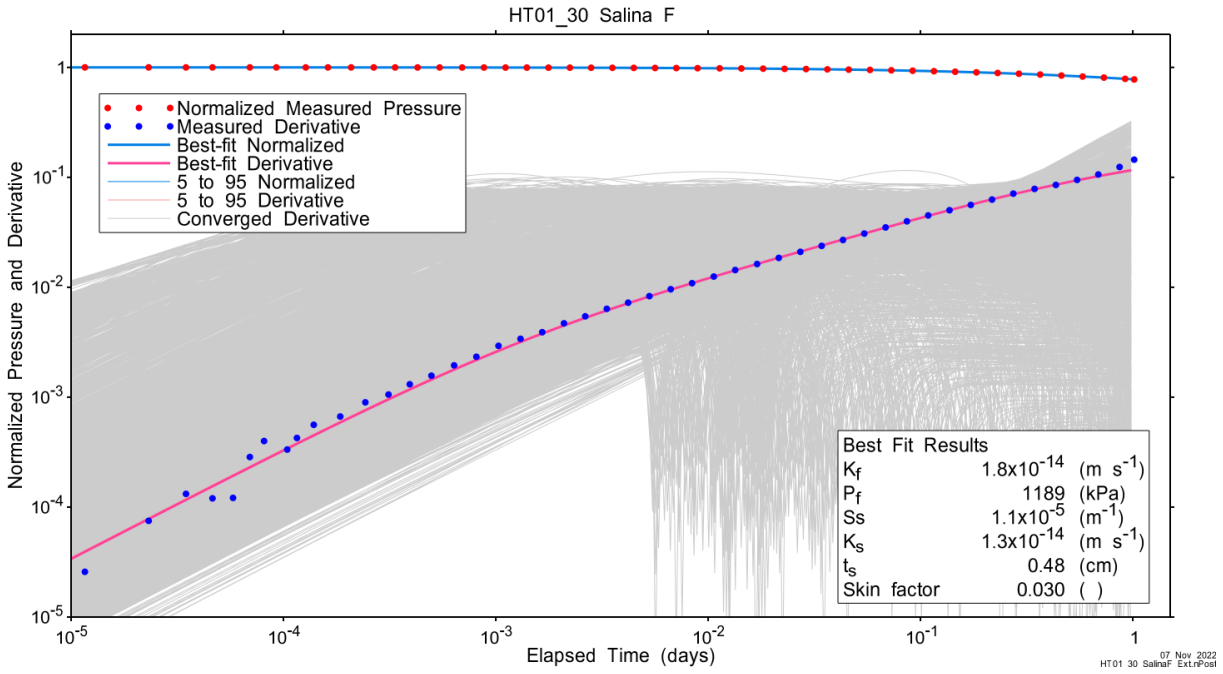

Figure A.94 – Log-log plot showing Ramey B and derivative response for all converged optimizations and those within 5% to 95% for all parameters.

A summary of best-fit and parameter ranges is given in Table A.9.

Table A.29 - Summary of the HT01_30 parameter estimates.

Parameter	Best Fit	5%	Median	95%
K_f (m/s)	1.8E-14	1.0E-14	5.7E-14	8.7E-14
P_f (kPa)	1189	846	1718	1850
Ss (1/m)	1.1E-05	4.6E-07	2.8E-06	1.8E-05
K_s (m/s)	1.3E-14	7.5E-15	4.4E-14	1.1E-13
t_s (cm)	0.48	0.25	1.88	20.92
s (-)	0.030	-0.550	0.041	0.105

Parameter correlations for all perturbations with all parameters within the 5% to 95% limits are given in Table A.5.

Table A.30 – Pearson cross-correlations of 5% to 95% parameters

	Log(K_f)	P_f	Log(Ss)	Log(K_s)	t_s	s
Log(K_f)	1.000	0.961	-0.919	0.969	0.579	-0.409
Pf	0.961	1.000	-0.810	0.886	0.466	-0.280
Log(S_s)	-0.919	-0.810	1.000	-0.988	-0.832	0.723
Log(K_s)	0.969	0.886	-0.988	1.000	0.750	-0.615
t_s	0.579	0.466	-0.832	0.750	1.000	-0.969
s	-0.409	-0.280	0.723	-0.615	-0.969	1.000

A.6.4 Additional Figures

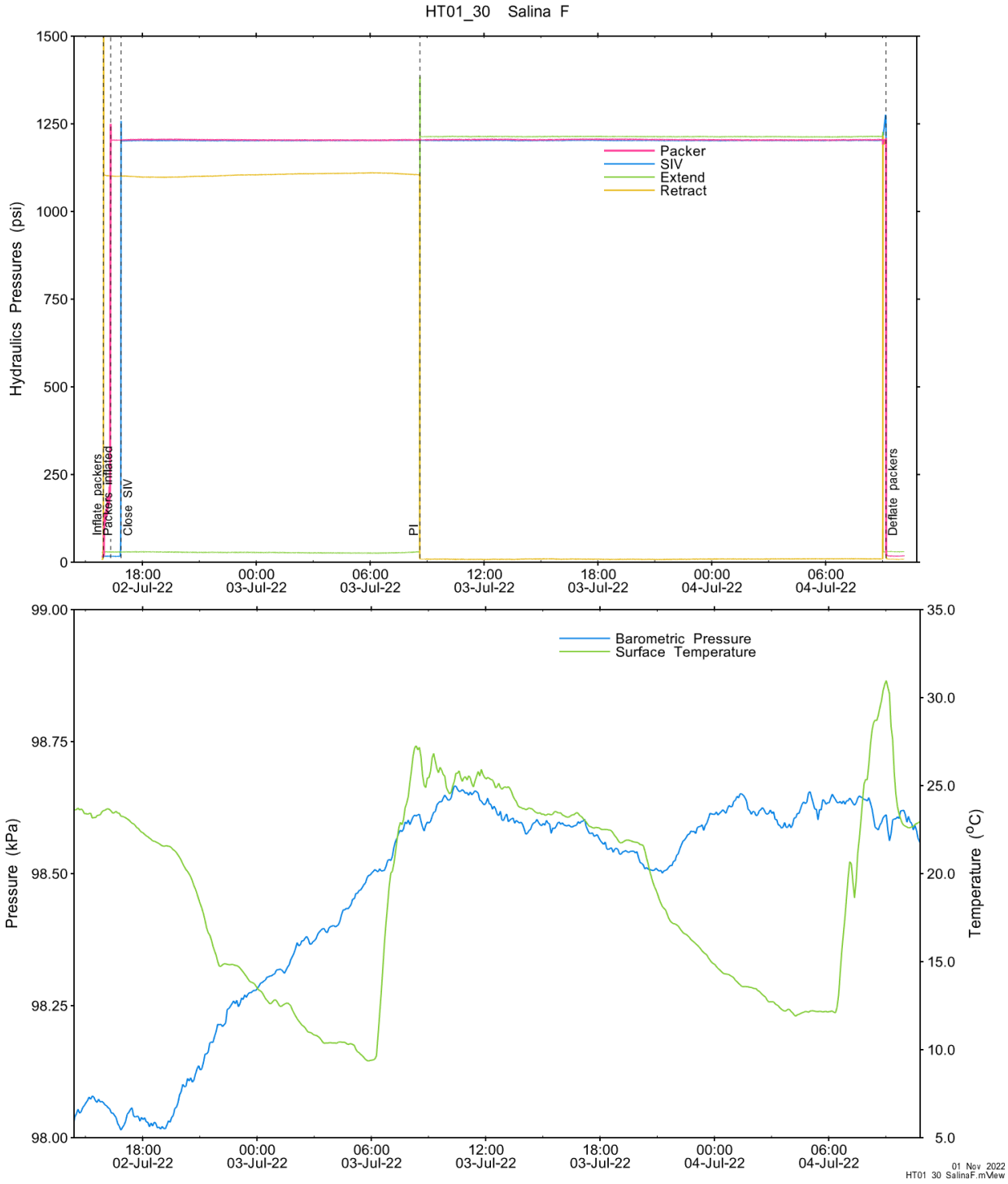

Figure A.95 - Hydraulics pressures and surface temperature/barometric pressure.

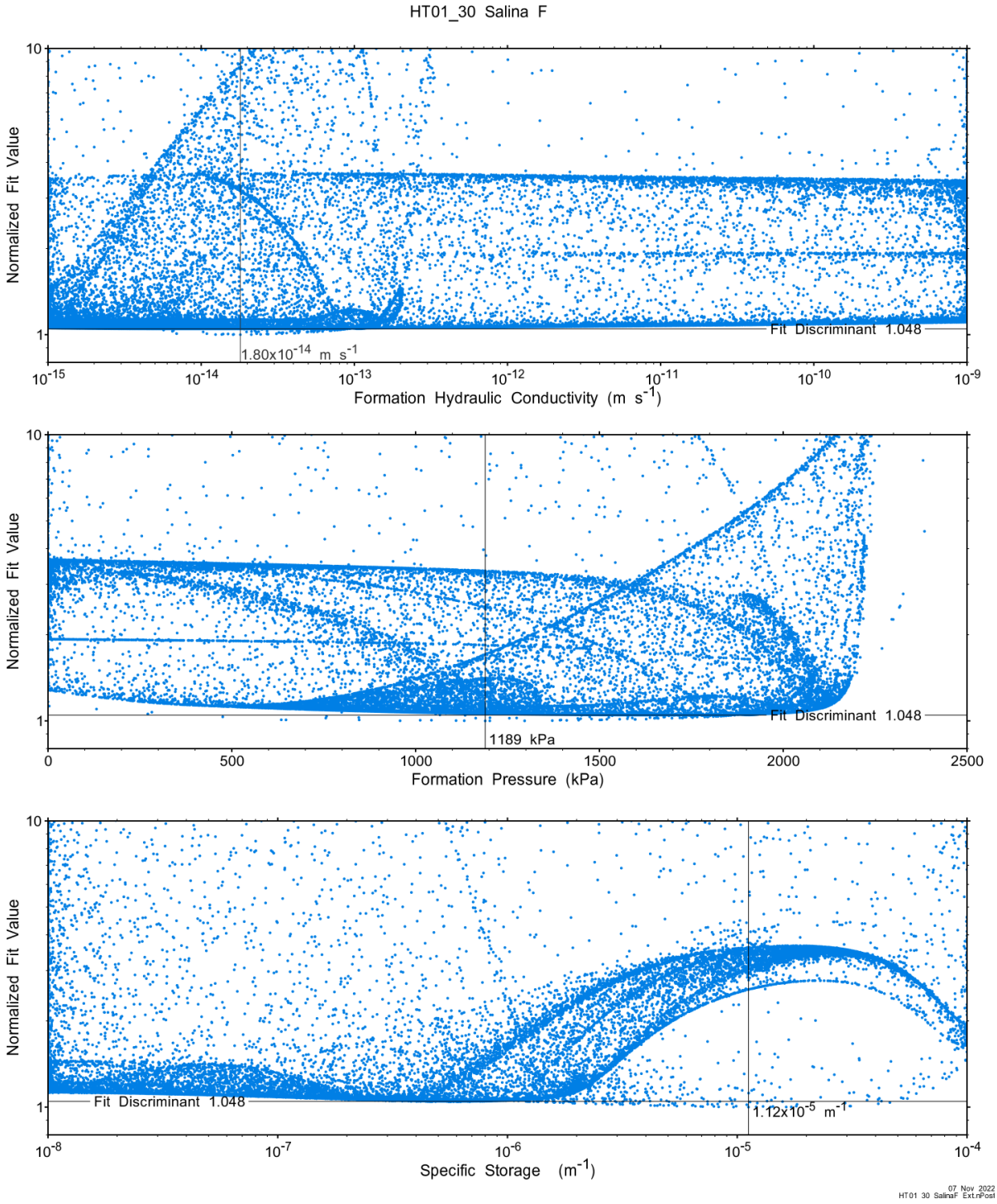

Figure A.96 - XY-scatter plot showing the formation parameter space normalized fit values.

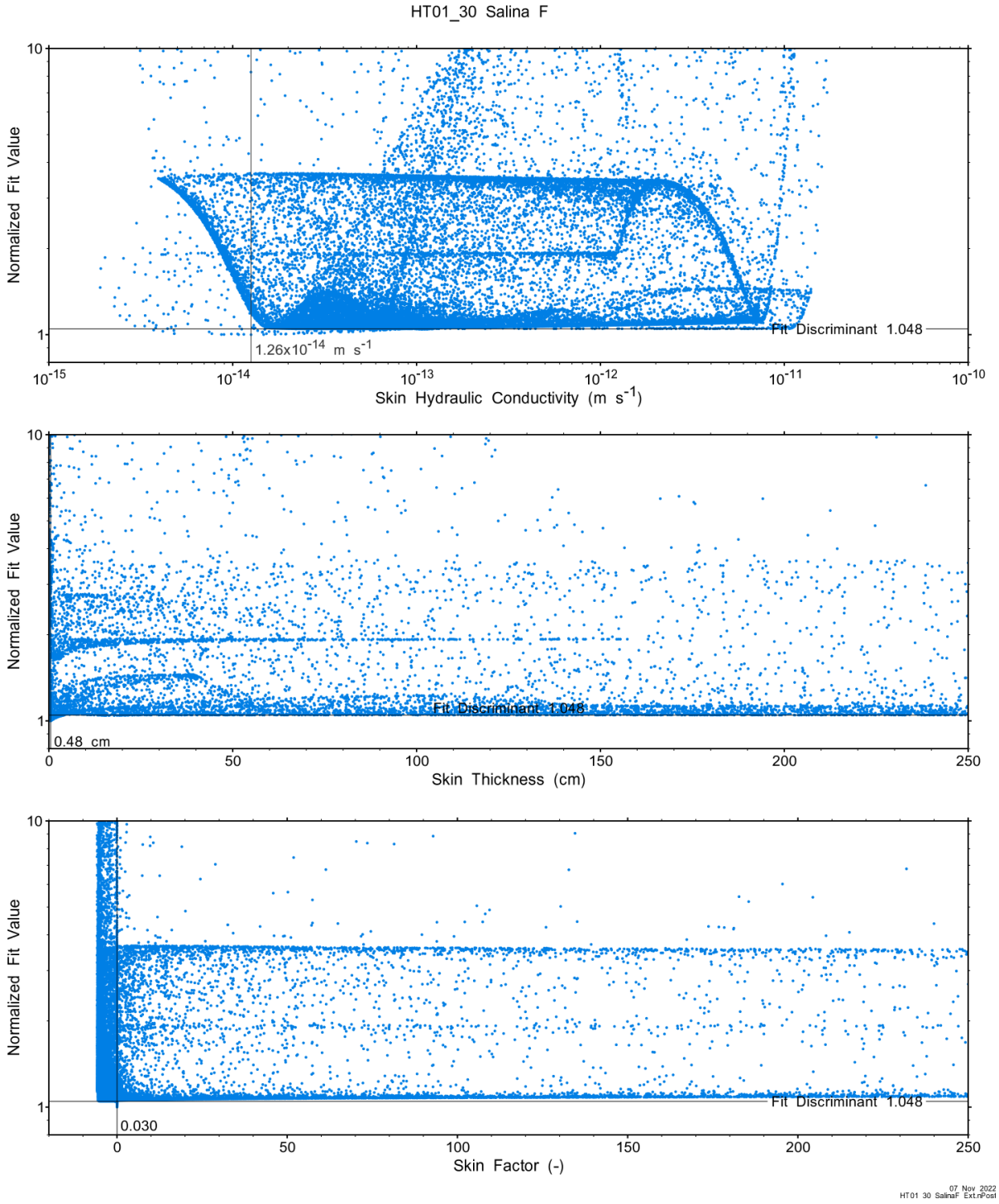

Figure A.97 - XY-scatter plot showing the skin parameter space normalized fit values.

A.7 HT02_30 Salina A1

The SB BH02 interval from 340.00 to 369.96 mBGS tested in HT02_30 includes the majority of the A1 Carbonate Unit of the Salina Group. A PI test with a duration of one day was conducted.

A.7.1 Test Data Summary

Table A.6 and Figure A.1 provide a summary of test events and a plot of pressures measured while testing respectively. Previous testing of this unit in other boreholes indicated the potential for a high permeability response. Accordingly, the tubing was swabbed and the test set up for an initial SW (Attempted SW on Figure A.1). After initiating the SW, the response was monitored for approximately 90 minutes. There was virtually no recovery, so the shut-valve was closed and the PI initiated 15 minutes later.

Table A.31 - Summary of Test Events.

Event	Start Date & Time	Duration (days)	TZ Pressure (kPa)
Drilling intercept	22-01-04 06:03	186.32	3585
Shut-in	22-07-09 13:37	0.86	3584
Pulse injection	22-07-10 10:21	1.01	3853
Test end	22-07-11 10:31		3464

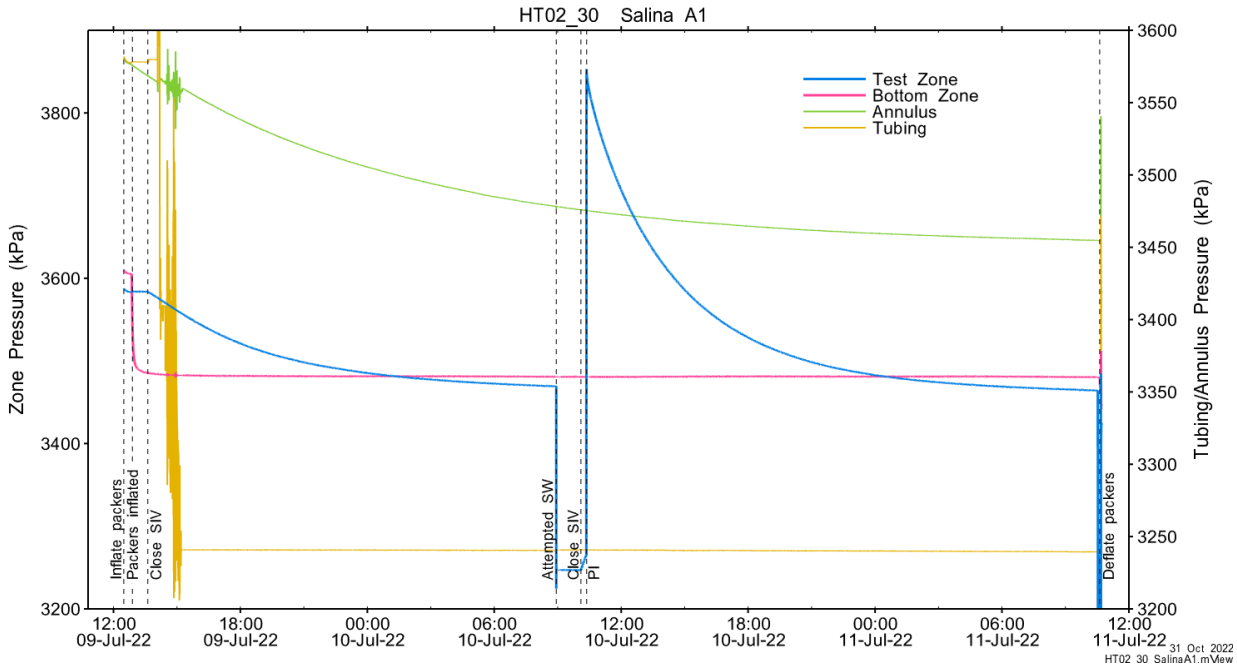

Figure A.98 - Test events and pressures.

A.7.2 Test Analyses

Table A.7 is a summary of test-specific input parameters used in the analyses, while Table A.8 presents the optimized parameters and allowed ranges.

Table A.32 – nSIGHTS Input Parameters.

Parameter	Value	Units
Test zone radius	6.73	cm
Test zone compressibility	4.13E-10	1/Pa
Test zone length	29.96	m

Table A.33 – nSIGHTS Parameter Optimization Ranges.

Parameter	Minimum	Maximum	Units	Type
Formation hydraulic conductivity (K_f)	1E-15	1E-09	m/s	log
Formation pressure (P_f)	1000	5000	kPa	linear
Specific storage (S_s)	1E-08	1E-04	1/m	log
Skin hydraulic conductivity (K_s)	1E-15	1E-09	m/s	log
Skin thickness (t_s)	0.013	1000	cm	linear

Figure A.18 shows the measured test zone pressure record (with reduced data density for clarity) used in the analysis along with the best-fit simulation and parameter values. Figure A.19 presents the pre-test history, and Figure A.20 shows the Ramey B normalized best-fit pressure and pressure derivatives.

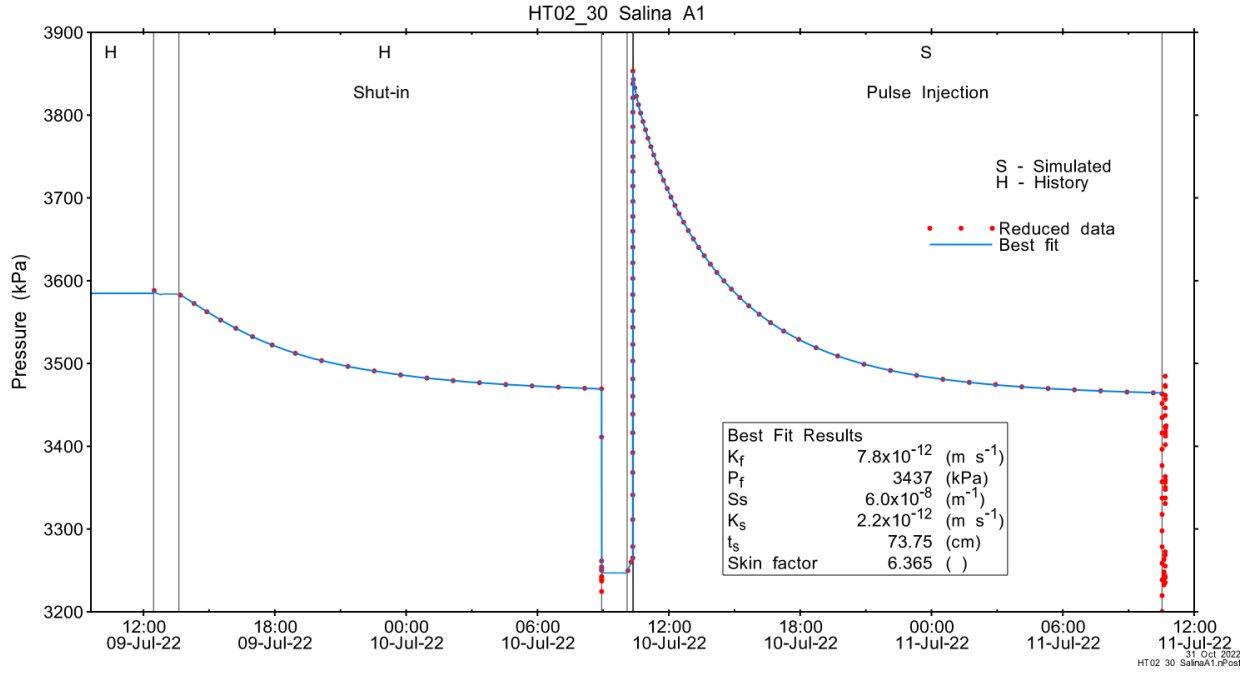

Figure A.99 - Annotated testing sequence showing best-fit simulation and parameter estimates.

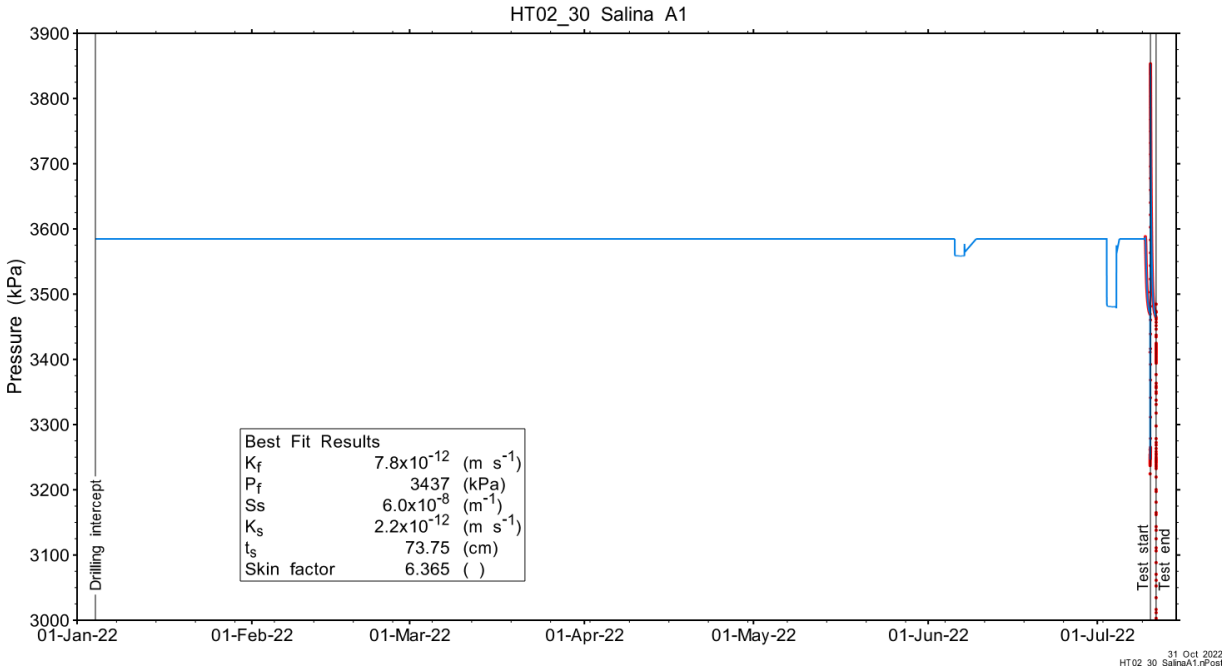

Figure A.100 - Annotated HT02_30 testing sequence showing pre-test history, best-fit simulation and parameter estimates.

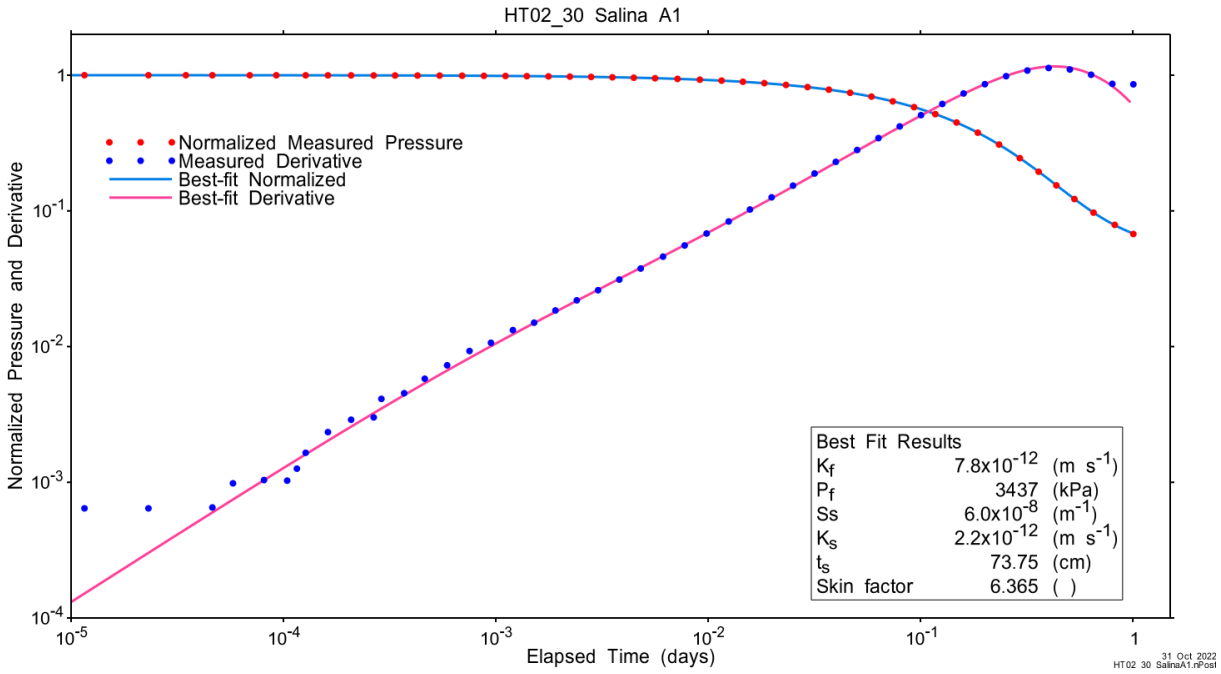

Figure A.101 - Log-log plot showing Ramey B and derivative response for best-fit simulation.

Figure A.21 shows the normalized parameter sensitivity response for the best fit. Sensitivity for all fitting parameters was relatively constant by the end of the test, indicating that the test duration was sufficient for well-constrained parameter estimation.

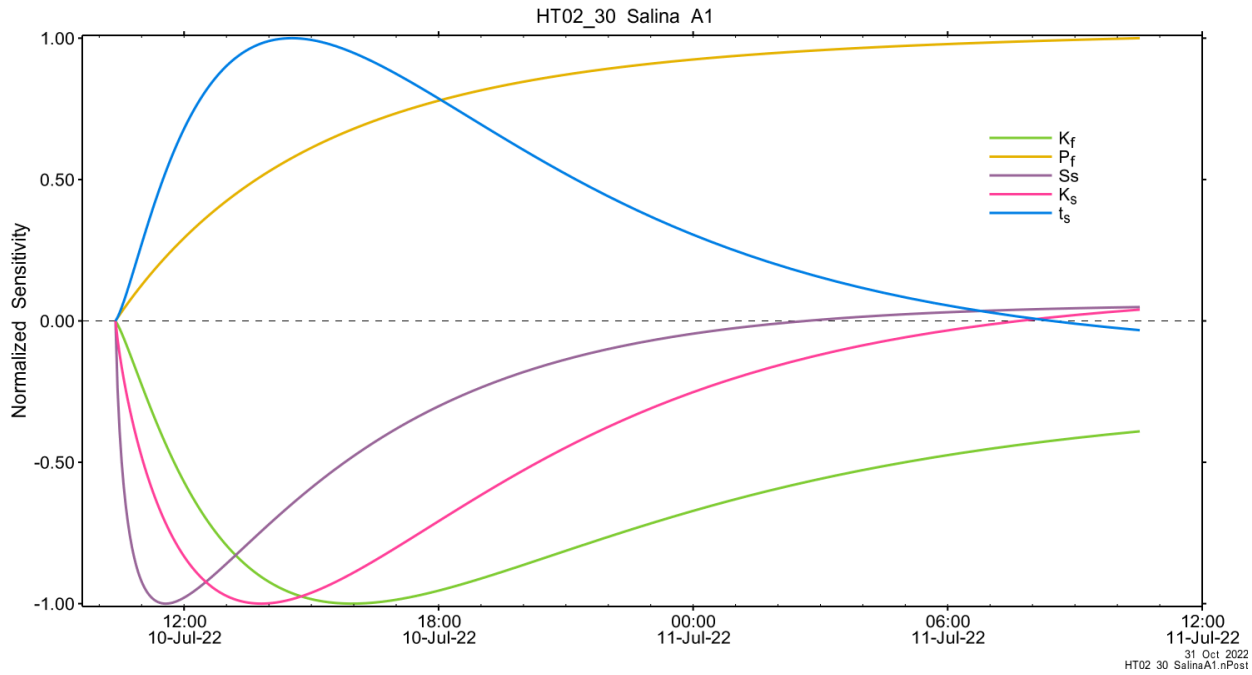

Figure A.102 - Normalized Jacobian for best-fit simulation.

A.7.3 Uncertainty Analyses

The CDF of normalized fit values for all converged simulations and the selected fit discriminant are shown in Figure A.22.

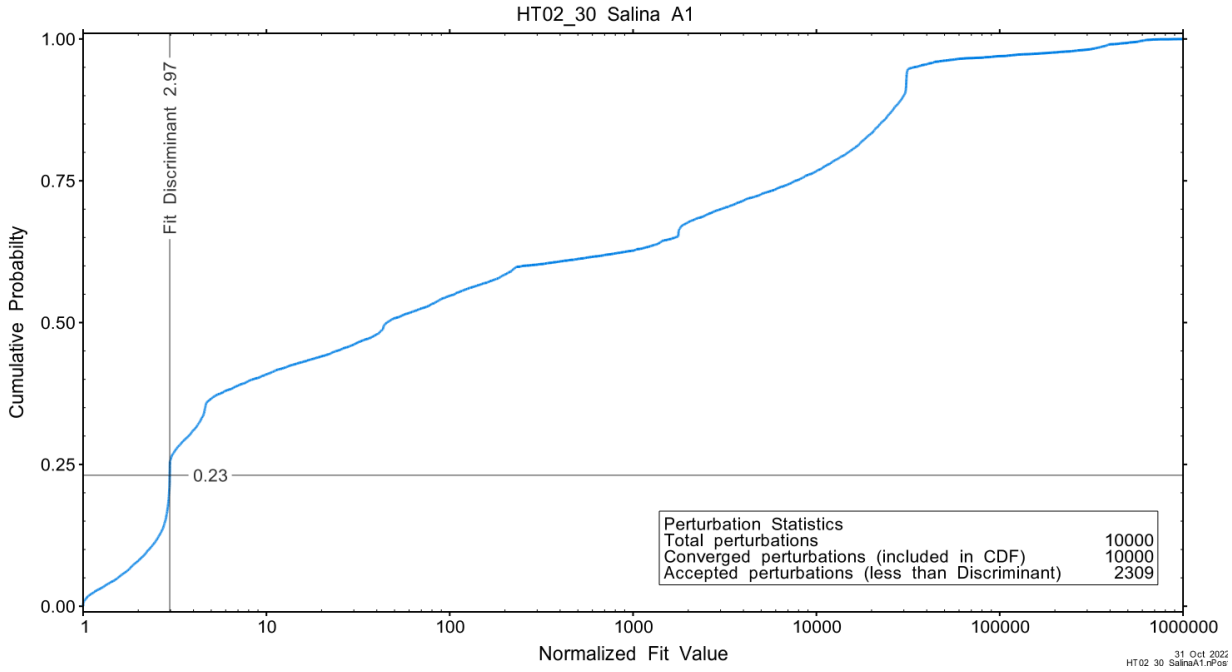

Figure A.103 - Fit value cumulative distribution function.

Summary cross parameter scatter plots for selected formation and skin parameters are given in Figure A.24 and Figure A.25. The light pink dots on the figures are the initial parameter estimates, with red dots overlaying those initial parameter values that resulted in accepted optimization results. The grey dots are converged optimizations which did not meet the fit discriminant. Larger varying color symbols represent the fit value of accepted optimizations, with the blue values representing the best fit.

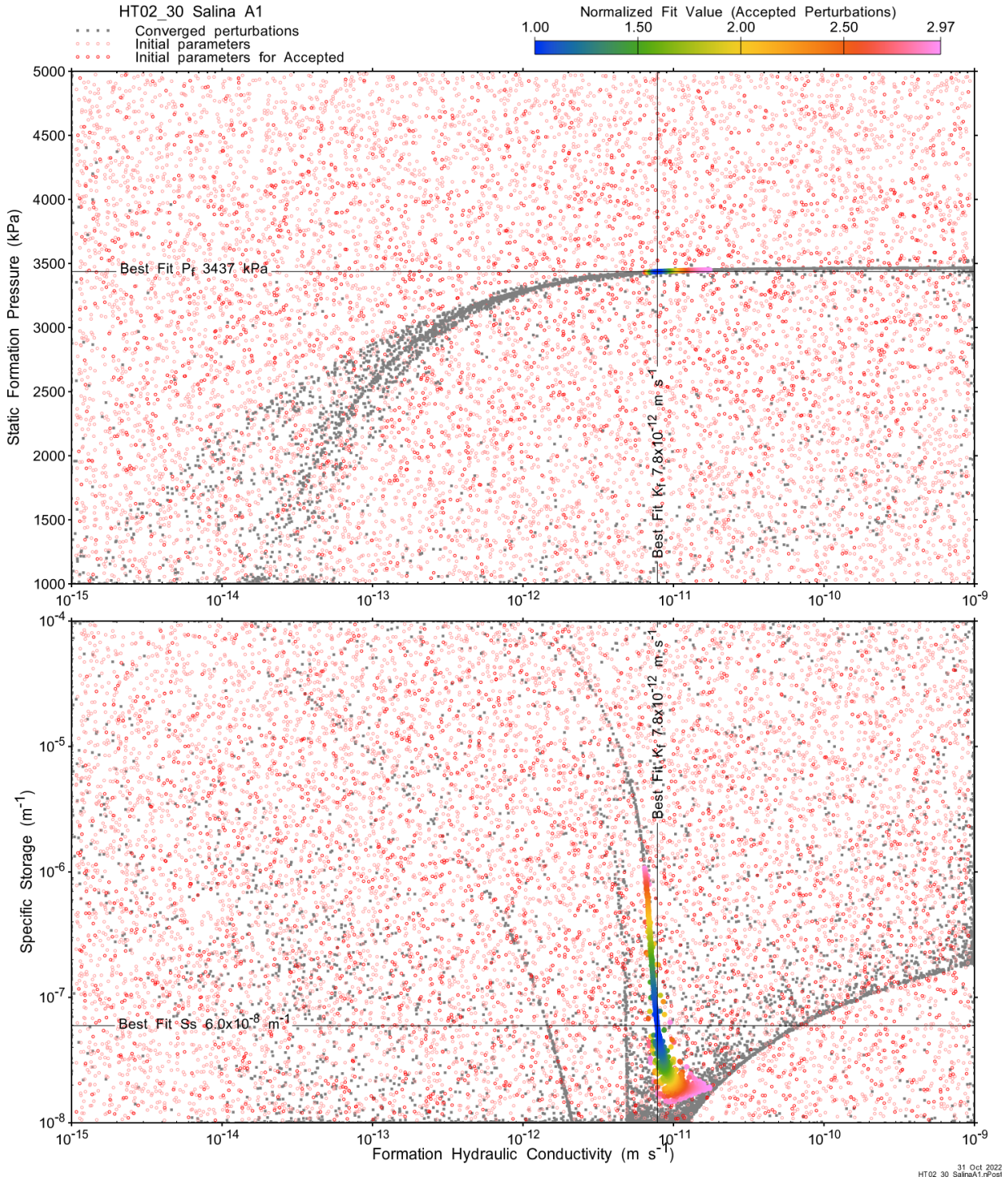

Figure A.104 - XY-scatter plot showing estimates of formation hydraulic conductivity (K_f) vs static formation pressure (P_f) (top panel) and specific storage (Ss) (bottom panel).

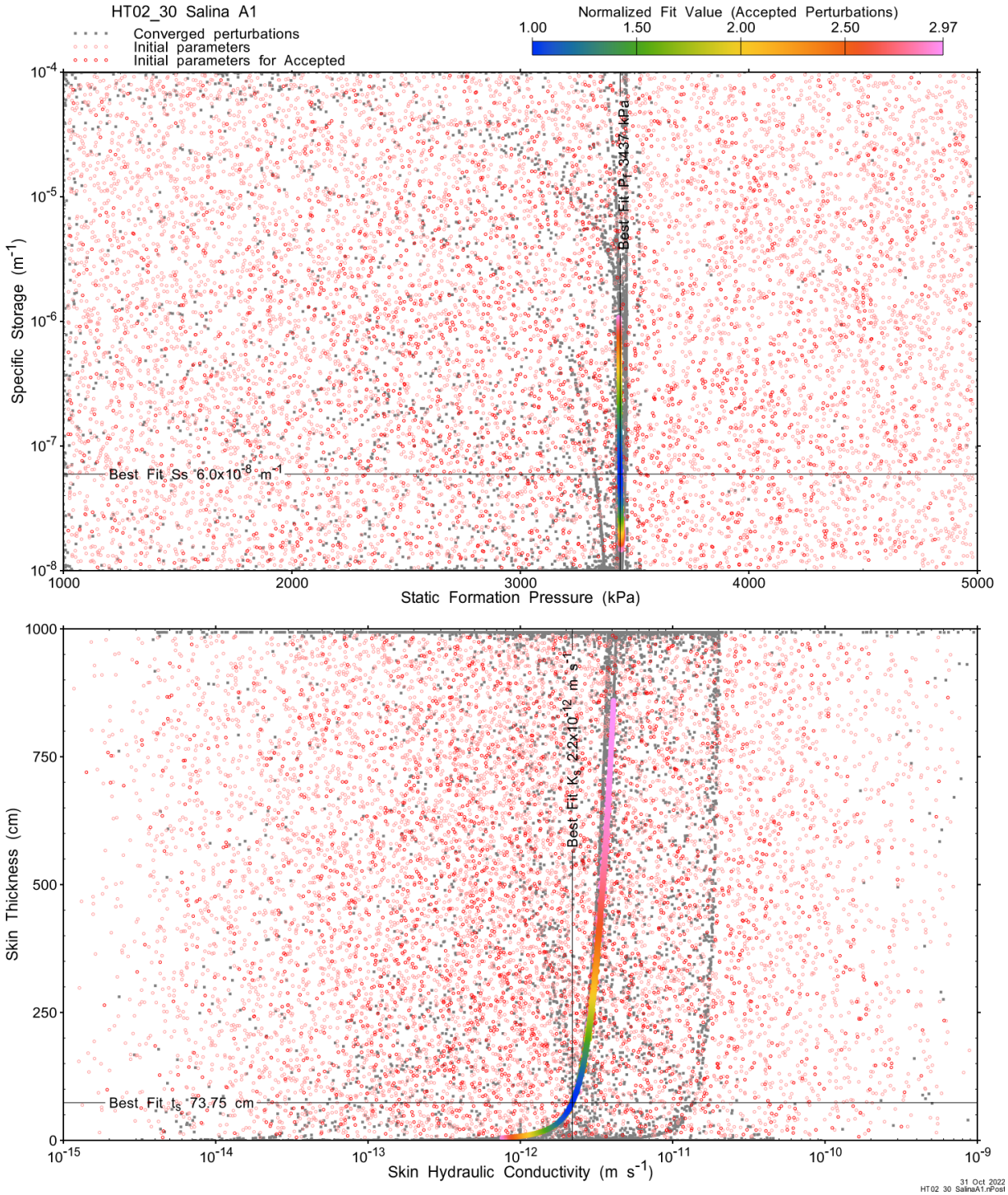

Figure A.105 - XY-scatter plot showing estimates of static formation pressure (P_f) vs specific storage (Ss) (top panel) and skin hydraulic conductivity (K_s) vs skin thickness (t_s) (bottom panel).

Confidence limits and median values are determined from the CDF of accepted optimization results (i.e. the varying color values in the above figures), with best fit value, 5% and 95% confidence indicated on Figure A.26 and Figure A.27.

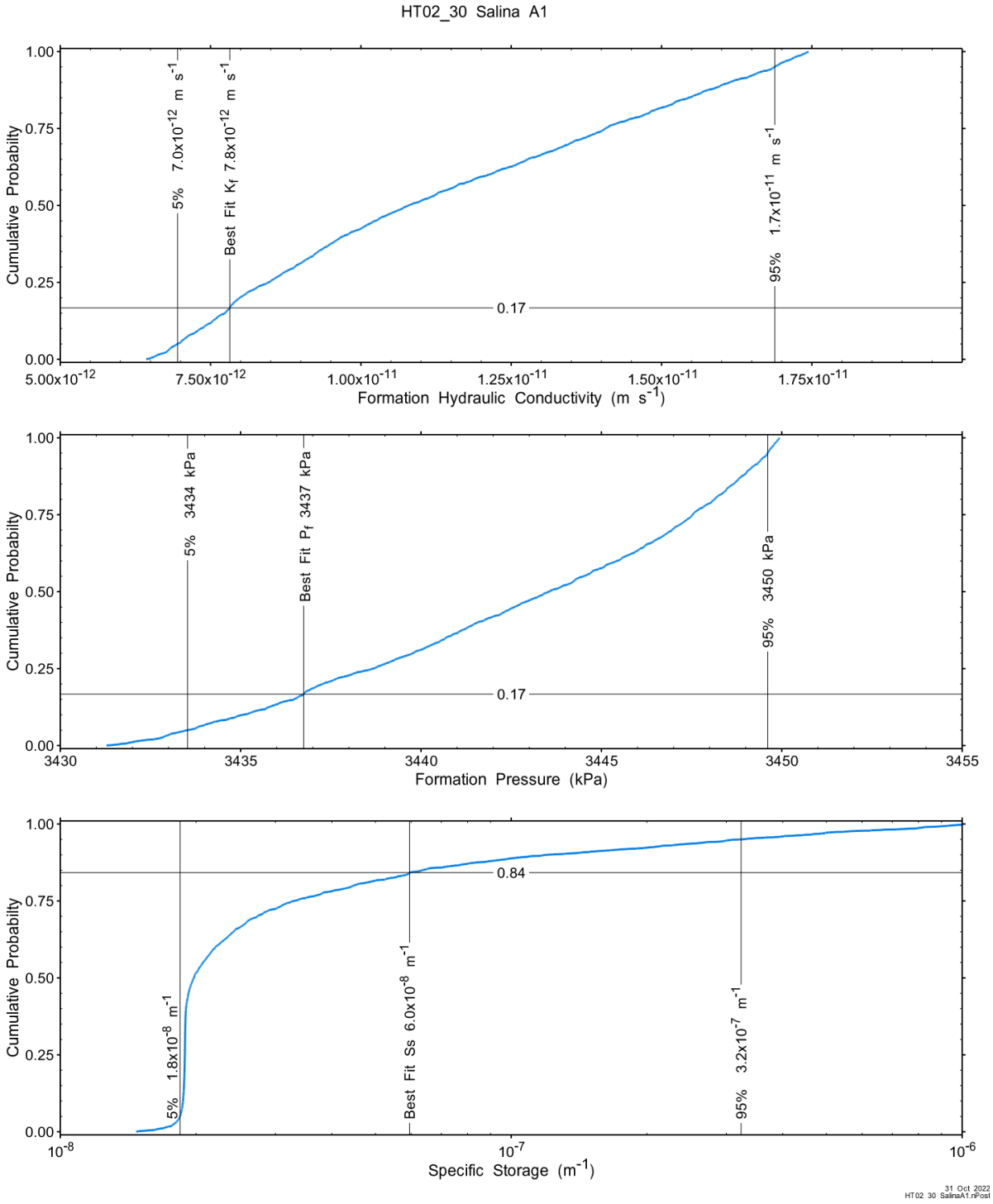

Figure A.106 – Cumulative distribution functions and parameter limits for formation hydraulic conductivity (K_f) (top panel), static formation pressure (P_f) (middle panel) and specific storage (Ss) (bottom panel).

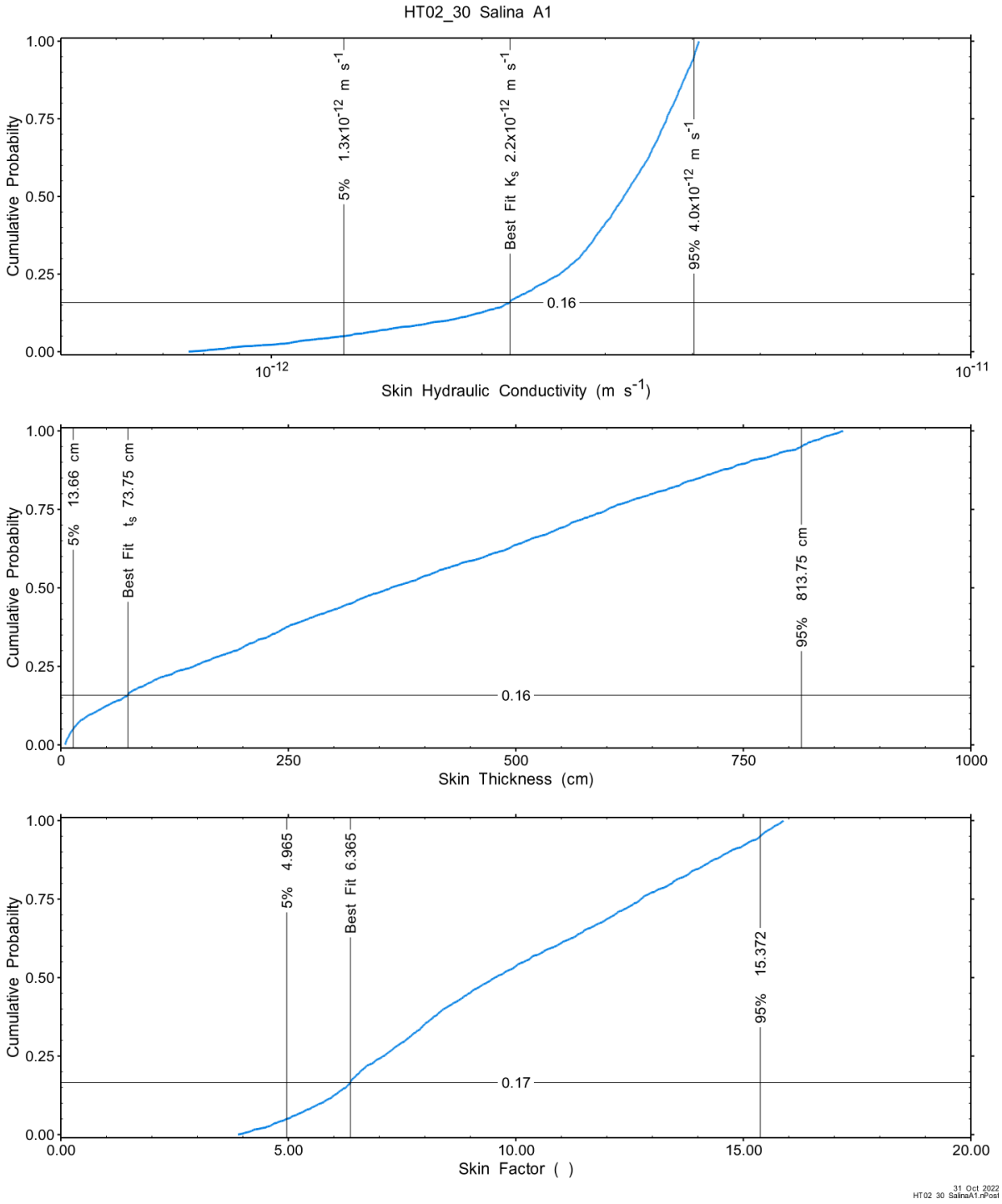

Figure A.107 – Cumulative distribution functions and parameter limits for skin hydraulic conductivity (K_s) (top panel), skin thickness (t_s) (middle panel) and skin factor (s) (bottom panel).

A summary of perturbation results is presented in Figure A.28, with Ramey-processed perturbations in Figure 12. Those perturbations (1953 of 10,000) with all parameters within the 5% and 95% range present a very good fit to the measured test zone data.

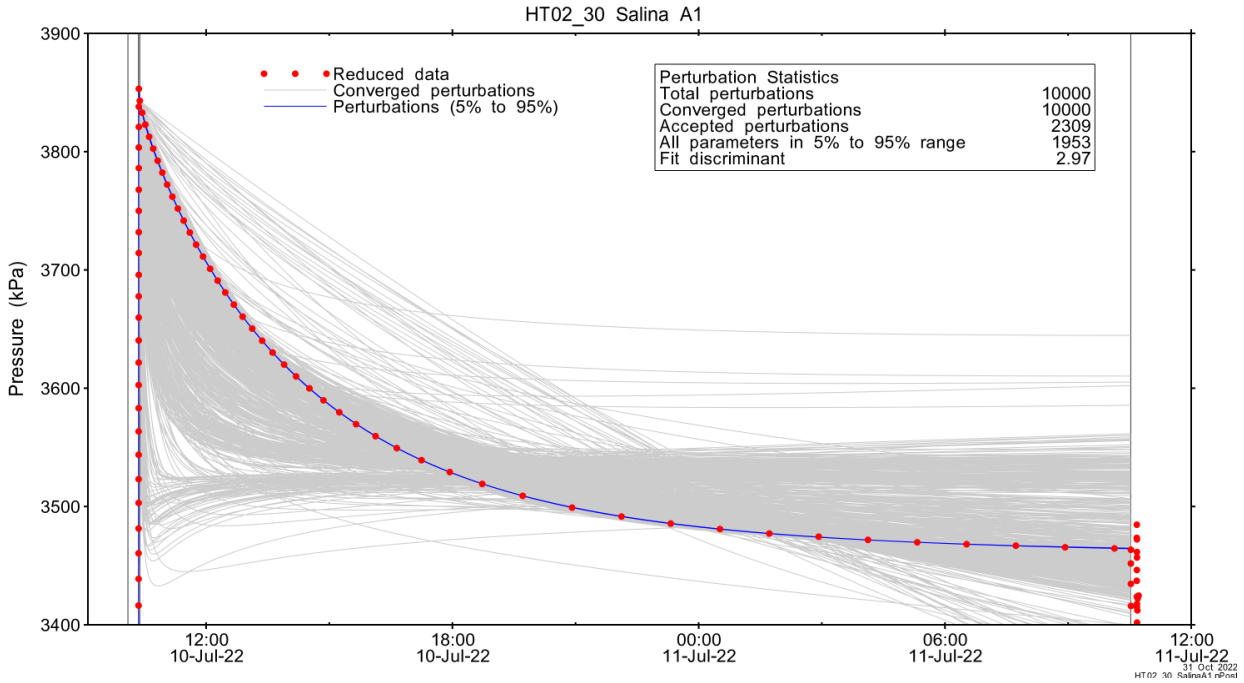

Figure A.108 – Perturbation results – all converged, accepted, and within 5% to 95% for all parameters.

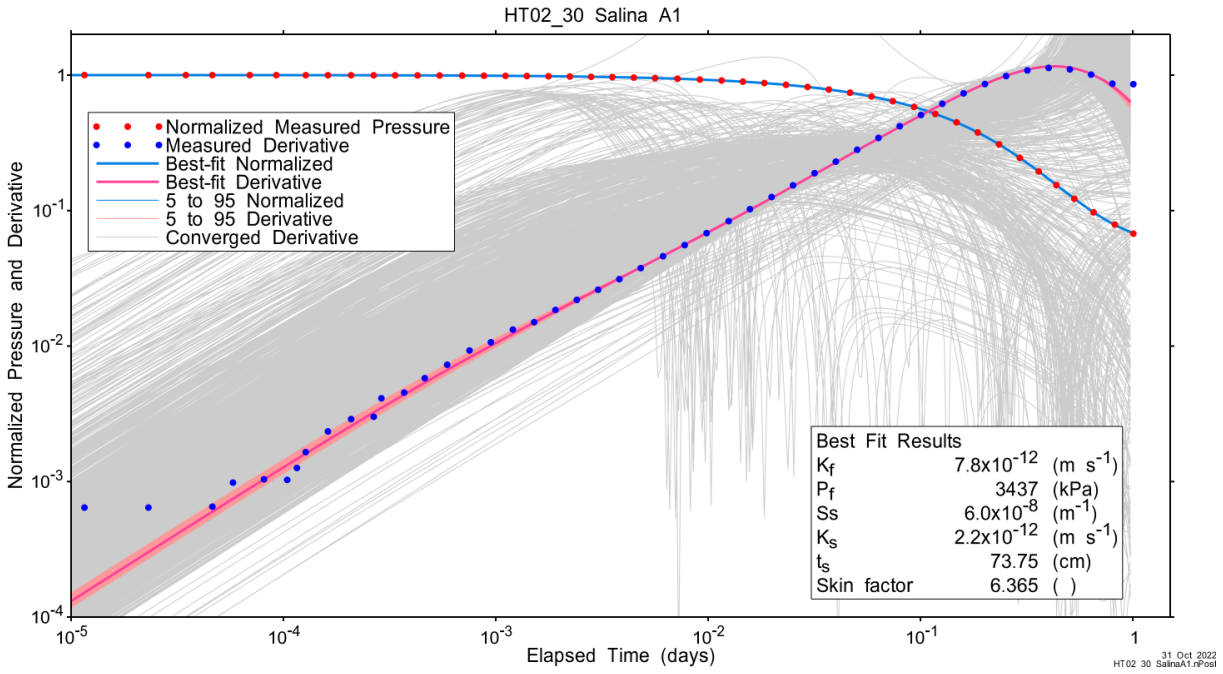

Figure A.109 – Log-log plot showing Ramey B and derivative response for all converged optimizations and those within 5% to 95% for all parameters.

A summary of best-fit and parameter ranges is given in Table A.9.

Table A.34 - Summary of the HT02_30 parameter estimates.

Parameter	Best Fit	5%	Median	95%
K_f (m/s)	7.8E-12	7.0E-12	1.1E-11	1.7E-11
P_f (kPa)	3437	3434	3444	3450
Ss (1/m)	6.0E-08	1.8E-08	2.0E-08	3.2E-07
K_s (m/s)	2.2E-12	1.3E-12	3.2E-12	4.0E-12
t_s (cm)	73.75	13.66	362.38	813.75
s (-)	6.365	4.965	9.538	15.372

Parameter correlations for all perturbations with all parameters within the 5% to 95% limits are given in Table A.5.

Table A.35 – Pearson cross-correlations of 5% to 95% parameters

	Log(K_f)	P_f	Log(Ss)	Log(K_s)	t_s	s
Log(K_f)	1.000	0.992	-0.753	0.916	0.995	0.997
Pf	0.992	1.000	-0.817	0.950	0.979	0.980
Log(S_s)	-0.753	-0.817	1.000	-0.952	-0.736	-0.723
Log(K_s)	0.916	0.950	-0.952	1.000	0.901	0.898
t_s	0.995	0.979	-0.736	0.901	1.000	0.997
s	0.997	0.980	-0.723	0.898	0.997	1.000

A.7.4 Additional Figures

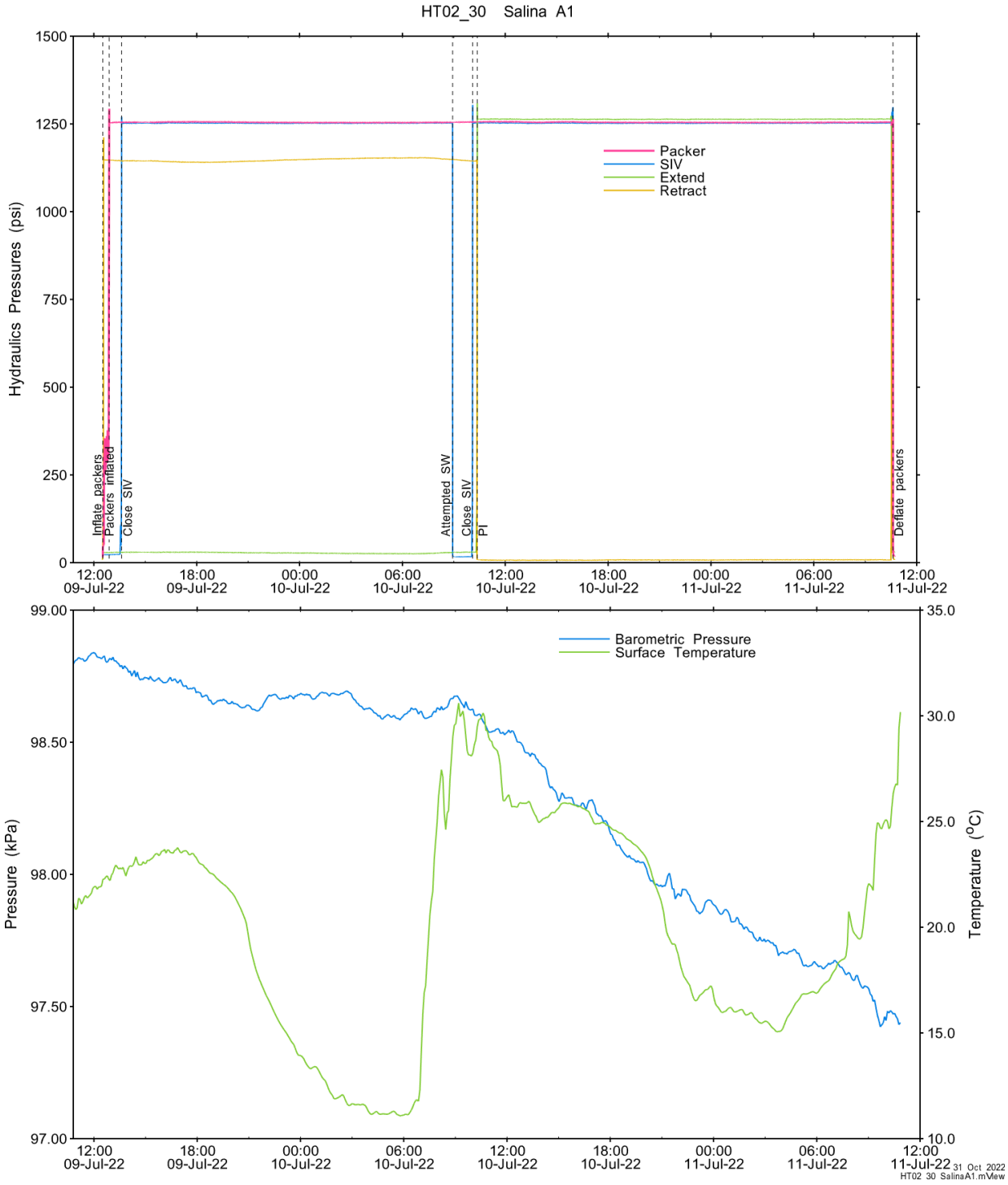

Figure A.110 - Hydraulics pressures and surface temperature/barometric pressure.

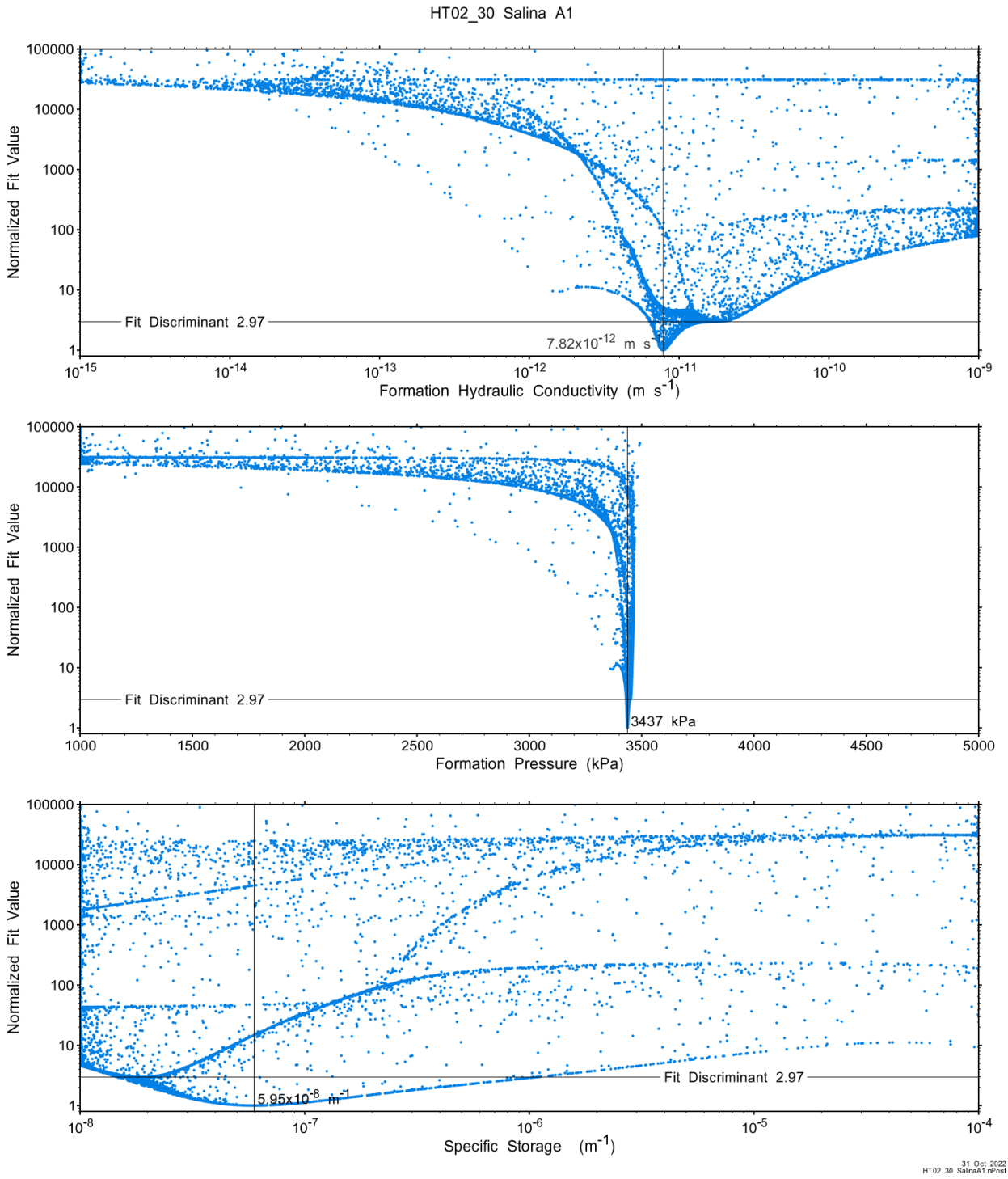

Figure A.111 - XY-scatter plot showing the formation parameter space normalized fit values.

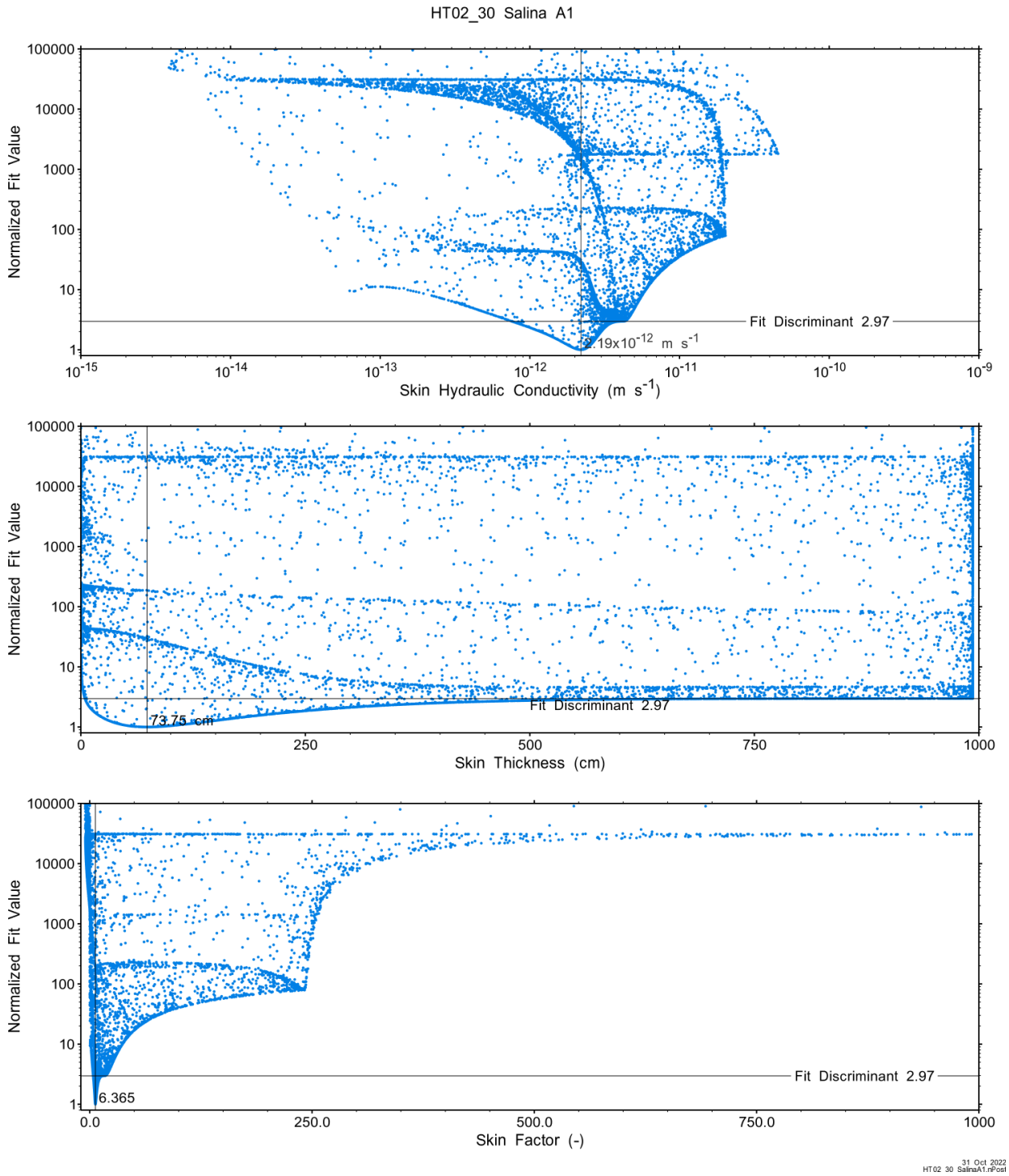

Figure A.112 - XY-scatter plot showing the skin parameter space normalized fit values.

A.8 HT03_30 Goat Island

The SB BH02 interval from 393.00 to 422.96 mBGS tested in HT03_30 includes the Goat Island, Gasport, Lions Head, and Fossil Hill Formations, as well as 3m of the upper Cabot Head Formation. A PI test was originally intended for the interval, however after the test zone was shut-in, the rapid equilibration of the test zone indicated relatively high permeability. Consequently, the tubing was swabbed and a one day duration SW test was conducted.

A.8.1 Test Data Summary

Table A.6 and Figure A.1 provide a summary of test events and a plot of pressures measured while testing respectively.

Table A.36 - Summary of Test Events.

Event	Start Date & Time	Duration (days)	TZ Pressure (kPa)
Drilling intercept	22-01-05 10:12	187.16	4044
Shut-in	22-07-11 14:02	0.78	4055
Slug withdrawal	22-07-12 08:41	1.00	3849
Test end	22-07-13 08:43		4035

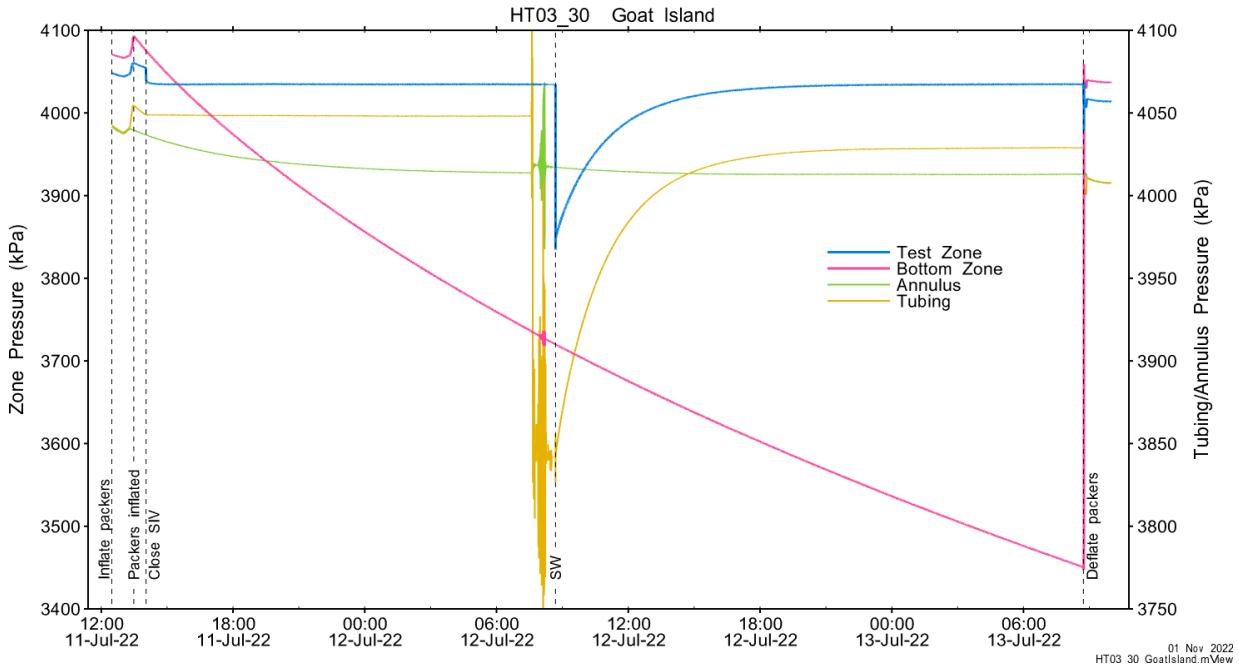

Figure A.113 - Test events and pressures.

A.8.2 Test Analyses

Table A.7 is a summary of test-specific input parameters used in the analyses, while Table A.8 presents the optimized parameters and allowed ranges.

Table A.37 – nSIGHTS Input Parameters.

Parameter	Value	Units
Test zone radius	6.71	cm
Tubing string radius	2.54	cm
Test zone length	29.96	m

Table A.38 – nSIGHTS Parameter Optimization Ranges.

Parameter	Minimum	Maximum	Units	Type
Formation hydraulic conductivity (K_f)	1E-12	1E-05	m/s	log
Formation pressure (P_f)	3000	5000	kPa	linear
Specific storage (S_s)	1E-08	1E-04	1/m	log
Skin hydraulic conductivity (K_s)	1E-12	1E-05	m/s	log
Skin thickness (t_s)	0.013	10000	cm	linear

Figure A.18 shows the measured test zone pressure record (with reduced data density for clarity) used in the analysis along with the best-fit simulation and parameter values. Figure A.19 presents the pre-test history, and Figure A.20 shows the Ramey B normalized best-fit pressure and pressure derivatives.

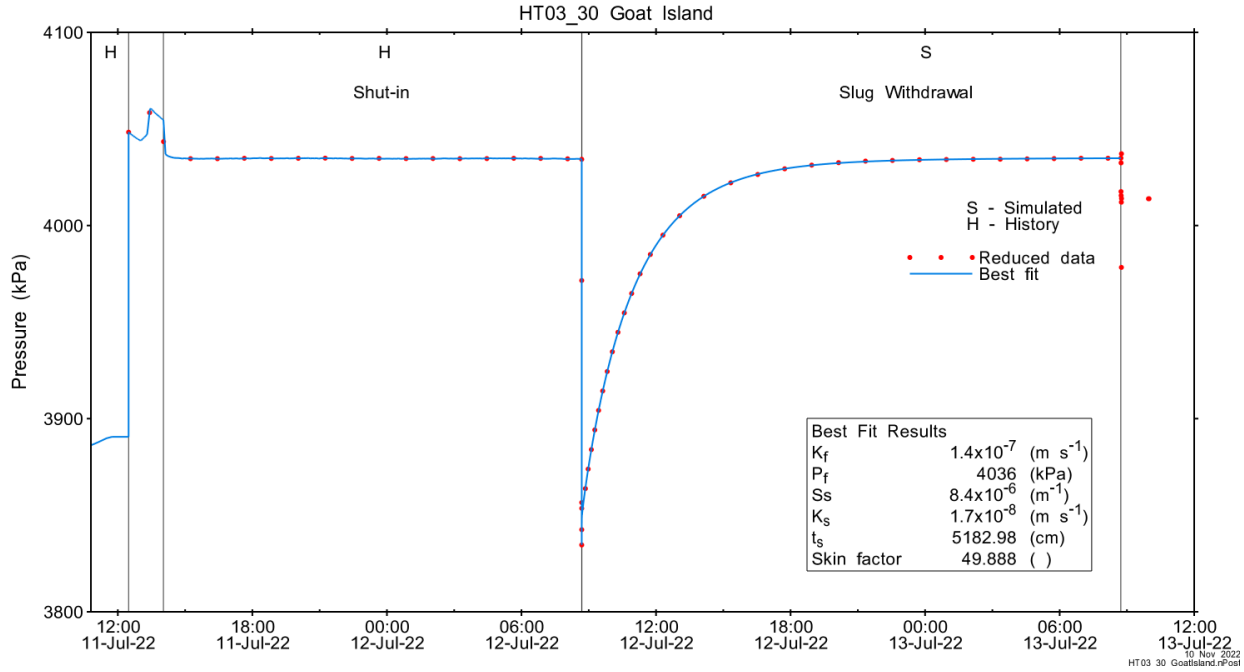

Figure A.114 - Annotated testing sequence showing best-fit simulation and parameter estimates.

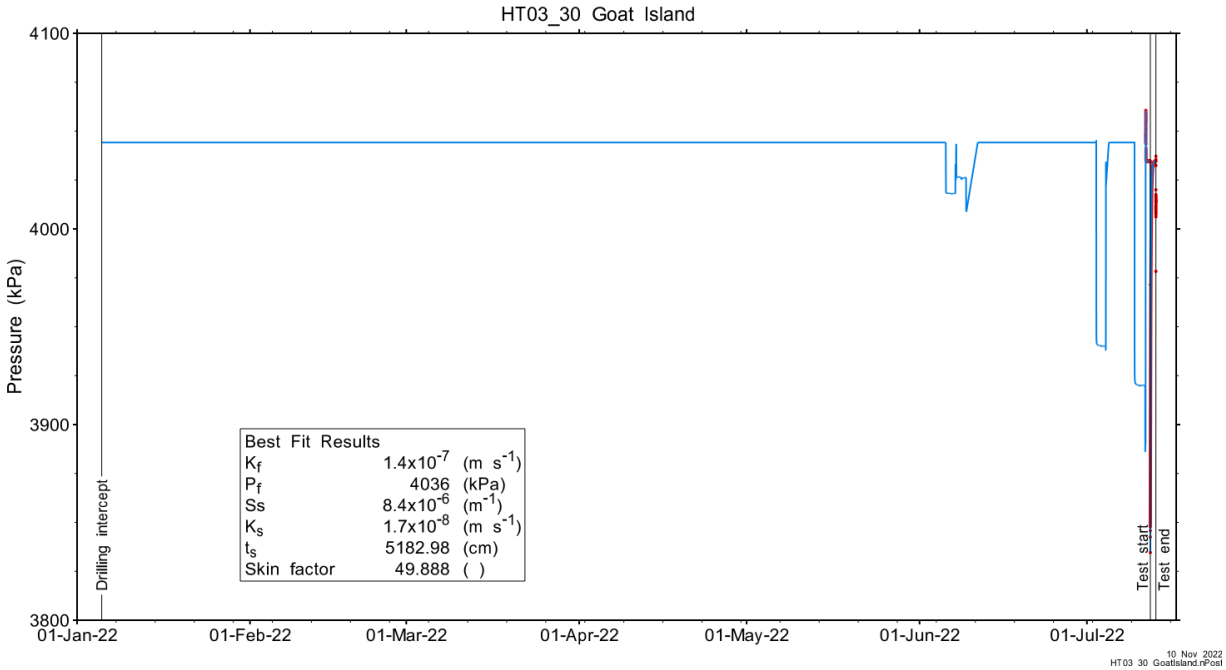

Figure A.115 - Annotated HT03_30 testing sequence showing pre-test history, best-fit simulation and parameter estimates.

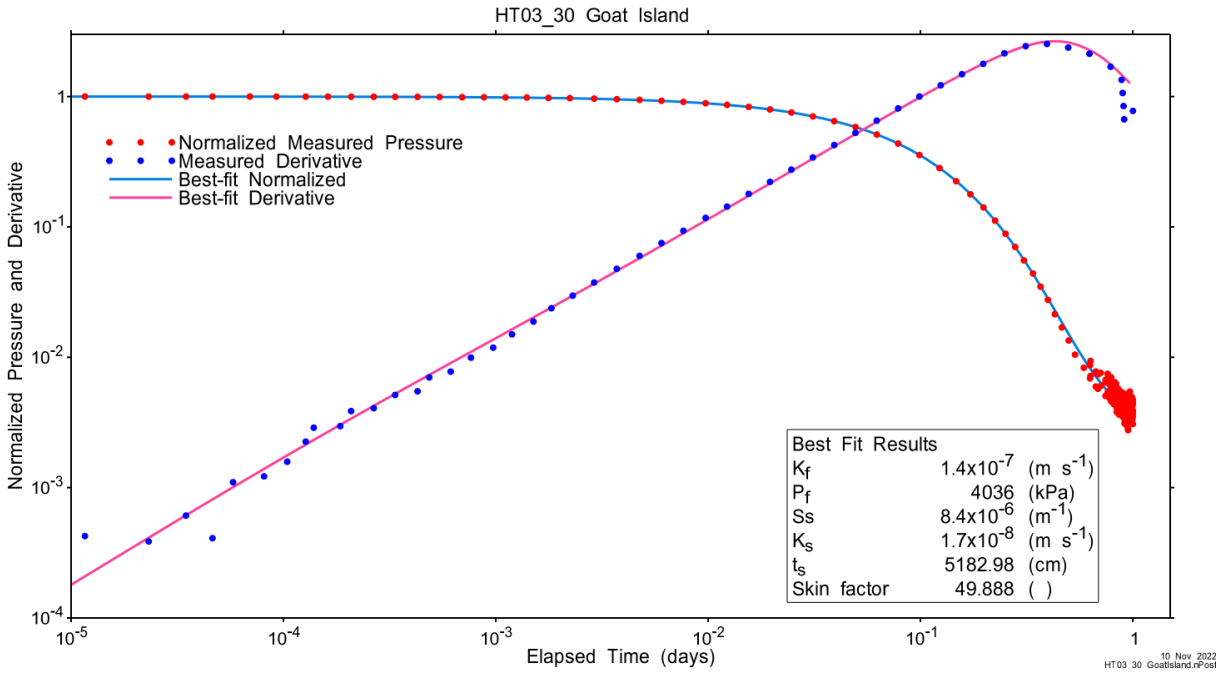

Figure A.116 - Log-log plot showing Ramey B and derivative response for best-fit simulation.

Figure A.21 shows the normalized parameter sensitivity response for the best fit. Sensitivity for all fitting parameters was relatively constant by the end of the test, indicating that the test duration was sufficient for well-constrained parameter estimation.

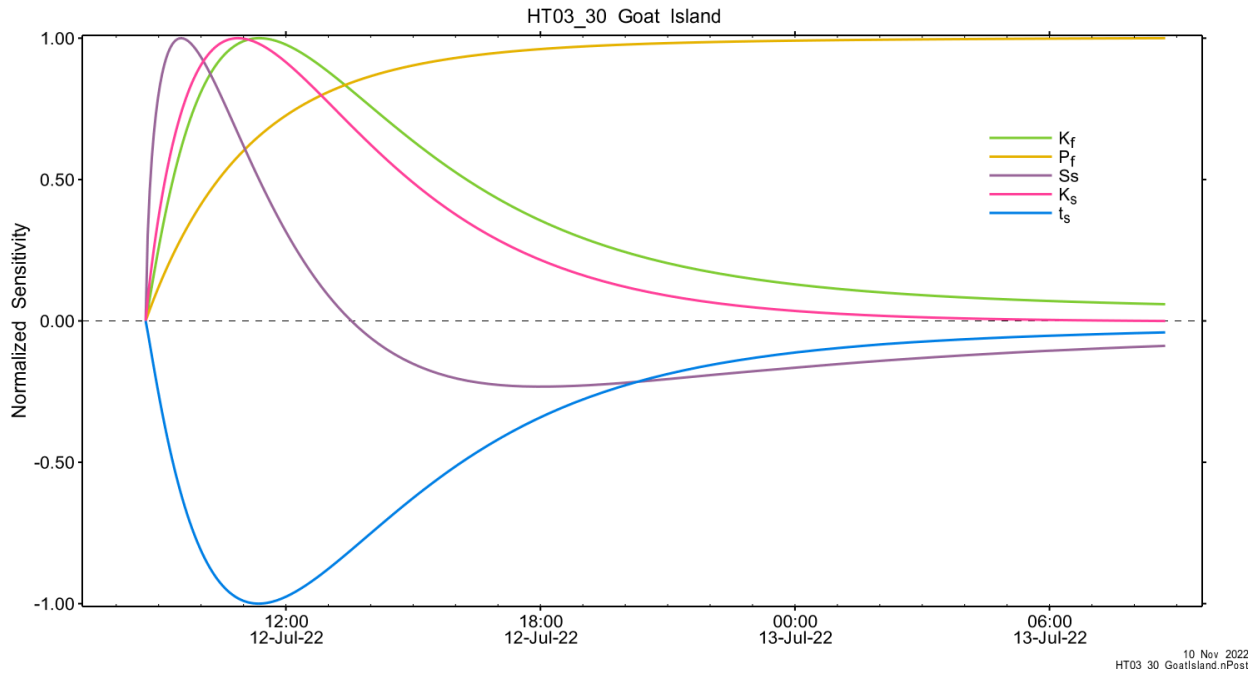

Figure A.117 - Normalized Jacobian for best-fit simulation.

A.8.3 Uncertainty Analyses

The CDF of normalized fit values for all converged simulations and the selected fit discriminant are shown in Figure A.22 and Figure A.119.

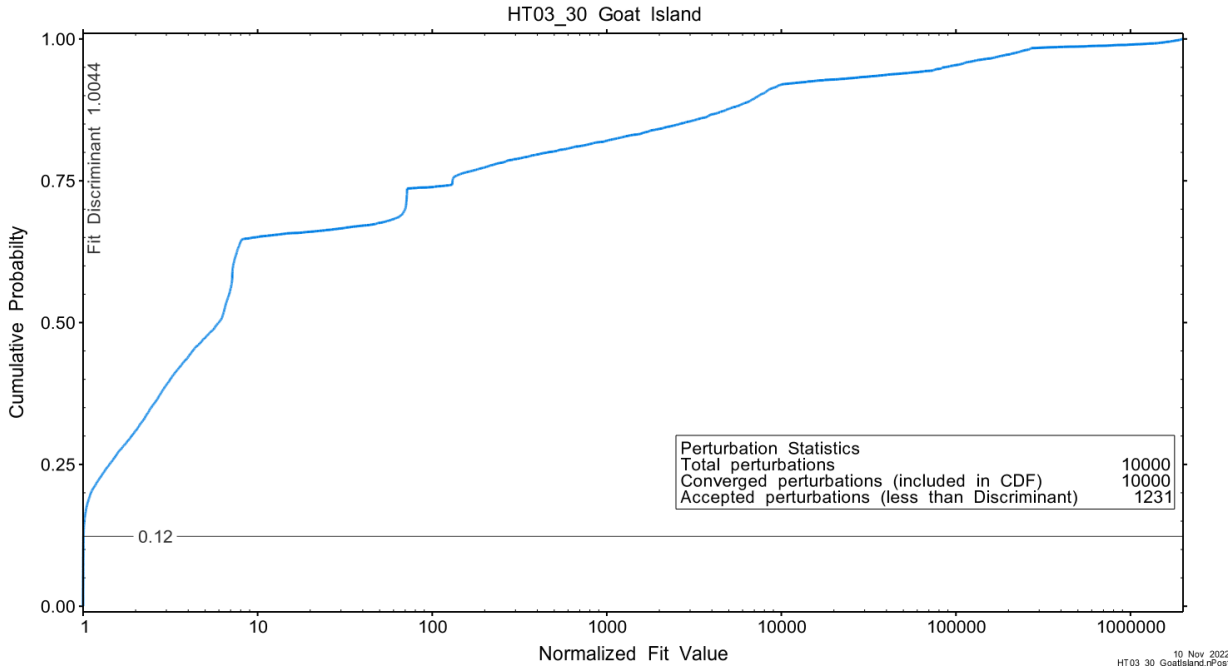

Figure A.118 - Fit value cumulative distribution function.

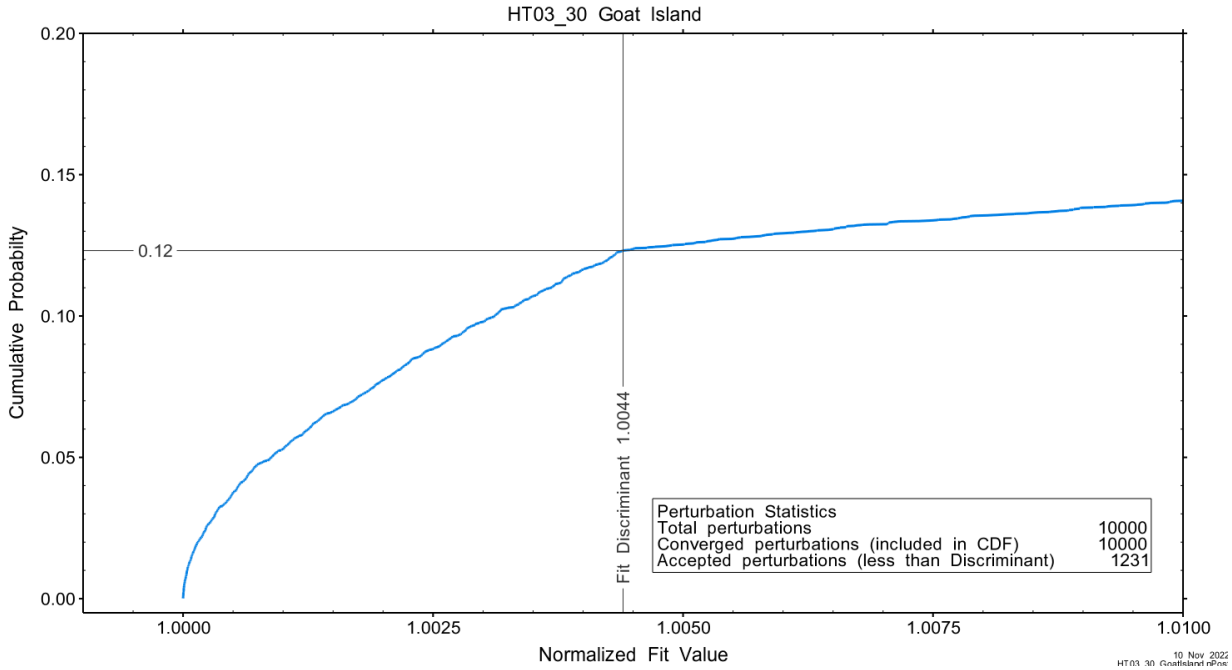

Figure A.119 – Detail - fit value cumulative distribution function.

Summary cross parameter scatter plots for selected formation and skin parameters are given in Figure A.24 and Figure A.25. The light pink dots on the figures are the initial parameter estimates, with red dots overlaying those initial parameter values that resulted in accepted optimization results. The grey dots are converged optimizations which did not meet the fit discriminant. Larger varying color symbols represent the fit value of accepted optimizations, with the blue values representing the best fit.

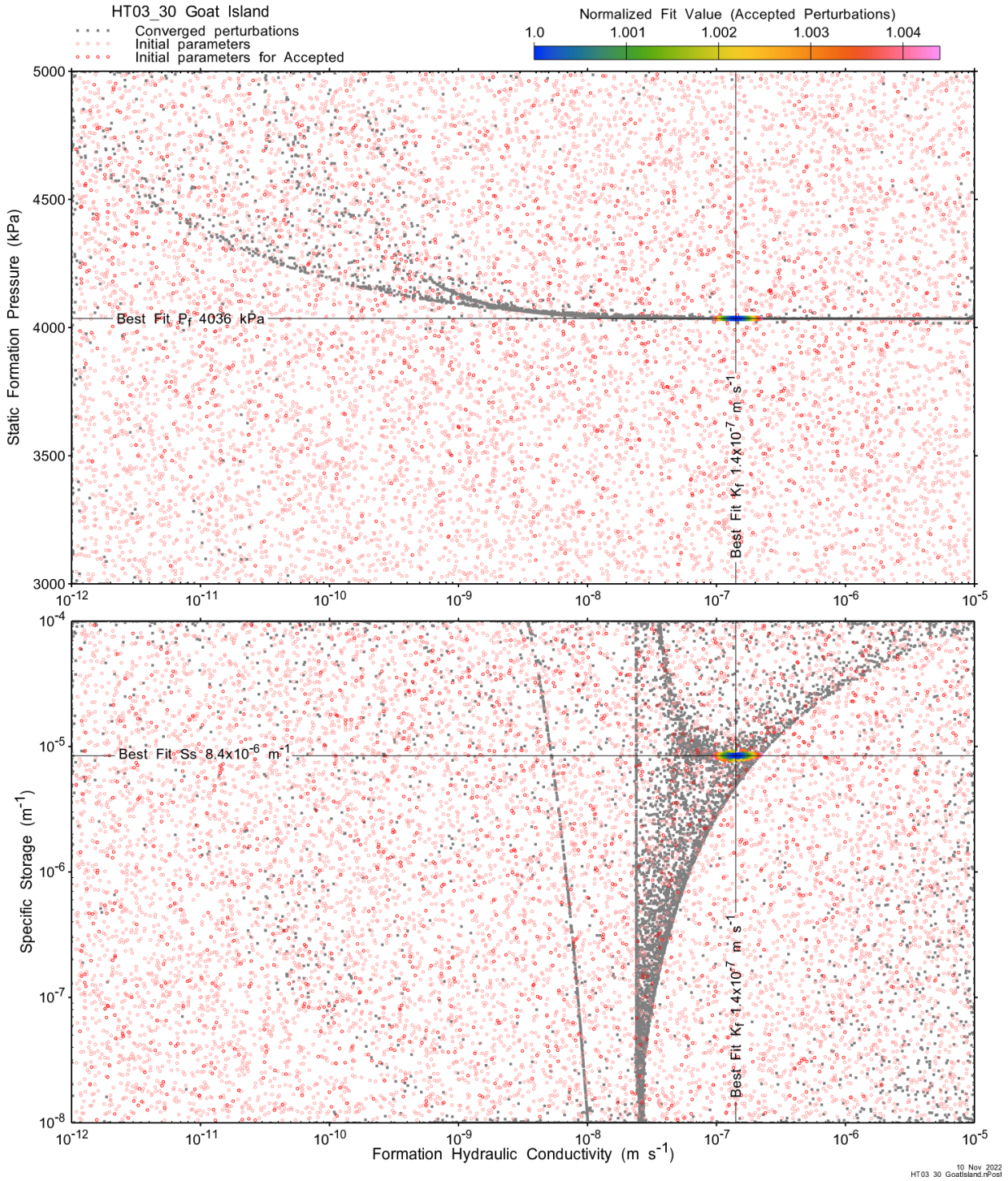

Figure A.120 - XY-scatter plot showing estimates of formation hydraulic conductivity (K_f) vs static formation pressure (P_f) (top panel) and specific storage (Ss) (bottom panel).

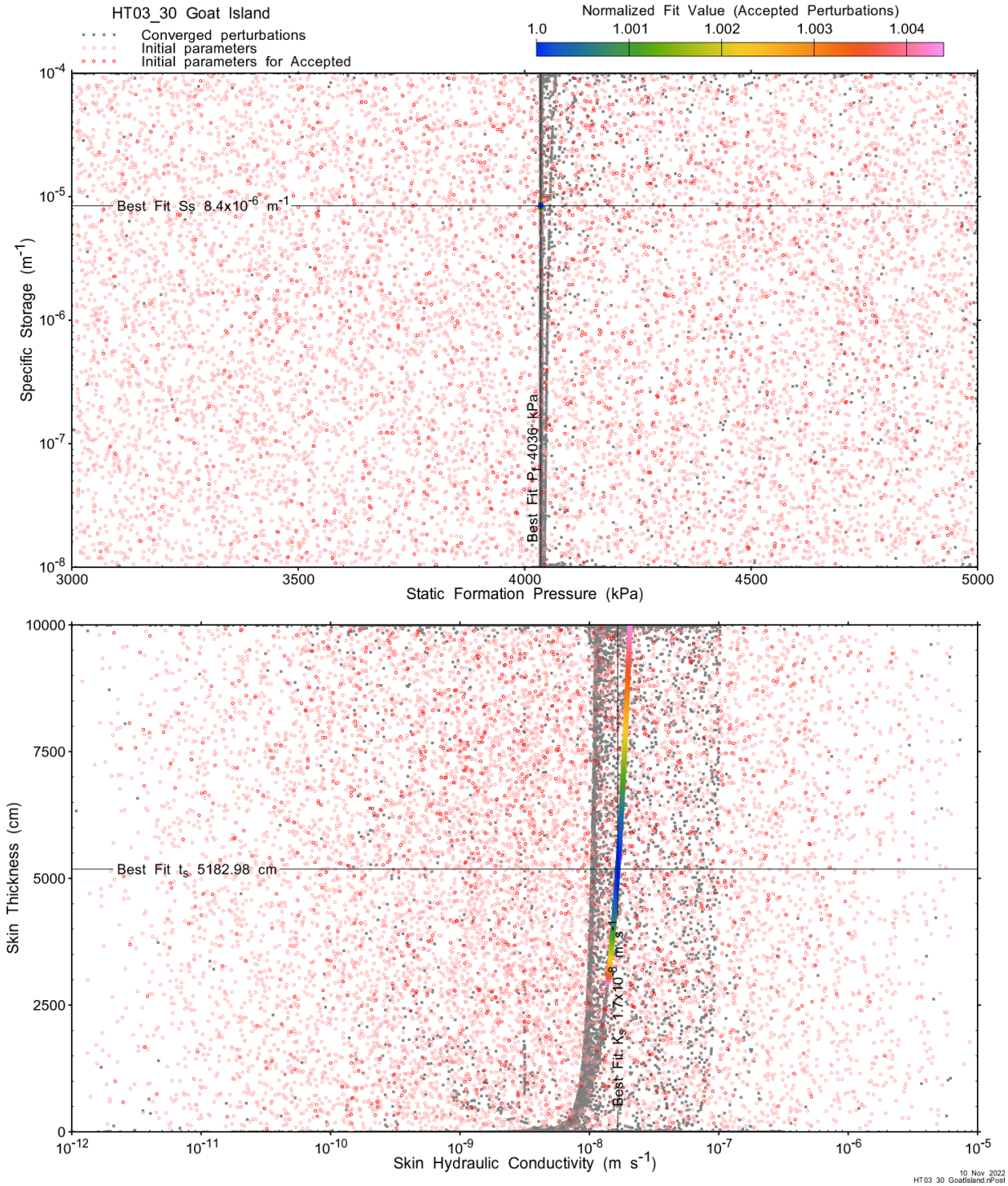

Figure A.121 - XY-scatter plot showing estimates of static formation pressure (P_f) vs specific storage (Ss) (top panel) and skin hydraulic conductivity (K_s) vs skin thickness (t_s) (bottom panel).

Confidence limits and median values are determined from the CDF of accepted optimization results (i.e. the varying color values in the above figures), with best fit value, 5% and 95% confidence indicated on Figure A.26 and Figure A.27.

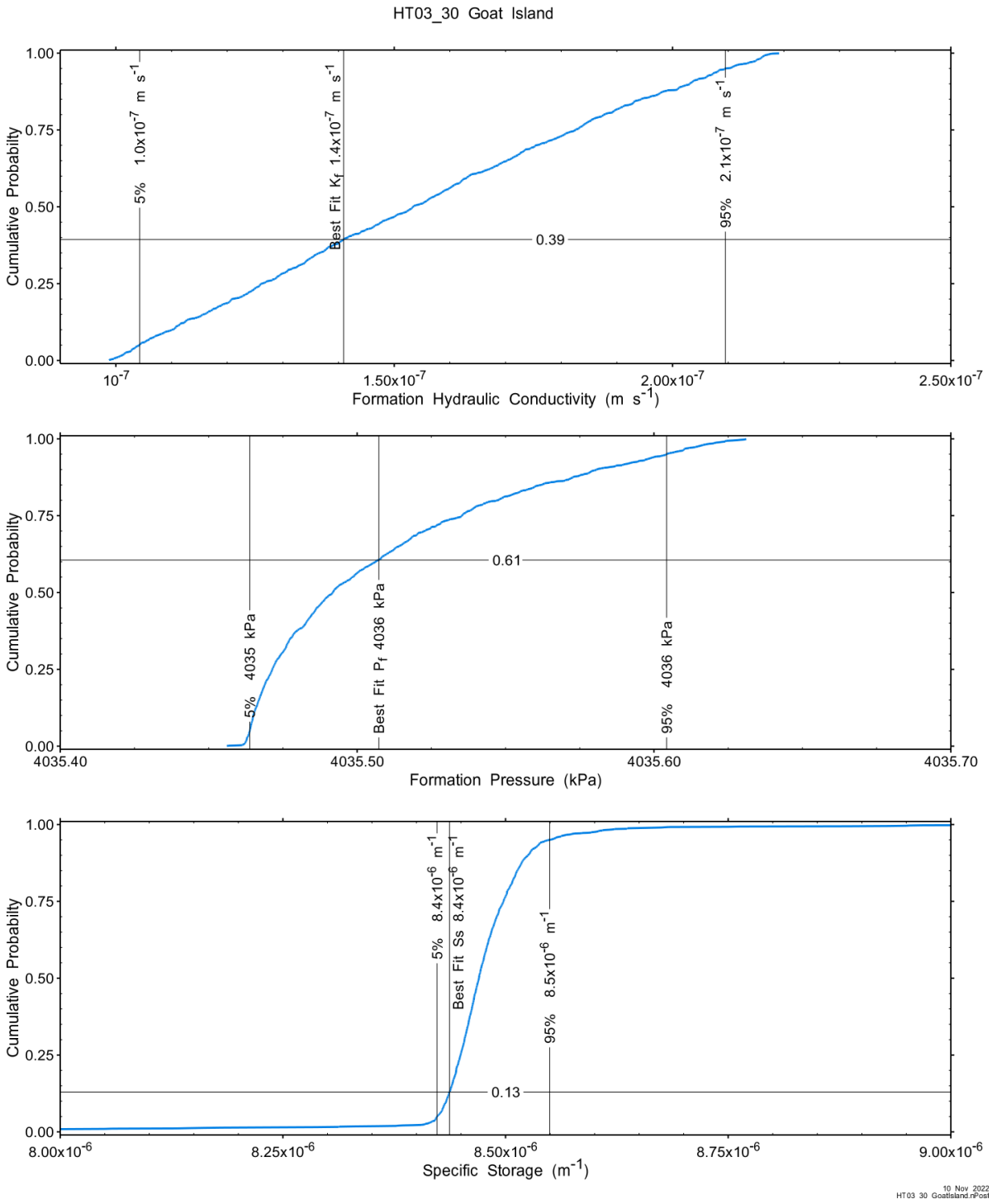

Figure A.122 – Cumulative distribution functions and parameter limits for formation hydraulic conductivity (K_f) (top panel), static formation pressure (P_f) (middle panel) and specific storage (Ss) (bottom panel).

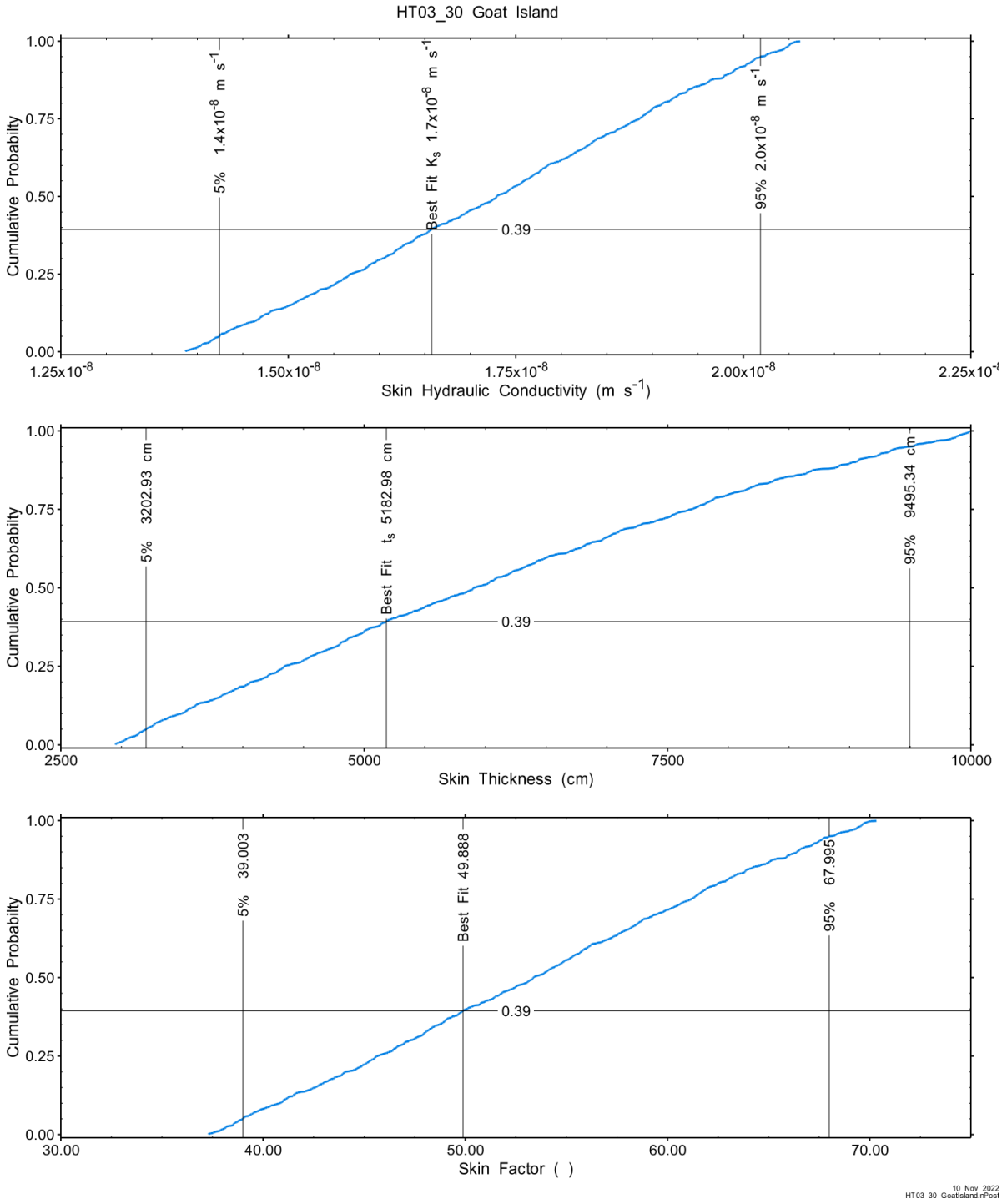

Figure A.123 – Cumulative distribution functions and parameter limits for skin hydraulic conductivity (K_s) (top panel), skin thickness (t_s) (middle panel) and skin factor (s) (bottom panel).

A summary of perturbation results is presented in Figure A.28, with Ramey-processed perturbations in Figure 12. Those perturbations (999 of 10,000) with all parameters within the 5% and 95% range present a very good fit to the measured test zone data.

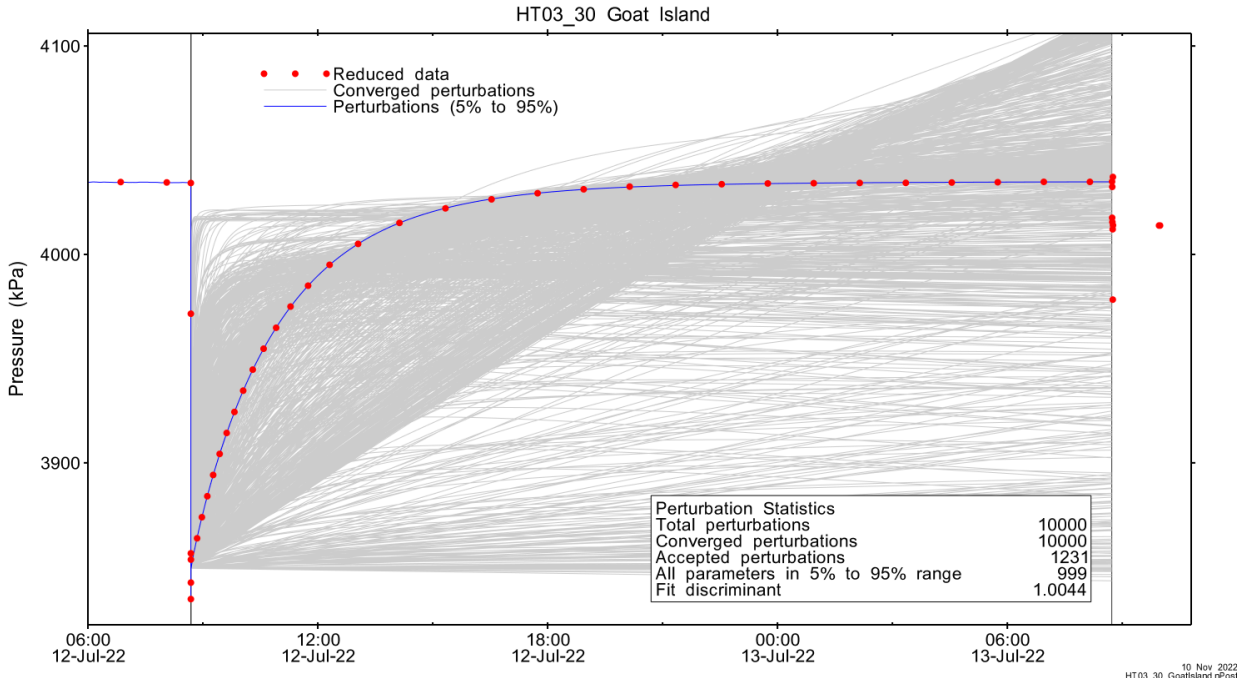

Figure A.124 – Perturbation results – all converged, accepted, and within 5% to 95% for all parameters.

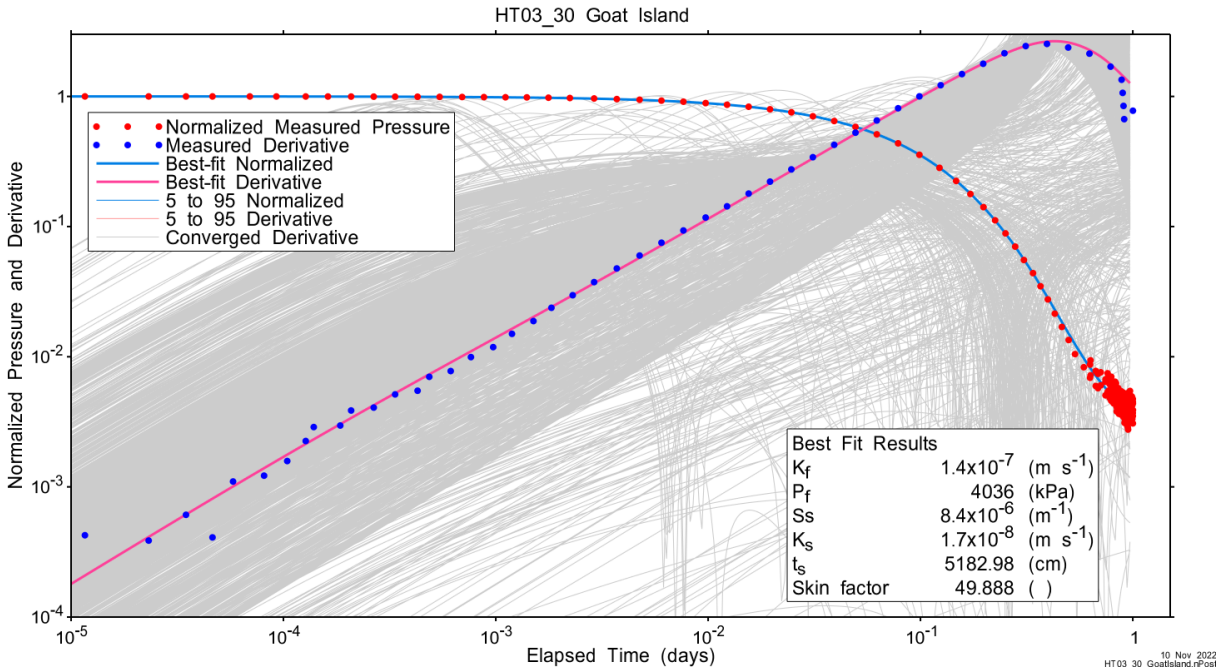

Figure A.125 – Log-log plot showing Ramey B and derivative response for all converged optimizations and those within 5% to 95% for all parameters.

A summary of best-fit and parameter ranges is given in Table A.9.

Table A.39 - Summary of the HT03_30 parameter estimates.

Parameter	Best Fit	5%	Median	95%
K_f (m/s)	1.4E-07	1.0E-07	1.5E-07	2.1E-07
P_f (kPa)	4036	4035	4035	4036
Ss (1/m)	8.4E-06	8.4E-06	8.5E-06	8.5E-06
K_s (m/s)	1.7E-08	1.4E-08	1.7E-08	2.0E-08
t_s (cm)	5182.98	3202.93	5900.29	9495.34
s (-)	49.888	39.003	53.377	67.995

Parameter correlations for all perturbations with all parameters within the 5% to 95% limits are given in Table A.5.

Table A.40 – Pearson cross-correlations of 5% to 95% parameters

	Log(K_f)	P_f	Log(Ss)	Log(K_s)	t_s	s
Log(K_f)	1.000	-0.980	-0.985	0.996	0.960	0.978
Pf	-0.980	1.000	0.997	-0.992	-0.888	-0.920
Log(S_s)	-0.985	0.997	1.000	-0.996	-0.905	-0.933
Log(K_s)	0.996	-0.992	-0.996	1.000	0.936	0.959
t_s	0.960	-0.888	-0.905	0.936	1.000	0.997
s	0.978	-0.920	-0.933	0.959	0.997	1.000

A.8.4 Additional Figures

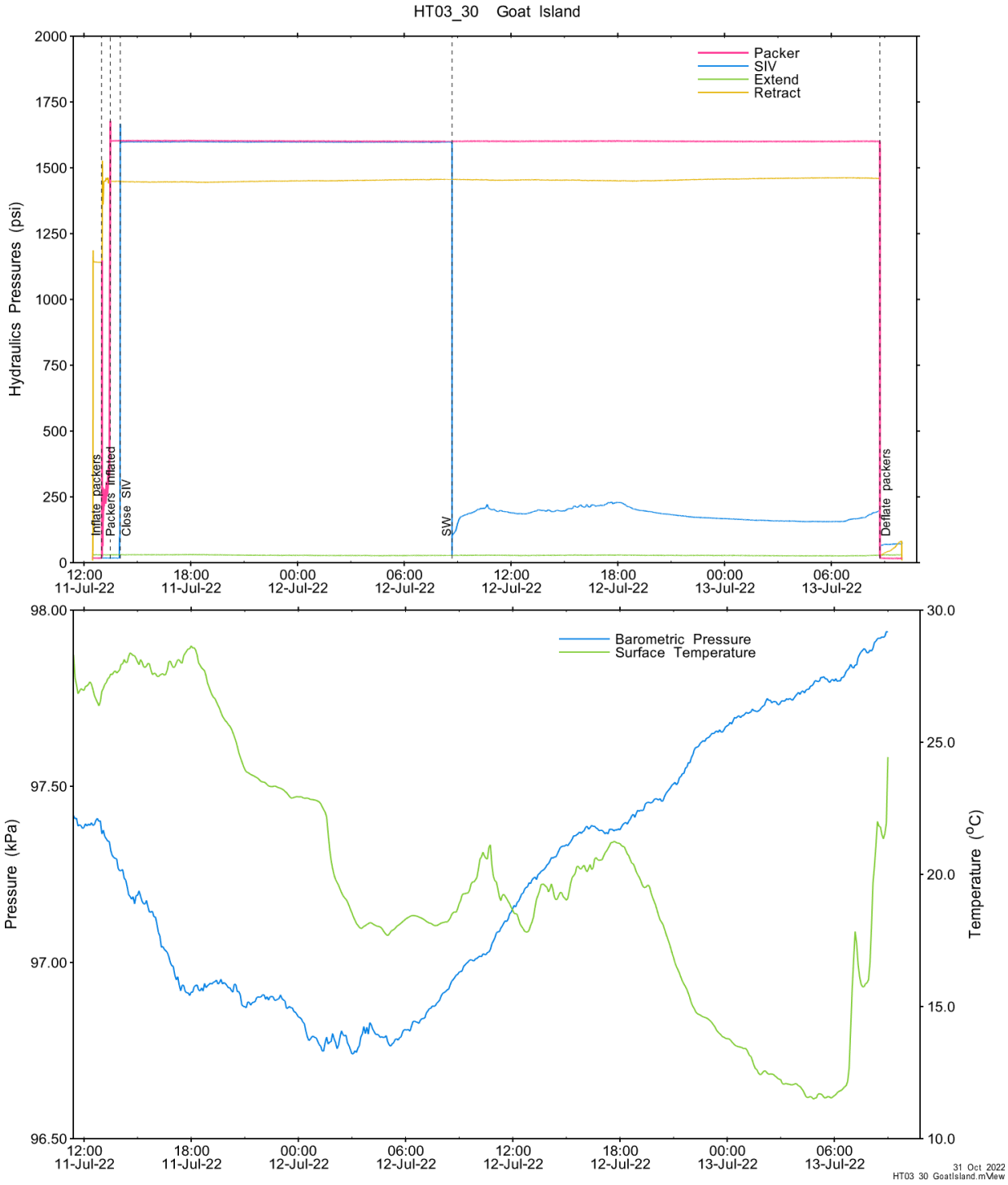

Figure A.126 - Hydraulics pressures and surface temperature/barometric pressure.

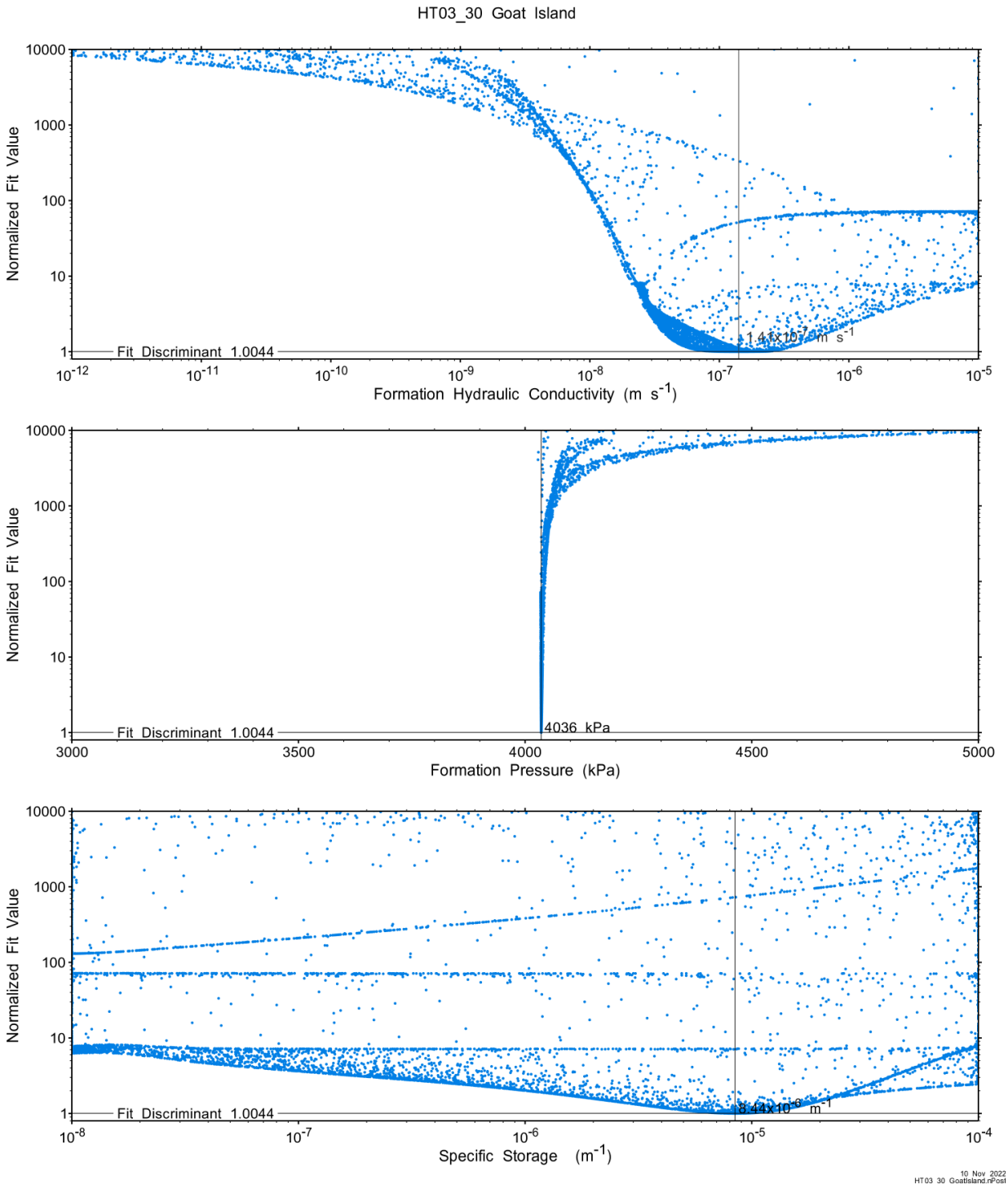

Figure A.127 - XY-scatter plot showing the formation parameter space normalized fit values.

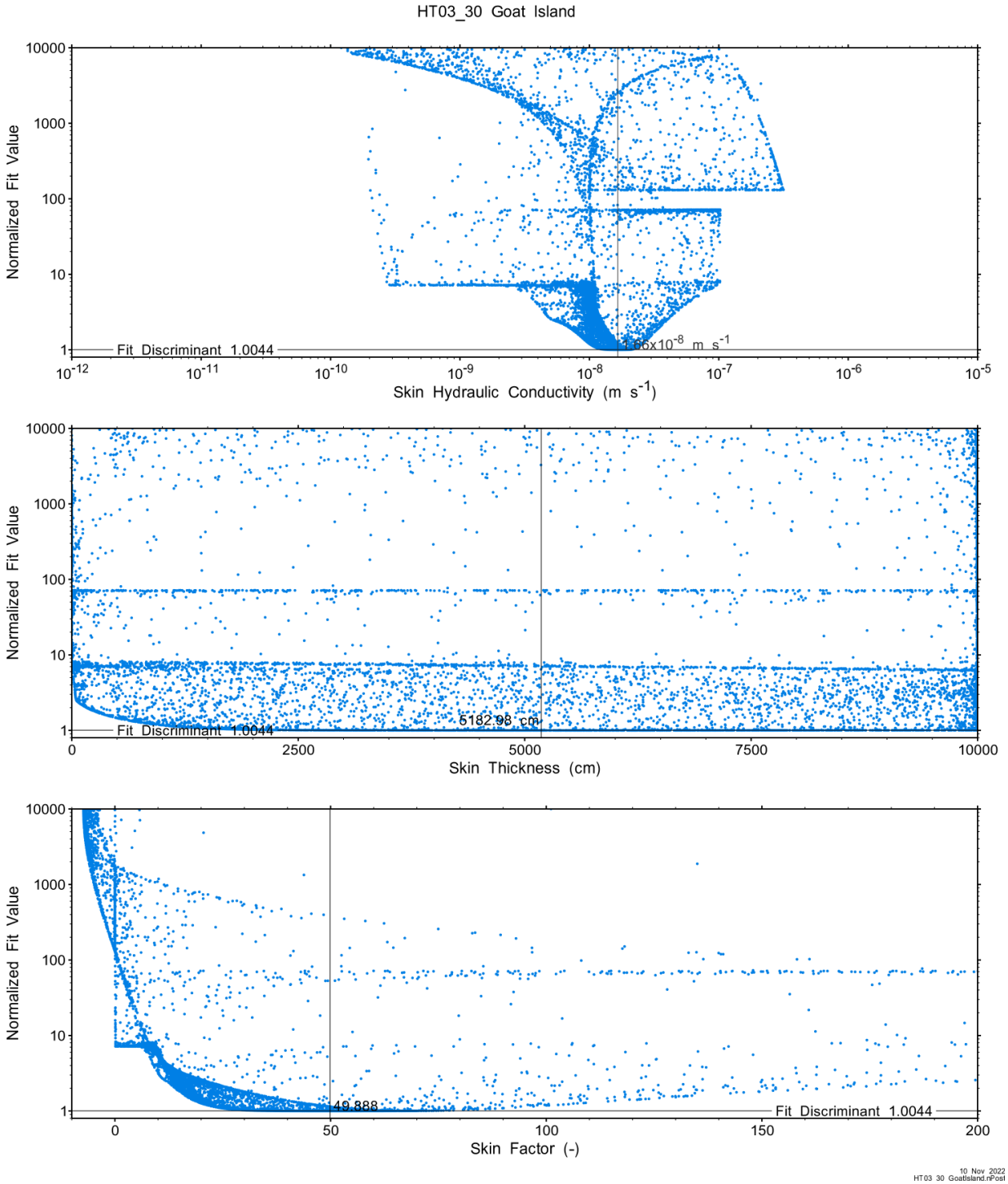

Figure A.128 - XY-scatter plot showing the skin parameter space normalized fit values.

A.9 HT04_30 Cabot Head

The SB BH02 interval from 420.00 to 449.96 mBGS tested in HT04_30 includes the entirety of the Cabot Head and Manitoulin Formations. A single PI test of one day duration was conducted.

A.9.1 Test Data Summary

Table A.6 and Figure A.1 provide a summary of test events and a plot of pressures measured while testing respectively.

Table A.41 - Summary of Test Events.

Event	Start Date & Time	Duration (days)	TZ Pressure (kPa)
Drilling intercept	22-01-05 23:57	188.48	4330
Shut-in	22-07-13 11:31	0.86	4337
Pulse injection	22-07-14 08:10	1.00	4906
Test end	22-07-15 08:15		4673

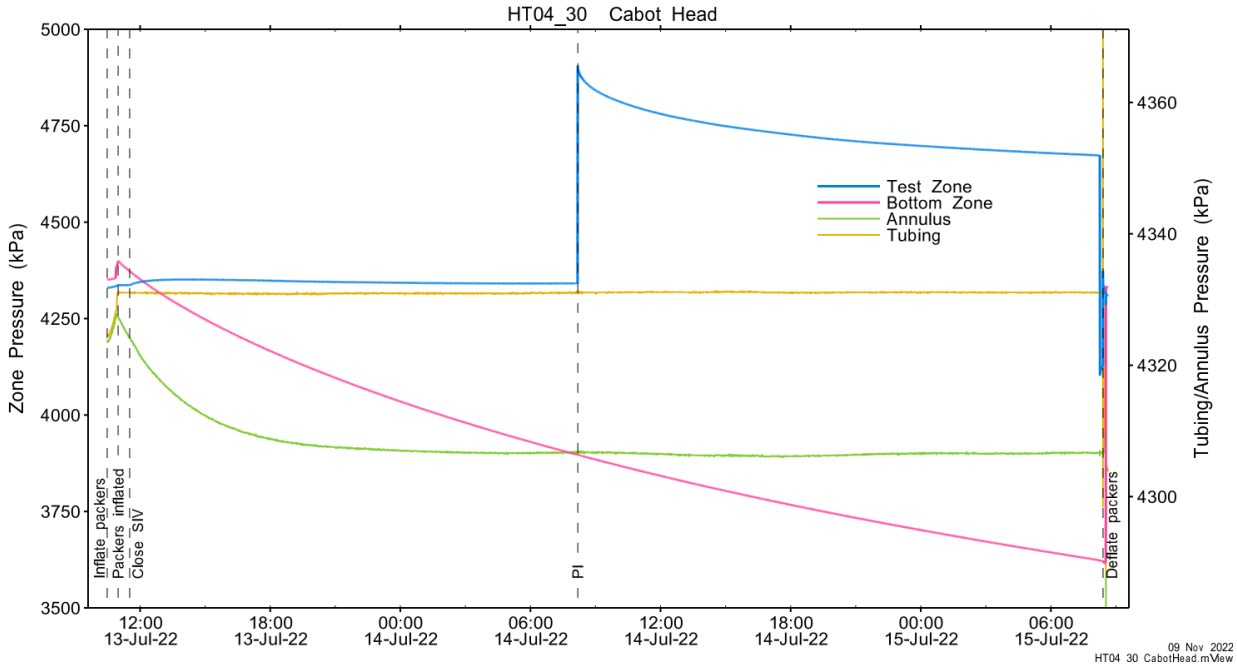

Figure A.129 - Test events and pressures.

A.9.2 Test Analyses

Table A.7 is a summary of test-specific input parameters used in the analyses, while Table A.8 presents the optimized parameters and allowed ranges.

Table A.42 – nSIGHTS Input Parameters.

Parameter	Value	Units
Test zone radius	6.67	cm
Test zone compressibility	4.38E-10	1/Pa
Test zone length	29.96	m

Table A.43 – nSIGHTS Parameter Optimization Ranges.

Parameter	Minimum	Maximum	Units	Type
Formation hydraulic conductivity (K_f)	1E-16	1E-08	m/s	log
Formation pressure (P_f)	2000	7000	kPa	linear
Specific storage (S_s)	1E-08	1E-04	1/m	log
Skin hydraulic conductivity (K_s)	1E-16	1E-08	m/s	log
Skin thickness (t_s)	0.013	1000	cm	linear

Figure A.18 shows the measured test zone pressure record (with reduced data density for clarity) used in the analysis along with the best-fit simulation and parameter values. Figure A.19 presents the pre-test history, and Figure A.20 shows the Ramey B normalized best-fit pressure and pressure derivatives.

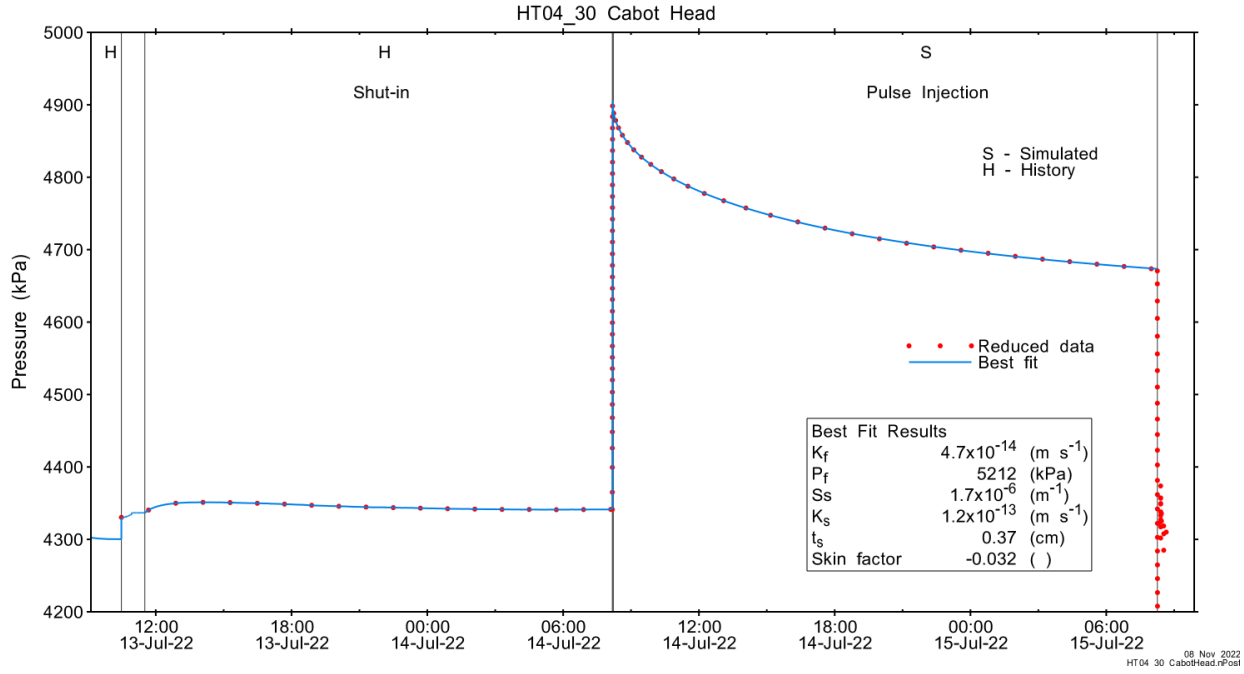

Figure A.130 - Annotated testing sequence showing best-fit simulation and parameter estimates.

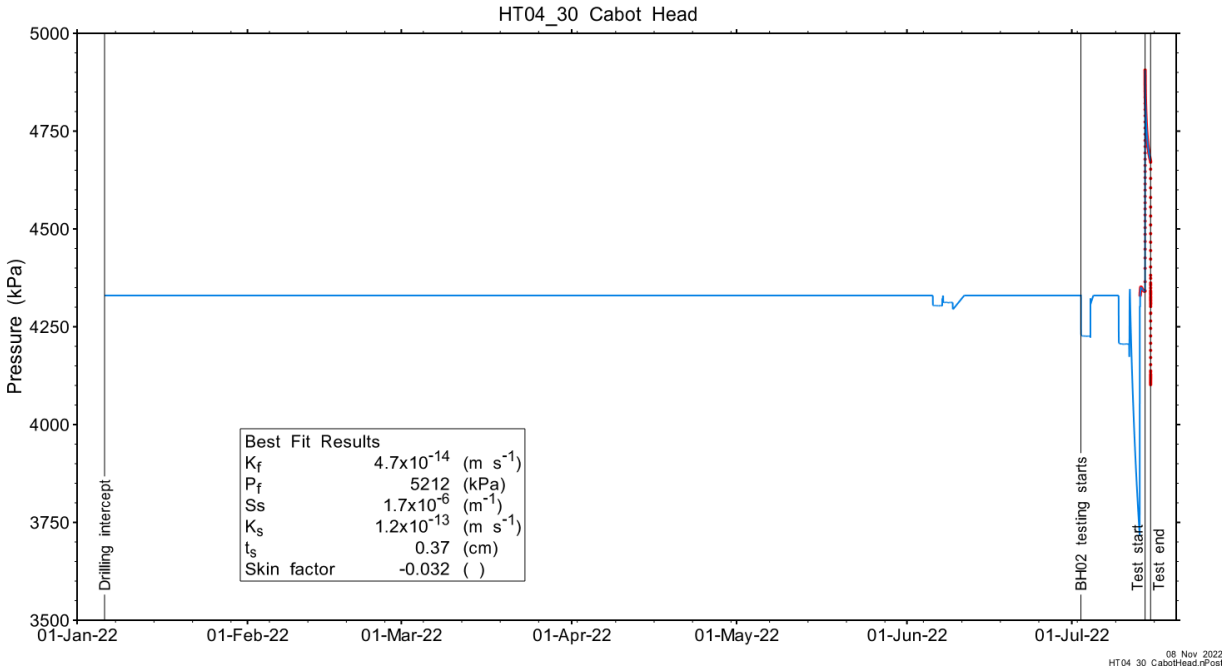

Figure A.131 - Annotated HT04_30 testing sequence showing pre-test history, best-fit simulation and parameter estimates.

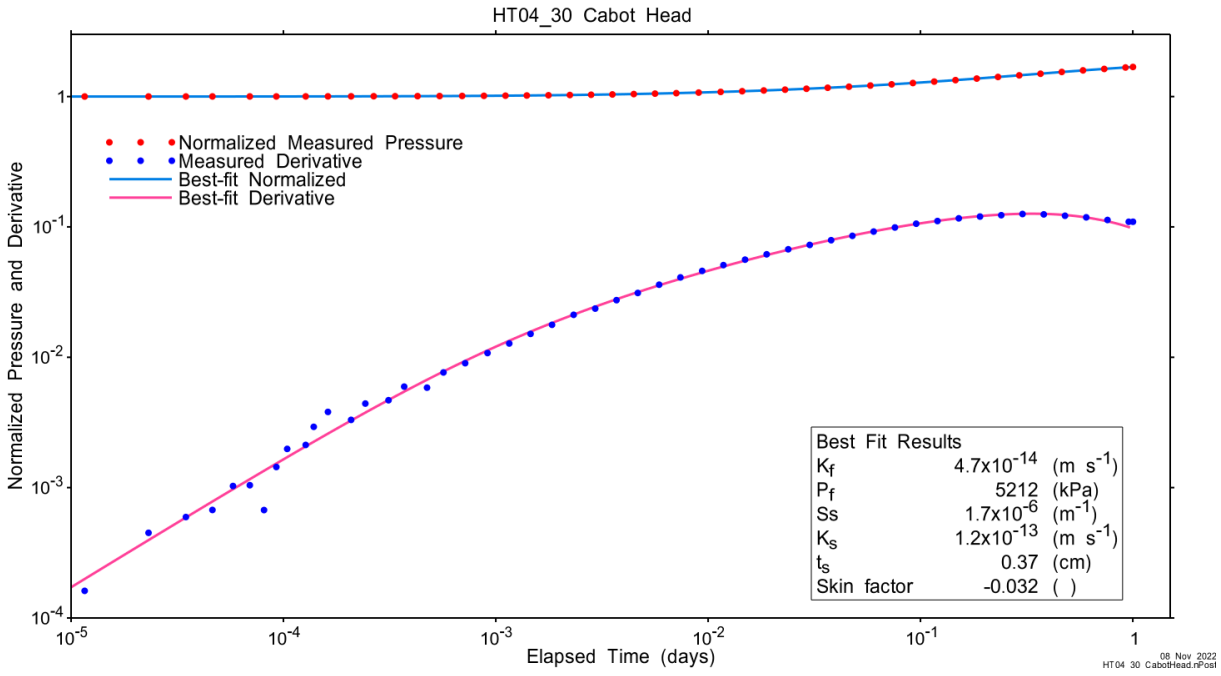

Figure A.132 - Log-log plot showing Ramey B and derivative response for best-fit simulation.

Figure A.21 shows the normalized parameter sensitivity response for the best fit. Sensitivity for all fitting parameters (except P_f) was relatively constant by the end of the test, indicating that the test duration was sufficient for well-constrained parameter estimation.

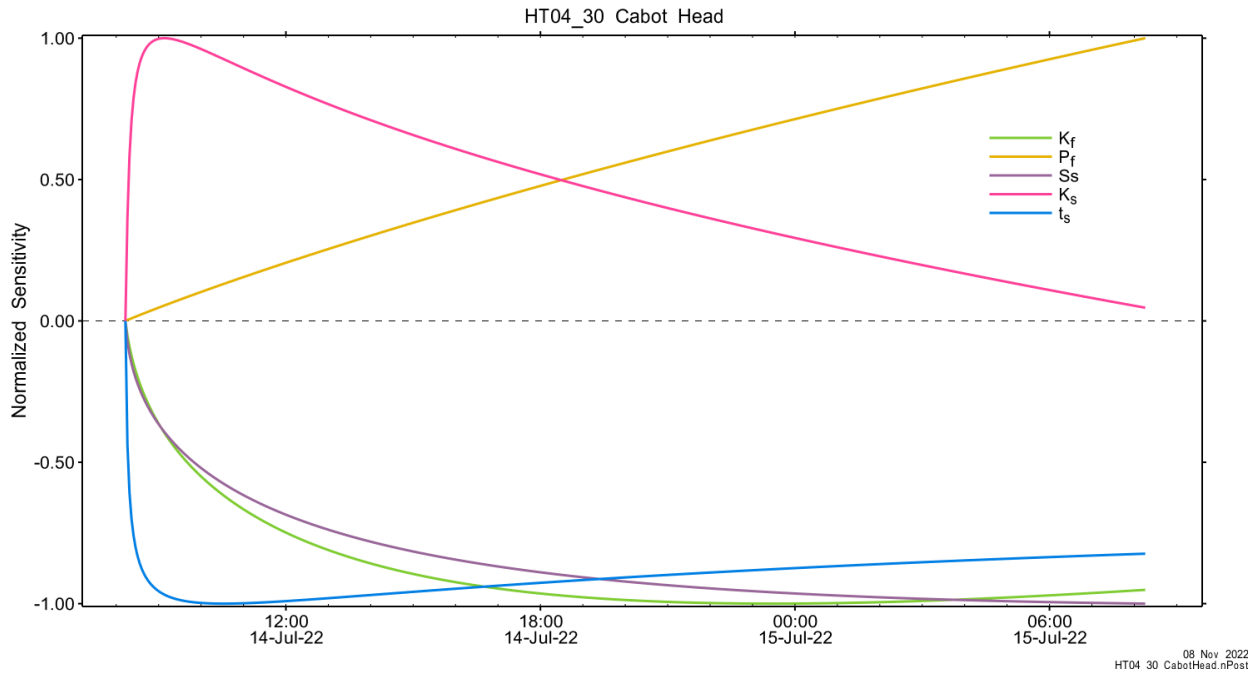

Figure A.133 - Normalized Jacobian for best-fit simulation.

A.9.3 Uncertainty Analyses

The CDF of normalized fit values for all converged simulations and the selected fit discriminant are shown in Figure A.22, with a detail of the fit discriminant in Figure A.135.

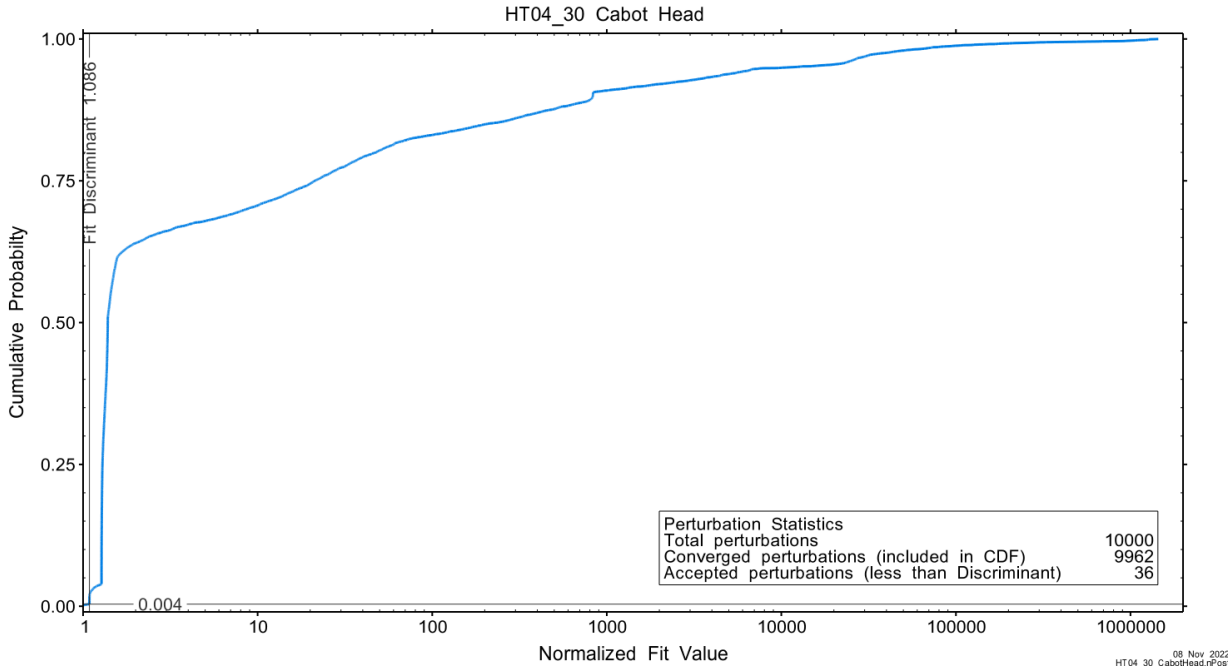

Figure A.134 - Fit value cumulative distribution function.

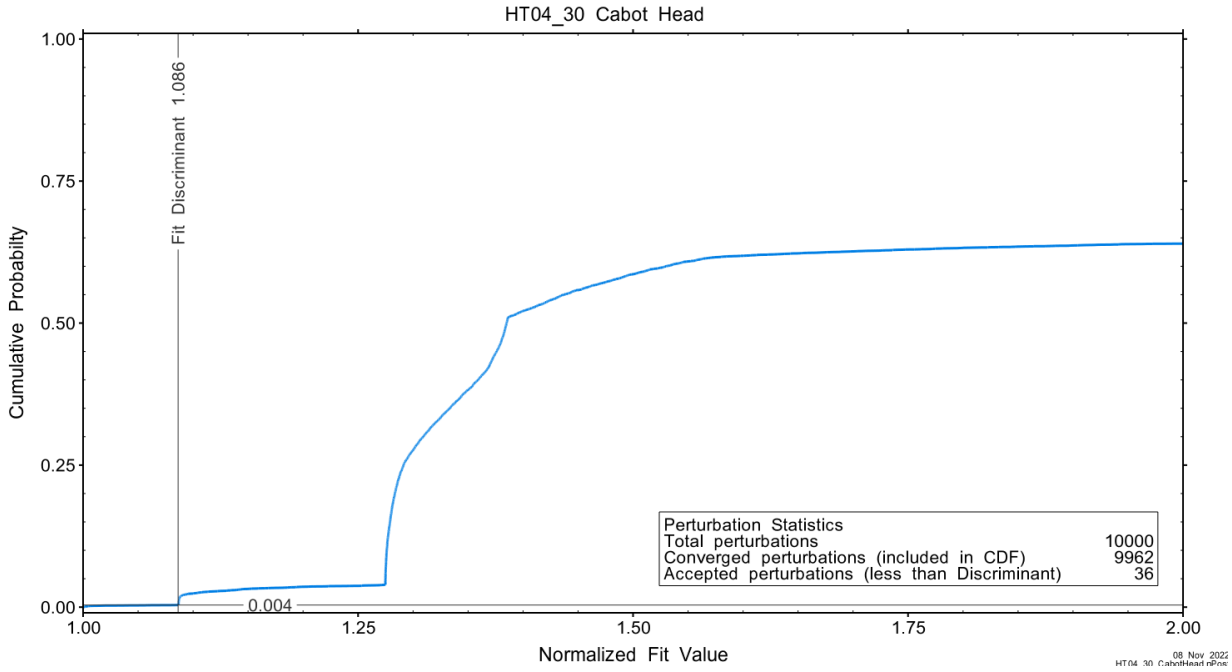

Figure A.135 – Detail of fit value cumulative distribution function.

Summary cross parameter scatter plots for selected formation and skin parameters are given in Figure A.24 and Figure A.25. The light pink dots on the figures are the initial parameter estimates, with red dots overlaying those initial parameter values that resulted in accepted optimization results. The grey dots are converged optimizations which did not meet the fit discriminant. Larger varying color symbols represent the fit value of accepted optimizations, with the blue values representing the best fit.

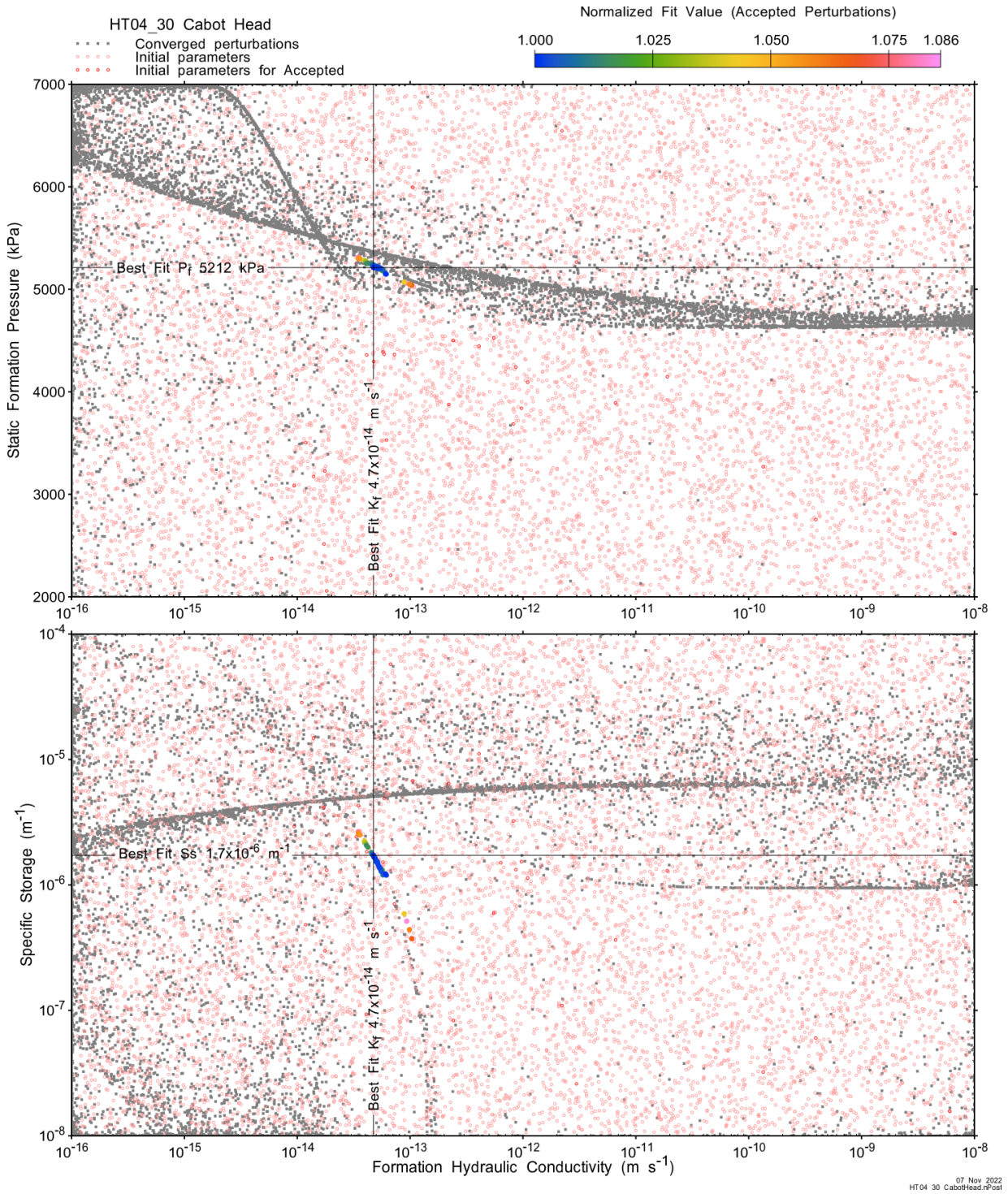

Figure A.136 - XY-scatter plot showing estimates of formation hydraulic conductivity (K_f) vs static formation pressure (P_f) (top panel) and specific storage (Ss) (bottom panel).

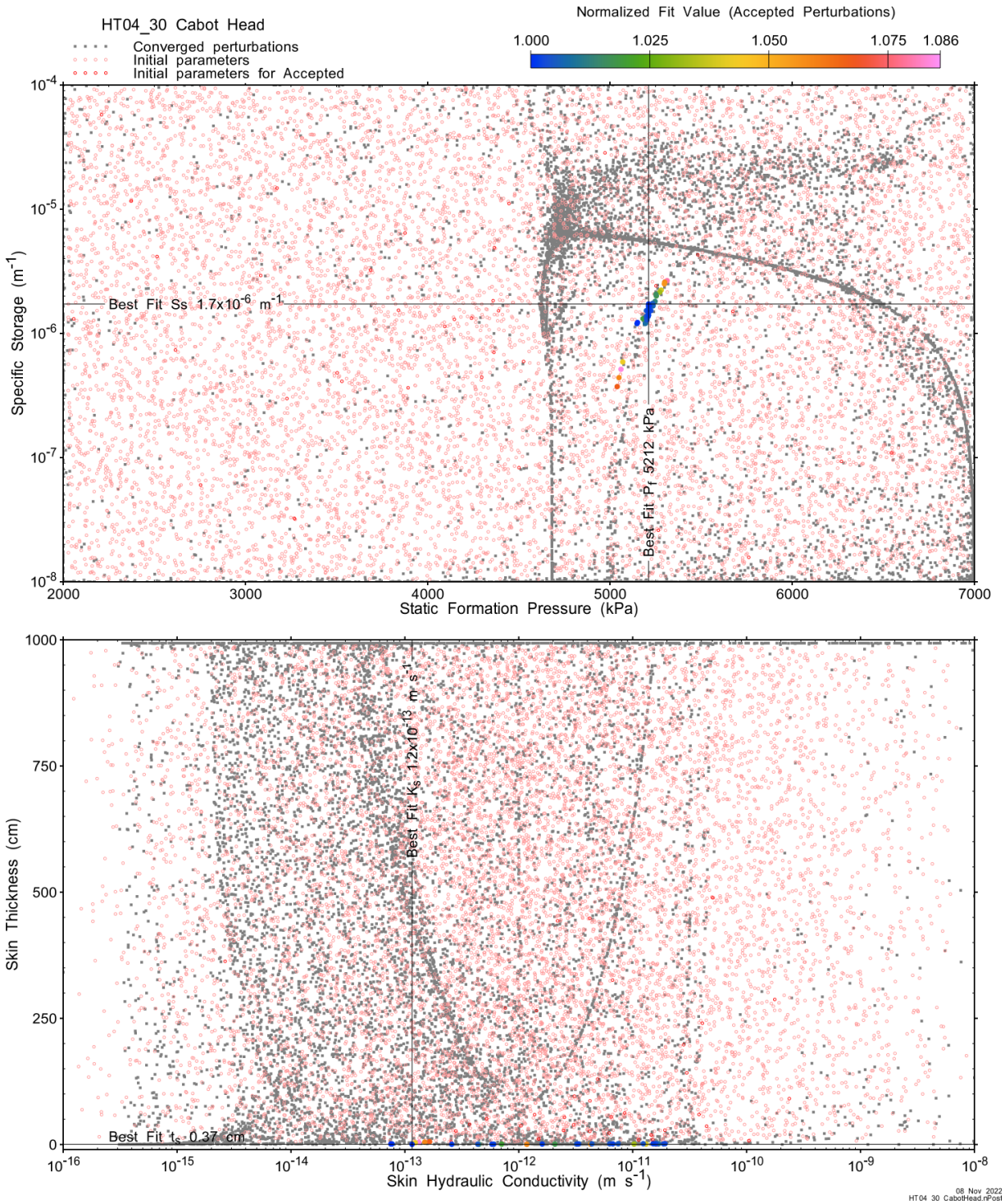

Figure A.137 - XY-scatter plot showing estimates of static formation pressure (P_f) vs specific storage (Ss) (top panel) and skin hydraulic conductivity (K_s) vs skin thickness (t_s) (bottom panel).

Confidence limits and median values are determined from the CDF of accepted optimization results (i.e. the varying color values in the above figures), with best fit value, 5% and 95% confidence indicated on Figure A.26 and Figure A.27.

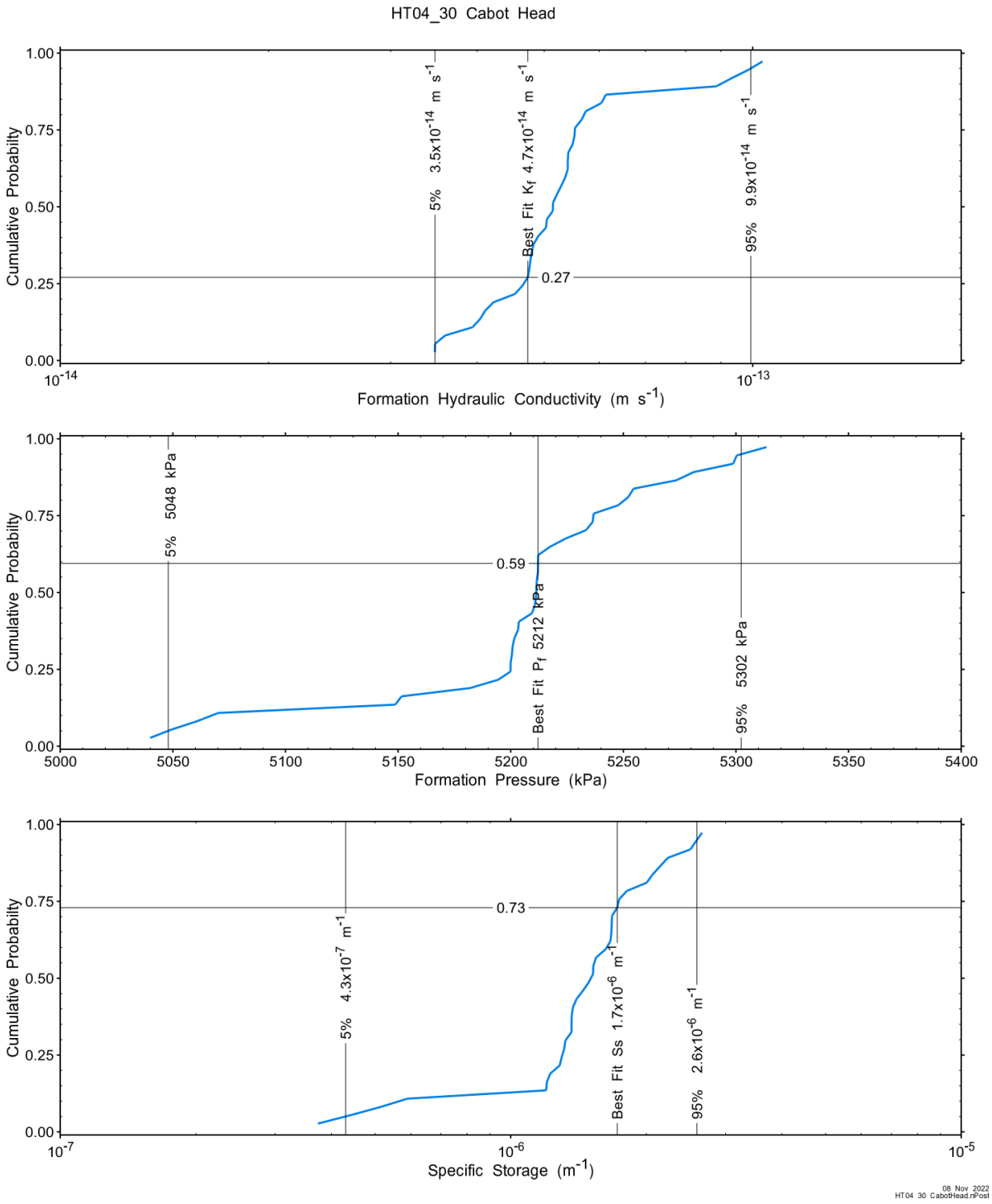

Figure A.138 – Cumulative distribution functions and parameter limits for formation hydraulic conductivity (K_f) (top panel), static formation pressure (P_f) (middle panel) and specific storage (Ss) (bottom panel).

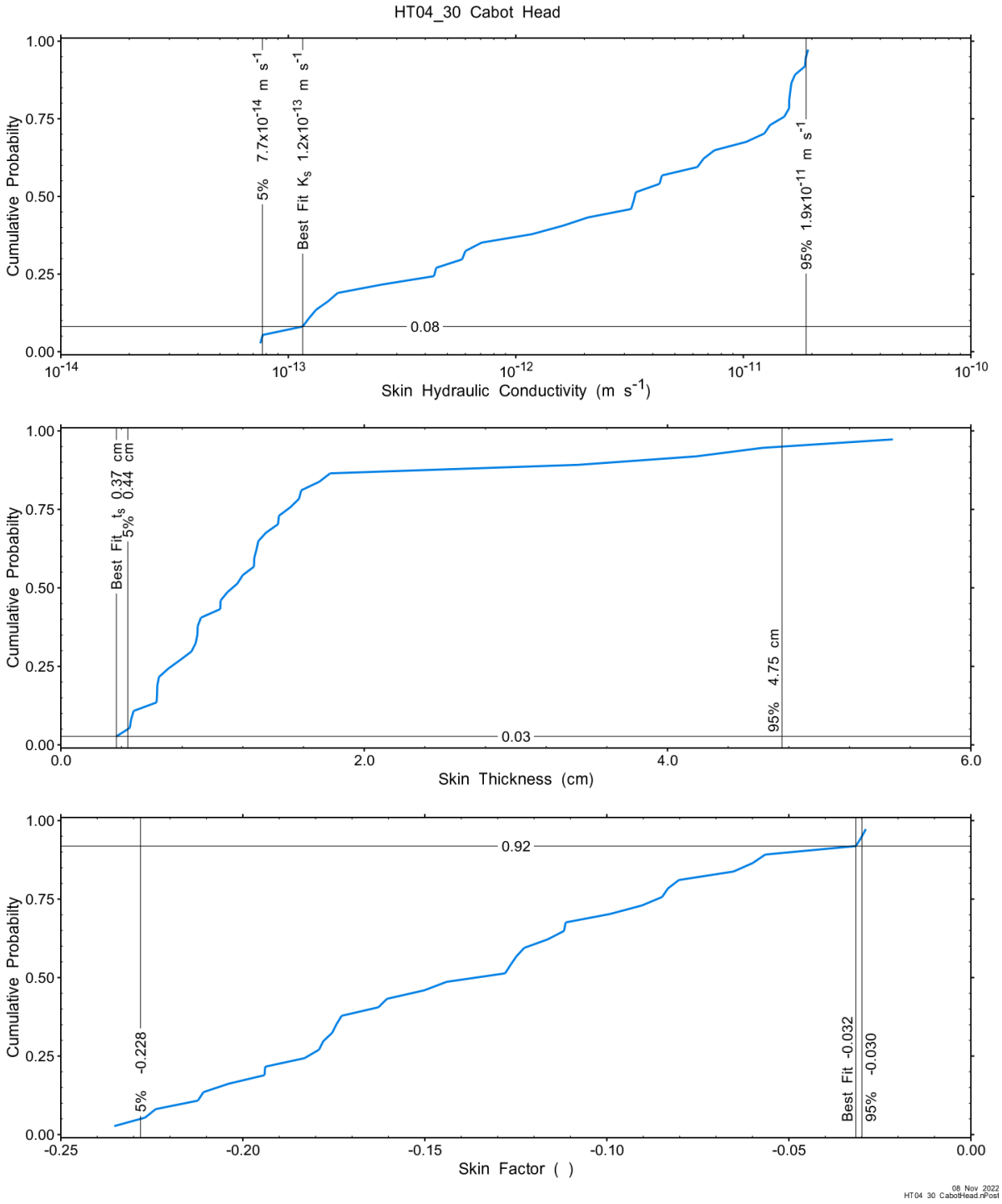

Figure A.139 – Cumulative distribution functions and parameter limits for skin hydraulic conductivity (K_s) (top panel), skin thickness (t_s) (middle panel) and skin factor (s) (bottom panel).

A summary of perturbation results is presented in Figure A.28, with Ramey-processed perturbations in Figure 12. Those perturbations (29 of 10,000) with all parameters within the 5% and 95% range present a very good fit to the measured test zone data.

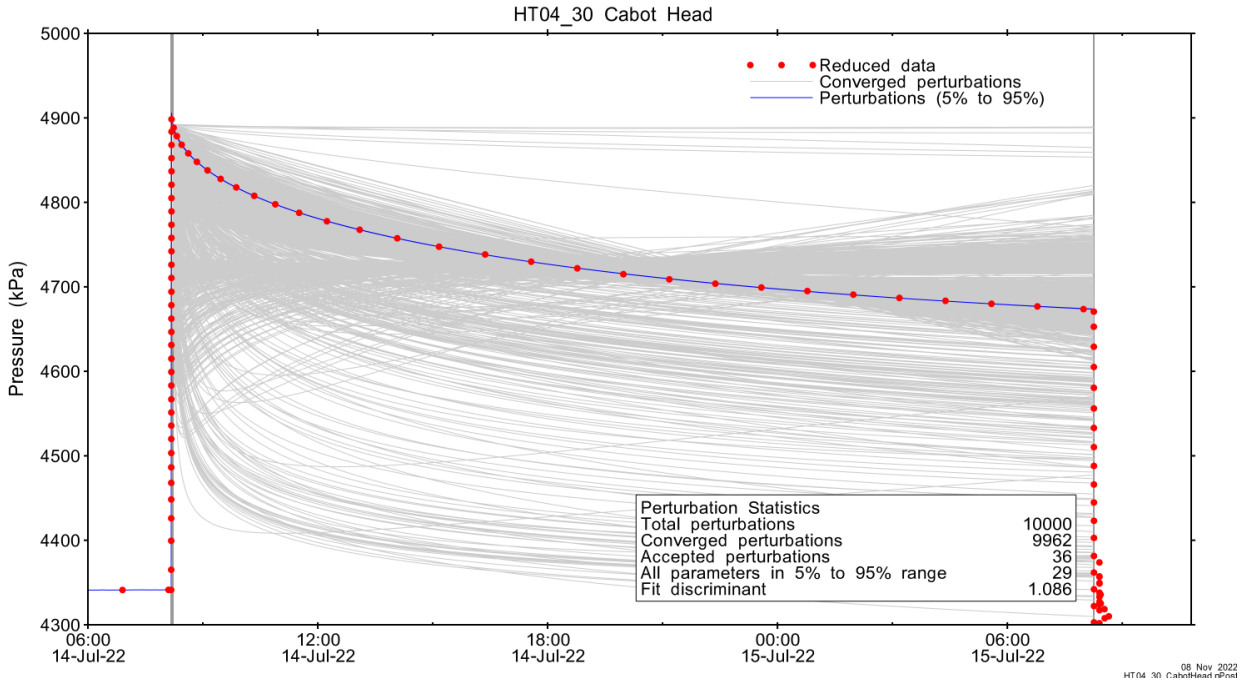

Figure A.140 – Perturbation results – all converged, accepted, and within 5% to 95% for all parameters.

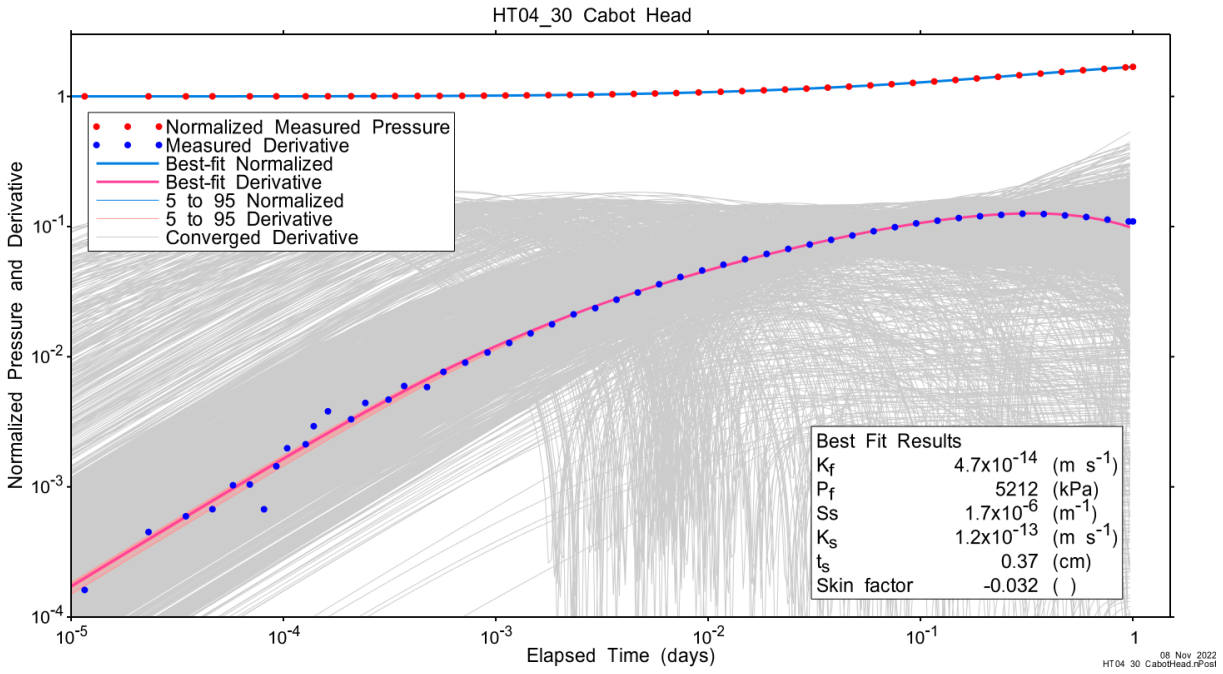

Figure A.141 – Log-log plot showing Ramey B and derivative response for all converged optimizations and those within 5% to 95% for all parameters.

A summary of best-fit and parameter ranges is given in Table A.9.

Table A.44 - Summary of the HT04_30 parameter estimates.

Parameter	Best Fit	5%	Median	95%
K_f (m/s)	4.7E-14	3.5E-14	5.1E-14	9.9E-14
P_f (kPa)	5212	5048	5211	5302
Ss (1/m)	1.7E-06	4.3E-07	1.5E-06	2.6E-06
K_s (m/s)	1.2E-13	7.7E-14	3.3E-12	1.9E-11
t_s (cm)	0.37	0.44	1.13	4.75
s (-)	-0.032	-0.228	-0.136	-0.030

Parameter correlations for all perturbations with all parameters within the 5% to 95% limits are given in Table A.5.

Table A.45 – Pearson cross-correlations of 5% to 95% parameters

	Log(K_f)	P_f	Log(Ss)	Log(K_s)	t_s	s
Log(K_f)	1.000	-0.991	-0.996	-0.549	0.897	-0.207
Pf	-0.991	1.000	0.983	0.654	-0.856	0.079
Log(S_s)	-0.996	0.983	1.000	0.533	-0.929	0.227
Log(K_s)	-0.549	0.654	0.533	1.000	-0.327	-0.685
t_s	0.897	-0.856	-0.929	-0.327	1.000	-0.369
s	-0.207	0.079	0.227	-0.685	-0.369	1.000

A.9.4 Additional Figures

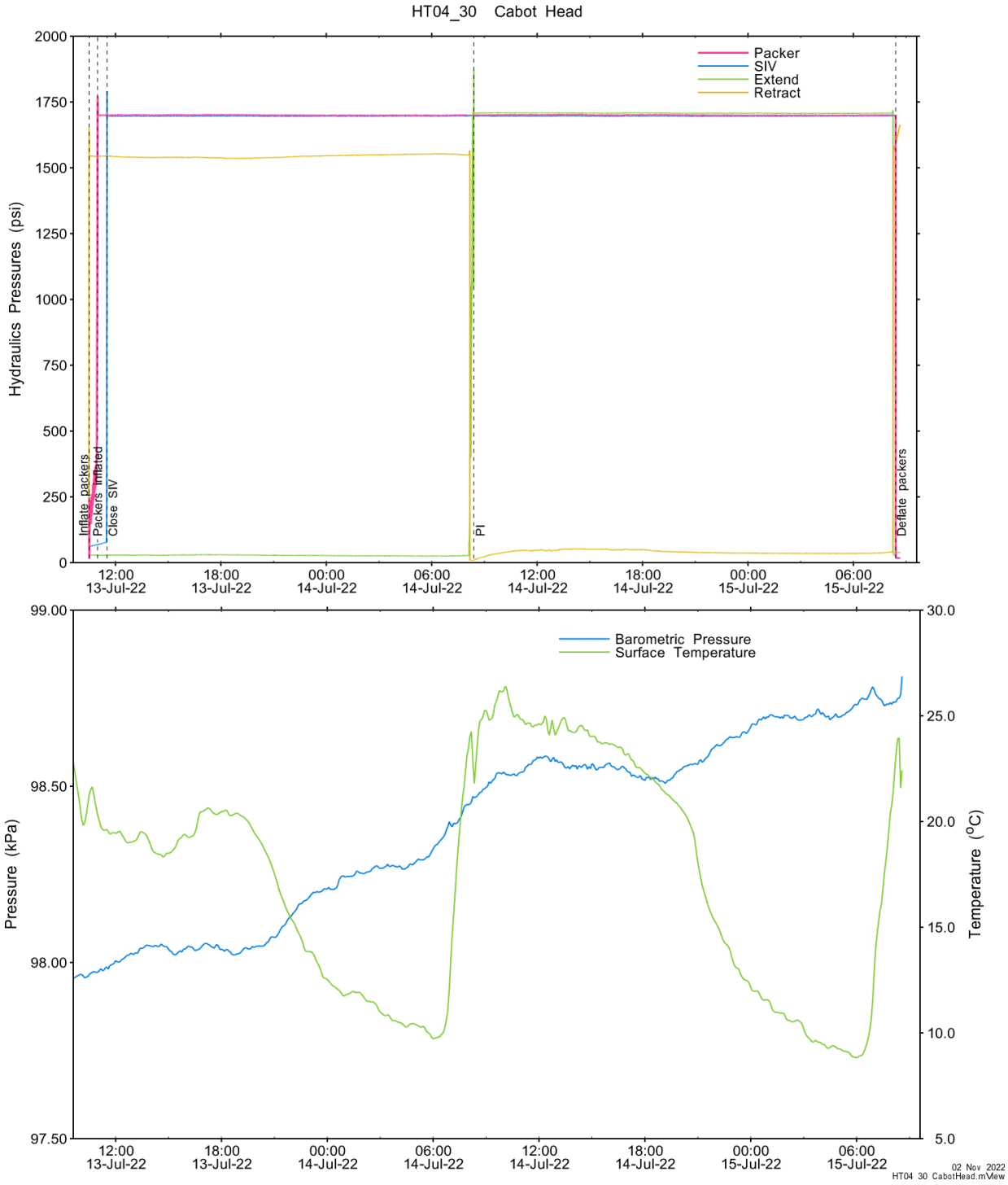

Figure A.142 - Hydraulics pressures and surface temperature/barometric pressure.

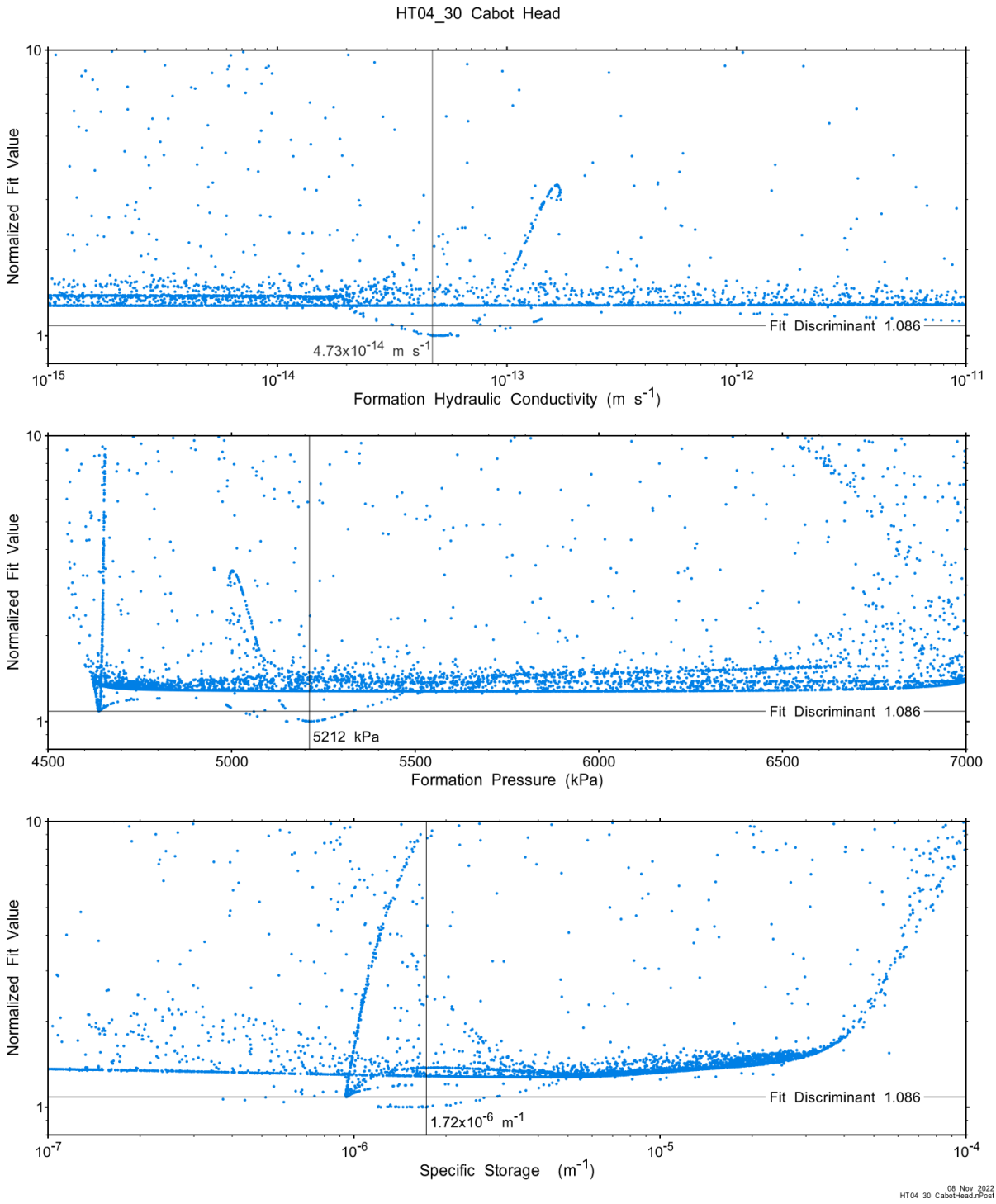

Figure A.143 - XY-scatter plot showing the formation parameter space normalized fit values.

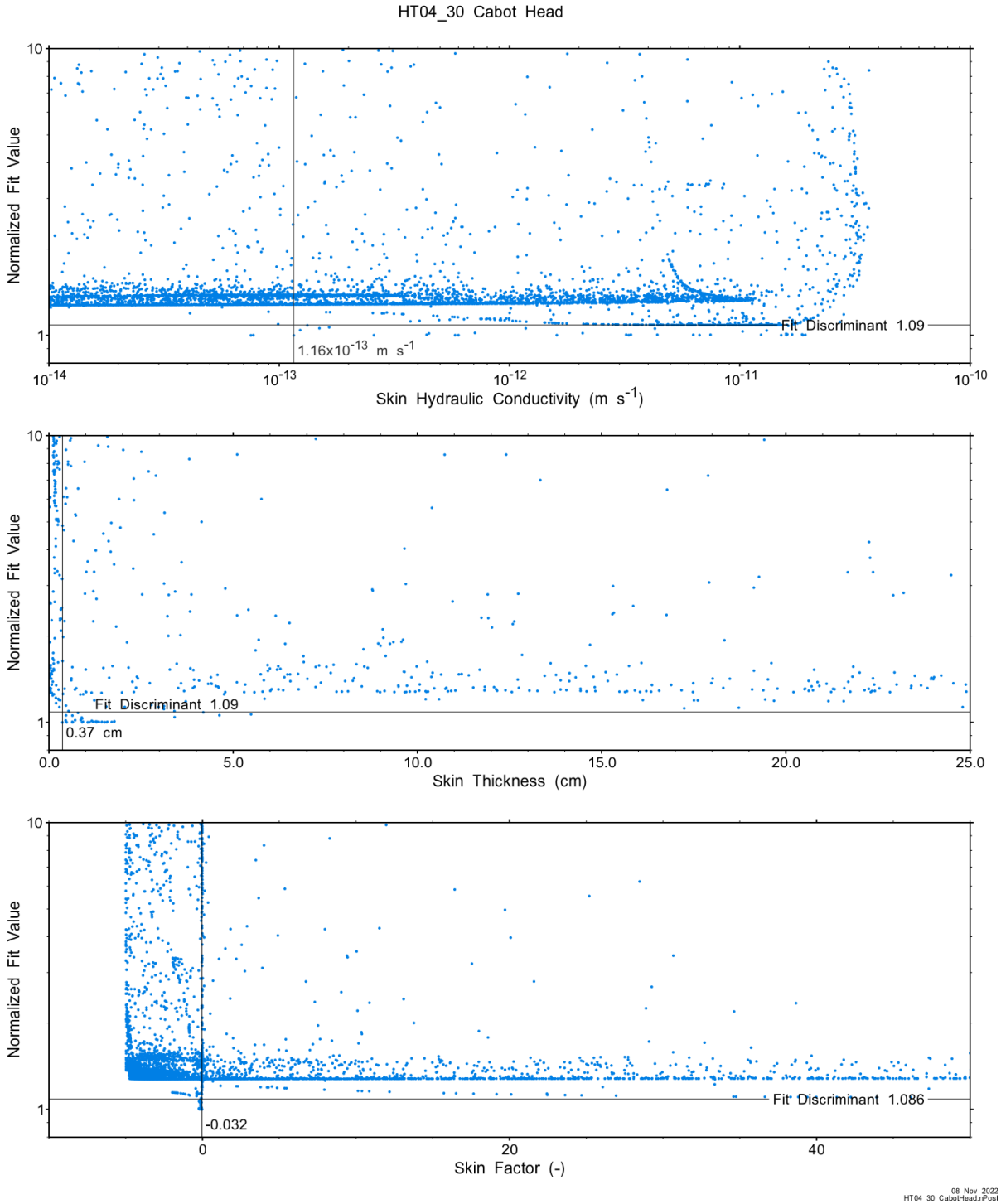

Figure A.144 - XY-scatter plot showing the skin parameter space normalized fit values.

A.10 HT05_30 Upper Queenston

The SB BH02 interval from 450.00 to 479.96 mBGS tested in HT05_30 consists of the upper 30m of the Queenston Formation. A single PI test of two days duration was conducted.

A.10.1 Test Data Summary

Table A.6 and Figure A.1 provide a summary of test events and a plot of pressures measured while testing respectively.

Table A.46 - Summary of Test Events.

Event	Start Date & Time	Duration (days)	TZ Pressure (kPa)
Drilling intercept	22-01-06 00:39	190.45	4654
Shut-in	22-07-15 11:30	0.86	4667
Pulse injection	22-07-16 08:06	2.00	5122
Test end	22-07-18 08:09		4962

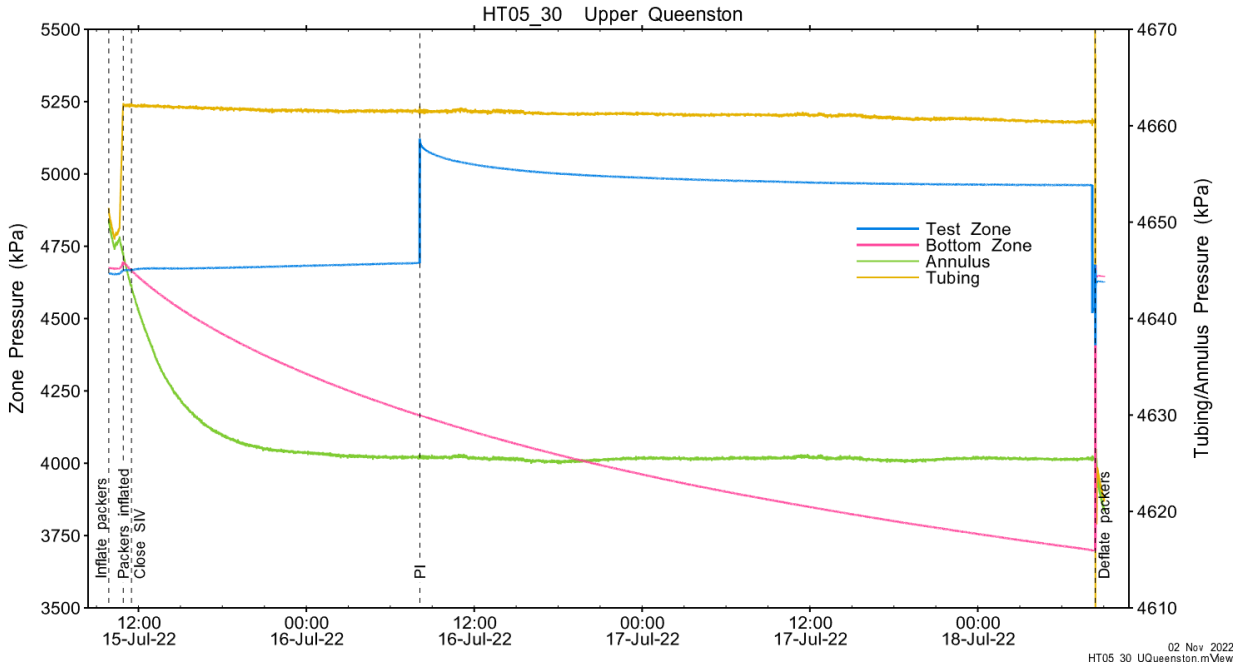

Figure A.145 - Test events and pressures.

A.10.2 Test Analyses

Table A.7 is a summary of test-specific input parameters used in the analyses, while Table A.8 presents the optimized parameters and allowed ranges.

Table A.47 – nSIGHTS Input Parameters.

Parameter	Value	Units
Test zone radius	7.45	cm
Test zone compressibility	4.58E-10	1/Pa
Test zone length	29.96	m

Table A.48 – nSIGHTS Parameter Optimization Ranges.

Parameter	Minimum	Maximum	Units	Type
Formation hydraulic conductivity (K_f)	1E-16	1E-09	m/s	log
Formation pressure (P_f)	3000	9000	kPa	linear
Specific storage (S_s)	1E-08	1E-04	1/m	log
Skin hydraulic conductivity (K_s)	1E-16	1E-09	m/s	log
Skin thickness (t_s)	0.013	1000	cm	linear

Figure A.18 shows the measured test zone pressure record (with reduced data density for clarity) used in the analysis along with the best-fit simulation and parameter values. Figure A.19 presents the pre-test history, and Figure A.20 shows the Ramey B normalized best-fit pressure and pressure derivatives.

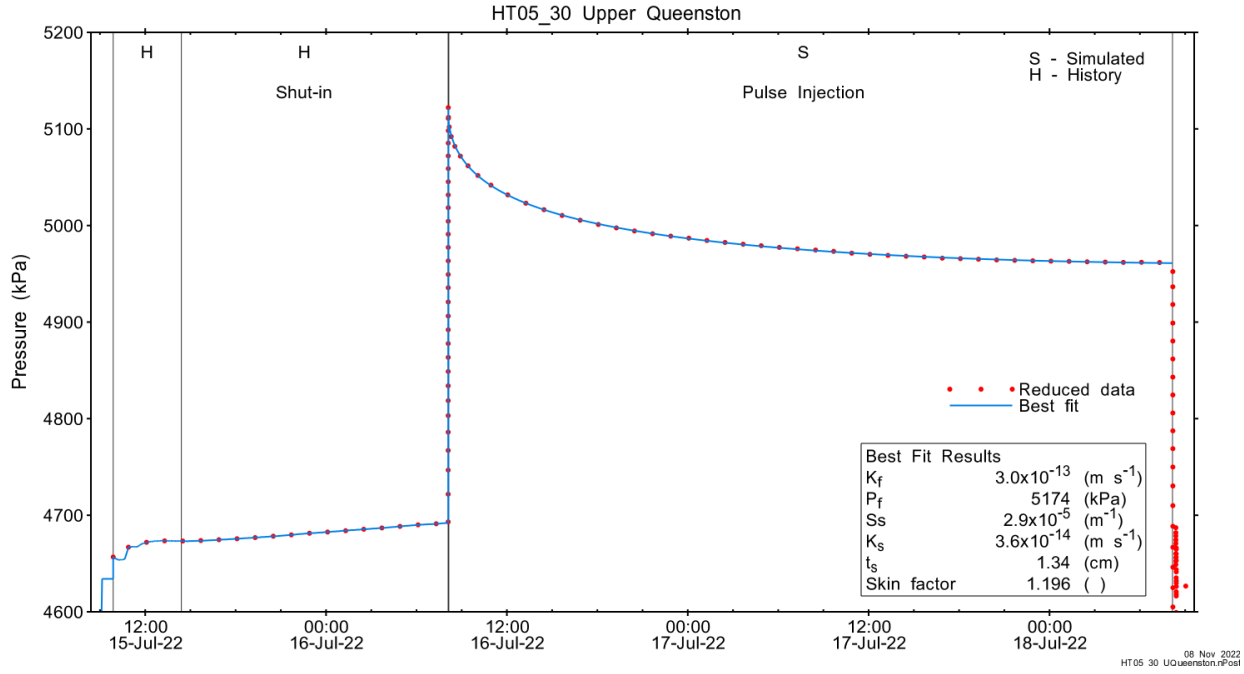

Figure A.146 - Annotated testing sequence showing best-fit simulation and parameter estimates.

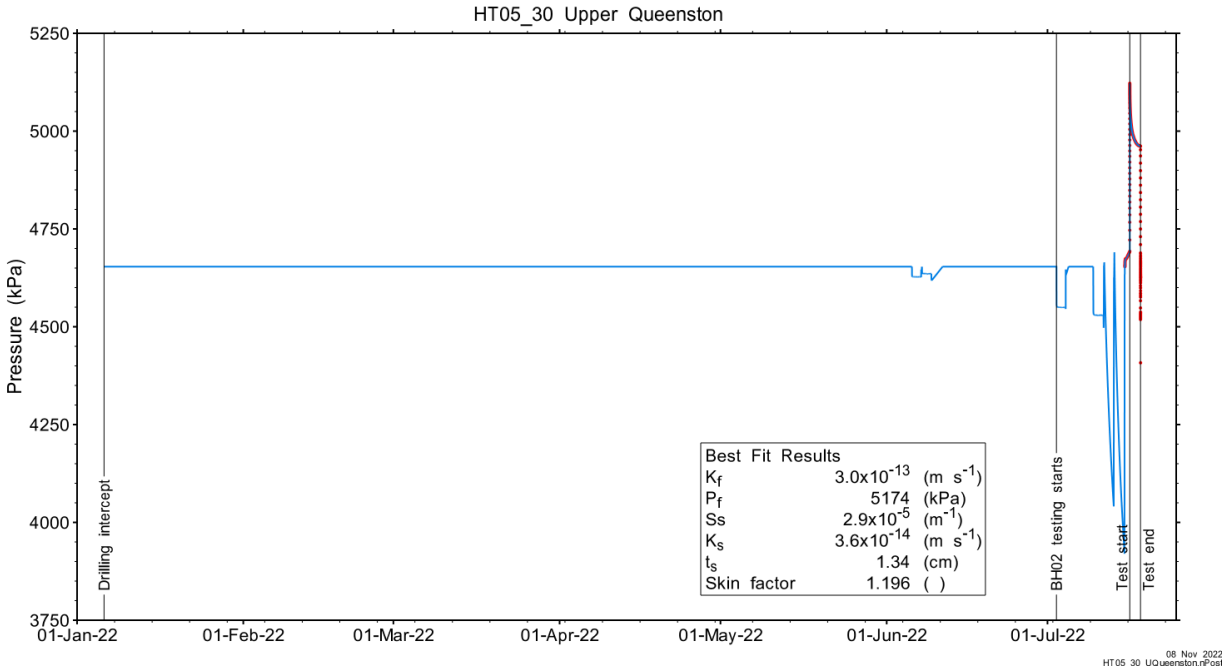

Figure A.147 - Annotated HT05_30 testing sequence showing pre-test history, best-fit simulation and parameter estimates.

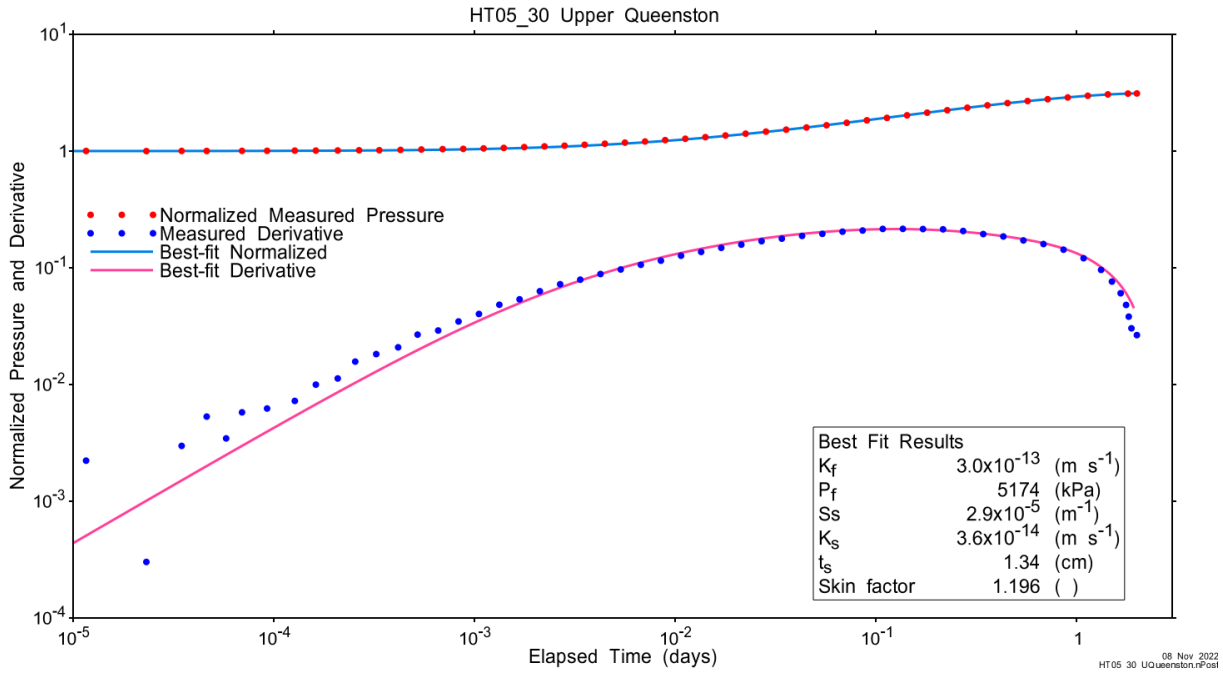

Figure A.148 - Log-log plot showing Ramey B and derivative response for best-fit simulation.

Figure A.21 shows the normalized parameter sensitivity response for the best fit. Sensitivity for all fitting parameters (except S_s) was rising at the end of the test, indicating that a longer test may have returned more precise results.

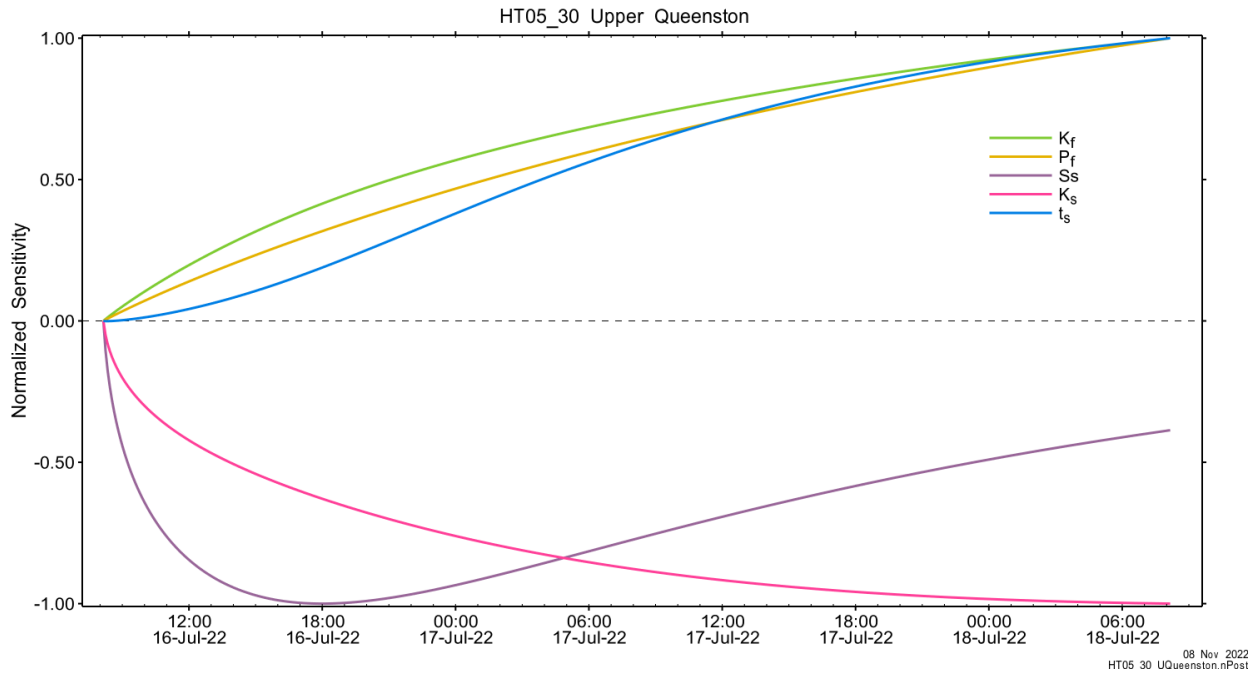

Figure A.149 - Normalized Jacobian for best-fit simulation.

A.10.3 Uncertainty Analyses

The CDF of normalized fit values for all converged simulations and the selected fit discriminant are shown in Figure A.22. The initial fit discriminant selected was somewhat higher (1.55), however, this resulted in inclusion of a local minimum (see Appendix plots). The fit value was adjusted downward to 1.25, at which point only the global minimum remained.

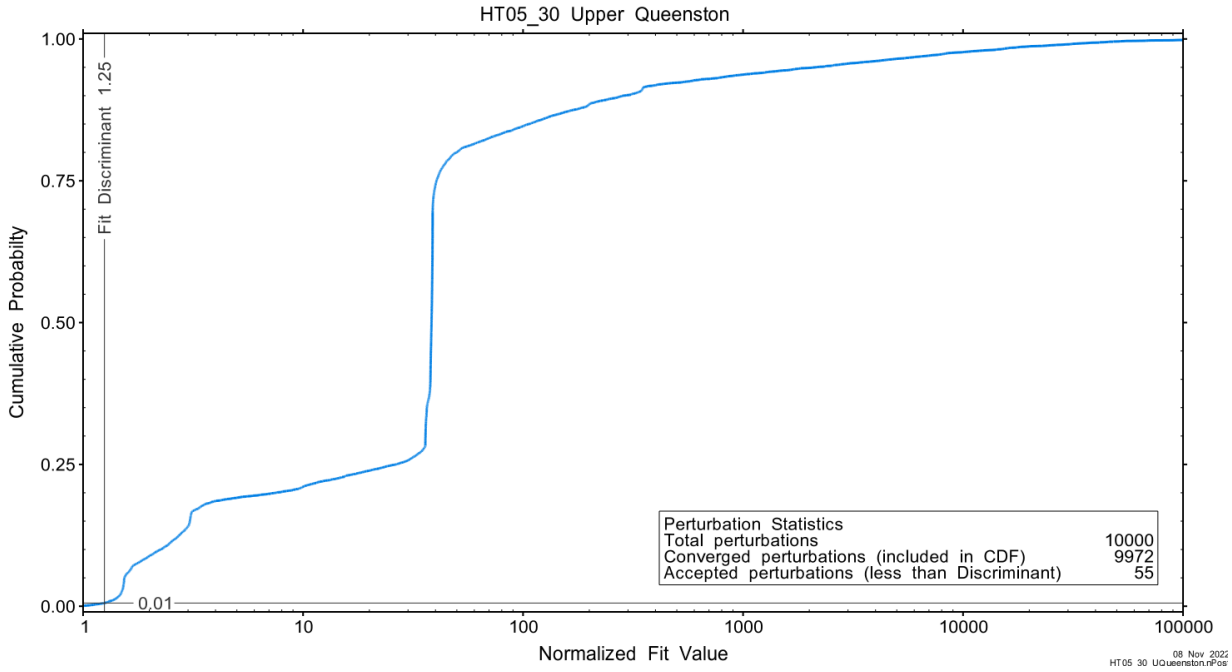

Figure A.150 - Fit value cumulative distribution function.

Summary cross parameter scatter plots for selected formation and skin parameters are given in Figure A.24 and Figure A.25. The light pink dots on the figures are the initial parameter estimates, with red dots overlaying those initial parameter values that resulted in accepted optimization results. The grey dots are converged optimizations which did not meet the fit discriminant. Larger varying color symbols represent the fit value of accepted optimizations, with the blue values representing the best fit.

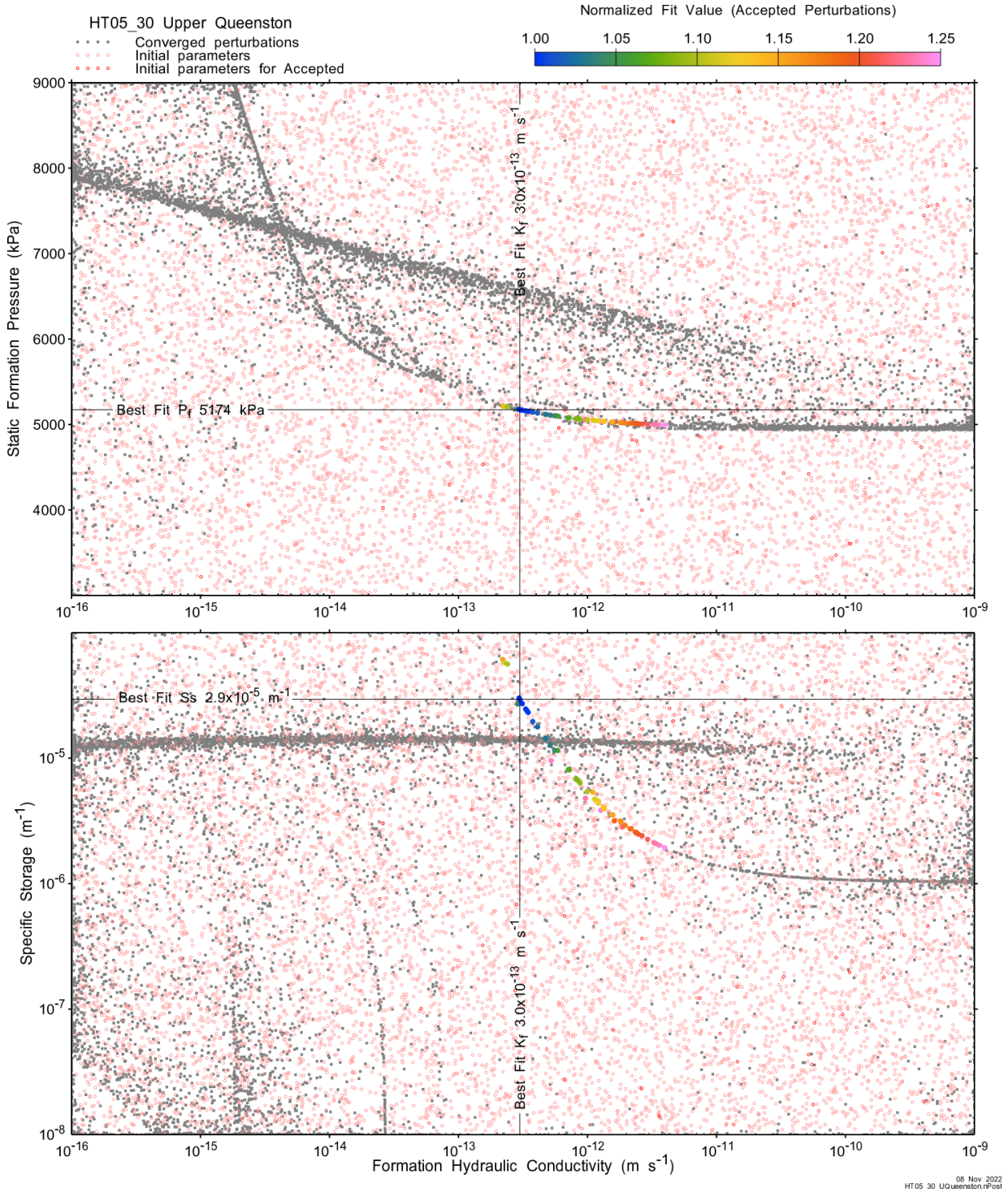

Figure A.151 - XY-scatter plot showing estimates of formation hydraulic conductivity (K_f) vs static formation pressure (P_f) (top panel) and specific storage (Ss) (bottom panel).

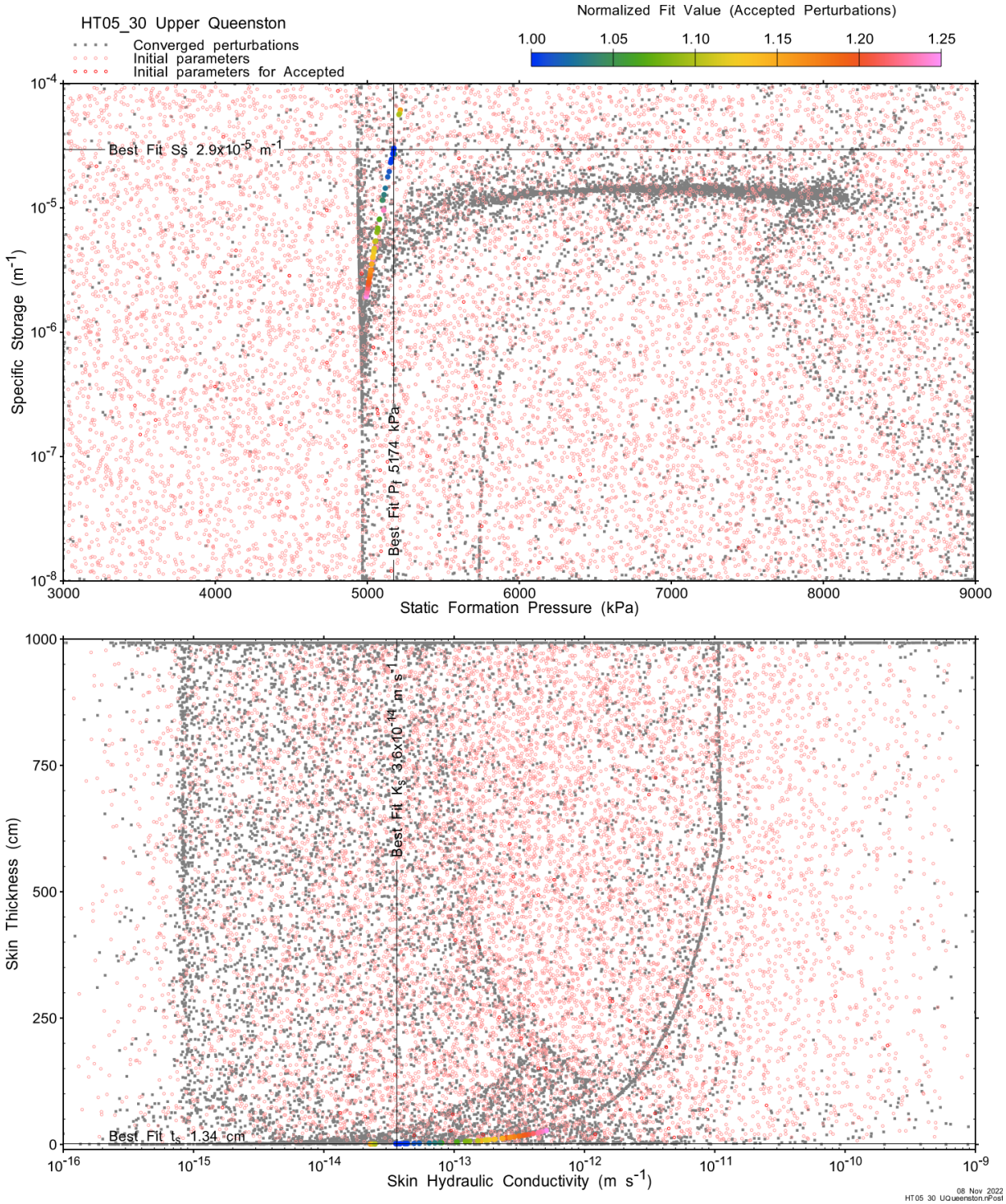

Figure A.152 - XY-scatter plot showing estimates of static formation pressure (P_f) vs specific storage (Ss) (top panel) and skin hydraulic conductivity (K_s) vs skin thickness (t_s) (bottom panel).

Confidence limits and median values are determined from the CDF of accepted optimization results (i.e. the varying color values in the above figures), with best fit value, 5% and 95% confidence indicated on Figure A.26 and Figure A.27.

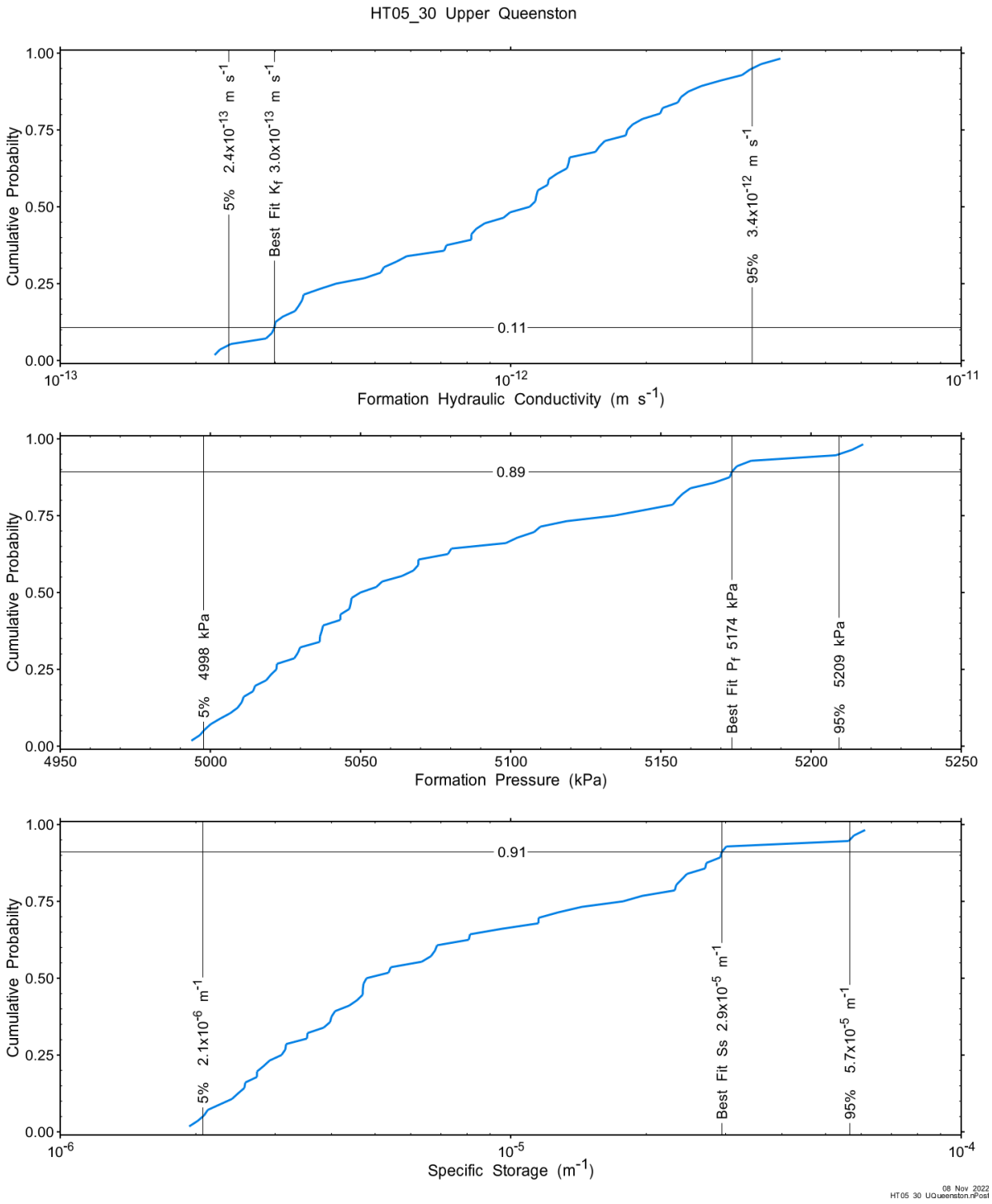

Figure A.153 – Cumulative distribution functions and parameter limits for formation hydraulic conductivity (K_f) (top panel), static formation pressure (P_f) (middle panel) and specific storage (Ss) (bottom panel).

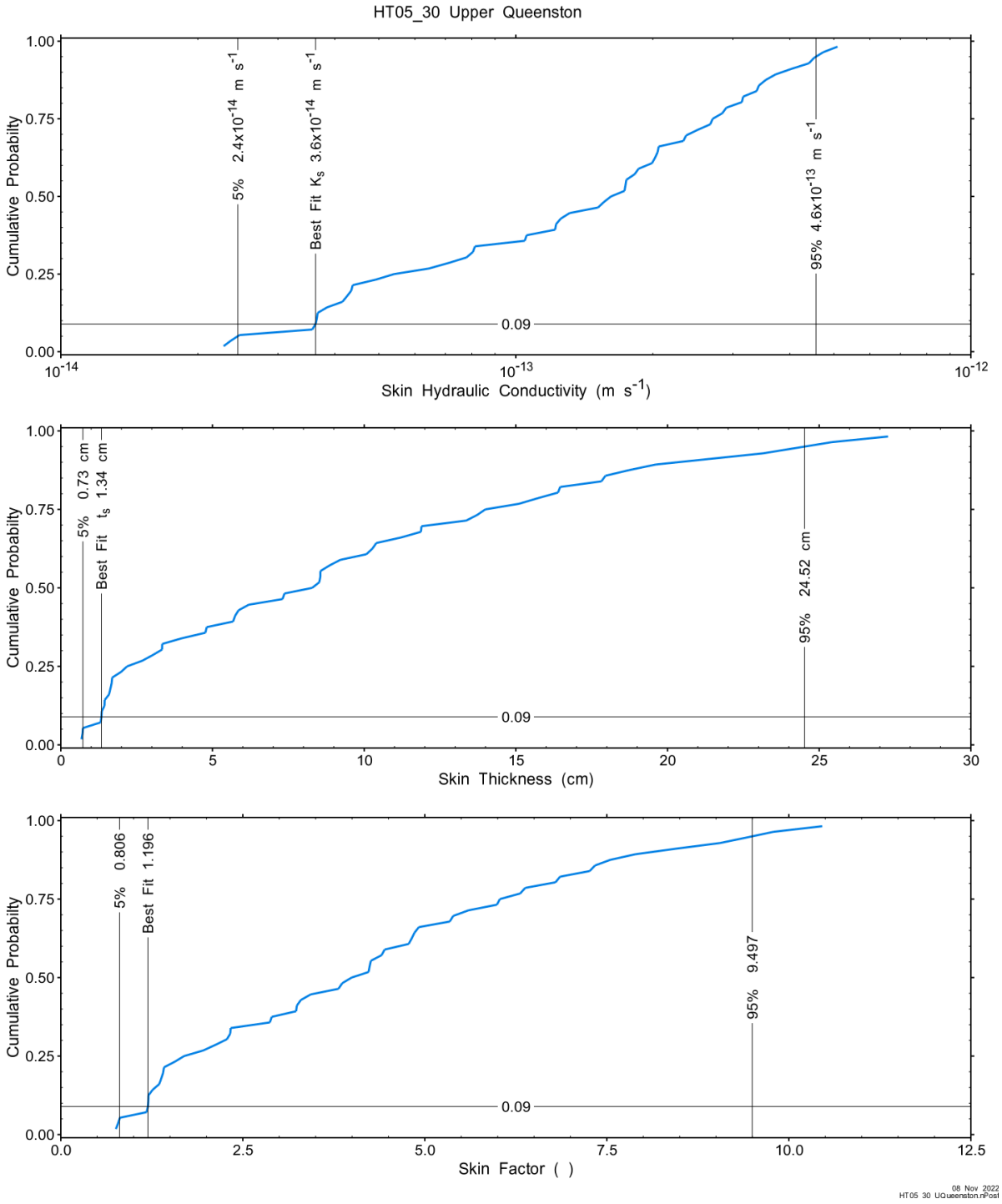

Figure A.154 – Cumulative distribution functions and parameter limits for skin hydraulic conductivity (K_s) (top panel), skin thickness (t_s) (middle panel) and skin factor (s) (bottom panel).

A summary of perturbation results is presented in Figure A.28, with Ramey-processed perturbations in Figure 12. Those perturbations (51 of 10,000) with all parameters within the 5% and 95% range present a very good fit to the measured test zone data.

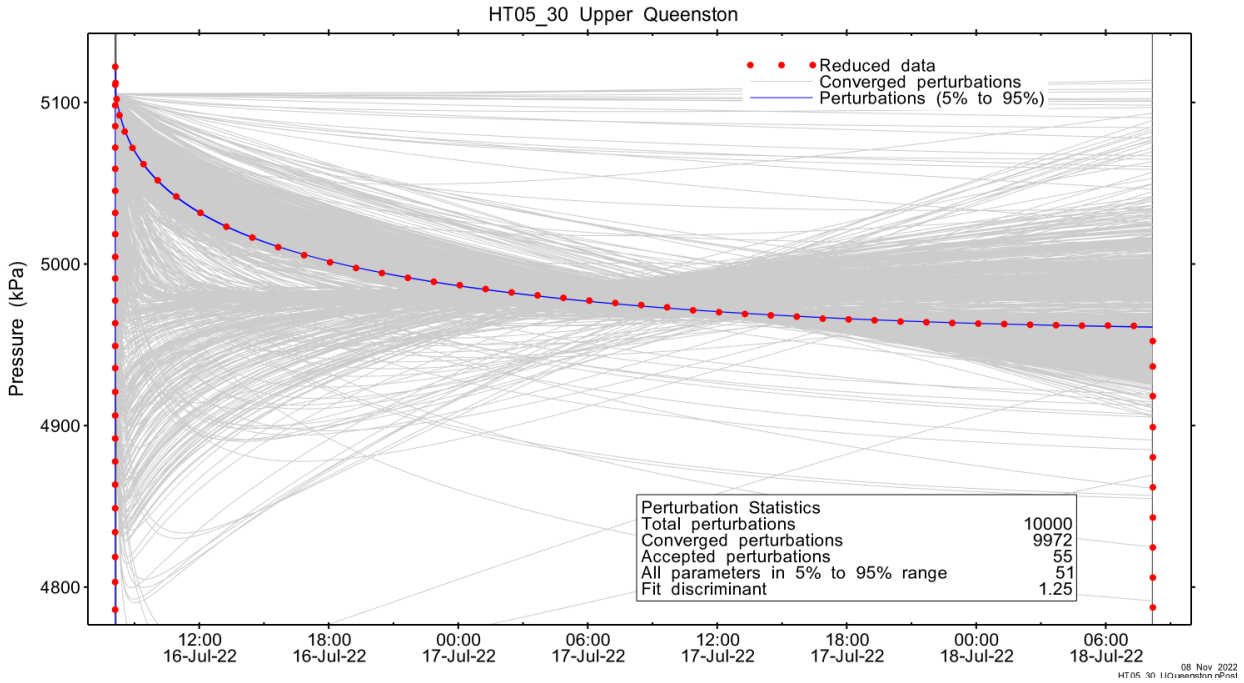

Figure A.155 – Perturbation results – all converged, accepted, and within 5% to 95% for all parameters.

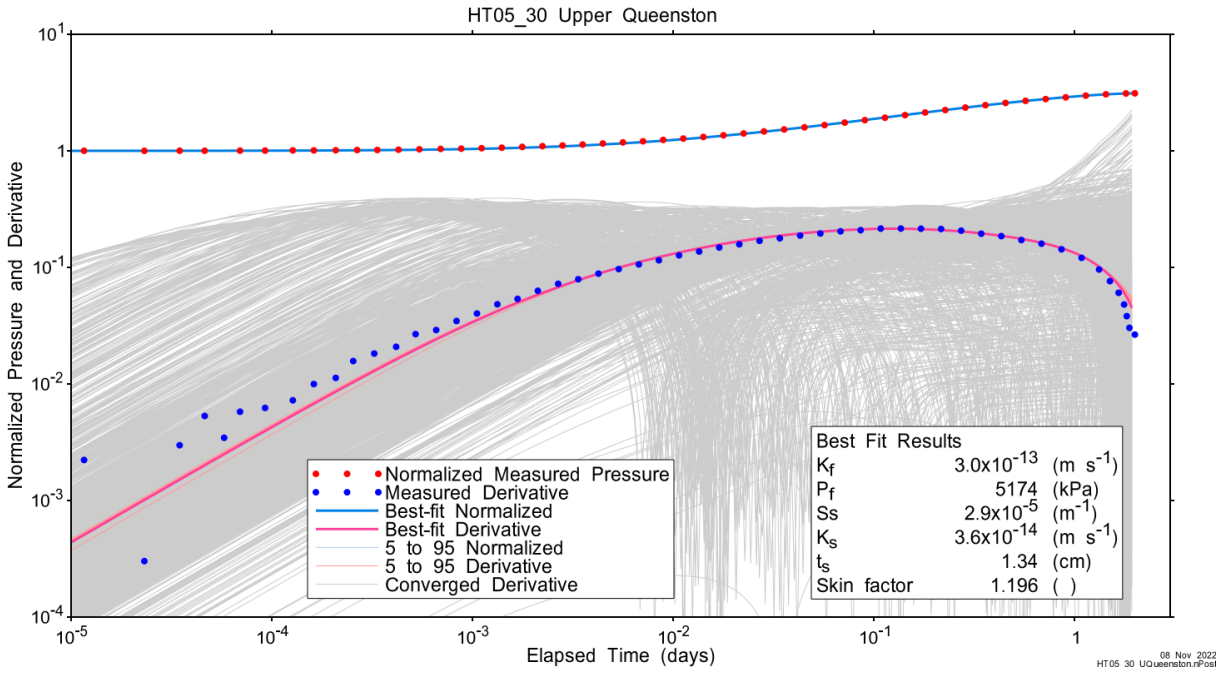

Figure A.156 – Log-log plot showing Ramey B and derivative response for all converged optimizations and those within 5% to 95% for all parameters.

A summary of best-fit and parameter ranges is given in Table A.9.

Table A.49 - Summary of the HT05_30 parameter estimates.

Parameter	Best Fit	5%	Median	95%
K_f (m/s)	3.0E-13	2.4E-13	1.1E-12	3.4E-12
P_f (kPa)	5174	4998	5050	5209
Ss (1/m)	2.9E-05	2.1E-06	4.8E-06	5.7E-05
K_s (m/s)	3.6E-14	2.4E-14	1.6E-13	4.6E-13
t_s (cm)	1.34	0.73	8.28	24.52
s (-)	1.196	0.806	3.994	9.497

Parameter correlations for all perturbations with all parameters within the 5% to 95% limits are given in Table A.5.

Table A.50 – Pearson cross-correlations of 5% to 95% parameters

	Log(K_f)	P_f	Log(Ss)	Log(K_s)	t_s	s
Log(K_f)	1.000	-0.980	-0.985	0.996	0.960	0.978
Pf	-0.980	1.000	0.997	-0.992	-0.888	-0.920
Log(S_s)	-0.985	0.997	1.000	-0.996	-0.905	-0.933
Log(K_s)	0.996	-0.992	-0.996	1.000	0.936	0.959
t_s	0.960	-0.888	-0.905	0.936	1.000	0.997
s	0.978	-0.920	-0.933	0.959	0.997	1.000

A.10.4 Additional Figures

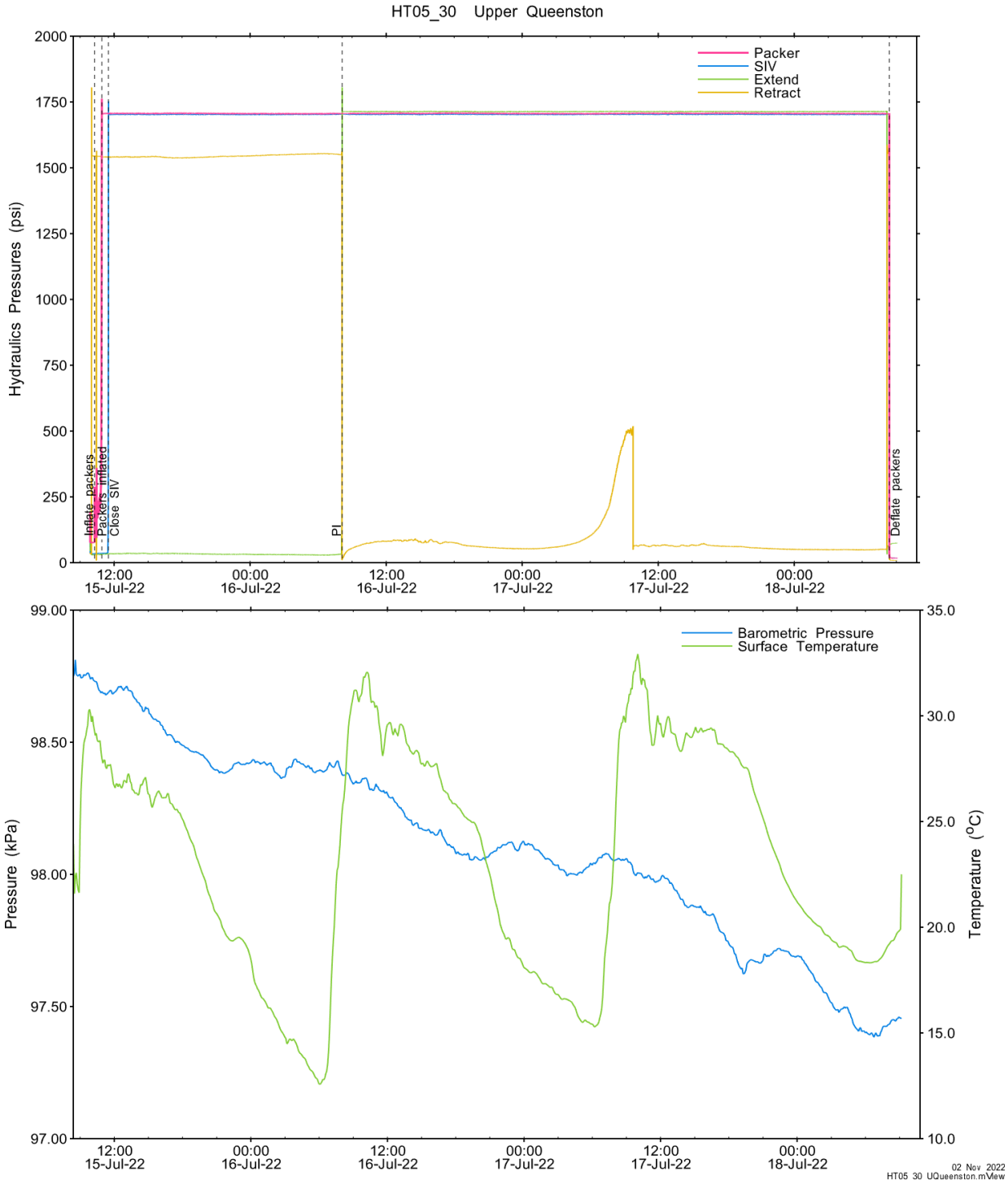

Figure A.157 - Hydraulics pressures and surface temperature/barometric pressure.

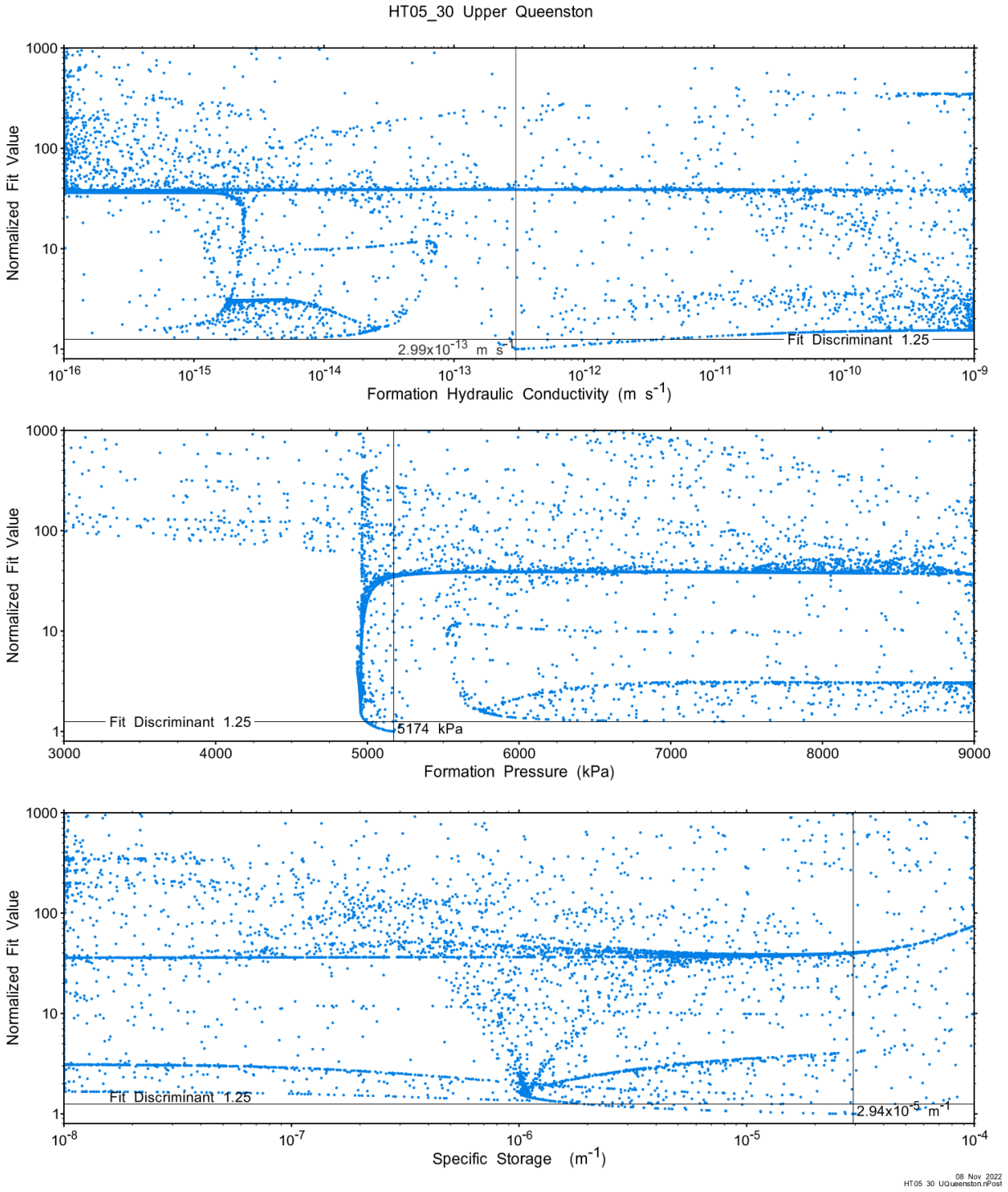

Figure A.158 - XY-scatter plot showing the formation parameter space normalized fit values.

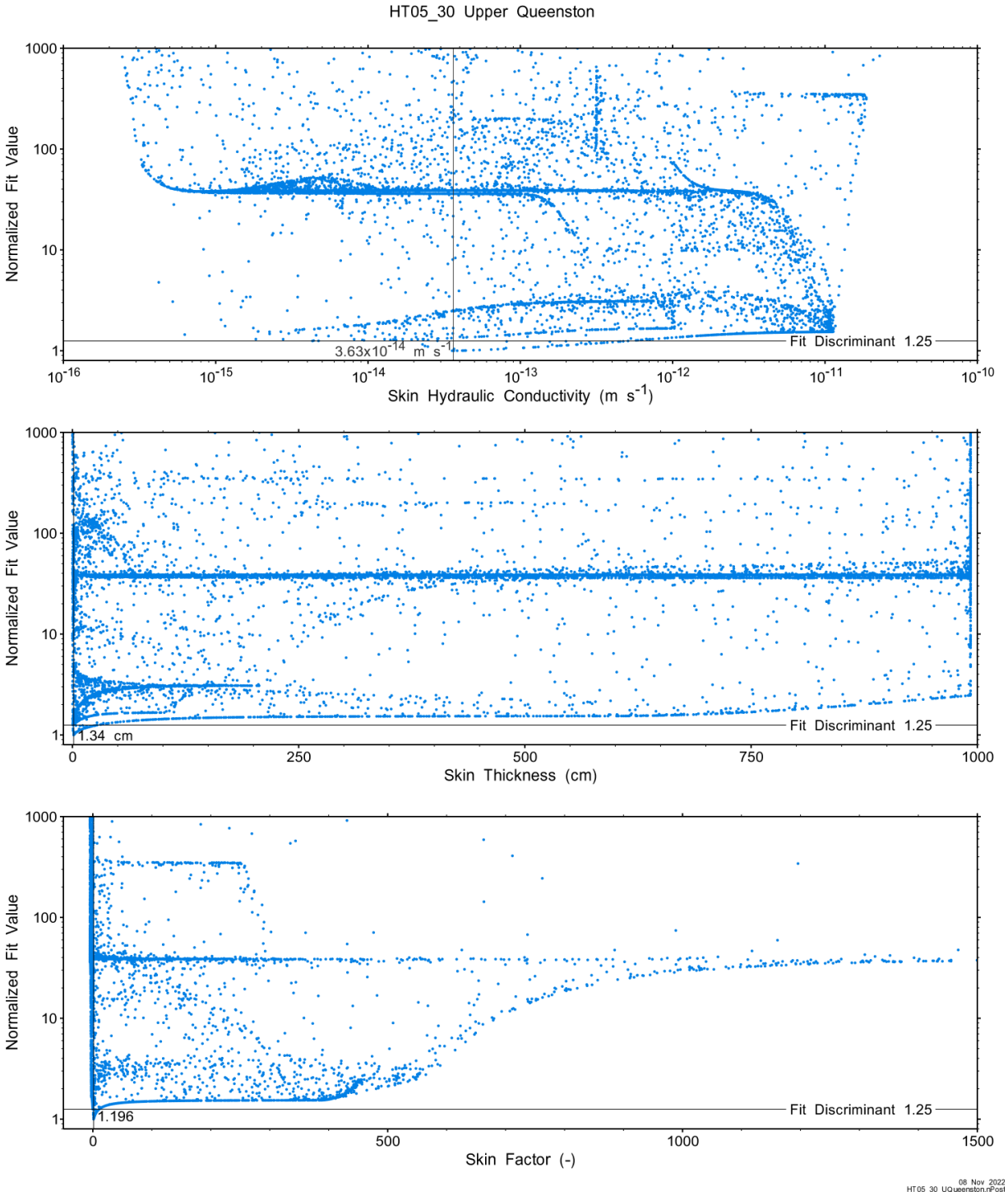

Figure A.159 - XY-scatter plot showing the skin parameter space normalized fit values.

A.11 HT06_30 Lower Queenston

The SB BH02 interval from 490.00 to 519.96 mBGS tested in HT06_30 consists of the upper 30m of the lower half of the Queenston Formation. A single PI test of two days duration was conducted.

A.11.1 Test Data Summary

Table A.6 and Figure A.1 provide a summary of test events and a plot of pressures measured while testing respectively. The excursions in the annulus response in the afternoon/evening of 21 July are due to a heavy rainstorm passing over the site, with some precipitation falling into the open surface casing.

Table A.51 - Summary of Test Events.

Event	Start Date & Time	Duration (days)	TZ Pressure (kPa)
Drilling intercept	22-03-01 08:52	139.10	5087
Shut-in	22-07-18 11:14	0.87	5092
Pulse injection	22-07-19 08:08	2.00	5436
Test end	22-07-21 08:09		5216

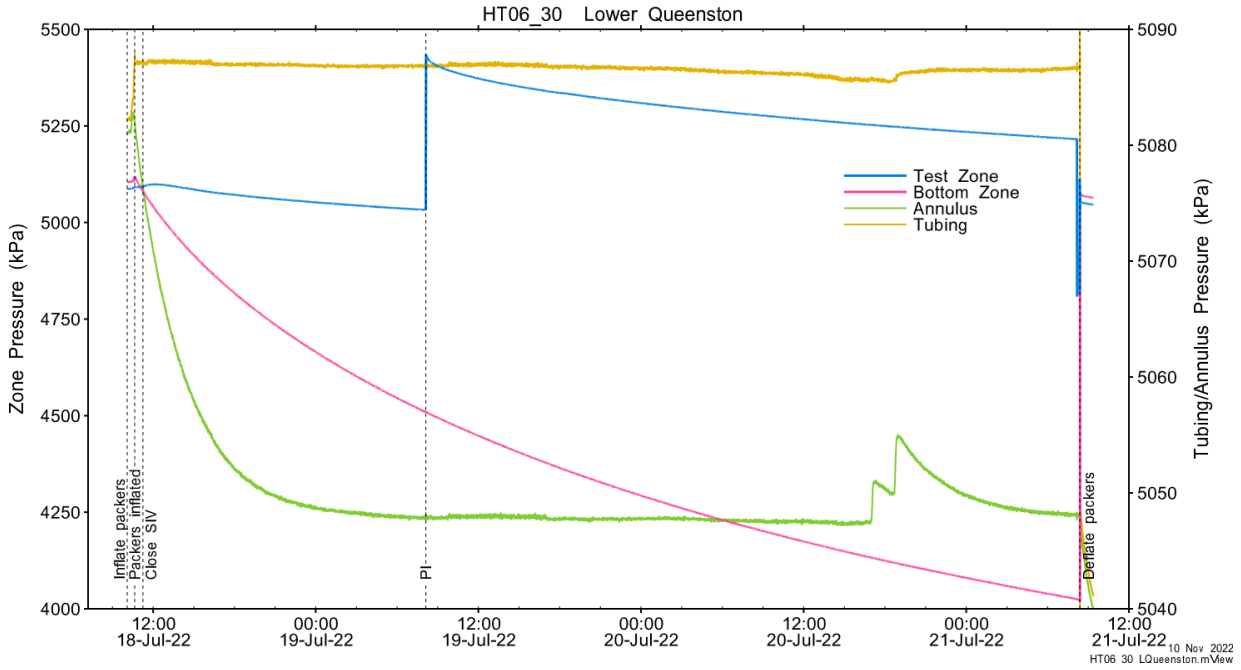

Figure A.160 - Test events and pressures.

A.11.2 Test Analyses

Table A.7 is a summary of test-specific input parameters used in the analyses, while Table A.8 presents the optimized parameters and allowed ranges.

Table A.52 – nSIGHTS Input Parameters.

Parameter	Value	Units
Test zone radius	7.61	cm
Test zone compressibility	4.67E-10	1/Pa
Test zone length	29.96	m

Table A.53 – nSIGHTS Parameter Optimization Ranges.

Parameter	Minimum	Maximum	Units	Type
Formation hydraulic conductivity (K_f)	1E-15	1E-08	m/s	log
Formation pressure (P_f)	3000	6000	kPa	linear
Specific storage (S_s)	1E-08	1E-04	1/m	log
Skin hydraulic conductivity (K_s)	1E-15	1E-08	m/s	log
Skin thickness (t_s)	0.013	500	cm	linear

Figure A.18 shows the measured test zone pressure record (with reduced data density for clarity) used in the analysis along with the best-fit simulation and parameter values. Figure A.19 presents the pre-test history, and Figure A.20 shows the Ramey B normalized best-fit pressure and pressure derivatives.

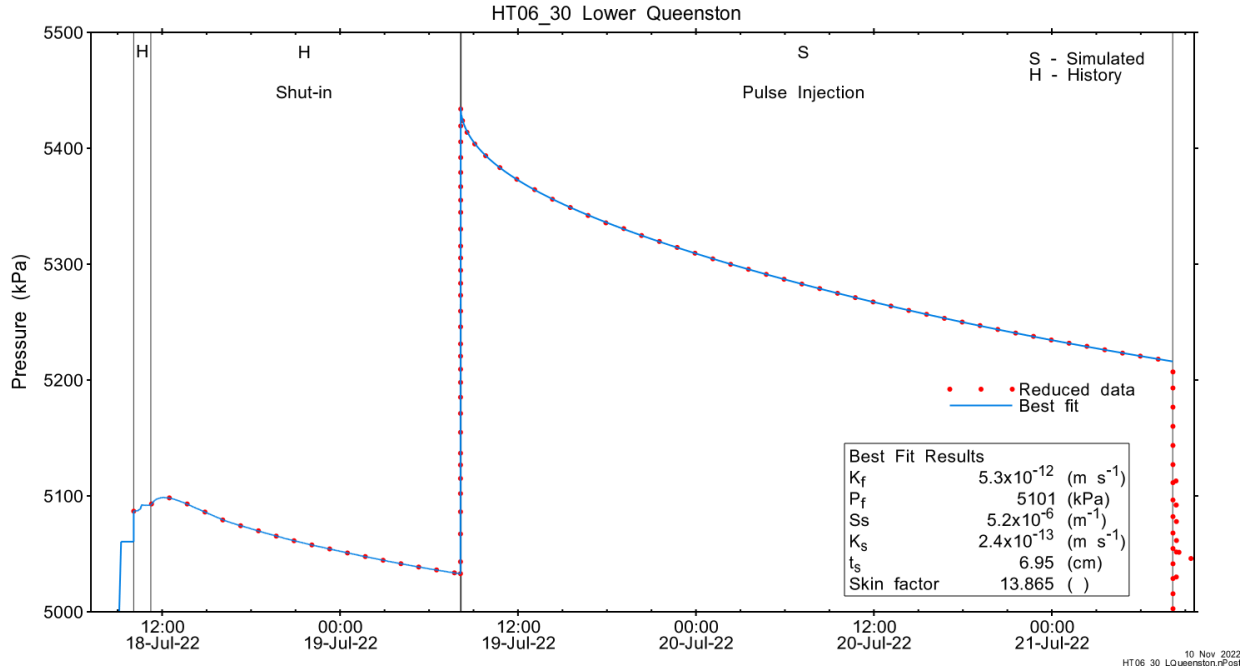

Figure A.161 - Annotated testing sequence showing best-fit simulation and parameter estimates.

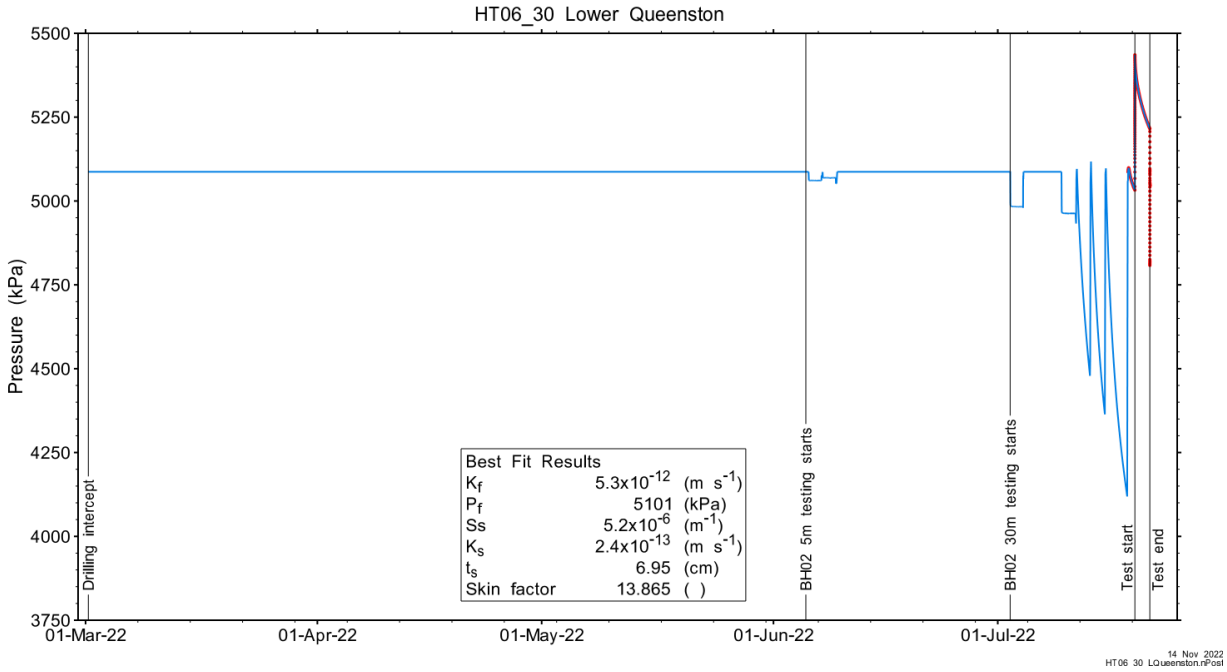

Figure A.162 - Annotated testing sequence showing pre-test history, best-fit simulation and parameter estimates.

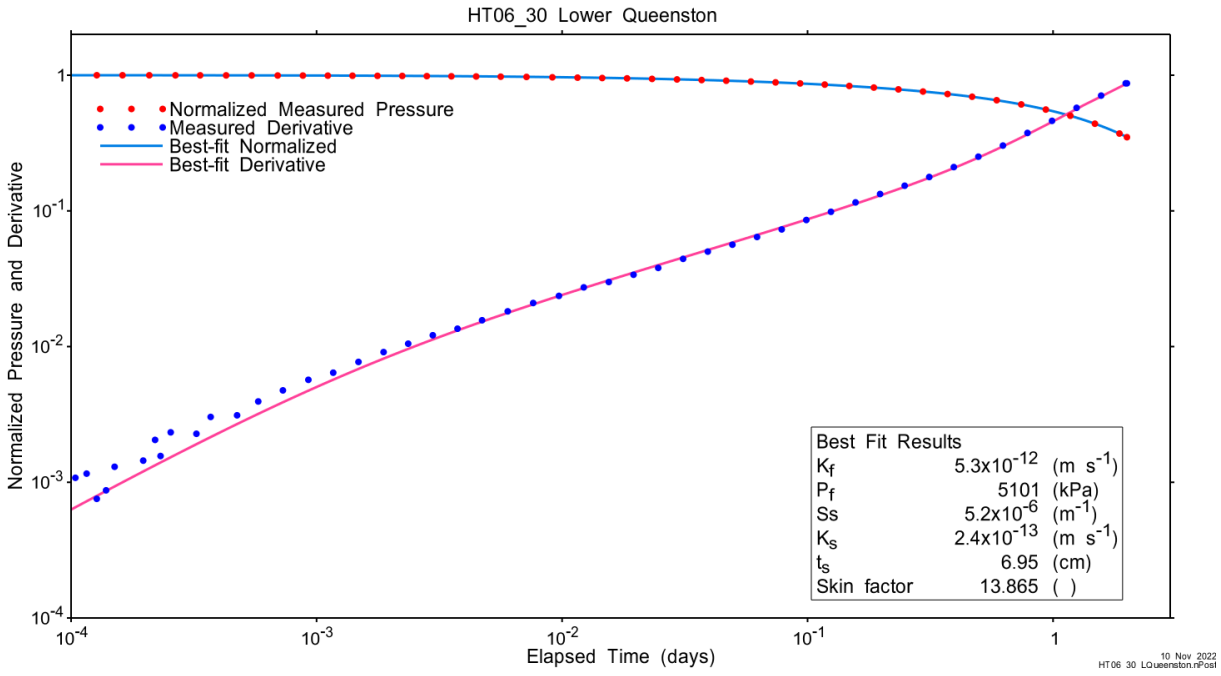

Figure A.163 - Log-log plot showing Ramey B and derivative response for best-fit simulation.

Figure A.21 shows the normalized parameter sensitivity response for the best fit. Sensitivity for all formation fitting parameters (except S_s) was rising at the end of the test, indicating that a longer test may have returned more precise results.

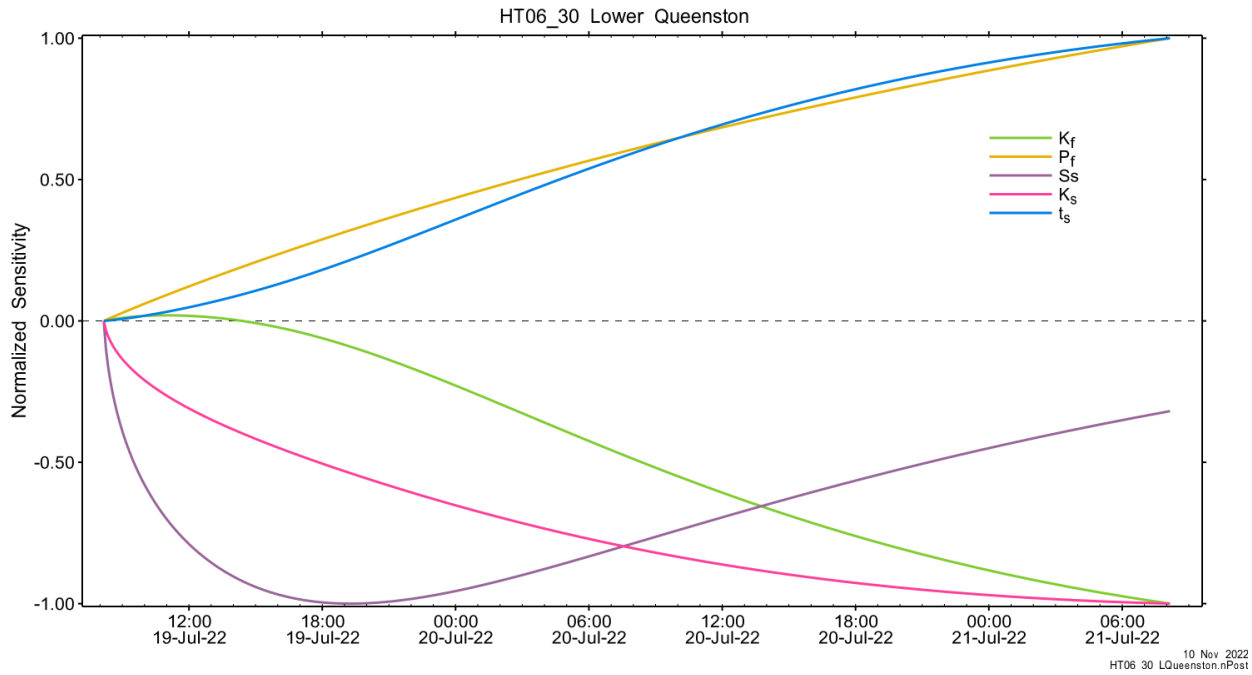

Figure A.164 - Normalized Jacobian for best-fit simulation.

A.11.3 Uncertainty Analyses

The CDF of normalized fit values for all converged simulations and the selected fit discriminant are shown in Figure A.22 and, in detail, in Figure A.166.

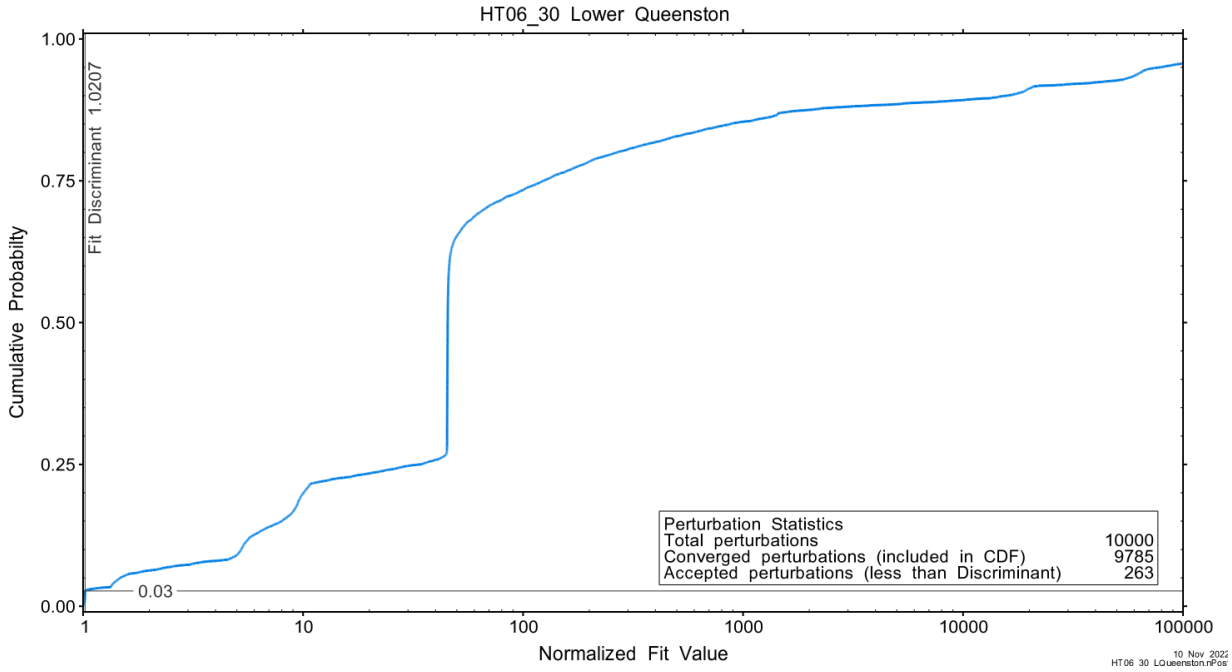

Figure A.165 - Fit value cumulative distribution function.

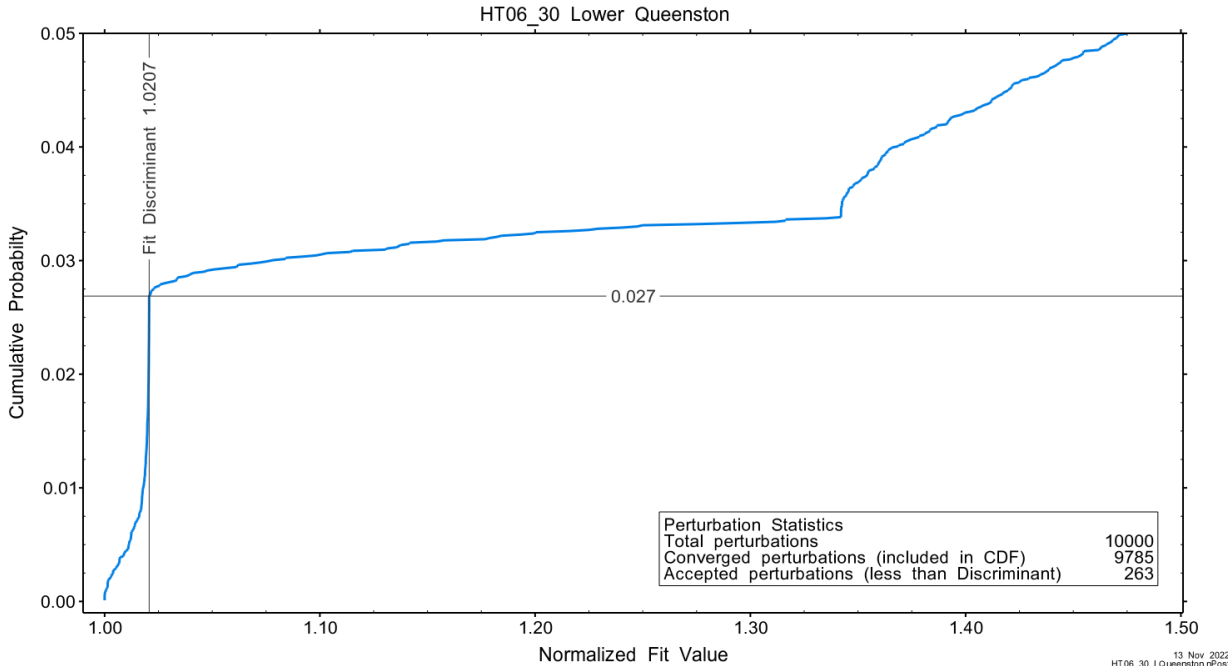

Figure A.166 – Detail of fit value cumulative distribution function.

Summary cross parameter scatter plots for selected formation and skin parameters are given in Figure A.24 and Figure A.25. The light pink dots on the figures are the initial parameter estimates, with red dots overlaying those initial parameter values that resulted in accepted optimization results. The grey dots are converged optimizations which did not meet the fit discriminant. Larger varying color symbols represent the fit value of accepted optimizations, with the blue values representing the best fit.

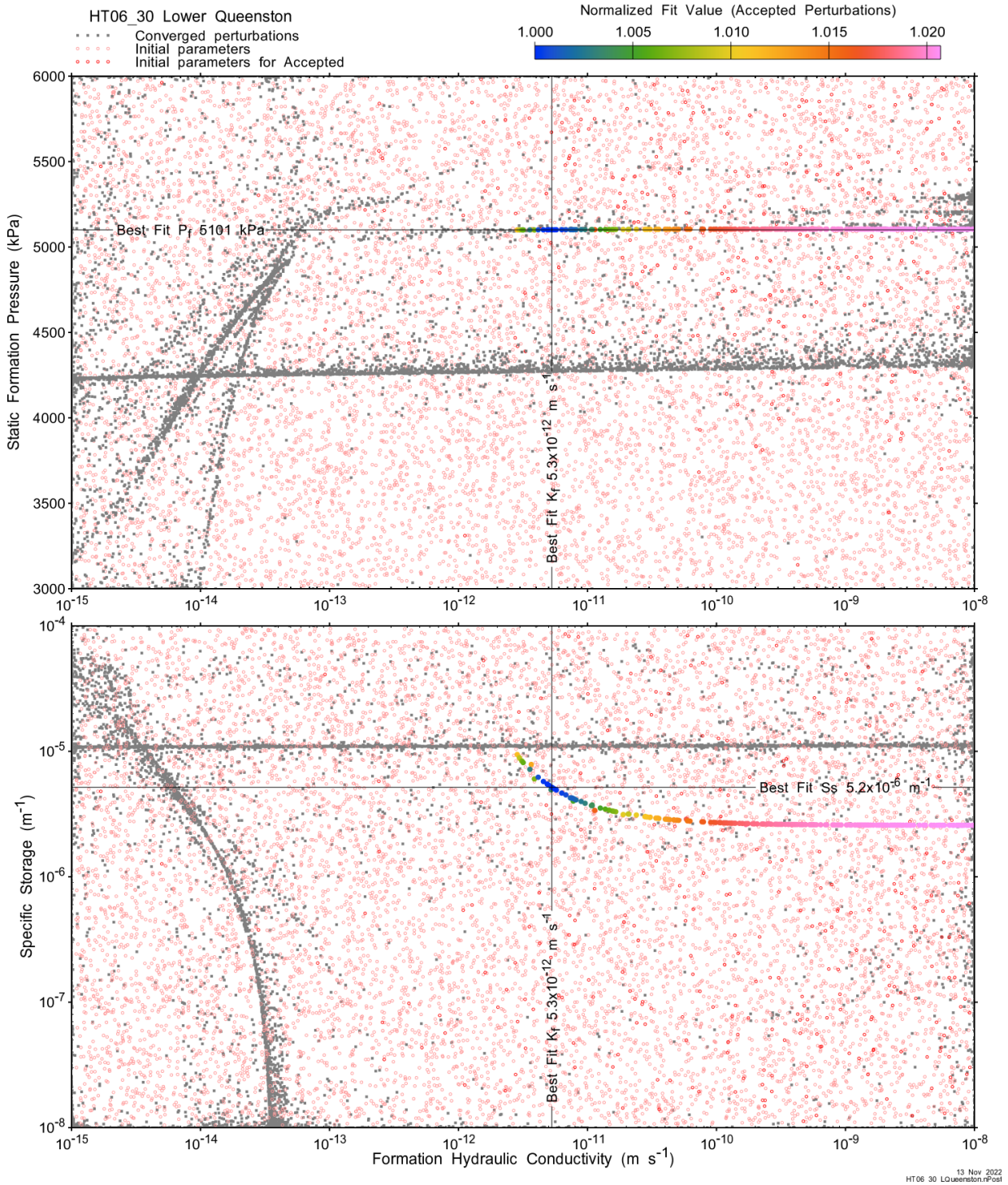

Figure A.167 - XY-scatter plot showing estimates of formation hydraulic conductivity (K_f) vs static formation pressure (P_f) (top panel) and specific storage (Ss) (bottom panel).

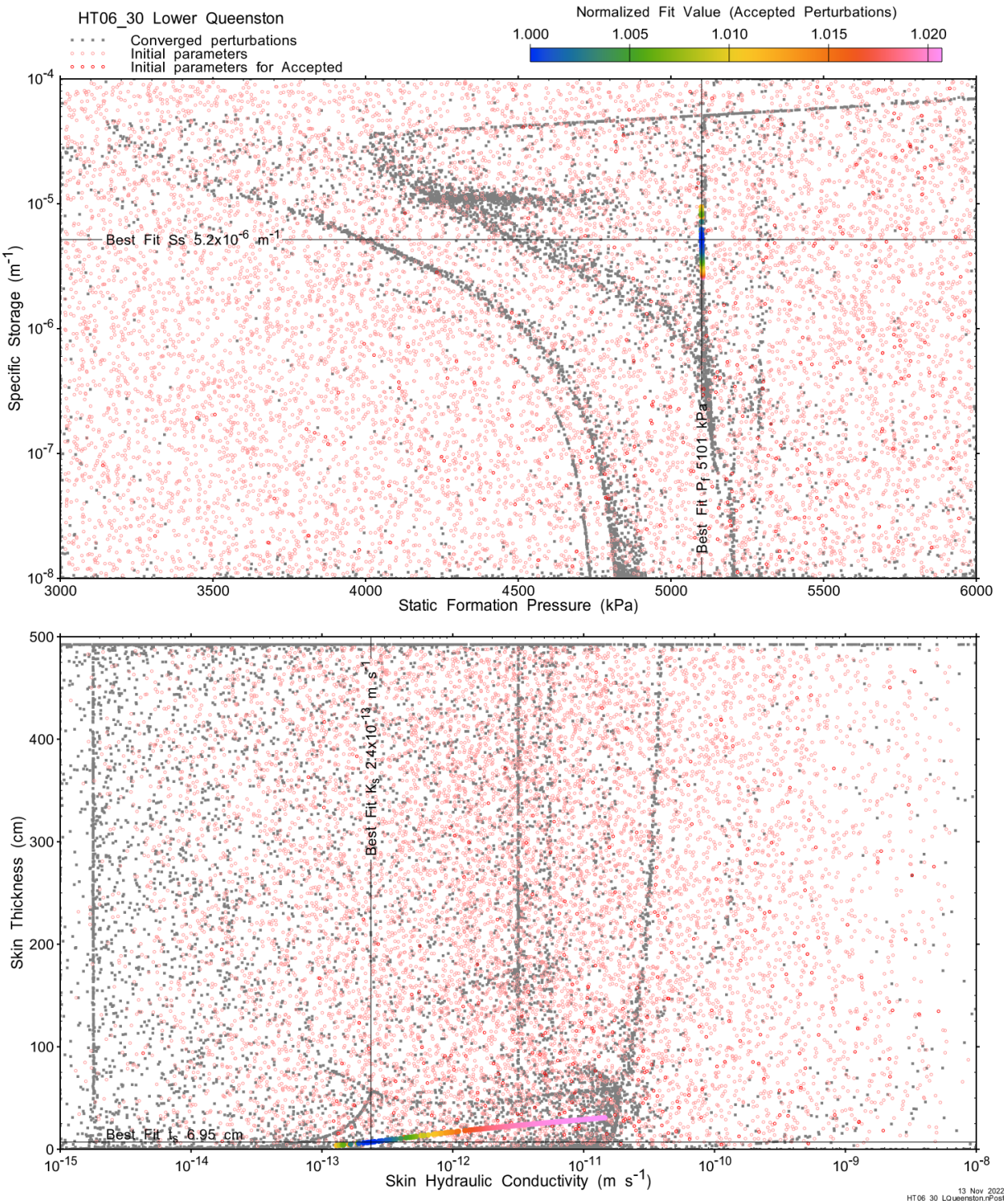

Figure A.168 - XY-scatter plot showing estimates of static formation pressure (P_f) vs specific storage (Ss) (top panel) and skin hydraulic conductivity (K_s) vs skin thickness (t_s) (bottom panel).

Confidence limits and median values are determined from the CDF of accepted optimization results (i.e. the varying color values in the above figures), with best fit value, 5% and 95% confidence indicated on Figure A.26 and Figure A.27.

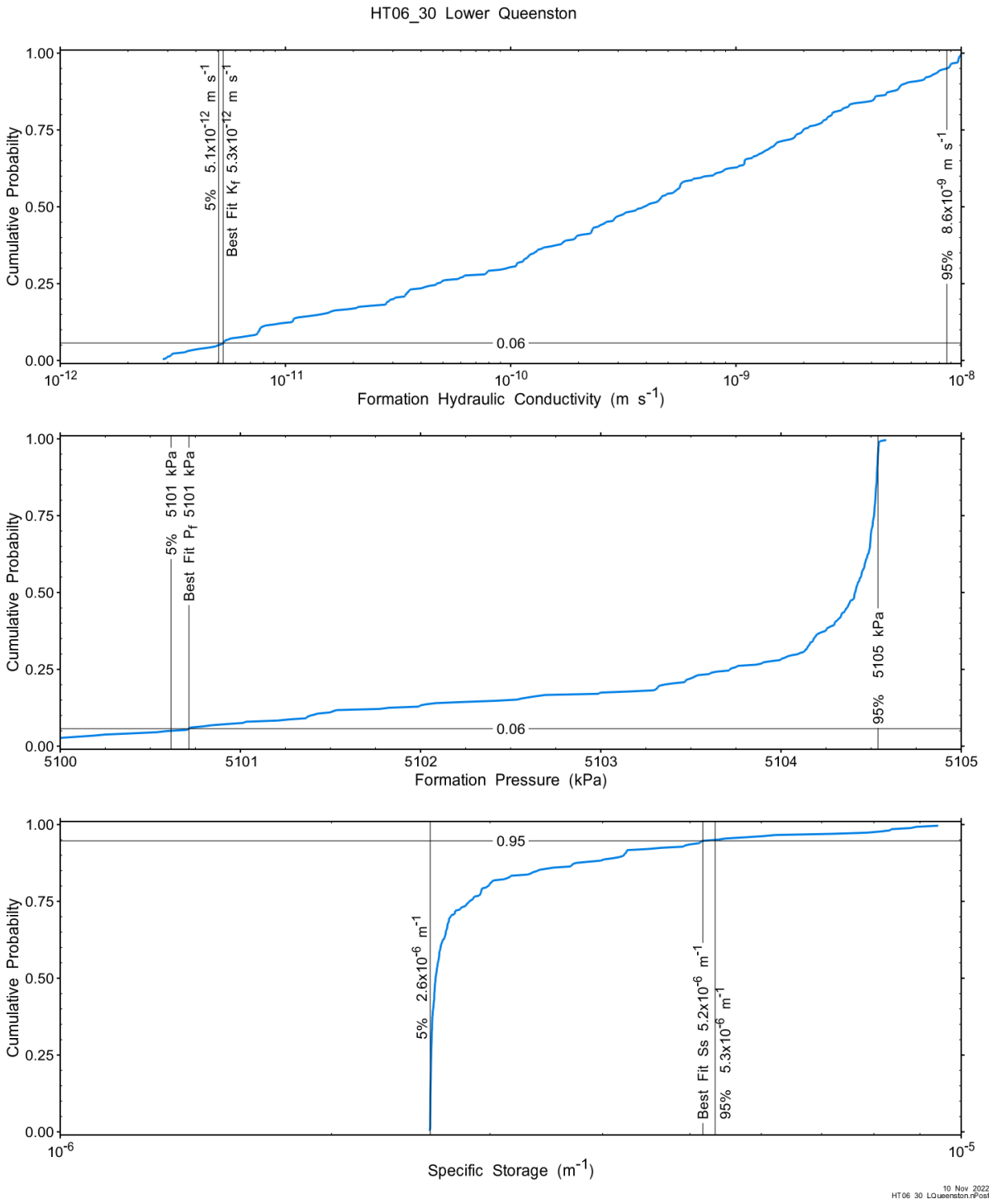

Figure A.169 – Cumulative distribution functions and parameter limits for formation hydraulic conductivity (K_f) (top panel), static formation pressure (P_f) (middle panel) and specific storage (Ss) (bottom panel).

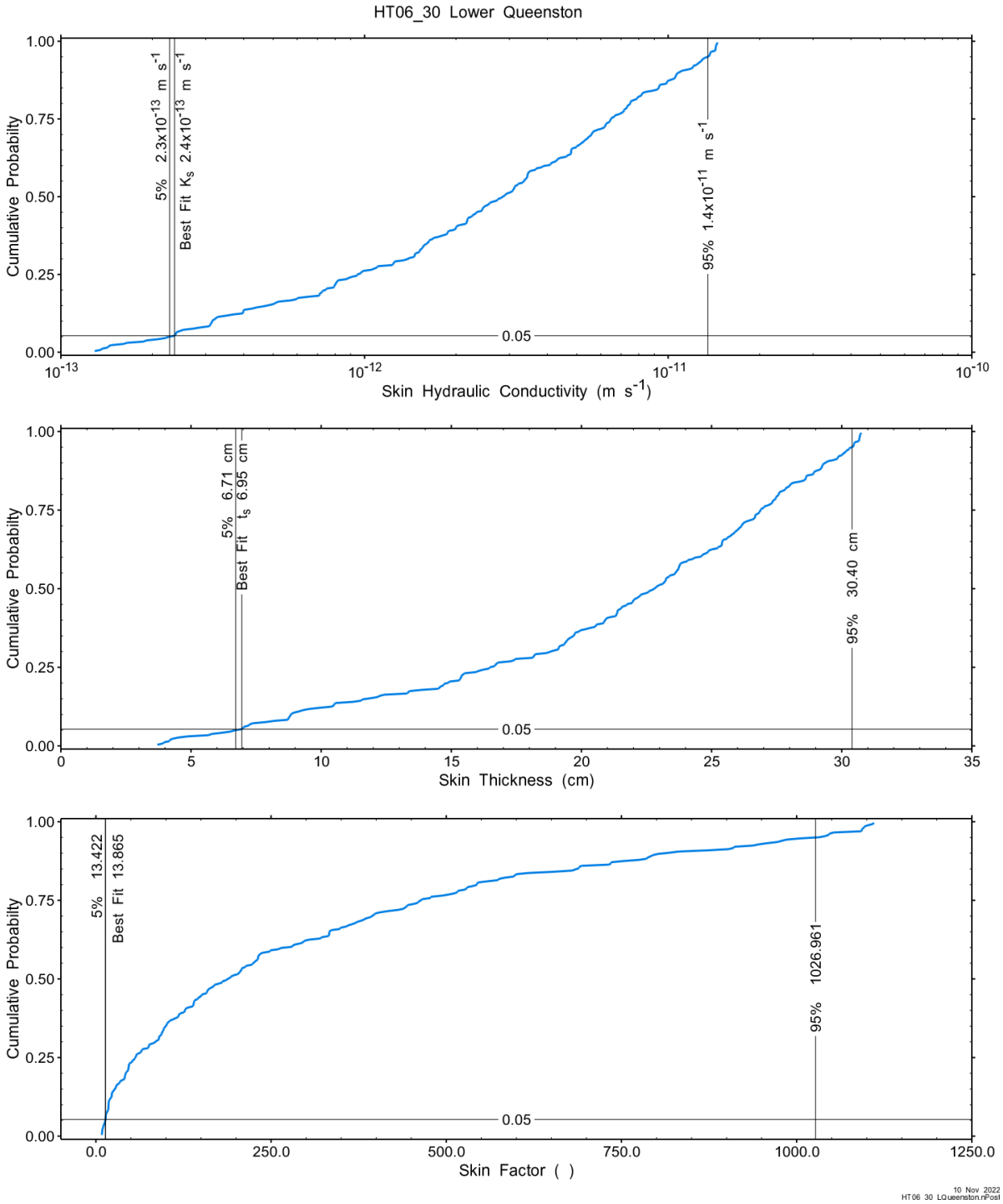

Figure A.170 – Cumulative distribution functions and parameter limits for skin hydraulic conductivity (K_s) (top panel), skin thickness (t_s) (middle panel) and skin factor (s) (bottom panel).

A summary of perturbation results is presented in Figure A.28, with Ramey-processed perturbations in Figure 12. Those perturbations (225 of 10,000) with all parameters within the 5% and 95% range present a very good fit to the measured test zone data.

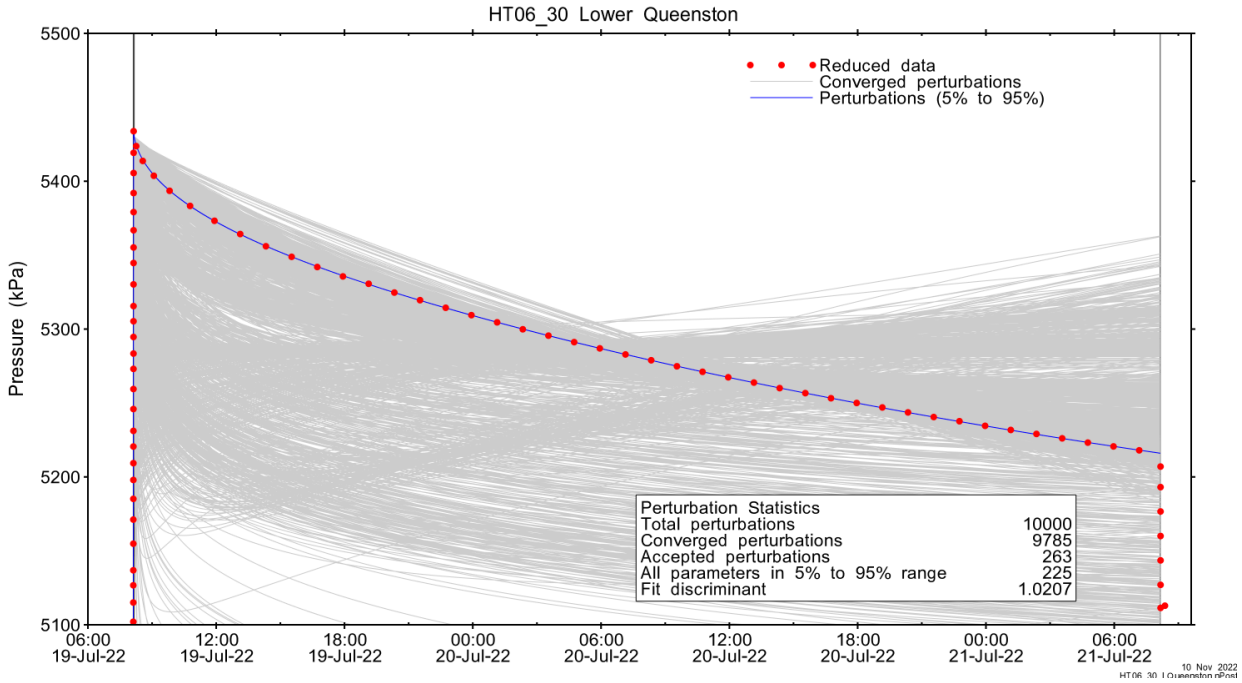

Figure A.171 – Perturbation results – all converged, accepted, and within 5% to 95% for all parameters.

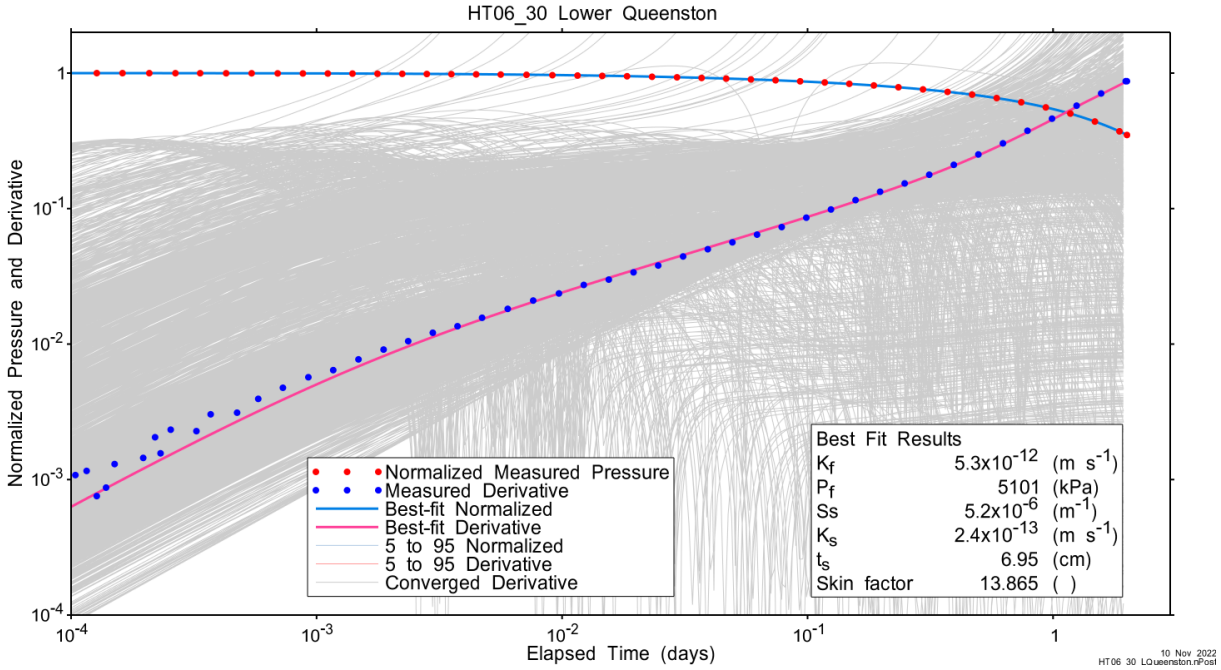

Figure A.172 – Log-log plot showing Ramey B and derivative response for all converged optimizations and those within 5% to 95% for all parameters.

A summary of best-fit and parameter ranges is given in Table A.9.

Table A.54 - Summary of the HT06_30 parameter estimates.

Parameter	Best Fit	5%	Median	95%
K_f (m/s)	5.3E-12	5.1E-12	3.9E-10	8.6E-09
P_f (kPa)	5101	5101	5104	5105
Ss (1/m)	5.2E-06	2.6E-06	2.6E-06	5.3E-06
K_s (m/s)	2.4E-13	2.3E-13	2.8E-12	1.4E-11
t_s (cm)	6.95	6.71	22.79	30.40
s (-)	13.865	13.422	187.910	1026.961

Parameter correlations for all perturbations with all parameters within the 5% to 95% limits are given in Table A.5.

Table A.55 – Pearson cross-correlations of 5% to 95% parameters

	Log(K_f)	P_f	Log(Ss)	Log(K_s)	t_s	s
Log(K_f)	1.000	0.843	-0.797	0.999	0.992	0.897
Pf	0.843	1.000	-0.987	0.865	0.901	0.565
Log(S_s)	-0.797	-0.987	1.000	-0.823	-0.863	-0.518
Log(K_s)	0.999	0.865	-0.823	1.000	0.997	0.882
t_s	0.992	0.901	-0.863	0.997	1.000	0.845
s	0.897	0.565	-0.518	0.882	0.845	1.000

A.11.4 Additional Figures

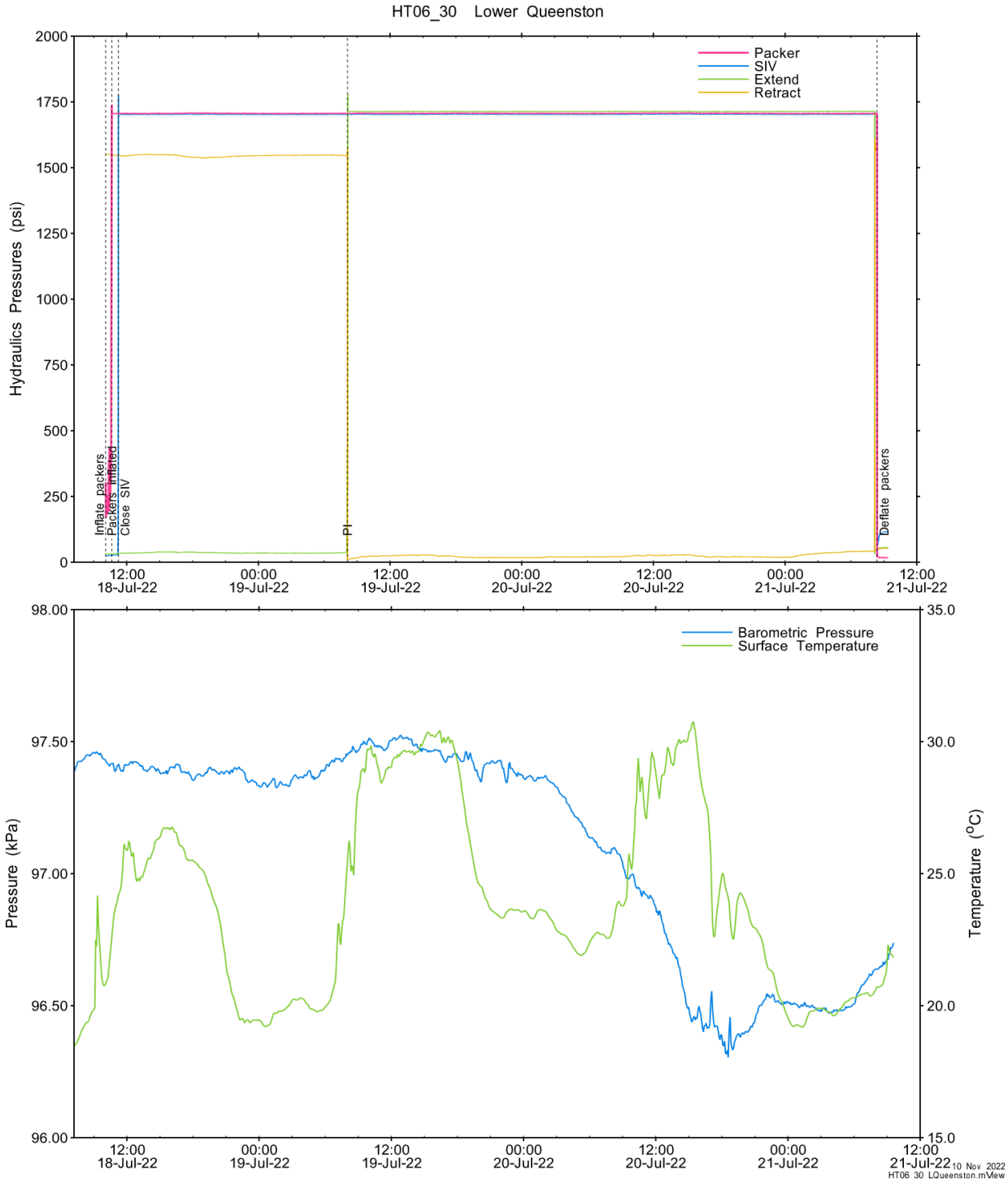

Figure A.173 - Hydraulics pressures and surface temperature/barometric pressure.

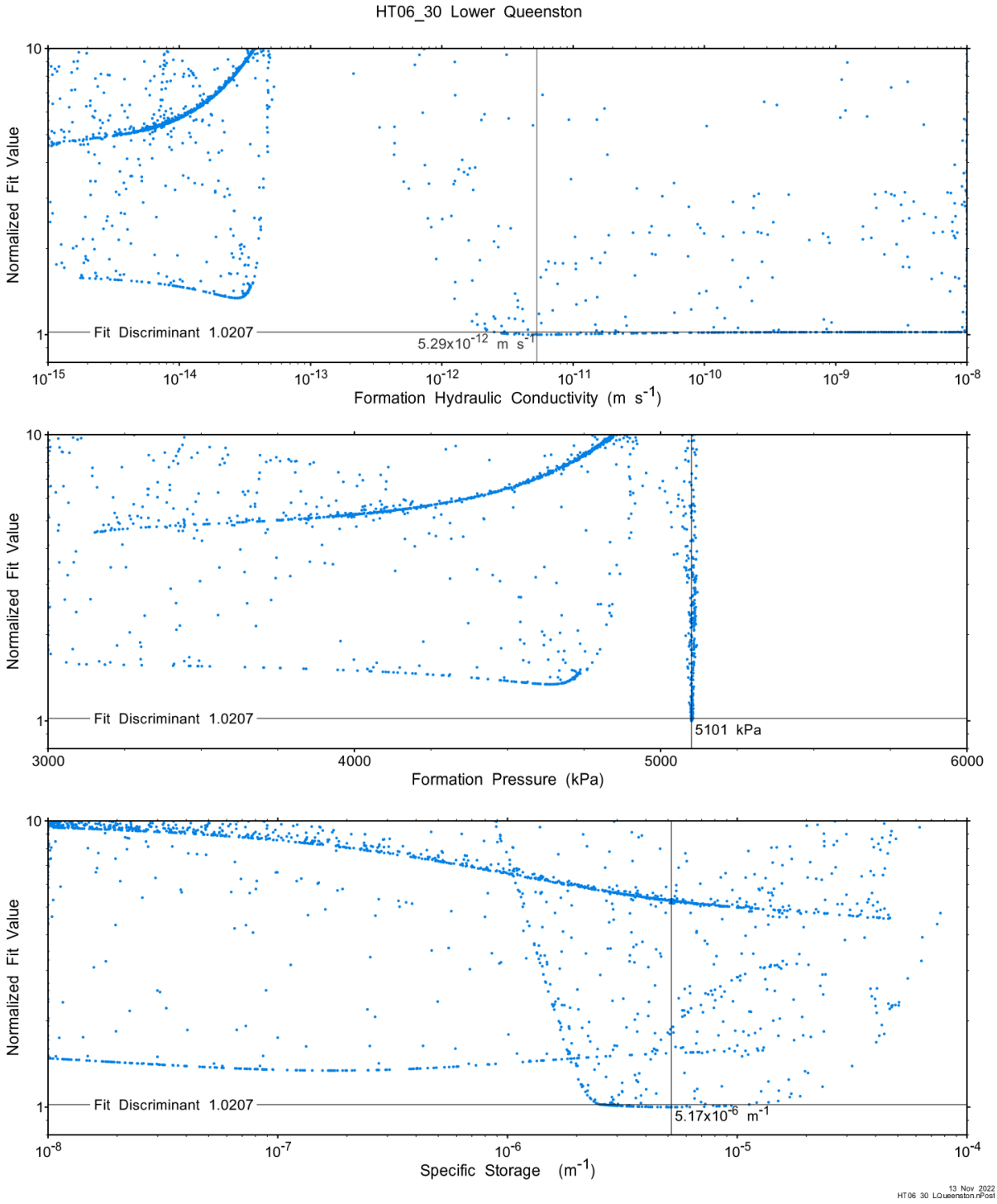

Figure A.174 - XY-scatter plot showing the formation parameter space normalized fit values.

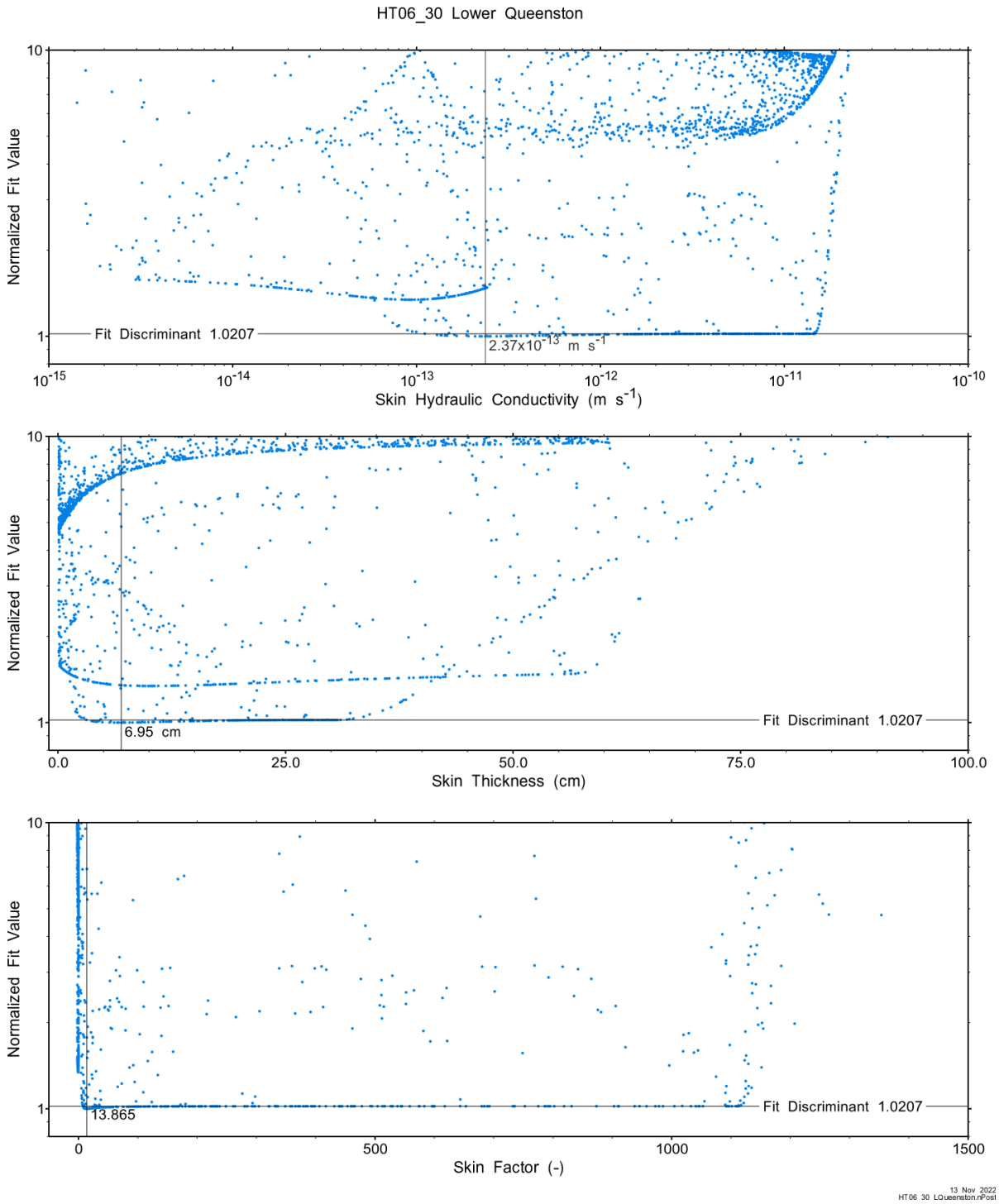

Figure A.175 - XY-scatter plot showing the skin parameter space normalized fit values.

A.12 HT07_30 Upper Georgian Bay

The SB BH02 interval from 532.00 to 561.96 mBGS tested in HT07_30 is located in the middle of the upper half of the Georgian Bay Formation. A single PI test of two days duration was conducted.

A.12.1 Test Data Summary

Table A.6 and Figure A.1 provide a summary of test events and a plot of pressures measured while testing respectively.

Table A.56 - Summary of Test Events.

Event	Start Date & Time	Duration (days)	TZ Pressure (kPa)
Drilling intercept	22-03-04 23:27	138.54	5526
Shut-in	22-07-21 12:17	0.80	5530
Pulse injection	22-07-22 07:34	2.00	5582
Test end	22-07-24 07:39		5474

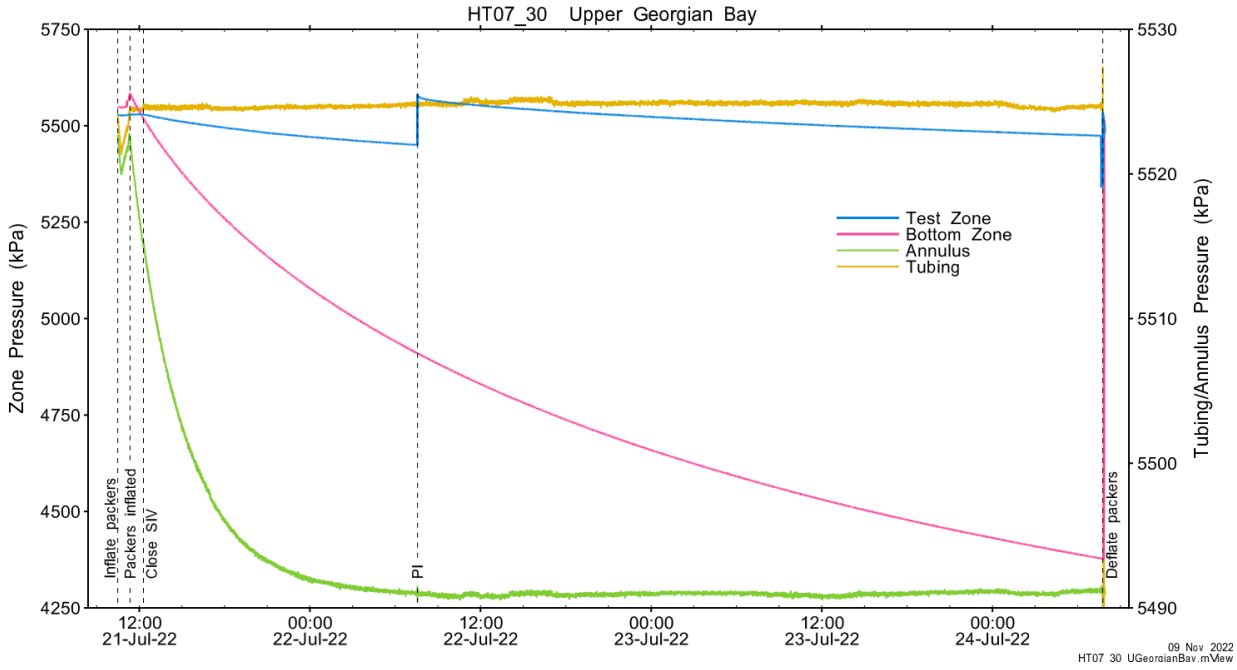

Figure A.176 - Test events and pressures.

A.12.2 Test Analyses

Table A.7 is a summary of test-specific input parameters used in the analyses, while Table A.8 presents the optimized parameters and allowed ranges.

Table A.57 – nSIGHTS Input Parameters.

Parameter	Value	Units
Test zone radius	6.62	cm
Test zone compressibility	1.90E-09	1/Pa
Test zone length	29.96	m

Table A.58 – nSIGHTS Parameter Optimization Ranges.

Parameter	Minimum	Maximum	Units	Type
Formation hydraulic conductivity (K_f)	1E-16	1E-08	m/s	log
Formation pressure (P_f)	0	6000	kPa	linear
Specific storage (S_s)	1E-08	1E-04	1/m	log
Skin hydraulic conductivity (K_s)	1E-16	1E-08	m/s	log
Skin thickness (t_s)	0.013	500	cm	linear

Figure A.18 shows the measured test zone pressure record (with reduced data density for clarity) used in the analysis along with the best-fit simulation and parameter values. Figure A.19 presents the pre-test history, and Figure A.20 shows the Ramey B normalized best-fit pressure and pressure derivatives.

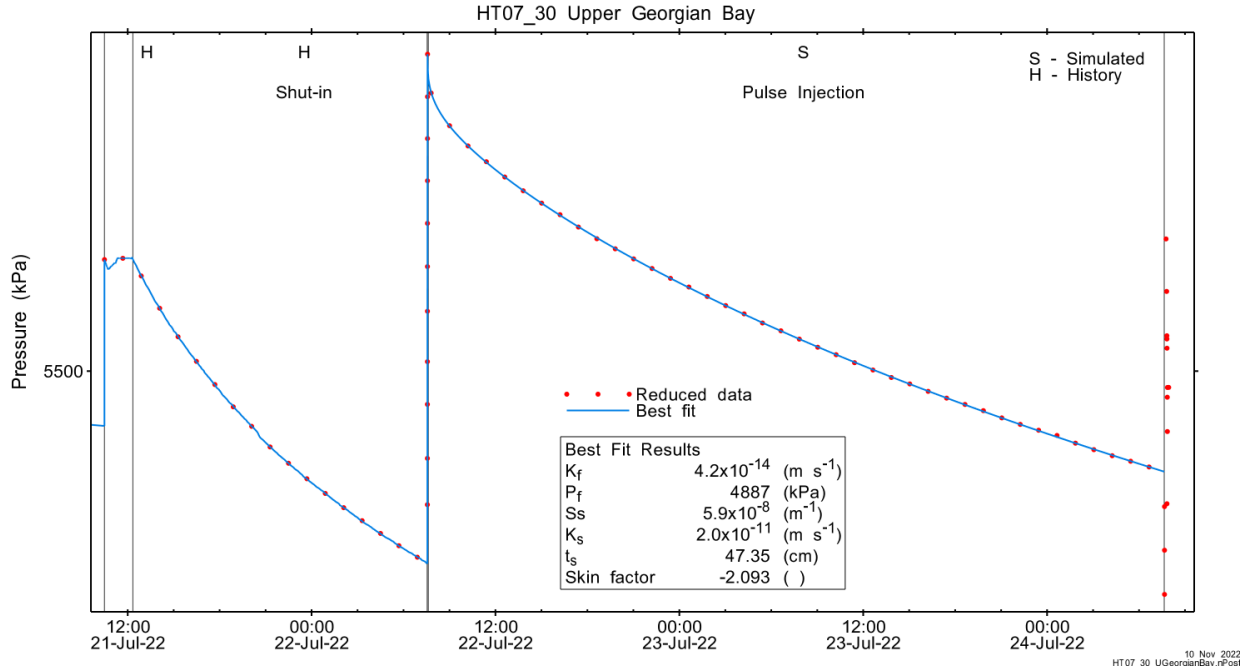

Figure A.177 - Annotated testing sequence showing best-fit simulation and parameter estimates.

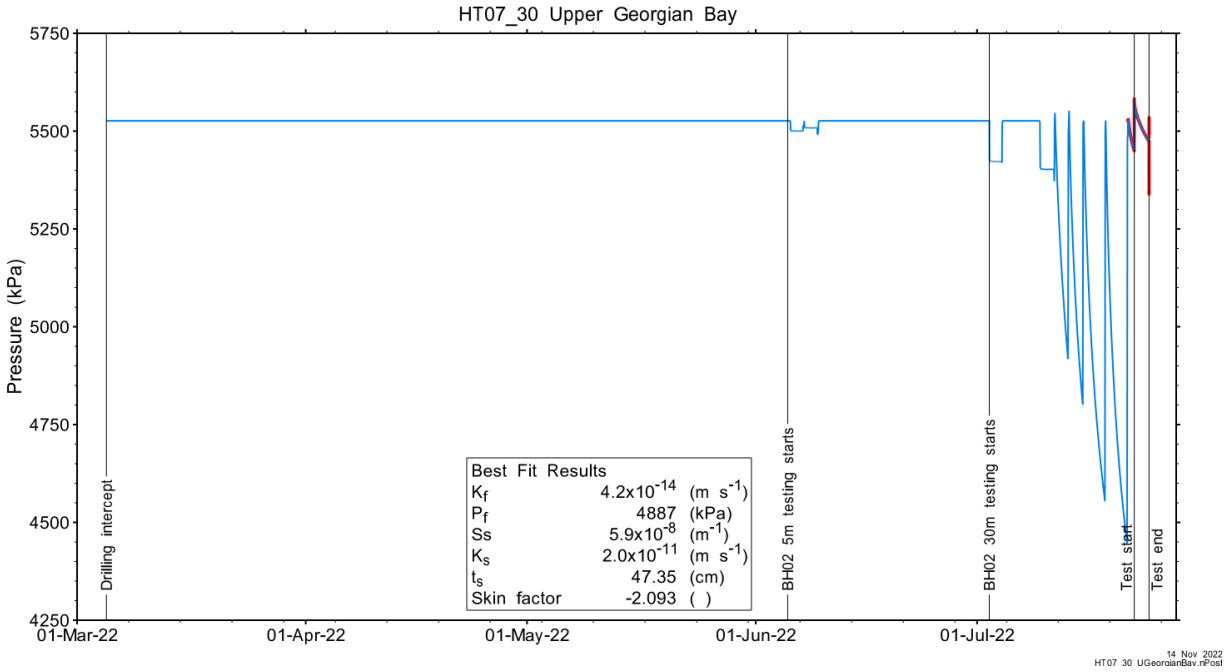

Figure A.178 - Annotated HT07_30 testing sequence showing pre-test history, best-fit simulation and parameter estimates.

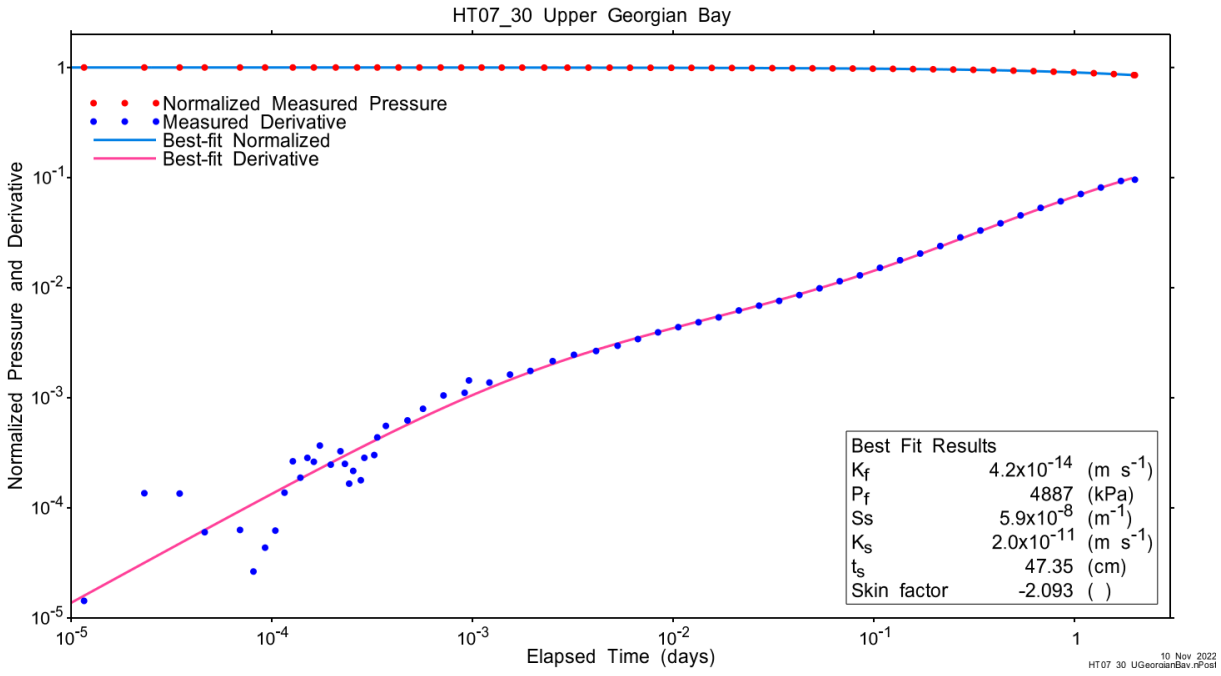

Figure A.179 - Log-log plot showing Ramey B and derivative response for best-fit simulation.

Figure A.21 shows the normalized parameter sensitivity response for the best fit. Sensitivity for all fitting parameters (except K_s) was rising at the end of the test, indicating that a longer test may have returned more precise results.

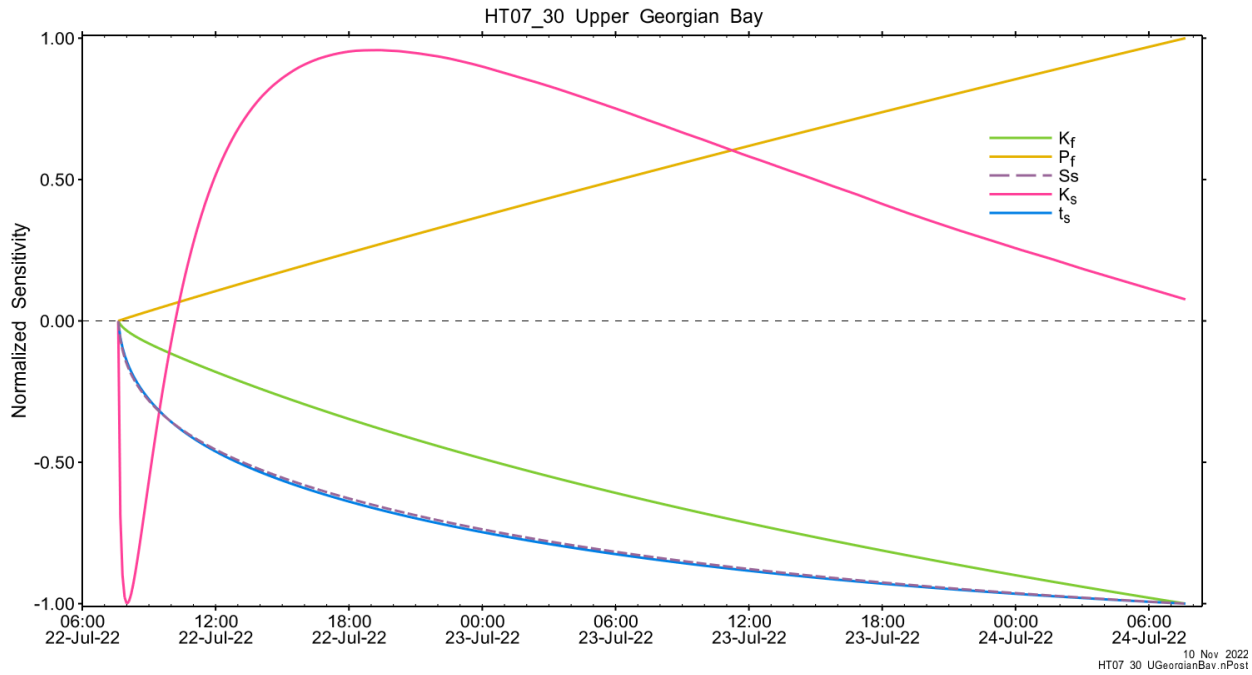

Figure A.180 - Normalized Jacobian for best-fit simulation.

A.12.3 Uncertainty Analyses

The CDF of normalized fit values for all converged simulations and the selected fit discriminant are shown in Figure A.22, and, in detail, in Figure A.182. The fit criterion was originally set higher, but this resulted in the inclusion of fits that were clearly associated with several local minima. The discriminant was adjusted downwards to include only global minimum associated fits (see Appendix plots).

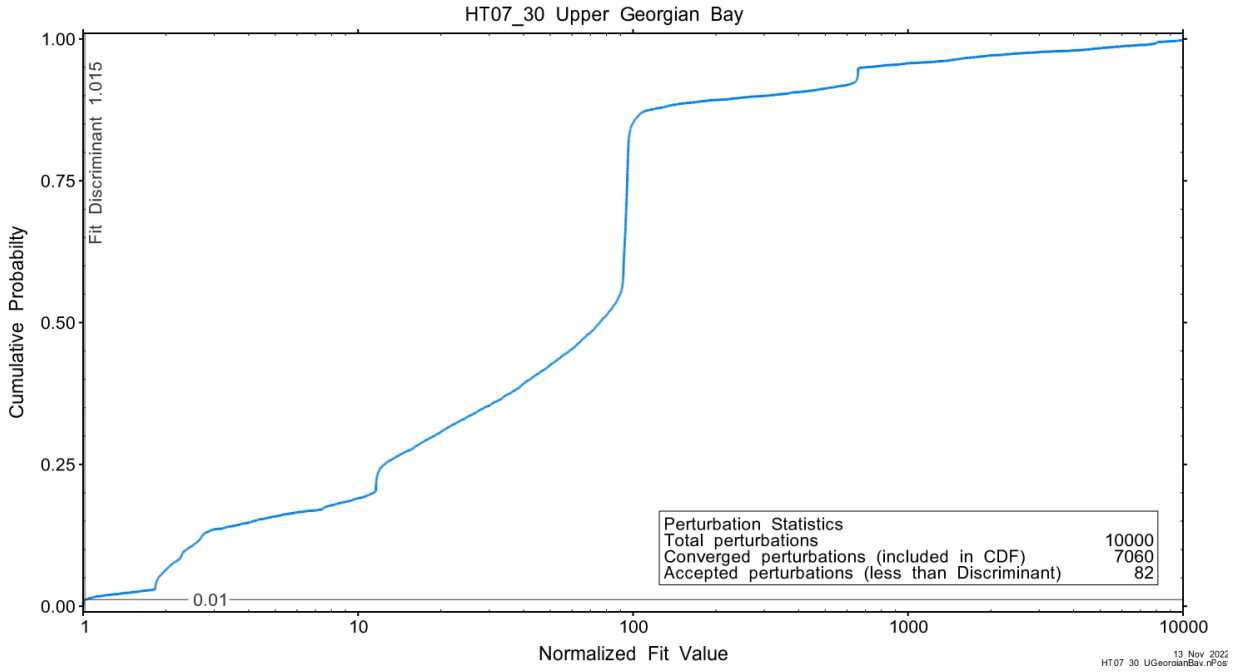

Figure A.181 - Fit value cumulative distribution function.

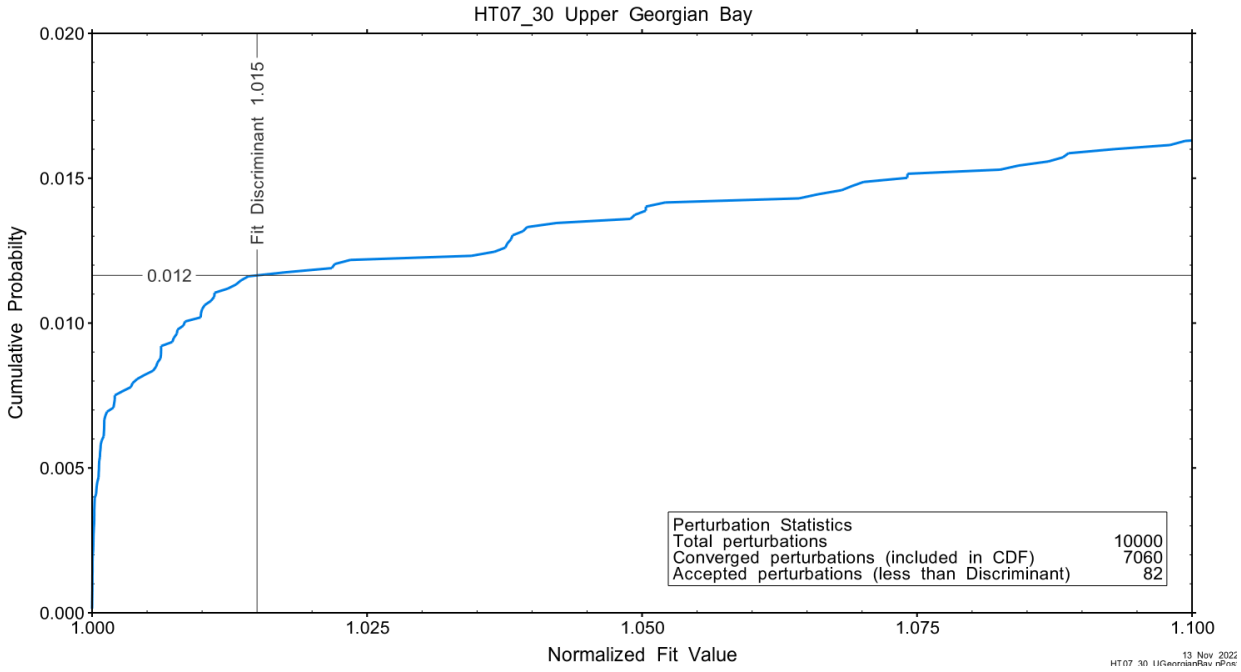

Figure A.182 – Detail of fit value cumulative distribution function.

Summary cross parameter scatter plots for selected formation and skin parameters are given in Figure A.24 and Figure A.25. The light pink dots on the figures are the initial parameter estimates, with red dots overlaying those initial parameter values that resulted in accepted optimization results. The grey dots are converged optimizations which did not meet the fit discriminant. Larger varying color symbols represent the fit value of accepted optimizations, with the blue values representing the best fit.

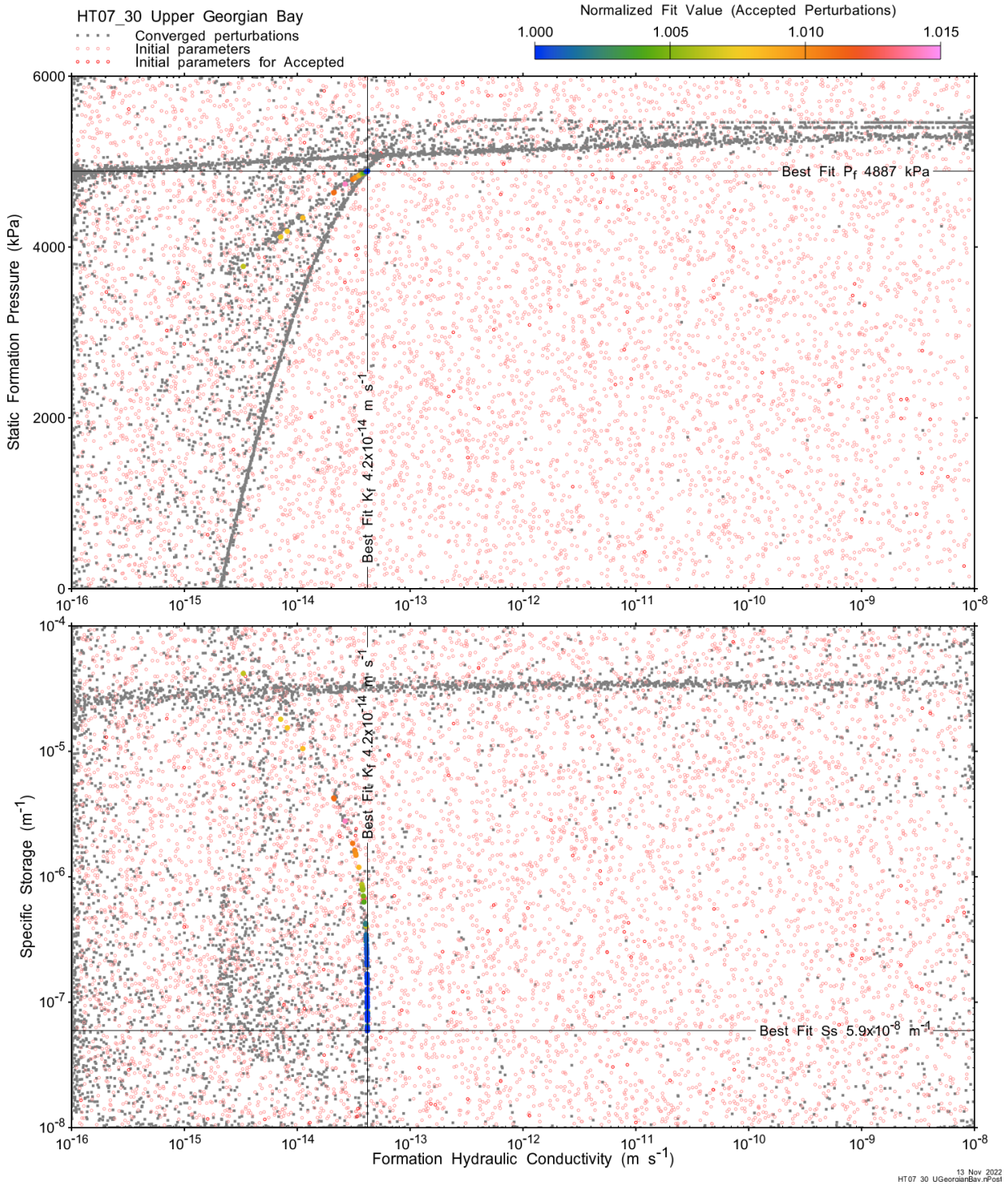

Figure A.183 - XY-scatter plot showing estimates of formation hydraulic conductivity (K_f) vs static formation pressure (P_f) (top panel) and specific storage (Ss) (bottom panel).

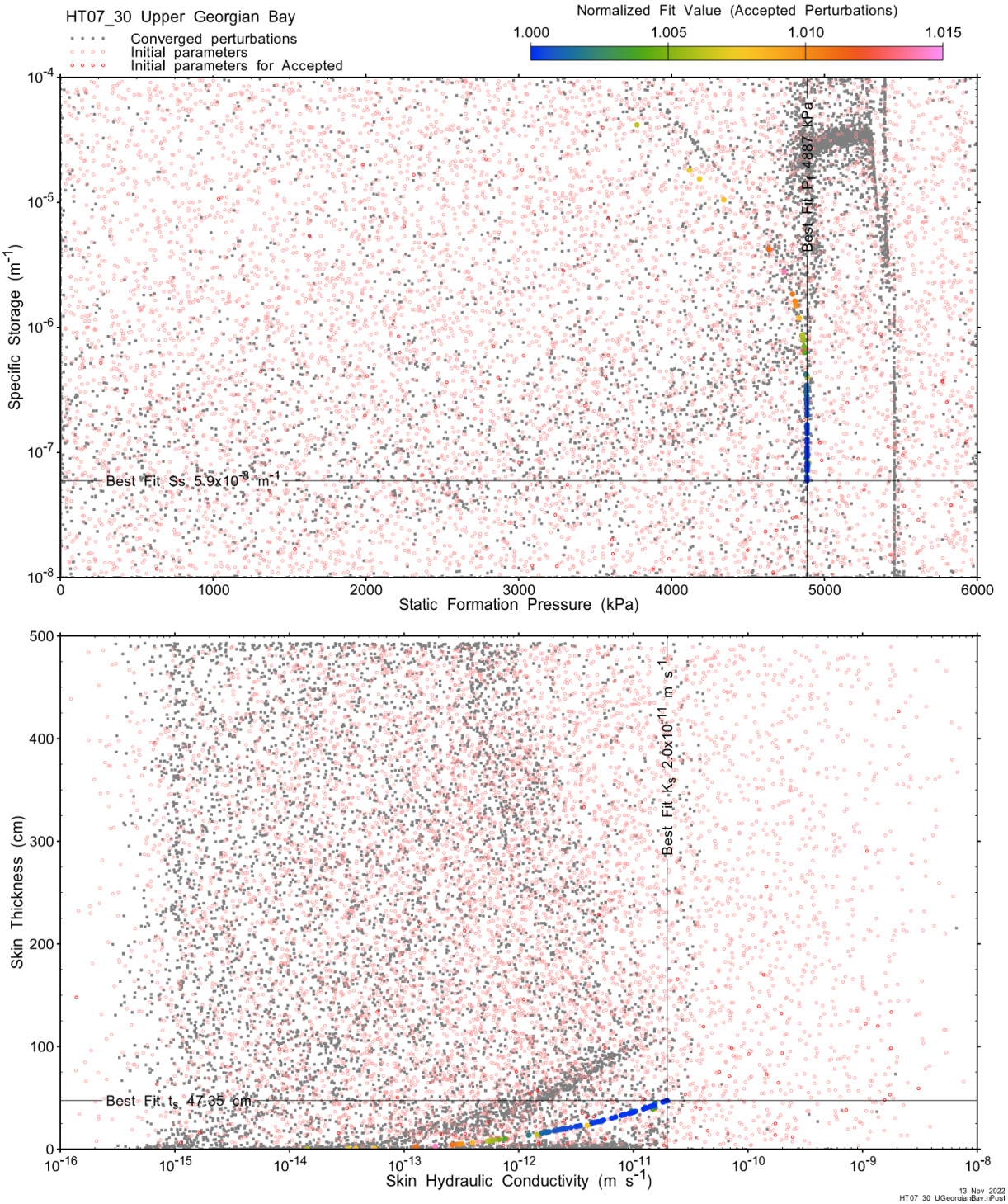

Figure A.184 - XY-scatter plot showing estimates of static formation pressure (P_f) vs specific storage (Ss) (top panel) and skin hydraulic conductivity (K_s) vs skin thickness (t_s) (bottom panel).

Confidence limits and median values are determined from the CDF of accepted optimization results (i.e. the varying color values in the above figures), with best fit value, 5% and 95% confidence indicated on Figure A.26 and Figure A.27.

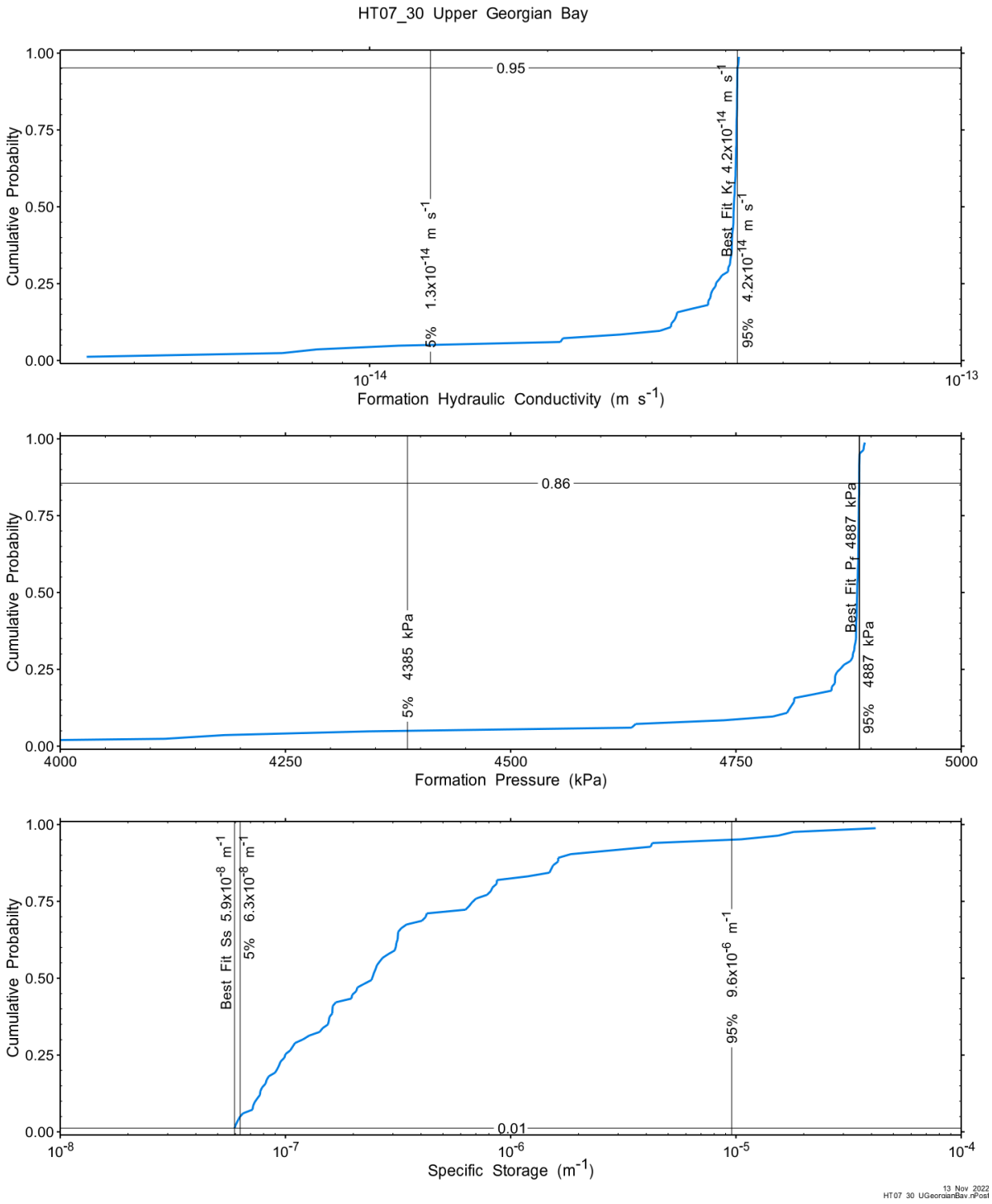

Figure A.185 – Cumulative distribution functions and parameter limits for formation hydraulic conductivity (K_f) (top panel), static formation pressure (P_f) (middle panel) and specific storage (Ss) (bottom panel).

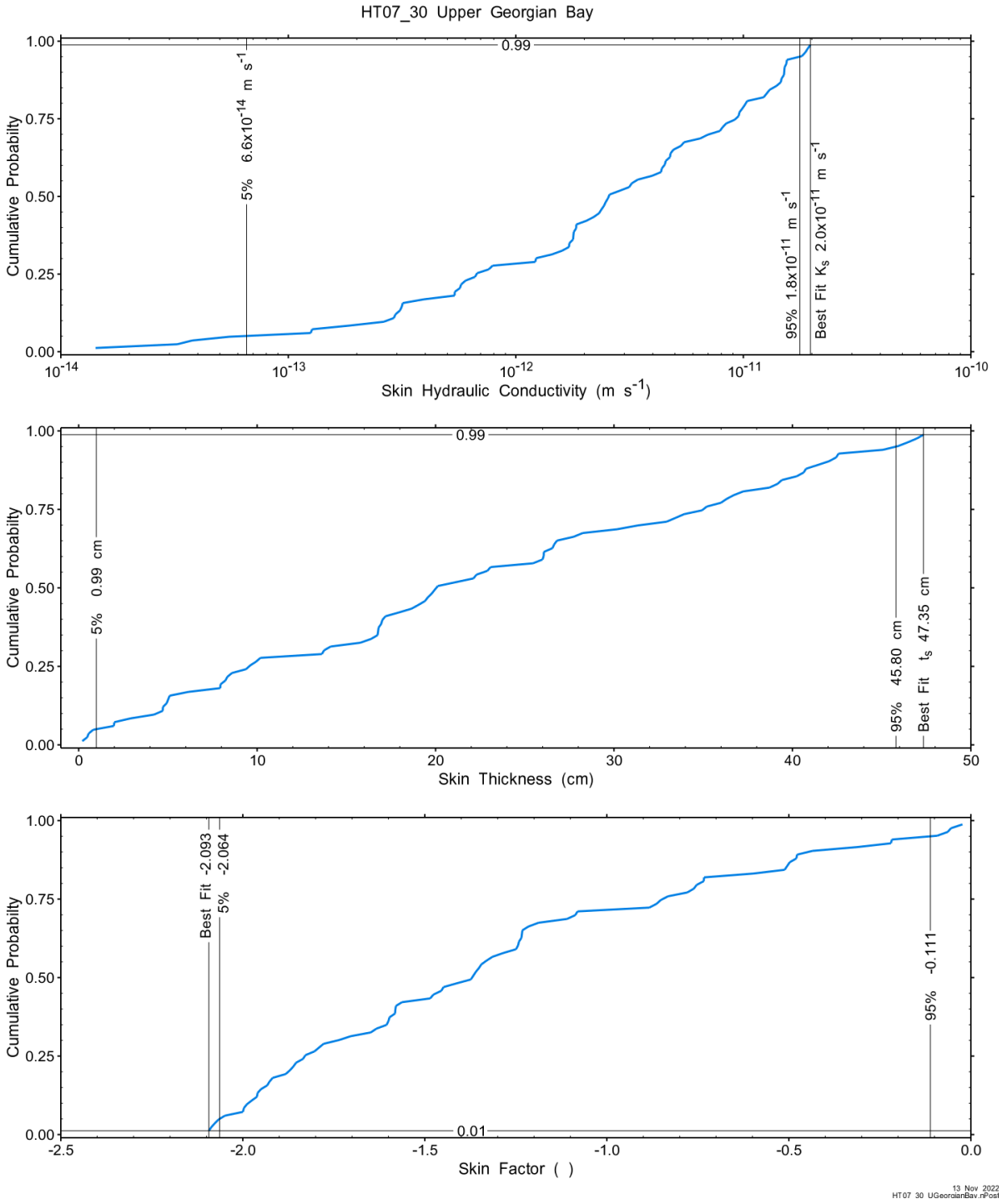

Figure A.186 – Cumulative distribution functions and parameter limits for skin hydraulic conductivity (K_s) (top panel), skin thickness (t_s) (middle panel) and skin factor (s) (bottom panel).

A summary of perturbation results is presented in Figure A.28, with Ramey-processed perturbations in Figure 12. Those perturbations (156 of 10,000) with all parameters within the 5% and 95% range present a very good fit to the measured test zone data.

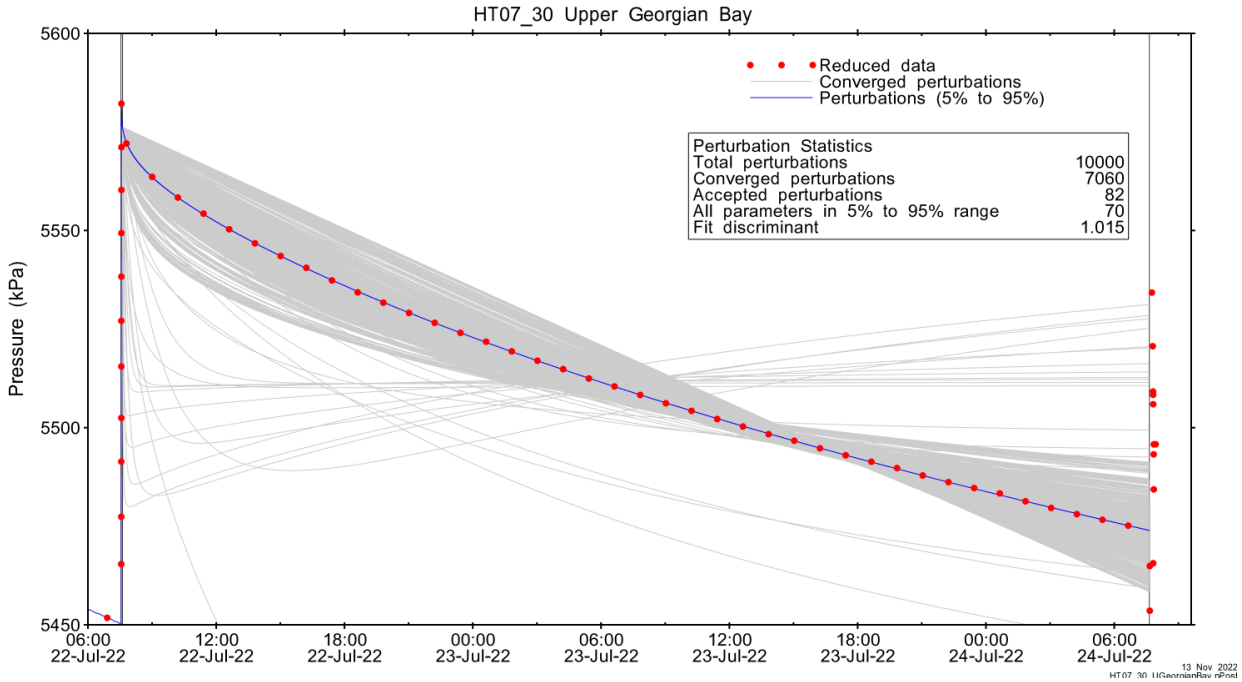

Figure A.187 – Perturbation results – all converged, accepted, and within 5% to 95% for all parameters.

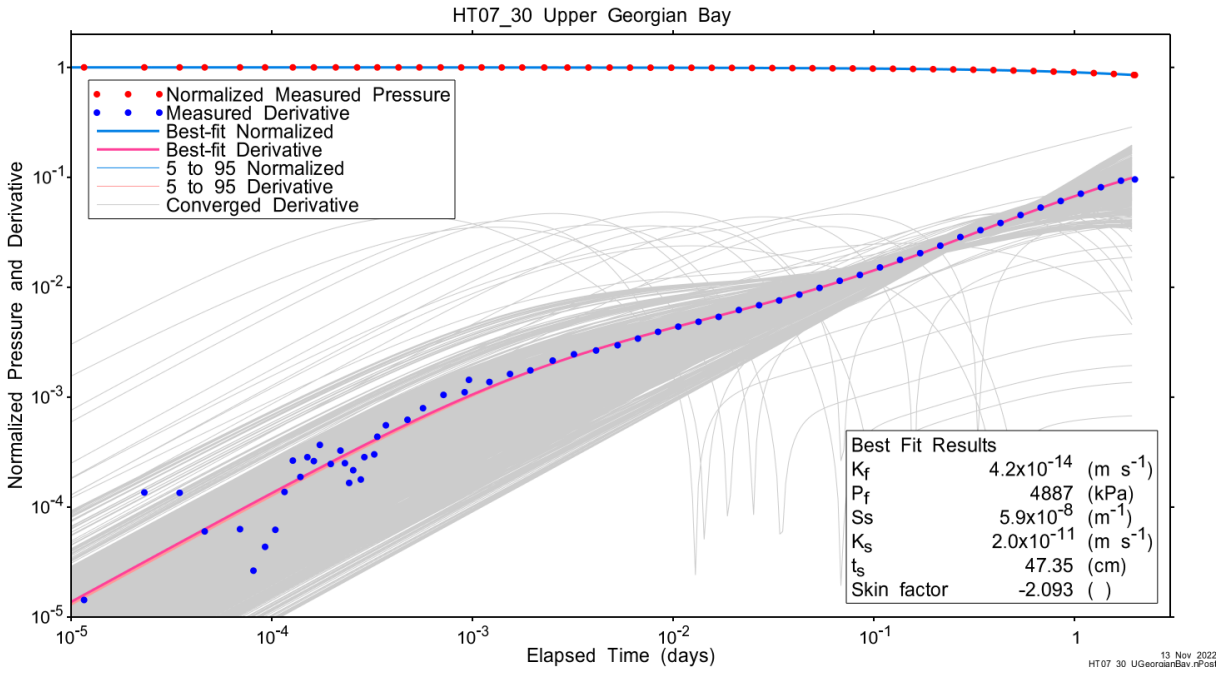

Figure A.188 – Log-log plot showing Ramey B and derivative response for all converged optimizations and those within 5% to 95% for all parameters.

A summary of best-fit and parameter ranges is given in Table A.9.

Table A.59 - Summary of the HT07_30 parameter estimates.

Parameter	Best Fit	5%	Median	95%
K_f (m/s)	4.2E-14	1.3E-14	4.1E-14	4.2E-14
P_f (kPa)	4887	4385	4885	4887
Ss (1/m)	5.9E-08	6.3E-08	2.4E-07	9.6E-06
K_s (m/s)	2.0E-11	6.6E-14	2.6E-12	1.8E-11
t_s (cm)	47.35	0.99	20.04	45.80
s (-)	-2.093	-2.064	-1.370	-0.111

Parameter correlations for all perturbations with all parameters within the 5% to 95% limits are given in Table A.5.

Table A.60 – Pearson cross-correlations of 5% to 95% parameters

	Log(K_f)	P_f	Log(Ss)	Log(K_s)	t_s	s
Log(K_f)	1.000	0.980	-0.803	0.781	0.507	-0.683
Pf	0.980	1.000	-0.715	0.745	0.415	-0.588
Log(S_s)	-0.803	-0.715	1.000	-0.895	-0.903	0.982
Log(K_s)	0.781	0.745	-0.895	1.000	0.780	-0.883
t_s	0.507	0.415	-0.903	0.780	1.000	-0.954
s	-0.683	-0.588	0.982	-0.883	-0.954	1.000

A.12.4 Additional Figures

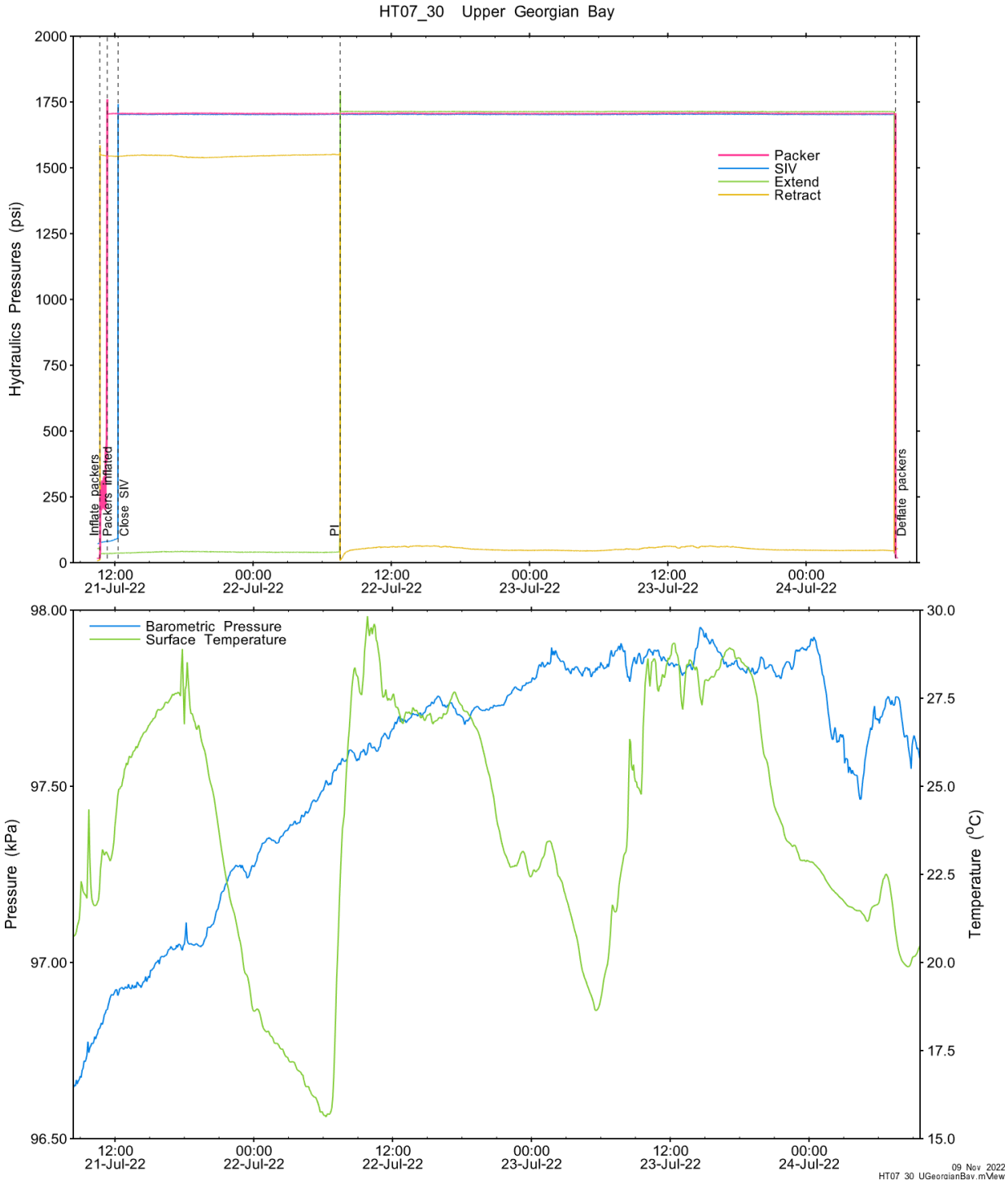

Figure A.189 - Hydraulics pressures and surface temperature/barometric pressure.

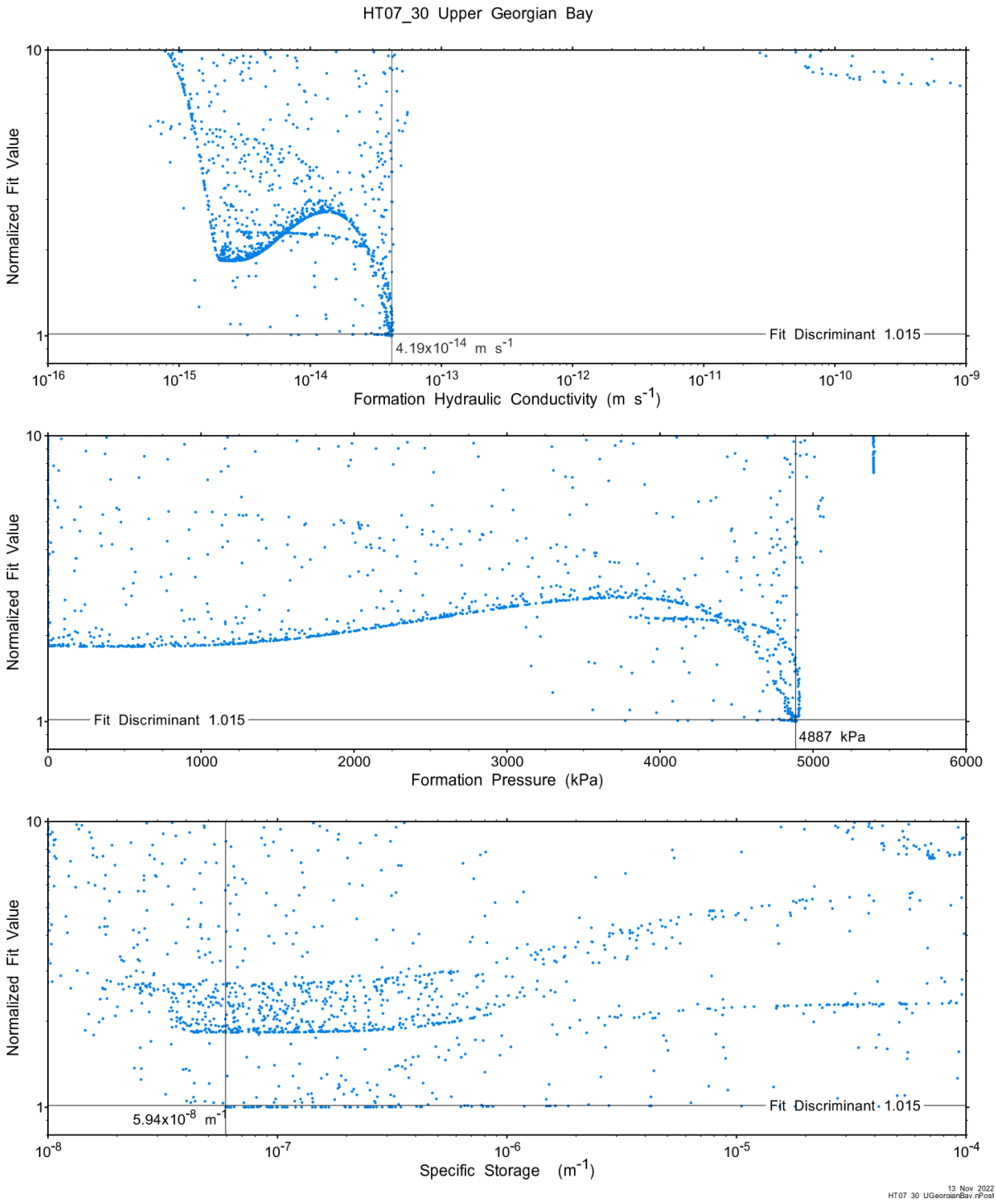

Figure A.190 - XY-scatter plot showing the formation parameter space normalized fit values.

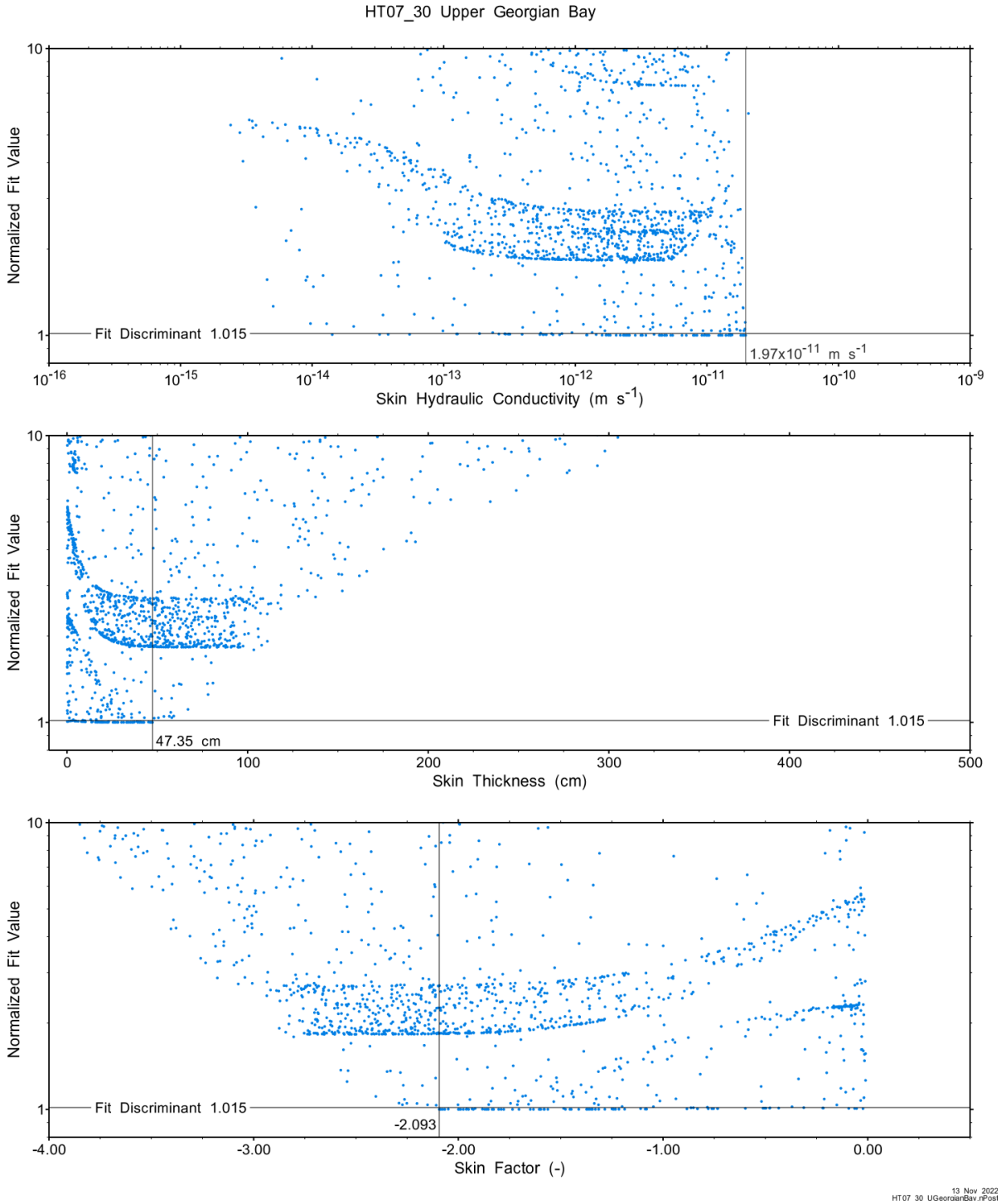

Figure A.191 - XY-scatter plot showing the skin parameter space normalized fit values.

A.13 HT08_30 Lower Georgian Bay

The SB BH02 interval from 580.00 to 609.96 mBGS tested in HT08_30 is located in the middle of the lower half of the Georgian Bay Formation. A single PI test of two days duration was conducted.

A.13.1 Test Data Summary

Table A.6 and Figure A.1 provide a summary of test events and a plot of pressures measured while testing respectively.

Table A.61 - Summary of Test Events.

Event	Start Date & Time	Duration (days)	TZ Pressure (kPa)
Drilling intercept	22-03-09 02:28	137.35	6053
Shut-in	22-07-24 10:48	0.90	6057
Pulse injection	22-07-25 08:23	2.01	5989
Test end	22-07-27 08:33		5758

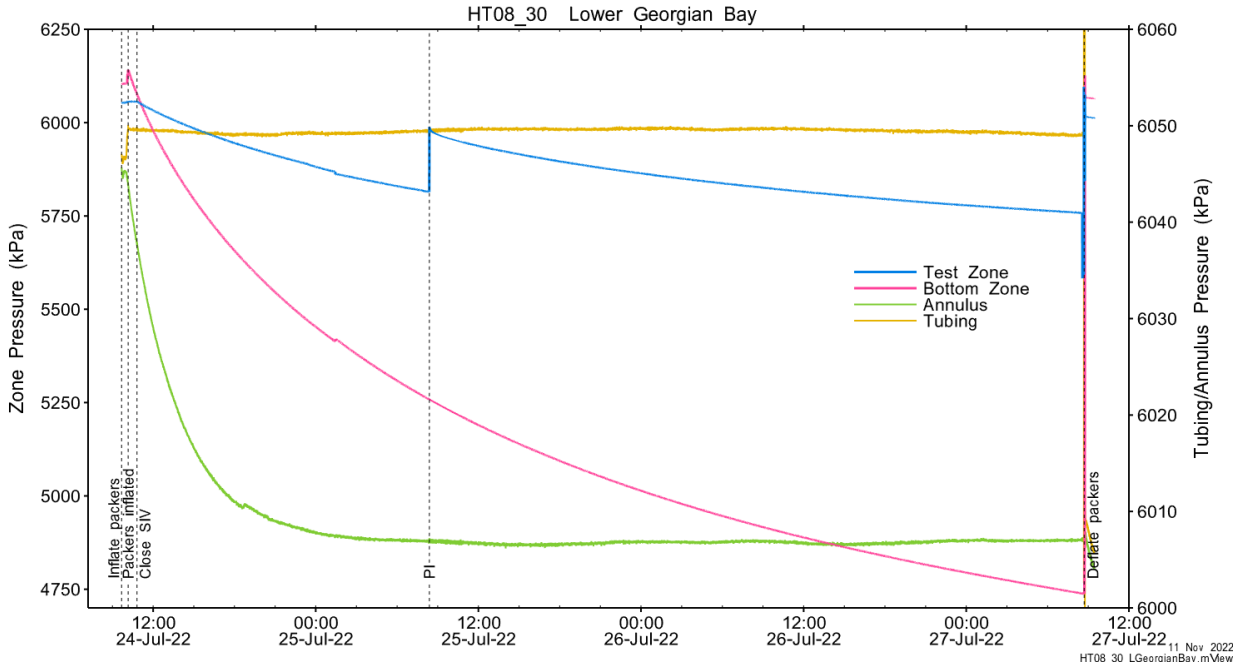

Figure A.192 - Test events and pressures.

A.13.2 Test Analyses

Table A.7 is a summary of test-specific input parameters used in the analyses, while Table A.8 presents the optimized parameters and allowed ranges.

Table A.62 – nSIGHTS Input Parameters.

Parameter	Value	Units
Test zone radius	6.47	cm
Test zone compressibility	1.50E-09	1/Pa
Test zone length	29.96	m

Table A.63 – nSIGHTS Parameter Optimization Ranges.

Parameter	Minimum	Maximum	Units	Type
Formation hydraulic conductivity (K_f)	1E-15	1E-07	m/s	log
Formation pressure (P_f)	2000	7000	kPa	linear
Specific storage (S_s)	1E-08	1E-04	1/m	log
Skin hydraulic conductivity (K_s)	1E-15	1E-07	m/s	log
Skin thickness (t_s)	0.013	500	cm	linear

Figure A.18 shows the measured test zone pressure record (with reduced data density for clarity) used in the analysis along with the best-fit simulation and parameter values. Figure A.19 presents the pre-test history, and Figure A.20 shows the Ramey B normalized best-fit pressure and pressure derivatives.

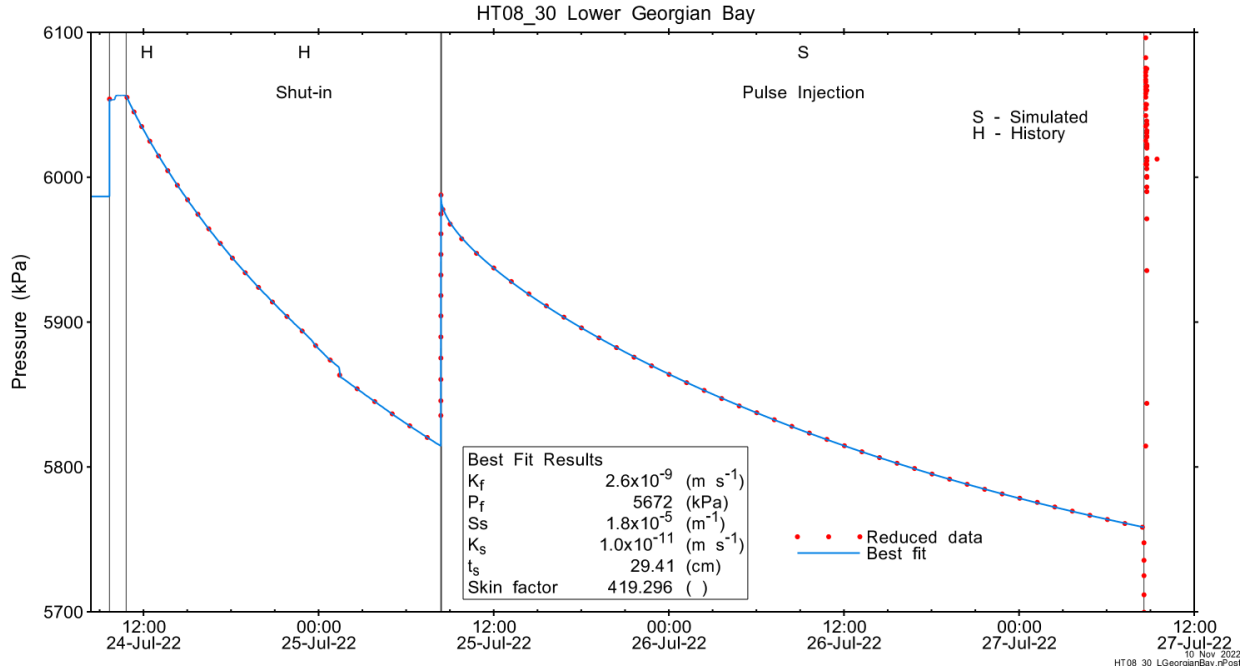

Figure A.193 - Annotated testing sequence showing best-fit simulation and parameter estimates.

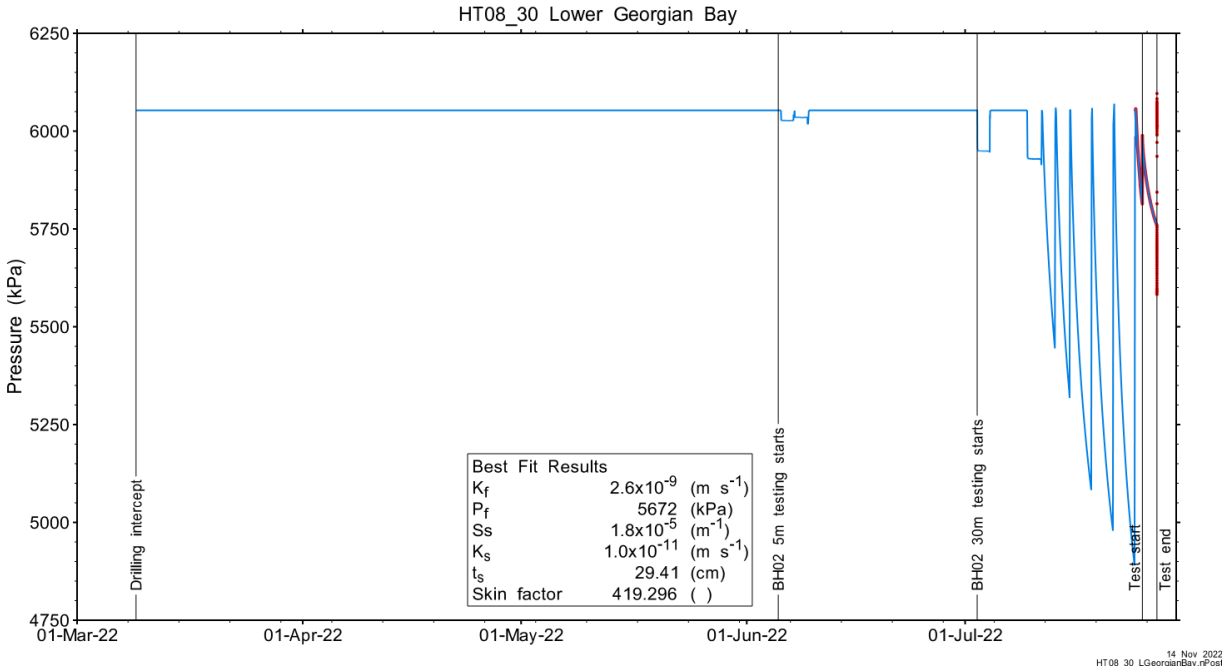

Figure A.194 - Annotated testing sequence showing pre-test history, best-fit simulation and parameter estimates.

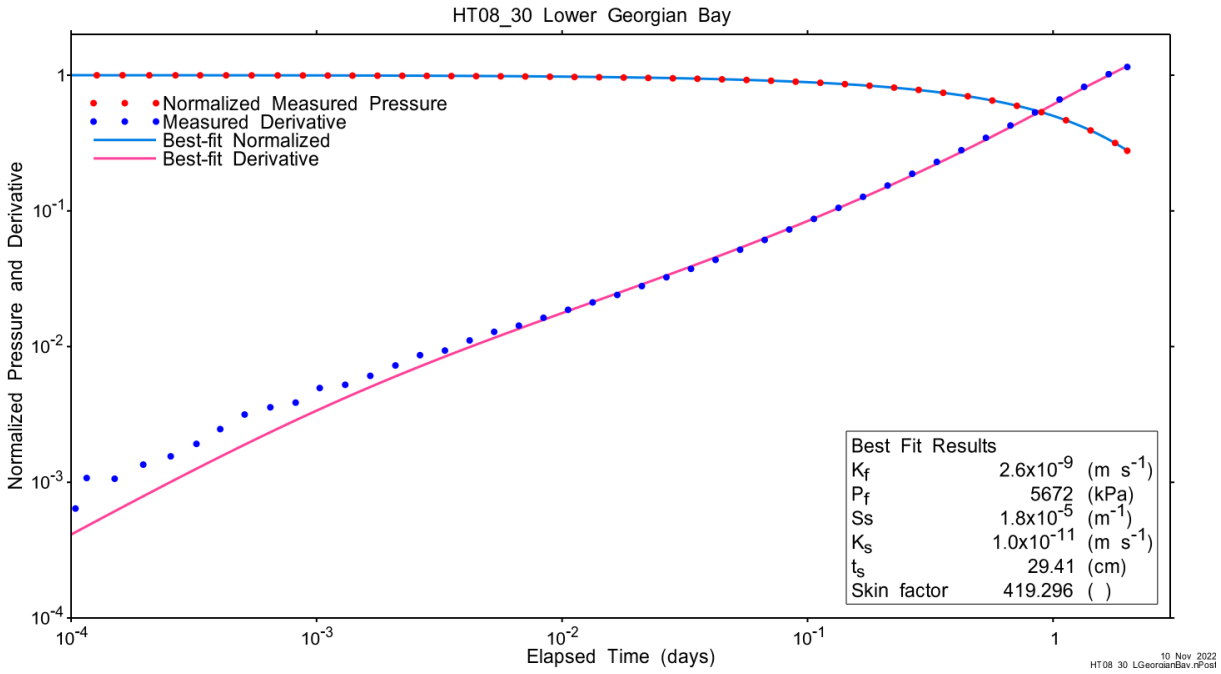

Figure A.195 - Log-log plot showing Ramey B and derivative response for best-fit simulation.

Figure A.21 shows the normalized parameter sensitivity response for the best fit. Sensitivity for most fitting parameters (except S_s and P_f) was relatively flat at the end of the test, indicating that test duration was adequate.

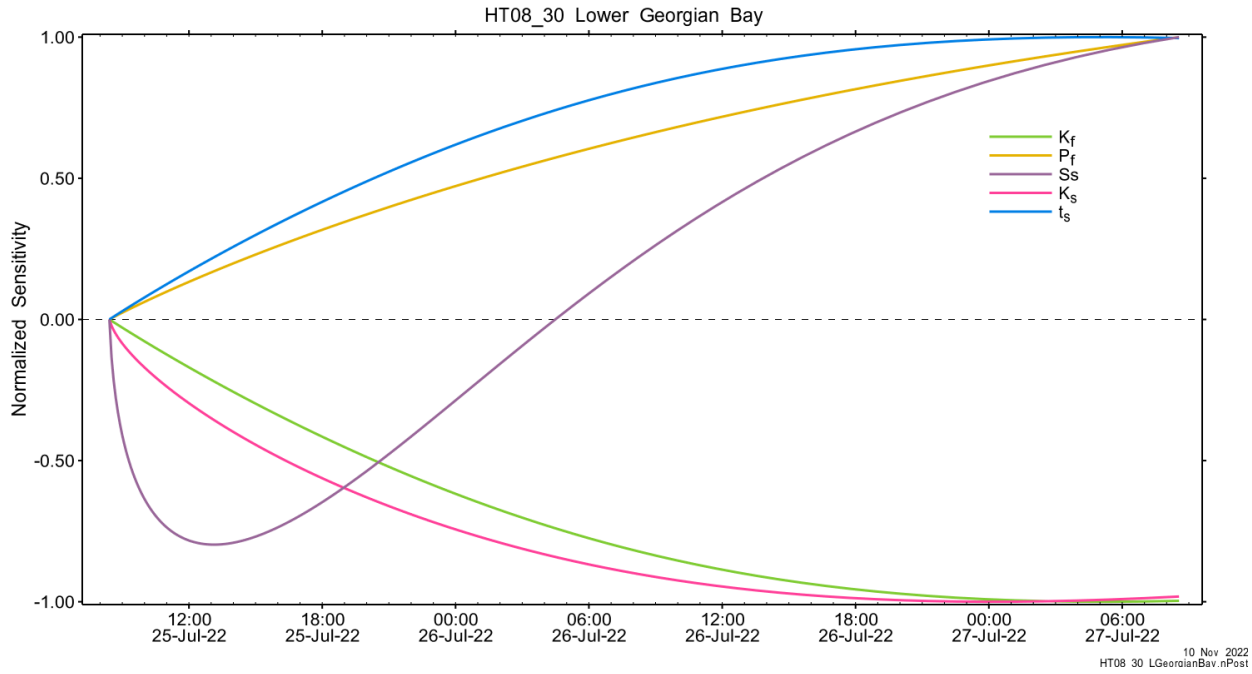

Figure A.196 - Normalized Jacobian for best-fit simulation.

A.13.3 Uncertainty Analyses

The CDF of normalized fit values for all converged simulations and the selected fit discriminant are shown in Figure A.22 and, in detail, in Figure A.198. The fit discriminant is set very low to avoid inclusion of a local minimum (see Appendix plots).

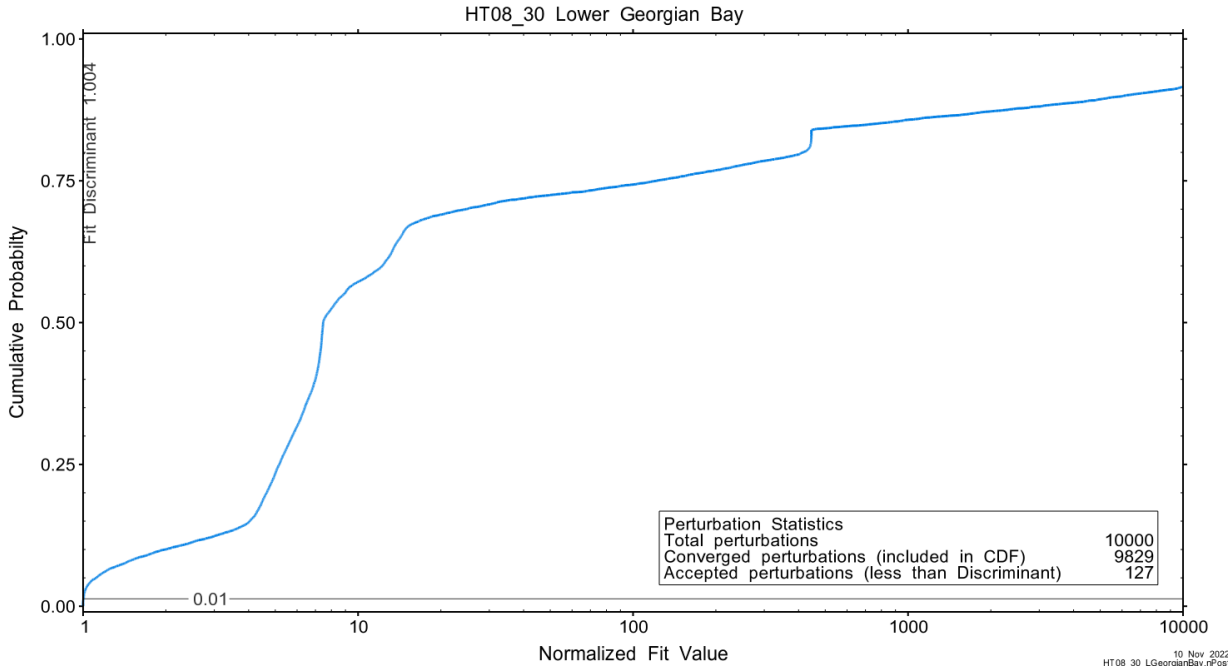

Figure A.197 - Fit value cumulative distribution function.

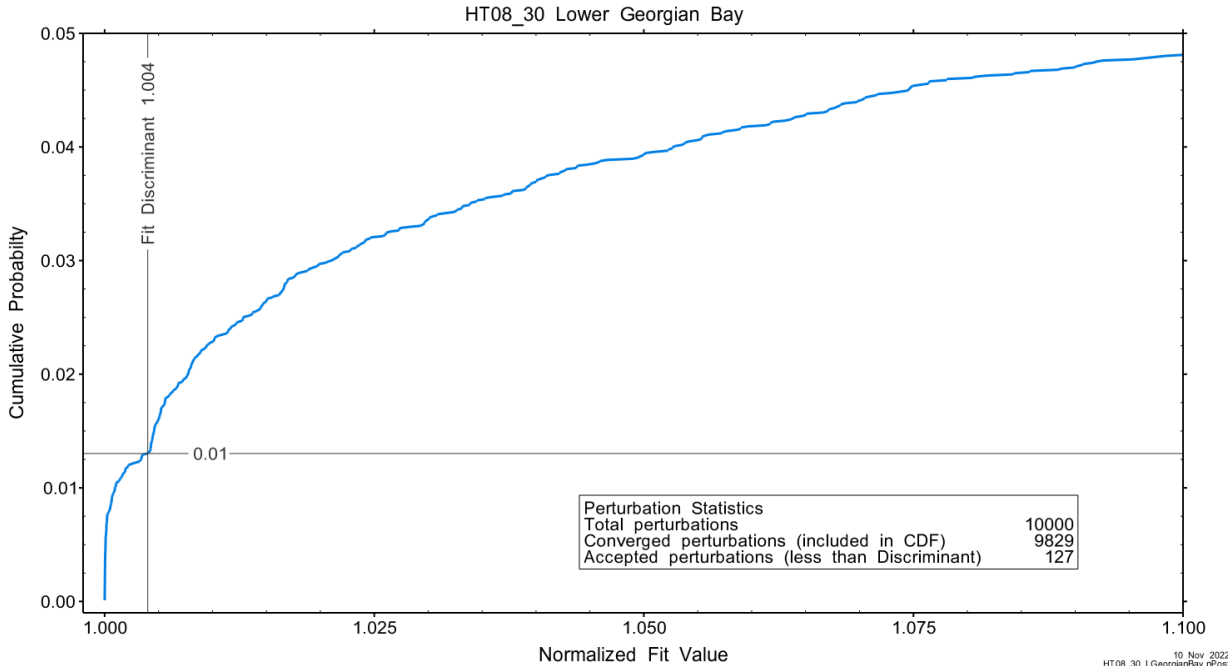

Figure A.198 – Detail fit value cumulative distribution function.

Summary cross parameter scatter plots for selected formation and skin parameters are given in Figure A.24 and Figure A.25. The light pink dots on the figures are the initial parameter estimates, with red dots overlaying those initial parameter values that resulted in accepted optimization results. The grey dots are converged optimizations which did not meet the fit discriminant. Larger varying color symbols represent the fit value of accepted optimizations, with the blue values representing the best fit.

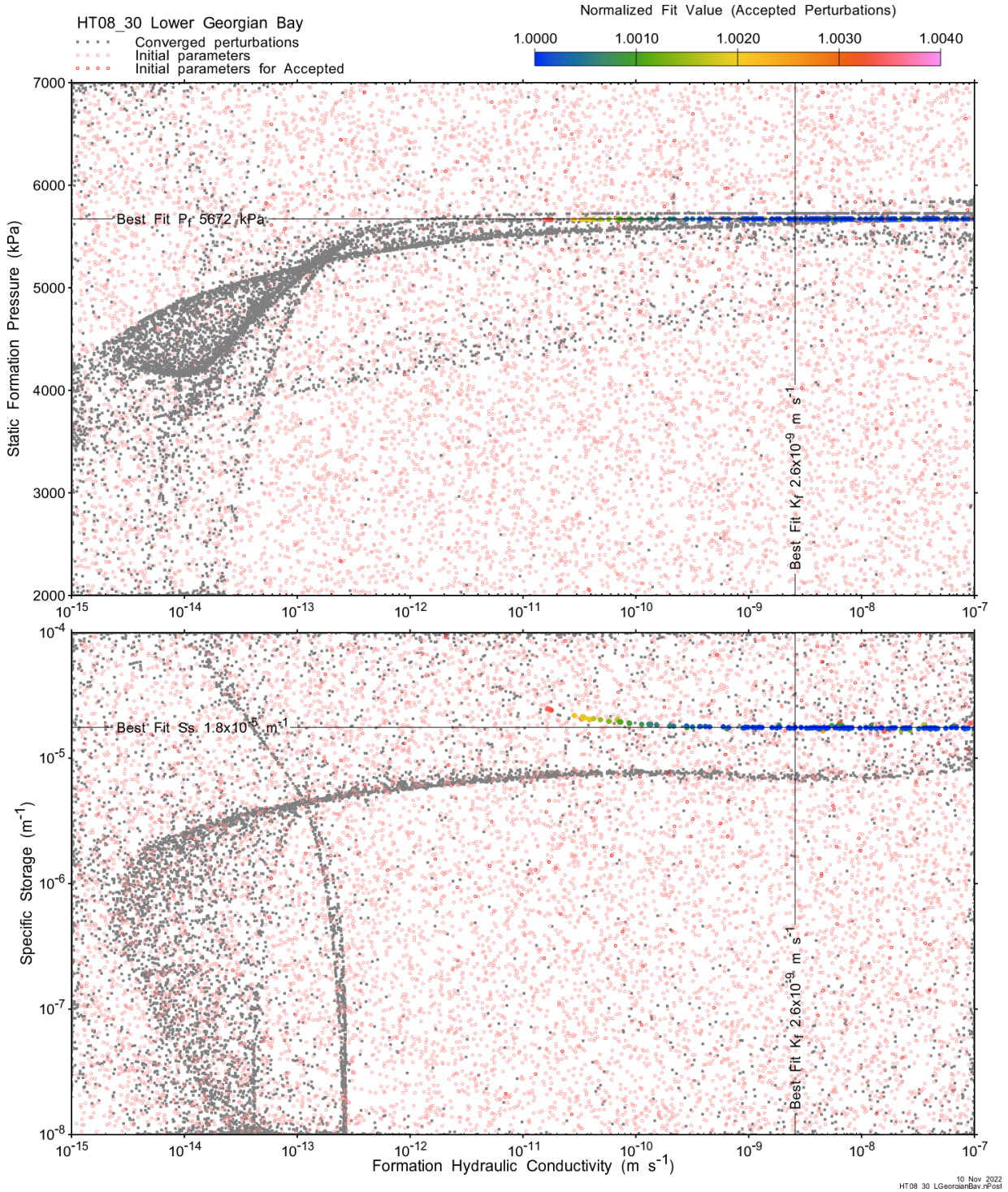

Figure A.199 - XY-scatter plot showing estimates of formation hydraulic conductivity (K_f) vs static formation pressure (P_f) (top panel) and specific storage (Ss) (bottom panel).

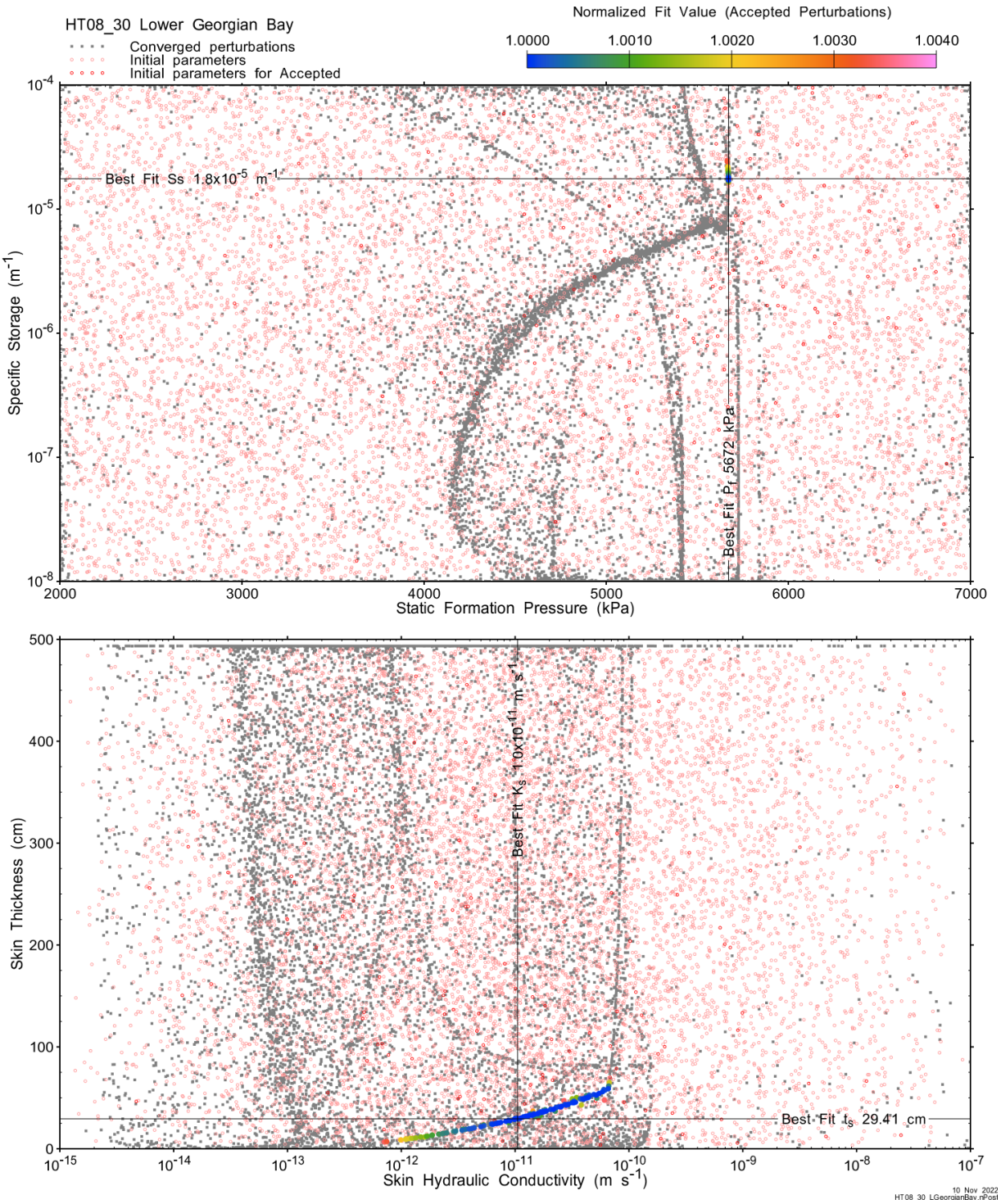

Figure A.200 - XY-scatter plot showing estimates of static formation pressure (P_f) vs specific storage (Ss) (top panel) and skin hydraulic conductivity (K_s) vs skin thickness (t_s) (bottom panel).

Confidence limits and median values are determined from the CDF of accepted optimization results (i.e. the varying color values in the above figures), with best fit value, 5% and 95% confidence indicated on Figure A.26 and Figure A.27.

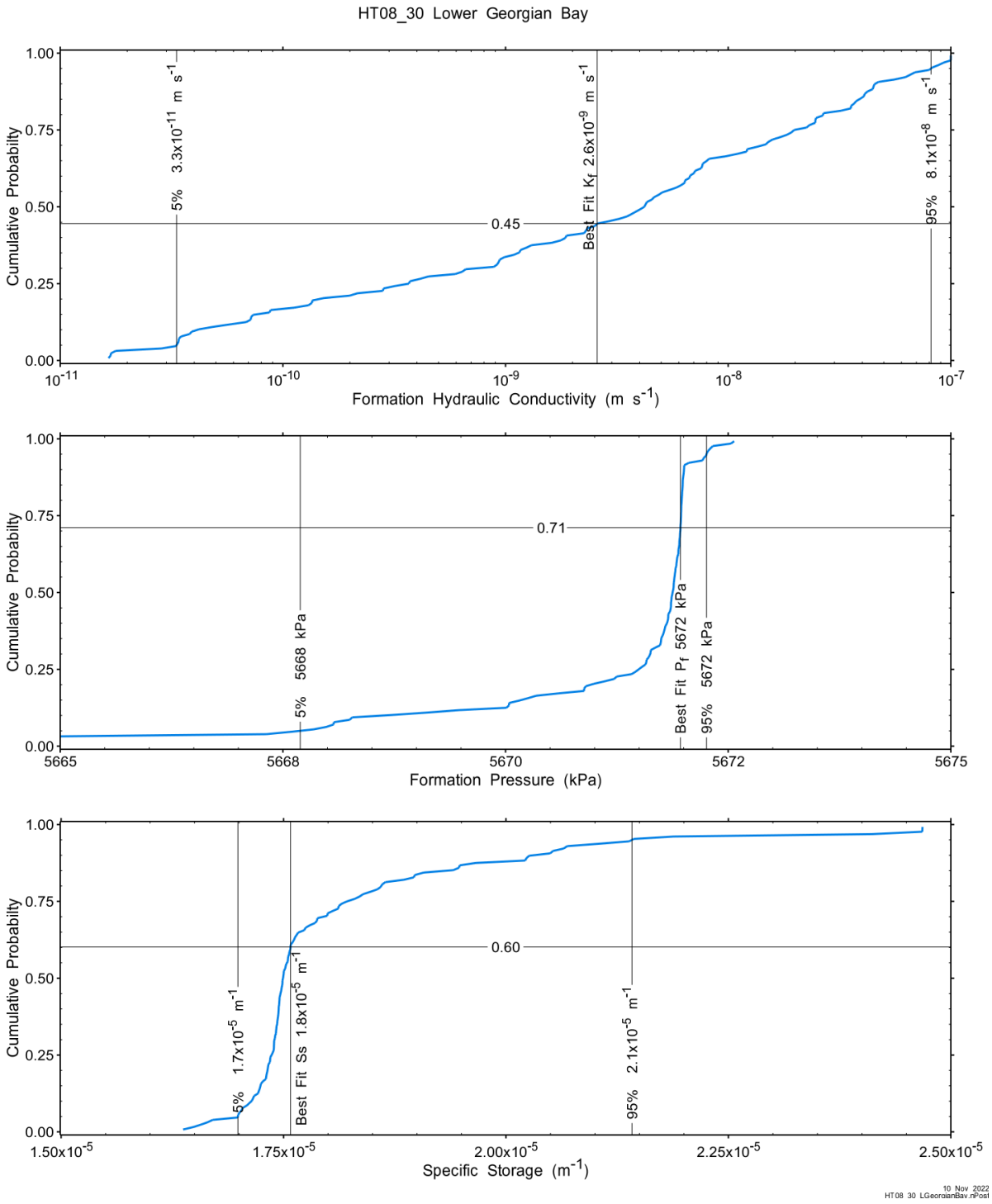

Figure A.201 – Cumulative distribution functions and parameter limits for formation hydraulic conductivity (K_f) (top panel), static formation pressure (P_f) (middle panel) and specific storage (Ss) (bottom panel).

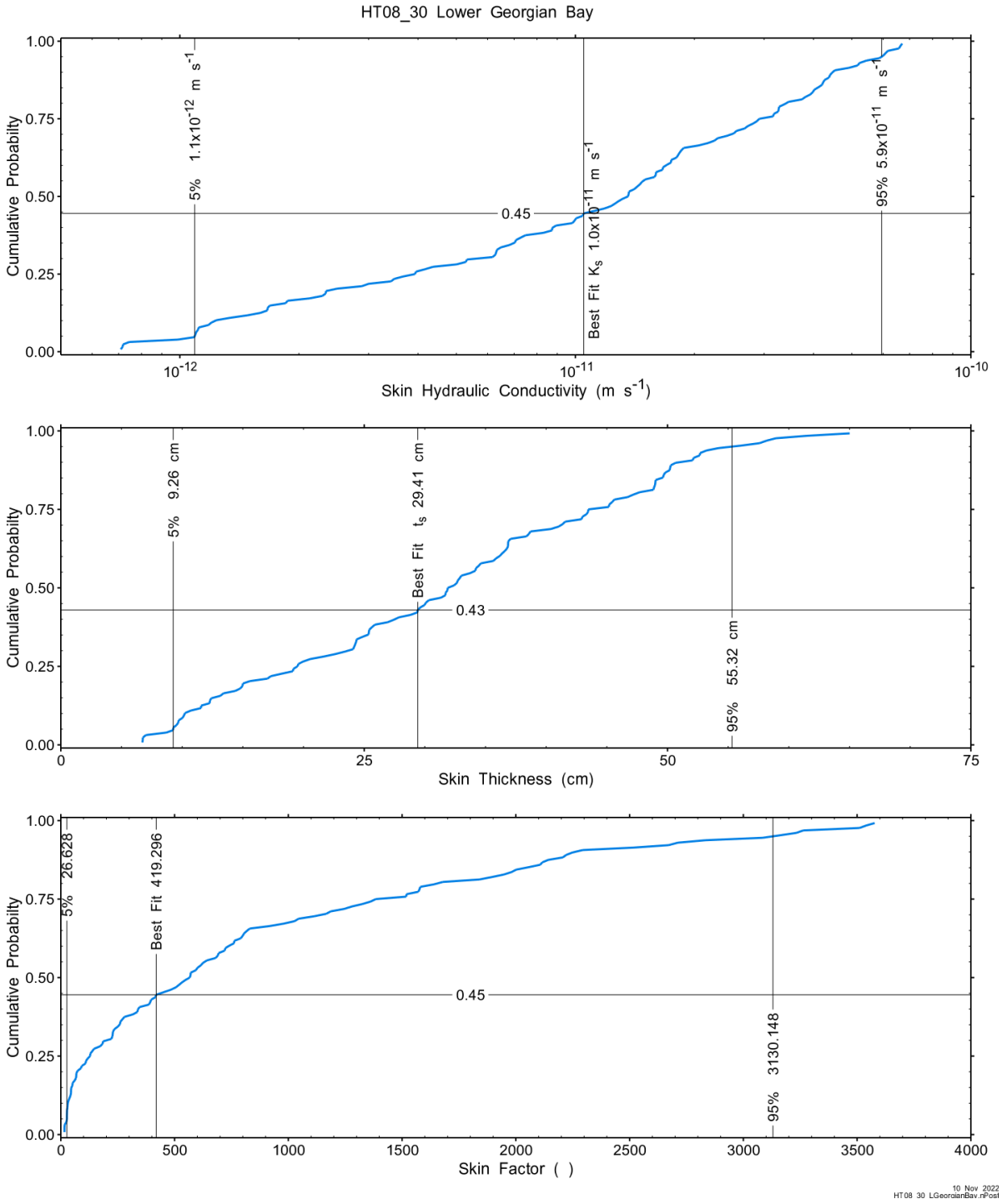

Figure A.202 – Cumulative distribution functions and parameter limits for skin hydraulic conductivity (K_s) (top panel), skin thickness (t_s) (middle panel) and skin factor (s) (bottom panel).

A summary of perturbation results is presented in Figure A.28, with Ramey-processed perturbations in Figure A.204. Those perturbations (103 of 10,000) with all parameters within the 5% and 95% range present a very good fit to the measured test zone data.

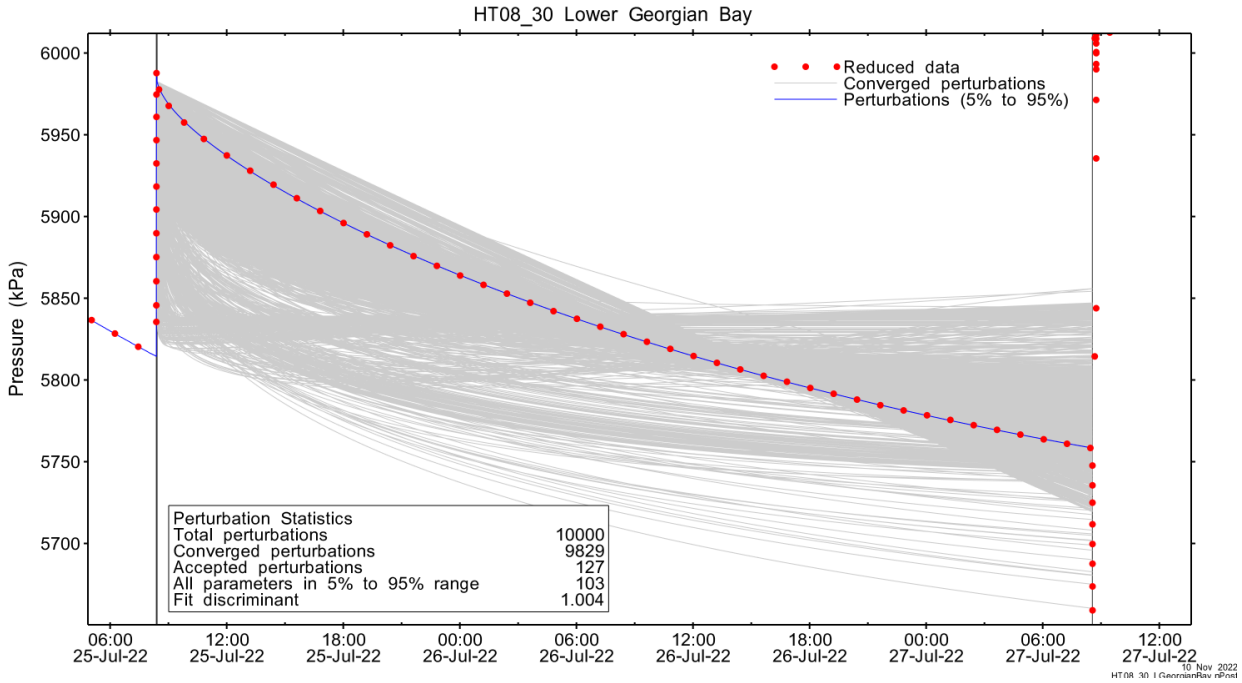

Figure A.203 – Perturbation results – all converged, accepted, and within 5% to 95% for all parameters.

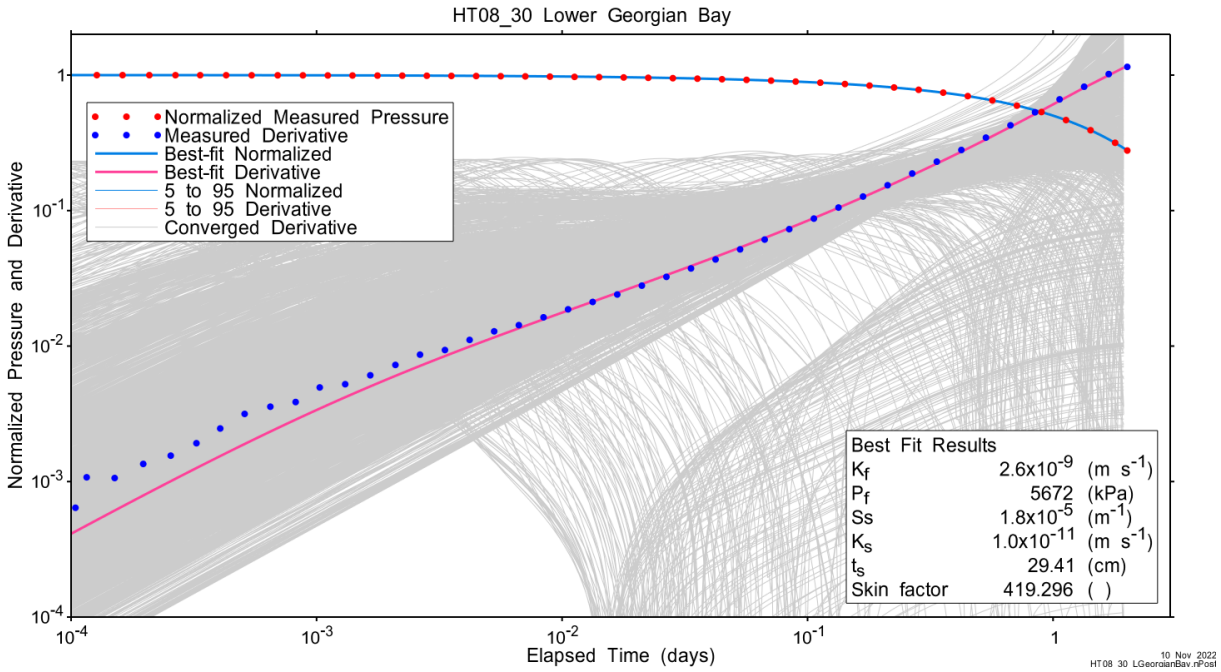

Figure A.204 – Log-log plot showing Ramey B and derivative response for all converged optimizations and those within 5% to 95% for all parameters.

A summary of best-fit and parameter ranges is given in Table A.9.

Table A.64 - Summary of the HT08_30 parameter estimates.

Parameter	Best Fit	5%	Median	95%
K_f (m/s)	2.6E-09	3.3E-11	4.2E-09	8.1E-08
P_f (kPa)	5672	5668	5672	5672
Ss (1/m)	1.8E-05	1.7E-05	1.7E-05	2.1E-05
K_s (m/s)	1.0E-11	1.1E-12	1.4E-11	5.9E-11
t_s (cm)	29.41	9.26	31.88	55.32
s (-)	419.296	26.628	566.389	3130.148

Parameter correlations for all perturbations with all parameters within the 5% to 95% limits are given in Table A.5.

Table A.65 – Pearson cross-correlations of 5% to 95% parameters

	Log(K_f)	P_f	Log(Ss)	Log(K_s)	t_s	s
Log(K_f)	1.000	0.771	-0.788	1.000	0.989	0.875
Pf	0.771	1.000	-0.936	0.778	0.691	0.456
Log(S_s)	-0.788	-0.936	1.000	-0.796	-0.730	-0.492
Log(K_s)	1.000	0.778	-0.796	1.000	0.988	0.871
t_s	0.989	0.691	-0.730	0.988	1.000	0.931
s	0.875	0.456	-0.492	0.871	0.931	1.000

A.13.4 Additional Figures

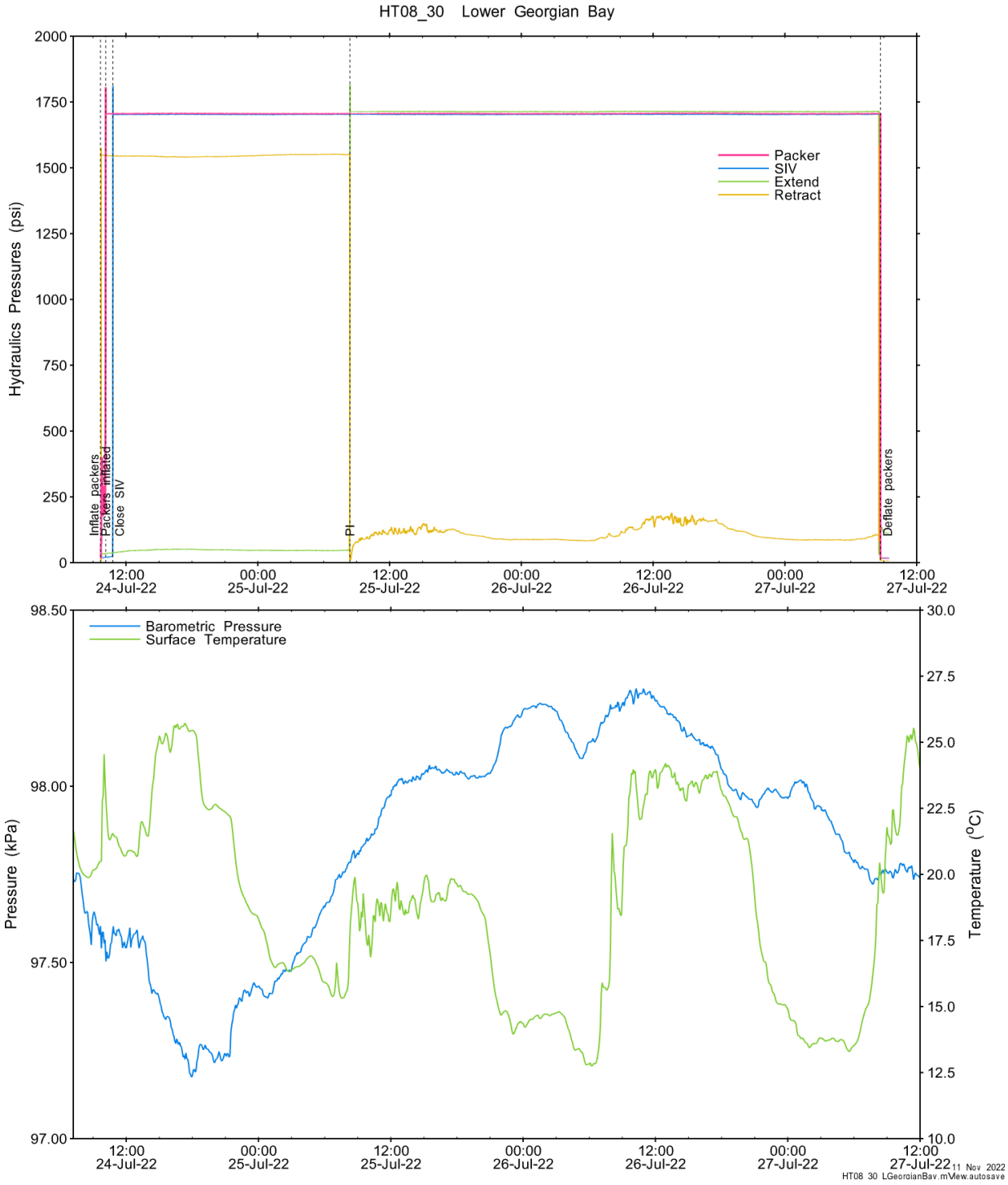

Figure A.205 - Hydraulics pressures and surface temperature/barometric pressure.

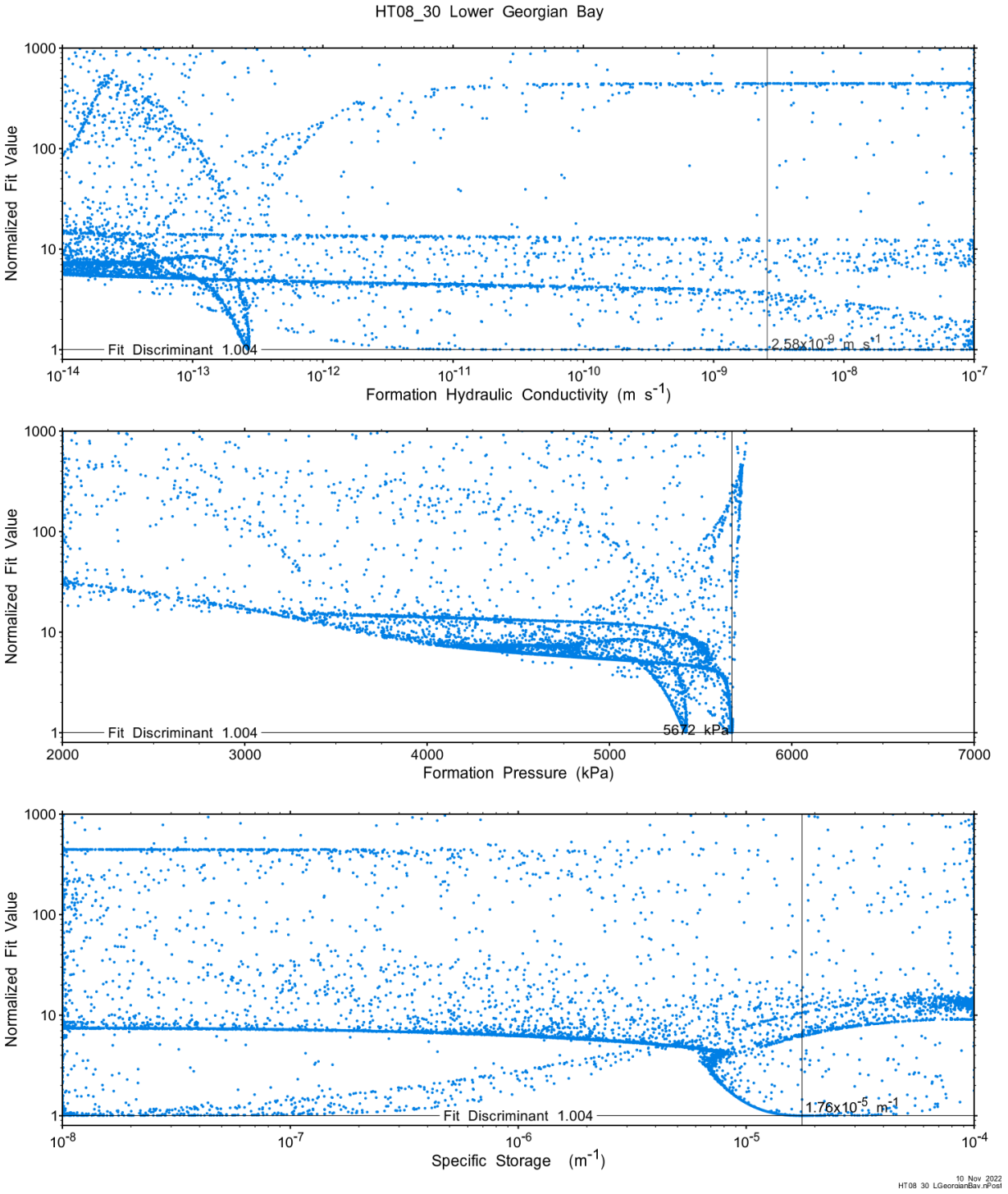

Figure A.206 - XY-scatter plot showing the formation parameter space normalized fit values.

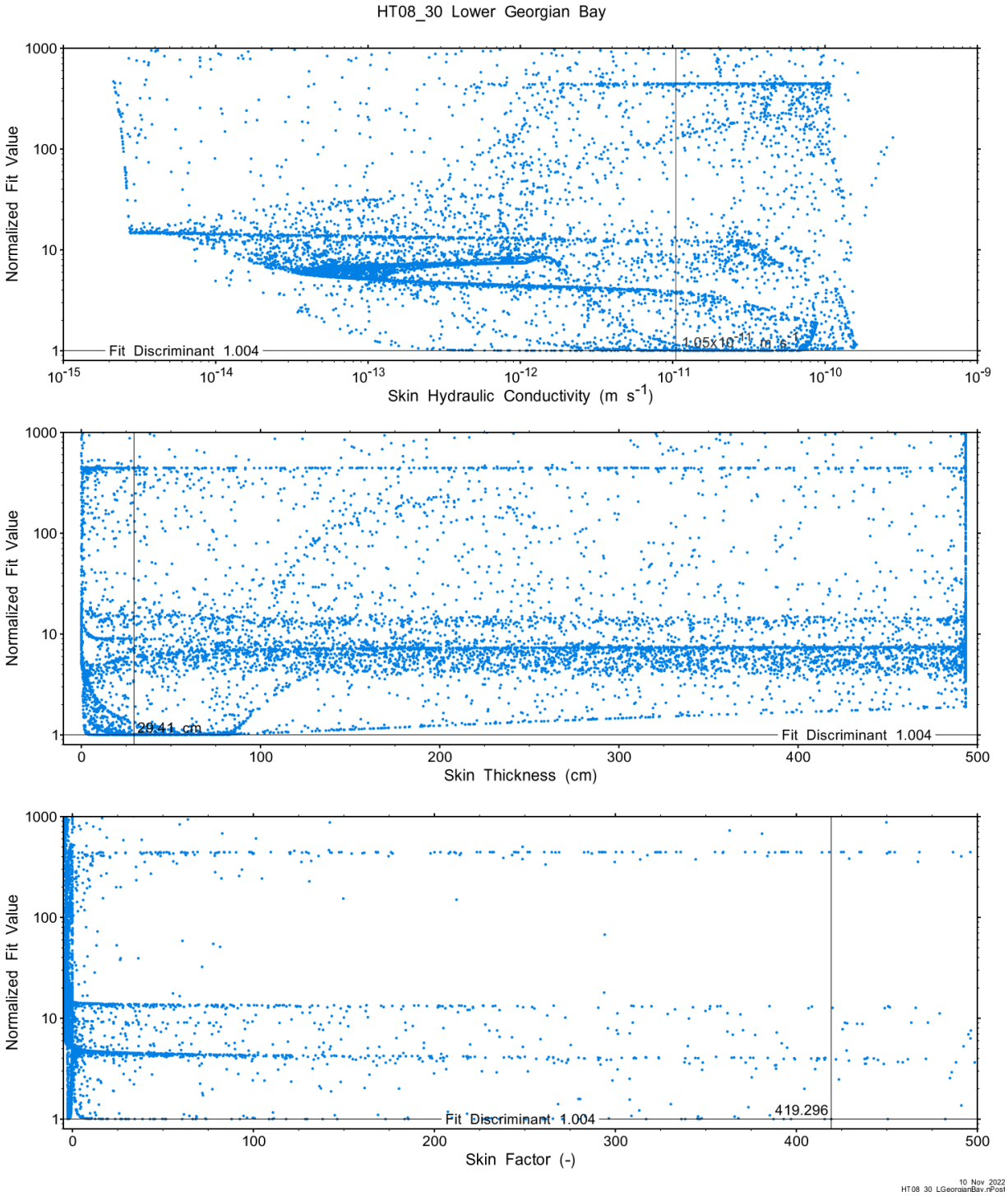

Figure A.207 - XY-scatter plot showing the skin parameter space normalized fit values.

A.14 HT09_30 Blue Mountain

The SB BH02 interval from 630.00 to 659.96 mBGS tested in HT09_30 covers the majority of the Blue Mountain Formation. A single PI test of two days duration was conducted.

A.14.1 Test Data Summary

Table A.6 and Figure A.1 provide a summary of test events and a plot of pressures measured while testing respectively.

Table A.66 - Summary of Test Events.

Event	Start Date & Time	Duration (days)	TZ Pressure (kPa)
Drilling intercept	22-03-11 10:47	143.21	6639
Shut-in	22-08-01 15:44	0.70	6705
Pulse injection	22-08-02 08:33	2.00	6840
Test end	22-08-04 08:32		6628

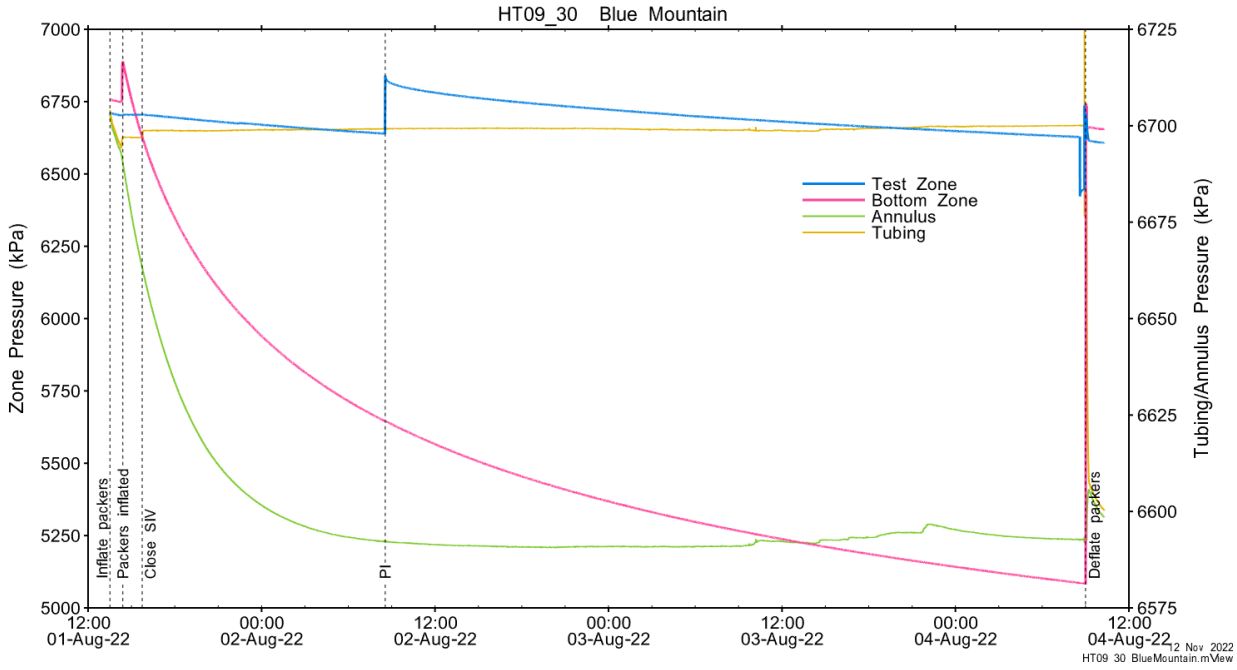

Figure A.208 - Test events and pressures.

A.14.2 Test Analyses

Table A.7 is a summary of test-specific input parameters used in the analyses, while Table A.8 presents the optimized parameters and allowed ranges. The specific storage parameter range was increased based on initial perturbation results.

Table A.67 – nSIGHTS Input Parameters.

Parameter	Value	Units
Test zone radius	6.49	cm
Test zone compressibility	1.30E-09	1/Pa
Test zone length	29.96	m

Table A.68 – nSIGHTS Parameter Optimization Ranges.

Parameter	Minimum	Maximum	Units	Type
Formation hydraulic conductivity (K_f)	1E-16	1E-08	m/s	log
Formation pressure (P_f)	2000	7000	kPa	linear
Specific storage (S_s)	1E-08	1E-03	1/m	log
Skin hydraulic conductivity (K_s)	1E-16	1E-08	m/s	log
Skin thickness (t_s)	0.013	500	cm	linear

Figure A.18 shows the measured test zone pressure record (with reduced data density for clarity) used in the analysis along with the best-fit simulation and parameter values. Figure A.19 presents the pre-test history, and Figure A.20 shows the Ramey B normalized best-fit pressure and pressure derivatives.

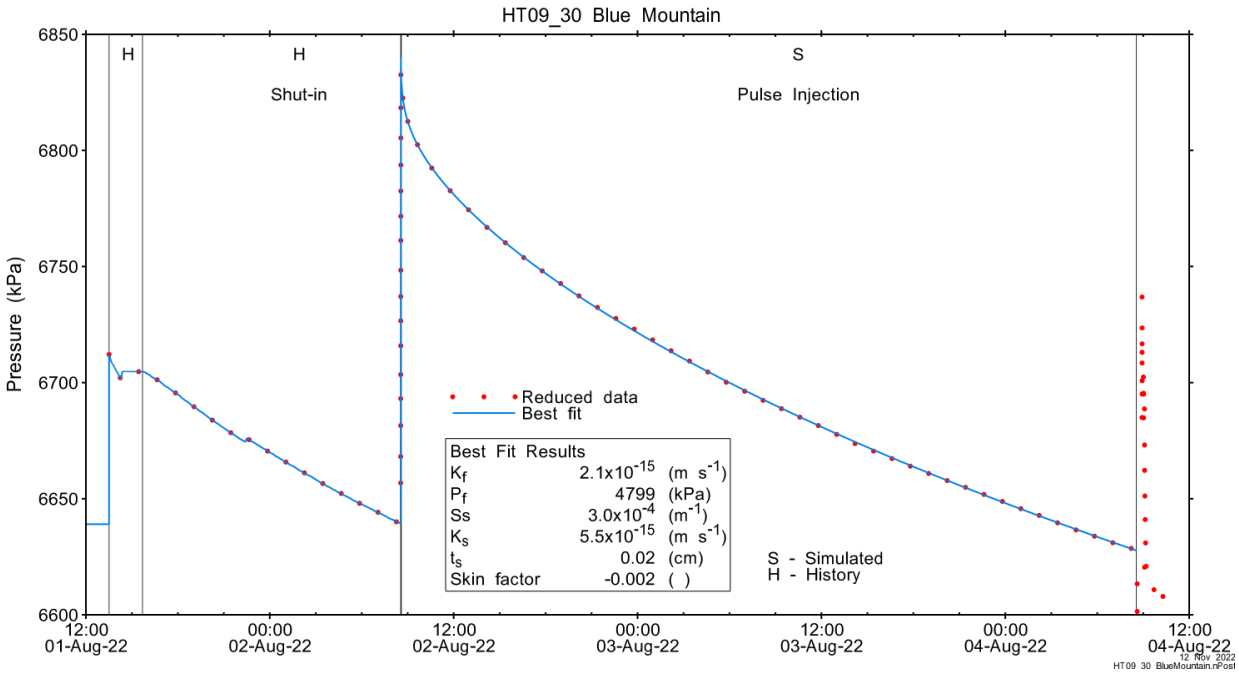

Figure A.209 - Annotated testing sequence showing best-fit simulation and parameter estimates.

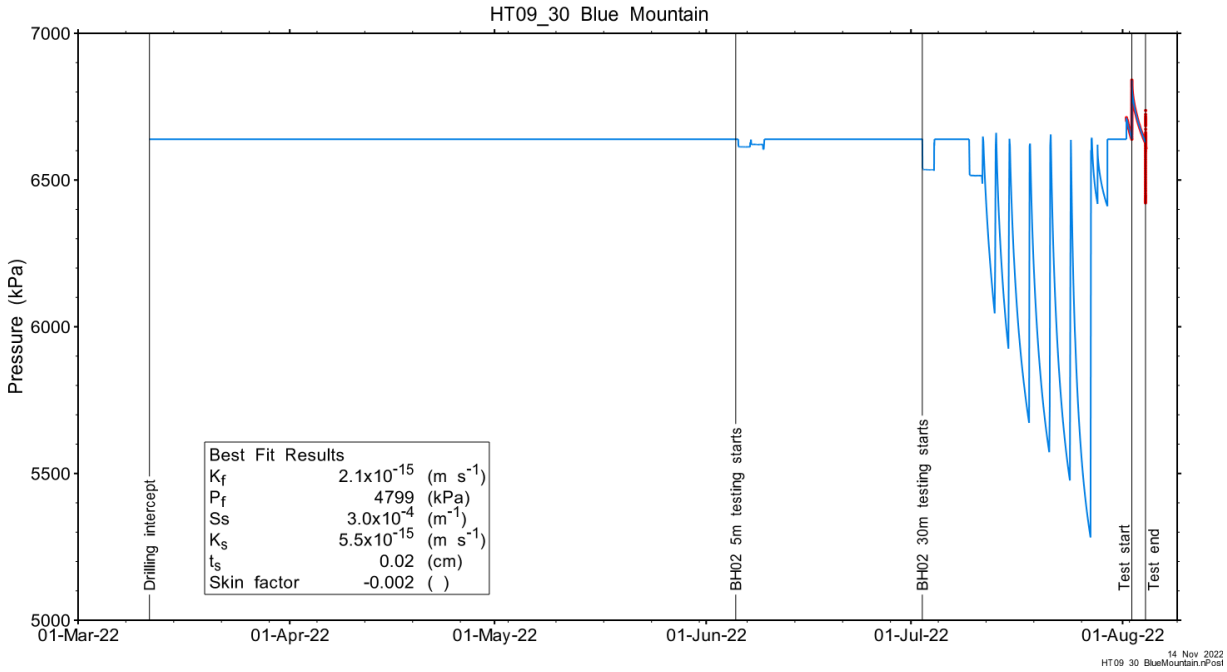

Figure A.210 - Annotated testing sequence showing pre-test history, best-fit simulation and parameter estimates.

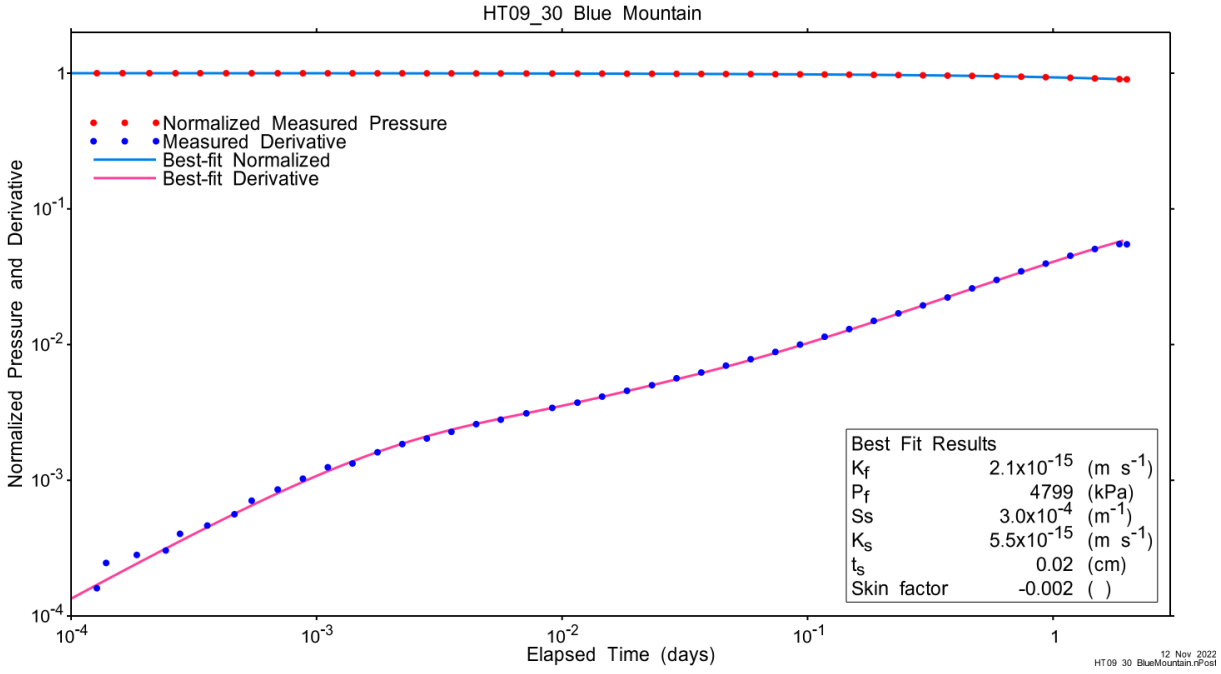

Figure A.211 - Log-log plot showing Ramey B and derivative response for best-fit simulation.

Figure A.21 shows the normalized parameter sensitivity response for the best fit. Sensitivity for most fitting parameters was increasing at the end of the test, indicating that lengthening the test may have improved the precision of the analysis.

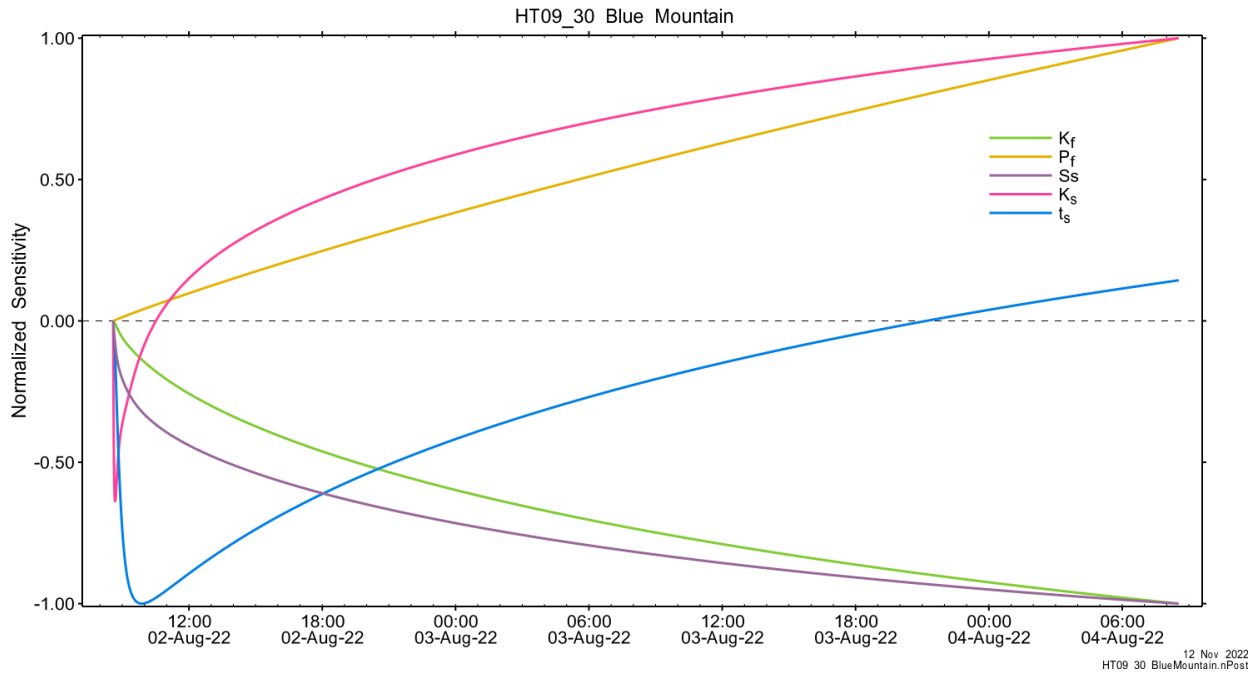

Figure A.212 - Normalized Jacobian for best-fit simulation.

A.14.3 Uncertainty Analyses

The CDF of normalized fit values for all converged simulations and the selected fit discriminant are shown in Figure A.22.

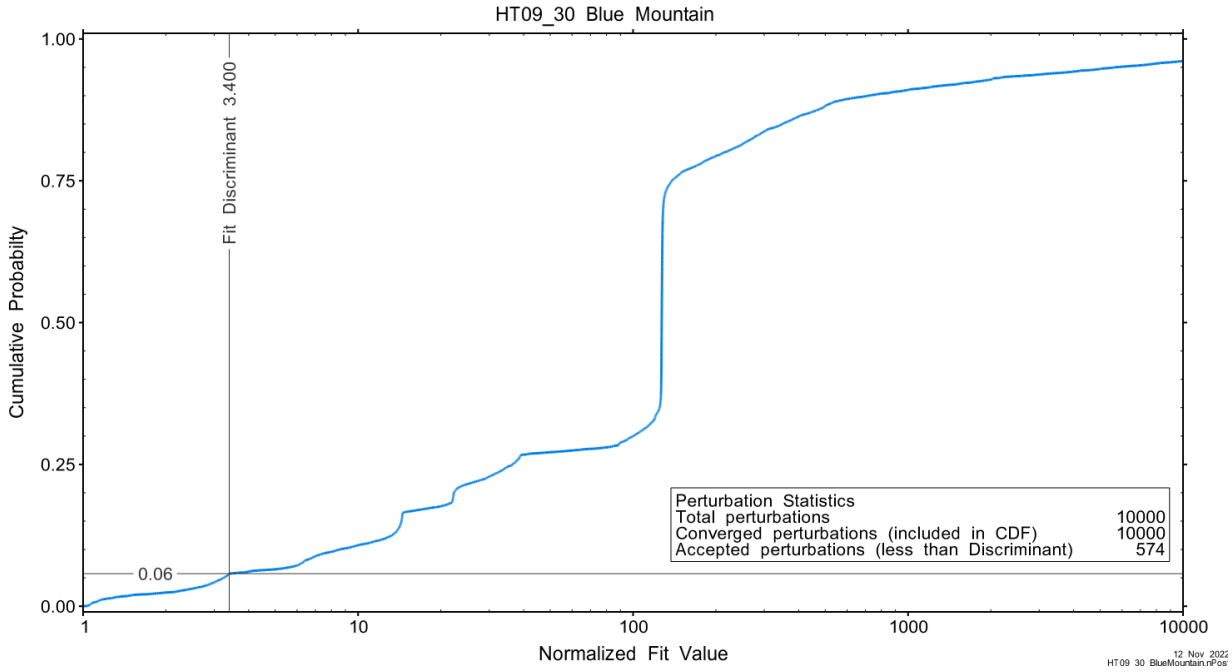

Figure A.213 - Fit value cumulative distribution function.

Summary cross parameter scatter plots for selected formation and skin parameters are given in Figure A.24 and Figure A.25. The light pink dots on the figures are the initial parameter estimates, with red dots overlaying those initial parameter values that resulted in accepted optimization results. The grey dots are converged optimizations which did not meet the fit discriminant. Larger varying color symbols represent the fit value of accepted optimizations, with the blue values representing the best fit.

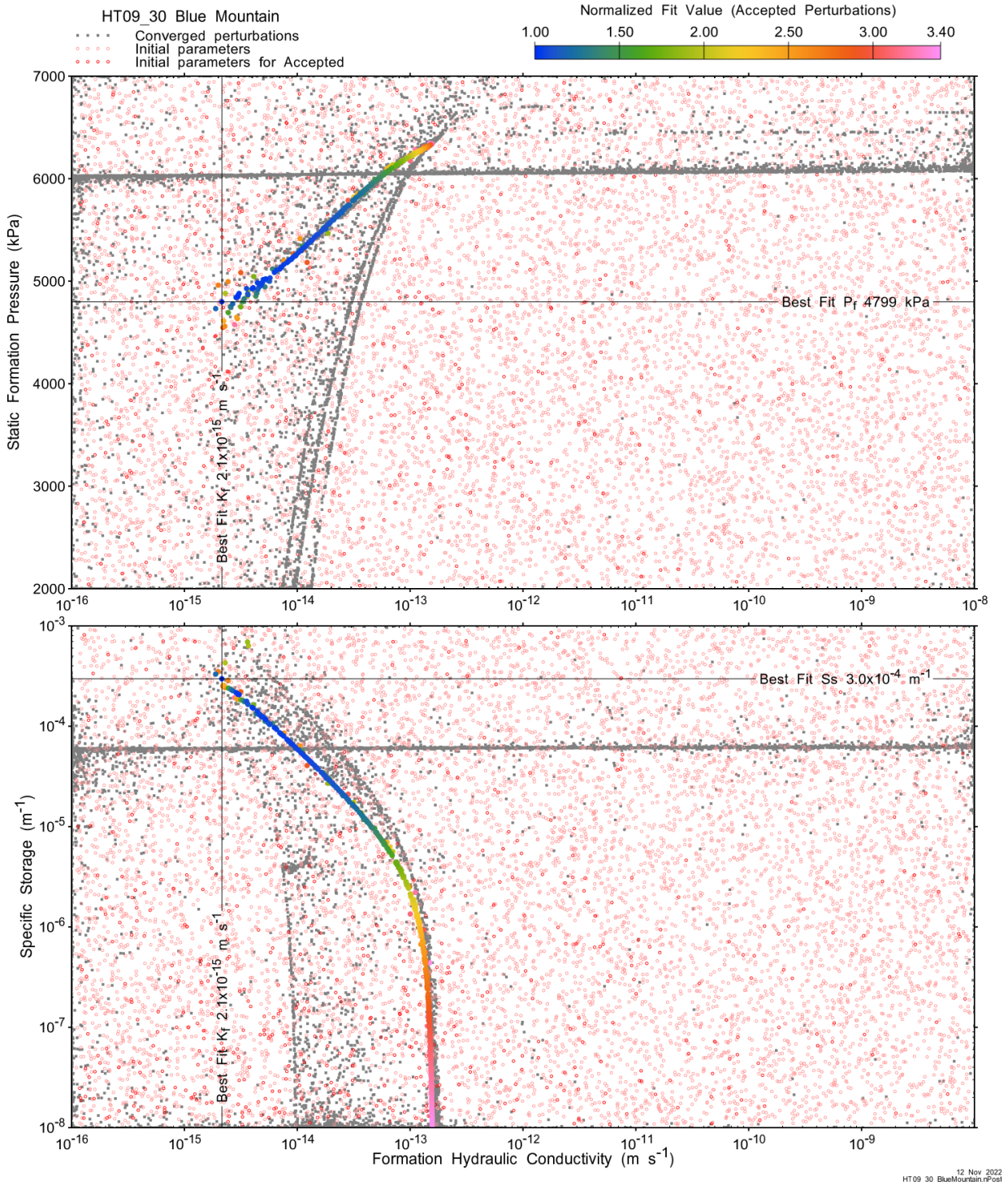

Figure A.214 - XY-scatter plot showing estimates of formation hydraulic conductivity (K_f) vs static formation pressure (P_f) (top panel) and specific storage (Ss) (bottom panel).

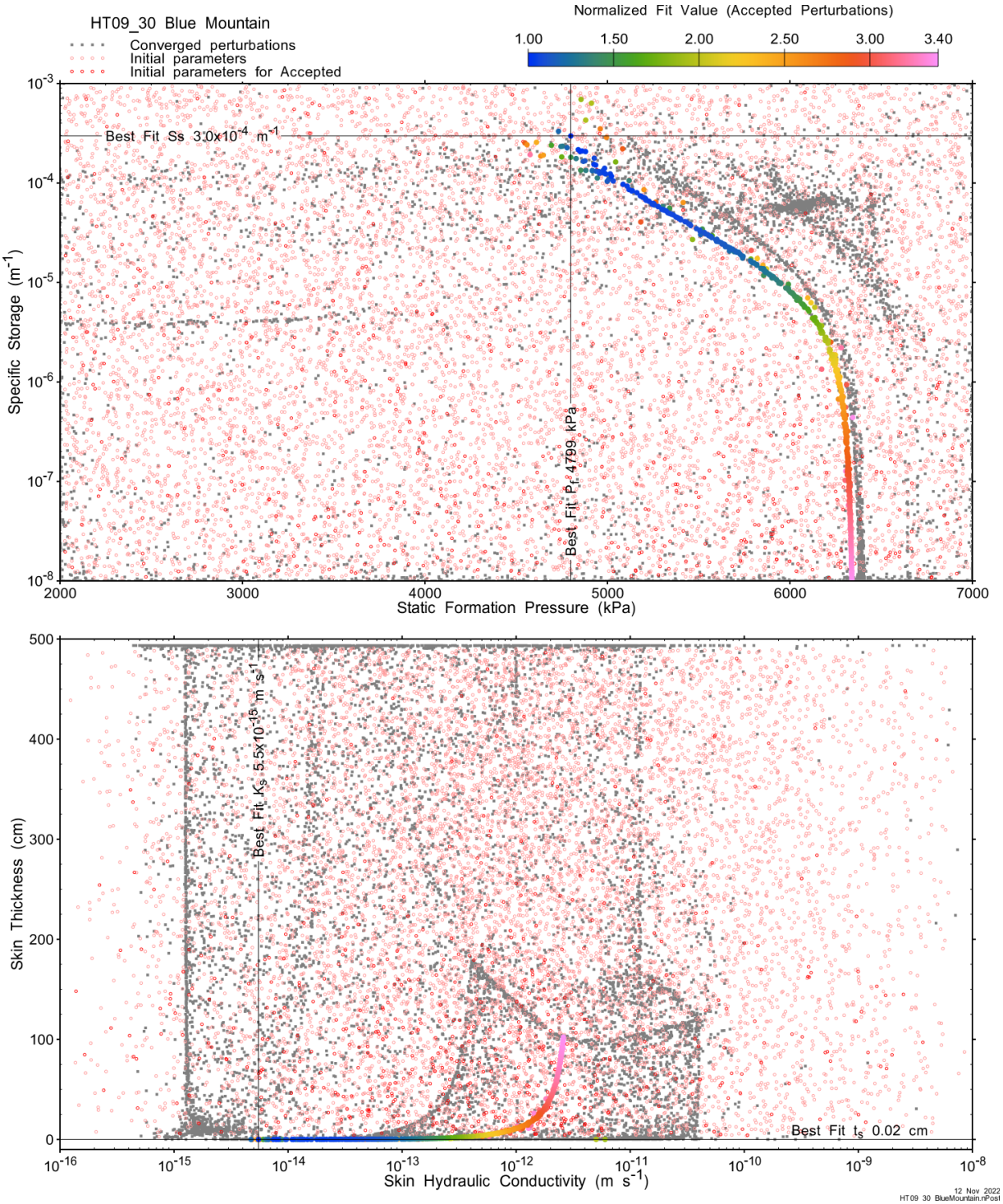

Figure A.215 - XY-scatter plot showing estimates of static formation pressure (P_f) vs specific storage (Ss) (top panel) and skin hydraulic conductivity (K_s) vs skin thickness (t_s) (bottom panel).

Confidence limits and median values are determined from the CDF of accepted optimization results (i.e. the varying color values in the above figures), with best fit value, 5% and 95% confidence indicated on Figure A.26 and Figure A.27.

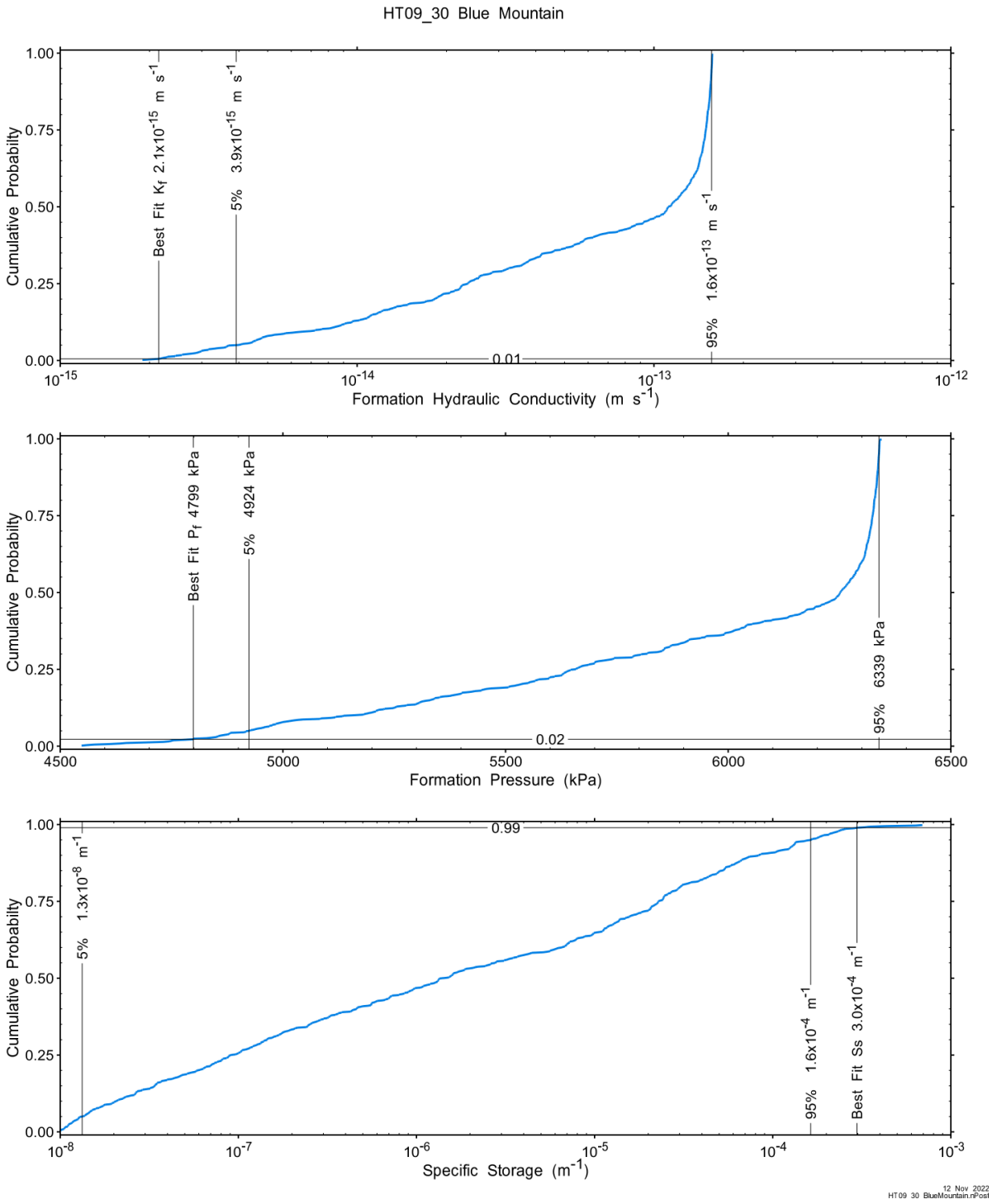

Figure A.216 – Cumulative distribution functions and parameter limits for formation hydraulic conductivity (K_f) (top panel), static formation pressure (P_f) (middle panel) and specific storage (Ss) (bottom panel).

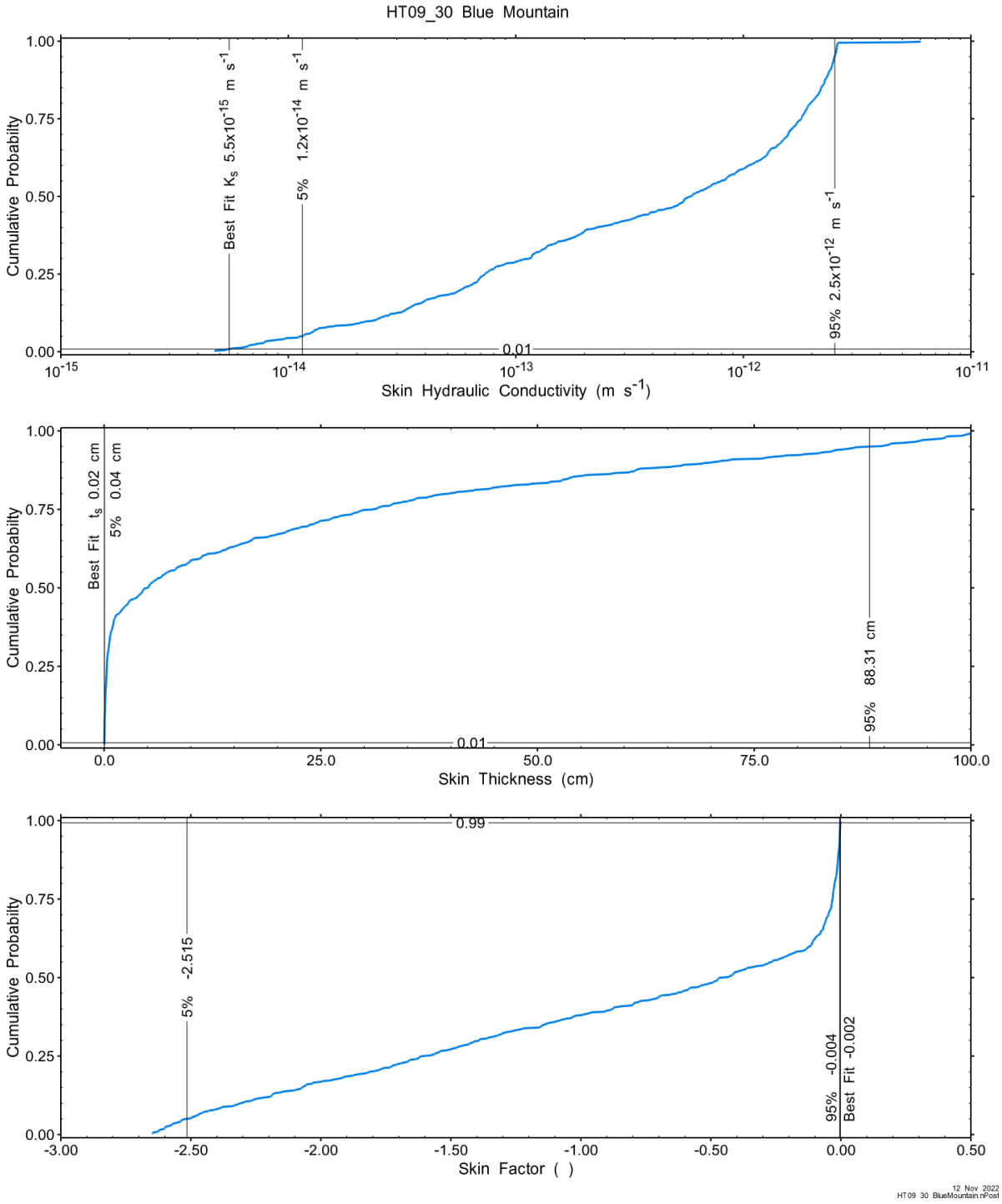

Figure A.217 – Cumulative distribution functions and parameter limits for skin hydraulic conductivity (K_s) (top panel), skin thickness (t_s) (middle panel) and skin factor (s) (bottom panel).

A summary of perturbation results is presented in Figure A.28, with Ramey-processed perturbations in Figure A.219. Those perturbations (508 of 10,000) with all parameters within the 5% and 95% range present a good fit to the measured test zone data.

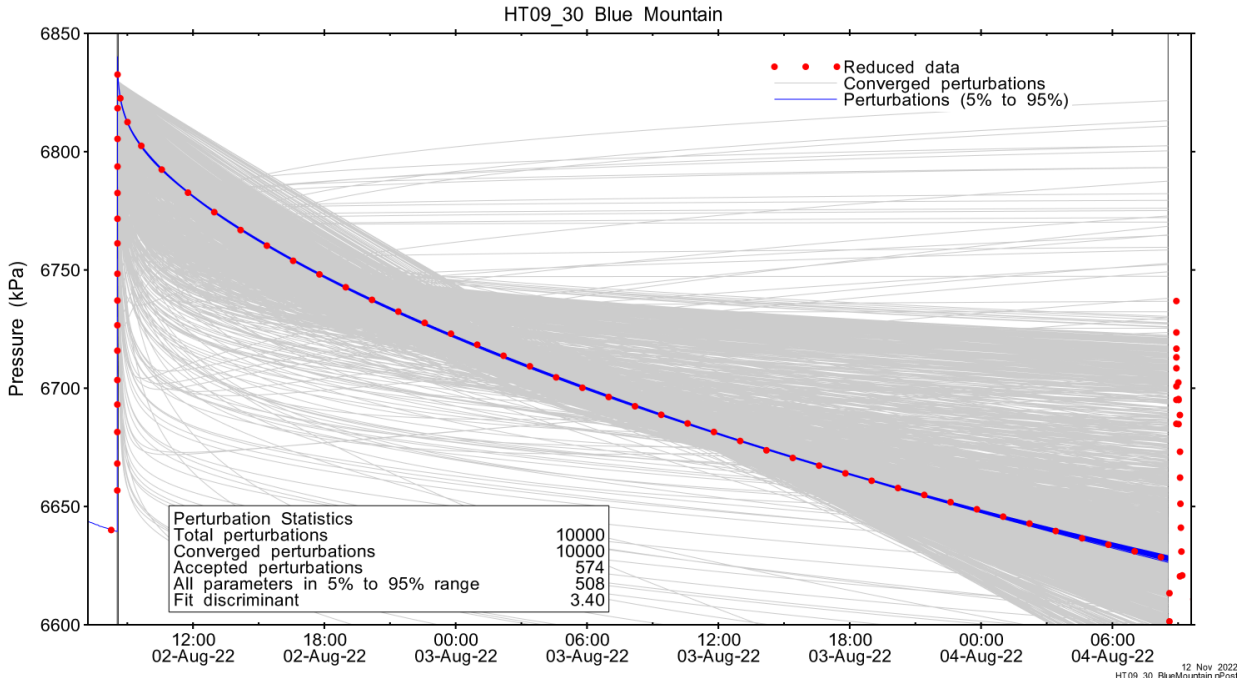

Figure A.218 – Perturbation results – all converged, accepted, and within 5% to 95% for all parameters.

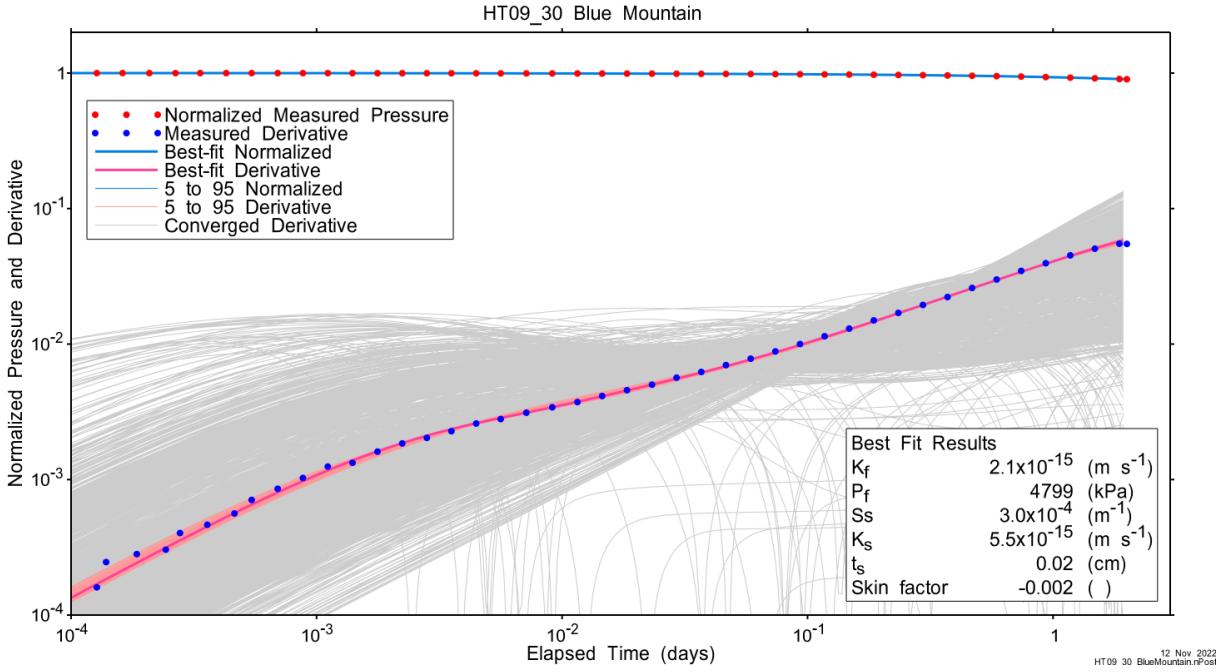

Figure A.219 – Log-log plot showing Ramey B and derivative response for all converged optimizations and those within 5% to 95% for all parameters.

A summary of best-fit and parameter ranges is given in Table A.9.

Table A.69 - Summary of the HT09_30 parameter estimates.

Parameter	Best Fit	5%	Median	95%
K_f (m/s)	2.1E-15	3.9E-15	1.1E-13	1.6E-13
P_f (kPa)	4799	4924	6252	6339
Ss (1/m)	3.0E-04	1.3E-08	1.4E-06	1.6E-04
K_s (m/s)	5.5E-15	1.2E-14	5.9E-13	2.5E-12
t_s (cm)	0.02	0.04	4.95	88.31
s (-)	-0.002	-2.515	-0.457	-0.004

Parameter correlations for all perturbations with all parameters within the 5% to 95% limits are given in Table A.5.

Table A.70 – Pearson cross-correlations of 5% to 95% parameters

	Log(K_f)	P_f	Log(Ss)	Log(K_s)	t_s	s
Log(K_f)	1.000	0.996	-0.905	0.976	0.596	-0.743
Pf	0.996	1.000	-0.875	0.958	0.558	-0.700
Log(S_s)	-0.905	-0.875	1.000	-0.973	-0.861	0.957
Log(K_s)	0.976	0.958	-0.973	1.000	0.732	-0.867
t_s	0.596	0.558	-0.861	0.732	1.000	-0.954
s	-0.743	-0.700	0.957	-0.867	-0.954	1.000

A.14.4 Additional Figures

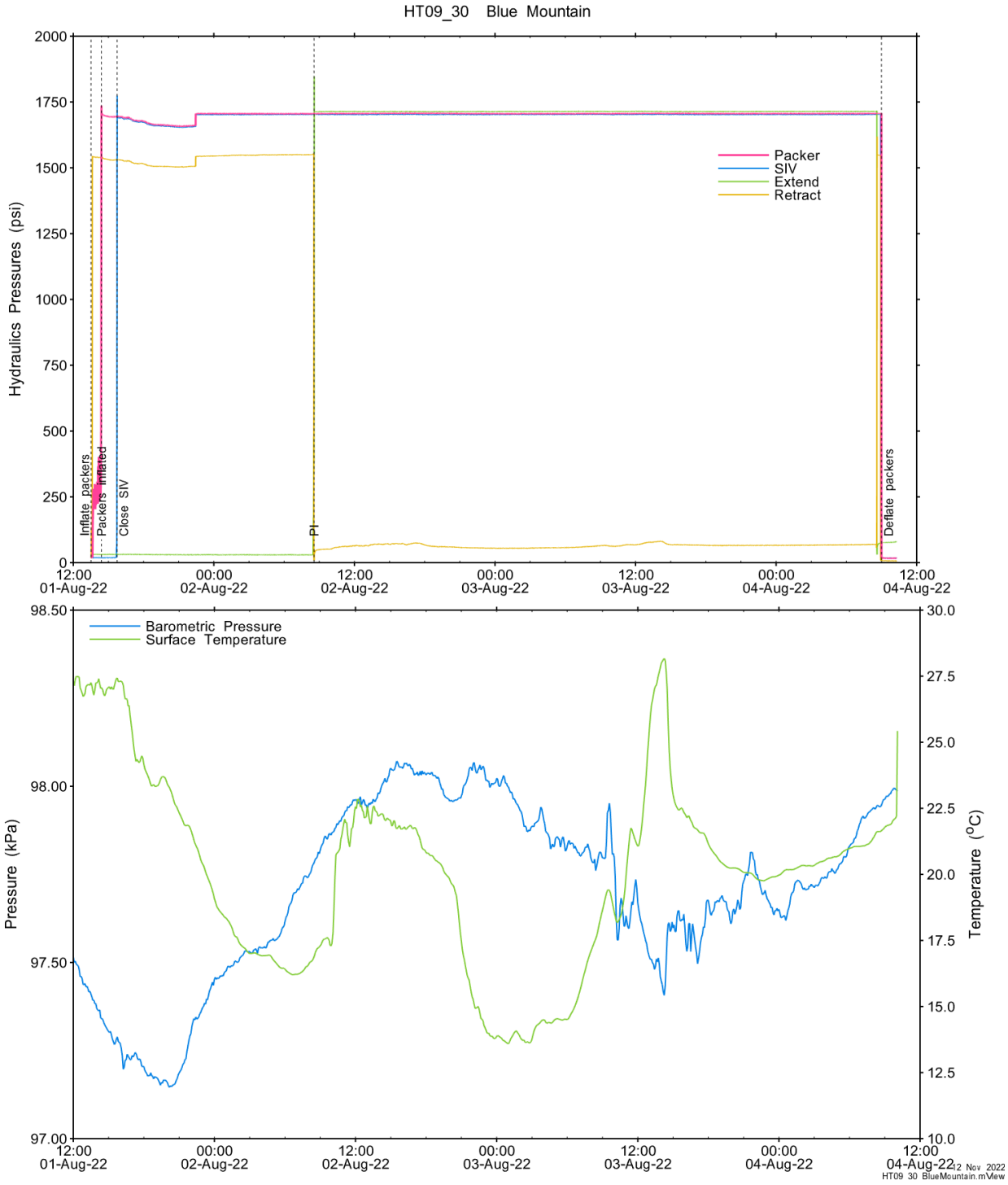

Figure A.220 - Hydraulics pressures and surface temperature/barometric pressure.

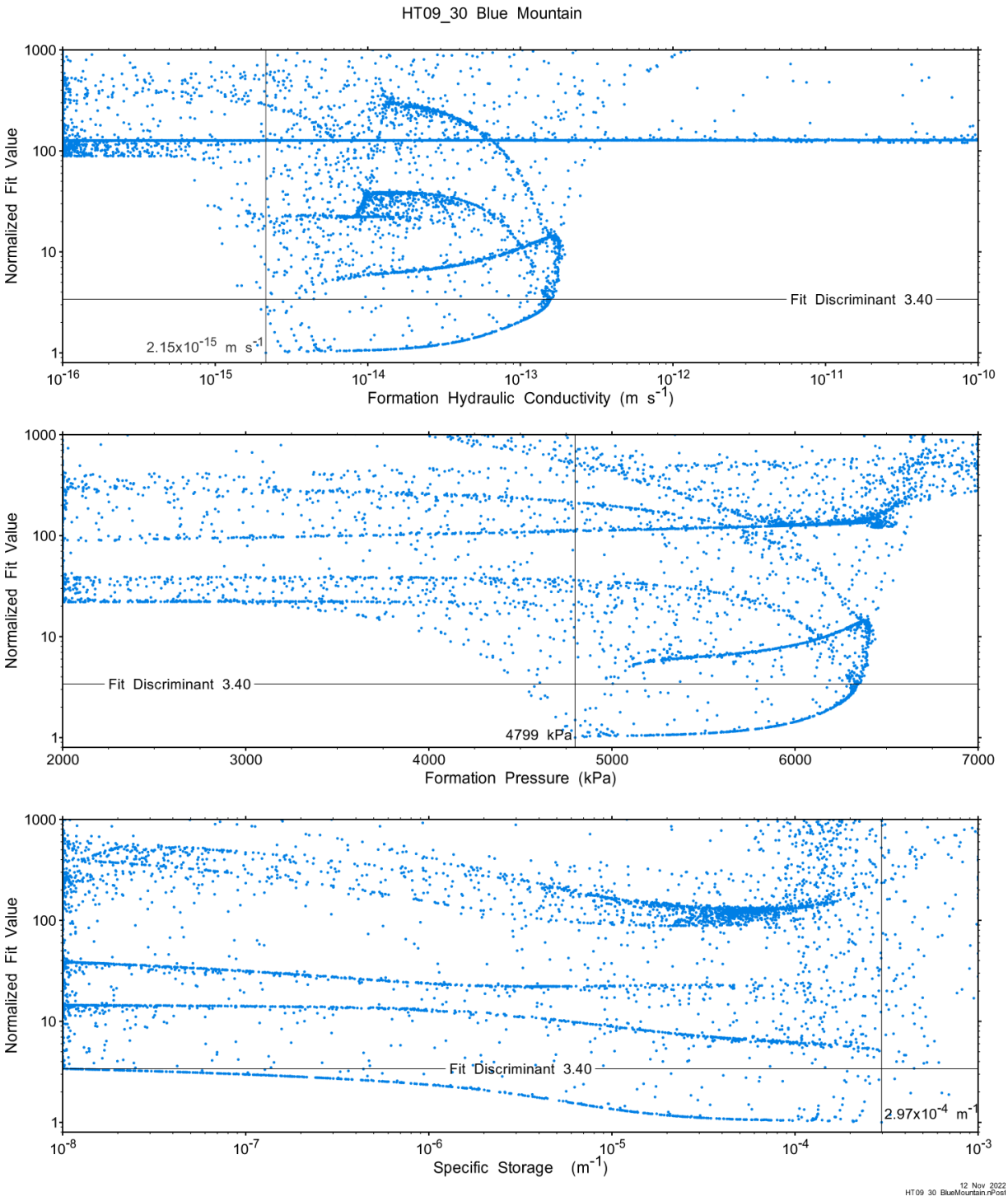

Figure A.221 - XY-scatter plot showing the formation parameter space normalized fit values.

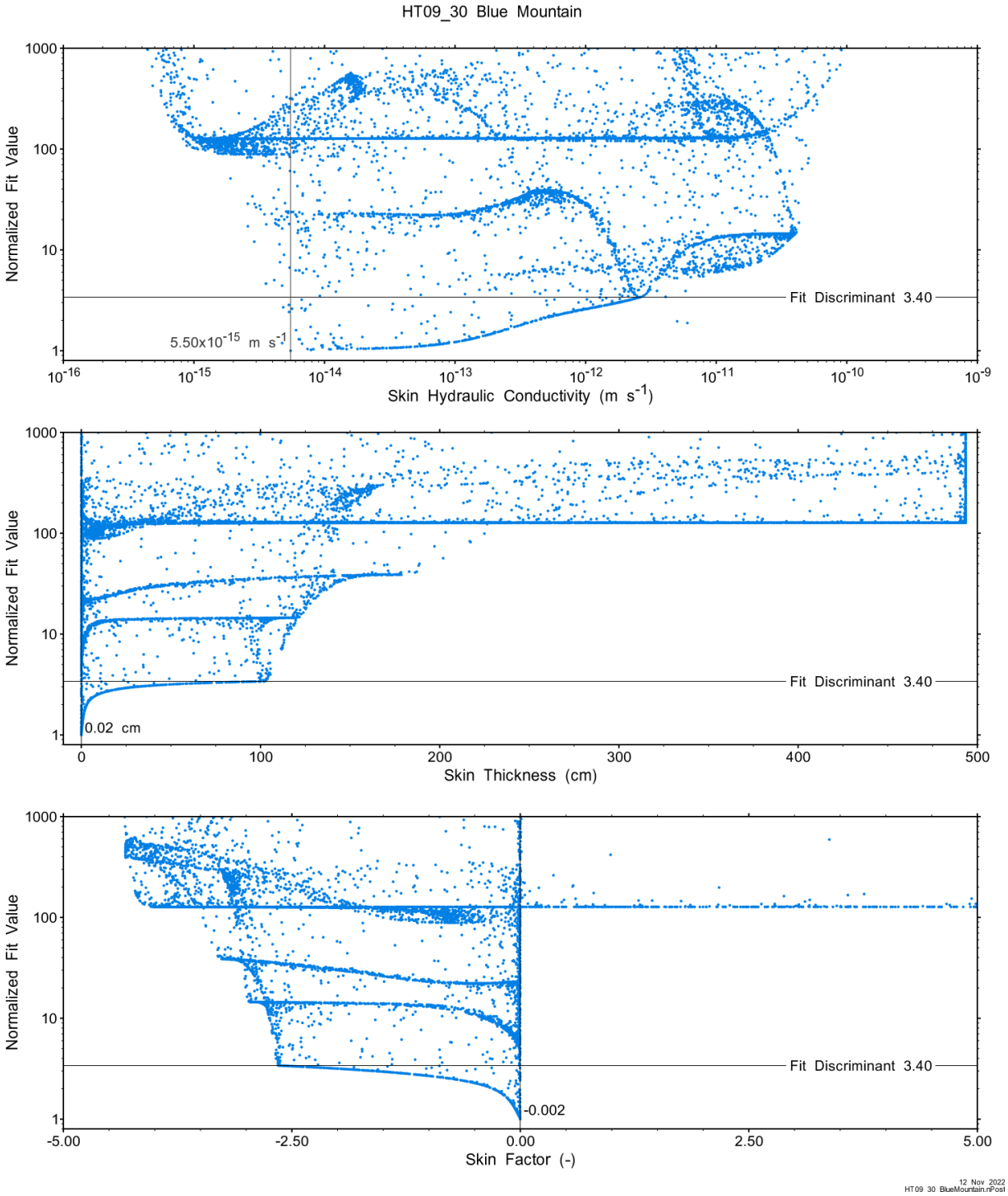

Figure A.222 - XY-scatter plot showing the skin parameter space normalized fit values.

A.15 HT10_30 Collingwood/Cobourg

The SB BH02 interval from 671.00 to 700.96 mBGS tested in HT10_30 covers nearly the entirety of the Collingwood formation (6.54 m of 7.85 m) and the upper 60% of the Cobourg Formation (23.39 m of 38.83 m). A single PI test of two days duration was conducted.
The response for this test indicated extremely low permeability with virtually no recovery. The analyses presented below confirms this assessment but indicates an anomalously high formation pressure. We believe that this pressure is incorrect and in fact indicates equipment effects that are apparent due to the extremely low conductivity. For this reason, we believe results from this test should be qualified. A formation hydraulic conductivity of less than 10^{-15} m/s is a reasonable assumption, but other analyses values, in particular formation pressure should not be used/reported.

A.15.1 Test Data Summary

Table A.6 and Figure A.1 provide a summary of test events and a plot of pressures measured while testing respectively.

Table A.71 - Summary of Test Events.

Event	Start Date & Time	Duration (days)	TZ Pressure (kPa)
Drilling intercept	22-03-13 12:10	144.06	7114
Shut-in	22-08-04 13:35	0.79	7120
Pulse injection	22-08-05 08:31	2.00	7875
Test end	22-08-07 08:37		7778

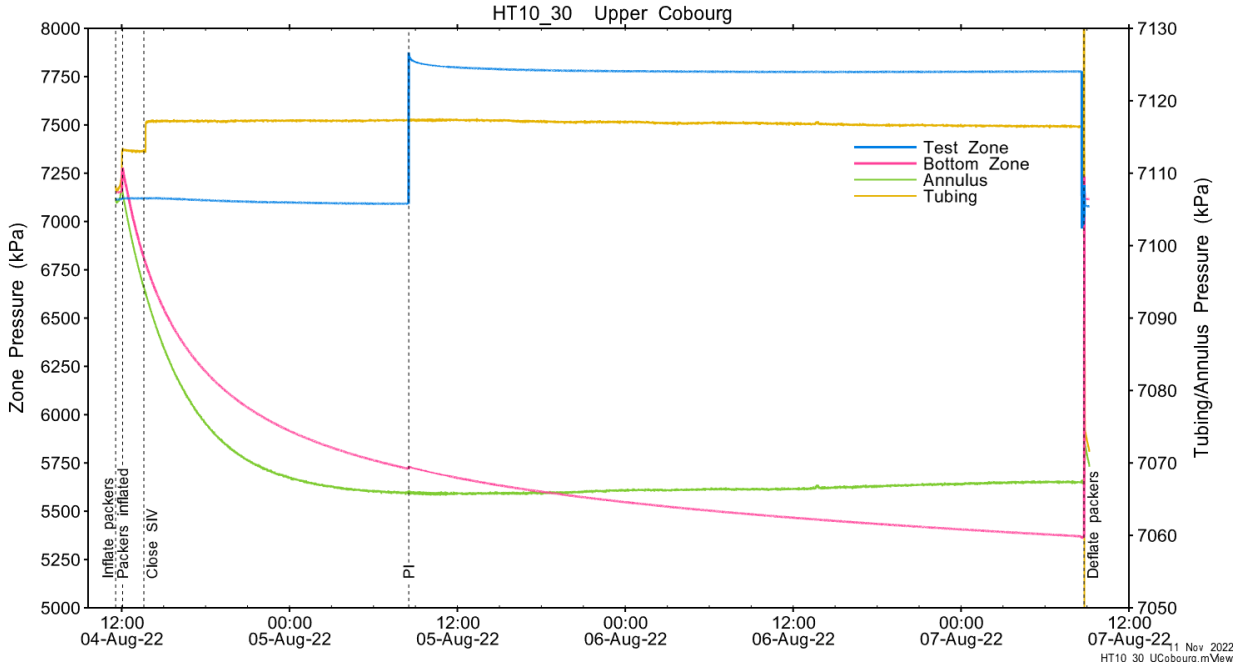

Figure A.223 - Test events and pressures.

A.15.2 Test Analyses

Table A.7 is a summary of test-specific input parameters used in the analyses, while Table A.8 presents the optimized parameters and allowed ranges.

Table A.72 – nSIGHTS Input Parameters.

Parameter	Value	Units
Test zone radius	6.32	cm
Test zone compressibility	3.53E-10	1/Pa
Test zone length	29.96	m

Table A.73 – nSIGHTS Parameter Optimization Ranges.

Parameter	Minimum	Maximum	Units	Type
Formation hydraulic conductivity (K_f)	1E-16	1E-07	m/s	log
Formation pressure (P_f)	4000	20000	kPa	linear
Specific storage (S_s)	1E-08	1E-04	1/m	log
Skin hydraulic conductivity (K_s)	1E-16	1E-07	m/s	log
Skin thickness (t_s)	0.013	500	cm	linear

Figure A.18 shows the measured test zone pressure record (with reduced data density for clarity) used in the analysis along with the best-fit simulation and parameter values. Figure A.19 presents the pre-test history, and Figure A.20 shows the Ramey B normalized best-fit pressure and pressure derivatives.

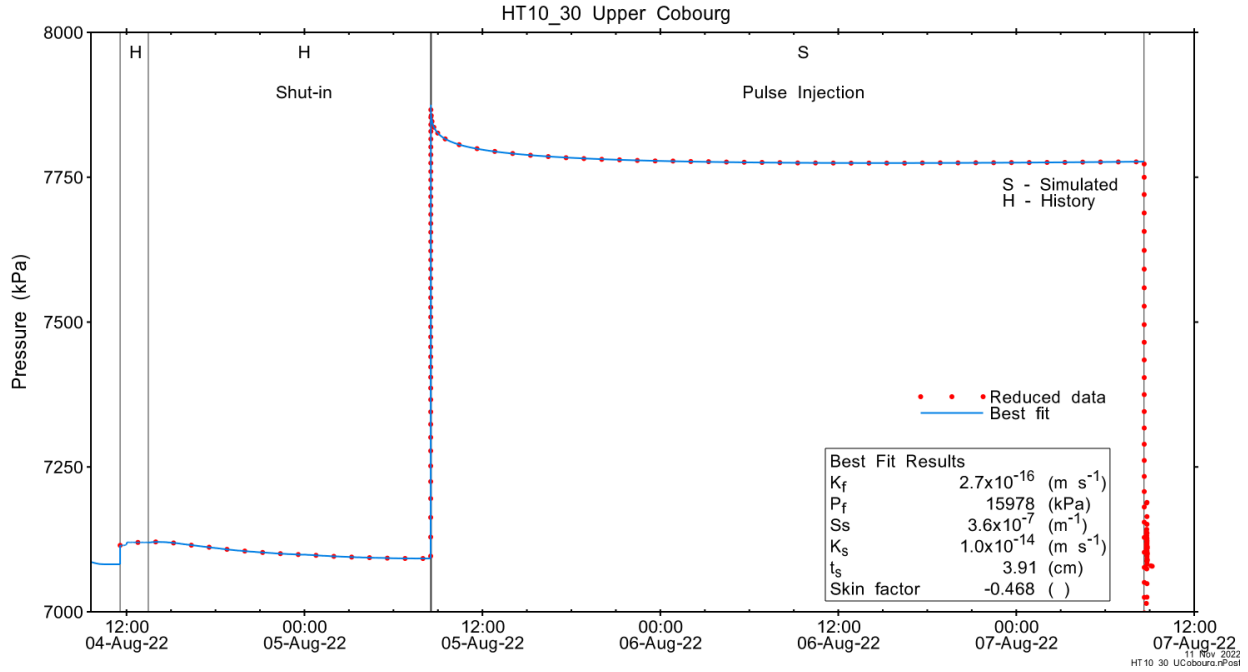

Figure A.224 - Annotated testing sequence showing best-fit simulation and parameter estimates.

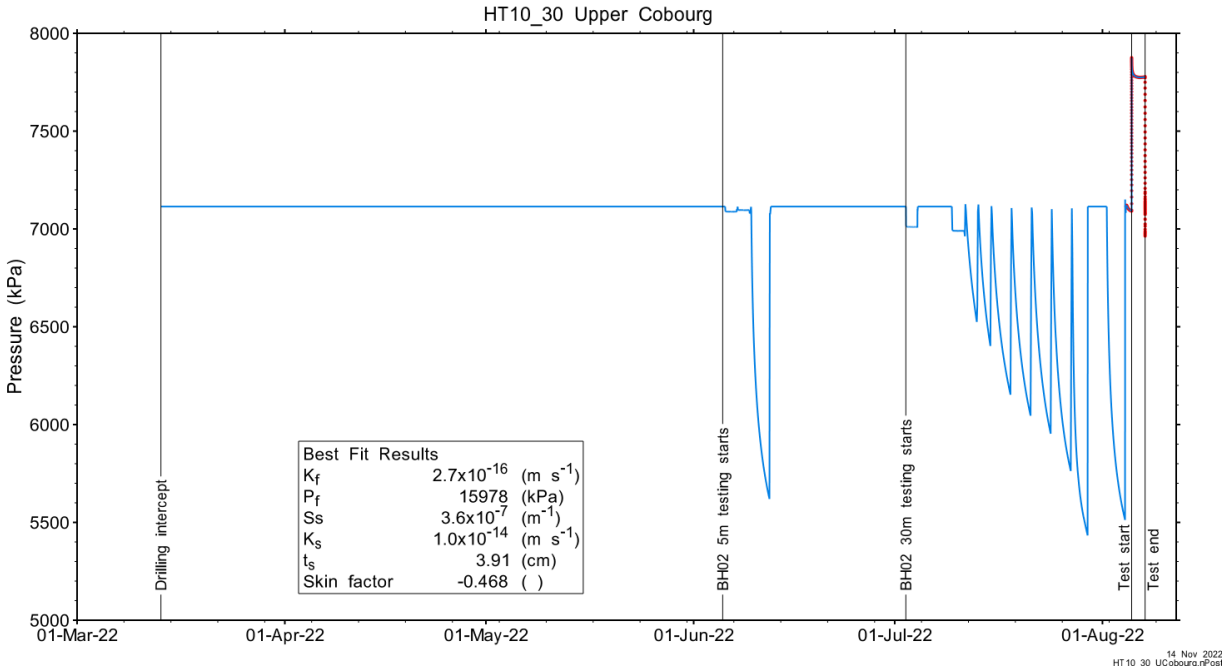

Figure A.225 - Annotated testing sequence showing pre-test history, best-fit simulation and parameter estimates.

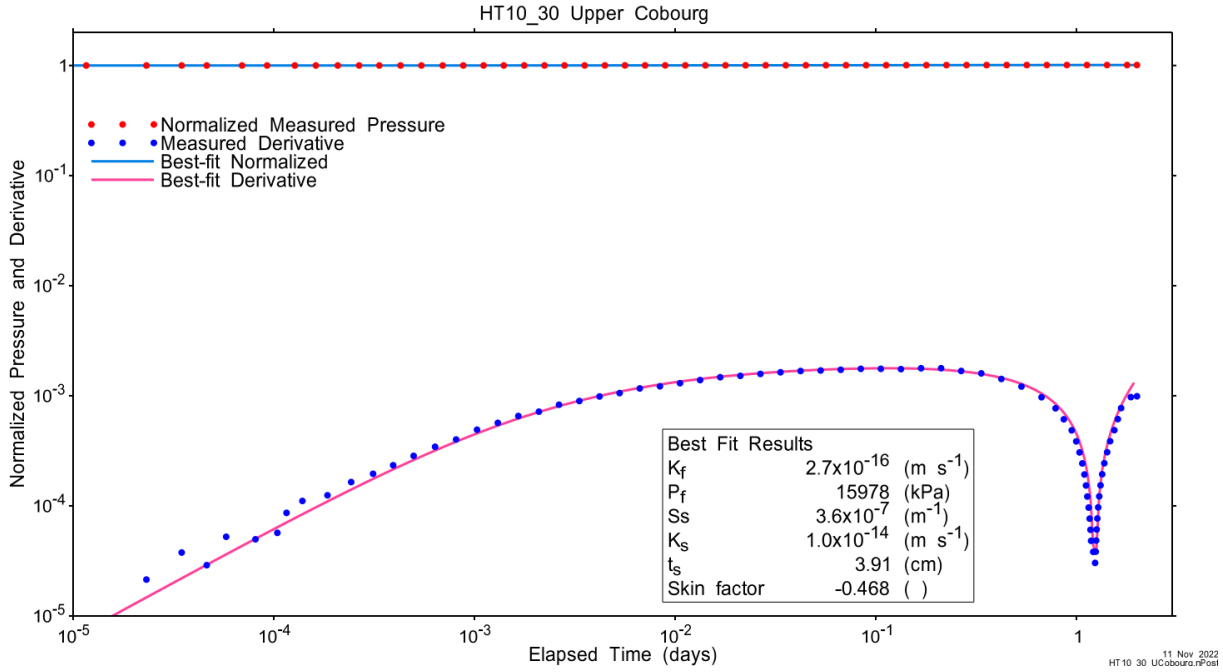

Figure A.226 - Log-log plot showing Ramey B and derivative response for best-fit simulation.

Figure A.21 shows the normalized parameter sensitivity response for the best fit. Sensitivity for all fitting parameters is increasing at the end of the test, indicating that increased test duration may have yielded more precise results.

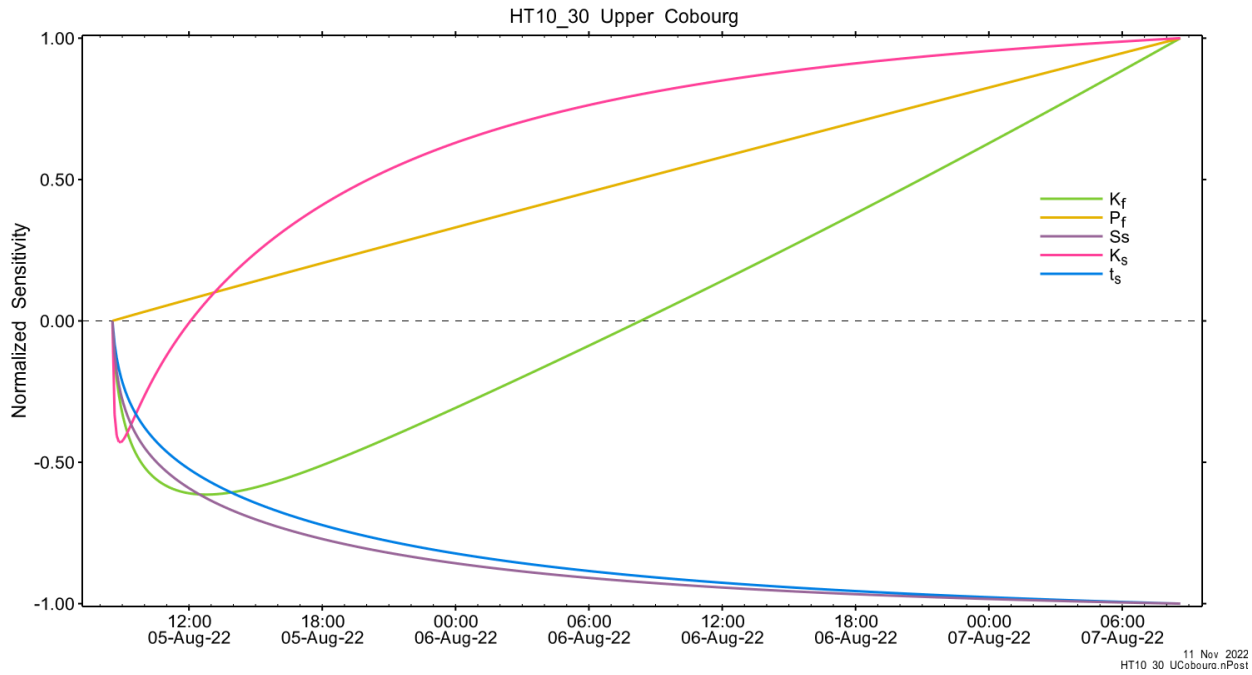

Figure A.227 - Normalized Jacobian for best-fit simulation.

A.15.3 Uncertainty Analyses

The CDF of normalized fit values for all converged simulations and the selected fit discriminant are shown in Figure A.22.

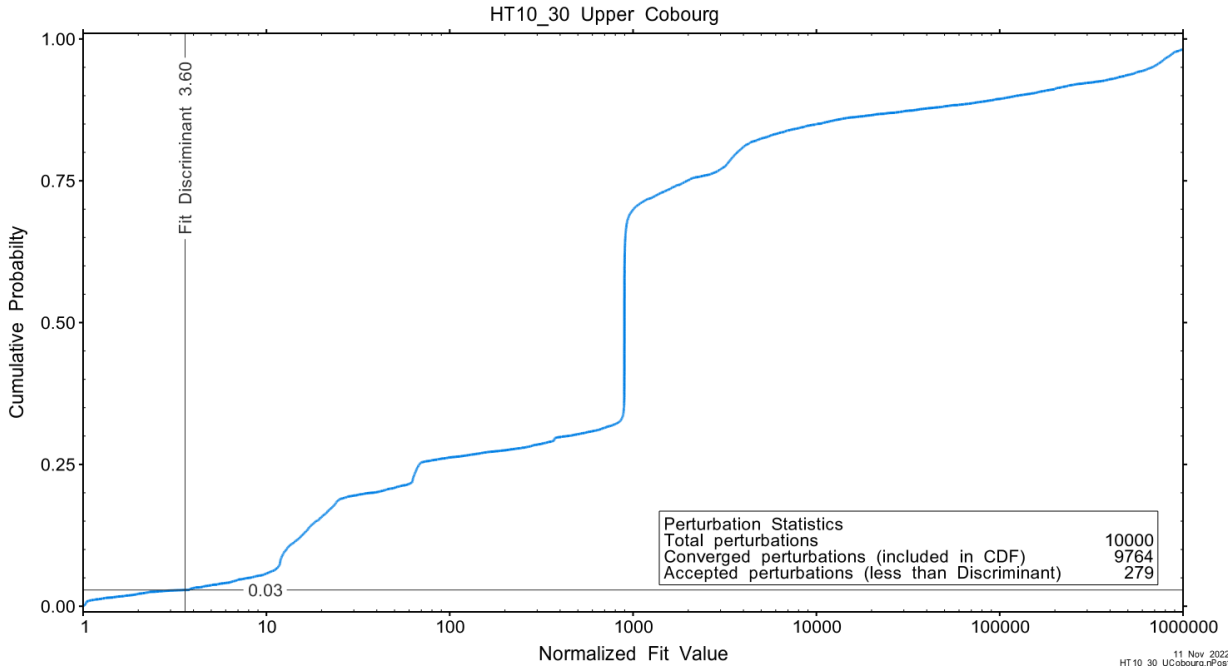

Figure A.228 - Fit value cumulative distribution function.

Summary cross parameter scatter plots for selected formation and skin parameters are given in Figure A.24 and Figure A.25. The light pink dots on the figures are the initial parameter estimates, with red dots overlaying those initial parameter values that resulted in accepted optimization results. The grey dots are converged optimizations which did not meet the fit discriminant. Larger varying color symbols represent the fit value of accepted optimizations, with the blue values representing the best fit.

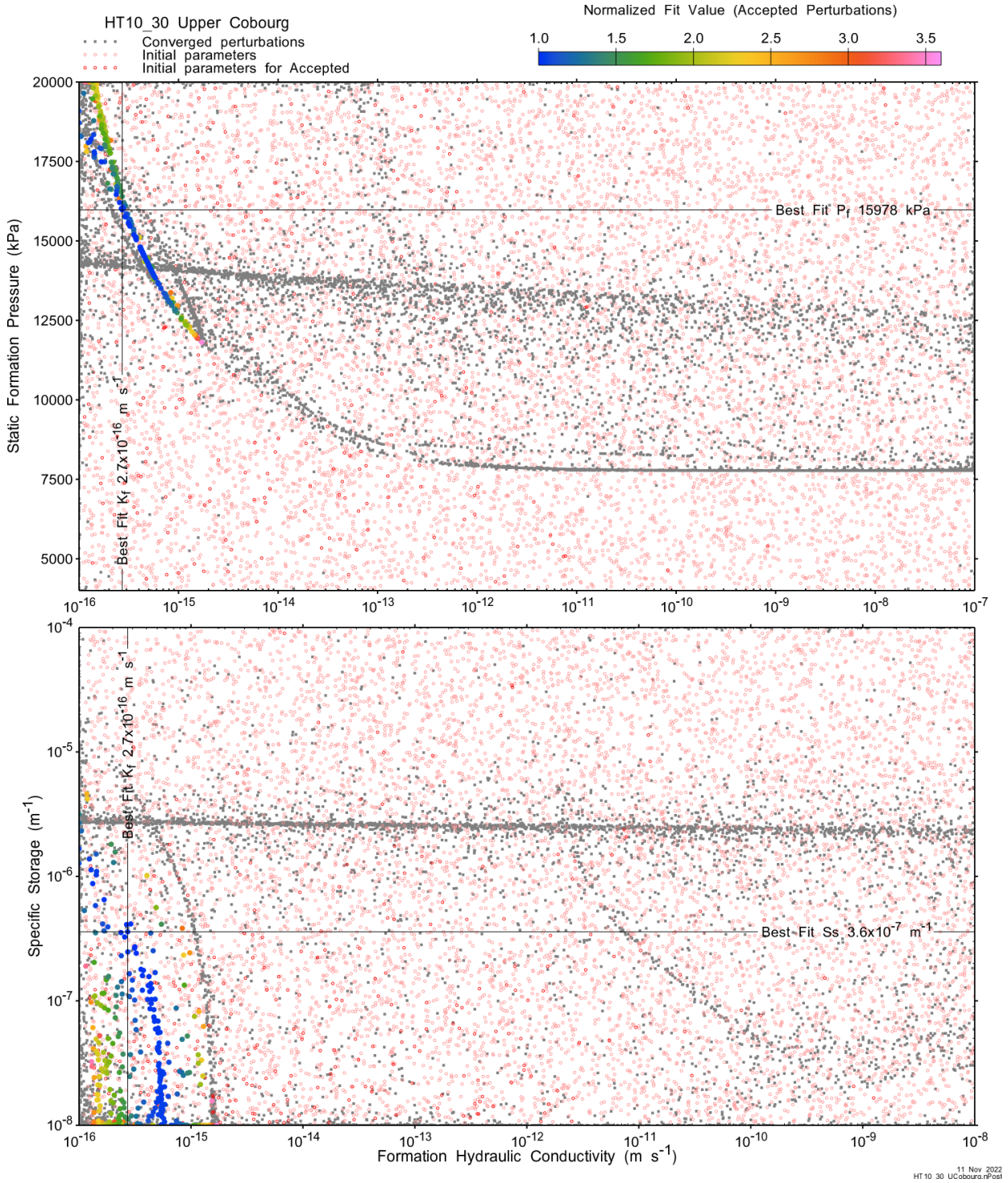

Figure A.229 - XY-scatter plot showing estimates of formation hydraulic conductivity (K_f) vs static formation pressure (P_f) (top panel) and specific storage (Ss) (bottom panel).

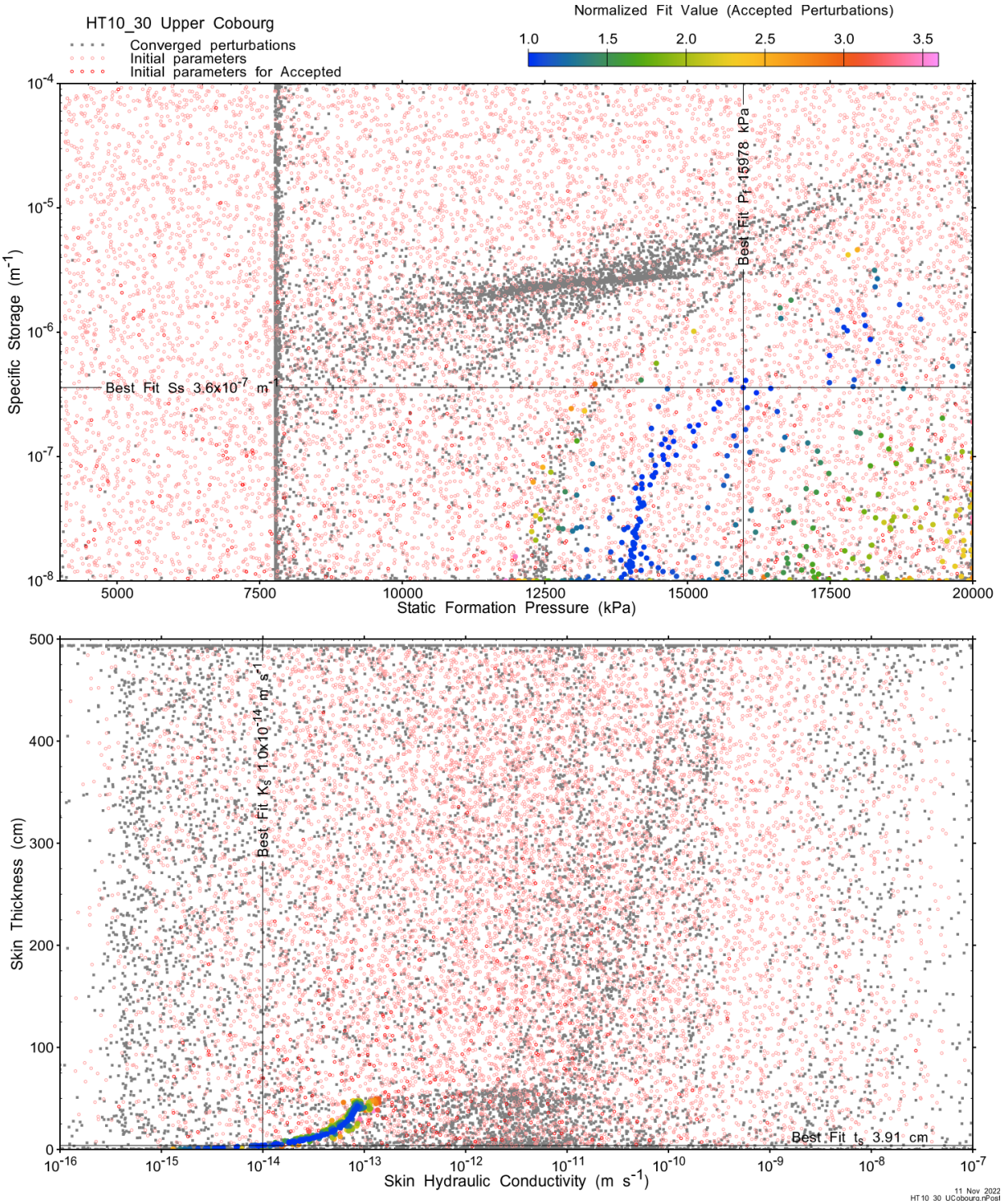

Figure A.230 - XY-scatter plot showing estimates of static formation pressure (P_f) vs specific storage (Ss) (top panel) and skin hydraulic conductivity (K_s) vs skin thickness (t_s) (bottom panel).

Confidence limits and median values are determined from the CDF of accepted optimization results (i.e. the varying color values in the above figures), with best fit value, 5% and 95% confidence indicated on Figure A.26 and Figure A.27.

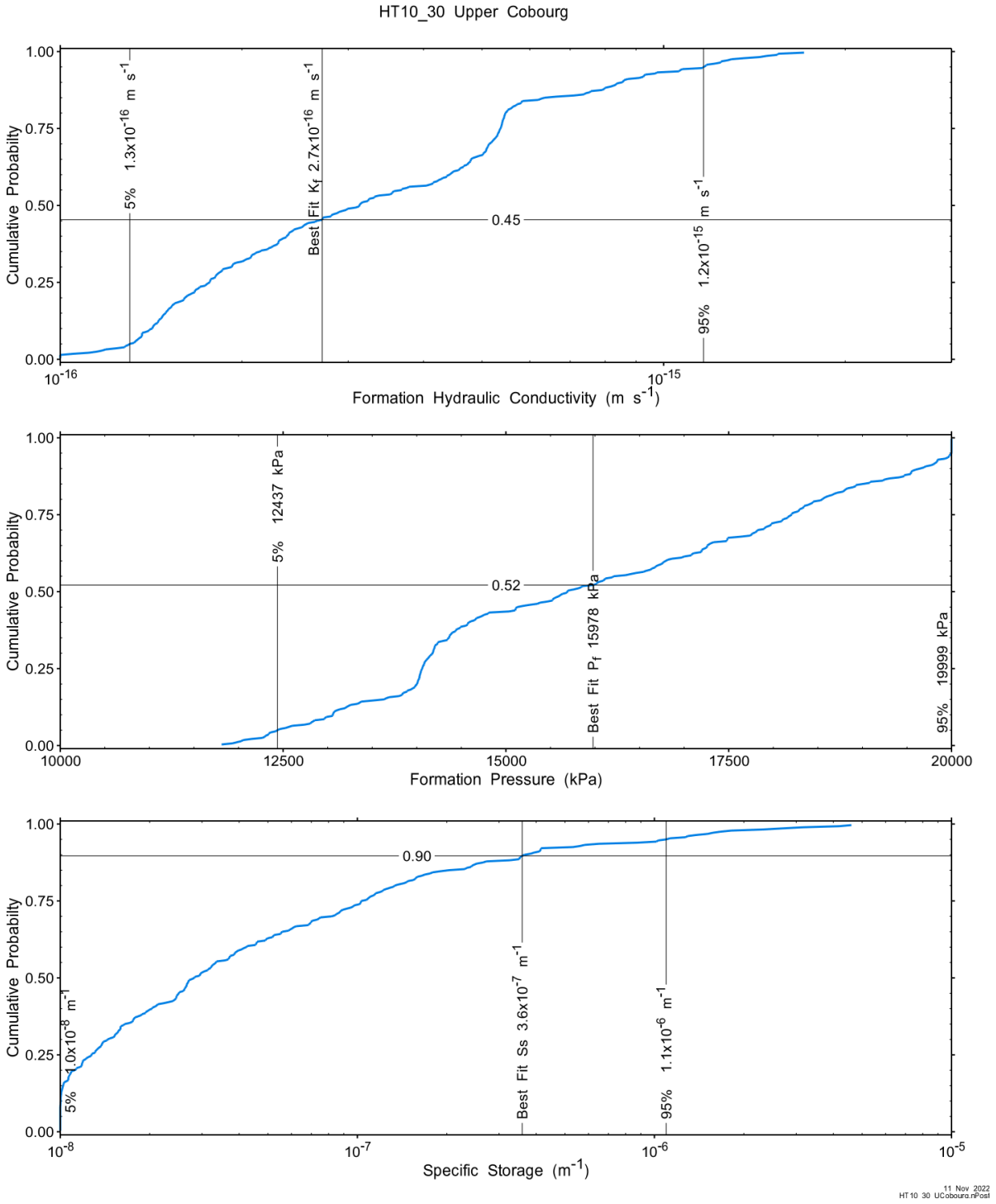

Figure A.231 – Cumulative distribution functions and parameter limits for formation hydraulic conductivity (K_f) (top panel), static formation pressure (P_f) (middle panel) and specific storage (Ss) (bottom panel).

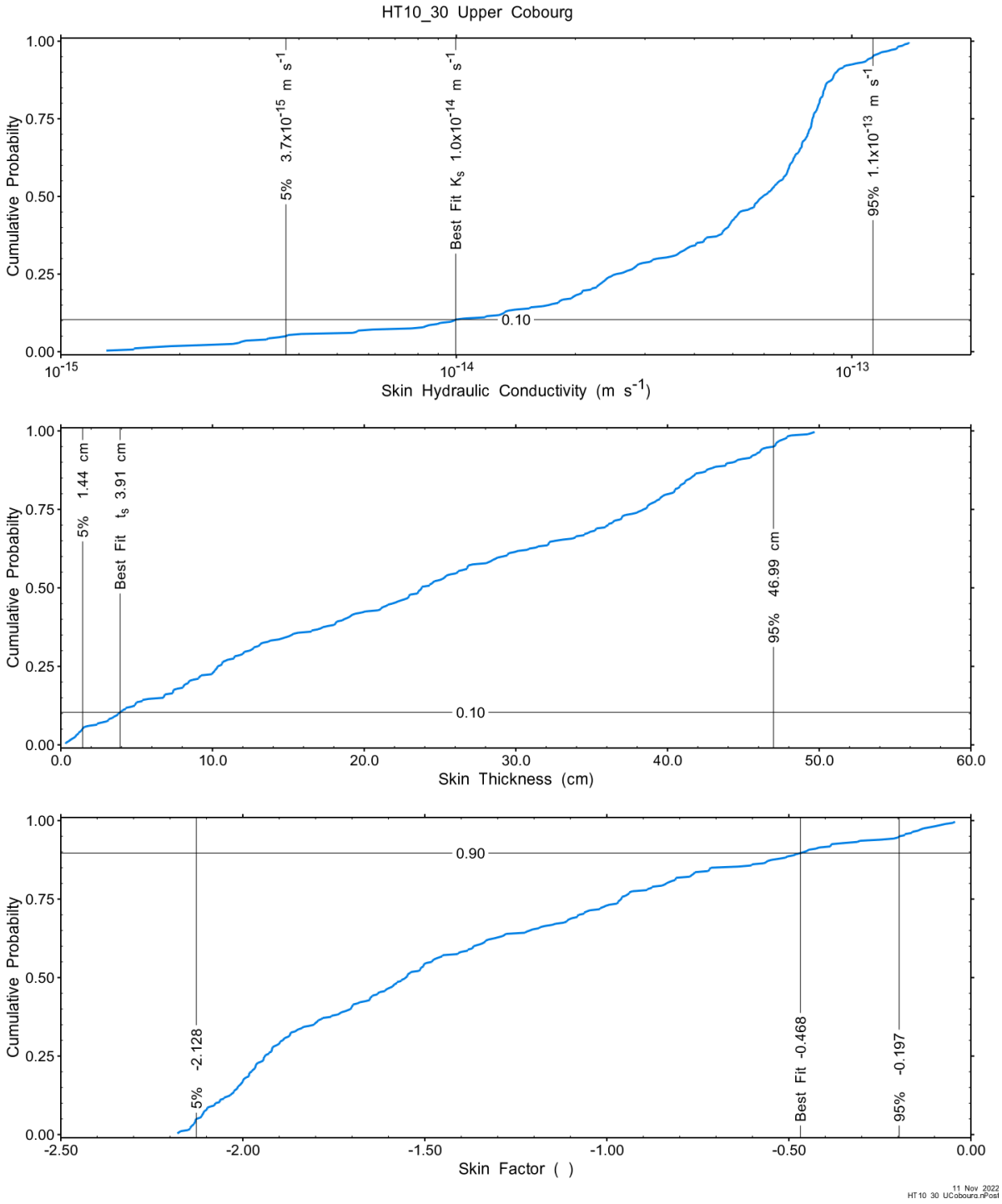

Figure A.232 – Cumulative distribution functions and parameter limits for skin hydraulic conductivity (K_s) (top panel), skin thickness (t_s) (middle panel) and skin factor (s) (bottom panel).

A summary of perturbation results is presented in Figure A.28, with Ramey-processed perturbations in Figure 12. Those perturbations (217 of 10,000) with all parameters within the 5% and 95% range present a very good fit to the measured test zone data.

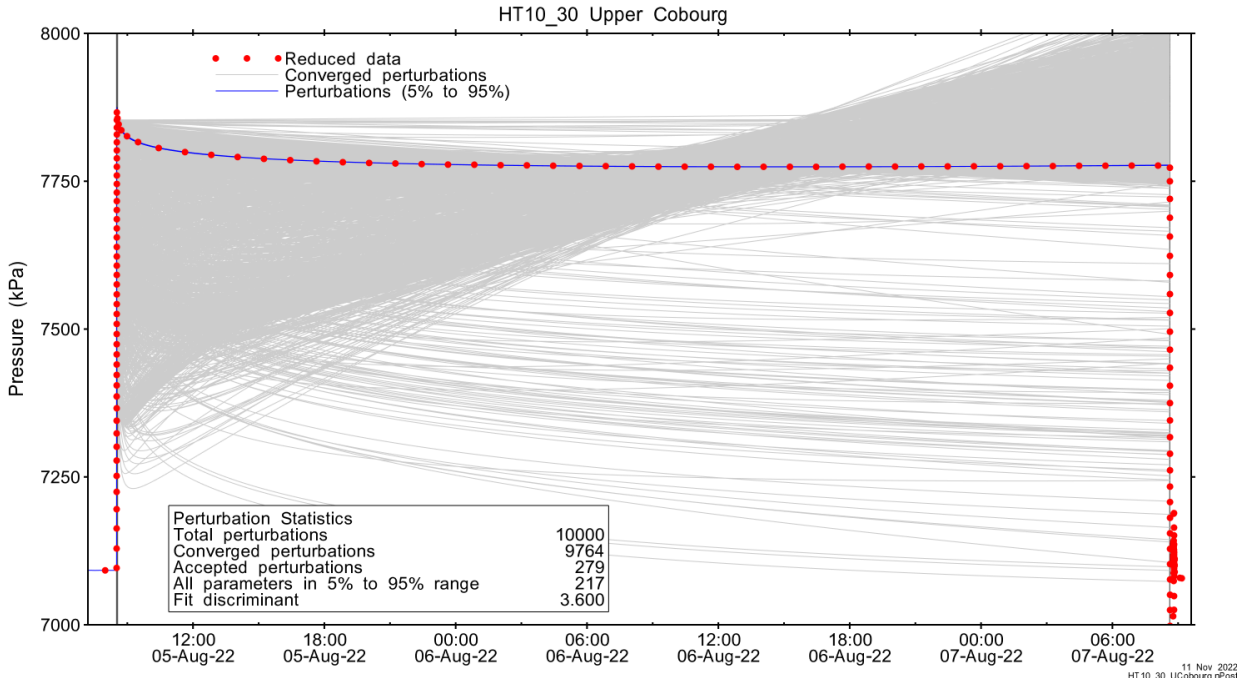

Figure A.233 – Perturbation results – all converged, accepted, and within 5% to 95% for all parameters.

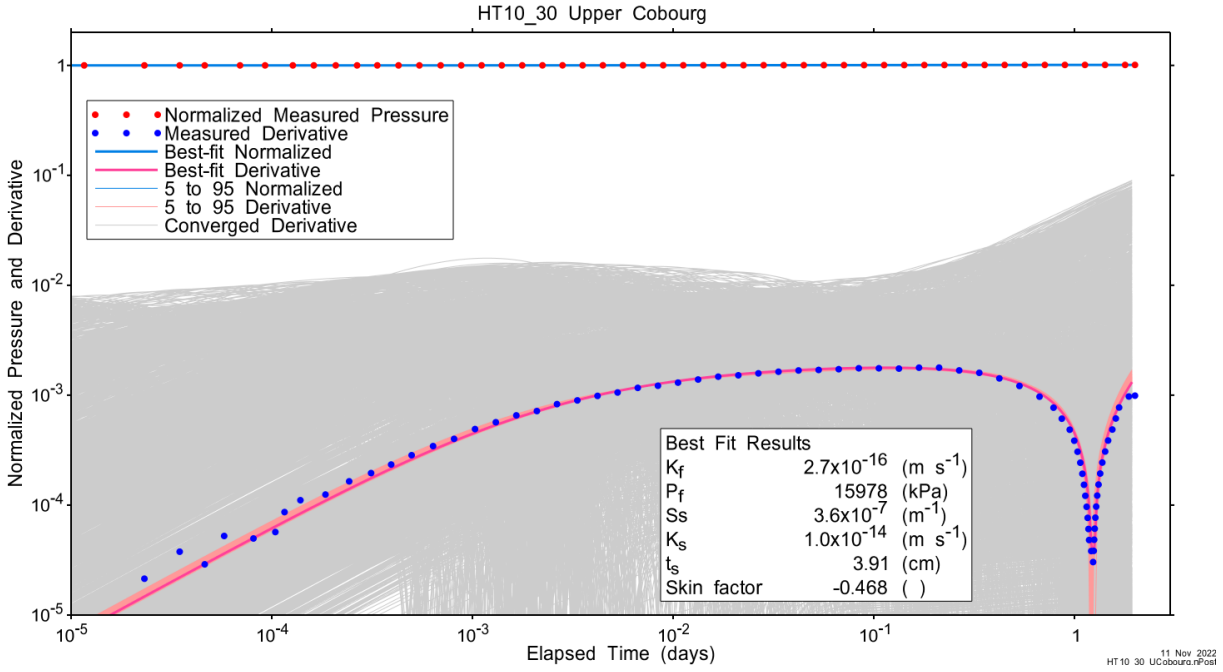

Figure A.234 – Log-log plot showing Ramey B and derivative response for all converged optimizations and those within 5% to 95% for all parameters.

A summary of best-fit and parameter ranges is given in Table A.9.

Table A.74 - Summary of the HT10_30 parameter estimates.

Parameter	Best Fit	5%	Median	95%
K_f (m/s)	2.7E-16	1.3E-16	3.1E-16	1.2E-15
P_f (kPa)	15978	12437	15691	19999
Ss (1/m)	3.6E-07	1.0E-08	2.8E-08	1.1E-06
K_s (m/s)	1.0E-14	3.7E-15	6.0E-14	1.1E-13
t_s (cm)	3.91	1.44	23.80	46.99
s (-)	-0.468	-2.128	-1.553	-0.197

Parameter correlations for all perturbations with all parameters within the 5% to 95% limits are given in Table A.5.

Table A.75 – Pearson cross-correlations of 5% to 95% parameters

	Log(K_f)	P_f	Log(Ss)	Log(K_s)	t_s	s
Log(K_f)	1.000	-0.978	-0.187	0.292	0.074	-0.096
Pf	-0.978	1.000	0.108	-0.196	-0.011	0.020
Log(S_s)	-0.187	0.108	1.000	-0.978	-0.958	0.994
Log(K_s)	0.292	-0.196	-0.978	1.000	0.891	-0.955
t_s	0.074	-0.011	-0.958	0.891	1.000	-0.976
s	-0.096	0.020	0.994	-0.955	-0.976	1.000

A.15.4 Additional Figures

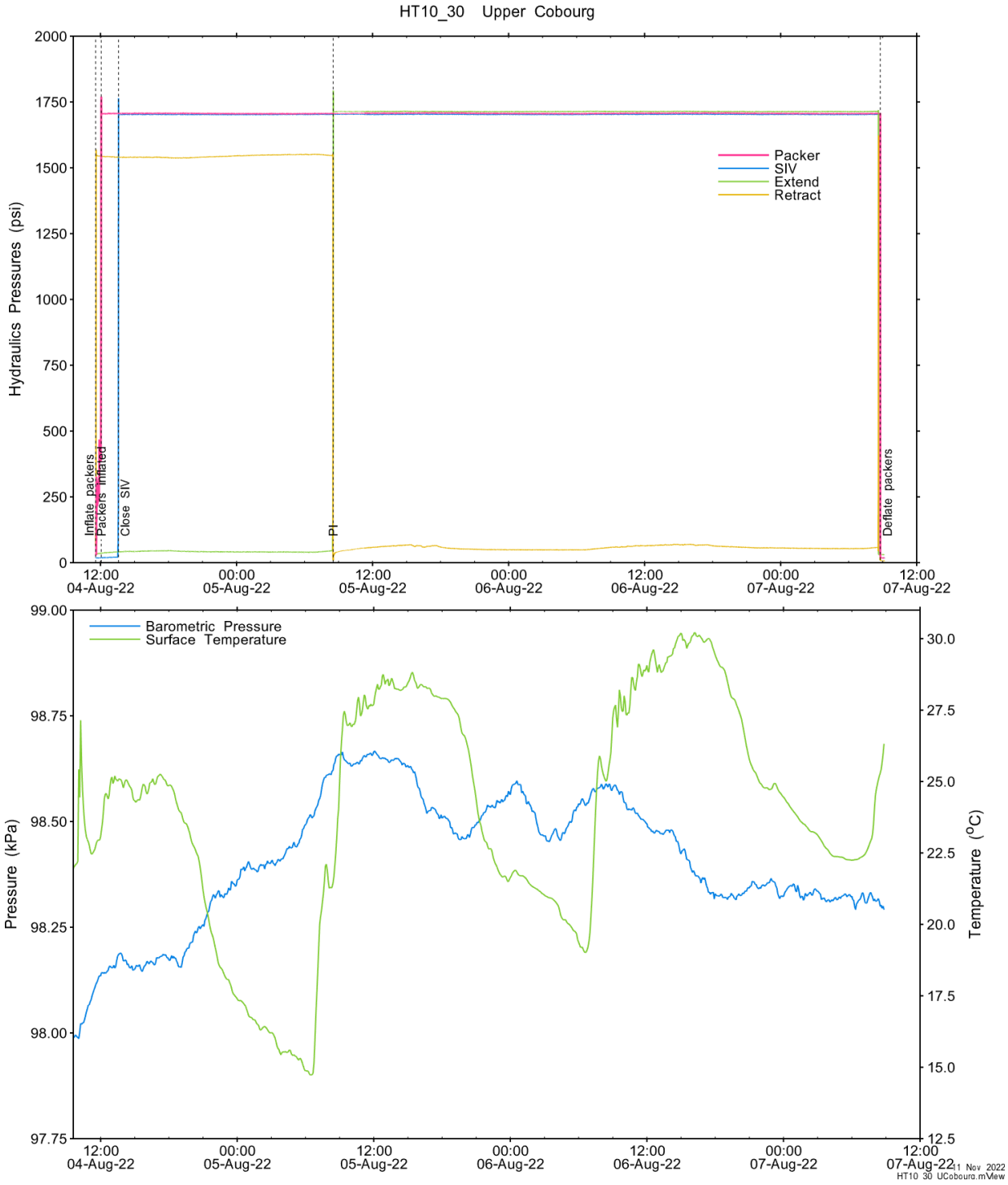

Figure A.235 - Hydraulics pressures and surface temperature/barometric pressure.

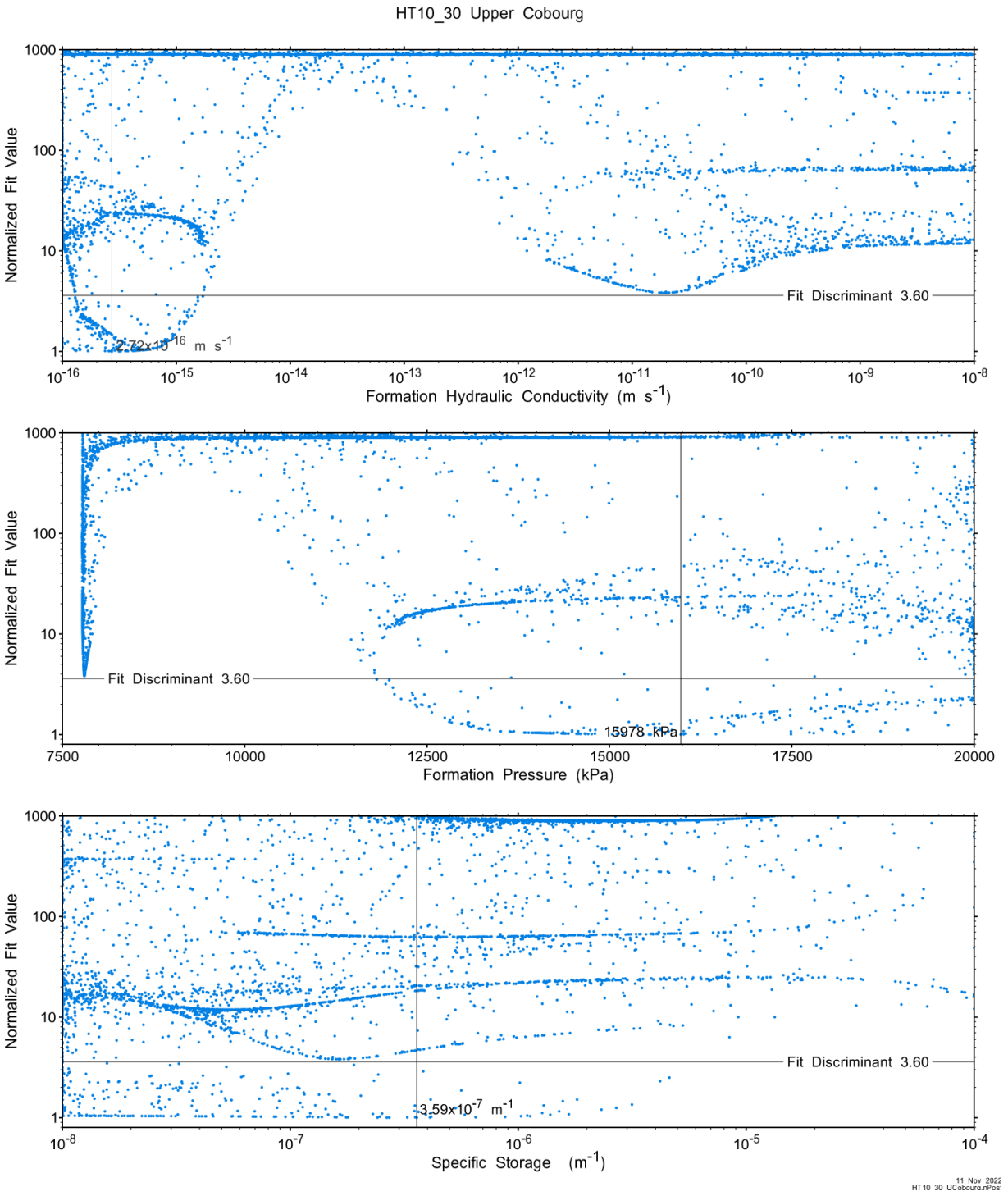

Figure A.236 - XY-scatter plot showing the formation parameter space normalized fit values.

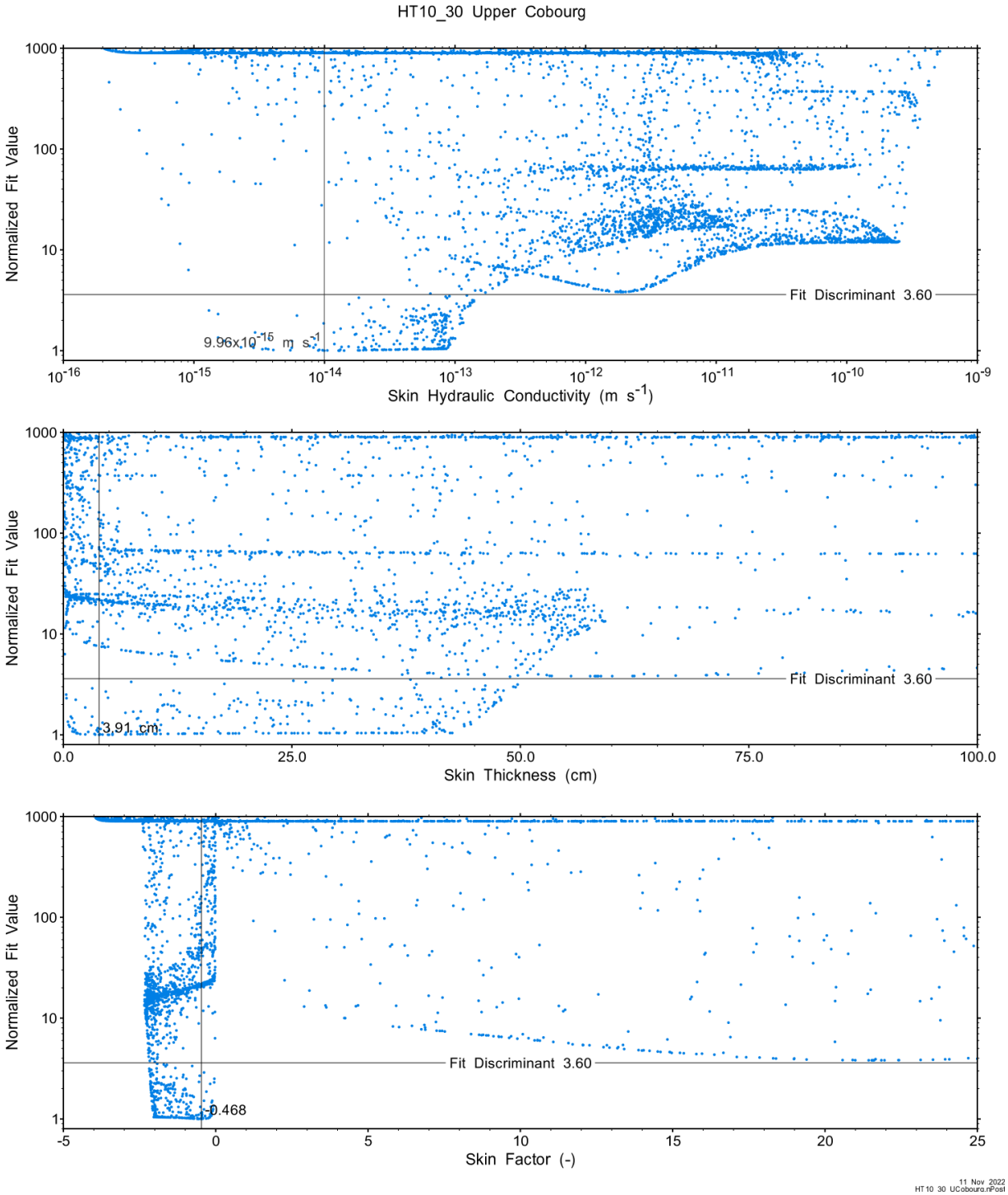

Figure A.237 - XY-scatter plot showing the skin parameter space normalized fit values.

A.16 HT11_30 Lower Cobourg

The SB BH02 interval from 686.00 to 715.96 mBGS tested in HT11_30 covers approximately the lower 65% of the Cobourg Formation. A single PI test of two days duration was conducted.

A.16.1 Test Data Summary

Table A.6 and Figure A.1 provide a summary of test events and a plot of pressures measured while testing respectively.

Table A.76 - Summary of Test Events.

Event	Start Date & Time	Duration (days)	TZ Pressure (kPa)
Drilling intercept	22-03-13 21:53	146.66	7114
Shut-in	22-08-07 13:49	0.79	7262
Pulse injection	22-08-08 08:40	2.00	8743
Test end	22-08-10 08:42		8445

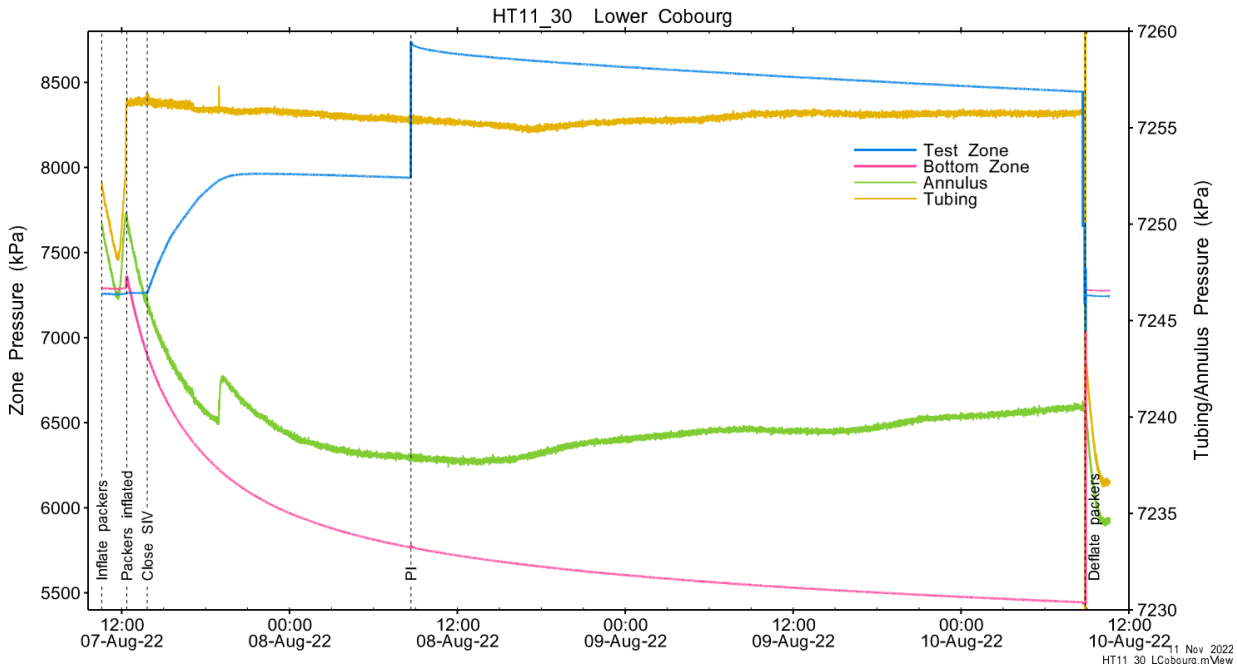

Figure A.238 - Test events and pressures.

A.16.2 Test Analyses

Table A.7 is a summary of test-specific input parameters used in the analyses, while Table A.8 presents the optimized parameters and allowed ranges.

Table A.77 – nSIGHTS Input Parameters.

Parameter	Value	Units
Test zone radius	6.33	cm
Test zone compressibility	3.43E-10	1/Pa
Test zone length	29.96	m

Table A.78 – nSIGHTS Parameter Optimization Ranges.

Parameter	Minimum	Maximum	Units	Type
Formation hydraulic conductivity (K_f)	1E-16	1E-08	m/s	log
Formation pressure (P_f)	0	12000	kPa	linear
Specific storage (S_s)	1E-08	1E-04	1/m	log
Skin hydraulic conductivity (K_s)	1E-16	1E-08	m/s	log
Skin thickness (t_s)	0.013	500	cm	linear

Figure A.18 shows the measured test zone pressure record (with reduced data density for clarity) used in the analysis along with the best-fit simulation and parameter values. Figure A.19 presents the pre-test history, and Figure A.20 shows the Ramey B normalized best-fit pressure and pressure derivatives.

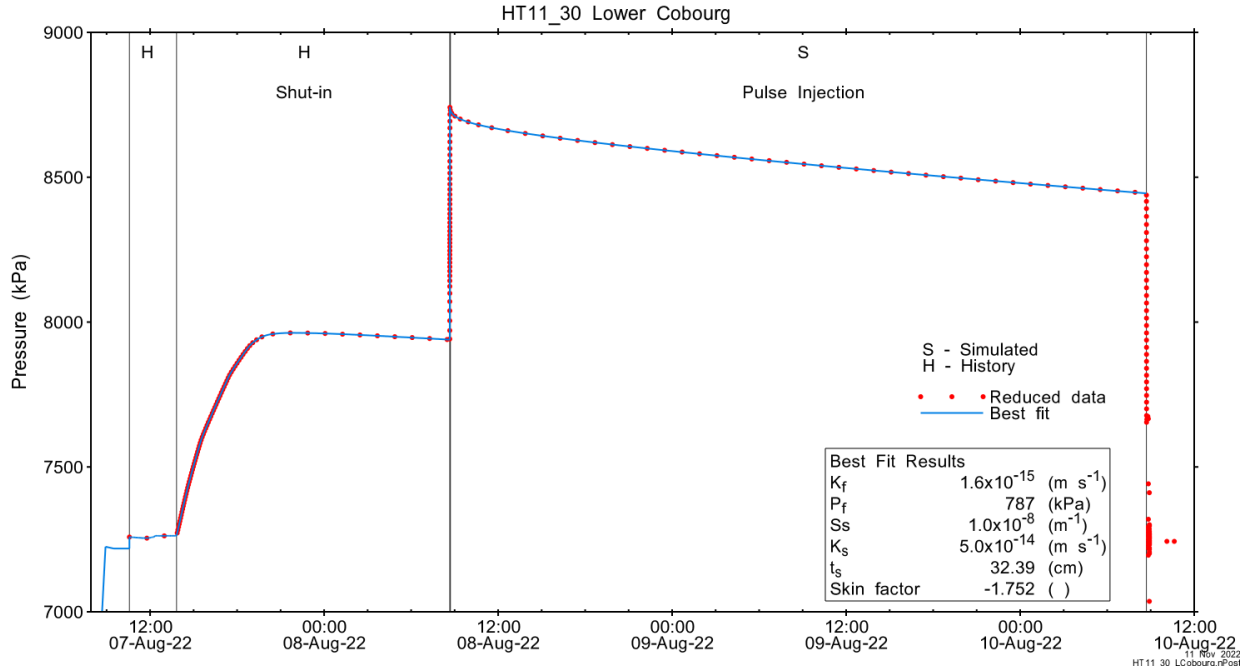

Figure A.239 - Annotated testing sequence showing best-fit simulation and parameter estimates.

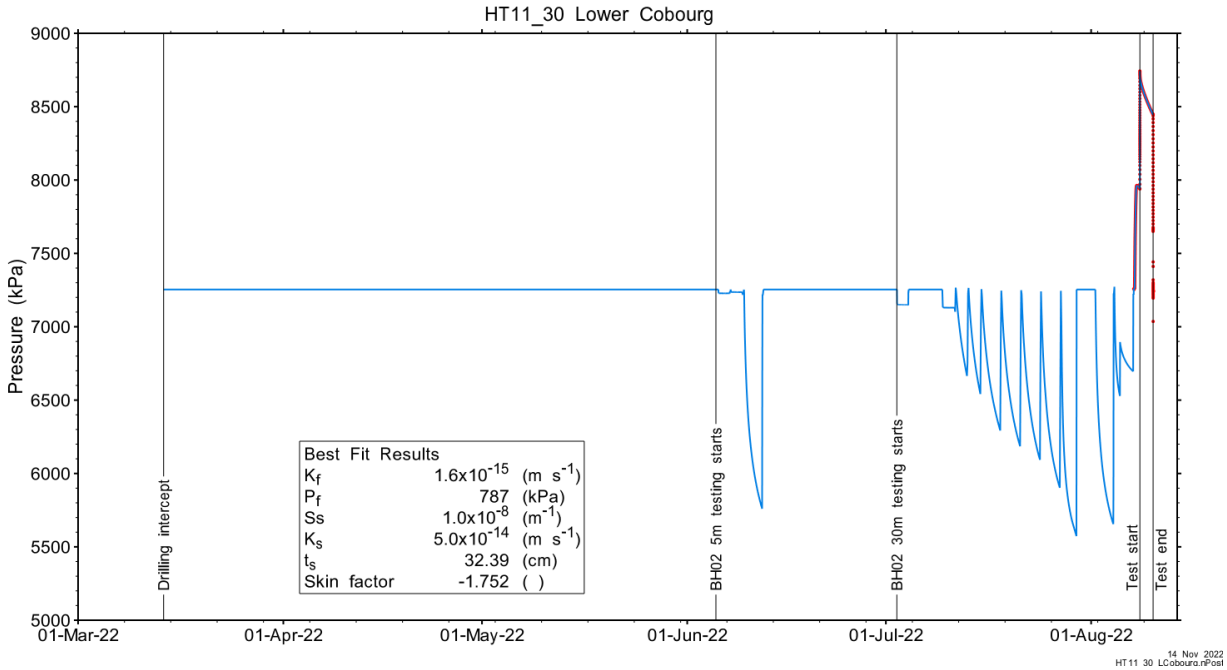

Figure A.240 - Annotated testing sequence showing pre-test history, best-fit simulation and parameter estimates.

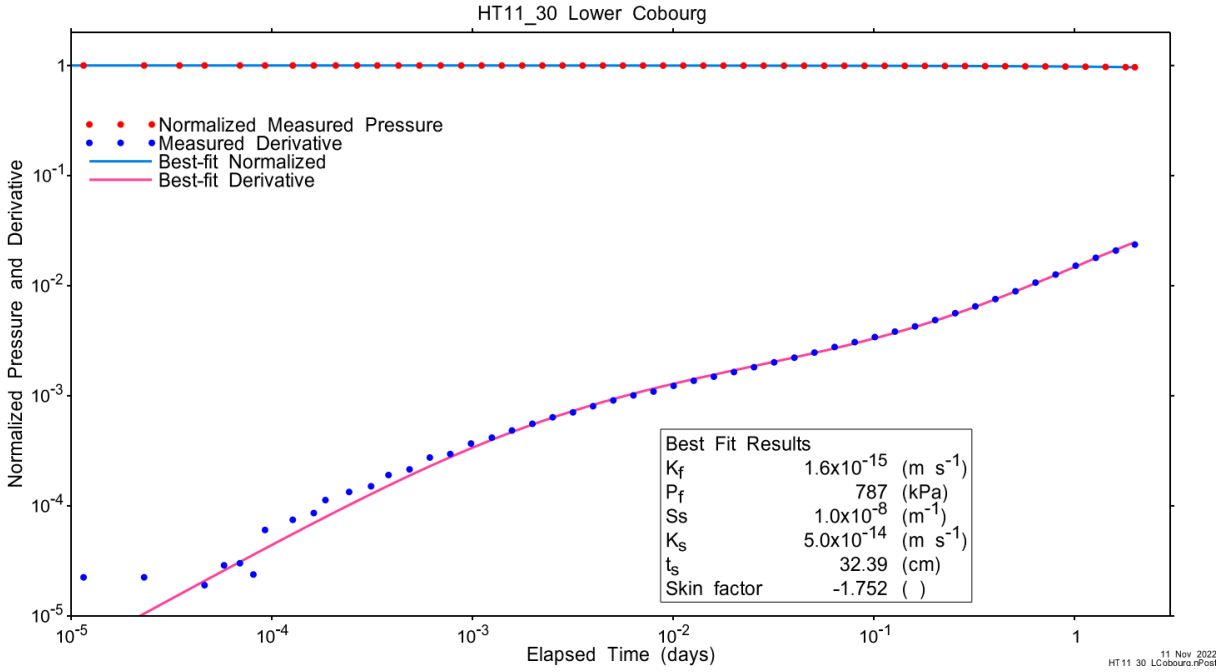

Figure A.241 - Log-log plot showing Ramey B and derivative response for best-fit simulation.

Figure A.21 shows the normalized parameter sensitivity response for the best fit. Sensitivity for most fitting parameters is increasing at the end of the test, indicating that increased test duration may have yielded more precise results.

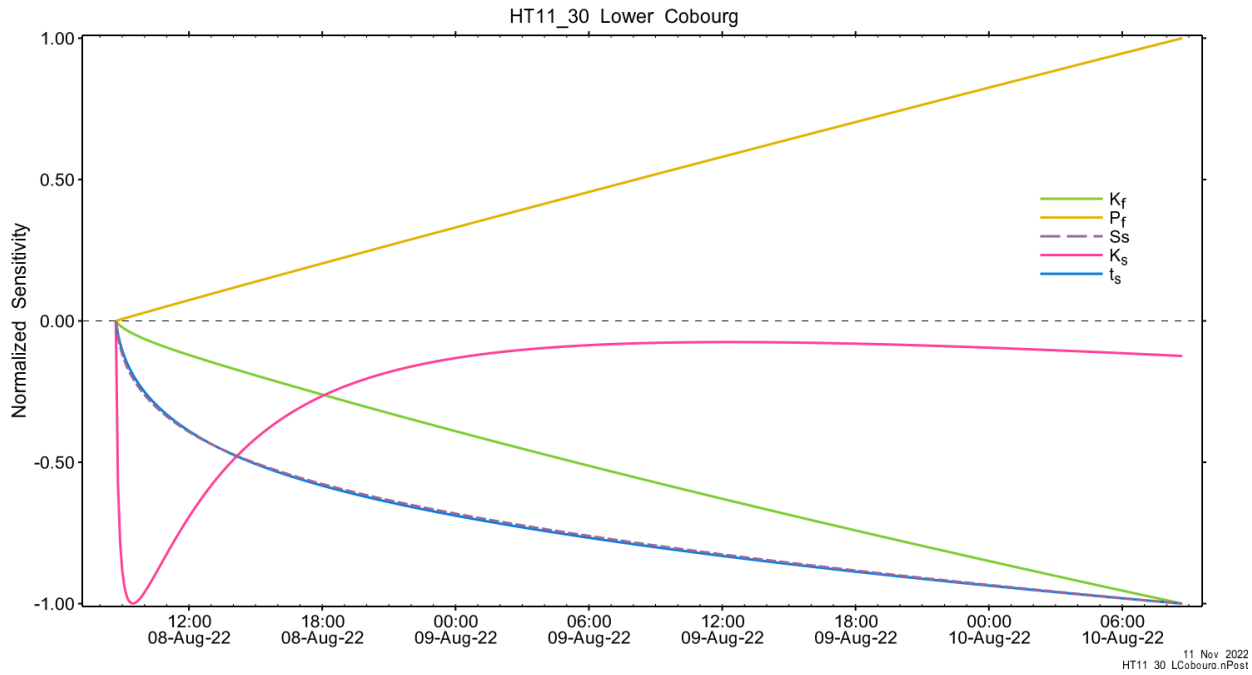

Figure A.242 - Normalized Jacobian for best-fit simulation.

A.16.3 Uncertainty Analyses

The CDF of normalized fit values for all converged simulations and the selected fit discriminant are shown in Figure A.22.

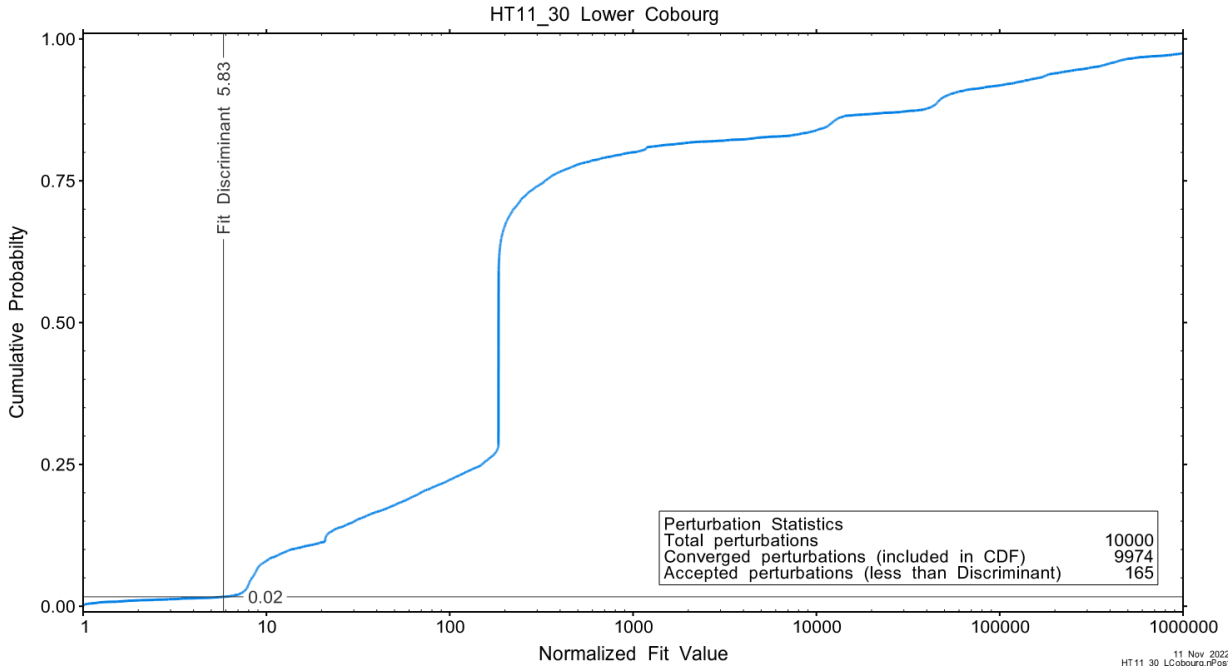

Figure A.243 - Fit value cumulative distribution function.

Summary cross parameter scatter plots for selected formation and skin parameters are given in Figure A.24 and Figure A.25. The light pink dots on the figures are the initial parameter estimates, with red dots overlaying those initial parameter values that resulted in accepted optimization results. The grey dots are converged optimizations which did not meet the fit discriminant. Larger varying color symbols represent the fit value of accepted optimizations, with the blue values representing the best fit.

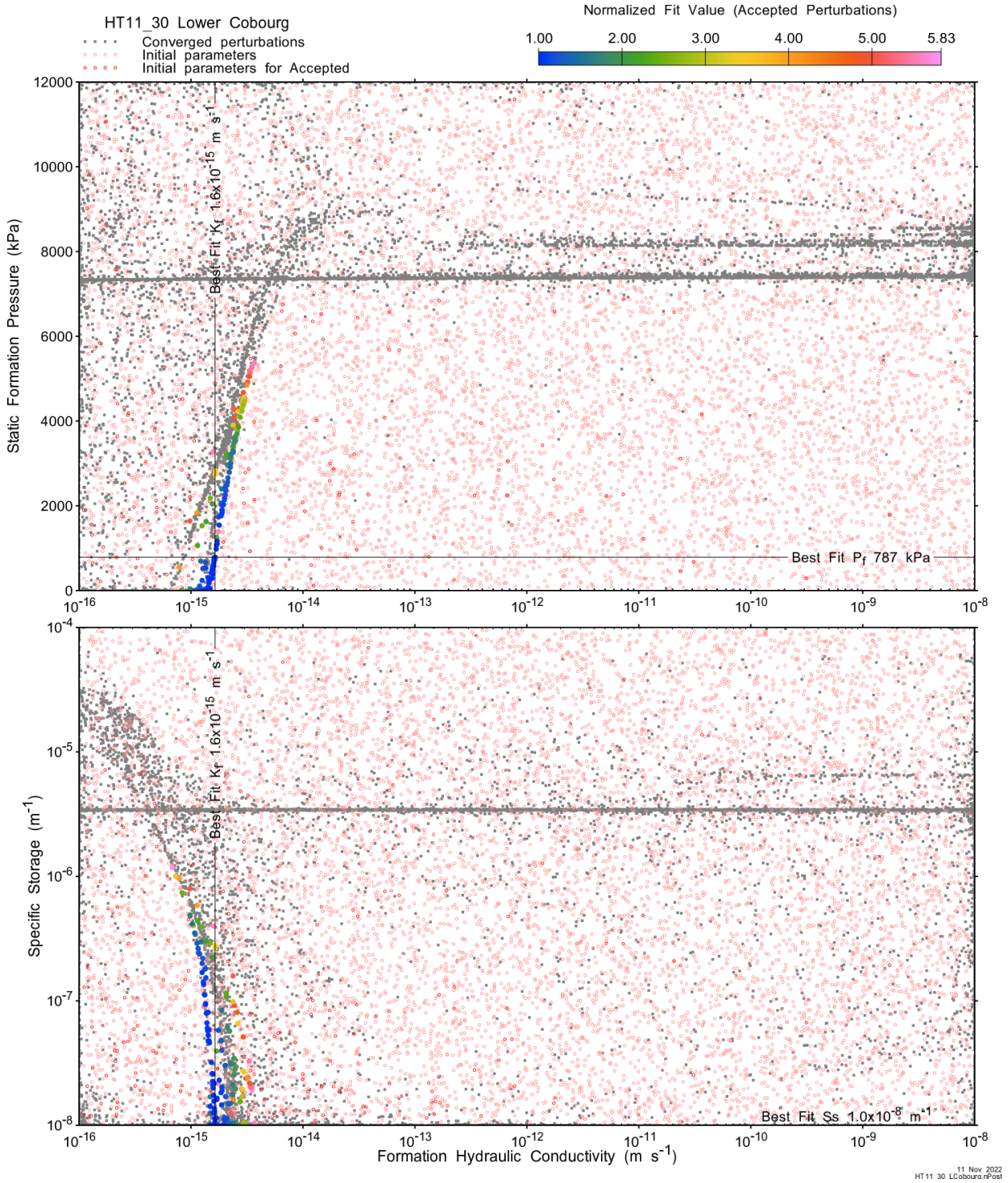

Figure A.244 - XY-scatter plot showing estimates of formation hydraulic conductivity (K_f) vs static formation pressure (P_f) (top panel) and specific storage (Ss) (bottom panel).

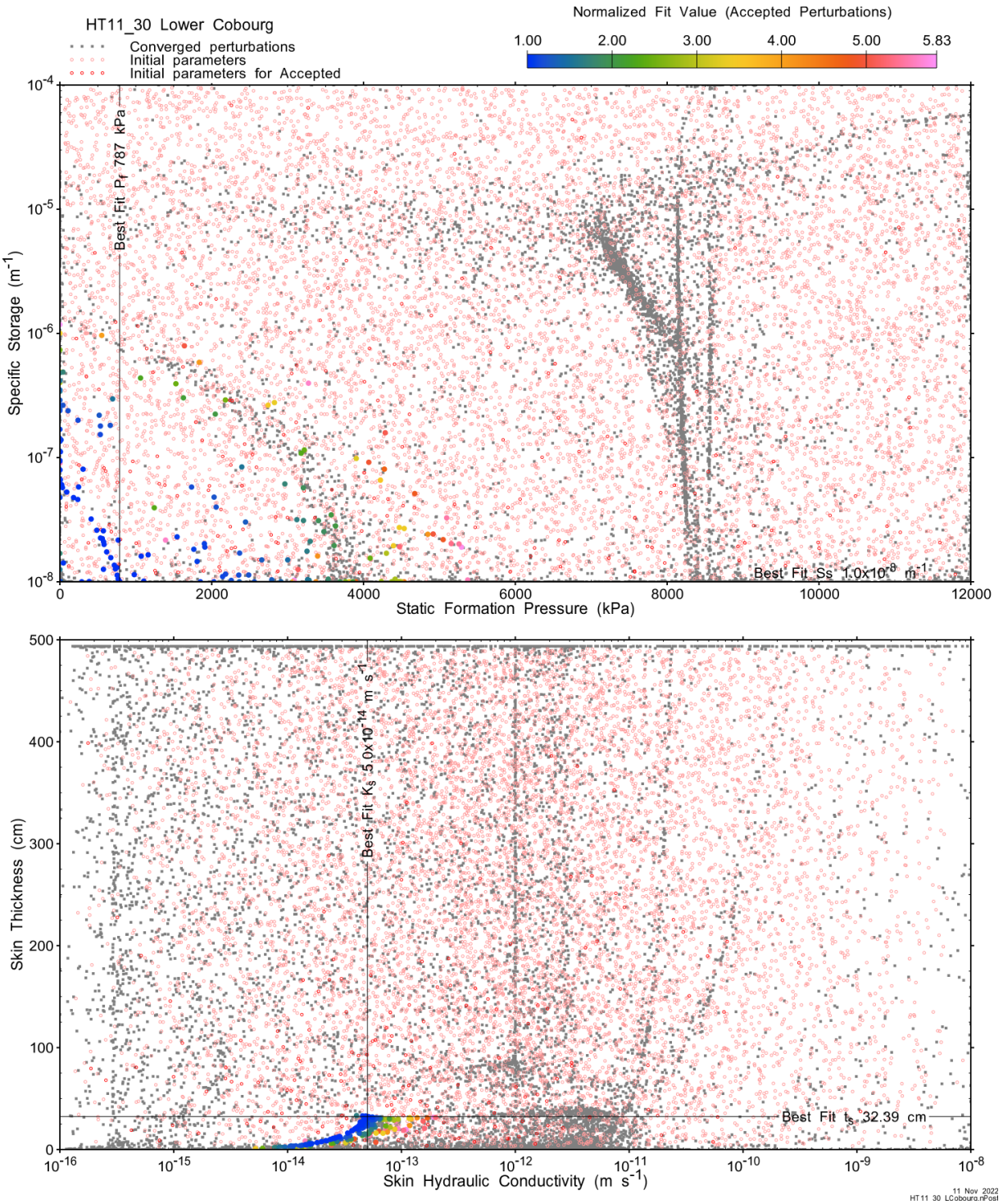

Figure A.245 - XY-scatter plot showing estimates of static formation pressure (P_f) vs specific storage (Ss) (top panel) and skin hydraulic conductivity (K_s) vs skin thickness (t_s) (bottom panel).

Confidence limits and median values are determined from the CDF of accepted optimization results (i.e. the varying color values in the above figures), with best fit value, 5% and 95% confidence indicated on Figure A.26 and Figure A.27.

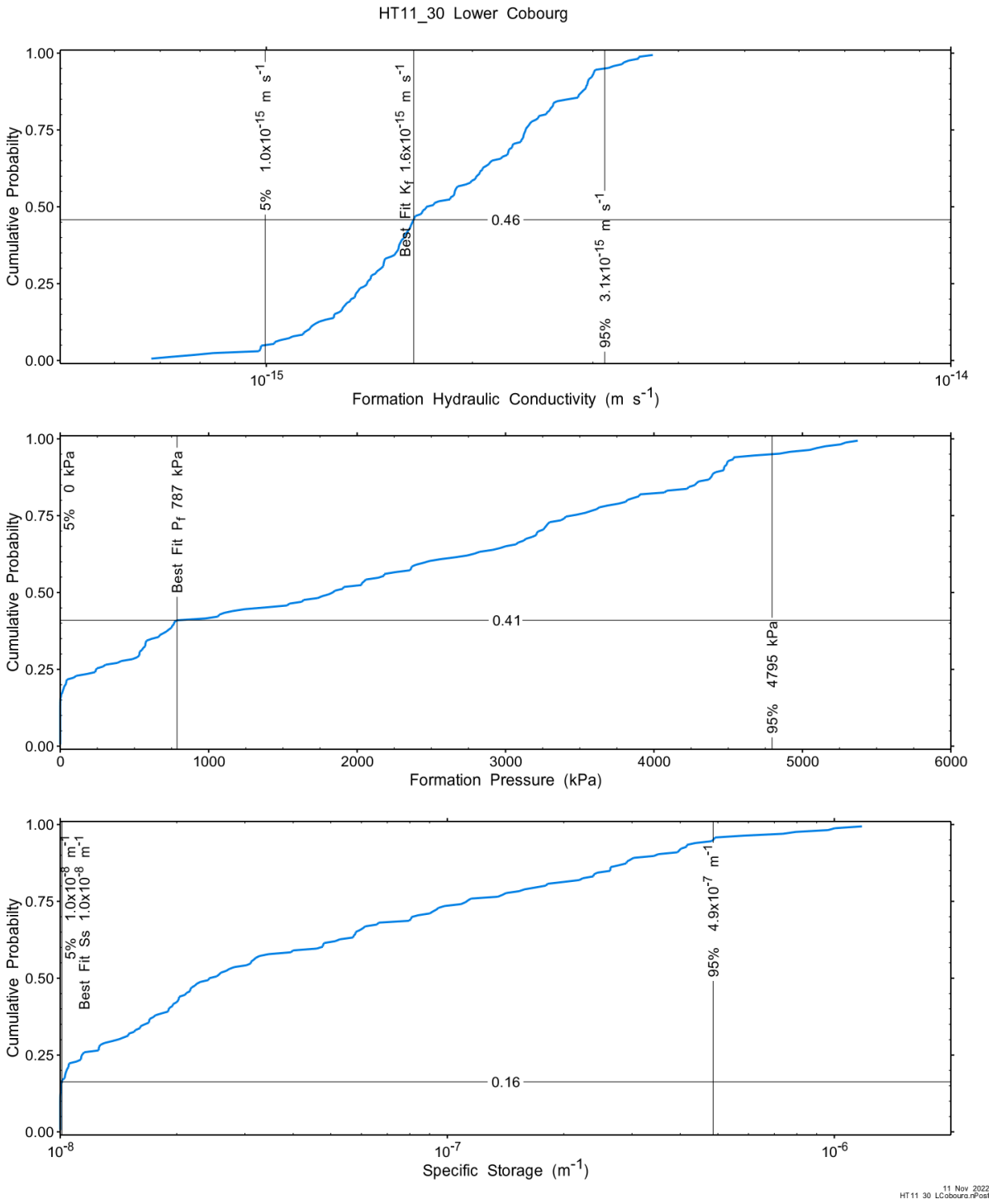

Figure A.246 – Cumulative distribution functions and parameter limits for formation hydraulic conductivity (K_f) (top panel), static formation pressure (P_f) (middle panel) and specific storage (Ss) (bottom panel).

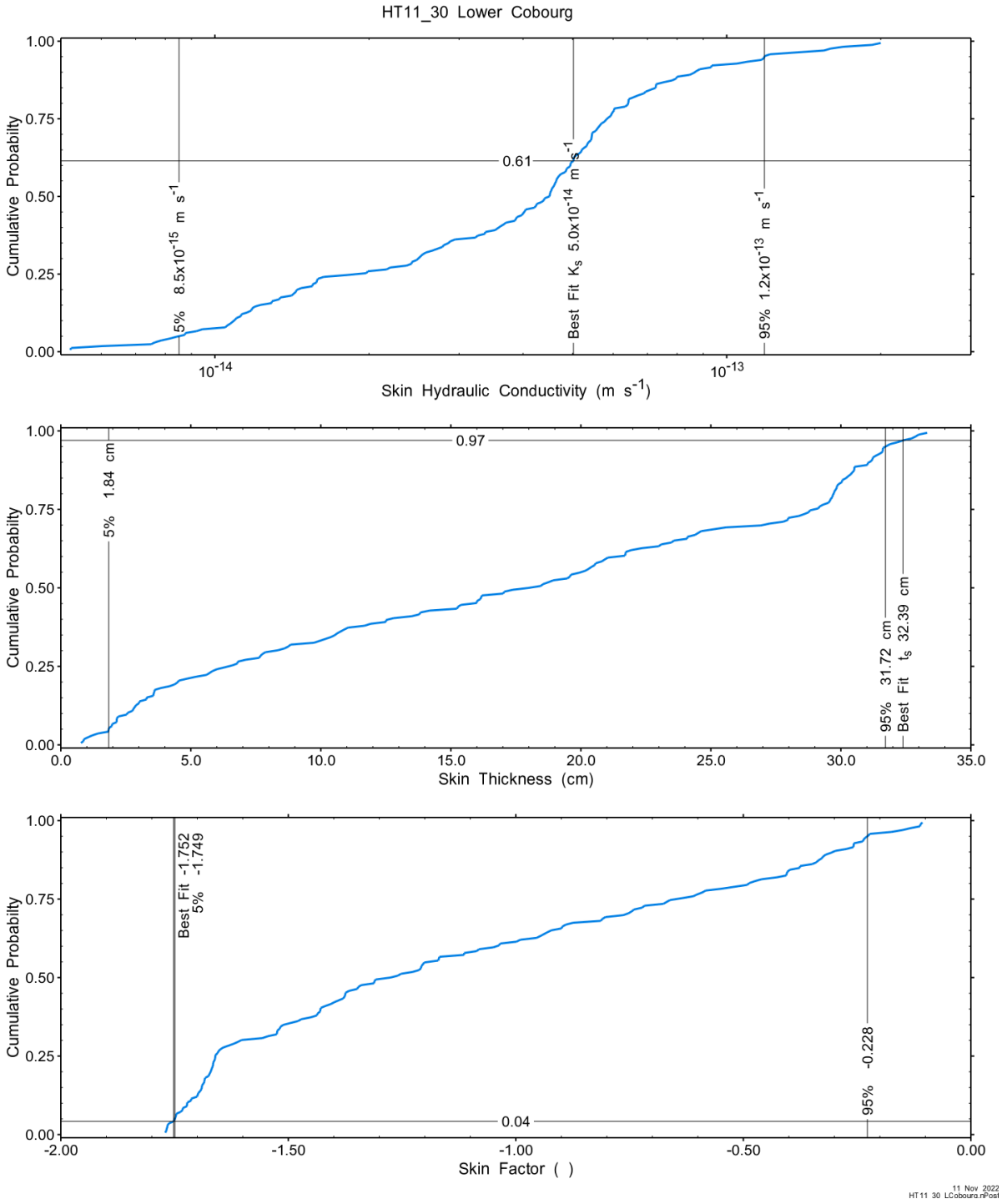

Figure A.247 – Cumulative distribution functions and parameter limits for skin hydraulic conductivity (K_s) (top panel), skin thickness (t_s) (middle panel) and skin factor (s) (bottom panel).

A summary of perturbation results is presented in Figure A.28, with Ramey-processed perturbations in Figure A.249. Those perturbations (121 of 10,000) with all parameters within the 5% and 95% range present a good fit to the measured test zone data.

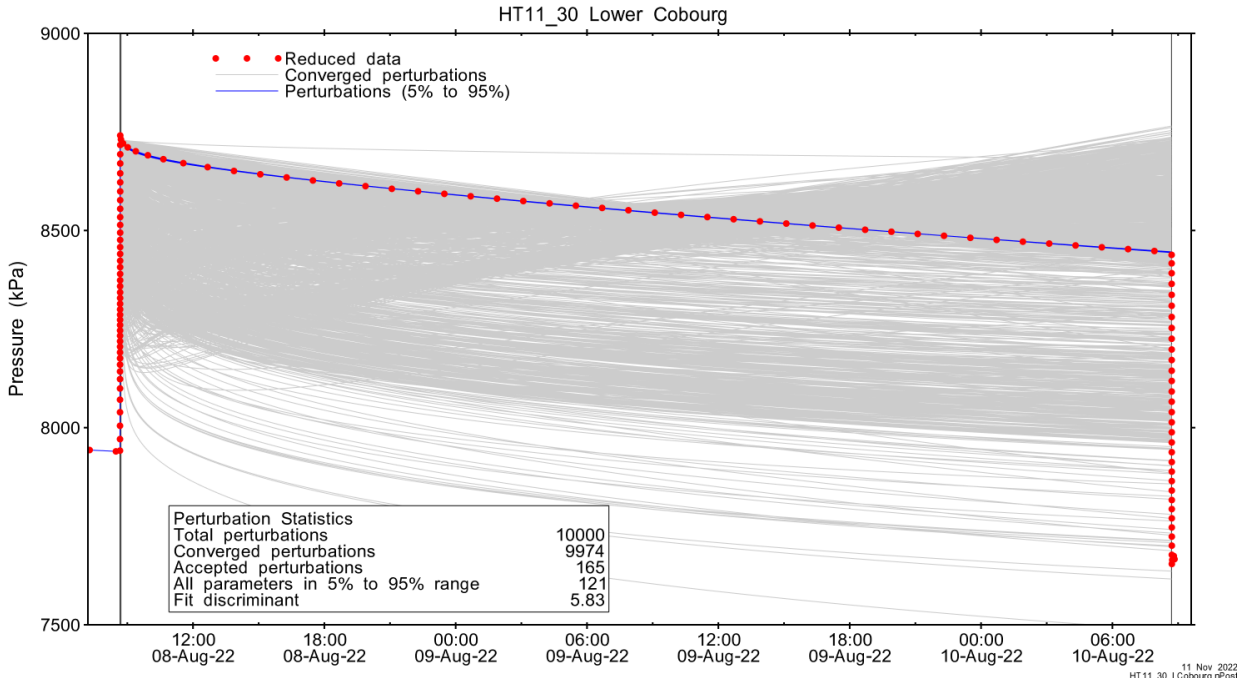

Figure A.248 – Perturbation results – all converged, accepted, and within 5% to 95% for all parameters.

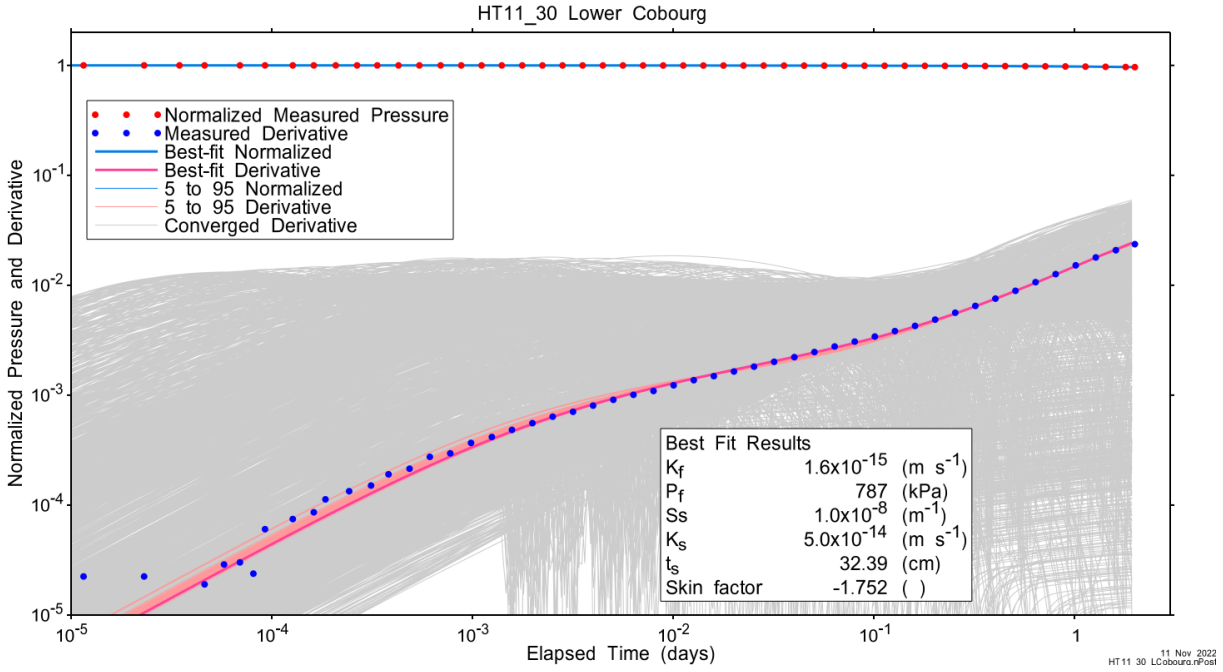

Figure A.249 – Log-log plot showing Ramey B and derivative response for all converged optimizations and those within 5% to 95% for all parameters.

A summary of best-fit and parameter ranges is given in Table A.9.

Table A.79 - Summary of the HT11_30 parameter estimates.

Parameter	Best Fit	5%	Median	95%
K_f (m/s)	1.6E-15	1.0E-15	1.7E-15	3.1E-15
P_f (kPa)	787	0	1836	4795
Ss (1/m)	1.0E-08	1.0E-08	2.4E-08	4.9E-07
K_s (m/s)	5.0E-14	8.5E-15	4.5E-14	1.2E-13
t_s (cm)	32.39	1.84	18.00	31.72
s (-)	-1.752	-1.749	-1.276	-0.228

Parameter correlations for all perturbations with all parameters within the 5% to 95% limits are given in Table A.5.

Table A.80 – Pearson cross-correlations of 5% to 95% parameters

	Log(K_f)	P_f	Log(Ss)	Log(K_s)	t_s	s
Log(K_f)	1.000	-0.978	-0.187	0.292	0.074	-0.096
Pf	-0.978	1.000	0.108	-0.196	-0.011	0.020
Log(S_s)	-0.187	0.108	1.000	-0.978	-0.958	0.994
Log(K_s)	0.292	-0.196	-0.978	1.000	0.891	-0.955
t_s	0.074	-0.011	-0.958	0.891	1.000	-0.976
s	-0.096	0.020	0.994	-0.955	-0.976	1.000

A.16.4 Additional Figures

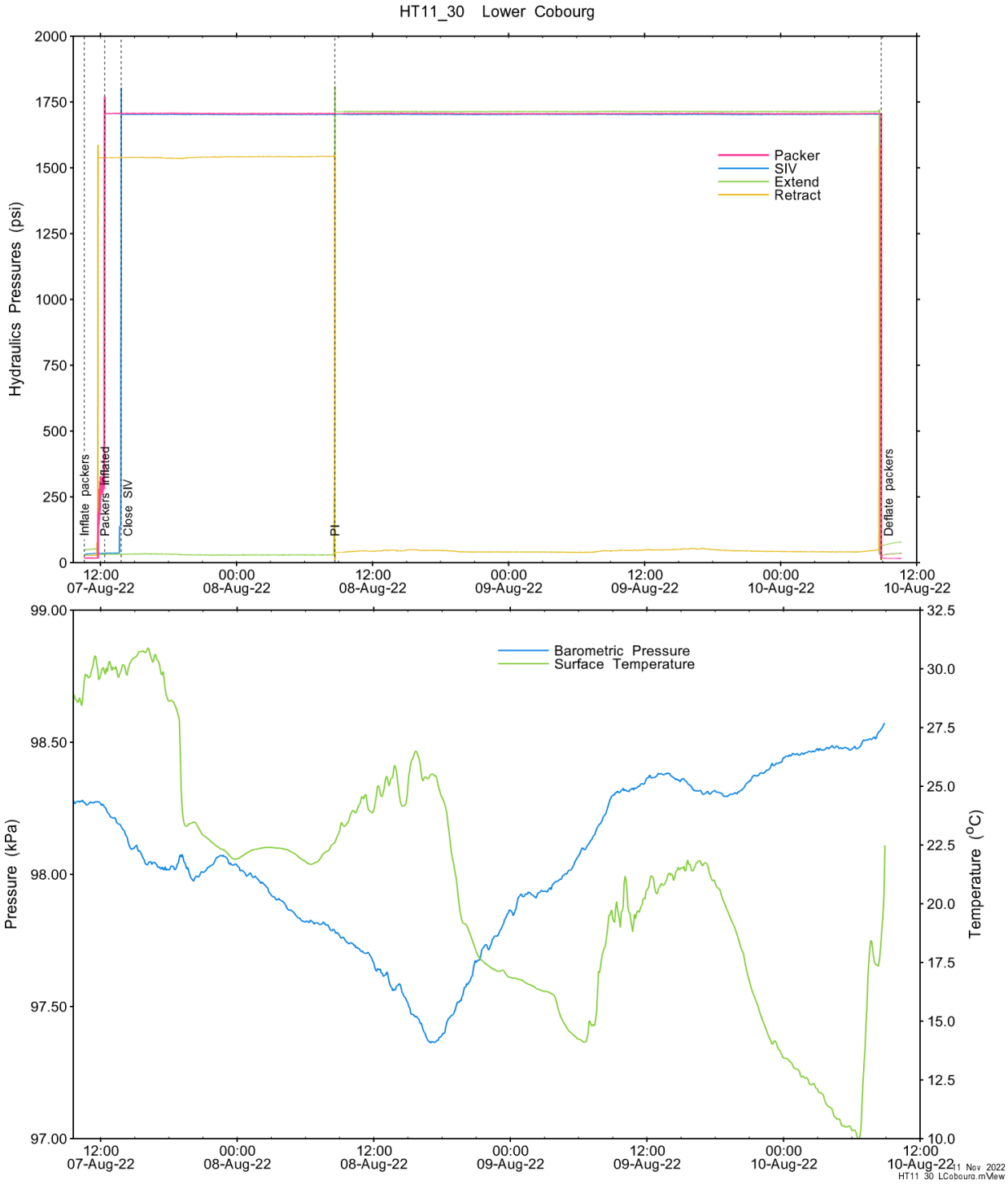

Figure A.250 - Hydraulics pressures and surface temperature/barometric pressure.

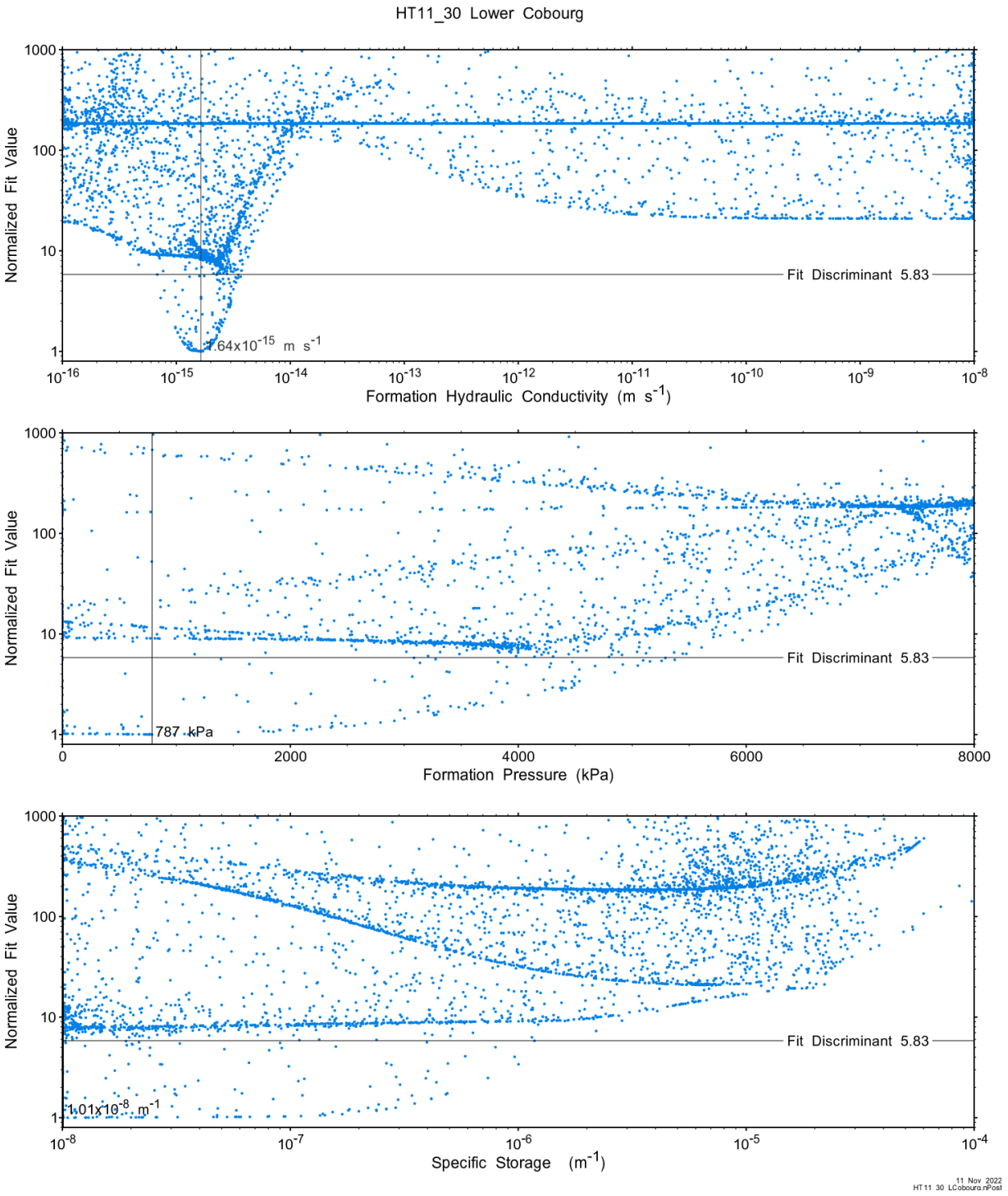

Figure A.251 - XY-scatter plot showing the formation parameter space normalized fit values.

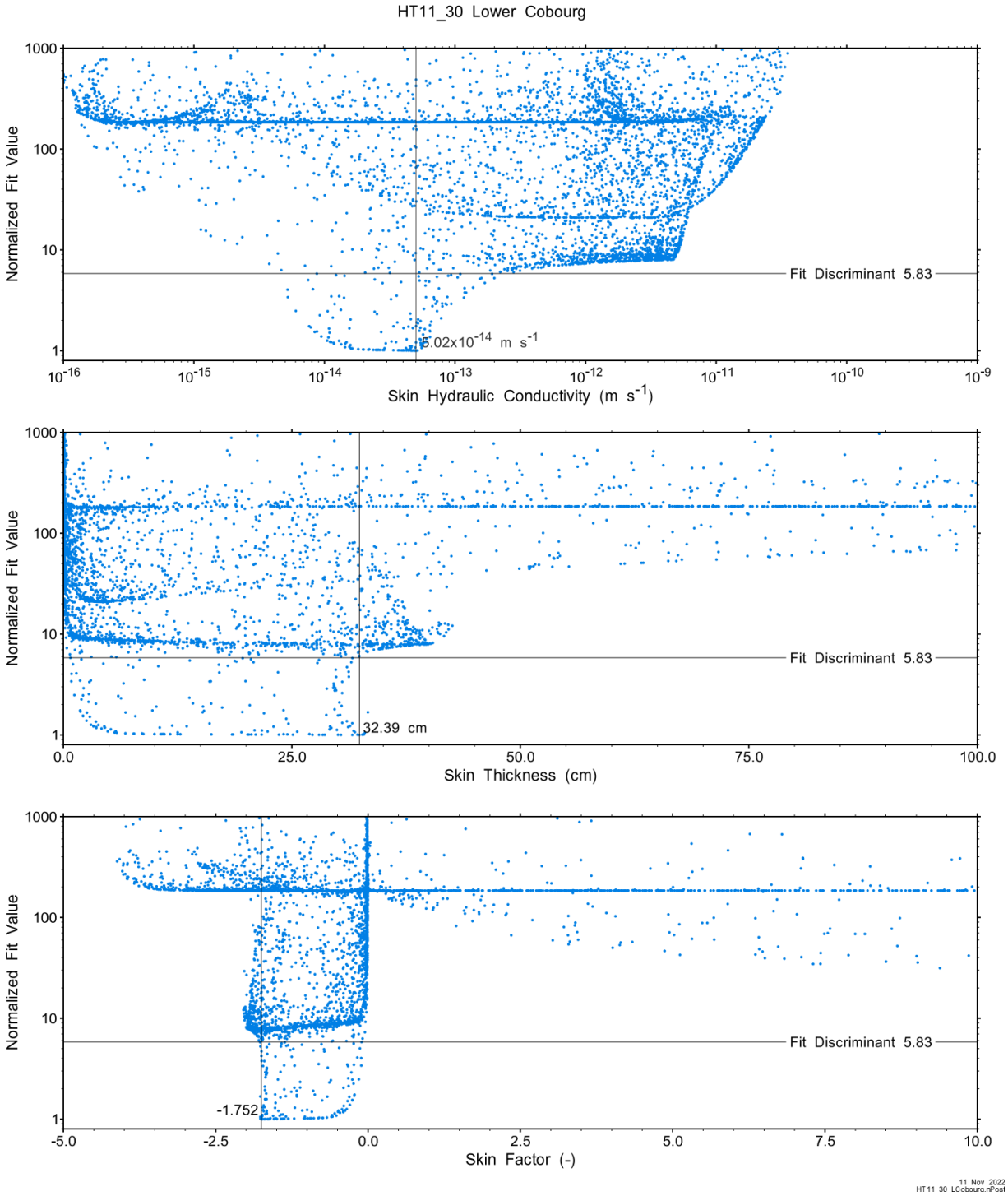

Figure A.252 - XY-scatter plot showing the skin parameter space normalized fit values.

A.17 HT12_30 Sherman Fall

The SB BH02 interval from 725.00 to 754.96 mBGS tested in HT12_30 covers the majority of the Sherman Fall Formation. A single PI test of two days duration was conducted.

A.17.1 Test Data Summary

Table A.6 and Figure A.1 provide a summary of test events and a plot of pressures measured while testing respectively.

Table A.81 - Summary of Test Events.

Event	Start Date & Time	Duration (days)	TZ Pressure (kPa)
Drilling intercept	22-03-14 22:11	148.64	7702
Shut-in	22-08-10 13:32	0.80	7709
Pulse injection	22-08-11 08:41	2.00	8239
Test end	22-08-13 08:47		7867

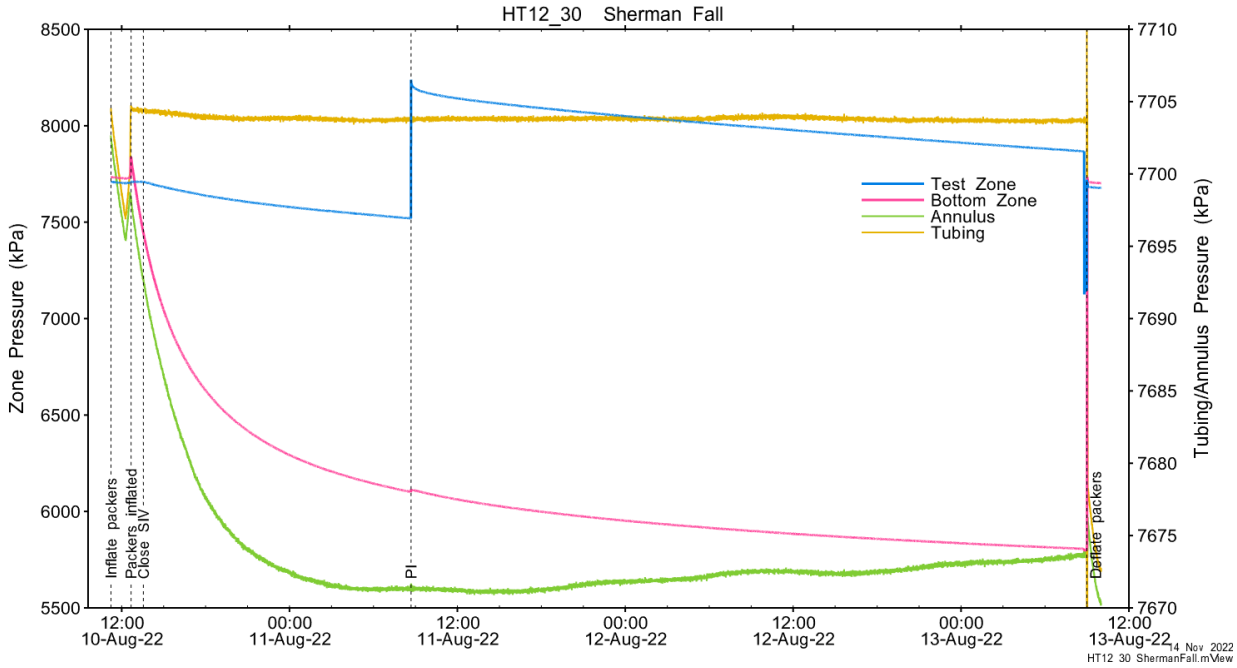

Figure A.253 - Test events and pressures.

A.17.2 Test Analyses

Table A.7 is a summary of test-specific input parameters used in the analyses, while Table A.8 presents the optimized parameters and allowed ranges.

Table A.82 – nSIGHTS Input Parameters.

Parameter	Value	Units
Test zone radius	6.33	cm
Test zone compressibility	3.82E-10	1/Pa
Test zone length	29.96	m

Table A.83 – nSIGHTS Parameter Optimization Ranges.

Parameter	Minimum	Maximum	Units	Type
Formation hydraulic conductivity (K_f)	1E-16	1E-08	m/s	log
Formation pressure (P_f)	0	8000	kPa	linear
Specific storage (S_s)	1E-08	1E-04	1/m	log
Skin hydraulic conductivity (K_s)	1E-16	1E-08	m/s	log
Skin thickness (t_s)	0.013	500	cm	linear

Figure A.18 shows the measured test zone pressure record (with reduced data density for clarity) used in the analysis along with the best-fit simulation and parameter values. Figure A.19 presents the pre-test history, and Figure A.20 shows the Ramey B normalized best-fit pressure and pressure derivatives.

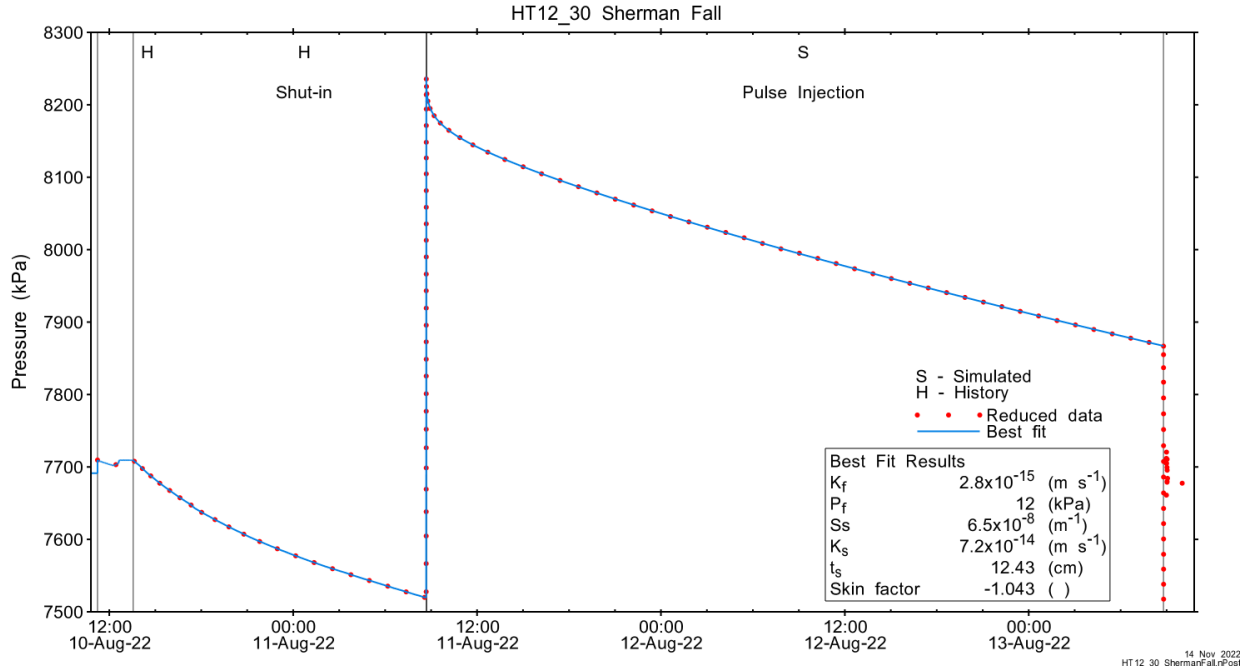

Figure A.254 - Annotated testing sequence showing best-fit simulation and parameter estimates.

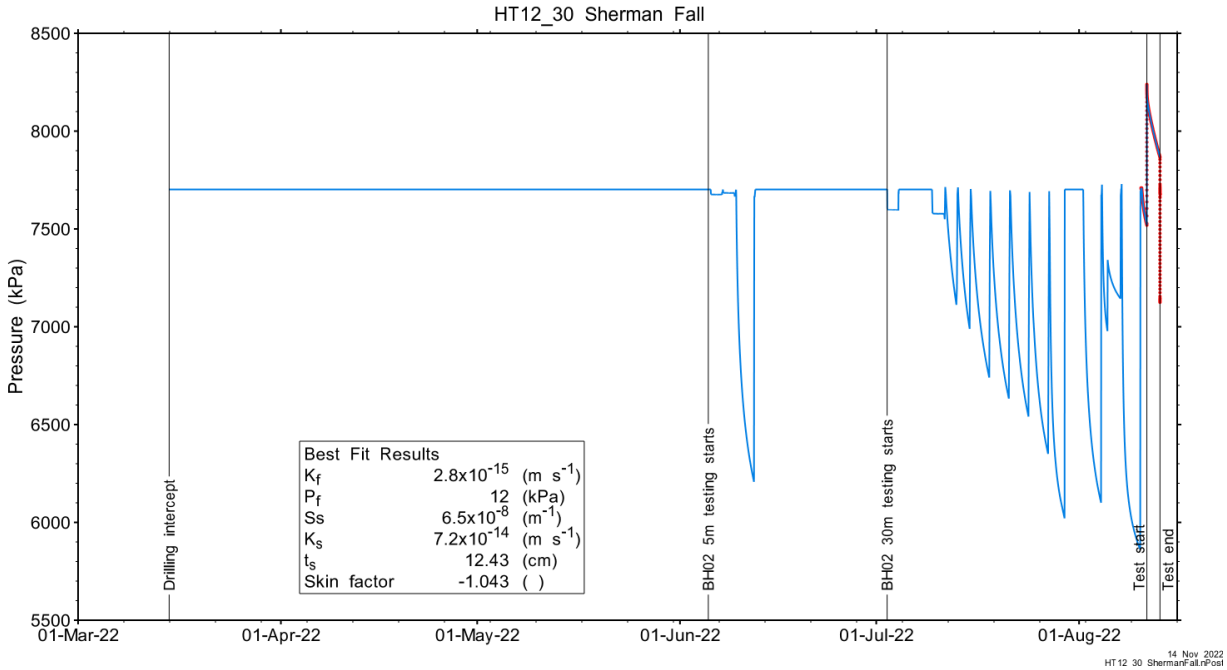

Figure A.255 - Annotated testing sequence showing pre-test history, best-fit simulation and parameter estimates.

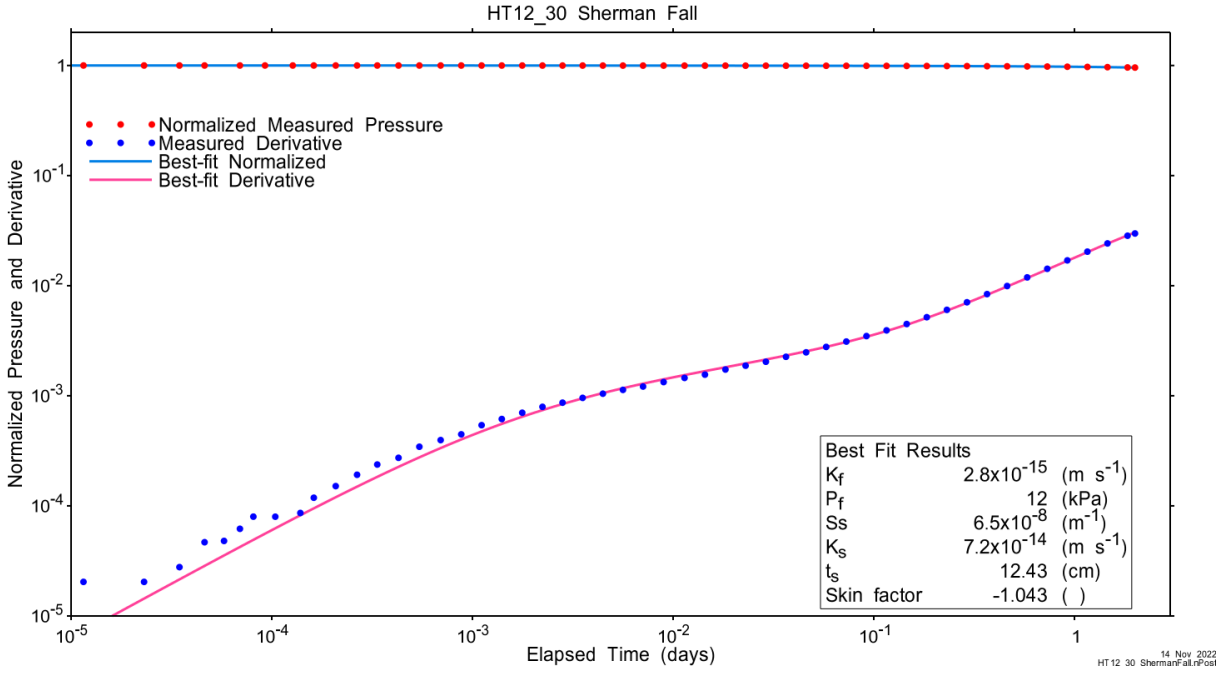

Figure A.256 - Log-log plot showing Ramey B and derivative response for best-fit simulation.

Figure A.21 shows the normalized parameter sensitivity response for the best fit. Sensitivity for most fitting parameters is increasing at the end of the test, indicating that increased test duration may have yielded more precise results.

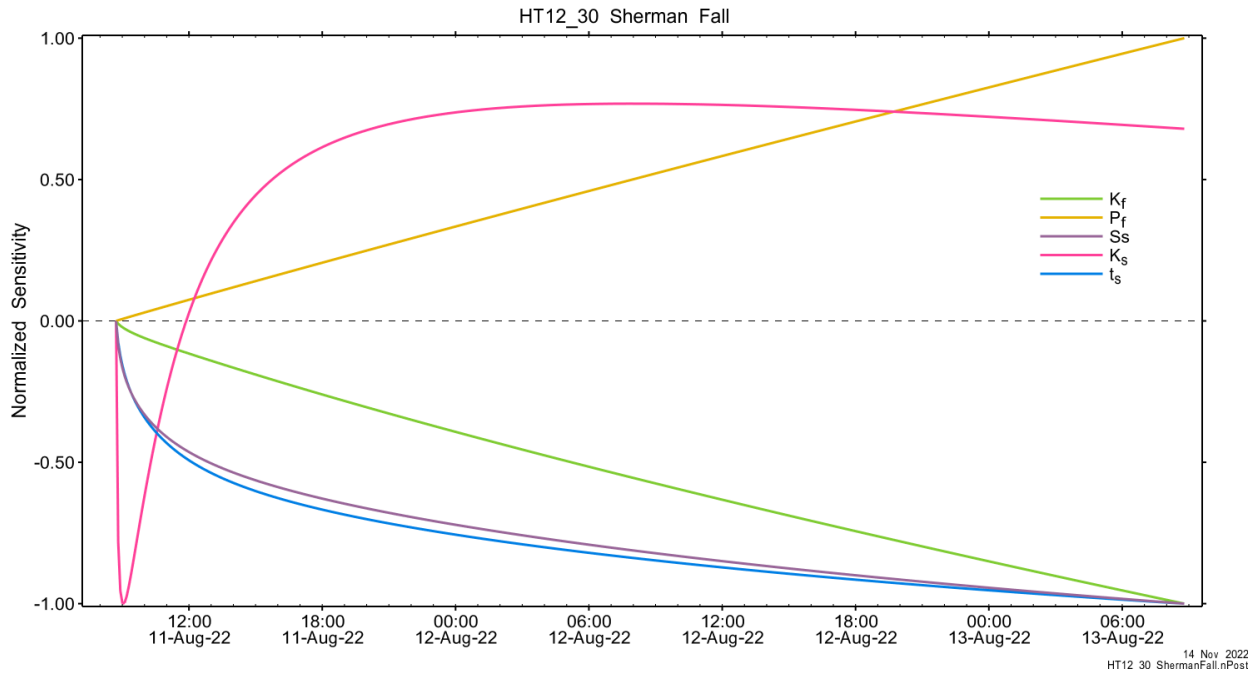

Figure A.257 - Normalized Jacobian for best-fit simulation.

A.17.3 Uncertainty Analyses

The CDF of normalized fit values for all converged simulations and the selected fit discriminant are shown in Figure A.22. Initially, the fit discriminant was set somewhat higher, but was reduced to remove local minima and to include the global minimum only.

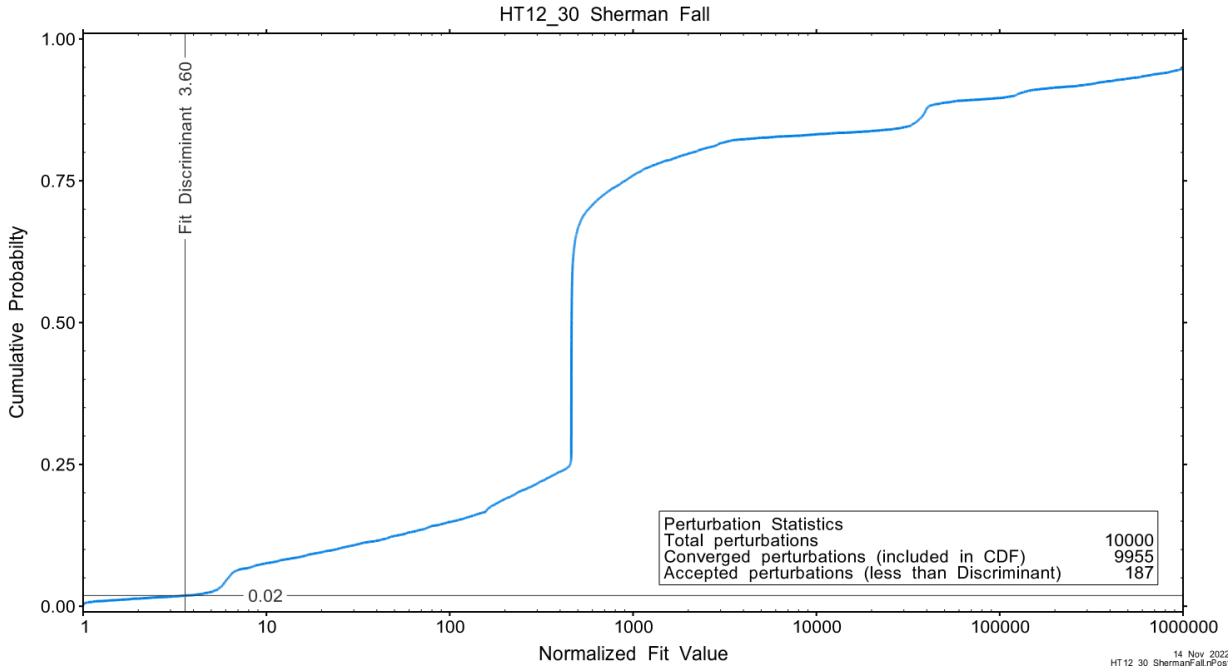

Figure A.258 - Fit value cumulative distribution function.

Summary cross parameter scatter plots for selected formation and skin parameters are given in Figure A.24 and Figure A.25. The light pink dots on the figures are the initial parameter estimates, with red dots overlaying those initial parameter values that resulted in accepted optimization results. The grey dots are converged optimizations which did not meet the fit discriminant. Larger varying color symbols represent the fit value of accepted optimizations, with the blue values representing the best fit.

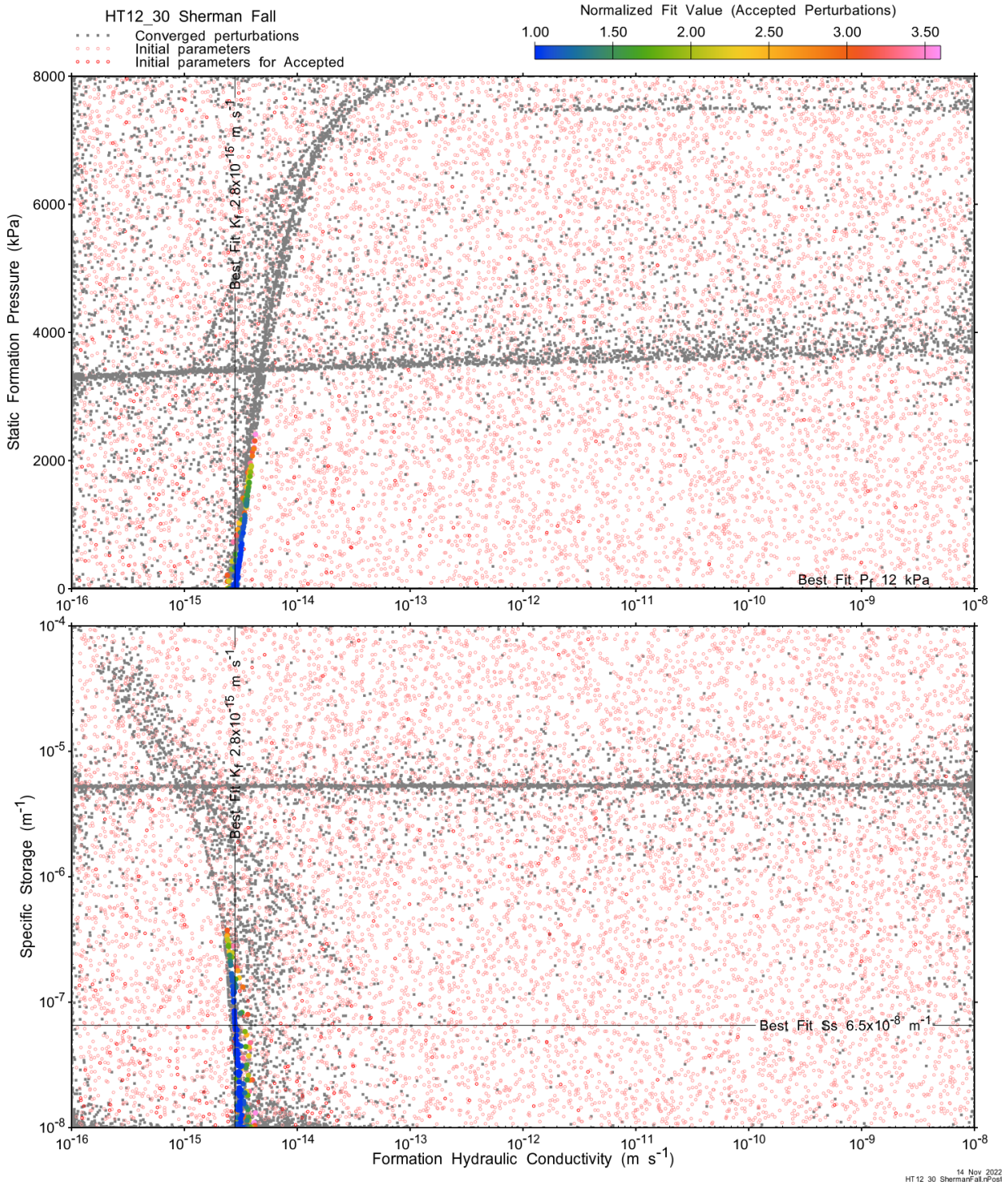

Figure A.259 - XY-scatter plot showing estimates of formation hydraulic conductivity (K_f) vs static formation pressure (P_f) (top panel) and specific storage (Ss) (bottom panel).

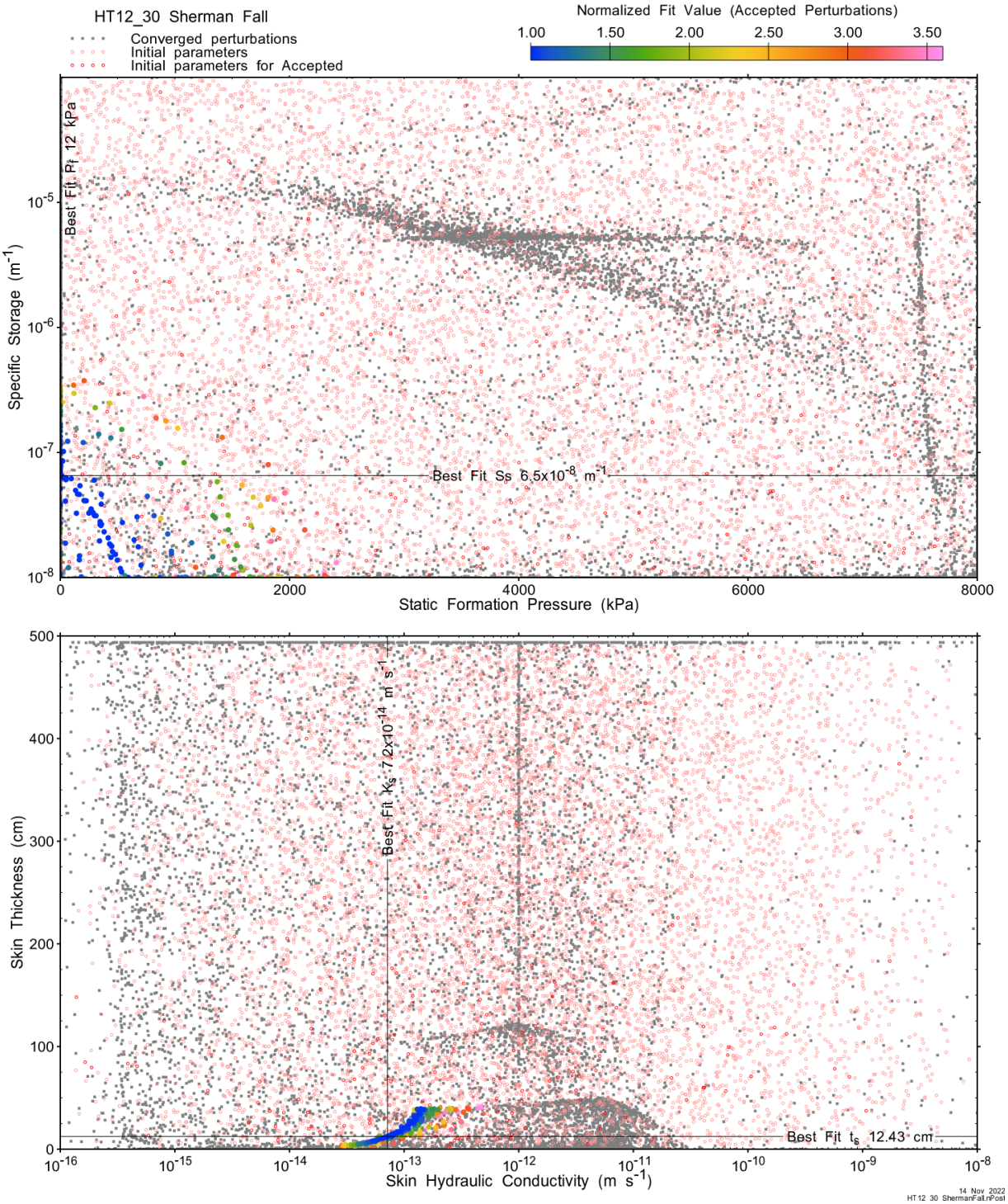

Figure A.260 - XY-scatter plot showing estimates of static formation pressure (P_f) vs specific storage (Ss) (top panel) and skin hydraulic conductivity (K_s) vs skin thickness (t_s) (bottom panel).

Confidence limits and median values are determined from the CDF of accepted optimization results (i.e. the varying color values in the above figures), with best fit value, 5% and 95% confidence indicated on Figure A.26 and Figure A.27.

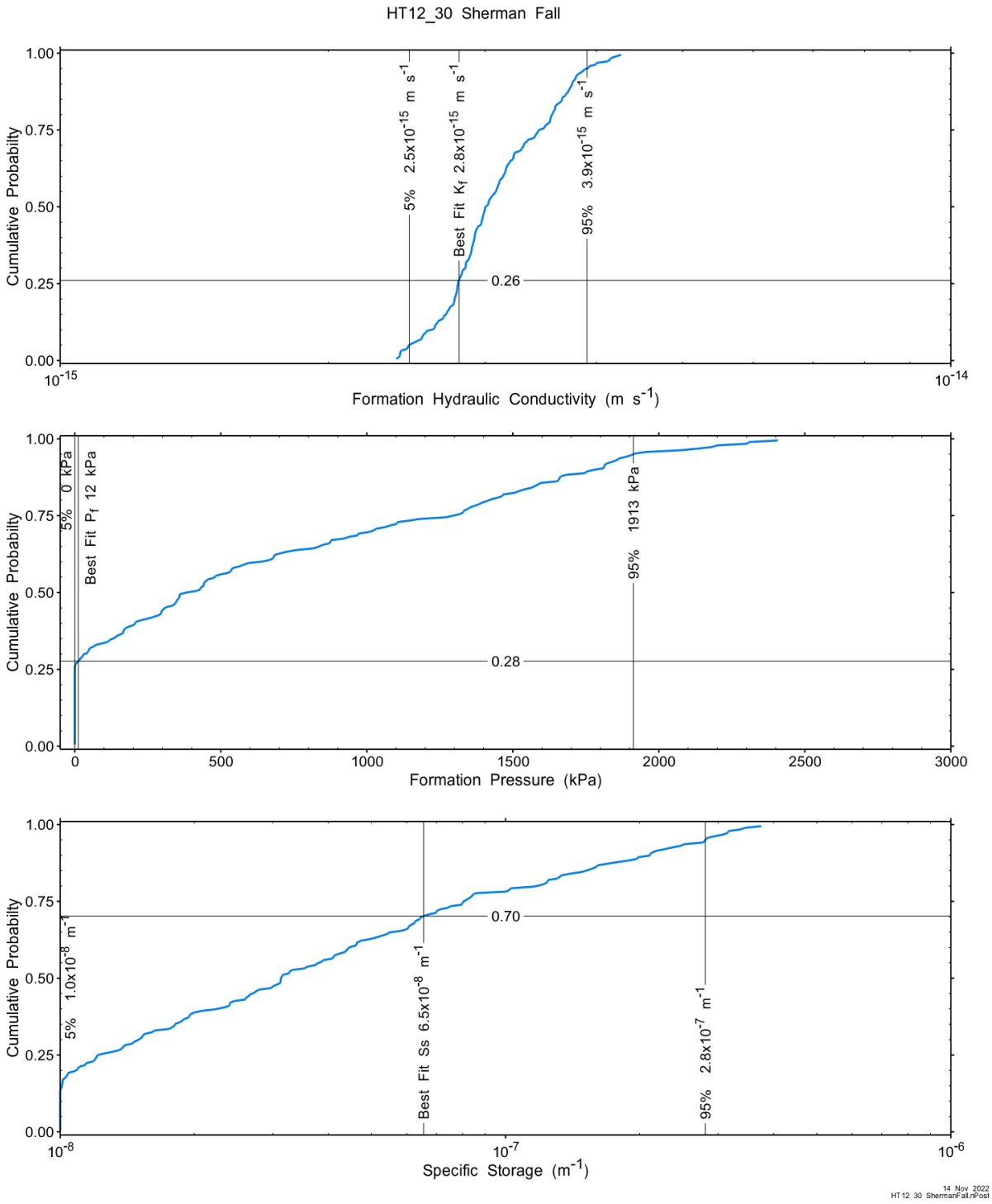

Figure A.261 – Cumulative distribution functions and parameter limits for formation hydraulic conductivity (K_f) (top panel), static formation pressure (P_f) (middle panel) and specific storage (Ss) (bottom panel).

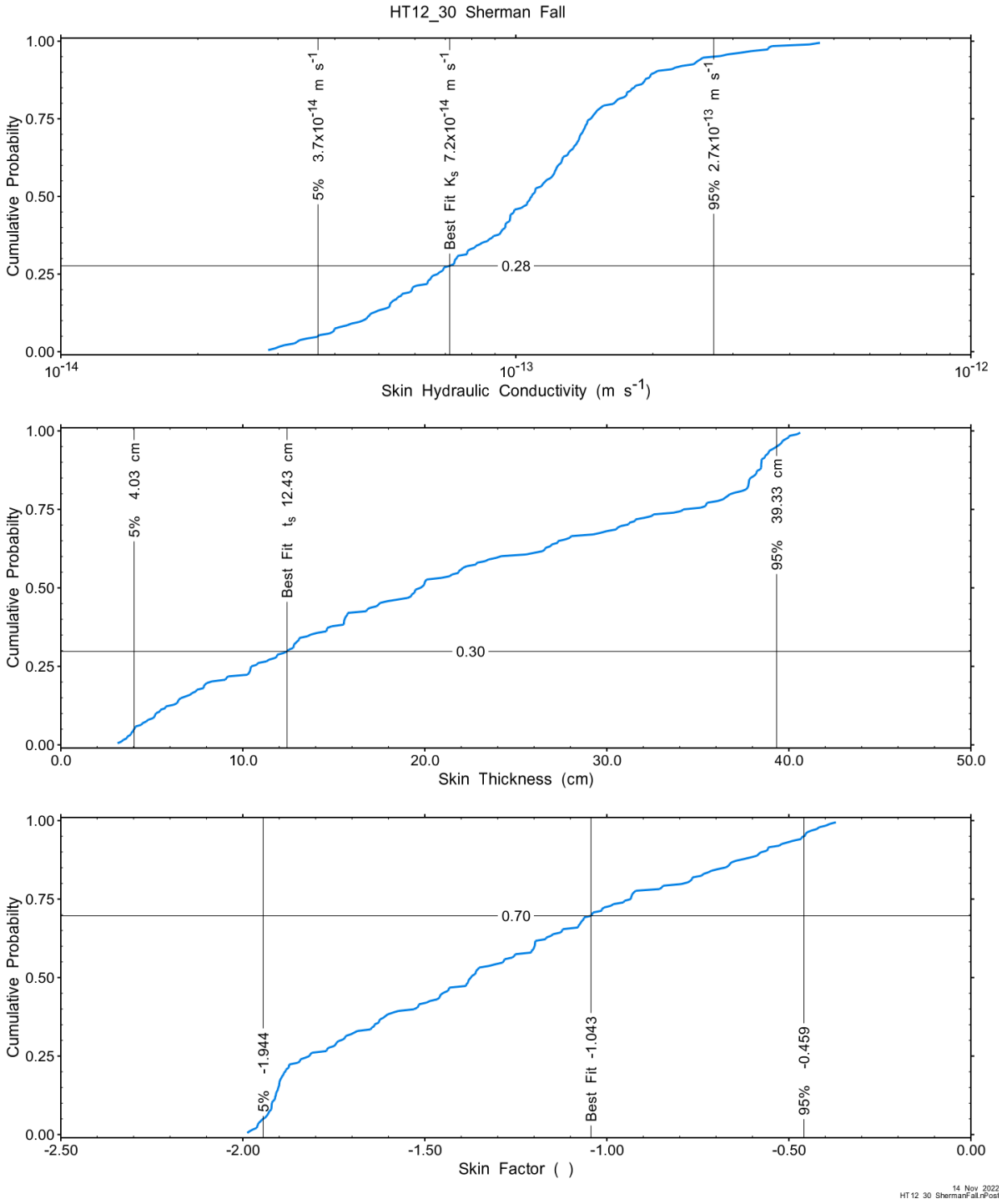

Figure A.262 – Cumulative distribution functions and parameter limits for skin hydraulic conductivity (K_s) (top panel), skin thickness (t_s) (middle panel) and skin factor (s) (bottom panel).

A summary of perturbation results is presented in Figure A.28, with Ramey-processed perturbations in Figure A.13. Those perturbations (139 of 10,000) with all parameters within the 5% and 95% range present a good fit to the measured test zone data.

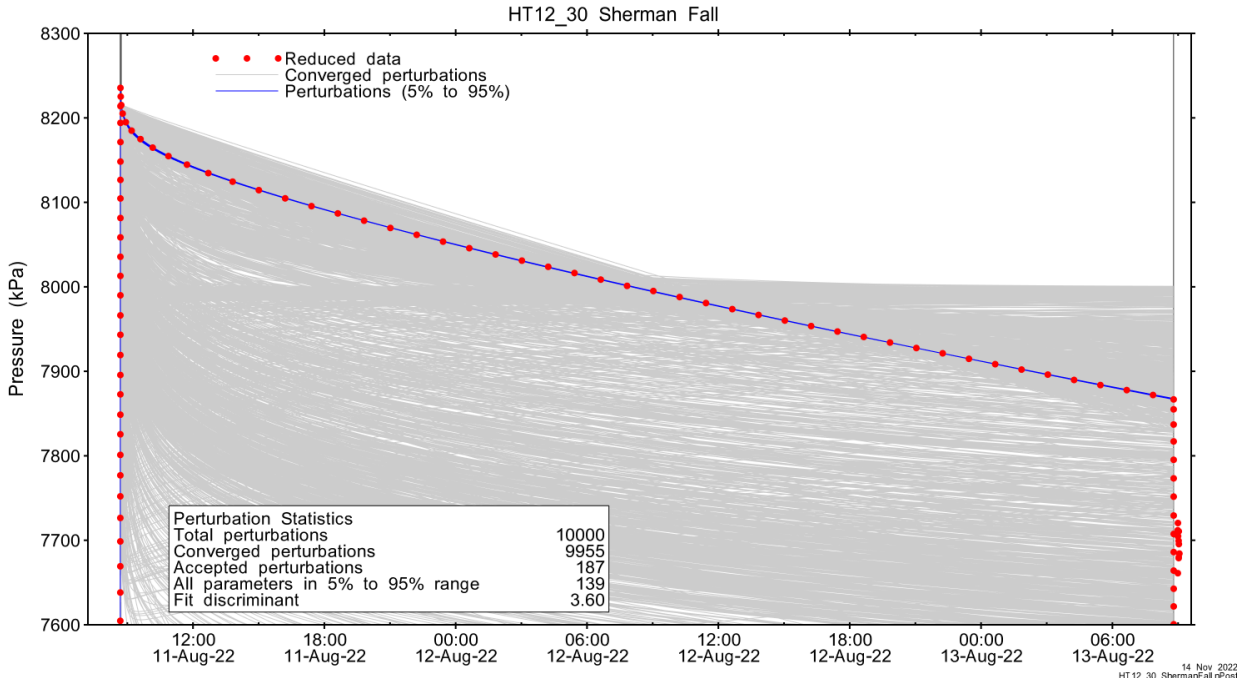

Figure A.263 – Perturbation results – all converged, accepted, and within 5% to 95% for all parameters.

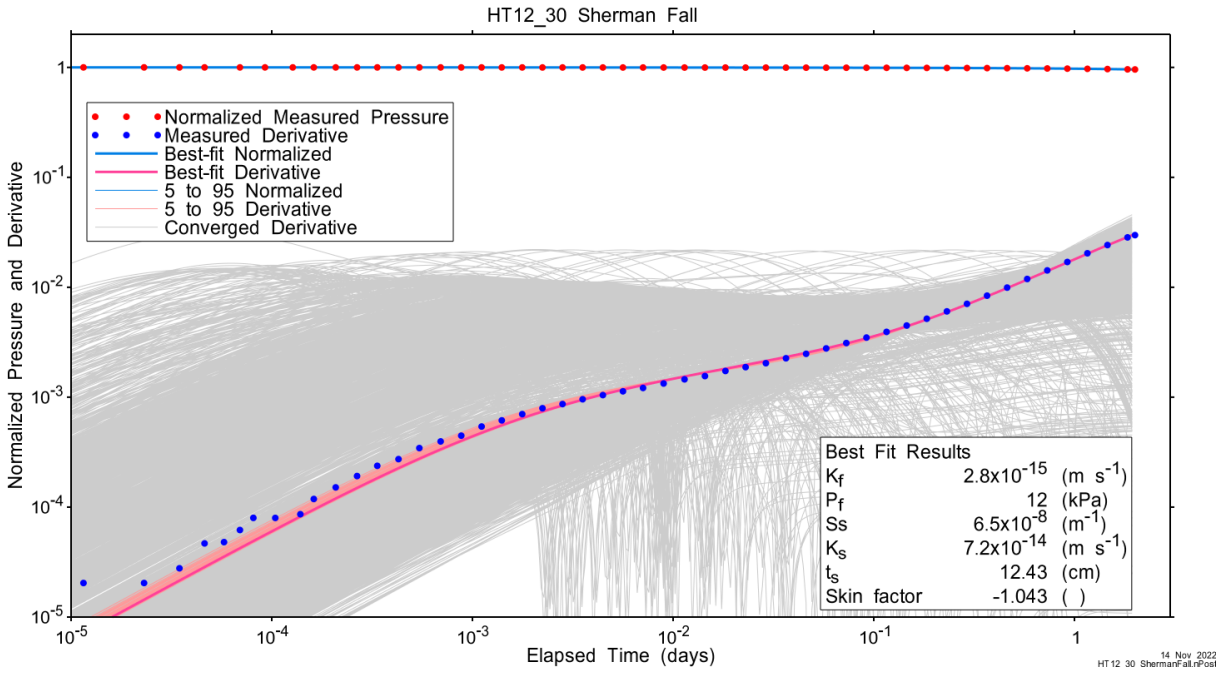

Figure A.264 – Log-log plot showing Ramey B and derivative response for all converged optimizations and those within 5% to 95% for all parameters.

A summary of best-fit and parameter ranges is given in Table A.9.

Table A.84 - Summary of the HT12_30 parameter estimates.

Parameter	Best Fit	5%	Median	95%
K_f (m/s)	2.8E-15	2.5E-15	3.0E-15	3.9E-15
P_f (kPa)	12	0	383	1913
Ss (1/m)	6.5E-08	1.0E-08	3.1E-08	2.8E-07
K_s (m/s)	7.2E-14	3.7E-14	1.1E-13	2.7E-13
t_s (cm)	12.43	4.03	19.75	39.33
s (-)	-1.043	-1.944	-1.373	-0.459

Parameter correlations for all perturbations with all parameters within the 5% to 95% limits are given in Table A.5.

Table A.85 – Pearson cross-correlations of 5% to 95% parameters

	Log(K_f)	P_f	Log(Ss)	Log(K_s)	t_s	s
Log(K_f)	1.000	0.943	-0.644	0.744	0.592	-0.625
Pf	0.943	1.000	-0.382	0.539	0.360	-0.365
Log(S_s)	-0.644	-0.382	1.000	-0.902	-0.976	0.999
Log(K_s)	0.744	0.539	-0.902	1.000	0.860	-0.904
t_s	0.592	0.360	-0.976	0.860	1.000	-0.982
s	-0.625	-0.365	0.999	-0.904	-0.982	1.000

A.17.4 Additional Figures

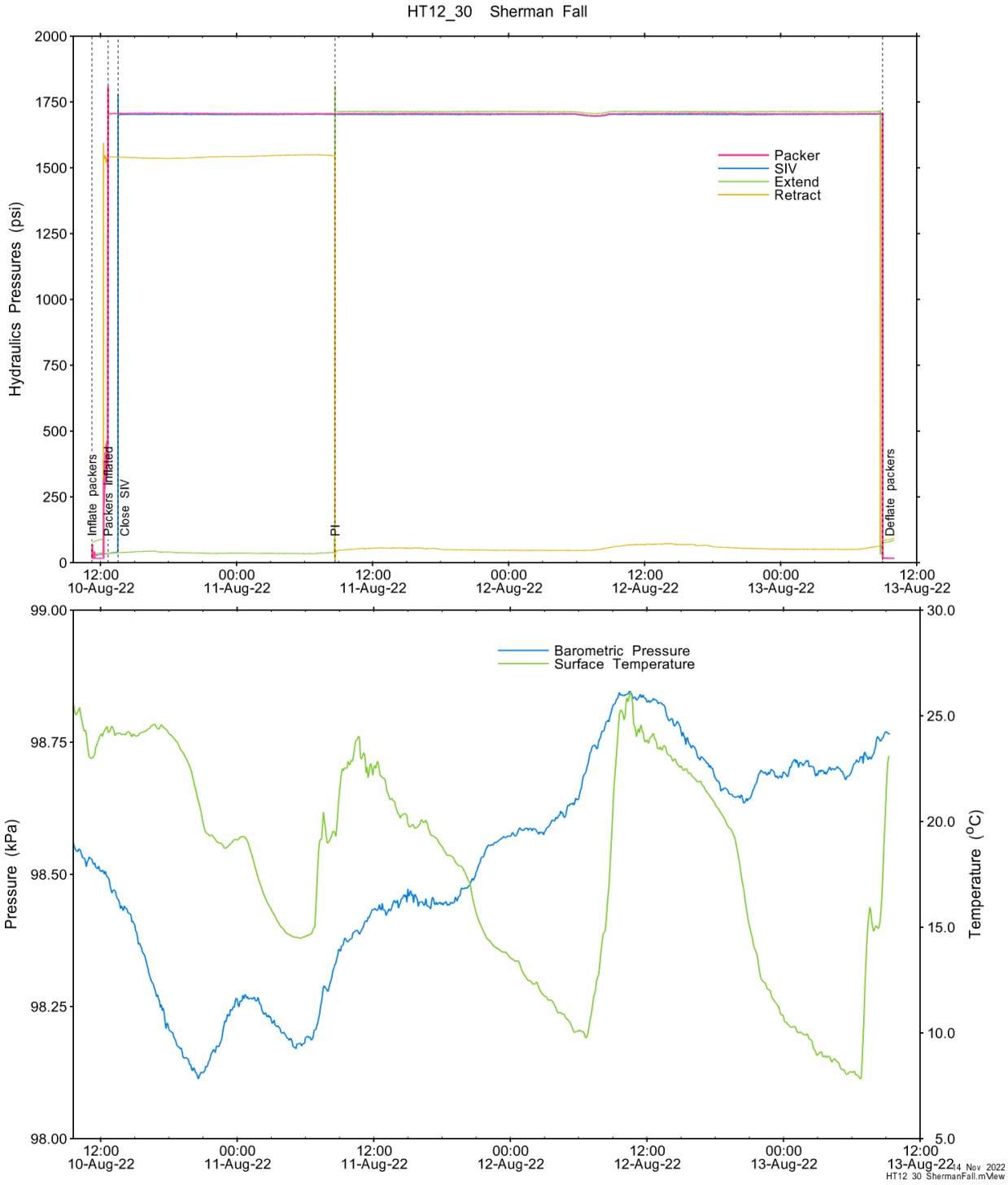

Figure A.265 - Hydraulics pressures and surface temperature/barometric pressure.

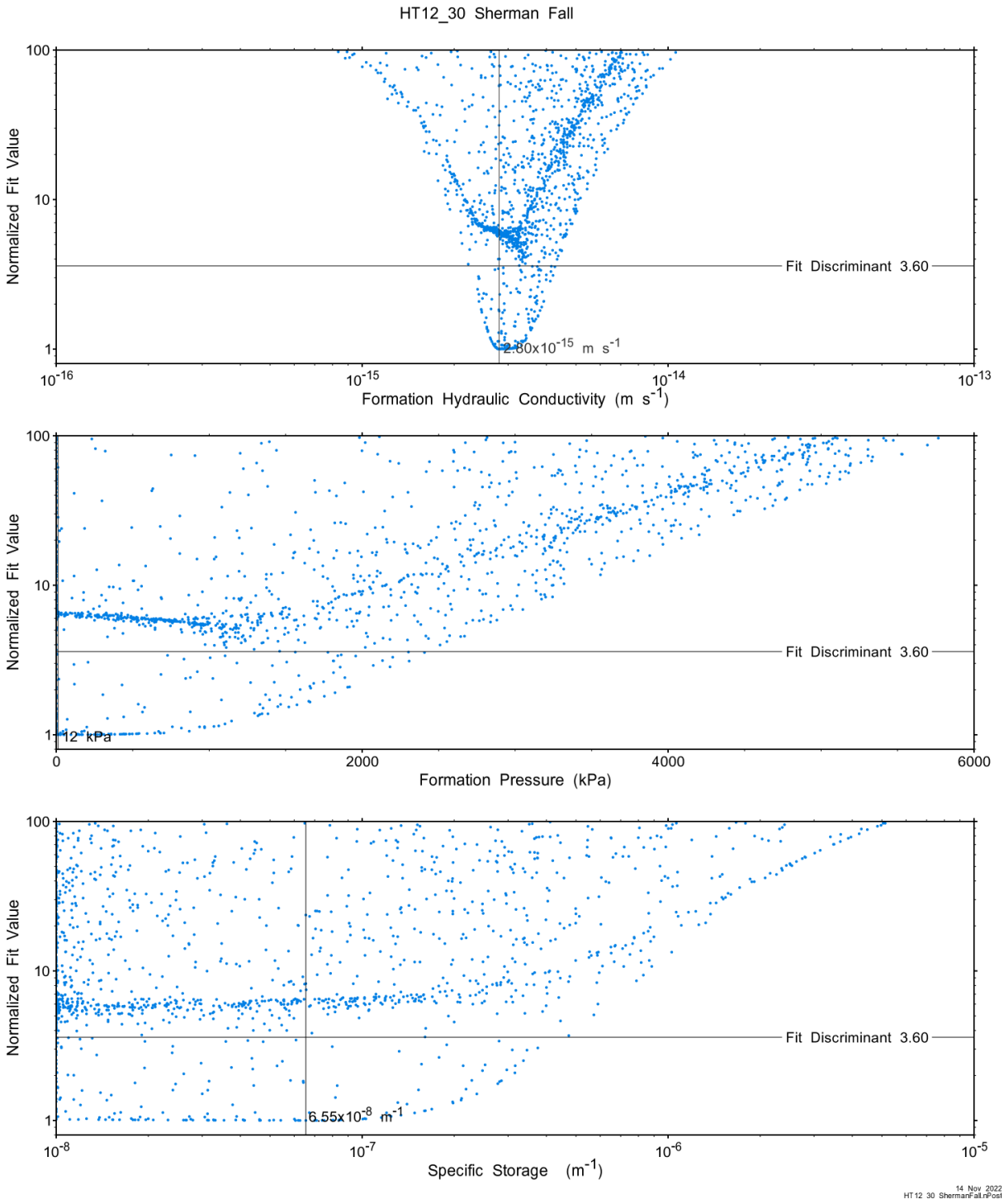

Figure A.266 - XY-scatter plot showing the formation parameter space normalized fit values.

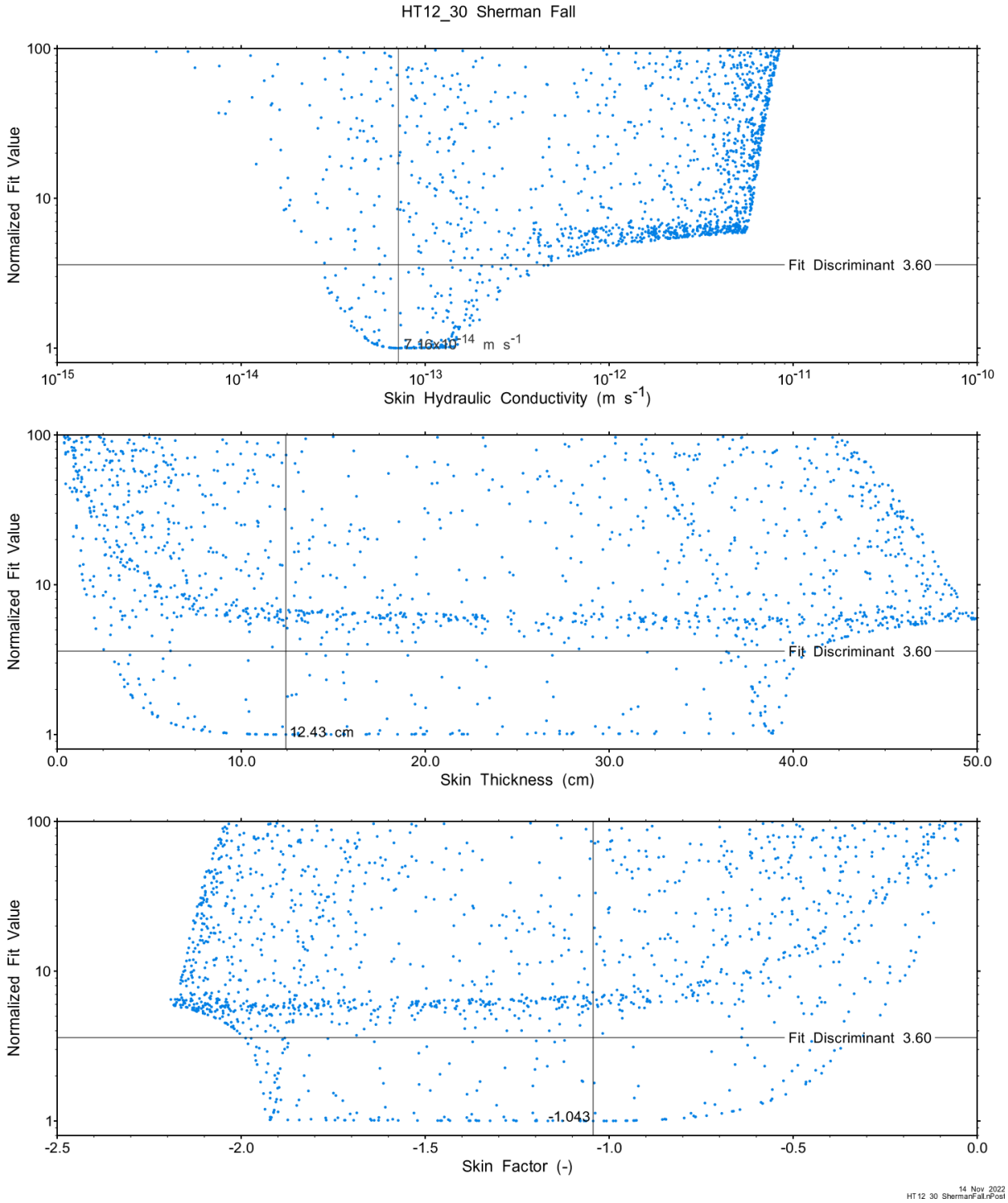

Figure A.267 - XY-scatter plot showing the skin parameter space normalized fit values.

A.18 HT13_30 Kirkfield

The SB BH02 interval from 770.00 to 799.96 mBGS tested in HT13_30 covers the majority of the Kirkfield Formation. A single PI test of two days duration was conducted.

A.18.1 Test Data Summary

Table A.6 and Figure A.1 provide a summary of test events and a plot of pressures measured while testing respectively.

Table A.86 - Summary of Test Events.

Event	Start Date & Time	Duration (days)	TZ Pressure (kPa)
Drilling intercept	22-03-18 01:14	148.53	7702
Shut-in	22-08-13 14:01	0.77	8197
Pulse injection	22-08-14 08:30	2.00	8785
Test end	22-08-16 08:36		8481

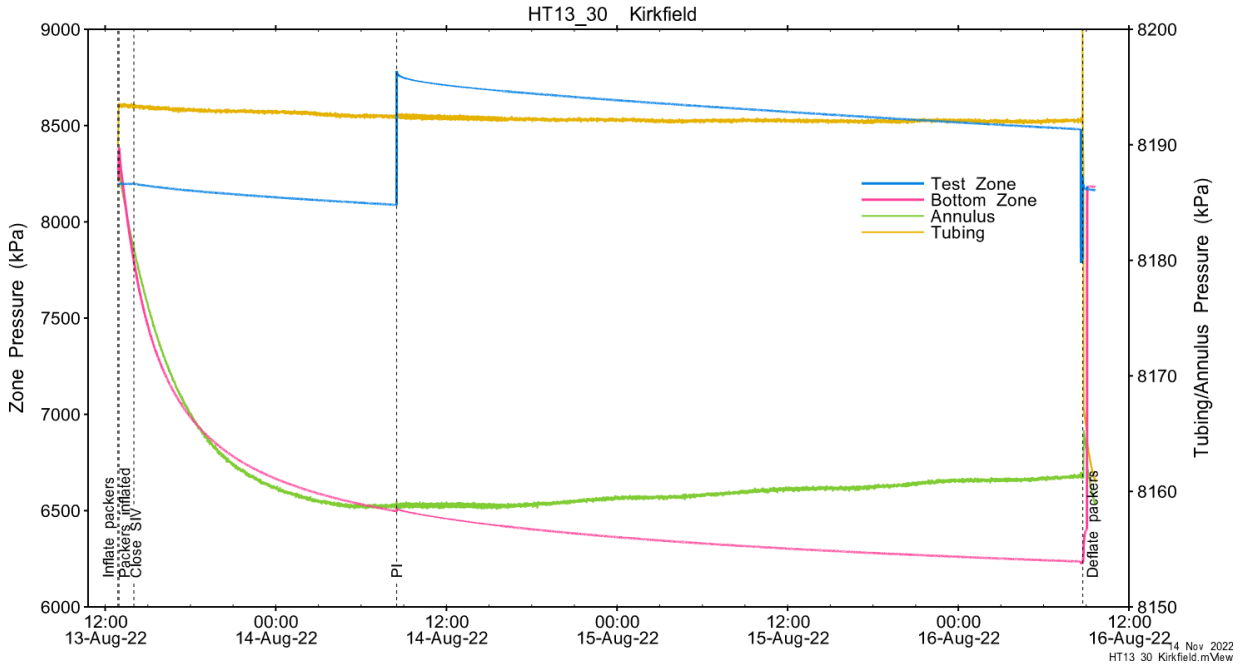

Figure A.268 - Test events and pressures.

A.18.2 Test Analyses

Table A.7 is a summary of test-specific input parameters used in the analyses, while Table A.8 presents the optimized parameters and allowed ranges.

Table A.87 – nSIGHTS Input Parameters.

Parameter	Value	Units
Test zone radius	6.37	cm
Test zone compressibility	3.91E-10	1/Pa
Test zone length	29.96	m

Table A.88 – nSIGHTS Parameter Optimization Ranges.

Parameter	Minimum	Maximum	Units	Type
Formation hydraulic conductivity (K_f)	1E-16	1E-07	m/s	log
Formation pressure (P_f)	0	10000	kPa	linear
Specific storage (S_s)	1E-08	1E-04	1/m	log
Skin hydraulic conductivity (K_s)	1E-16	1E-07	m/s	log
Skin thickness (t_s)	0.013	500	cm	linear

Figure A.18 shows the measured test zone pressure record (with reduced data density for clarity) used in the analysis along with the best-fit simulation and parameter values. Figure A.19 presents the pre-test history, and Figure A.20 shows the Ramey B normalized best-fit pressure and pressure derivatives.

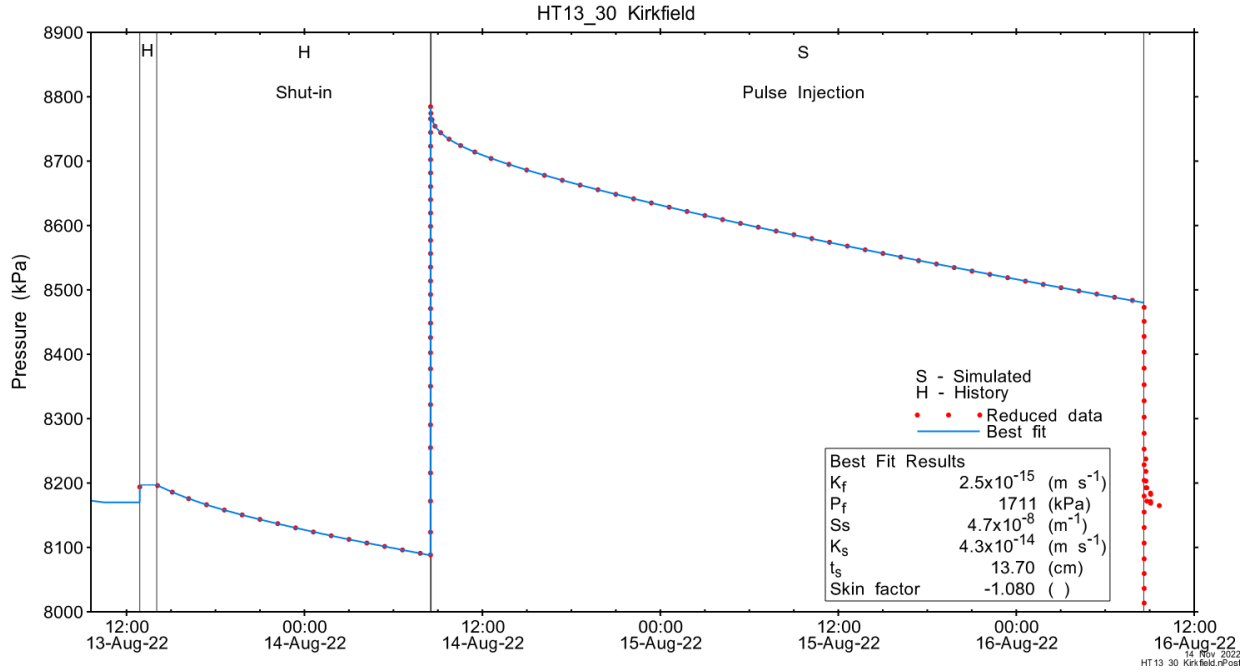

Figure A.269 - Annotated testing sequence showing best-fit simulation and parameter estimates.

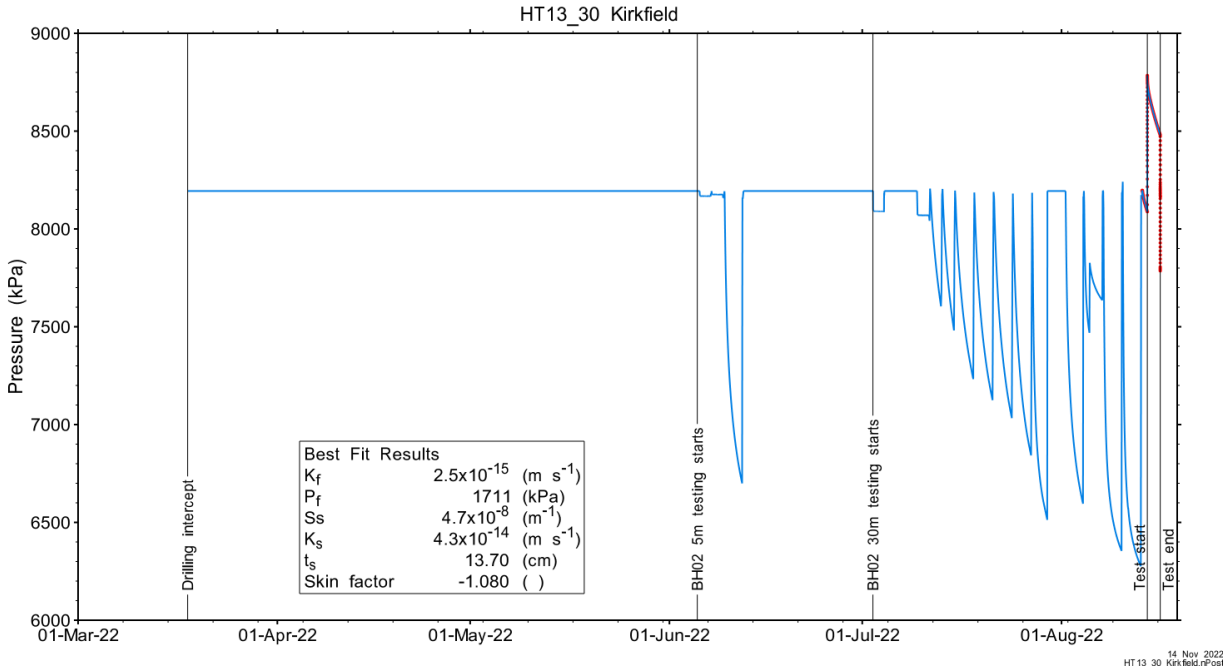

Figure A.270 - Annotated testing sequence showing pre-test history, best-fit simulation and parameter estimates.

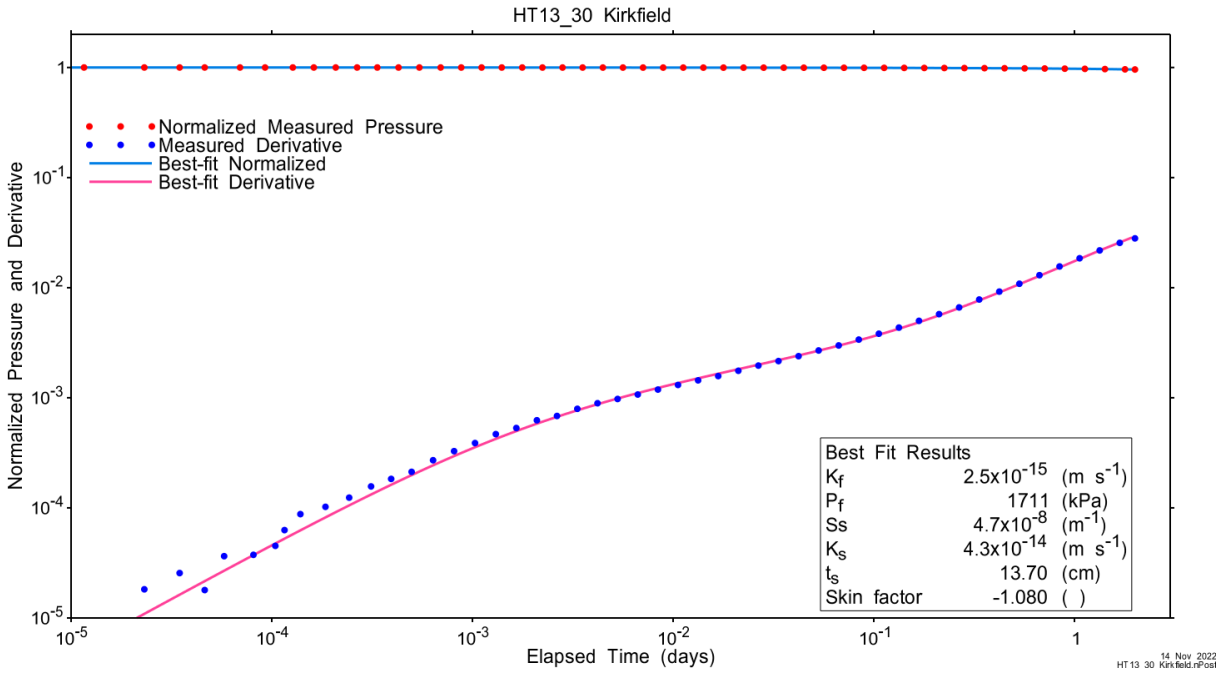

Figure A.271 - Log-log plot showing Ramey B and derivative response for best-fit simulation.

Figure A.21 shows the normalized parameter sensitivity response for the best fit. Sensitivity for most fitting parameters is increasing at the end of the test, indicating that increased test duration may have yielded more precise results.

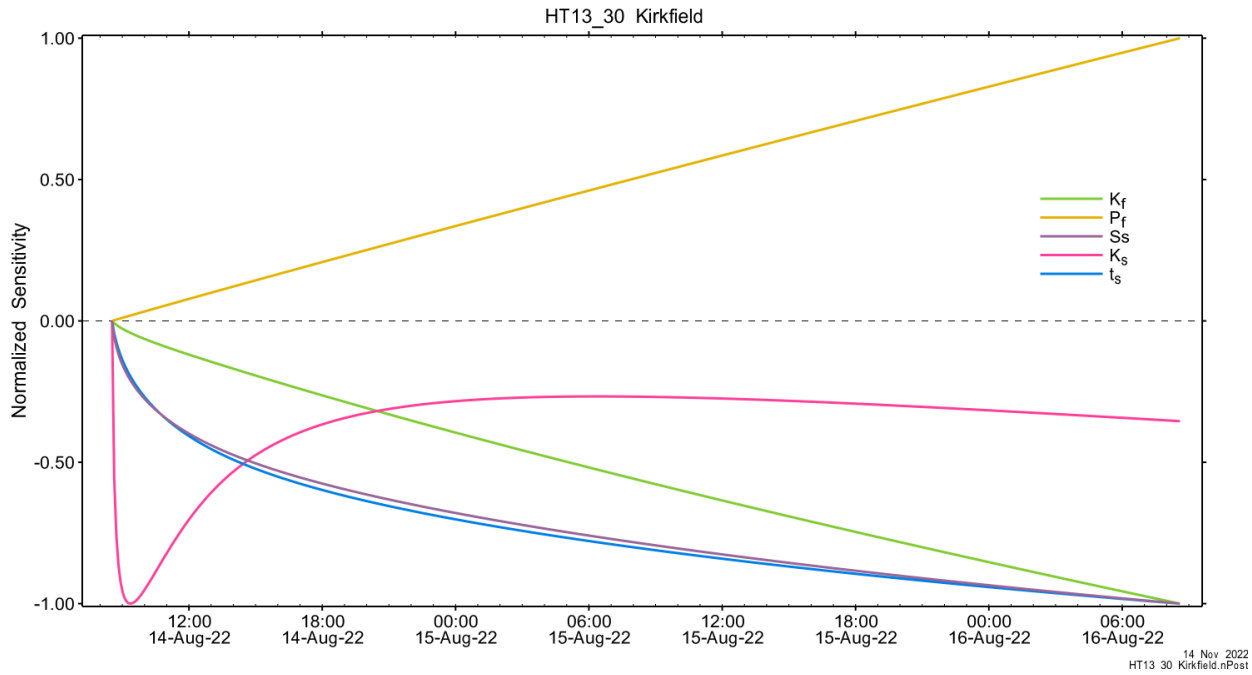

Figure A.272 - Normalized Jacobian for best-fit simulation.

A.18.3 Uncertainty Analyses

The CDF of normalized fit values for all converged simulations and the selected fit discriminant are shown in Figure A.22. Initially, the fit discriminant was set somewhat higher, but was reduced to remove local minima and to include the global minimum only.

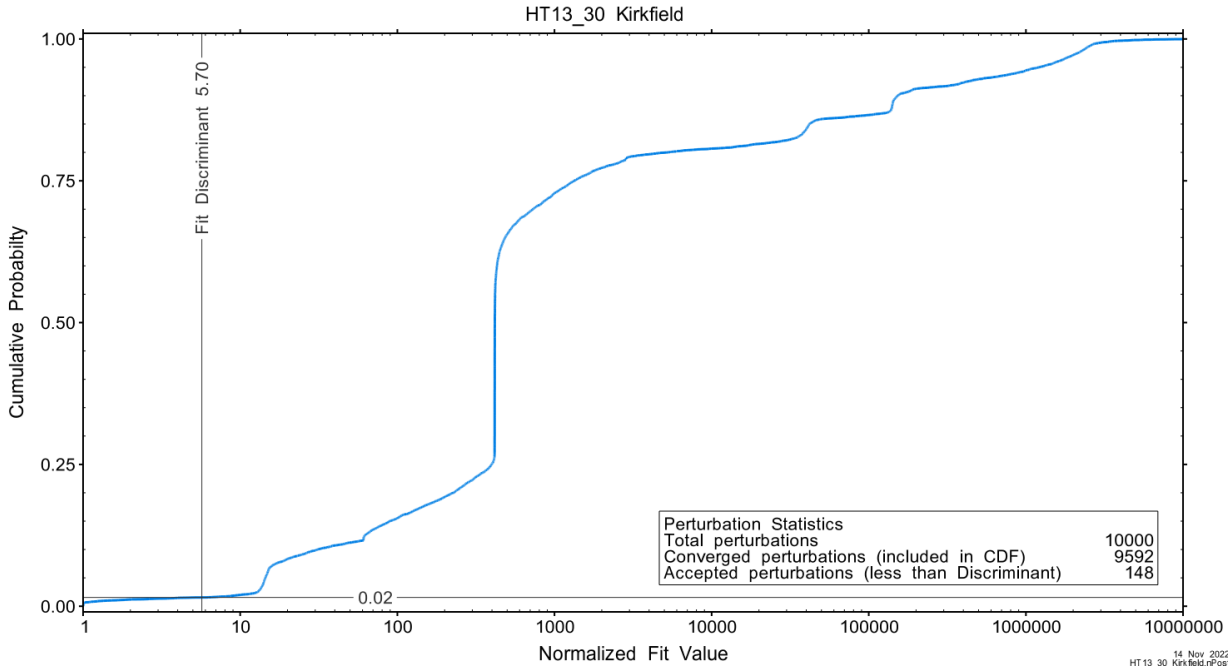

Figure A.273 - Fit value cumulative distribution function.

Summary cross parameter scatter plots for selected formation and skin parameters are given in Figure A.24 and Figure A.25. The light pink dots on the figures are the initial parameter estimates, with red dots overlaying those initial parameter values that resulted in accepted optimization results. The grey dots are converged optimizations which did not meet the fit discriminant. Larger varying color symbols represent the fit value of accepted optimizations, with the blue values representing the best fit.

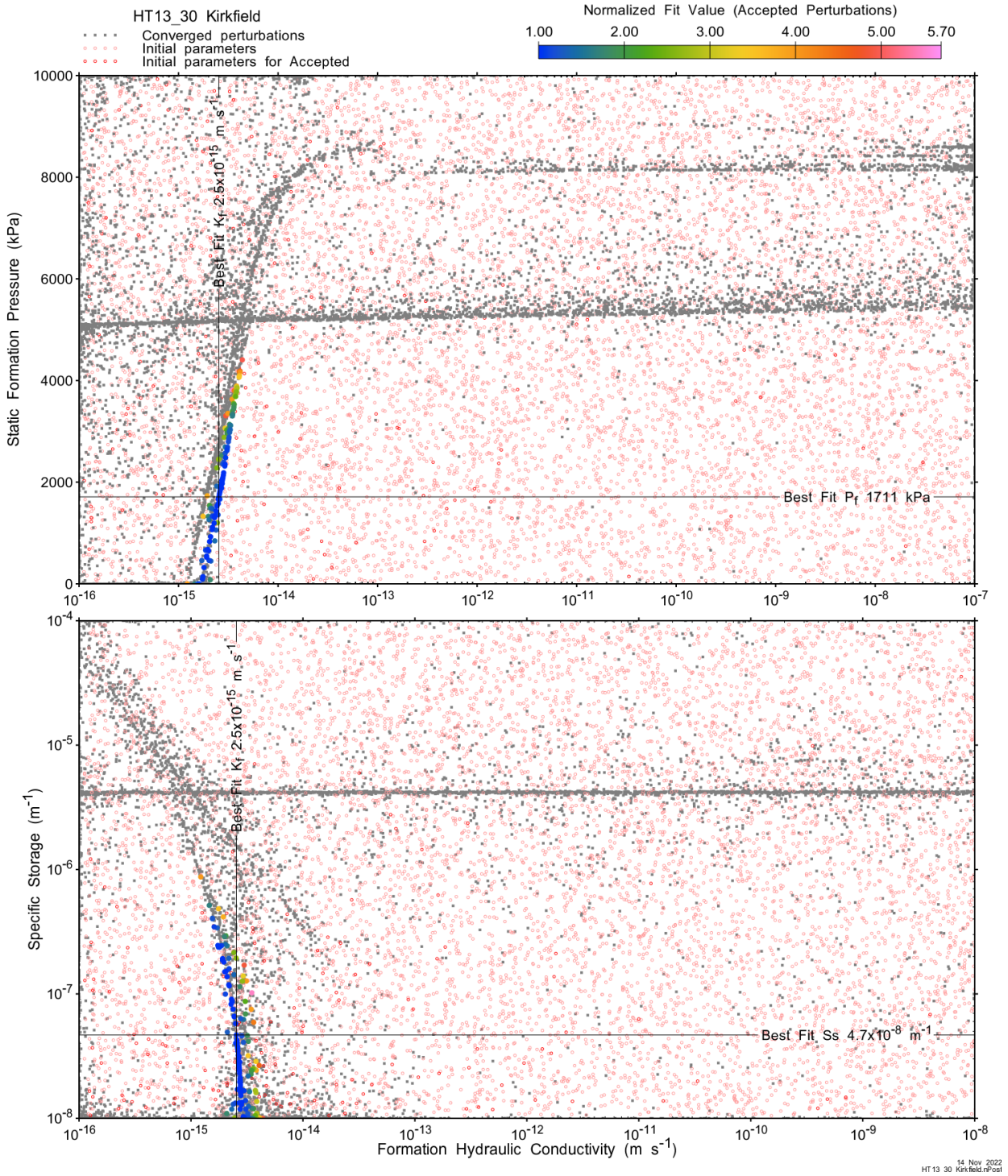

Figure A.274 - XY-scatter plot showing estimates of formation hydraulic conductivity (K_f) vs static formation pressure (P_f) (top panel) and specific storage (Ss) (bottom panel).

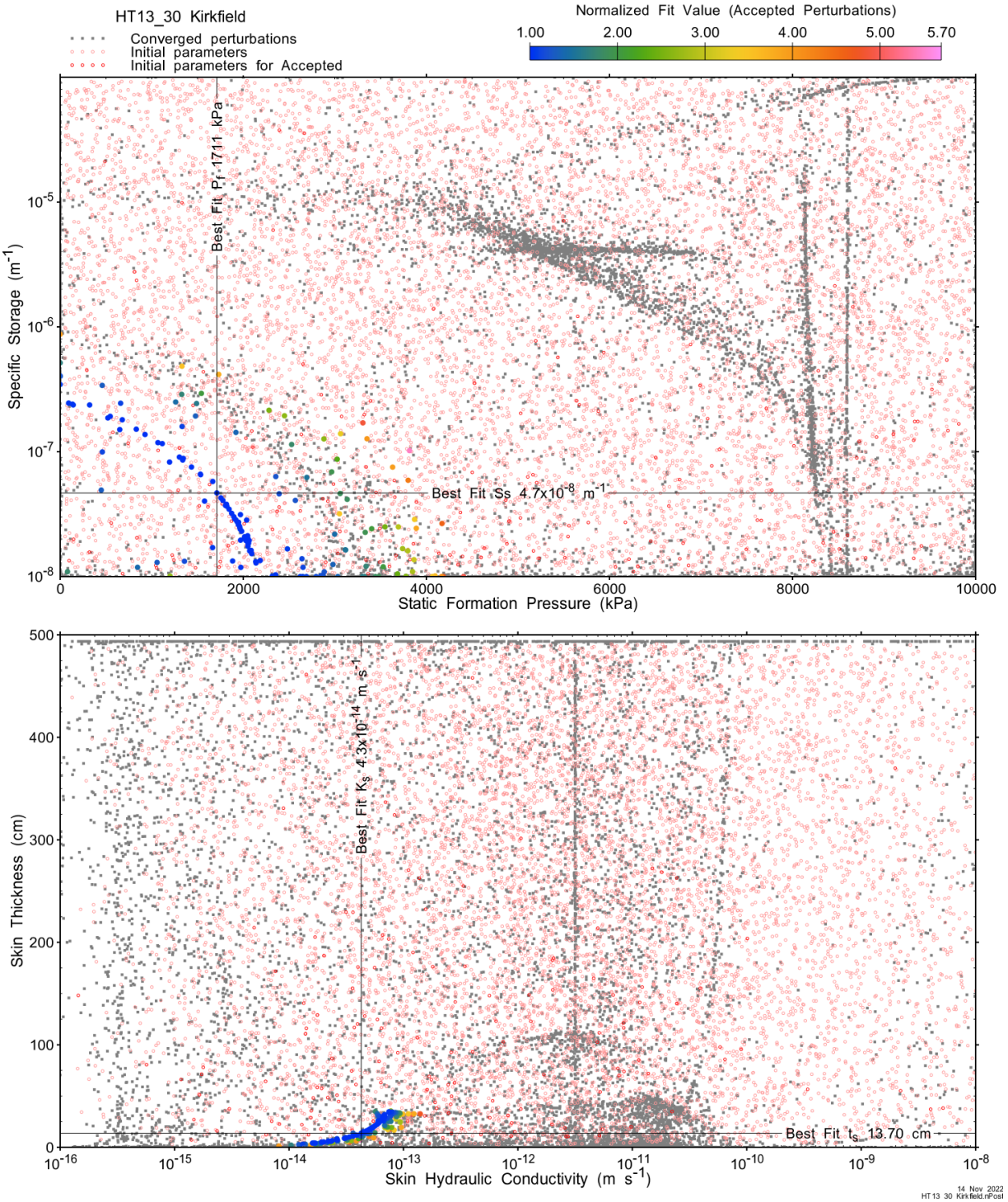

Figure A.275 - XY-scatter plot showing estimates of static formation pressure (P_f) vs specific storage (Ss) (top panel) and skin hydraulic conductivity (K_s) vs skin thickness (t_s) (bottom panel).

Confidence limits and median values are determined from the CDF of accepted optimization results (i.e. the varying color values in the above figures), with best fit value, 5% and 95% confidence indicated on Figure A.26 and Figure A.27.

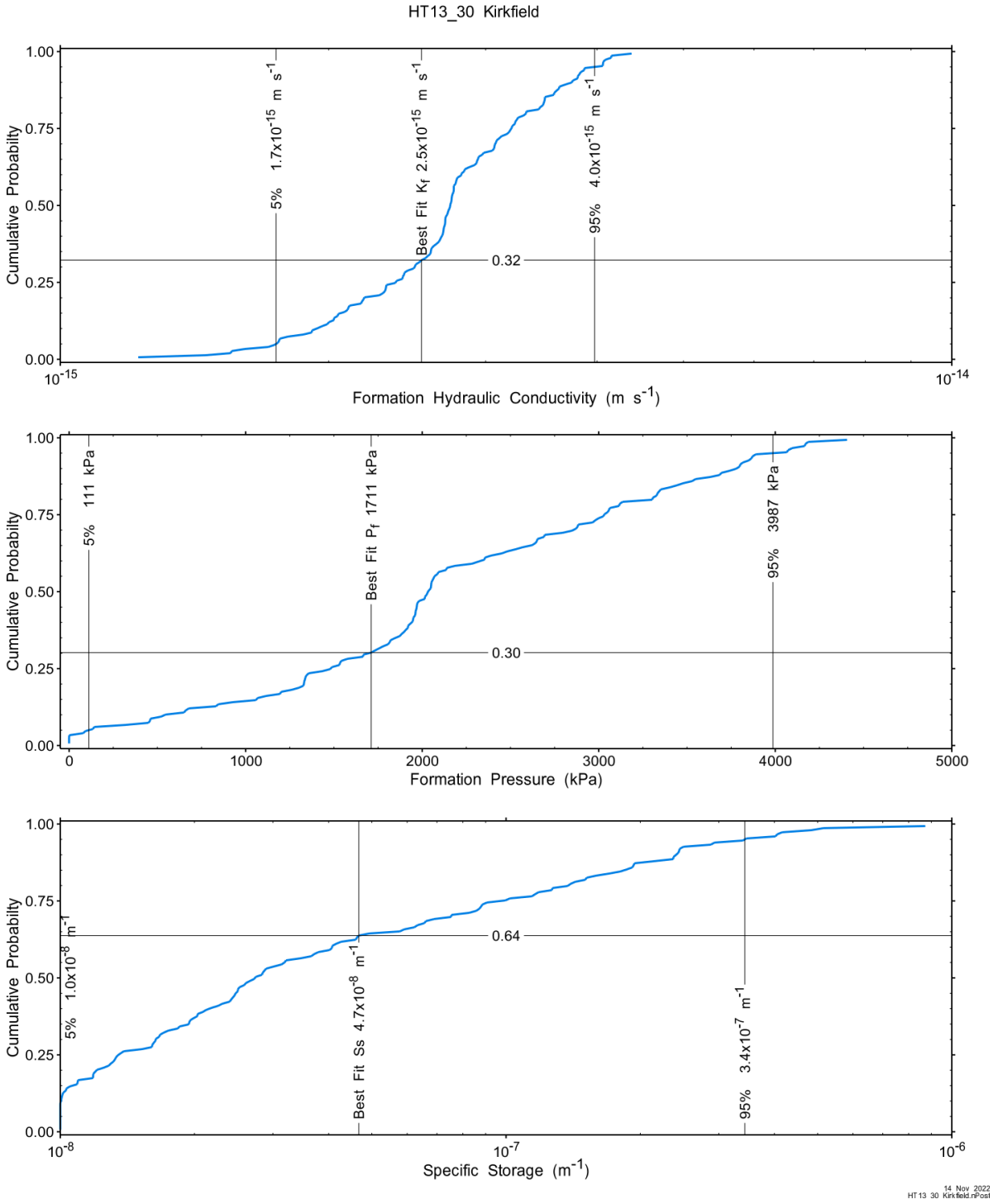

Figure A.276 – Cumulative distribution functions and parameter limits for formation hydraulic conductivity (K_f) (top panel), static formation pressure (P_f) (middle panel) and specific storage (Ss) (bottom panel).

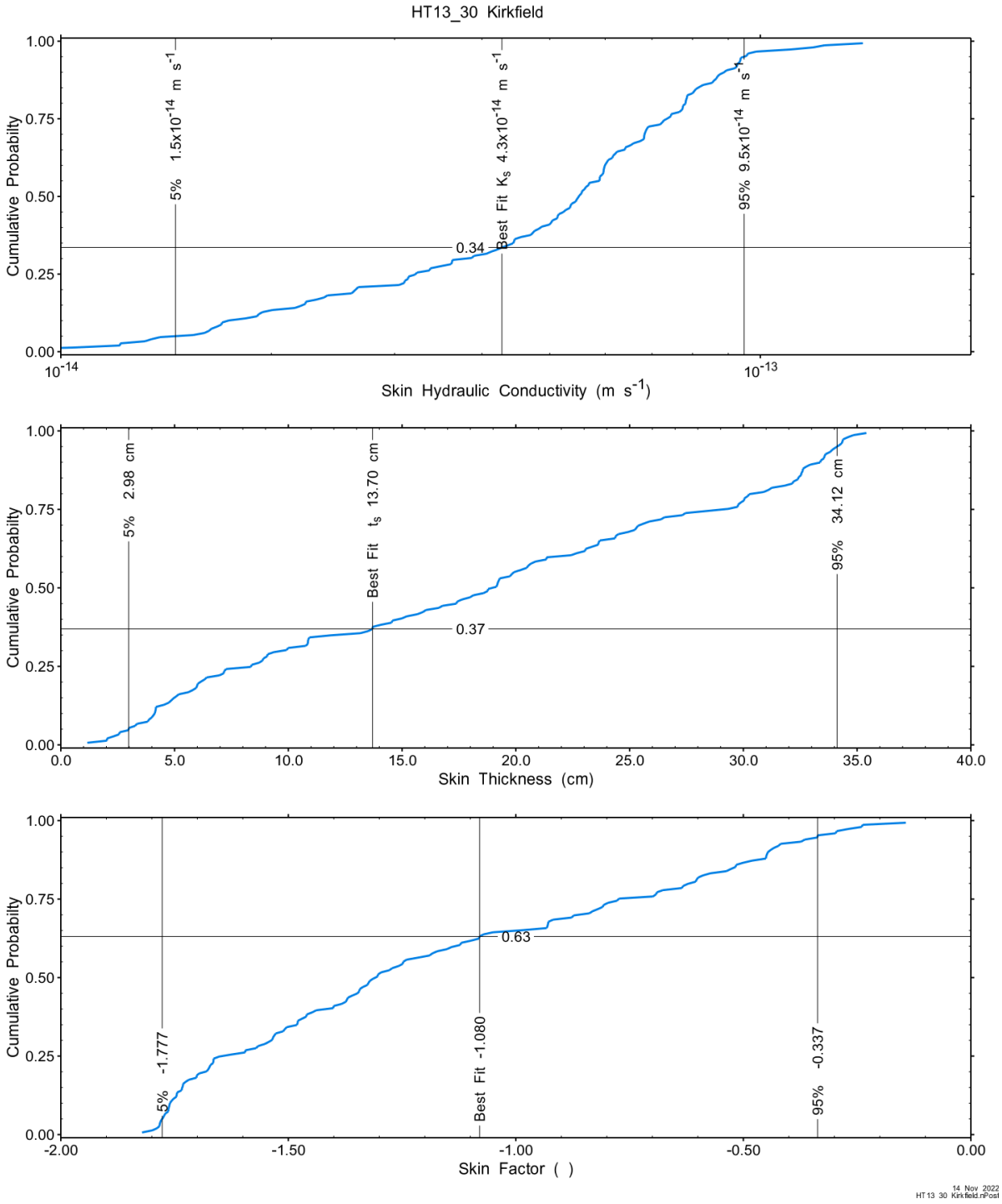

Figure A.277 – Cumulative distribution functions and parameter limits for skin hydraulic conductivity (K_s) (top panel), skin thickness (t_s) (middle panel) and skin factor (s) (bottom panel).

A summary of perturbation results is presented in Figure A.28, with Ramey-processed perturbations in Figure A.13. Those perturbations (123 of 10,000) with all parameters within the 5% and 95% range present a good fit to the measured test zone data.

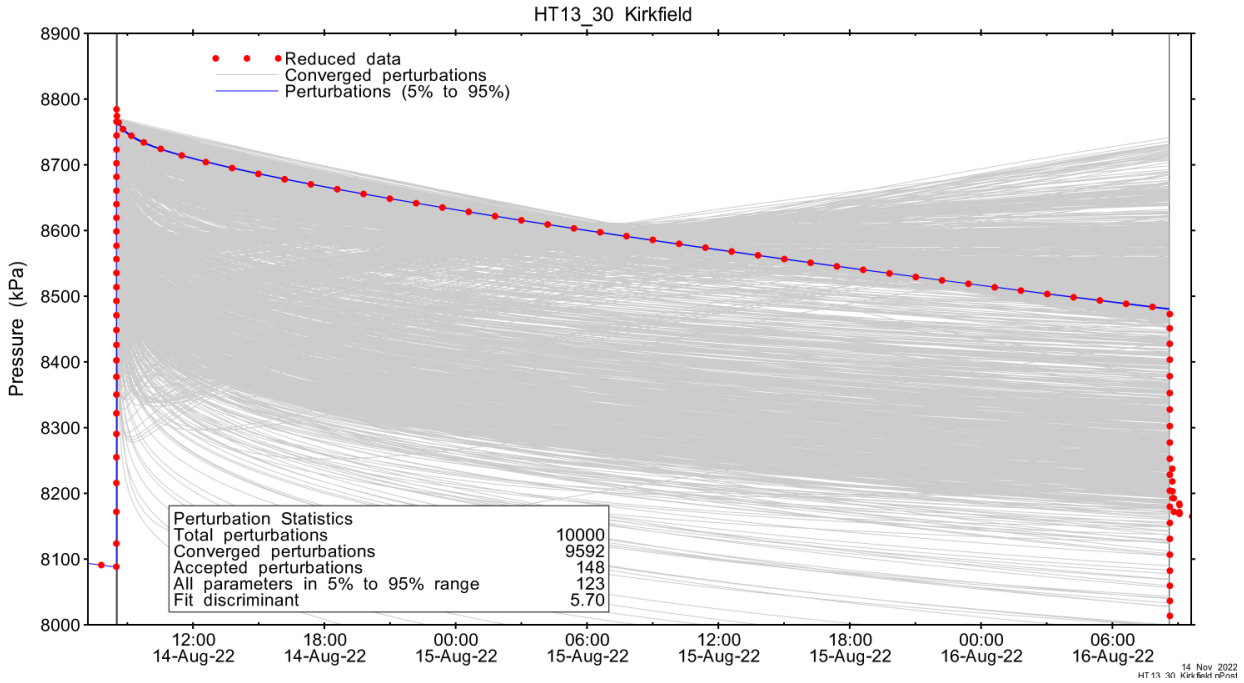

Figure A.278 – Perturbation results – all converged, accepted, and within 5% to 95% for all parameters.

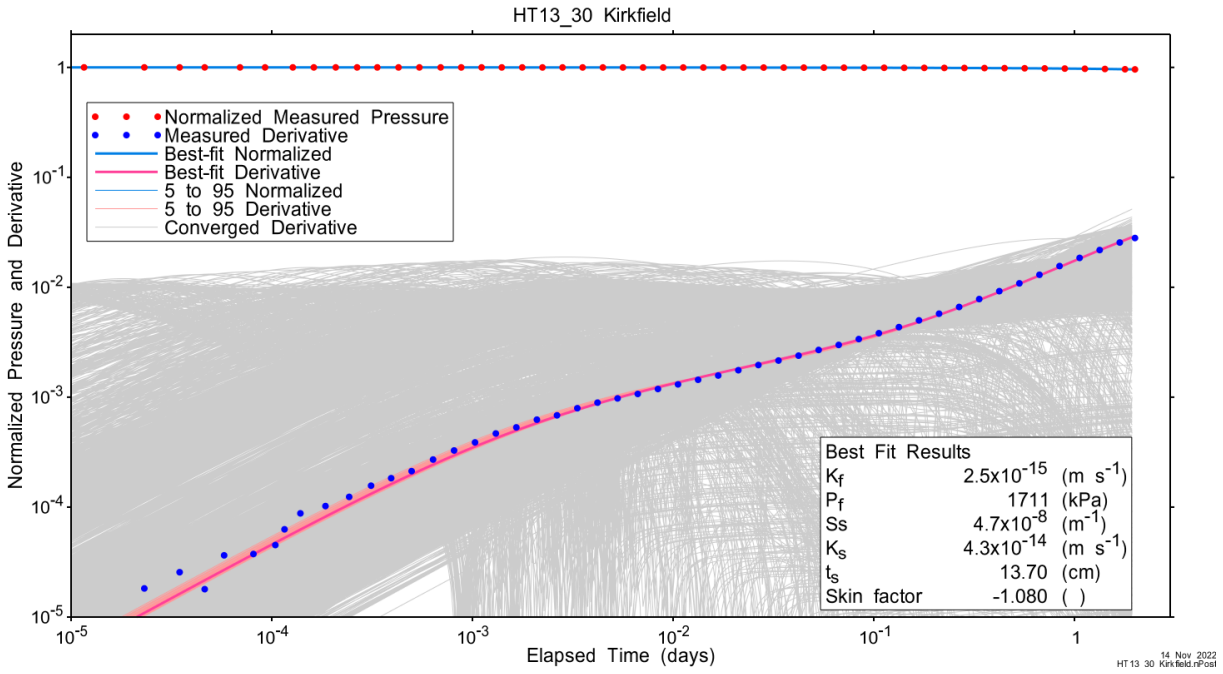

Figure A.279 – Log-log plot showing Ramey B and derivative response for all converged optimizations and those within 5% to 95% for all parameters.

A summary of best-fit and parameter ranges is given in Table A.9.

Table A.89 - Summary of the HT13_30 parameter estimates.

Parameter	Best Fit	5%	Median	95%
K_f (m/s)	2.5E-15	1.7E-15	2.7E-15	4.0E-15
P_f (kPa)	1711	111	2033	3987
Ss (1/m)	4.7E-08	1.0E-08	2.7E-08	3.4E-07
K_s (m/s)	4.3E-14	1.5E-14	5.5E-14	9.5E-14
t_s (cm)	13.70	2.98	18.96	34.12
s (-)	-1.080	-1.777	-1.309	-0.337

Parameter correlations for all perturbations with all parameters within the 5% to 95% limits are given in Table A.5.

Table A.90 – Pearson cross-correlations of 5% to 95% parameters

	Log(K_f)	P_f	Log(Ss)	Log(K_s)	t_s	s
Log(K_f)	1.000	0.965	-0.686	0.859	0.617	-0.647
Pf	0.965	1.000	-0.493	0.708	0.439	-0.452
Log(S_s)	-0.686	-0.493	1.000	-0.954	-0.976	0.998
Log(K_s)	0.859	0.708	-0.954	1.000	0.897	-0.936
t_s	0.617	0.439	-0.976	0.897	1.000	-0.984
s	-0.647	-0.452	0.998	-0.936	-0.984	1.000

A.18.4 Additional Figures

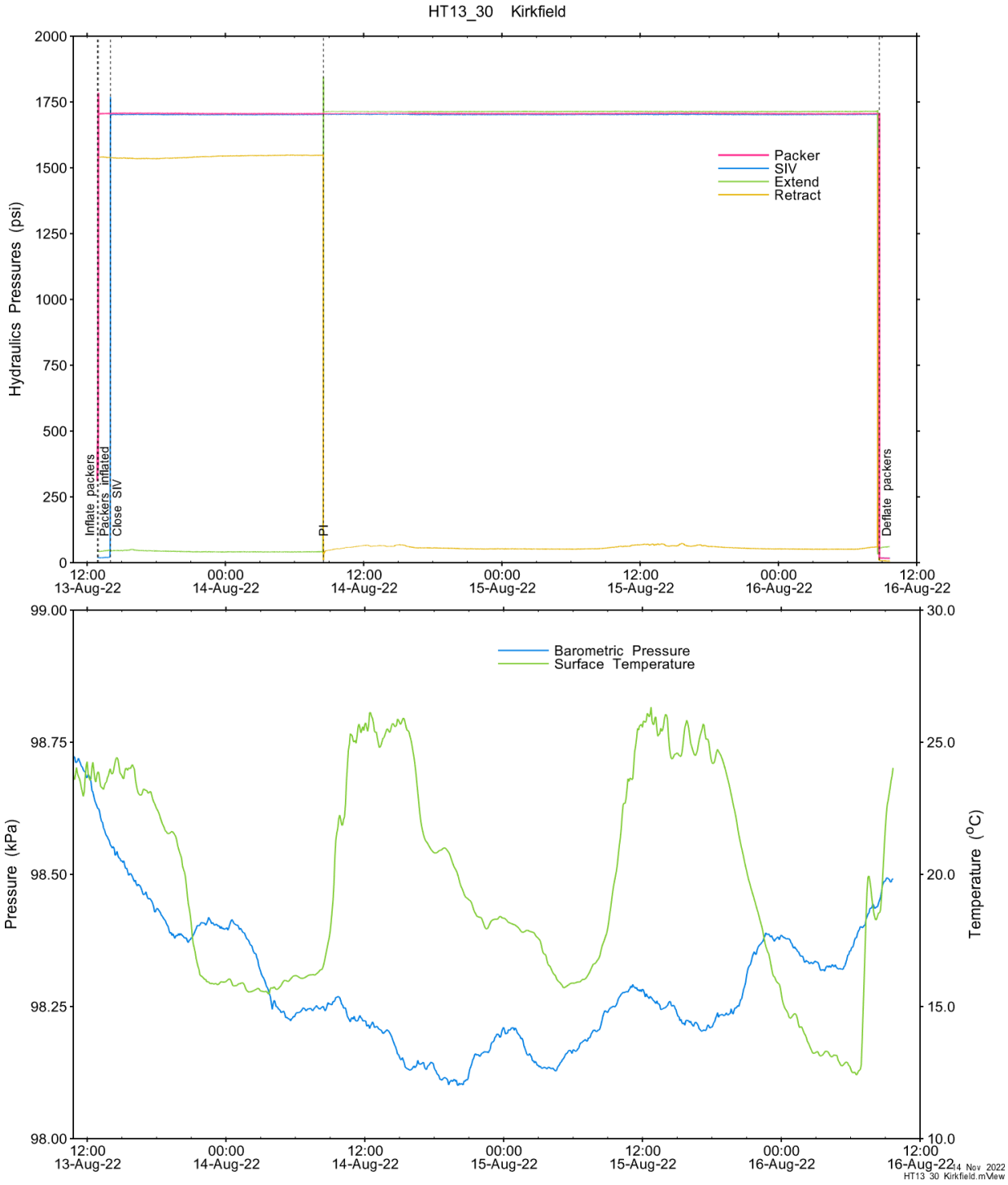

Figure A.280 - Hydraulics pressures and surface temperature/barometric pressure.

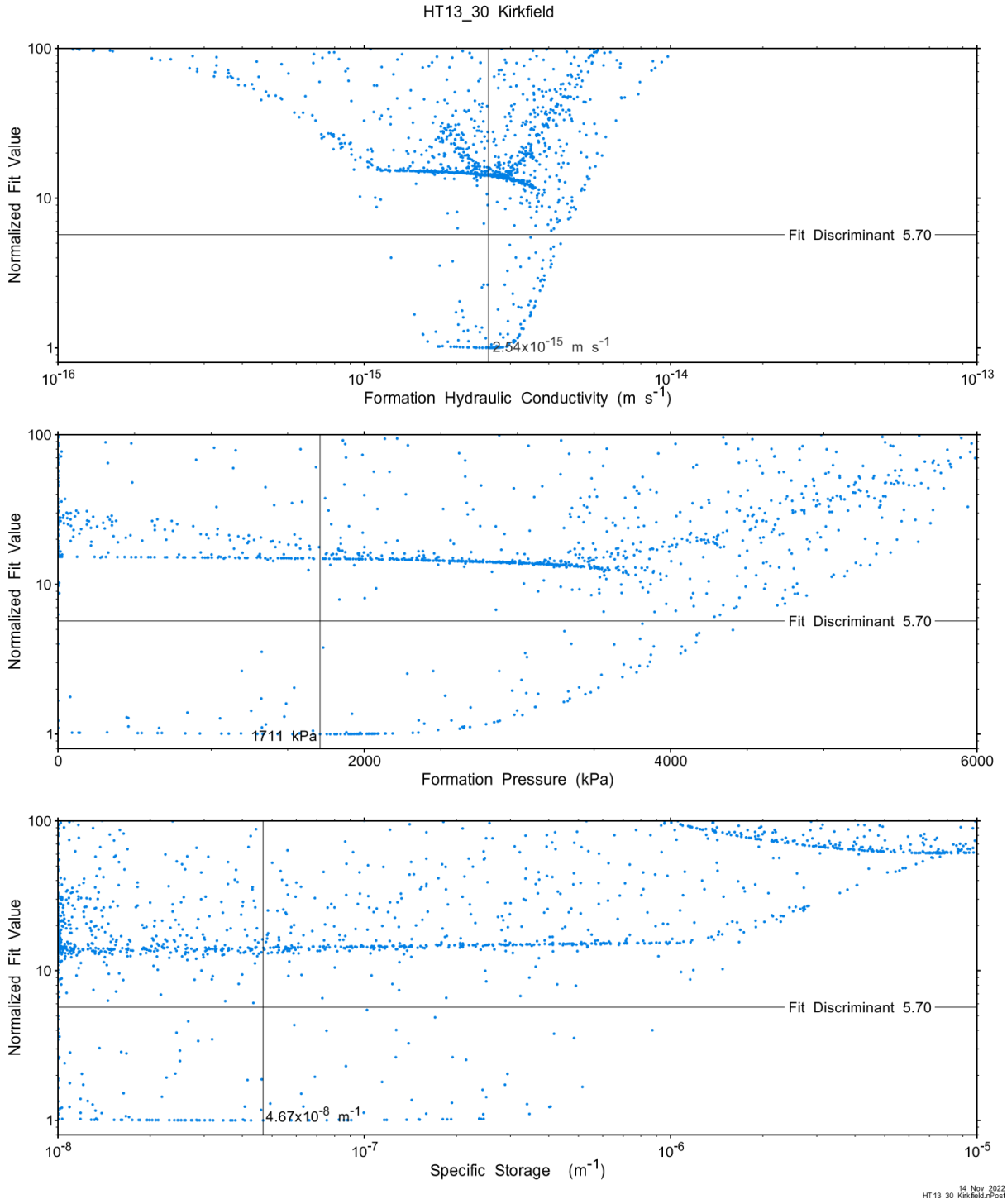

Figure A.281 - XY-scatter plot showing the formation parameter space normalized fit values.

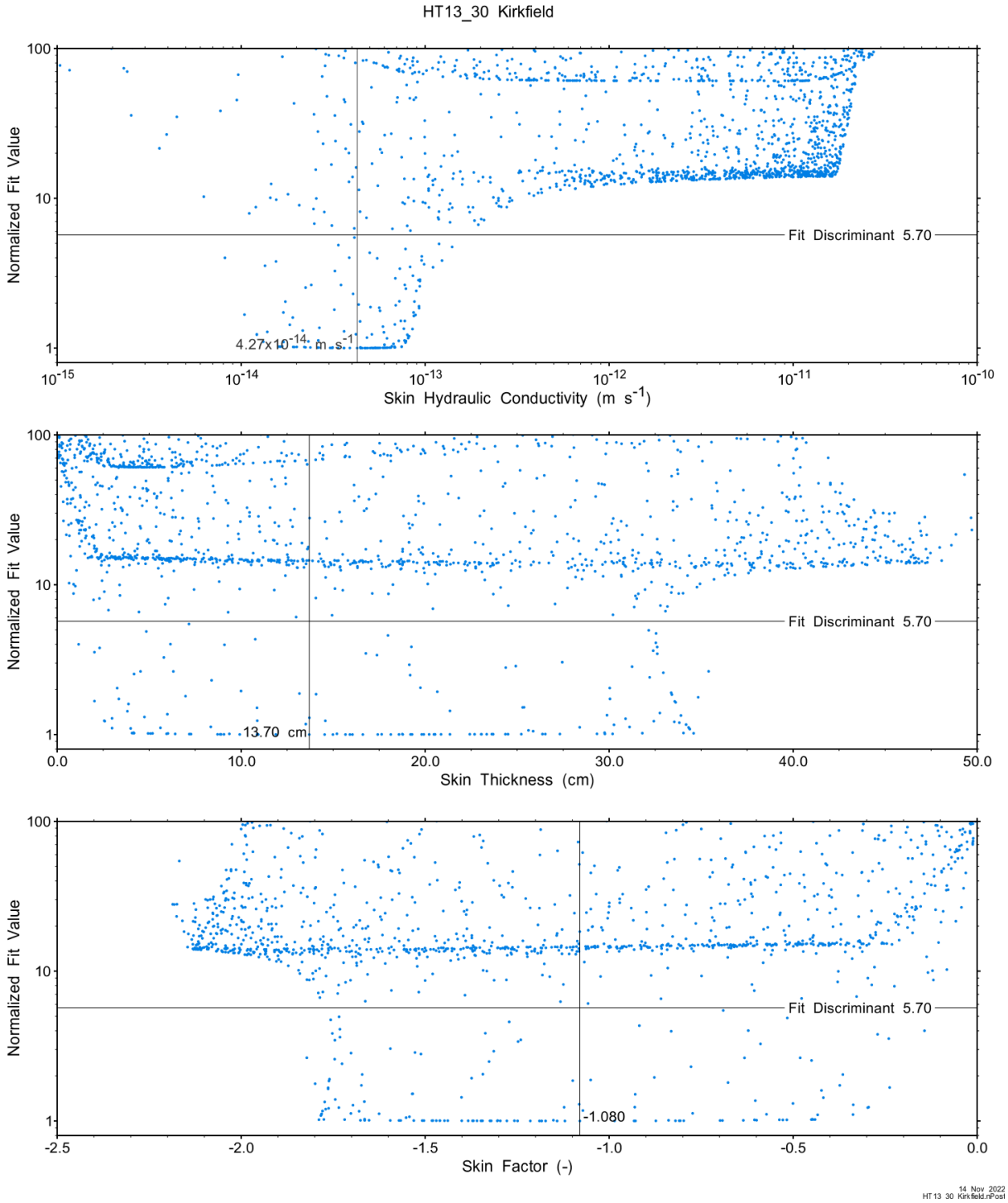

Figure A.282 - XY-scatter plot showing the skin parameter space normalized fit values.

A.19 HT14_30 Coboconk

The SB BH02 interval from 797.00 to 826.96 mBGS tested in HT14_30 covers the entirety of the of the Cobokonk Formation and the bottom 8m of the Kirkfield Formation. A single PI test of two days duration was conducted.

A.19.1 Test Data Summary

Table A.6 and Figure A.1 provide a summary of test events and a plot of pressures measured while testing respectively.

Table A.91 - Summary of Test Events.

Event	Start Date & Time	Duration (days)	TZ Pressure (kPa)
Drilling intercept	22-03-19 03:46	150.43	8468
Shut-in	22-08-16 14:03	0.82	8474
Pulse injection	22-08-17 09:50	2.01	7456
Test end	22-08-19 10:01		6668

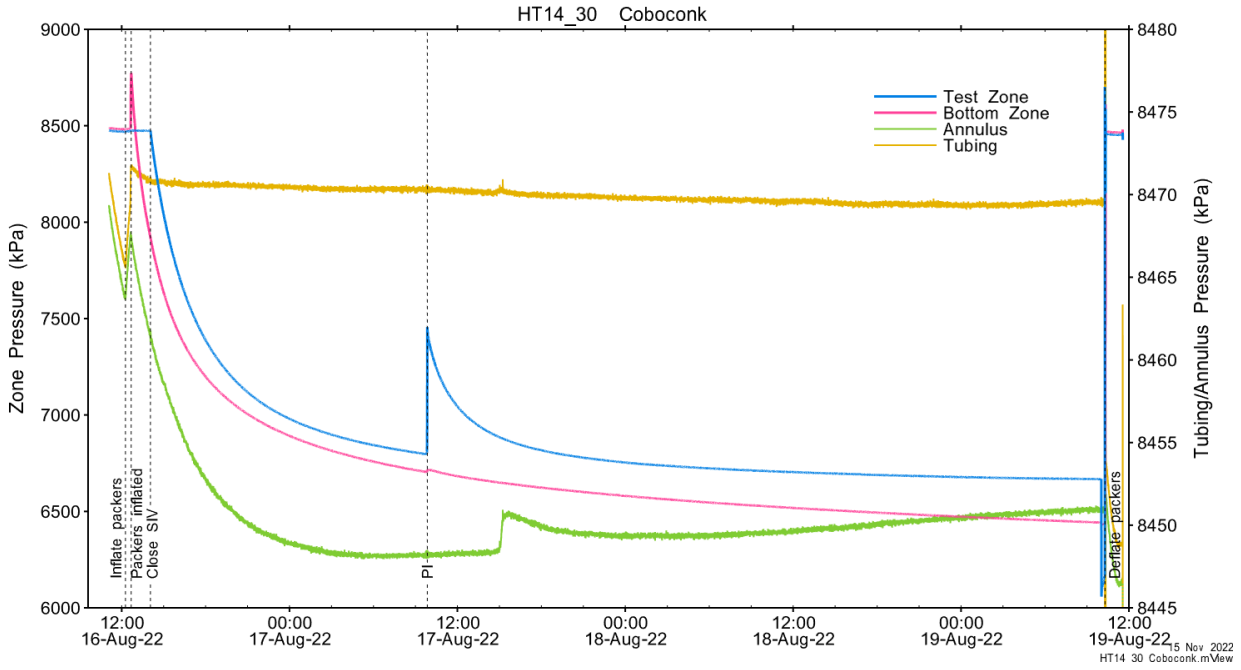

Figure A.283 - Test events and pressures.

A.19.2 Test Analyses

Table A.7 is a summary of test-specific input parameters used in the analyses, while Table A.8 presents the optimized parameters and allowed ranges. Perturbations were originally performed with a wider conductivity range and a maximum 500 cm skin thickness. Conductivity ranges were reduced and skin thickness increased to 1000 cm based on review of initial results.

Table A.92 – nSIGHTS Input Parameters.

Parameter	Value	Units
Test zone radius	6.27	cm
Test zone compressibility	4.27E-10	1/Pa
Test zone length	29.96	m

Table A.93 – nSIGHTS Parameter Optimization Ranges.

Parameter	Minimum	Maximum	Units	Type
Formation hydraulic conductivity (K_f)	1E-14	1E-08	m/s	log
Formation pressure (P_f)	4000	80000	kPa	linear
Specific storage (S_s)	1E-08	1E-04	1/m	log
Skin hydraulic conductivity (K_s)	1E-14	1E-08	m/s	log
Skin thickness (t_s)	0.013	1000	cm	linear

Figure A.18 shows the measured test zone pressure record (with reduced data density for clarity) used in the analysis along with the best-fit simulation and parameter values. Figure A.19 presents the pre-test history, and Figure A.20 shows the Ramey B normalized best-fit pressure and pressure derivatives.

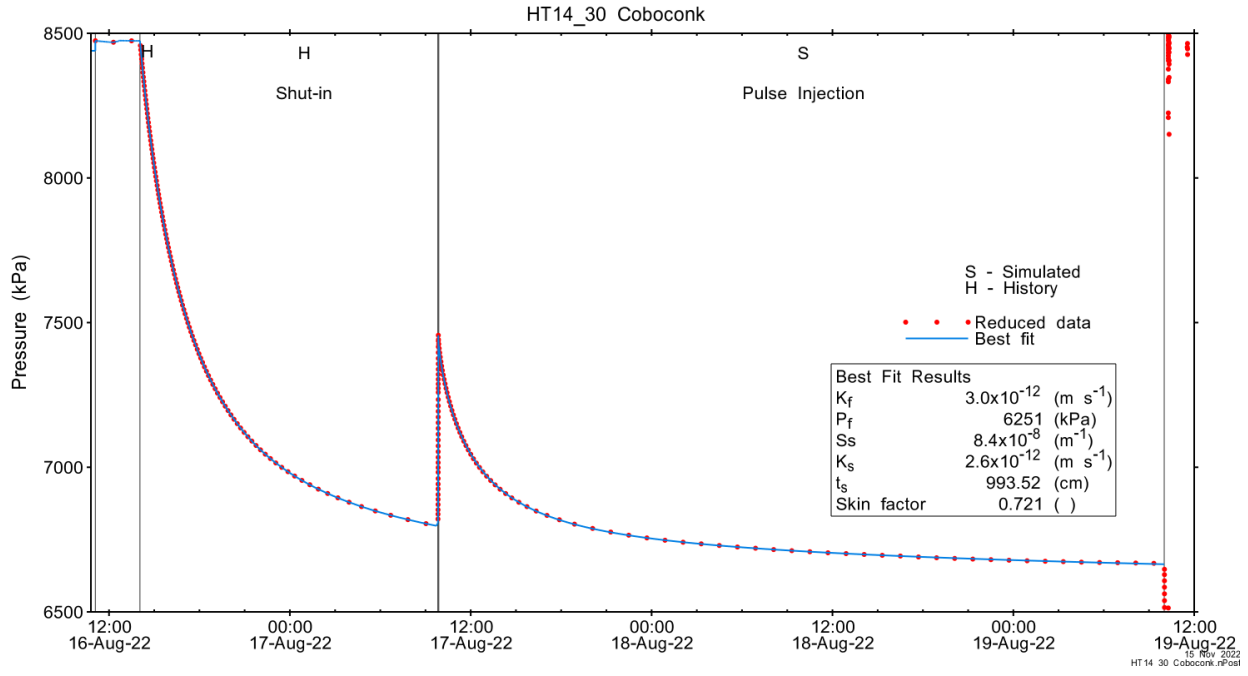

Figure A.284 - Annotated testing sequence showing best-fit simulation and parameter estimates.

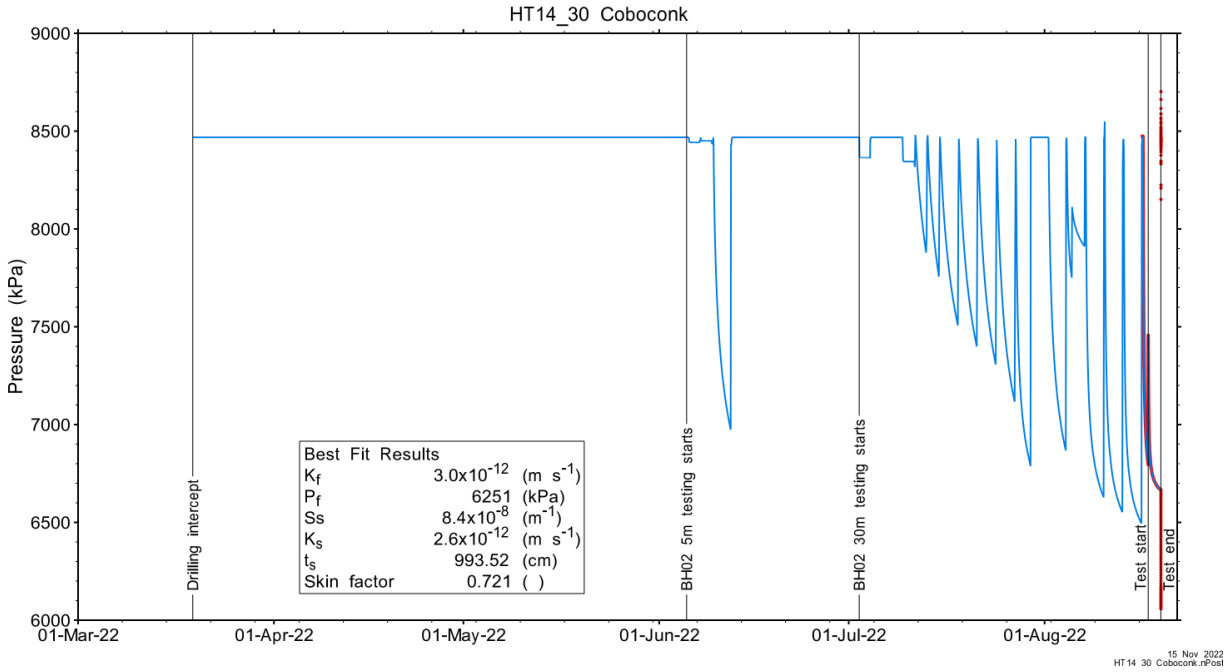

Figure A.285 - Annotated testing sequence showing pre-test history, best-fit simulation and parameter estimates.

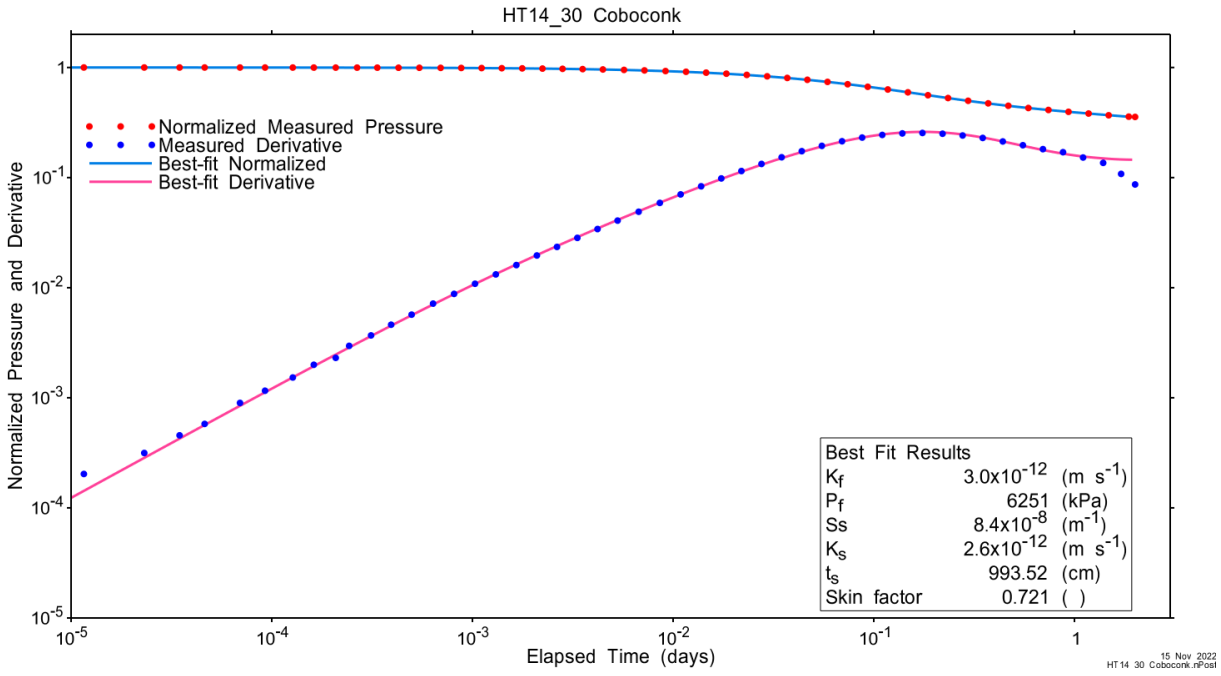

Figure A.286 - Log-log plot showing Ramey B and derivative response for best-fit simulation.

Figure A.21 shows the normalized parameter sensitivity response for the best fit. Sensitivity for fitting parameters is flat at the end of the test, indicating that test duration was sufficient.

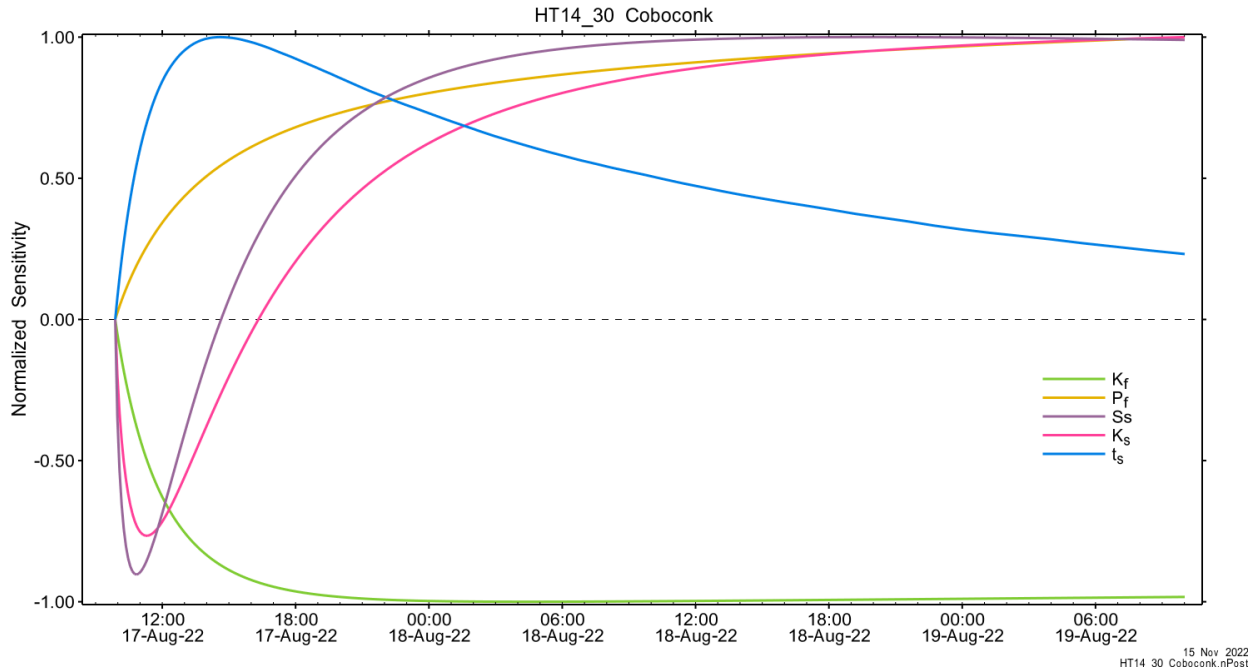

Figure A.287 - Normalized Jacobian for best-fit simulation.

A.19.3 Uncertainty Analyses

The CDF of normalized fit values for all converged simulations and the selected fit discriminant are shown in Figure A.22.

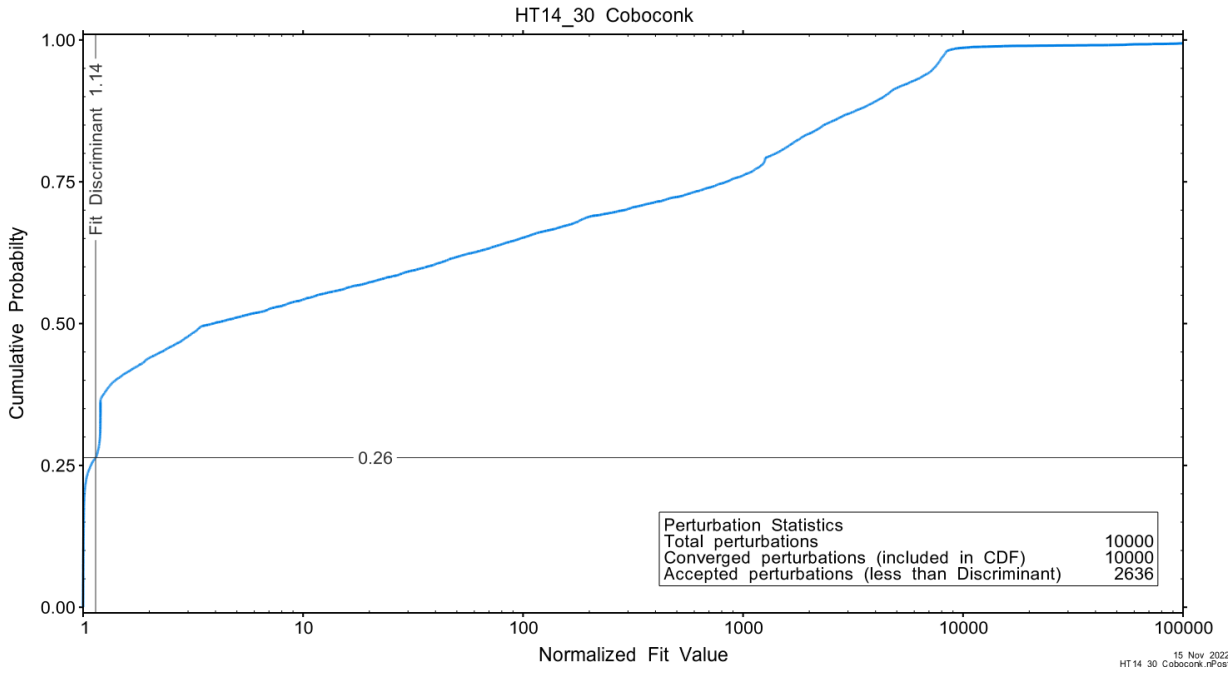

Figure A.288 - Fit value cumulative distribution function.

Summary cross parameter scatter plots for selected formation and skin parameters are given in Figure A.24 and Figure A.25. The light pink dots on the figures are the initial parameter estimates, with red dots overlaying those initial parameter values that resulted in accepted optimization results. The grey dots are converged optimizations which did not meet the fit discriminant. Larger varying color symbols represent the fit value of accepted optimizations, with the blue values representing the best fit.

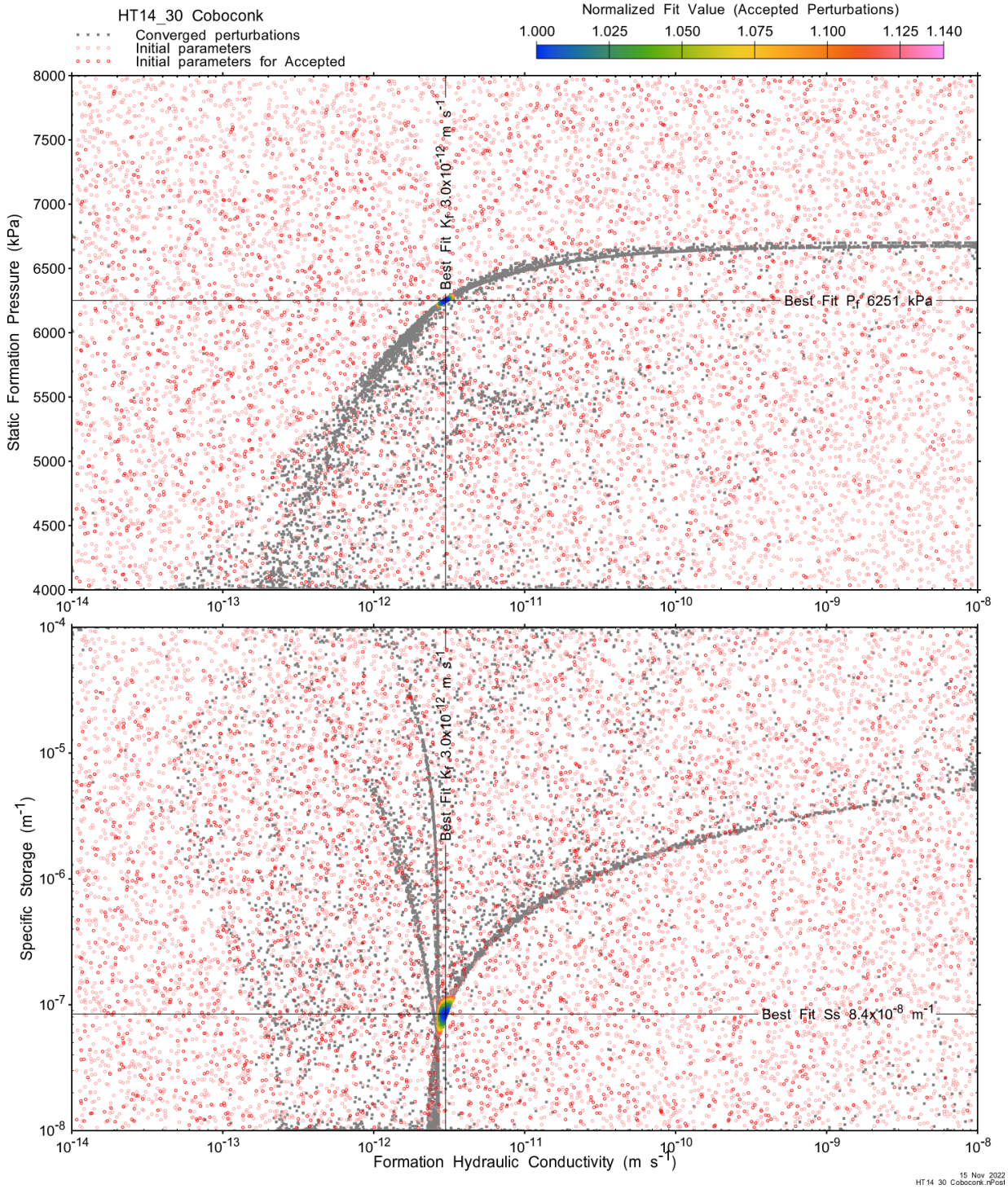

Figure A.289 - XY-scatter plot showing estimates of formation hydraulic conductivity (K_f) vs static formation pressure (P_f) (top panel) and specific storage (Ss) (bottom panel).

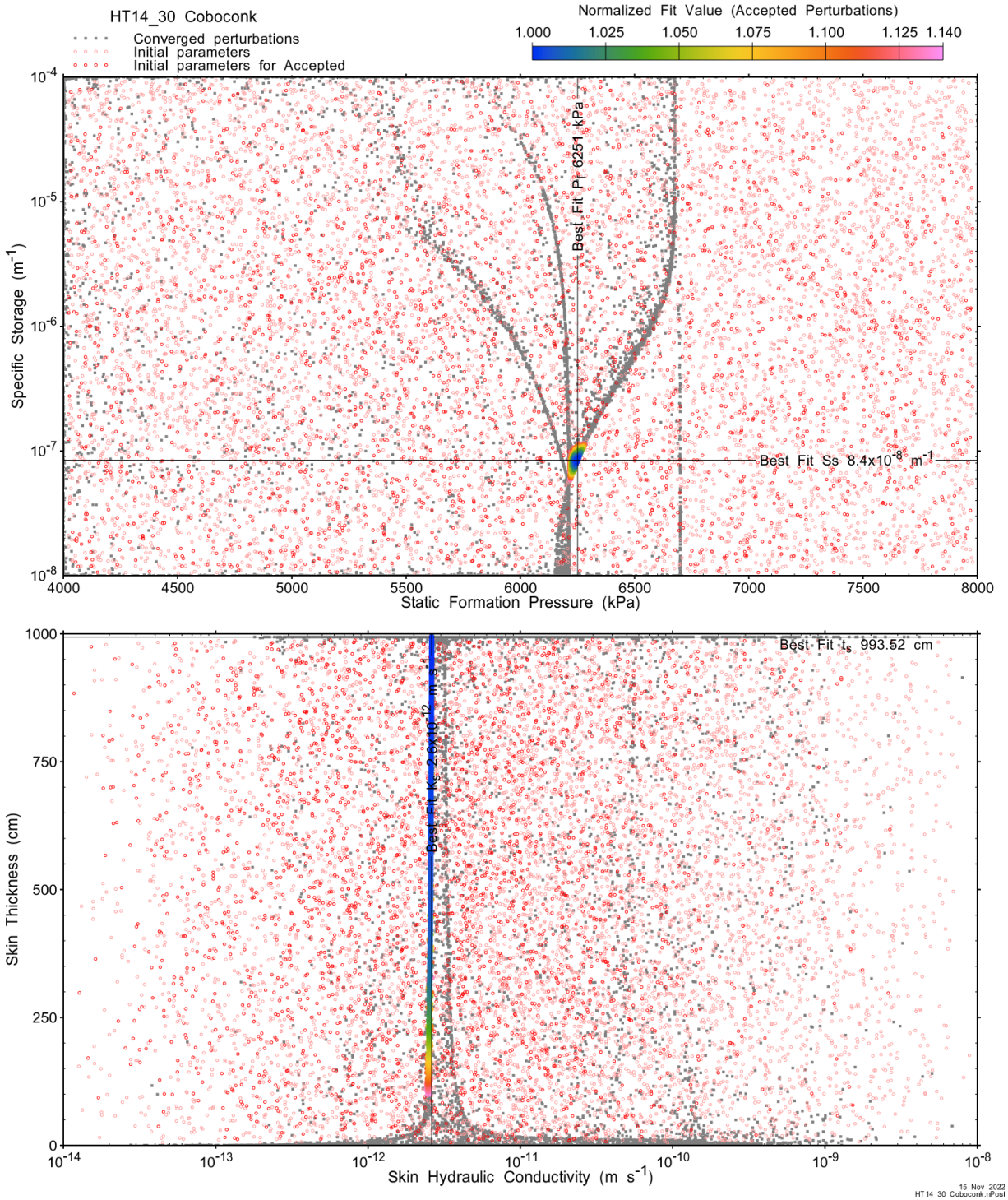

Figure A.290 - XY-scatter plot showing estimates of static formation pressure (P_f) vs specific storage (Ss) (top panel) and skin hydraulic conductivity (K_s) vs skin thickness (t_s) (bottom panel).

Confidence limits and median values are determined from the CDF of accepted optimization results (i.e. the varying color values in the above figures), with best fit value, 5% and 95% confidence indicated on Figure A.26 and Figure A.27.

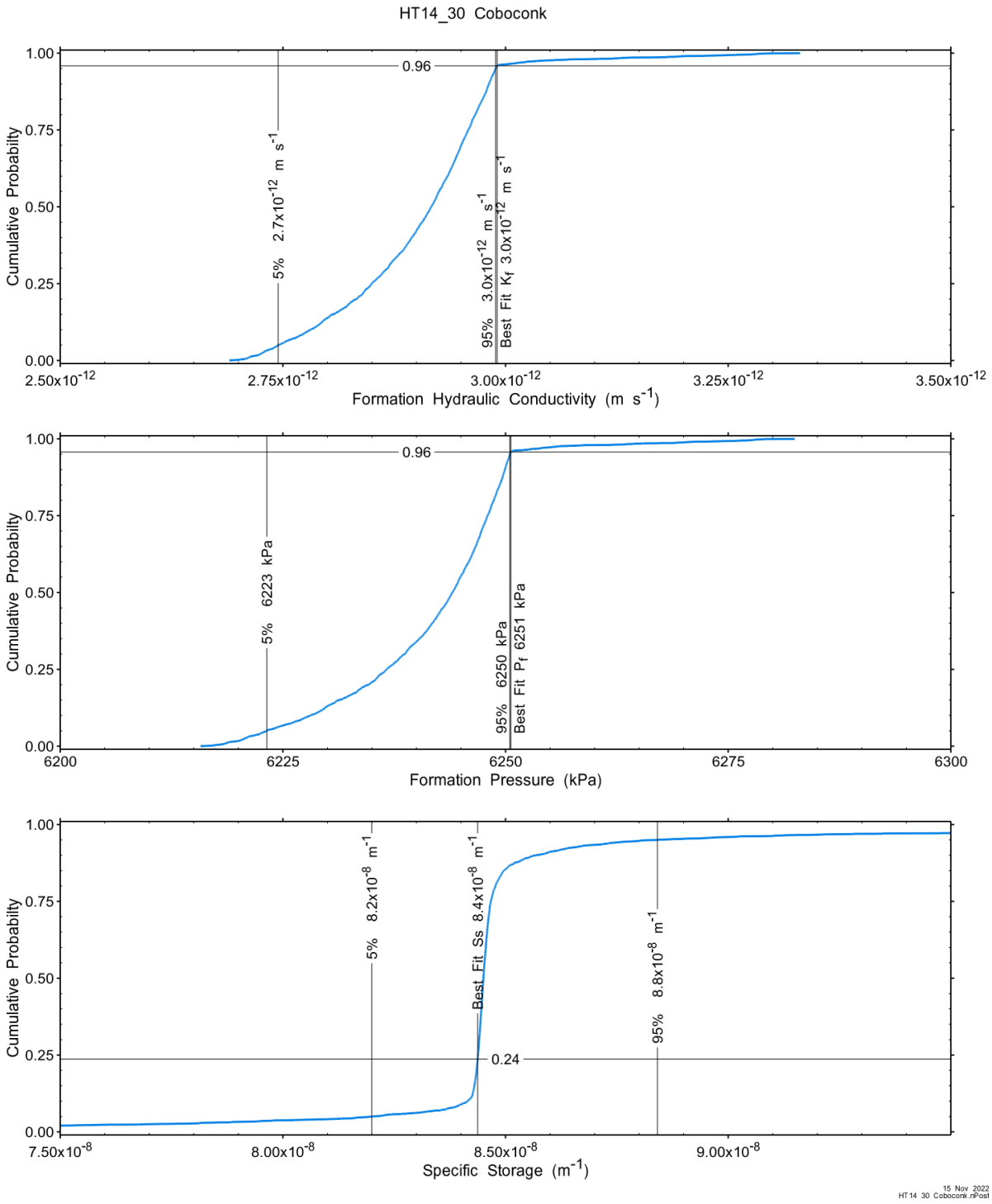

Figure A.291 – Cumulative distribution functions and parameter limits for formation hydraulic conductivity (K_f) (top panel), static formation pressure (P_f) (middle panel) and specific storage (Ss) (bottom panel).

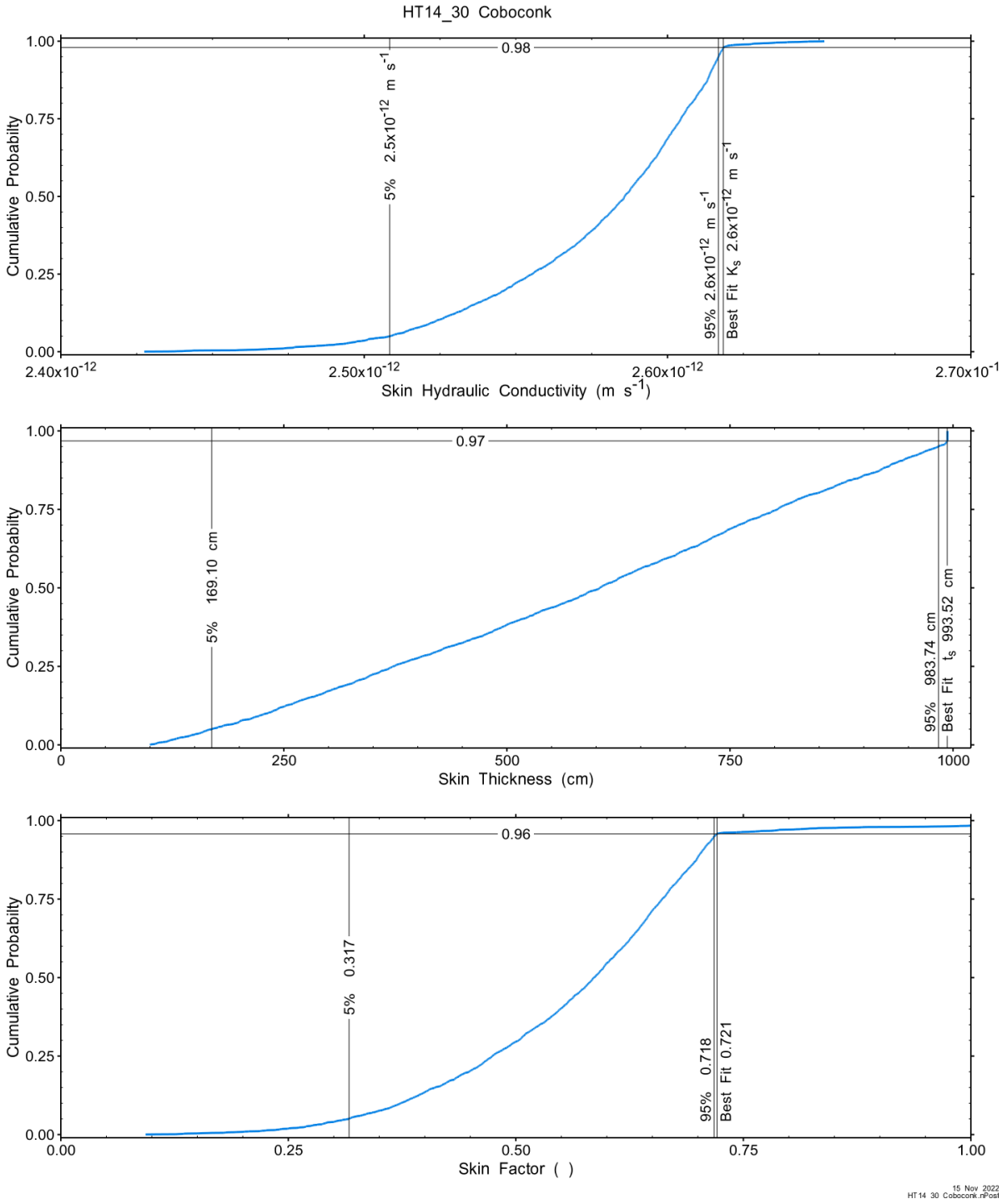

Figure A.292 – Cumulative distribution functions and parameter limits for skin hydraulic conductivity (K_s) (top panel), skin thickness (t_s) (middle panel) and skin factor (s) (bottom panel).

A summary of perturbation results is presented in Figure A.28, with Ramey-processed perturbations in Figure A.13. Those perturbations (2190 of 10,000) with all parameters within the 5% and 95% range present an excellent fit to the measured test zone data.

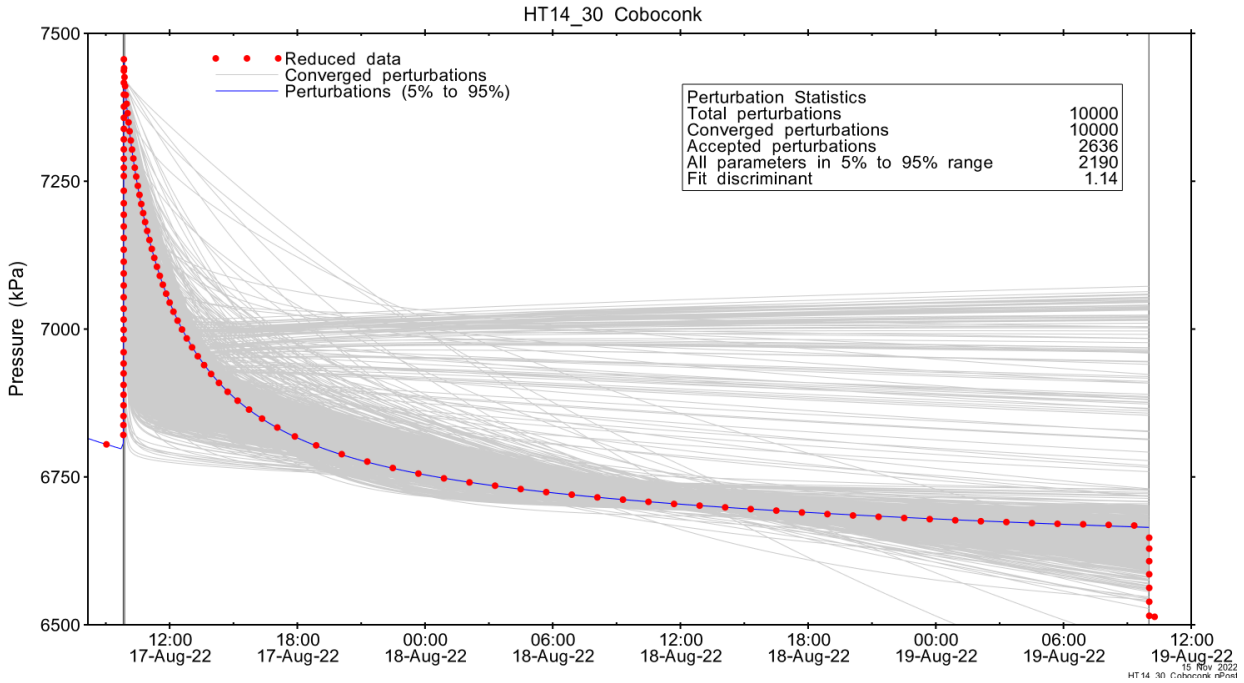

Figure A.293 – Perturbation results – all converged, accepted, and within 5% to 95% for all parameters.

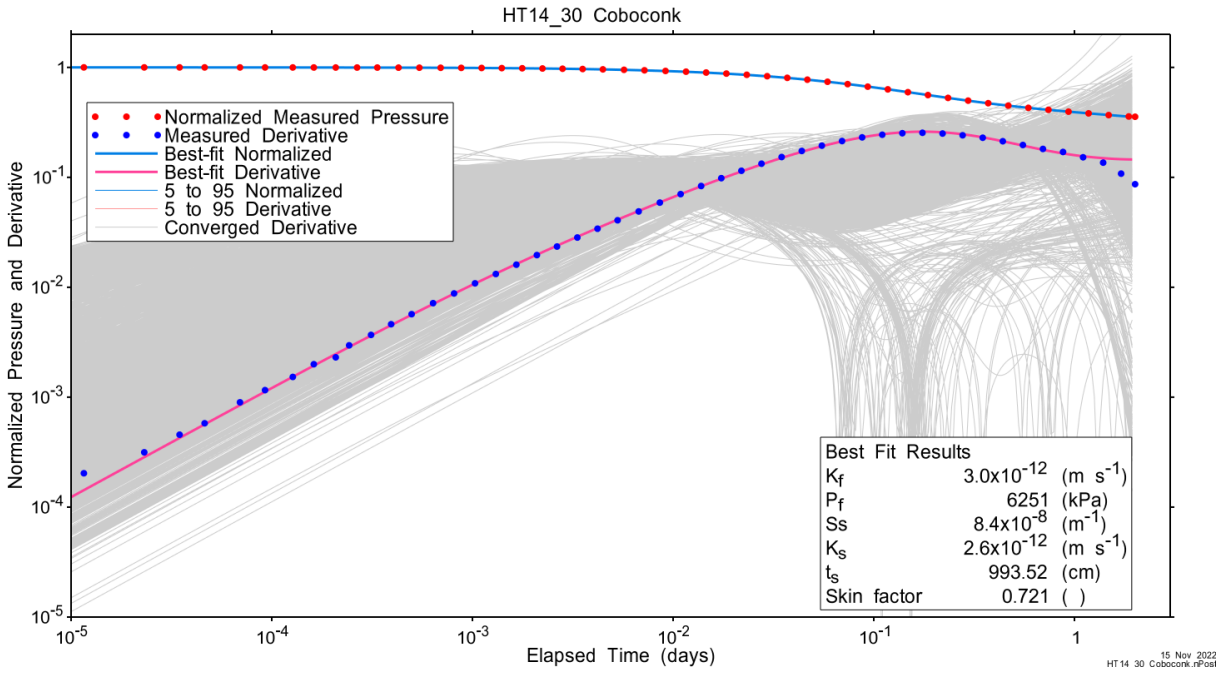

Figure A.294 – Log-log plot showing Ramey B and derivative response for all converged optimizations and those within 5% to 95% for all parameters.

A summary of best-fit and parameter ranges is given in Table A.9.

Table A.94 - Summary of the HT14_30 parameter estimates.

Parameter	Best Fit	5%	Median	95%
K_f (m/s)	3.0E-12	2.7E-12	2.9E-12	3.0E-12
P_f (kPa)	6251	6223	6244	6250
Ss (1/m)	8.4E-08	8.2E-08	8.5E-08	8.8E-08
K_s (m/s)	2.6E-12	2.5E-12	2.6E-12	2.6E-12
t_s (cm)	993.52	169.10	603.73	983.74
s (-)	0.721	0.317	0.586	0.718

Parameter correlations for all perturbations with all parameters within the 5% to 95% limits are given in Table A.5.

Table A.95 – Pearson cross-correlations of 5% to 95% parameters

	Log(K_f)	P_f	Log(Ss)	Log(K_s)	t_s	s
Log(K_f)	1.000	0.229	0.969	-0.968	-0.881	0.967
Pf	0.229	1.000	0.175	-0.153	-0.246	0.182
Log(S_s)	0.969	0.175	1.000	-0.999	-0.959	1.000
Log(K_s)	-0.968	-0.153	-0.999	1.000	0.951	-0.999
t_s	-0.881	-0.246	-0.959	0.951	1.000	-0.963
s	0.967	0.182	1.000	-0.999	-0.963	1.000

A.19.4 Additional Figures

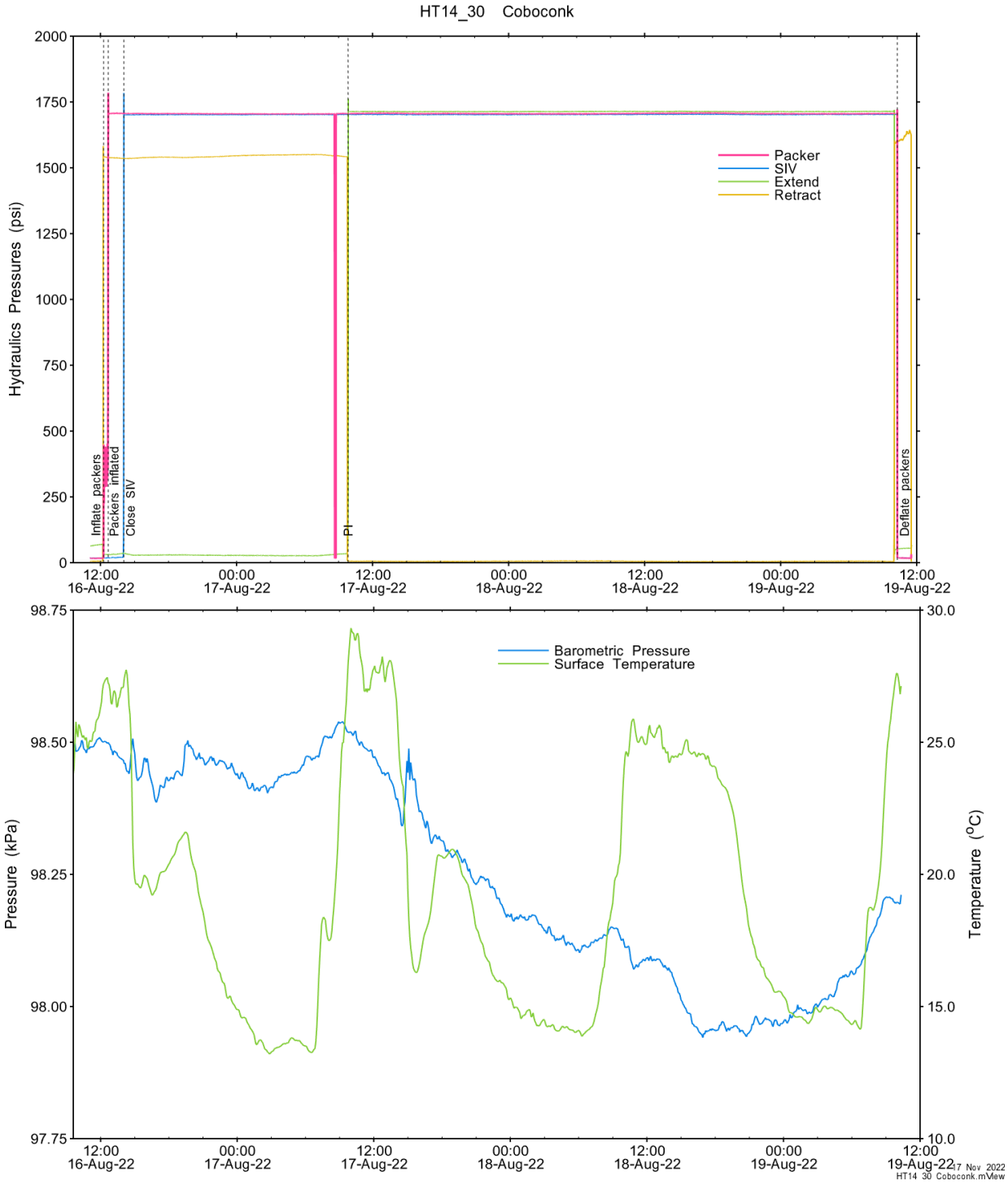

Figure A.295 - Hydraulics pressures and surface temperature/barometric pressure.

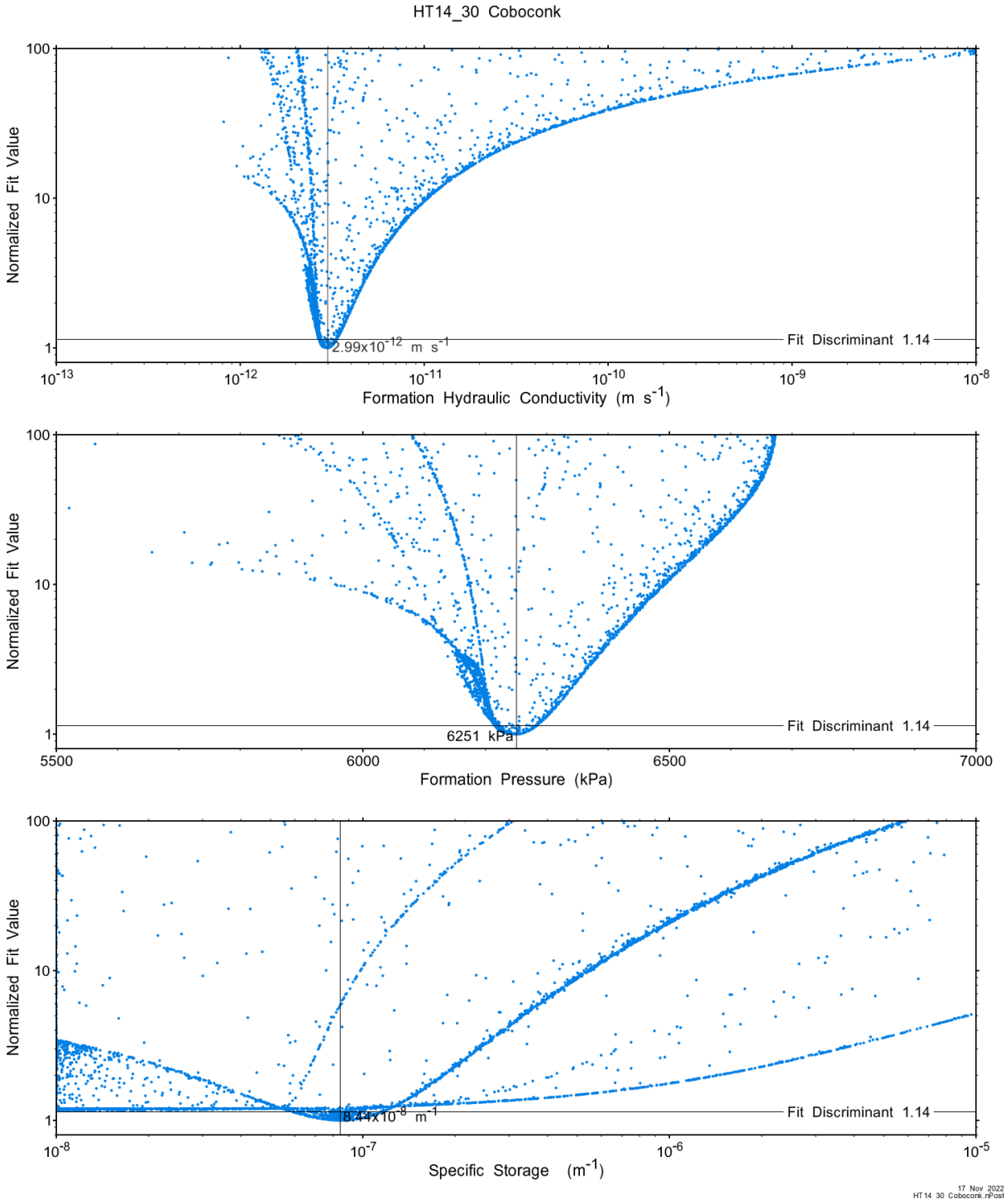

Figure A.296 - XY-scatter plot showing the formation parameter space normalized fit values.

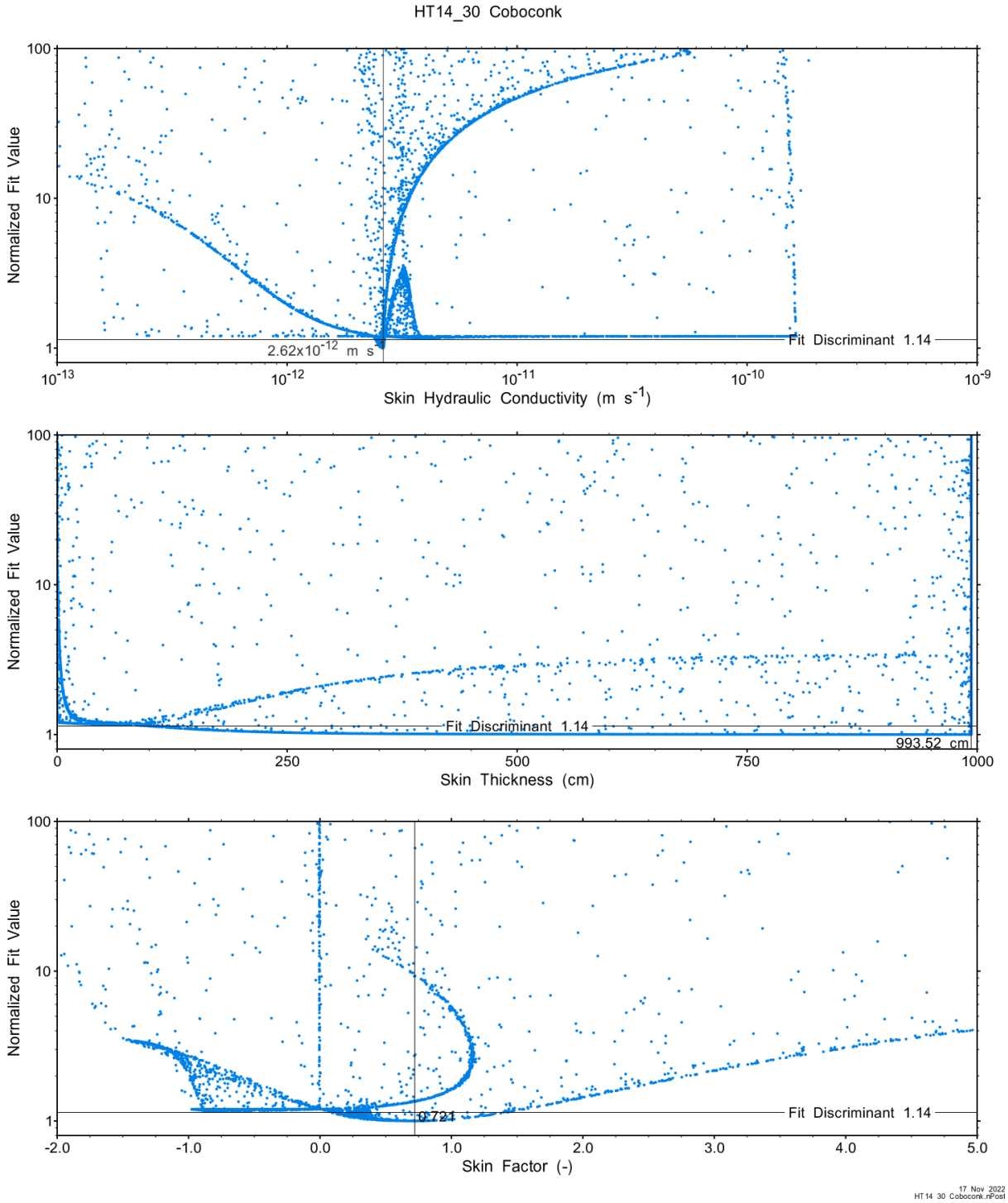

Figure A.297 - XY-scatter plot showing the skin parameter space normalized fit values.

A.20 HT15_30 Gull River

The SB BH02 interval from 840.00 to 869.96 mBGS tested in HT15_30 covers the majority of the Gull River Formation. The test plan called for a single PI test of two days duration. However, a malfunction of the SIV occurred approximately 20 hours into the PI. After cycling the SIV a second PI was initiated, and monitored for two days to successful completion. Both PI tests were included in the optimization and results presented here represent the best combined fit.

A.20.1 Test Data Summary

Table A.6 and Figure A.1 provide a summary of test events and a plot of pressures measured while testing respectively.

Table A.96 - Summary of Test Events.

Event	Start Date & Time	Duration (days)	TZ Pressure (kPa)
Drilling intercept	22-03-20 23:16	151.63	8935
Shut-in	22-08-19 14:26	0.75	8936
Pulse injection #1	22-08-20 08:21	0.84	7713
SIV leak	22-08-21 04:25	1.25	6907
SIV cycle	22-08-22 10:32	0.06	7083
Pulse injection #2	22-08-22 12:01	2.19	8064
Test end	22-08-24 16:33		6779

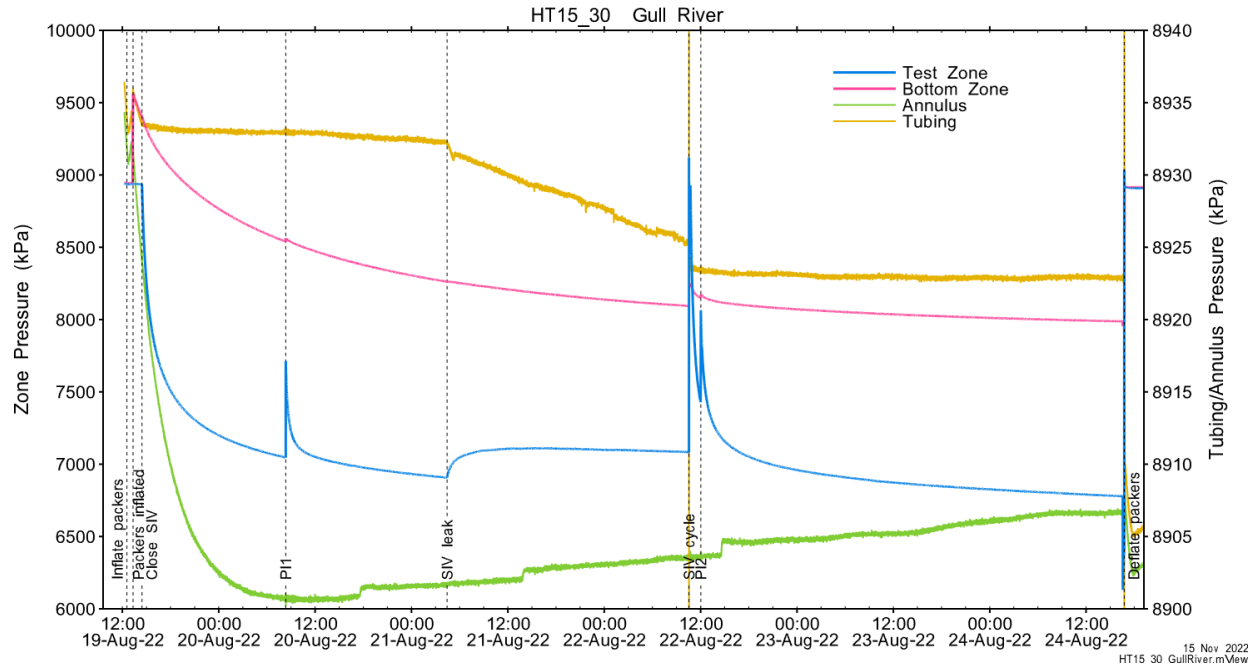

Figure A.298 - Test events and pressures.

A.20.2 Test Analyses

Table A.7 is a summary of test-specific input parameters used in the analyses, while Table A.8 presents the optimized parameters and allowed ranges.

Table A.97 – nSIGHTS Input Parameters.

Parameter	Value	Units
Test zone radius	6.25	cm
Test zone compressibility	4.46E-10	1/Pa
Test zone length	29.96	m

Table A.98 – nSIGHTS Parameter Optimization Ranges.

Parameter	Minimum	Maximum	Units	Type
Formation hydraulic conductivity (K_f)	1E-15	1E-07	m/s	log
Formation pressure (P_f)	3000	8000	kPa	linear
Specific storage (S_s)	1E-08	1E-04	1/m	log
Skin hydraulic conductivity (K_s)	1E-15	1E-07	m/s	log
Skin thickness (t_s)	0.013	1000	cm	linear

Figure A.18 shows the measured test zone pressure record (with reduced data density for clarity) used in the analysis along with the best-fit simulation and parameter values. Figure A.19 presents the pre-test history, and Figure A.20 and Figure A.302 show the Ramey B normalized best-fit pressure and pressure derivatives for test sequences PI1 and PI2, respectively.

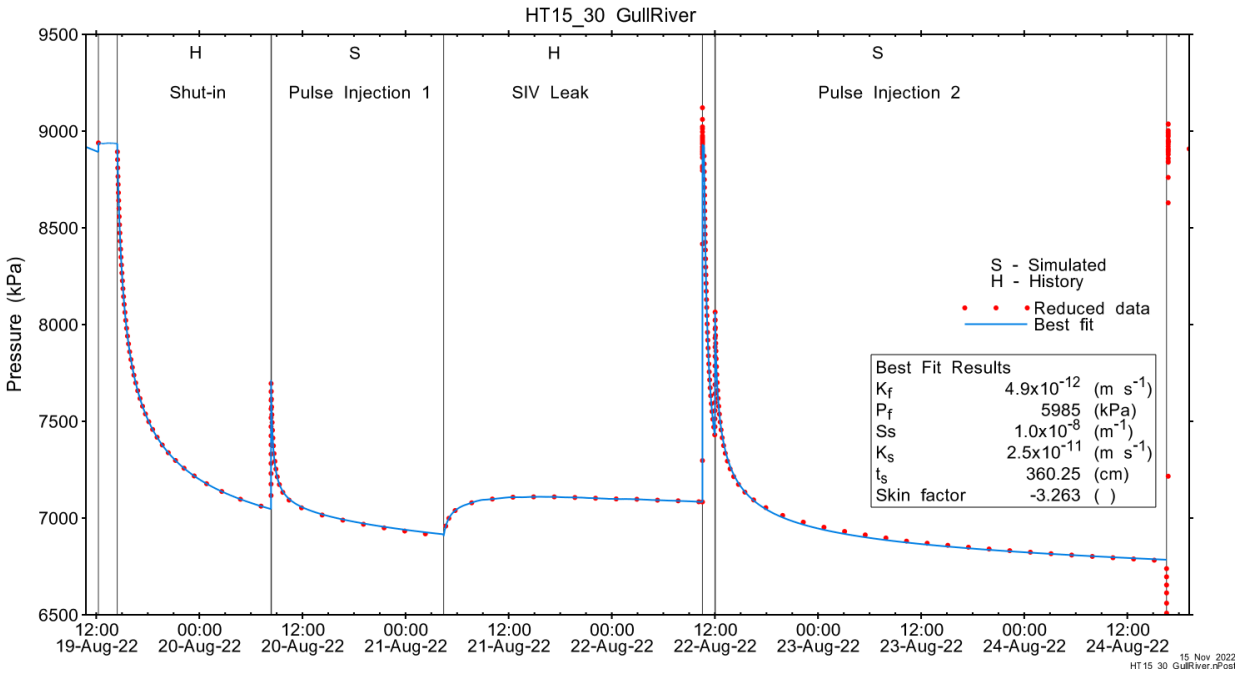

Figure A.299 - Annotated testing sequence showing best-fit simulation and parameter estimates.

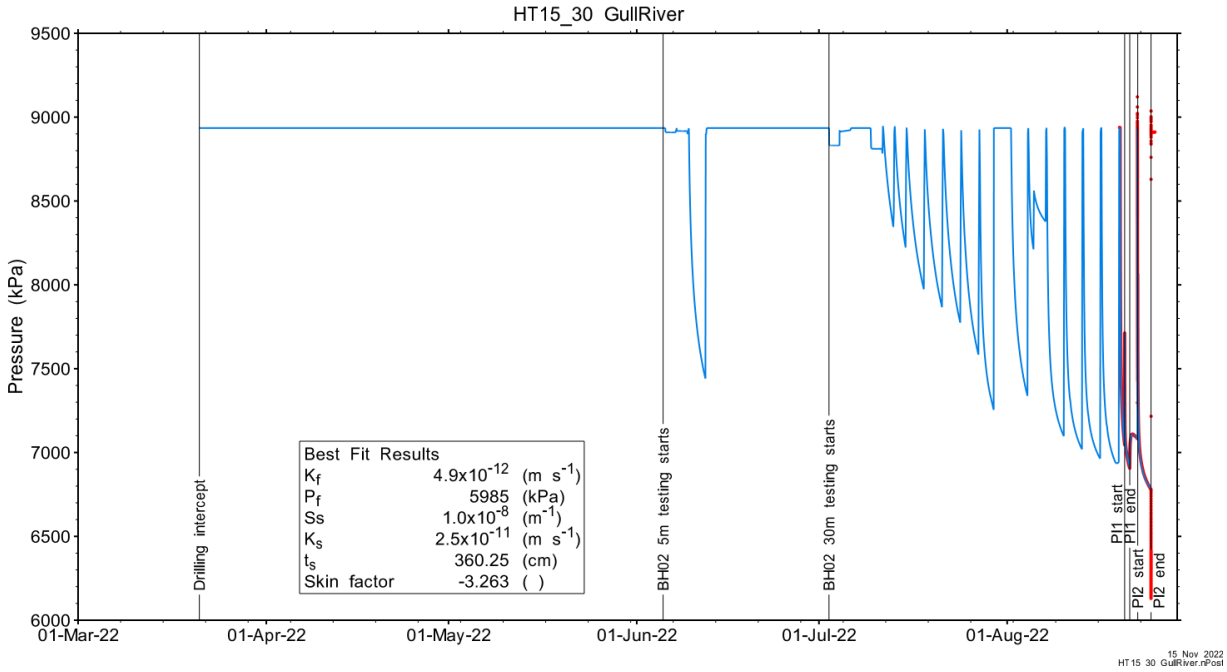

Figure A.300 - Annotated testing sequence showing pre-test history, best-fit simulation and parameter estimates.

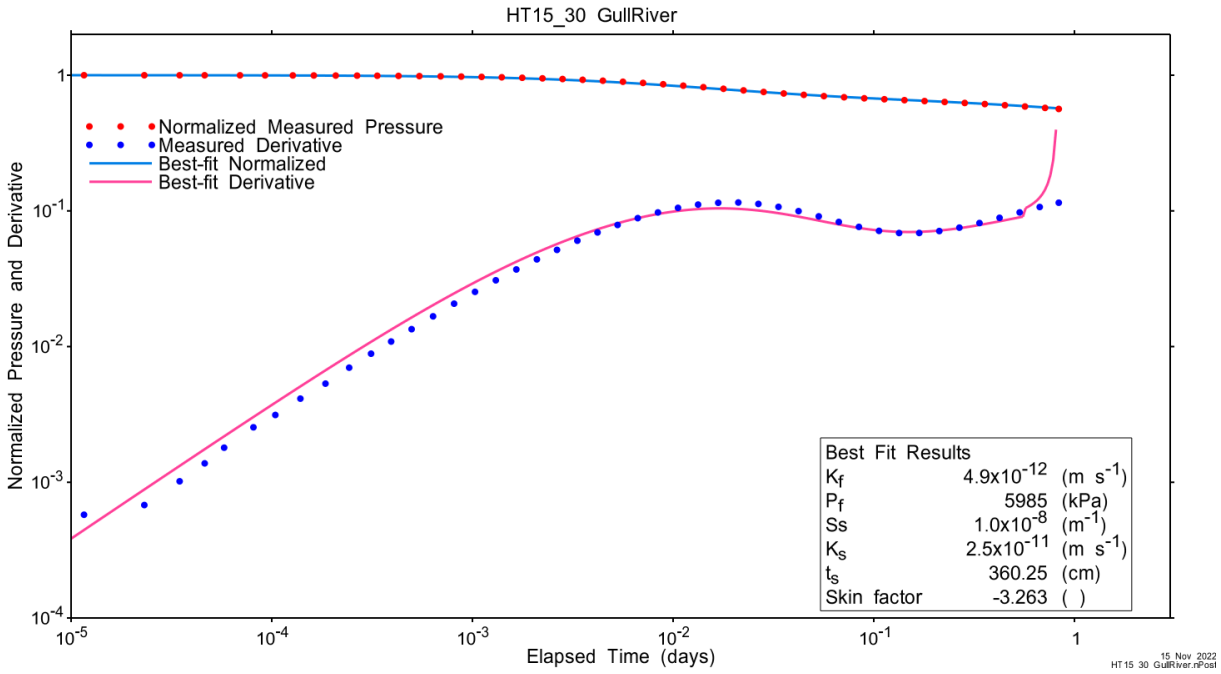

Figure A.301 - Log-log plot showing Ramey B and derivative response for best-fit simulation for test sequence PI1.

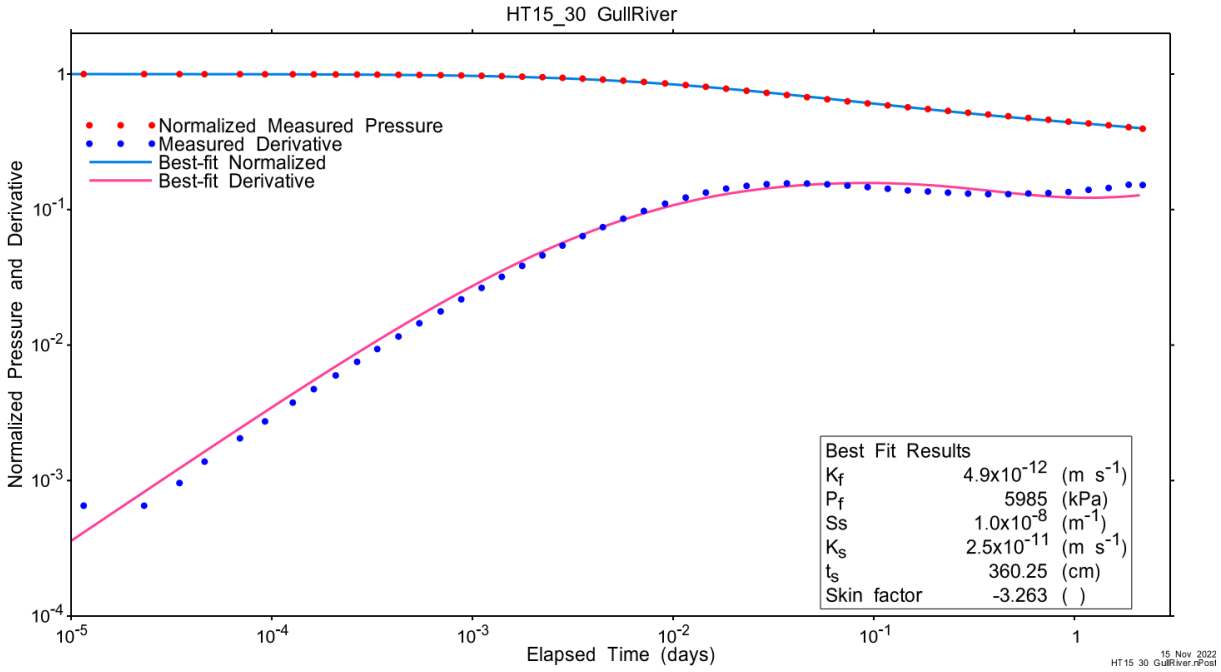

Figure A.302 - Log-log plot showing Ramey B and derivative response for best-fit simulation for test sequence PI2.

Figure A.21 and Figure A.304 show the normalized parameter sensitivity response for the best fit for test sequences PI1 and PI2 respectively. Sensitivity for all fitting parameters is nearly flat at the end of the test, indicating that test duration was sufficient.

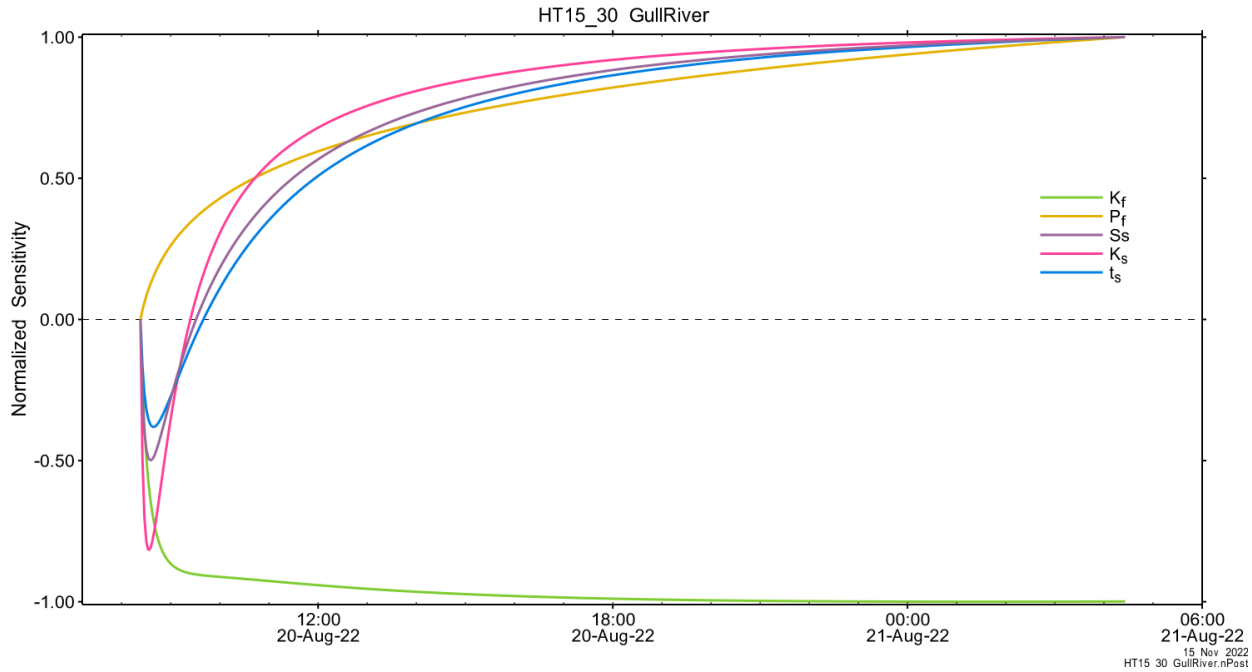

Figure A.303 - Normalized Jacobian for best-fit simulation for test sequence PI1.

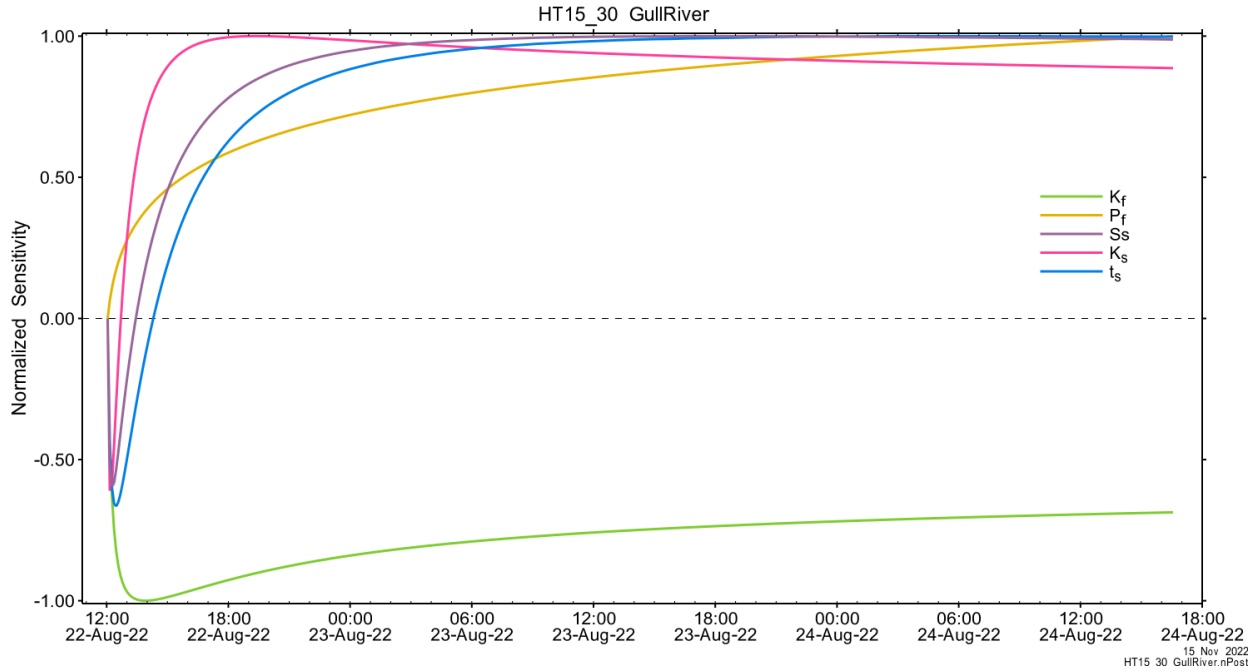

Figure A.304 - Normalized Jacobian for best-fit simulation for test sequence PI2.

A.20.3 Uncertainty Analyses

The CDF of normalized fit values for all converged simulations and the selected fit discriminant are shown in Figure A.22.

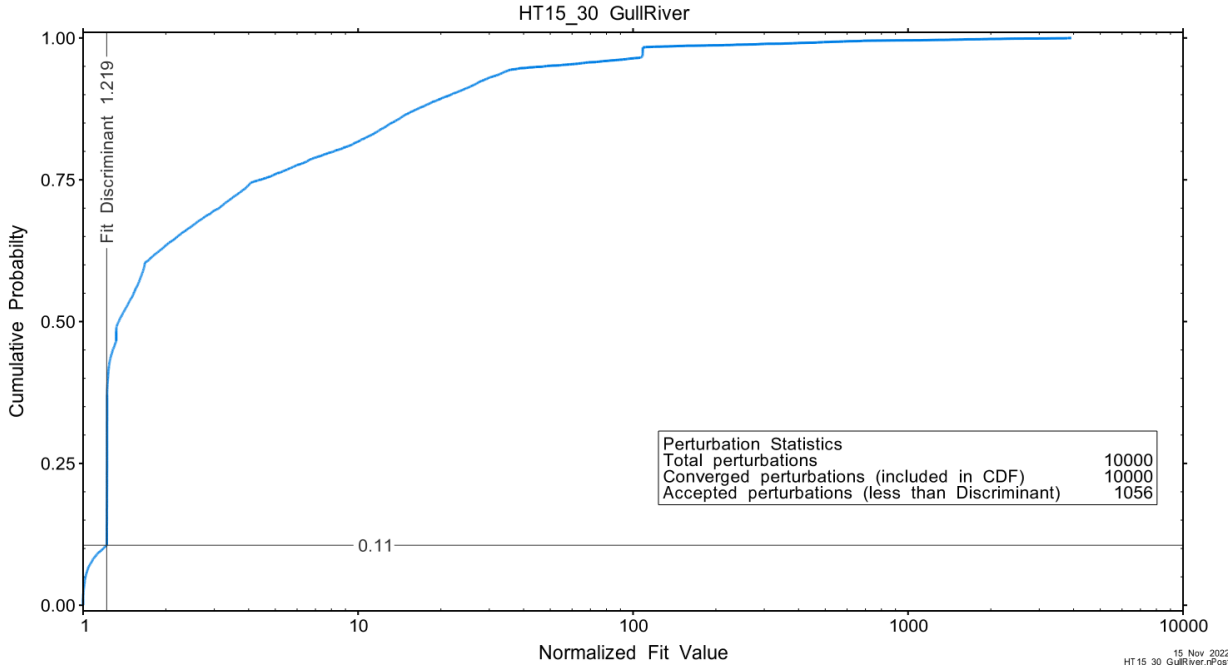

Figure A.305 - Fit value cumulative distribution function.

Summary cross parameter scatter plots for selected formation and skin parameters are given in Figure A.24 and Figure A.25. The light pink dots on the figures are the initial parameter estimates, with red dots overlaying those

initial parameter values that resulted in accepted optimization results. The grey dots are converged optimizations which did not meet the fit discriminant. Larger varying color symbols represent the fit value of accepted optimizations, with the blue values representing the best fit.

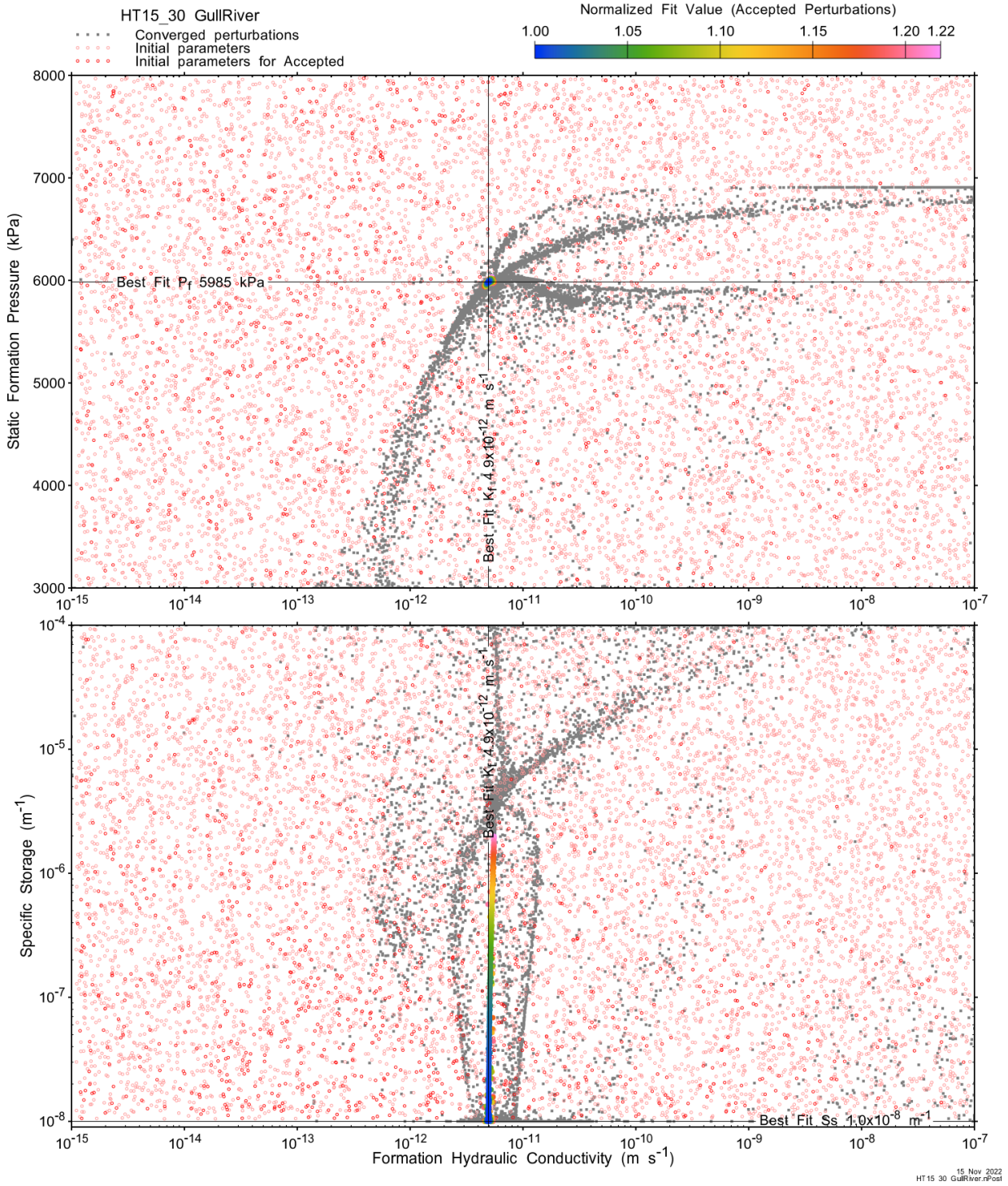

Figure A.306 - XY-scatter plot showing estimates of formation hydraulic conductivity (K_f) vs static formation pressure (P_f) (top panel) and specific storage (Ss) (bottom panel).

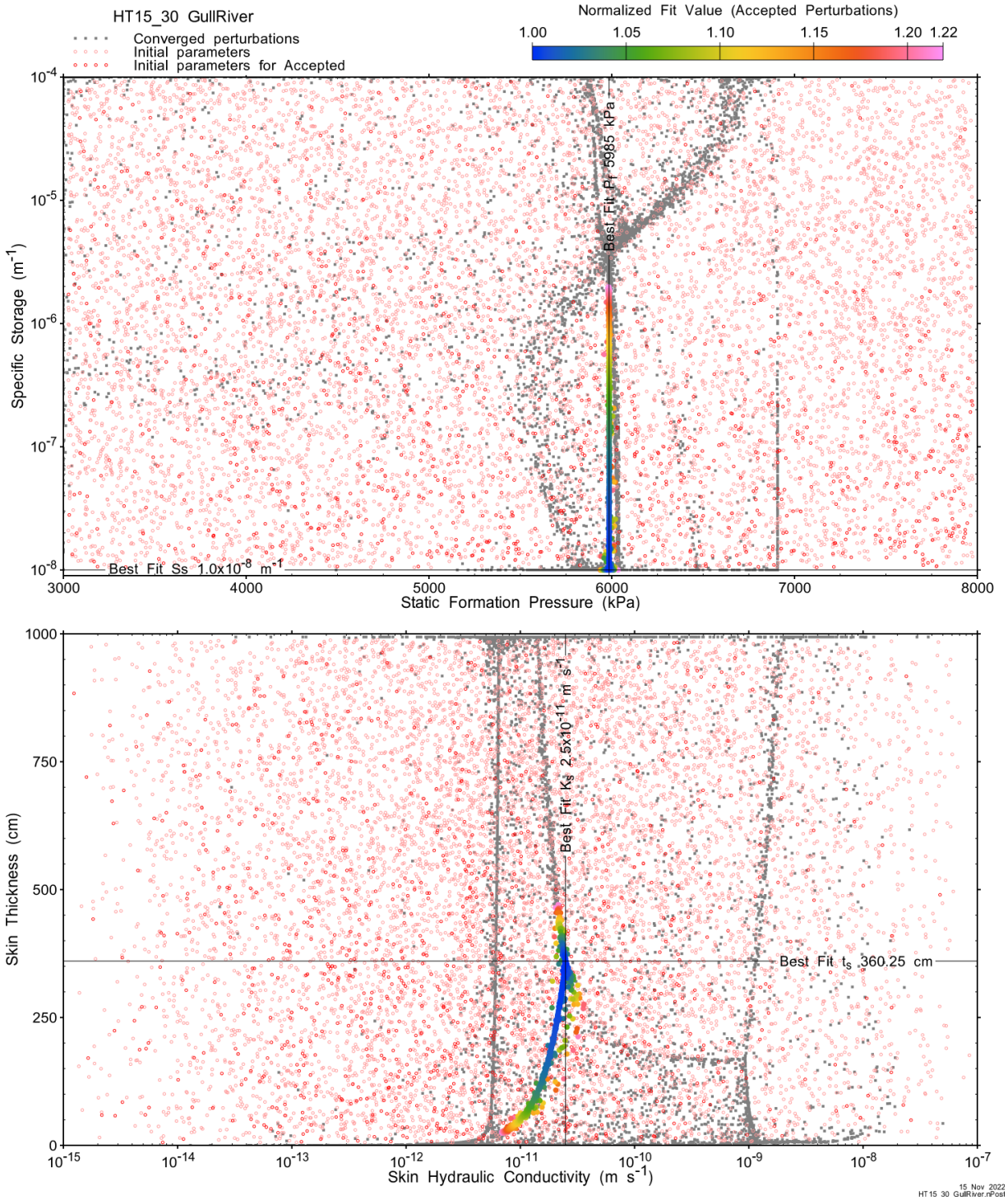

Figure A.307 - XY-scatter plot showing estimates of static formation pressure (P_f) vs specific storage (Ss) (top panel) and skin hydraulic conductivity (K_s) vs skin thickness (t_s) (bottom panel).

Confidence limits and median values are determined from the CDF of accepted optimization results (i.e. the varying color values in the above figures), with best fit value, 5% and 95% confidence indicated on Figure A.26 and Figure A.27.

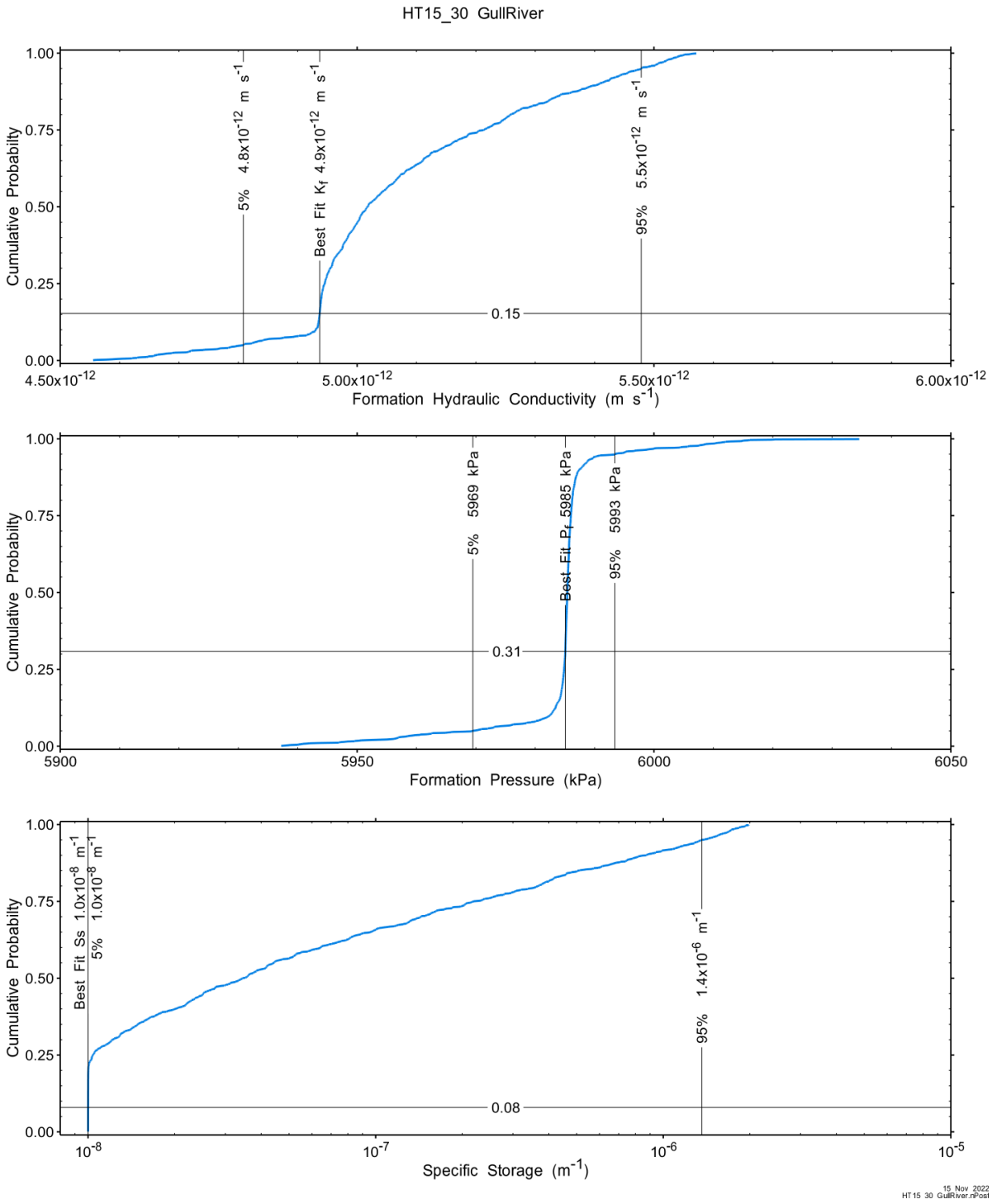

Figure A.308 – Cumulative distribution functions and parameter limits for formation hydraulic conductivity (K_f) (top panel), static formation pressure (P_f) (middle panel) and specific storage (Ss) (bottom panel).

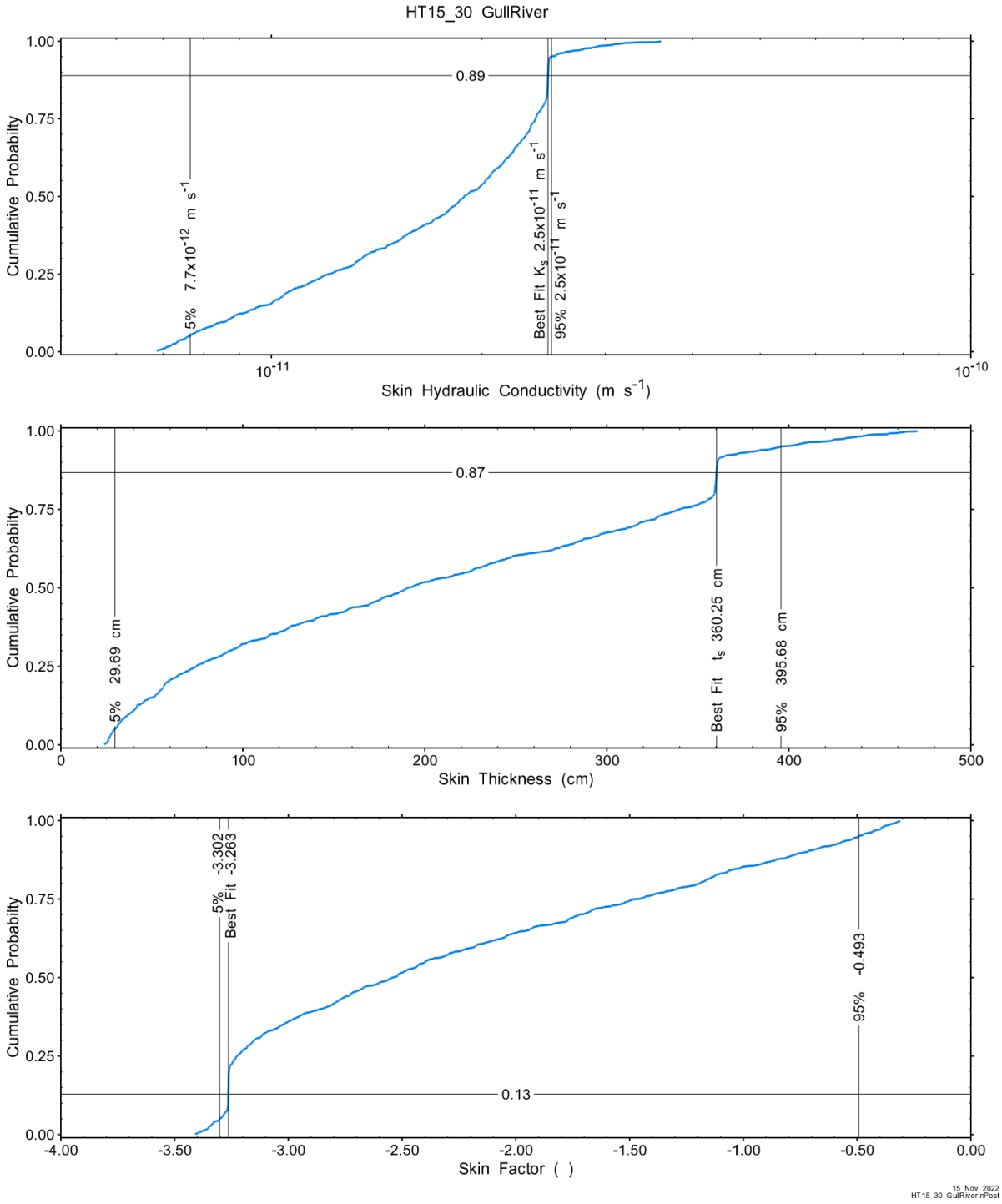

Figure A.309 – Cumulative distribution functions and parameter limits for skin hydraulic conductivity (K_s) (top panel), skin thickness (t_s) (middle panel) and skin factor (s) (bottom panel).

A summary of perturbation results is presented in Figure A.28, with Ramey-processed perturbations in Figure A.13. Those perturbations (851 of 10,000) with all parameters within the 5% and 95% range present a good fit to the measured test zone data, considering that it is the product of a simultaneous fit to two test sequences.

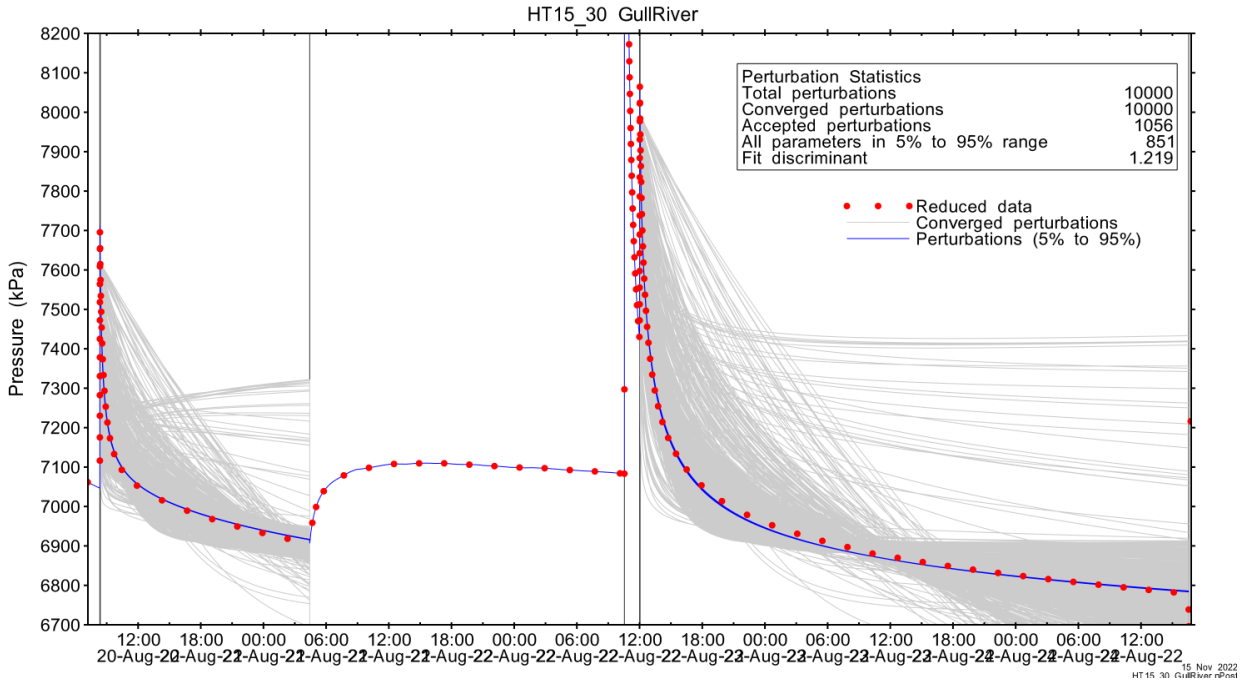

Figure A.310 – Perturbation results – all converged, accepted, and within 5% to 95% for all parameters.

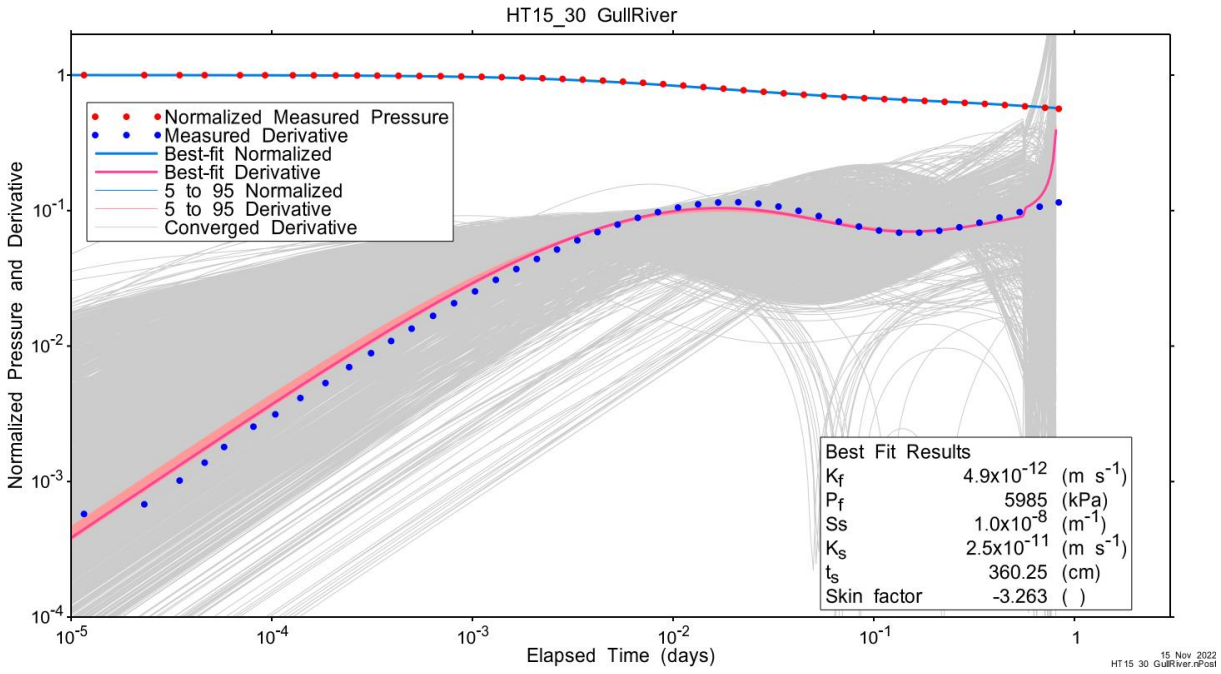

Figure A.311 – Log-log plot showing Ramey B and derivative response for all converged optimizations and those within 5% to 95% for all parameters for test sequence PI1.

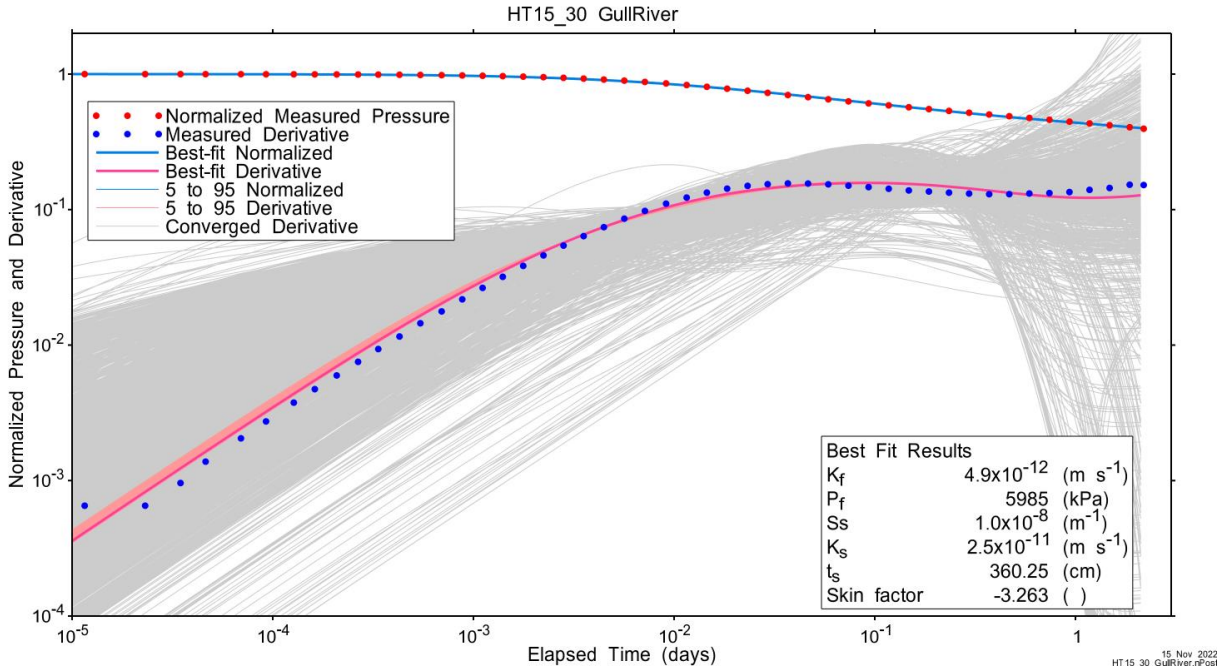

Figure A.312 – Log-log plot showing Ramey B and derivative response for all converged optimizations and those within 5% to 95% for all parameters for test sequence PI2.

A summary of best-fit and parameter ranges is given in Table A.9.

Table A.99 - Summary of the HT15_30 parameter estimates.

Parameter	Best Fit	5%	Median	95%
K_f (m/s)	4.9E-12	4.8E-12	5.0E-12	5.5E-12
P_f (kPa)	5985	5969	5985	5993
Ss (1/m)	1.0E-08	1.0E-08	3.5E-08	1.4E-06
K_s (m/s)	2.5E-11	7.7E-12	1.9E-11	2.5E-11
t_s (cm)	360.25	29.69	190.60	395.68
s (-)	-3.263	-3.302	-2.543	-0.493

Parameter correlations for all perturbations with all parameters within the 5% to 95% limits are given in Table A.5.

Table A.100 – Pearson cross-correlations of 5% to 95% parameters

	Log(K_f)	P_f	Log(Ss)	Log(K_s)	t_s	s
Log(K_f)	1.000	0.229	0.969	-0.968	-0.881	0.967
Pf	0.229	1.000	0.175	-0.153	-0.246	0.182
Log(S_s)	0.969	0.175	1.000	-0.999	-0.959	1.000
Log(K_s)	-0.968	-0.153	-0.999	1.000	0.951	-0.999
t_s	-0.881	-0.246	-0.959	0.951	1.000	-0.963
s	0.967	0.182	1.000	-0.999	-0.963	1.000

A.20.4 Additional Figures

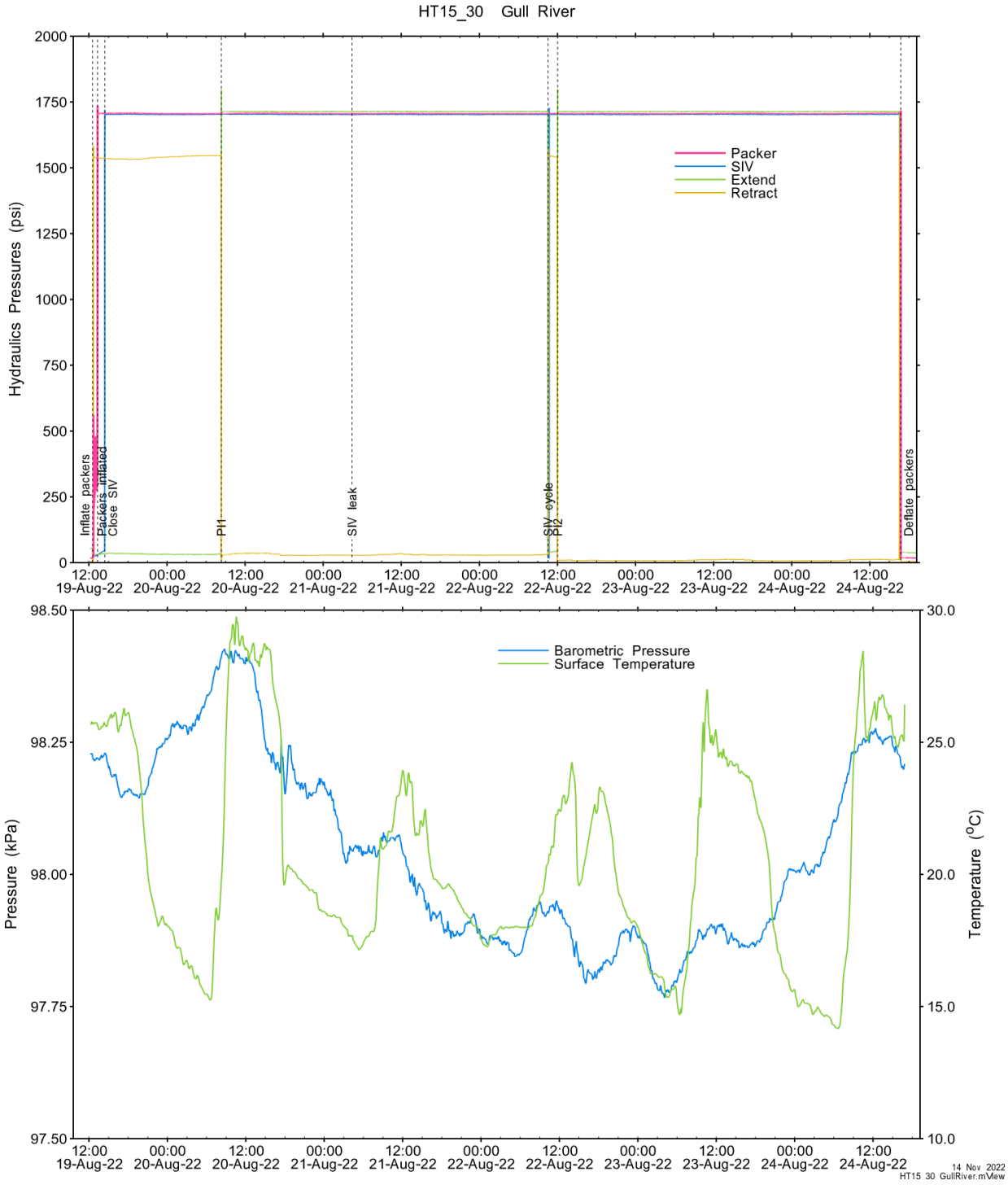

Figure A.313 - Hydraulics pressures and surface temperature/barometric pressure.

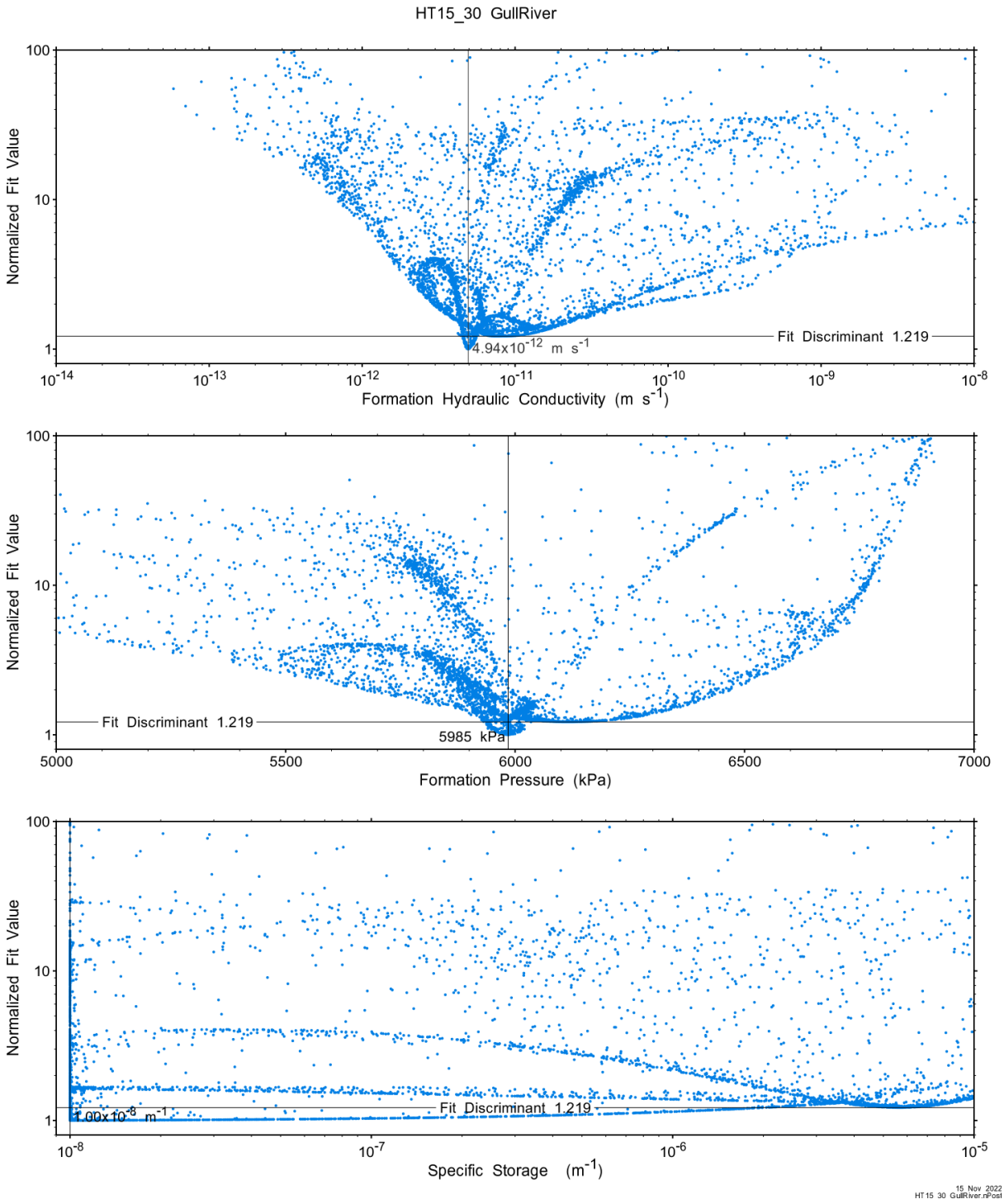

Figure A.314 - XY-scatter plot showing the formation parameter space normalized fit values.

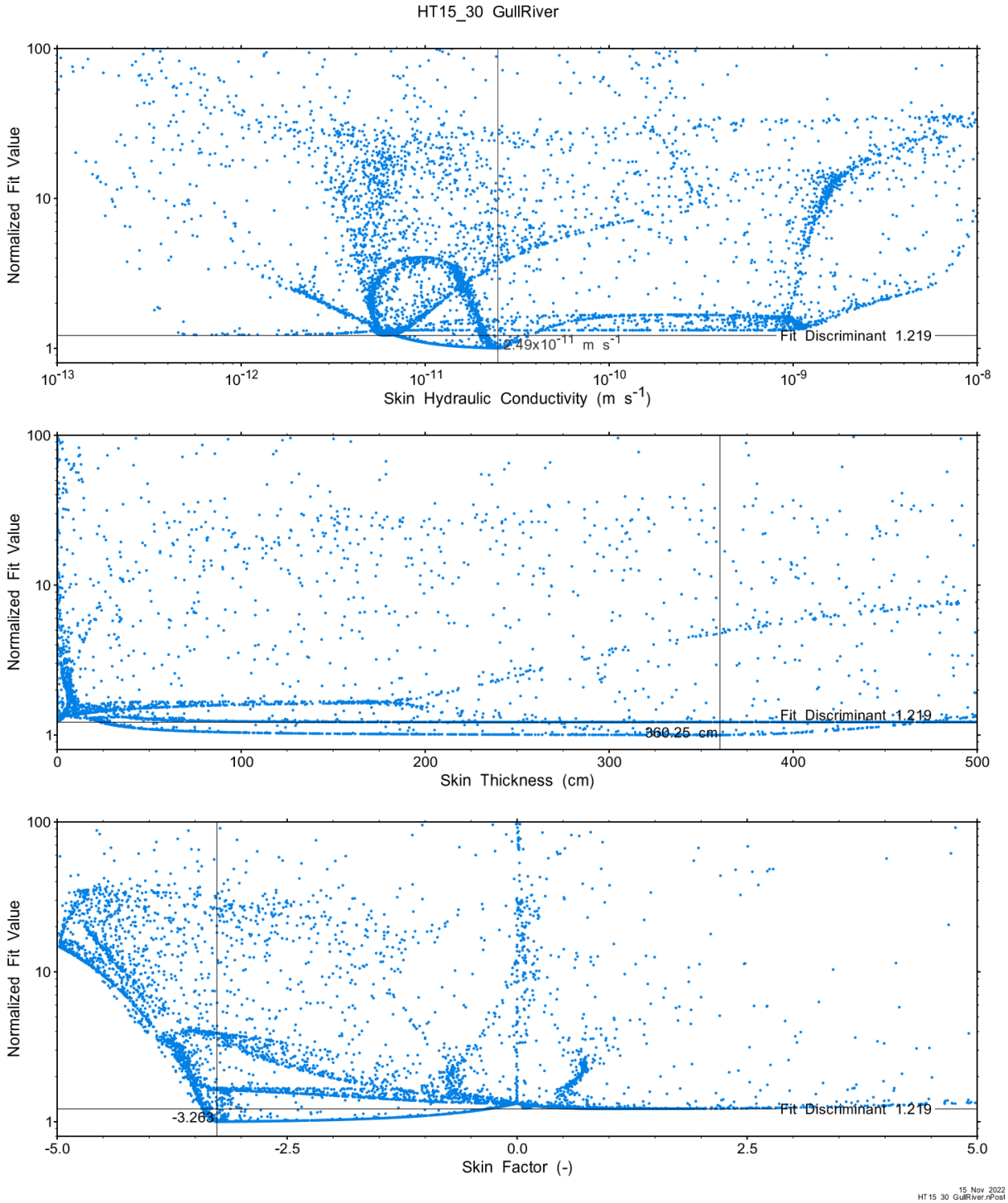

Figure A.315 - XY-scatter plot showing the skin parameter space normalized fit values.